Atiqur Rahman · Shouraseni Sen Roy ·
Swapan Talukdar · Shahfahad *Editors*

Advancements in Urban Environmental Studies

Application of Geospatial Technology and Artificial Intelligence in Urban Studies

MOREMEDIA ▶

Springer

GIScience and Geo-environmental Modelling

Series Editors

Biswajeet Pradhan, School of Information, System and Modelling, University of Technology Sydney, Sydney, Australia

Pravat Kumar Shit , Postgraduate Department of Geography, Raja Narendra Lal Khan Women's College (Autonomous), Midnapore, West Bengal, India

Gouri Sankar Bhunia , GIS, Randstad India Private Ltd, New Delhi, India

Partha Pratim Adhikary , Groundwater Management, ICAR Indian Institute of Water Management, Bhubaneswar, Odisha, India

Hamid Reza Pourghasemi, Department of Natural Resources and Environmental Engineering, Shiraz University, Shiraz, Iran

The "GIScience and Geo-environmental Modelling" book series seeks to publish a broad portfolio of scientific books addressing the interface between geography and the environment. The aim of the book series is to present geospatial technology approaches to data mining techniques, data analytics, modeling, risk assessment, visualization, and management strategies. The series includes peer-reviewed monographs, edited volumes, textbooks, and conference proceedings. The focus of Geo-environmental is on geospatial modelling in the frontier area of earth-environment related fields, such as urban and peri-urban environmental issues, ecology, hydrology, basin management, geohazards, estuarine-ecology, groundwater, agriculture, climate change, land-water, and forest resources, and related topics.

Geo-environmental modelling techniques have enjoyed an overwhelming interest in recent decades among the earth environmental and social sciences research communities for their powerful ability to solve and understand various complex problems and develop novel approaches toward sustainable earth and human society. Geo-environmental modelling using data mining, machine learning, and cloud computing technology is focused on spatiotemporal data analysis and modeling for sustainability in our environment.

Atiqur Rahman · Shouraseni Sen Roy ·
Swapan Talukdar · Shahfahad
Editors

Advancements in Urban Environmental Studies

Application of Geospatial
Technology and Artificial
Intelligence in Urban Studies

Editors
Atiqur Rahman
Department of Geography
Faculty of Natural Sciences
Jamia Millia Islamia
New Delhi, Delhi, India

Shouraseni Sen Roy
Department of Geography
and Sustainable Development
University of Miami
Coral Gables, FL, USA

Swapan Talukdar
Department of Geography
Faculty of Natural Sciences
Jamia Millia Islamia
New Delhi, Delhi, India

Shahfahad
Department of Geography
Faculty of Natural Sciences
Jamia Millia Islamia
New Delhi, Delhi, India

Dedicated to

***Our Teachers Who Make it Possible
to Reach us, Where We are Today***

Foreword

As per United Nations Development Program (UNDP) about 55 per cent of the world's population ($\sim$ 4 billion people) live in urban areas and nearly 2 billion more people are expected to migrate to the cities by 2030, putting unprecedented strain on the infrastructure, environment and natural resources in urban landscape. The scale and pace of urbanisation, as well as demographic change, pose direct threats to the urban system, challenging the efficiency of essential services and, most importantly, jeopardising the environmental quality. Urban environmental issues have become crucial in the twenty-first century for sustainable development. Today space based remote sensing is playing an important role for assessing many components of the urban environment and ecosystem cycles through measurements, monitoring, and modelling. The remote sensing technique has emerged as a new frontier in the urban studies. With the advancement in geospatial technology during recent past in terms of speed of data collection, resolution of sensors and accessibility has made it possible to understand various facets of urban systems. It has made us to monitor the dynamics of urban systems, such as urban landscape pattern and urban sprawl, urban environment and ecology, urban morphology, urban design, etc. Further geospatial technology together with artificial intelligence (AI) based machine leaning and deep learning techniques has made it possible to analyse and model various facets of urban environment at various scales across various disciplines.

I am delighted to introduce this book volume on *Advances in Urban Studies-Application of Geospatial Technology and Artificial Intelligence in Urban Studies*. The book contains twenty-eight research papers compiled as chapters, contributed by the experts of various disciplines across the globe. These papers are technically sound and focused on the application of geospatial techniques and AI for urban environmental management. The primary goal of this book is to improve the coordination of urban observations, monitoring forecasting, and assessment initiatives; to generate up-to-date information on the status and development of urban systems at various scales; to fill existing gaps in integrating urban land observations with various urban ancillary datasets; and to develop innovative ideas and techniques like machine learning and deep learning to support effective and sustainable urban development.

In this regard, the current initiative is socially and scientifically significant in the context of large scale urban transformation and climate change. I am glad that the *editors* have the foresight and energy to bring out this book

volume on such an important topic. It supports rigorous research efforts, advances knowledge about the urban environment and encourages the use of contemporary approaches to deal with potential threats to the urban environment.

Dr. Prakash Chauhan, Director
National Remote Sensing Centre (ISRO)
Government of India
Hyderabad, India

Preface

Urbanisation has increased worldwide during the last 50 years, leading to an increase in urban population and land utilization as well as the transformation of urban and peri-urban land use pattern. Urban areas are predicted to account for almost all the world's overall population growth between 2000 and 2030. In developing countries, the urban population is predicted to rise significantly by 2030. Urban regions are becoming more significant for present and future human population.

Increasing urbanization has had global, regional, and local consequences on land use and land cover. Urbanization causes considerable landscape and environmental changes in most cities. Urban land uses turn natural areas into impermeable surfaces. These changes affect the environment by affecting surface temperature, soil moisture content, and vegetation coverage.

More rural lands are converted to urban lands as more people move to cities. Understanding how these environmental changes will affect our living situations and the ecosystem is critical. In the last 20 years, advances in satellite remote sensing technology and newly deployed satellites have shown the prospect of effectively monitoring environmental conditions in many urban areas. Furthermore, since the debut of Landsat in the 1980s, numerous satellite sensors, such as Landsat TM and ETM+, have been routinely capturing data for extensive areas of the globe. Consequently, a rich archive is available for assessing and monitoring urban land cover changes at local and regional scales. Furthermore, urban remote sensing has aided our knowledge of the biophysical features, pattern, and processes characterizing urban environments. With these decades of observations, remote sensing data for urban regions is becoming more relevant for many physical models of climatic, hydrological, and ecological processes that show how urban areas interact with local, regional, and even the global environment.

With 28 chapters, this book provides a comprehensive and detailed overview of the development and advancements in urban environment evaluation utilizing remote sensing datasets as well as application of GIS tool. The latest research in this field has been combined to better understand the many current geospatial and artificial intelligence technologies for studying urban systems and predicting environmental changes. Current satellite observation capabilities, the use of remote sensing data to describe the metropolitan size and land cover, and satellite-derived data applications for urban environmental evaluations are all discussed.

We are grateful to all the contributors who diligently finished their papers well on time. Their scholarly work has contributed significantly in creating this enlightening and valuable book. We feel that scientists, geographers, ecologists, geologists, climate scientist, urban planners, and others working on the subject of urban environmental management, such as research scholars, environmentalists, and policymakers, would find this a handy book. We also want to express our thanks to the Springer Publishing House, Prof. Prabhat Kumar Shit, Springer Series Editor, Doris Bleier, and her team very professionally, for working with us to have this book published so promptly.

New Delhi, India	Prof. Atiqur Rahman
Coral Gables, USA	Prof. Shouraseni Sen Roy
New Delhi, India	Dr. Swapan Talukdar
New Delhi, India	Mr. Shahfahad

Contents

Editors and Contributors

About the Editors

Dr. Atiqur Rahman is a Professor of Geography at Department of Geography, Faculty of Natural Sciences, Jamia Millia Islamia. He completed B.Sc. (Hons.), M.Sc., M.Phil., and Ph.D. from Aligarh Muslim University, Aligarh. His research interests are urban environmental management, water resources and use of remote sensing satellite data, GIS, and GPS. He was Post-Doctoral Fellow (PDF) at UFZ-Centre for Environmental Research, Leipzig, Germany (1999). He was Co-PI of Indo-Germany DST-DAAD major project. He is the recipient of prestigious Young Scientist Project Grant Award (2001–2004) from Department of Science and Technology (DST), Government of India. He worked as one a member of Scientific Research Team of NASA-funded UEM project on *Urban Ecology and Sustainability* (2004–2007). He is the Co-PI Indo-Canadian major research projects on *Economic Transformation and Childhood Obesity* funded by ICMR (India) and CHI (Canada) during 2010–2015. He was Co-PI of a major research project funded by Ministry of Environment and Forest, Governmtnt of India. He was the collaborating Scientist of another NASA-funded major project on *Impacts of Desert Urbanization on Climate using Remote Sensing and Numerical Modeling* (2012–2015). Prof. Rahman has also done professional development initiative training on *Climate Change and Its Impacts: Resilience and Adaptation to Changes in Precipitation*, at Brown University USA (2010). He served as a Steering Committee (SC) Member (2009–2012) of Population and Environment Research Network (PERN), CISIN, Columbia University, USA. He was the

Advisor-Technical-cum-Consultant on Remote Sensing & GIS for the project (2013–2018) in the PHFI and AIIMS, and Emory University, USA project. He also served as a Member, Governing Body (GB), of some colleges of University of Delhi as a University Nominee. He was the Faculty Coordinator, Inspired Teachers In-Residence Programme organized by the Office of the President of India at Rashtrapati Bhavan, New Delhi, during June 6–12, 2015. Prof. Rahman was Hony. Dy. Director, (Academic) of Jamia Millia Islamia, (2015–2018). Prof. Rahman is the Coordinator, UGC-DRS SAP-I, Special Assistance Programme (SAP-I), Department of Geography, JMI. Eleven students have been awarded Ph.D degrees under his supervision. He has published 15 books and 150 peer-reviewed research papers in the journals of international repute such as Applied Geography, Journal of Environmental Management, Journal of Cleaner Production, Ecological Indicators, Urban Climate, and Nature's Scientific Reports, etc. He has widely traveled across the globe. Prof. Rahman is among the top 2% Global Elite Scientists in a study by University of Stanford, USA, published in the journal *PLOS Biology in 2020, 2021 and 2022*.

Shouraseni Sen Roy received all her pre-doctoral education from the University of Delhi, including B.A., M.A., and M.Phil. In 2005, she completed her Ph.D. from the Arizona State University and joined the faculty in the Department of Geography and Sustainable Development, University of Miami. Her core area of research over the last two decades has concentrated on expanding our understanding of long-term trends in climatic processes, in view of impending climate change. Her research methodology incorporates extensive spatial analysis using advanced geostatistical techniques to analyze trends in climatic variables. In addition to researching on climate processes over the Indian subcontinent, she has addressed targeted climate-related research questions in other regions of the world including the USA, Myanmar, Burundi, China, and South Africa. In addition, she has recently started working on crime patterns in South Florida. Her research has been funded by the National Geographic Society,

American Association of Geographers, and American Institute of Indian Studies. She recently completed a 2018–2019 Fulbright Nehru U.S. Scholar in India to study the role of urbanization on groundwater levels in two megacities of India. Her researches have been published in *The International Journal of Climatology*, *Physical Geography*, *Monthly Weather Review*, *Geophysical Research Letters*, and *Journal of Geophysical Research*, *Weather and Climate Extremes*, *British Journal of Criminology*, *European Journal of Criminal Policy and Research*, *The Professional Geographer*, *Natural Hazards, Cities*, *Groundwater for Sustainable Development*, and *Applied Geography*. She has published several books to name a few, Climate Variability, Extreme Events and Agricultural Productivity in Mountain Regions, Oxford & IBH Publishing, and Linking Gender to Climate Change Impacts in the Global South. Springer.

Dr. Swapan Talukdar is currently working as Dr. D. S. Kothari Post-doctoral fellow in the Department of Geography, Faculty of Natural sciences, Jamia Millia Islamia, New Delhi. Dr. Talukdar completed his Ph.D. from the Department of Geography, University of Gour Banga, West Bengal, India, in 2020. He served as the junior research fellow (JRF) during 2015–2017 and senior research fellow (SRF) during 2017–2019 in the Department of Geography, University of Gour Banga. He has also completed several short- and long-term courses on remote sensing, machine learning, and AI from different Scientific Institutes of India such as IITs and NITs. Dr. Talukdar has completed two international projects as Co-PI in collaboration with the King Khalid University, Saudi Arabia. He has published more than 85 scientific research articles in the journals of international repute such as Journal of Cleaner Production, Environmental Pollution, Scientific Reports, Ecological Indicators, Sustainable Cities and Society, Remote Sensing, etc. His main areas of research are urban environment, urban wetlands, natural hazards, remote sensing, and AI and their applications in environmental management. He has served as the reviewer for several reputed international journals.

Dr. Shahfahad completed his B.A. (Hons.) Geography in 2015, M.A. Geography in 2017 and Ph.D. in 2022 from the Department of Geography, Jamia Millia Islamia, New Delhi. Currently, he is working as senior researcher in the Department of Geography, Faculty of Natural sciences, Jamia Millia Islamia, New Delhi. He has served as the junior research fellow (JRF) during 2017–2019 and senior research fellow (SRF) during 2019–2022 in the Department of Geography, Jamia Millia Islamia. His core areas of research are urban expansion, urban climate change, urban hydrology as well as applications of geospatial techniques and artificial intelligence in urban studies. He has extensively studied the climate pattern and change over the metropolitan cities of Indian subcontinent. He has published more than 50 scientific research articles in the journals of international repute such as *Journal of Environmental Management, Journal of Cleaner Production*, *Urban Climate*, *Scientific Reports*, *Ecological Indicators*, *Remote Sensing*, *Geocarto International*, *Ecological Informatics*, etc. He has served as the reviewer for several reputed international journals.

Contributors

Shukla Acharjee Centre for Studies in Geography, Dibruragh University, Dibrugarh, Assam, India

Ateeque Ahmad Department of Geography, Faculty of Science, Aligarh Muslim University, Aligarh, India

Mansoor Ahmad Department of Geography, University of Jammu, Jammu, Jammu and Kashmir, India

Uzma Ajmal Department of Geography, Faculty of Science, Aligarh Muslim University, Aligarh, India

Vaseem Akram Economics and Business Environment Area, Indian Institute of Management Jammu, Jammu, Jammu and Kashmir, India

MD Tushar Ali Department of Geography, University of Gour Banga, Malda, West Bengal, India

Sk Ajim Ali Department of Geography, Faculty of Science, Aligarh Muslim University, Aligarh, India

Salman Amin Department of Architecture, Faculty of Architecture & Ekistics, Jamia Millia Islamia, New Delhi, India

Mangalasseril Mohammad Anees School of Environmental Sciences, Jawaharlal Nehru University, New Delhi, India

Asif Department of Geography, Faculty of Natural Sciences, Jamia Millia Islamia, New Delhi, India

Rohit Kumar Azad Department of Geography, Faculty of Natural Sciences, Jamia Millia Islamia, New Delhi, India

Vladimir Berg BCC Geospatial Center of the CUNY CREST Institute, City University of New York, Bronx, USA

Sunil Bhaskaran BCC Geospatial Center of the CUNY CREST Institute, City University of New York, Bronx, USA

Sanjiv Bhatia Department of Mathematics and Computer Science, University of Missouri-St. Louis, St. Louis, MO, USA

Eshita Boral Department of Geography and Disaster Management, Tripura University, Suryamaninagar, Tripura, India

Subrata Chattopadhyay Department of Architecture and Regional Planning, Indian Institute of Technology,, Kharagpur, West Bengal, India

Andrella Collins BCC Geospatial Center of the CUNY CREST Institute, City University of New York, Bronx, USA

Arijit Das Department of Geography, University of Gour Banga, Malda, West Bengal, India

Manob Das Department of Geography, University of Gour Banga, Malda, West Bengal, India

Rajib Tarani Das Centre for Studies in Geography, Dibruragh University, Dibrugarh, Assam, India

Tanmoy Das Department of Geography, Faculty of Natural Sciences, Jamia Millia Islamia, New Delhi, India

Sandipta Debanshi Department of Geography, University of Gour Banga, Malda, West Bengal, India

Jatan Debnath Department of Geography, Gauhati University, Guwahati, Assam, India

Prajnamita Debnath Department of Geography and Disaster Management, Tripura University, Suryamaninagar, Tripura, India

Ipsita Dutta Department of Geography, University of Gour Banga, Malda, West Bengal, India

Mrinalendra Narayan Dutta Department of Applied Geology, Dibruragh University, Dibrugarh, Assam, India

Kulsum Fatima Department of Architecture, Faculty of Architecture and Ekistics, New Delhi, India;
SAPL, University of Calgary, Calgary, AB, Canada

Sajal Ghosh Department of Geography and Disaster Management, Tripura University, Suryamaninagar, Tripura, India

Aakriti Grover Department of Geography, Central University of Tamil Nadu, Thiruvarur, India

Rajan Dev Gupta Civil Engineering Department and GIS Cell, Motilal Nehru National Institute of Technology Allahabad, Prayagraj, India

Parvez Hayat Centre for Disaster Management, Department of Geography, Faculty of Natural Sciences, Jamia Millia Islamia, New Delhi, India

Mujahid Husain Department of Geography, Faculty of Natural Sciences, Jamia Millia Islamia, New Delhi, India

Qamar Irshad Department of Architecture, Faculty of Architecture & Ekistics, Jamia Millia Islamia, New Delhi, India

Mohammad Ishtiaque Department of Geography, Faculty of Natural Sciences, Jamia Millia Islamia, New Delhi, India

Saleha Jamal Department of Geography, Faculty of Science, Aligarh Muslim University, Aligarh, India

Pawan K. Joshi School of Environmental Sciences (SES), Jawaharlal Nehru University, New Delhi, India;
Special Centre for Disaster Research (SCDR), Jawaharlal Nehru University, New Delhi, India

Chitrarekha Kabre Department of Architecture, School of Planning and Architecture, New Delhi, India

Jayant Kumar BCC Geospatial Center of the CUNY CREST Institute, City University of New York, Bronx, USA

Debasish Kundu Department of Geography and Disaster Management, Tripura University, Suryamaninagar, Tripura, India

Susanta Mahato Special Centre for Disaster Research (SCDR), Jawaharlal Nehru University, New Delhi, India

Sandeep Maithani Urban and Regional Studies Department, Indian Institute of Remote Sensing, Dehradun, Uttarakhand, India

Madhurima Majumdar Department of Geography, University of Gour Banga, Malda, West Bengal, India

Manisha D. Malcoti Faculty of Architecture and Ekistics, Jamia Millia Islamia, New Delhi, India

SK Mithun Department of Geography, Haldia Government College, Haldia, West Bengal, India

Prolay Mondal Department of Geography, Raiganj University, Raiganj, West Bengal, India

Md. Mushfiqus Saleheen Department of Geography and Environmental Science, Begum Rokeya University, Rangpur, Bangladesh

Shadman Nahid School of Environmental Sciences, Jawaharlal Nehru University, New Delhi, India

Mohd Waseem Naikoo Department of Geography, Faculty of Natural Sciences, Jamia Millia Islamia, New Delhi, India

Md. Naimur Rahman Department of Geography and Environmental Science, Begum Rokeya University, Rangpur, Bangladesh

S. Najmul Islam Hashmi Department of Geography, Faculty of Science, Aligarh Muslim University, Aligarh, India

Md. Omar Sarif Department of Geography, Lovely Professional University, Phagwara, India

Aruna Paarcha Department of Geography, Faculty of Natural Sciences, Jamia Millia Islamia, New Delhi, India

Swades Pal Department of Geography, University of Gour Banga, Malda, West Bengal, India

Deep Narayan Pandey Special Centre for Disaster Research (SCDR), Jawaharlal Nehru University, New Delhi, India

Samsad Parveen Department of Geography, Aligarh Muslim University, Aligarh, Uttar Pradesh, India

Shaghla Parveen National Institute of Urban Affairs, New Delhi, India

Farhana Parvin Department of Geography, Faculty of Science, Aligarh Muslim University, Aligarh, India

Bushra Praveen Department of Economics, IIT Indore, Indore, Madhya Pradesh, India

Atiqur Rahman Department of Geography, Faculty of Natural Sciences, Jamia Millia Islamia, New Delhi, India

Nitin Rathi Centre for the Study of Regional Development (CSRD), Jawaharlal Nehru University, New Delhi, India

Tuhin Kanti Ray Department of Geography, Vidyasagar College, Kolkata, West Bengal, India

Md. Rejaur Rahman Department of Geography and Environmental Studies, University of Rajshahi, Rajshahi, Bangladesh

Bhaswati Roy Department of Geography, Raiganj University, Raiganj, India

Sunil Saha Department of Geography, Raiganj University, Raiganj, West Bengal, India

Mehebub Sahana Department of Geography, The University of Manchester, Manchester, UK

Rajesh Sarda Department of Geography, University of Gour Banga, Malda, West Bengal, India

Debabrata Sarkar Department of Geography, Raiganj University, Raiganj, West Bengal, India

Shouraseni Sen Roy Department of Geography and Sustainable Development, University of Miami, Coral Gables, FL, USA

Shahfahad Department of Geography, Faculty of Natural Sciences, Jamia Millia Islamia, New Delhi, India

Hamde Narayan Shankar Urban and Regional Studies Department, Indian Institute of Remote Sensing, Dehradun, Uttarakhand, India

Sajjad Hossain Shozib Department Environmental Engineering, Nanjing Forestry University, Nanjing, China

Nisa Suhanee Department of Geography, Faculty of Natural Sciences, Jamia Millia Islamia, New Delhi, India

Swapan Talukdar Department of Geography, Faculty of Natural Sciences, Jamia Millia Islamia, New Delhi, India

Abu Reza Md. Towfiqul Islam Department of Disaster Management, Begum Rokeya University, Rangpur, Bangladesh

Ashique Vadakkuveettil Department of Geography, Central University of Tamil Nadu, Thiruvarur, India

Sundus Samreen Wani Department of Physical Planning, School of Planning and Architecture, New Delhi, India

Hina Zia Faculty of Architecture and Ekistics, Jamia Millia Islamia, New Delhi, India

Sk. Ziaul Department of Geography, University of Gour Banga, Malda, West Bengal, India

Remote Sensing and Artificial Intelligence for Urban Environmental Studies

Atiqur Rahman, Shouraseni Sen Roy, Swapan Talukdar, and Shahfahad

Abstract

This chapter offers an outline of the concept of the book and its importance to scientists, researchers, stakeholders, and authorities. It seeks to provide a framework for the subjects that have been selected to address the knowledge gap that exists between urban studies and remote sensing with machine learning by fostering a deeper understanding of the scientific principles that underpin both subfields. This chapter also provides an overview of 28 articles written by the world's leading experts in the different fields of urban research, using earth observation databases, statistical techniques, and artificial intelligence to solve urban environmental issues.

Keywords

Urban growth · Urban environment · Land use mapping · Earth observation data · Machine learning

A. Rahman (✉) · S. Talukdar · Shahfahad
Department of Geography, Faculty of Natural Sciences, Jamia Millia Islamia, New Delhi 110025, India
e-mail: arahman2@jmi.ac.in

S. S. Roy
Department of Geography and Sustainable Development, University of Miami, Coral Gables, FL, USA
e-mail: ssr@miami.edu

1.1 Introduction

The transformation of the natural landscape surroundings of urban areas into the urban landscape is referred to as "urban expansion," which causes cities to grow in size (Xu et al. 2021). The urban expansion or urbanization process has occurred on a large scale worldwide in recent decades because of rapid urban population growth, improved human well-being, and industrialization (Elvidge et al. 2012). Since urbanization in developed countries began with the industrial revolution, it has slowed down (Puga 1998). On the other hand, urbanization in developing countries has sped up significantly in the last four decades (Henderson 2002; Wang et al. 2018). As a result, the urban population surpassed 50% in 2008, marking the first time in history that this milestone has been attained (UN-Habitat 2008). However, urbanization significantly affects both local and global ecosystems because of the discharge of waste, the concentration of industries, and the intense use of energy and resources (Chen et al. 2019; Pan et al. 2019; Hu et al. 2018; Romero-Duque et al. 2020). The need for scientific study to give ecological solutions to issues caused by urbanization, the deterioration of freshwater supplies, and the transportation of materials across ecosystems has become important (Lyu et al. 2019; Das and Das 2019; Das et al. 2022).

Because of the rapid urbanization in developing countries, uncountable natural resources have been destroyed to make urbanized areas, which alter the landscape and functions of the ecosystems (Tang et al. 2021; Tu et al. 2021; Khan et al. 2021). India's urban population grew from 62 million (17.29%) in 1951 to 377 million (31.16%) in 2011 and is expected to reach 600 million by 2031. In India, cities grew primarily inside municipal limits throughout the first part of the twentieth century (Shaw 2005). Over the past several decades, the urban population boom has led to unprecedented peripheral growth in Class-I cities (Shaw 2005). According to Brears (2017), it is projected that two-thirds of the global population will live in urban areas by 2050 if the present urbanization trend continues. Because of the rapid urbanization and changes in demography in developing countries, especially in Asia and Africa, major threats like hunger, malnutrition, and food insecurity, have been observed (Sarker et al. 2021; Qayyum et al. 2021; Narain and Roth 2022; Wan et al. 2022; Islam and Kieu 2021; Blasi et al. 2022; Akinola 2021; Hemerijckx et al. 2022). This situation will worsen in the coming decades. Rapid peripheral expansion is unplanned, low density, fragmented, and haphazard, known as urban sprawl (Sarif and Gupta 2021; Chettry and Surawar 2021; Jia et al. 2022; Getu and Bhat 2021). The faster peripheral expansion changes natural land cover into urban impermeable surfaces, causing environmental and socioeconomic effects (Cengiz et al. 2022; Liu et al. 2022). The growth of cities worldwide has caused several environmental and ecological problems, such as global warming, greenhouse gas emissions, deforestation, loss of biodiversity, and soil, water, and air pollution (Ortiz et al. 2021; Xiong et al. 2021; Rastandeh and Jarchow 2021). Therefore, detecting urbanization's impact is considered a crucial topic for sustainability in urban research (Onanuga et al. 2022).

In order to perform accurate planning and monitoring of changes in urban areas, a large quantity of data about the surface of the earth is required. This is mainly done using earth observation data or remote sensing (RS) (Yin et al. 2021; Halder et al. 2021; Kowe et al. 2021). Recent developments in Earth observation data, technology, and theory have helped urban remote sensing, also known as urban applications of remote sensing, quickly acquire traction among scientists (Cetin et al. 2021; Yang 2021; Li et al. 2021). For urban and regional planners, remote sensing is becoming more critical because it provides information on the urban environment in a timely, comprehensive, and cost-effective manner that can be used for various planning and management purposes (Yeh et al. 2021; Singh 2021; Edan et al. 2021). Urban researchers have been employing remote sensing to collect information about the city's structure to build further theories and models of the morphology of a city's structure (Yang et al. 2021; Zhu et al. 2022; Zhou et al. 2022; Wang et al. 2022). Environmental scientists rely on remote sensing for extracting information on the urban land cover as a major boundary condition utilized in many spatially distributed models (Saran et al. 2021; Ndlovu et al. 2022; Fonseca et al. 2022). Researchers have also agreed that remote sensing can study the spatial dynamics and effects of urbanization, a significant type of global change.

Earth observation datasets, also called RS datasets, cover a wide range of scales, from the local to the global. Analyzing RS datasets is one approach to understanding the state and changes in both natural and artificial environments. RS sensors and methods have advanced significantly in recent decades. They may provide a significant amount of high-quality data with high spatial resolution, which can be used to explain and solve problems in urban research (Jung et al. 2021; Mellit and Kalogirou 2021; Yuan et al. 2021). Because of this, urban geographers have to deal with two big problems: a lot of data and complex data.

Therefore, translating this big data into helpful information is a big challenge. Because simple techniques cannot extract accurate and productive information. To overcome these issues, advanced remote sensing techniques and artificial intelligence (AI) have evolved. In recent years, the application of AI in different fields has gained attention (Rahman et al. 2021; Das et al. 2022;

Alqadhi et al. 2022). Many researchers have also used AI and machine learning algorithms to extract information related to urban studies (Kuras et al. 2021; Kwon and Kim 2021; Rahimpour et al. 2021; Luo 2021). These algorithms and advanced remote sensing techniques can handle complex and nonlinear real data to derive accurate and productive information related to urban studies, like rapid urbanization, climate change, heat island formation, poverty, hazards, and inequality (Suzuki and Amano 2021; He and Zheng 2021; Luo 2021; Das et al. 2022; Rahman et al. 2021).

Under the umbrella term "AI," machine learning algorithms can process enormous volumes of data in a nonlinear fashion. Because remote sensing generates a lot of data, machine learning techniques are an excellent way to analyze it. The machine learning algorithms can be implemented to resolve different issues in urban areas, such as precise urban land use mapping, urban sprawl modeling, urban hazards modeling, urban ecological quality modeling, and urban area forecasting (Luo 2021; Das et al. 2022; Rahman et al. 2021; AlQadhi et al. 2021; Bindajam et al. 2021; Mallick et al. 2021). Some vital machine learning algorithms, which have frequently been used in urban studies, are decision trees (Sang et al. 2019; Ranaweera et al. 2021; Nichols et al. 2020), random forests (Zhou et al. 2020; Ruiz and Shi 2018; Talukdar et al. 2021; Yoo et al. 2019), support vector machines (Jozdani et al. 2019; Ul Din and Mak 2021; Mustafa et al. 2018a, b; Rana and Suryanarayana 2020), artificial neural networks (Rana and Suryanarayana 2020; Gharaibeh et al. 2020; Liao et al. 2022; Talukdar et al. 2020), and fuzzy logic (Saadat Foomani and Malekmohammadi 2020; Das et al. 2022; Mrówczyńska et al. 2021). In urban research, process-based and data-based models are the two broad categories of machine learning models commonly employed for analyzing urban problems.

Cellular automata, sometimes known as CA, is one of the process-based models frequently used in urban development simulations (Batty et al. 1999). By modeling urban development based on the simulation of spatial processes as a discrete and dynamic system in space and time, CA is one way to model urban expansion (Alkheder and Shan 2005). The domain experts, specifically in modeling urban growth, use the CA model coupled with other techniques and models known as hybrid models that yield better performance. Among them, the neural network CA (Wu et al. 2022; Yatoo et al. 2020), Fuzzy-CA (Yang et al. 2018), logistic-CA (Guan et al. 2019), CA and partial swarm optimization (Mustafa et al. 2018a, b), CA and system dynamics (Liu et al. 2020), and CA-Markov (Mansour et al. 2020; Mohamed and Worku 2020; Aliani et al. 2019) are notable. Logistic regression and fuzzy logic are the typical approaches for objectively estimating occurrences' probability. It is based on data, a relatively new technique (Fang et al. 2005).

Therefore, to assess, monitor, and resolve the recent urban issues and problems, this book provides 27 scholarly scientific articles on the application of moderate-resolution to high-resolution satellite images with machine learning for urban mapping, monitoring, and solving urban environmental problems.

1.2 Urban Growth and Expansion Modeling Through Remote Sensing

A city, often known as an urban area, is a permanent human settlement that a local or regional government governs (Goodal 1987; Bailey et al. 2013). Residents, businesses, and activities may all interact owing to centralization. Because of their complex networks of facilities, services, and comforts, urban areas are emblems of civilization and modernity. The availability of communal facilities aids in the growth of cities (Banister 2012; Yamu et al. 2015). In actuality, towns and rural areas, and villages are separated by the concentration of these facilities and services. Urbanization is defined as changing natural settings to residential, commercial, and industrial land uses from an environmental standpoint

(Fang et al. 2005). According to Mubareka et al. (2011), urbanization is defined as increasing land demand over time.

Urbanization is a natural human behavior that aims to increase the quality of life, livability, and security. The complexity, breadth, and capacity of these qualities may be used to determine the degree of urbanization in metropolitan areas. Urbanization fosters industrialization and economic progress (Mahmood et al. 2020; Dong et al. 2021). The pace at which the population, land area, or effective land use in an urban region rises is considered as "urban growth" (Mallick et al. 2021; Das et al. 2022). It is also known as the rise of metropolitan regions or cities, and it began between the years 5000 and 6000 B.C. It was primarily caused by the migration of people from rural areas to urban areas, which are locations with a large human population, economic activity, and infrastructure (Shaw and Das 2018; Shukla and Jain 2019). The nineteenth century, in particular, was a defining moment in the development of genuine cities.

Since 1800, the urban revolution has been accelerating at an ever-increasing rate, and it has now reached unprecedented heights in the annals of human history (Burke and Pomeranz 2009; Foster 1999). There is a tight connection between urban growth and urbanization or urbanism, a word used to describe a rising percentage of people living in urban areas such as cities, suburbs, towns, and districts (Mdari et al. 2022). Urban growth is likewise closely tied to urbanization or urbanism (Lin 1998; Bernhardt 2005).

Urban expansion is consequently used to show both the economic health of a nation or region and its level of development. The expansion of metropolitan regions is often driven by several causes, including, but not limited to, an abundance of resources, the creation of new infrastructure, commercialization, educational opportunities, and mining (Wei and Ewing 2018).

Since the late 1950s, many developing countries have got freedom from colonization, which led to the transformation of the country through urbanization. After 1980s, globalization has accelerated the process of urbanization (Sassen 2000). Therefore, existing urban centers have gained more urban population and grew in size. On the other hand, many urban centers have been grown and decentralized, which rapid urbanization. Through this process, different forms of urban expansion and sprawl have been noticed, such as low density, leap-frog, infilling, etc. (Pramanik et al. 2021; Sahani and Raghavaswamy 2018; Antipova et al. 2022). In the case of big cities or metropolitans, due to huge migration from small cities and rural areas, several problems have been arise, such as poverty, inequality, loss of habitat quality, and crime.

The introduction of RS and GIS has made urban research more accessible and convenient. It offers multi-spectral, multi-temporal, and multi-spatial resolution data that can be utilized to analyze and simulate changes and dynamics in land cover (Sang et al. 2019; Zhou et al. 2020; Talukdar et al. 2021). In this way, satellite RS imagery can offer an overview of a landscape at regular intervals, provide views of locations not accessible by traditional surveying, and show clear patterns of a landscape's land use and land cover (AlQadhi et al. 2021; Luo 2021). The combination of RS with GIS technology provides a strong, cost-effective tool for detecting, mapping, monitoring, and analyzing the dynamics of urban expansion, urban habitat quality modeling, urban hazards modeling, and the generation and monitoring of urban heat islands (Mallick et al. 2021; Bindajam et al. 2021; Jung et al. 2021).

At the moment, remote sensing has been acknowledged as an effective method for viewing, monitoring, evaluating, describing, and mapping urban development and expansion (Das et al. 2022). Consequently, it has seen widespread use in recognizing and monitoring urban changes in various sizes, with fruitful results in each case (Yuan et al. 2021). Because of its great spatially and temporally precision and consistency, remote sensing is an essential source of data for studies on the growth of urban areas (Fonseca et al. 2022; Kuras et al. 2021). In addition, the data obtained by remote sensing is beneficial since they provide a synoptic image, repeating coverage, and real-time data collecting (Cetin et al. 2021; Li et al. 2021; Singh 2021).

Using digital data, often as satellite images, enables the correct distinction of land use, covers categories, and contributes to the maintenance of the spatial data infrastructure, which is vital for tracking the growth of metropolitan areas (Yeh et al. 2021; Edan et al. 2021; Xiong et al. 2021). A database will need to be compiled to illustrate the evolution of the urban landscape through time in a particular region at predetermined intervals and going as far back in time as feasible (Edan et al. 2021; Yin et al. 2021). It should be no surprise that satellite data, remote sensing, and Geographic Information Systems (GIS) are the technologies most pertinent to efficiently addressing these requirements.

Recently, most of the researchers have been used remote sensing database and GIS for investigating the urban sprawl and expansion at global, national, and regional scale (Liu et al. 2022; Ortiz et al. 2021).

1.3   Application of Machine Learning for Urban Mapping and Monitoring

In order to understand urban growth and human activities, mapping and monitoring urban expansion is critical in urban remote sensing (Yoo et al. 2019; Jozdani et al. 2019; Ul Din and Mak 2021). Complex monitoring systems are needed to keep pace with rapidly changing urban environments (Bindajam et al. 2021). Changing urban environments necessitates the use of remote sensing for mapping, monitoring, and analysis (Das et al. 2022). Geospatial technologies, such as remote sensing and GIS, have been essential in quantifying and analyzing urban growth (Mustafa et al. 2018a, b; Liao et al. 2022). GIS tracks and analyzes LULC and urban growth (Talukdar et al. 2020; Rana and Suryanarayana 2020).

Satellites, including Landsat, SPOT, ASTER, and MODIS have been used in recent decades to map, monitor, and forecast LULC dynamics (Xu et al. 2020; Sarif and Gupta 2022; Afrin et al. 2019; Seydi et al. 2021). For research and planning purposes, the use of hyperspectral satellite

sensors has increased several-fold since their inception.

LULC mapping using machine learning algorithms based on remotely sensed imagery has lately sparked considerable attention (Talukadr et al. 2020). There are two types of machine learning approaches: supervised and unsupervised (Abbas and Jaber 2020). Supervised classification techniques include support vector machines (SVMs) (Balha et al. 2021; Jamali 2020), random forests (RFs) (Shihab et al. 2020; Talukdar et al. 2020), spectral angle mappers (SAMs) (Zare Naghadehi et al. 2021; Singh et al. 2022), fuzzy adaptive resonance theory-supervised predictive mappings (Fuzzy ART-MAPs) (Han et al. 2018; Talukdar et al. 2020), decision trees (Sang et al. 2019; Ranaweera et al. 2021; Nichols et al. 2020), artificial neural networks (Rana and Suryanarayana 2020; Gharaibeh et al. 2020; Liao et al. 2022; Talukdar et al. 2020), and fuzzy logic (Saadat Foomani and Malekmohammadi 2020; Das et al. 2022; Mrówczyńska et al. 2021). On the other hand, cluster algorithms, fuzzy c-means algorithms, K-means algorithms, and ISODATA are unsupervised algorithms for urban mapping. Table 1.1 shows the application of machine learning algorithms for classifying urban areas with higher accuracy. Therefore, it can be stated that machine learning algorithms can classify the urban land use efficiently. For example, urban land use land cover classification for the study English Bazar city has been done using random forest classifier.

1.4   Application of Machine Learning and Earth Observation Data for Urban Environmental Studies

The environmental and socioeconomic effects that are related with recorded population expansion are only one of the many factors that have contributed to the fact that sustainable development has been recognized as one of the world's most pressing problems for many years. In 2018, there were 55% of the world's population living in urban regions, and this number is projected to

Table 1.1 Urban land use modeling using machine learning algorithms with higher accuracy

Urban areas	Method for mapping	Accuracy (%)	References
Gharbia Governorate, Egypt	Support vector machine	94.3	Sabzekar and Hasheminejad (2021)
Kumasi Metropolis, Ghana	Random forest	97	Frimpong and Molkenthin (2021)
Shiraz, Iran	Support vector machine	98	Jamali (2021)
South Africa	Random forest	97	Zeng et al. (2020)
Hyderabad, Pakistan	Support vector machine	98	Ul Din et al. (2021)
Gopalganj, Bangladesh	Artificial neural networking	89.4	Hossain and Moniruzzaman (2021)
New Juaben Municipality, Ghana	Random forest	96.3	Nyamekye et al. (2020)
Soviet cities	Support vector machine	94	Poghosyan (2018)
Islamabad, Pakistan	Random forest	98	Khan and Sudheer (2022)

rise to 68 percent by the year 2050 (Kaza et al. 2018; Ritchie and Roser 2018). The fundamental goal in tackling this problem is to offer a framework for a systematic and controlled urban growth with improve human well-being.

Evaluating sustainability allows for determining a level of development for urban ecosystems characterized by the interaction and coexistence of natural and artificial structures (Tan et al. 2021; Tu et al. 2021; Khan et al. 2021). The supply of goods and services by natural systems is referred to as "ecosystem services," and it is one way in which natural systems contribute to the sustainability of urban environments (Das and Das 2019). However, because of human activity and the development of urban settlements, several aspects of the natural environment are being changed, including air pollutants, trash, and wastewater.

It is essential, however, to monitor the urban land cover, urban green and blue cover, urban risks, and urban heat islands in order to propose management measures to address these challenges (Jung et al. 2021; Mellit and Kalogirou 2021; Yuan et al. 2021). When precise and reliable mapping and modeling are achieved, only then will it be possible to conduct monitoring with a high degree of accuracy. These levels of precision are attainable with the use of various machine learning techniques (Luo 2021; Das

et al. 2022; Rahman et al. 2021; AlQadhi et al. 2021; Bindajam et al. 2021; Mallick et al. 2021). These are able to extract relevant information from large datasets that are complicated.

Several studies have been conducted using machine learning methods to determine the degree of progress that has been made concerning the development of sustainable cities (Das et al. 2022; Mallick et al. 2021; Talukdar et al. 2020; Bindajam et al. 2021). These researches have provided techniques for the computation, aggregation, and comparison of indicators in various contexts. In addition, these studies have offered tools that might be beneficial for decision making.

Machine learning algorithms have been used for decades in various contexts to predict future input data behavior (Talukdar et al. 2020; Bindajam et al. 2021; Khan and Sudheer 2022; Jamali 2021). These techniques have become increasingly helpful in establishing development plans and assessing sustainability at all scales, from the smallest urban settings (organizations, homes) to the territorial level, because of the collection of vast data (Nyamekye et al. 2020; Singh et al. 2022). As a result, it is critical to recognize that attaining sustainable development requires not just a national policy perspective but also knowledge of the activities of territories that are part of cities and regions, urban microterritories (Shihab et al. 2020).

The assessment and modeling of urban ecological problems may be carried out with pinpoint accuracy because of machine learning. ML models, such as the decision trees (Sang et al. 2019; Ranaweera et al. 2021; Nichols et al. 2020), random forests (Zhou et al. 2020; Ruiz and Shi 2018; Talukdar et al. 2021; Yoo et al. 2019), support vector machines (Jozdani et al. 2019; Ul Din and Mak 2021; Mustafa et al. 2018a, b; Rana and Suryanarayana 2020), artificial neural networks (Rana and Suryanarayana 2020; Gharaibeh et al. 2020; Liao et al. 2022; Talukdar et al. 2020) are just some of the many that have been utilized in the investigation of ecological issues.

1.5   Organization of the Book

This book has been divided into four parts: urban land use and land cover, urban sprawl and growth, urban green and blue space, urban climate, heat island and hazards, and urban environmental planning and waste management, based on all the aspects of the urban environment. Each part comprises several articles. For example, the urban land use and land cover, urban sprawl, and growth parts consist of eight articles. On the other hand, the urban green and blue space part has six articles, while the urban climate, heat island, and hazards comprises six articles. The final part consists of seven articles.

The urban land use land cover, urban sprawl, and growth part is related to the urban growth in different cities around the world for different periods. For example, Grover and Vadakkuveettil (Chap. 4) have worked on the Kozhikode urban area to identify the growth of the urban areas by transforming the natural resources. Parcha et al. (Chap. 6) studied the urban sprawl in Kanpur city using geospatial technology between 2004 and 2021. They also used Shannon entropy and other advanced techniques to quantify the urban sprawl. Also, some leading scholars have used several machine learning algorithms with the Google Earth Engine to forecast the urban sprawl of different cities worldwide. For example, Saha et al. (Chap. 3)

used Google Earth Engine, cellular automata, and machine learning to predict the urban areas of Raiganj Municipality for 2025. Similarly, Naikoo et al. (Chap. 5) utilized cellular automata with an artificial neural network algorithm to predict the urban expansion of Mumbai metropolitan city for 2031. Rahman et al. (Chap. 8) have applied the Markov chain with cellular automata to predict the urban center of Barisal (Bangladesh) for 2031. On the other hand, this part has provided reviews of the evolution of machine learning algorithms and remote sensing for analyzing and predicting urban areas, such as Mithun et al. (Chap. 2) and Bushra et al. (Chap. 9).

The second part (urban green and blue spaces) deals with the dynamics of urban green (vegetation) and blue (wetland and water bodies) over time in different urban centers. Also, the dynamics of ecosystem services from the urban green and blue spaces can be tracked with the help of remote sensing and machine learning algorithms. For example, Rahman and Rahman (Chap. 10) have shown the dynamics of urban blue and green spaces using several advanced techniques and machine learning algorithms for Rajshahi Metropolitan City in Bangladesh. Dutta and Das (Chap. 11) have shown the dynamics of urban green spaces and land surface temperature in the English Bazar Municipality (India) from 1990 to 2015. Also, they showed the relationship between the dynamics of green space and land surface temperature. Using time-series Landsat imagery, Majumdar et al. (Chap. 12) have shown the influence of urbanization on the hydrological status and trophic state of the peri-urban wetland (Chatra wetland) during the 1990–2020 period. Sunil Bhaskaran et al. (Chap. 14) have developed a decarbonization planning tool for global cities. This work will help policymakers mitigate greenhouse gas emissions.

The third part concerns the urban climate, heat island, and hazards in different cities worldwide using machine learning and geostatistical techniques. For example, Ali et al. (Chap. 16) have proposed a GIS-based methodology, world urban database, and access portal tools for mapping local climate zones in the Kolkata Metropolitan

City for different periods. Sarda and Pal (Chap. 18) have shown the relationship between the anthropogenic heat flux (AHF), and urban heat island in the mining-dominated Asansol Durgapur Development Area (ADDA) of West Bengal from the period of 1990–2019. Rathi et al. (Chap. 20) have applied a statistical multi-criteria decision-making model to prepare an urban flood hazard index for Delhi. They also used hyperspectral remote sensing data for the study.

The last part (Urban environmental planning and waste management) covers the articles related to urban environmental planning and solid waste management in the different cities of the world. Gupta and Sarif (Chap. 26) have used machine learning and other geostatistical techniques to propose an urban planning perspective of UN Sustainable Development Goal-11 for the Kolkata megapolis. The concluding chapter by Rahman et al. (Chap. 28) has shown the progress of approaches and techniques for urban environmental studies since the advent of remote sensing and machine learning algorithms.

References

Abbas Z, Jaber HS (2020) Accuracy assessment of supervised classification methods for extraction land use maps using remote sensing and GIS techniques. IOP Confe Ser Mater Sci Eng 745(1):012166. IOP Publishing

Afrin S, Gupta A, Farjad B, Ahmed MR, Achari G, Hassan QK (2019) Development of land-use/land-cover maps using Landsat-8 and MODIS data, and their integration for hydro-ecological applications. Sensors 19(22):4891

Akinola AO (2021) Urbanization, poverty and the paradox of land reform in South Africa. In: The new political economy of land reform in South Africa. Palgrave Macmillan, Cham, pp 235–254

Aliani H, Malmir M, Sourodi M, Kafaky SB (2019) Change detection and prediction of urban land use changes by CA–Markov model (case study: Talesh County). Environ Earth Sci 78(17):1–12

Alkheder S, Shan J (2005) Urban growth simulation using remote sensing imagery and neural networks. In: Third international symposium remote sensing and data fusion over urban areas (URBAN 2005) and the 5th international symposium on remote sensing of urban areas (URS 2005), Arizona State University, Tempe, Arizona, pp 14–16

Alqadhi S, Mallick J, Talukdar S, Ahmed M, Khan RA, Sarkar SK, Rahman A (2022) Assessing the effect of future landslide on ecosystem services in Aqabat Al-Sulbat region, Saudi Arabia. Nat Hazards:1–31

AlQadhi S, Mallick J, Talukdar S, Bindajam AA, Shohan AAA, Shahfahad (2021) Quantification of urban sprawl for past-to-future in Abha City, Saudi Arabia. CMES-Comput Model Eng Sci 129(2):755–786

Antipova A, Momeni E, Banai R (2022) 15 Urban Sprawl, Blight, and the. In: Advances in urbanism, smart cities, and sustainability, p 263

Bailey PK, Tomson CR, Kinra S, Ebrahim S, Radhakrishna KV, Kuper H, Nitsch D, Ben Shlomo Y (2013) The effect of rural-to-urban migration on renal function in an Indian population: cross-sectional data from the Hyderabad arm of the Indian Migration Study. BMC Nephrol 14(1):1–9

Balha A, Mallick J, Pandey S, Gupta S, Singh CK (2021) A comparative analysis of different pixel and object-based classification algorithms using multi-source high spatial resolution satellite data for LULC mapping. Earth Sci Inf 14(4):2231–2247

Banister D (2012) Assessing the reality—Transport and land use planning to achieve sustainability. J Transp Land Use 5(3):1–14

Batty M, Xie Y, Sun Z (1999) Modeling urban dynamics through GIS-based cellular automata. Comput Environ Urban Syst 23(3):205–233

Bernhardt C (2005) Planning urbanization and urban growth in the socialist period: the case of East German New Towns, 1945–1989. J Urban Hist 32(1):104–119

Bindajam AA, Mallick J, Talukdar S, Islam ARM, Alqadhi S (2021) Integration of artificial intelligence–based LULC mapping and prediction for estimating ecosystem services for urban sustainability: past to future perspective. Arab J Geosci 14(18):1–23

Blasi S, Ganzaroli A, De Noni I (2022) Smartening sustainable development in cities: strengthening the theoretical linkage between smart cities and SDGs. Sustain Cities Soc 80:103793

Brears RC (2017) Singapore transitioning towards urban water security. Urban Water Secur:225–241

Burke E, Pomeranz K eds. (2009) The environment and world history, vol 9. Univ of California Press

Cengiz S, Görmüş S, Oğuz D (2022) Analysis of the urban growth pattern through spatial metrics Ankara City. Land Use Policy 112:105812

Cetin M, Aksoy T, Cabuk SN, Kurkcuoglu MAS, Cabuk A (2021) Employing remote sensing technique to monitor the influence of newly established universities in creating an urban development process on the respective cities. Land Use Policy 109:105705

Chen Y, Li X, Liu X, Zhang Y, Huang M (2019) Tele-connecting China's future urban growth to impacts on ecosystem services under the shared socioeconomic pathways. Sci Total Environ 652:765–779

Chettry V, Surawar M (2021) Assessment of urban sprawl characteristics in Indian cities using remote sensing: case studies of Patna, Ranchi, and Srinagar. Environ Dev Sustain 23(8):11913–11935

Das M, Das A (2019) Dynamics of urbanization and its impact on urban ecosystem services (UESs): a study of a medium size town of West Bengal. Eastern India J Urban Manag 8(3):420–434

Das T, Naikoo MW, Talukdar S, Parvez A, Rahman A, Pal S, Asgher MS, Islam ARM, Mosavi A (2022) Analysing process and probability of built-up expansion using machine learning and fuzzy logic in English bazar West Bengal. Remote Sensing 14 (10):2349

Dong H, Xue M, Xiao Y, Liu Y (2021) Do carbon emissions impact the health of residents? Considering China's industrialization and urbanization. Sci Total Environ 758:143688

Edan MH, Maarouf RM, Hasson J (2021) Predicting the impacts of land use/land cover change on land surface temperature using remote sensing approach in Al Kut, Iraq. Phys Chem Earth Parts a/b/c 123:103012

Elvidge CD, Sutton PC, Wagner TW, Ryzner R, Vogelmann JE, Goetz SJ, Smith AJ, Jantz C, Seto KC, Imhoff ML, Wang YQ (2012) Urbanization. In: Land change science. Springer, Dordrecht, pp 315–328

Fang S, Gertner GZ, Sun Z, Anderson AA (2005) The impact of interactions in spatial simulation of the dynamics of urban sprawl. Landscape Urban Plan 73 (4):294–306

Fonseca CABD, Al-Ansari N, Silva RMD, Santos CAG, Zerouali B, Oliveira DBD, Elbeltagi A (2022) Investigating relationships between runoff-erosion processes and land use and land cover using remote sensing multiple gridded datasets. ISPRS Int J Geo Inf 11(5):272

Foster JB (1999) The vulnerable planet: A short economic history of the environment. nyu Press

Frimpong BF, Molkenthin F (2021) Tracking urban expansion using random forests for the classification of Landsat imagery (1986–2015) and predicting urban/built-up areas for 2025: a Study of the Kumasi Metropolis Ghana. Land 10(1):44

Getu K, Bhat HG (2021) Analysis of spatio-temporal dynamics of urban sprawl and growth pattern using geospatial technologies and landscape metrics in Bahir Dar Northwest Ethiopia. Land Use Policy 109:105676

Gharaibeh A, Shaamala A, Obeidat R, Al Kofahi S (2020) Improving land-use change modeling by integrating ANN with cellular automata-Markov chain model. Heliyon 6(9):e05092

Goodal B (1987) The Penguin dictionary of human geography. London

Guan D, Zhao Z, Tan J (2019) Dynamic simulation of land use change based on logistic-CA-Markov and WLC-CA-Markov models: a case study in three gorges reservoir area of Chongqing China. Environ Sci Pollut Res 26(20):20669–20688

Habitat UN (2008) State of the world's cities 2008/2009: Harmonious cities. Earthscan, London, p 264

Halder B, Bandyopadhyay J, Banik P (2021) Monitoring the effect of urban development on urban heat island based on remote sensing and geo-spatial approach in Kolkata and adjacent areas India. Sustain Cities Soc 74:103186

Han M, Zhang C, Zhou Y (2018) Object-wise joint-classification change detection for remote sensing images based on entropy query-by fuzzy ARTMAP. Giscience Remote Sens 55(2):265–284

He J, Zheng H (2021) Prediction of crime rate in urban neighborhoods based on machine learning. Eng Appl Artif Intell 106:104460

Hemerijckx LM, Janusz K, Van Emelen S, Tumwesigye S, Davis J, Lwasa S, Van Rompaey A (2022) Food accessibility of different socioeconomic groups in sub-Saharan African cities: a mixed-method analysis in Kampala, Uganda. Food Secur:1–18

Henderson V (2002) Urbanization in developing countries. The World Bank Res Observer 17(1):89–112

Hossain F, Moniruzzaman M (2021) Environmental change detection through remote sensing technique: A study of Rohingya refugee camp area (Ukhia and Teknaf sub-district), Cox's Bazar Bangladesh. Environ Challenges 2:100024

Hu Y, Zhang Y, Ke X (2018) Dynamics of tradeoffs between economic benefits and ecosystem services due to urban expansion. Sustainability 10(7):2306

Islam MS, Kieu E (2021) Urban food security and sustainability in Asian Cities. In: Climate Change and Food Security in Asia Pacific. Palgrave Macmillan, Cham, pp 153–176

Jamali A (2020) Land use land cover mapping using advanced machine learning classifiers: a case study of Shiraz city Iran. Earth Sci Inf 13(4):1015–1030

Jamali A (2021) Improving land use land cover mapping of a neural network with three optimizers of multi-verse optimizer, genetic algorithm, and derivative-free function. Egypt J Remote Sens Space Sci 24(3):373–390

Jia M, Zhang H, Yang Z (2022) Compactness or sprawl: multi-dimensional approach to understanding the urban growth patterns in Beijing-Tianjin-Hebei region China. Ecol Indic 138:108816

Jozdani SE, Johnson BA, Chen D (2019) Comparing deep neural networks, ensemble classifiers, and support vector machine algorithms for object-based urban land use/land cover classification. Remote Sens 11 (14):1713

Jung J, Maeda M, Chang A, Bhandari M, Ashapure A, Landivar Bowles J (2021) The potential of remote sensing and artificial intelligence as tools to improve the resilience of agriculture production systems. Curr Opin Biotechnol 70:15–22

Kaza S, Yao L, Bhada-Tata P, Van Woerden F (2018) What a waste 2.0: a global snapshot of solid waste management to 2050. World Bank Publications

Khan A, Sudheer M (2022) Machine learning-based monitoring and modeling for spatio-temporal urban growth of Islamabad. Egypt J Remote Sens Space Sci 25(2):541–550

Khan I, Hou F, Le HP, Ali SA (2021) Do natural resources, urbanization, and value-adding manufacturing affect environmental quality? Evidence from the

top ten manufacturing countries. Resour Policy 72:102109

Kowe P, Mutanga O, Dube T (2021) Advancements in the remote sensing of landscape pattern of urban green spaces and vegetation fragmentation. Int J Remote Sens 42(10):3797–3832

Kuras A, Brell M, Rizzi J, Burud I (2021) Hyperspectral and lidar data applied to the urban land cover machine learning and neural-network-based classification: a review. Remote Sens 13(17):3393

Kwon SH, Kim JH (2021) Machine learning and urban drainage systems: state-of-the-art review. Water 13 (24):3545

Li J, Gong J, Guldmann JM, Yang J (2021) Assessment of urban ecological quality and spatial heterogeneity based on remote sensing: a case study of the rapid urbanization of Wuhan City. Remote Sens 13 (21):4440

Liao G, He P, Gao X, Lin Z, Huang C, Zhou W, Deng O, Xu C, Deng L (2022) Land use optimization of rural production–living–ecological space at different scales based on the BP–ANN and CLUE–S models. Ecol Ind 137:108710

Lin GCS (1998) China's industrialization with controlled urbanization: anti-urbanism or urban-biased? Issues Stud 34(6):98–116

Liu D, Zheng X, Wang H (2020) Land-use simulation and decision-support system (LandSDS): seamlessly integrating system dynamics, agent-based model, and cellular automata. Ecol Model 417:108924

Liu J, Xu Q, Yi J, Huang X (2022) Analysis of the heterogeneity of urban expansion landscape patterns and driving factors based on a combined multi-order adjacency index and geodetector model. Ecol Ind 136:108655

Luo J (2021) Online design of green urban garden landscape based on machine learning and computer simulation technology. Environ Technol Innov 24:101819

Lyu R, Clarke KC, Zhang J, Jia X, Feng J, Li J (2019) The impact of urbanization and climate change on ecosystem services: A case study of the city belt along the Yellow River in Ningxia, China. Comput Environ Urban Syst 77:101351

Mahmood H, Alkhateeb TTY, Furqan M (2020) Industrialization, urbanization and CO2 emissions in Saudi Arabia: asymmetry analysis. Energy Rep 6:1553–1560

Mallick J, Singh VP, Almesfer MK, Talukdar S, Alsubhi M, Ahmed M, Khan RA (2021) Spatio-temporal analysis and simulation of land cover changes and their impacts on land surface temperature in urban agglomeration of Bisha Watershed, Saudi Arabia. Geocarto Int:1–27

Mansour S, Al-Belushi M, Al Awadhi T (2020) Monitoring land use and land cover changes in the mountainous cities of Oman using GIS and CA-Markov modelling techniques. Land Use Policy 91:104414

Mdari YE, Daoud MA, Namir A, Hakdaoui M (2022) Casablanca smart city project: urbanization, urban growth, and sprawl challenges using remote sensing and spatial analysis. In: Proceedings of sixth international congress on information and communication technology. Springer, Singapore, pp 209–217

Mellit A, Kalogirou S (2021) Artificial intelligence and internet of things to improve efficacy of diagnosis and remote sensing of solar photovoltaic systems: challenges, recommendations and future directions. Renew Sustain Energy Rev 143:110889

Mohamed A, Worku H (2020) Simulating urban land use and cover dynamics using cellular automata and Markov chain approach in Addis Ababa and the surrounding. Urban Climate 31:100545

Mrówczyńska M, Skiba M, Sztubecka M, Bazan-Krzywoszańska A, Kazak JK, Gajownik P (2021) Scenarios as a tool supporting decisions in urban energy policy: the analysis using fuzzy logic, multi-criteria analysis and GIS tools. Renew Sustain Energy Rev 137:110598

Mubareka S, Koomen E, Estreguil C, Lavalle C (2011) Development of a composite index of urban compactness for land use modelling applications. Landscape Urban Plan 103(3–4):303–317

Mustafa A, Rienow A, Saadi I, Cools M, Teller J (2018a) Comparing support vector machines with logistic regression for calibrating cellular automata land use change models. Eur J Remote Sens 51(1):391–401

Mustafa AMES, Saadi I, Ebaid A, Cools M, Teller J, 2018b. Comparison among three automated calibration methods for cellular automata land use change model: GA, PSO and MCMC. In: AGILE conference 2018b

Narain V, Roth D (2022) Water security, conflict and cooperation in peri-urban South Asia: flows across boundaries. Springer Nature, p 180

Ndlovu HS, Sibanda M, Odindi J, Buthelezi S, Mutanga O (2022) Detecting and mapping the spatial distribution of Chromoleana odorata invasions in communal areas of South Africa using Sentinel-2 multispectral remotely sensed data. Phys Chem Earth, Parts a/b/c 126:103081

Nichols C, Hung MC, Wu YH (2020) Hierarchical classification and knowledge-based decision tree for land use/land cover classification with very high resolution imagery. Int J Geoinformatics 16(3)

Nyamekye C, Kwofie S, Ghansah B, Agyapong E, Boamah LA (2020) Assessing urban growth in Ghana using machine learning and intensity analysis: a case study of the New Juaben Municipality. Land Use Policy 99:105057

Onanuga MY, Eludoyin AO, Ofoezie IE (2022) Urbanization and its effects on land and water resources in Ijebuland, southwestern Nigeria. Environ Dev Sustain 24(1):592–616

Ortiz DI, Piche-Ovares M, Romero-Vega LM, Wagman J, Troyo A (2021) The impact of deforestation, urbanization, and changing land use patterns on the ecology of mosquito and tick-borne diseases in Central America. InSects 13(1):20

Pan H, Zhang L, Cong C, Deal B, Wang Y (2019) A dynamic and spatially explicit modeling approach to

identify the ecosystem service implications of complex urban systems interactions. Ecol Ind 102:426–436

Poghosyan A (2018) Quantifying urban growth in 10 post-Soviet cities using Landsat data and machine learning. Int J Remote Sens 39(23):8688–8702

Pramanik S, Butsch C, Punia M (2021) Post-liberal urban dynamics in India-the case of Gurugram, the 'Millennium City.' Remote Sens Appl Soc Environ 22:100504

Puga D (1998) Urbanization patterns: European versus less developed countries. J Reg Sci 38(2):231–252

Qayyum U, Sabir S, Anjum S (2021) Urbanization, informal economy, and ecological footprint quality in South Asia. Environ Sci Pollut Res 28(47):67011–67021

Rahimpour A, Amanollahi J, Tzanis CG (2021) Air quality data series estimation based on machine learning approaches for urban environments. Air Qual Atmos Health 14(2):191–201

Rahman MM, Paul KC, Hossain MA, Ali GMN, Rahman MS, Thill JC (2021) Machine learning on the COVID-19 pandemic, human mobility and air quality: a review. IEEE Access 9:72420–72450

Rana VK, Suryanarayana TMV (2020) Performance evaluation of MLE, RF and SVM classification algorithms for watershed scale land use/land cover mapping using sentinel 2 bands. Remote Sens Appl Soc Environ 19:100351

Ranaweera N, Jayasinghe A, Abenayake C (2021) Decision tree application for model built-up land fragmentation in urban areas

Rastandeh A, Jarchow M (2021) Urbanization and biodiversity loss in the post-COVID-19 era: complex challenges and possible solutions. Cities Health 5 (sup1):S37–S40

Ritchie H, Roser M (2018) Urbanization. Our world in data

Romero-Duque LP, Trilleras JM, Castellarini F, Quijas S (2020) Ecosystem services in urban ecological infrastructure of Latin America and the Caribbean: How do they contribute to urban planning? Sci Total Environ 728:138780

Ruiz Hernandez IE, Shi W (2018) A random forests classification method for urban land-use mapping integrating spatial metrics and texture analysis. Int J Remote Sens 39(4):1175–1198

Saadat Foomani M, Malekmohammadi B (2020) Site selection of sustainable urban drainage systems using fuzzy logic and multi-criteria decision-making. Water Environ J 34(4):584–599

Sabzekar M, Hasheminejad SMH (2021) Robust regression using support vector regressions. Chaos, Solitons Fractals 144:110738. https://doi.org/10.1016/j.chaos.2021.110738

Sahani S, Raghavaswamy V (2018) Decoding patterns of urban dynamics in class-1 city of Khammam, Telangana State, India. J Indian Soc Remote Sens 46 (5):749–759

Sang X, Guo Q, Wu X, Fu Y, Xie T, He C, Zang J (2019) Intensity and stationarity analysis of land use change based on CART algorithm. Sci Rep 9(1):1–12

Saran S, Sterk G, Aggarwal SP, Dadhwal VK (2021) Coupling remote sensing and GIS with KINEROS2 model for spatially distributed runoff modeling in a Himalayan watershed. J Indian Soc Remote Sens 49 (5):1121–1139

Sarif M, Gupta RD (2021) Modelling of trajectories in urban sprawl types and their dynamics (1988–2018): a case study of Prayagraj City (India). Arab J Geosci 14 (14):1–21

Sarif M, Gupta RD (2022) Evaluation of seasonal ecological vulnerability using LULC and thermal state dynamics using Landsat and MODIS data: a case study of Prayagraj City, India (1987–2018). Environ Sci Pollut Res:1–34

Sarker B, Keya KN, Mahir FI, Nahiun KM, Shahida S, Khan RA (2021) Surface and ground water pollution: causes and effects of urbanization and industrialization in South Asia. Sci Rev 7(3):32–41

Sassen S (2000) New frontiers facing urban sociology at the Millennium. Br J Sociol 51(1):143–159

Seydi ST, Akhoondzadeh M, Amani M, Mahdavi S (2021) Wildfire damage assessment over Australia using sentinel-2 imagery and MODIS land cover product within the google earth engine cloud platform. Remote Sens 13(2):220

Shaw, A., 2005. Peri-urban interface of Indian cities: growth, governance and local initiatives. *Economic and Political Weekly*, pp.129–136.

Shaw R, Das A (2018) Identifying peri-urban growth in small and medium towns using GIS and remote sensing technique: a case study of English Bazar Urban Agglomeration, West Bengal, India. Egypt J Remote Sens Space Sci 21(2):159–172

Shihab TH, Al Hameedawi AN, Hamza AM (2020) Random forest (RF) and artificial neural network (ANN) algorithms for LULC mapping. Eng Technol J 38(4):510–514

Shukla A, Jain K (2019) Modeling urban growth trajectories and spatiotemporal pattern: a case study of Lucknow City, India. J Indian Soc Remote Sens 47 (1):139–152

Singh KT, Singh NM, Devi TT (2022) A remote sensing, GIS based study on LULC change detection by different methods of classifiers on Landsat data. In: Innovative trends in hydrological and environmental systems. Springer, Singapore, pp 107–117

Singh R ed. (2021) Re-envisioning remote sensing applications: perspectives from developing countries. CRC Press

Suzuki T, Amano Y (2021) NLOS multipath classification of GNSS signal correlation output using machine learning. Sensors 21(7):2503

Talukdar S, Eibek KU, Akhter S, Ziaul SK, Islam ARMT, Mallick J (2021) Modeling fragmentation probability of land-use and land-cover using the bagging, random forest and random subspace in the Teesta River Basin Bangladesh. Ecol Indic 126:107612

Talukdar S, Singha P, Mahato S, Pal S, Liou YA, Rahman A (2020) Land-use land-cover classification

by machine learning classifiers for satellite observations—a review. Remote Sens 12(7):1135

Tang L, Ke X, Chen Y, Wang L, Zhou Q, Zheng W, Xiao B (2021) Which impacts more seriously on natural habitat loss and degradation? Cropland expansion or urban expansion? Land Degrad Dev 32 (2):946–964

Tu Y, Chen B, Yu L, Xin Q, Gong P, Xu B (2021) How does urban expansion interact with cropland loss? A comparison of 14 Chinese cities from 1980 to 2015. Landscape Ecol 36(1):243–263

Ul Din S, Mak HWL (2021) Retrieval of land-use/land cover change (LUCC) maps and urban expansion dynamics of Hyderabad, Pakistan via Landsat datasets and support vector machine framework. Remote Sens 13(16):3337

Wan G, Zhang X, Zhao M (2022) Urbanization can help reduce income inequality. npj Urban Sustainy 2(1):1–8

Wang J, Georganos S, Kuffer M, Abascal A, Vanhuysse S (2022) On the knowledge gain of urban morphology from space. Comput Environ Urban Syst 95:101831

Wang S, Li G, Fang C (2018) Urbanization, economic growth, energy consumption, and CO_2 emissions: empirical evidence from countries with different income levels. Renew Sustain Energy Rev 81:2144–2159

Wei YD, Ewing R (2018) Urban expansion, sprawl and inequality. Landscape Urban Plan 177:259–265

Wu X, Liu X, Zhang D, Zhang J, He J, Xu X (2022) Simulating mixed land-use change under multi-label concept by integrating a convolutional neural network and cellular automata: a case study of Huizhou China. Giscience Remote Sens 59(1):609–632

Xiong B, Chen R, An L, Zhang Q, Xia Z (2021) Telecoupling urbanization and mountain areas deforestation between 2000 and 2020: Evidence from Zhejiang Province China. Land Degrad Develop 32 (16):4727–4739

Xu D, Yang F, Yu L, Zhou Y, Li H, Ma J, Huang J, Wei J, Xu Y, Zhang C, Cheng J (2021) Quantization of the coupling mechanism between eco-environmental quality and urbanization from multi-source remote sensing data. J Clean Prod 321:128948

Xu Y, Yu L, Peng D, Zhao J, Cheng Y, Liu X, Li W, Meng R, Xu X, Gong P (2020) Annual 30-m land use/land cover maps of China for 1980–2015 from the integration of AVHRR, MODIS and Landsat data using the BFAST algorithm. Sci China Earth Sci 63 (9):1390–1407

Yamu C, Frankhauser P (2015) Spatial accessibility to amenities, natural areas and urban green spaces: using a multiscale, multifractal simulation model for managing urban sprawl. Environ Plann B Plann Des 42 (6):1054–1078

Yang C, Zhu W, Sun J, Xu X, Wang R, Lu Y, Zhang S, Zhou W (2021) Assessing the effects of 2D/3D urban morphology on the 3D urban thermal environment by using multi-source remote sensing data and UAV measurements: a case study of the snow-climate city of Changchun China. J Cleaner Prod 321:128956

Yang J, Liu W, Li Y, Li X, Ge Q (2018) Simulating intraurban land use dynamics under multiple scenarios based on fuzzy cellular automata: a case study of Jinzhou district, Dalian. Complexity

Yang XX ed. (2021) Urban remote sensing: monitoring, synthesis and modeling in the urban environment. Wiley

Yatoo SA, Sahu P, Kalubarme MH, Kansara BB (2020) Monitoring land use changes and its future prospects using cellular automata simulation and artificial neural network for Ahmedabad city, India. GeoJournal:1–22

Yeh AG, Li X, Xia C (2021) Cellular automata modeling for urban and regional planning. In: Urban informatics. Springer, Singapore, pp 865–883

Yin J, Dong J, Hamm NA, Li Z, Wang J, Xing H, Fu P (2021) Integrating remote sensing and geospatial big data for urban land use mapping: a review. Int J Appl Earth Obs Geoinf 103:102514

Yoo C, Han D, Im J, Bechtel B (2019) Comparison between convolutional neural networks and random forest for local climate zone classification in mega urban areas using Landsat images. ISPRS J Photogramm Remote Sens 157:155–170

Yuan X, Shi J, Gu L (2021) A review of deep learning methods for semantic segmentation of remote sensing imagery. Expert Syst Appl 169:114417

Zare Naghadehi S, Asadi M, Maleki M, Tavakkoli-Sabour SM, Van Genderen JL, Saleh SS (2021) Prediction of urban area expansion with implementation of MLC, SAM and SVMs' classifiers incorporating artificial neural network using Landsat data. ISPRS Int J Geo Inf 10(8):513

Zeng L, Li J, Zhou Z, Yu Y (2020) Optimizing land use patterns for the grain for Green Project based on the efficiency of ecosystem services under different objectives. Ecol Ind 114:106347

Zhou L, Dang X, Sun Q, Wang S (2020) Multi-scenario simulation of urban land change in Shanghai by random forest and CA-Markov model. Sustain Cities Soc 55:102045

Zhou L, Yuan B, Hu F, Wei C, Dang X, Sun D (2022) Understanding the effects of 2D/3D urban morphology on land surface temperature based on local climate zones. Build Environ 208:108578

Zhu XX, Qiu C, Hu J, Shi Y, Wang Y, Schmitt M, Taubenböck H (2022) The urban morphology on our planet–global perspectives from space. Remote Sens Environ 269:112794

Part I

Land Use Land Cover, Urban Growth and Sprawl

A Systematic Review on the Application of Geospatial Technology and Artificial Intelligence in Urban Growth Modeling

SK Mithun, Samsad Parveen, Mehebub Sahana, and Subrata Chattopadhyay

Abstract

Understanding urban growth in rapidly changing cities is critical to city planners and administrators. Urban growth is a wide-ranging concept defined in many ways by different scholars. The existing literature on urban growth and urban sprawl is voluminous. The concept of sprawl suffers from difficulty in definition and is 'lost in a semantic wilderness.' In this present chapter, an attempt has been made to briefly document the important aspects of urban growth and urban sprawl pertaining to nature and dimensions of the studies on urban growth, issues associated with rapid built-up growth, particularly in developing countries like India, the role of remote sensing (RS) and geographic informa-

tion system (GIS) in urban growth studies, preprocessing, classification, and accuracy assessment of the used satellite images, techniques of measuring and monitoring urban growth, especially the entropy approach, change detection analysis, landscape metrics, the goodness of urban growth, and other quantitative and qualitative indices employed by global researchers highlighting their merits and demerits, modeling urban growth dynamics and its recent trends. It also highlights similar studies conducted in the Indian context. The bibliometric analysis finds that USA tops urban growth research as per Scopus database followed by China, while India ranks 49th position in the ladder. Modeling approaches, like Markov chain, cellular automata, and SLEUTH, are frequently deployed modeling approaches often integrated with RS-GIS. Furthermore, very recently, some machine learning approaches (e.g., multi-layer perceptron) are reportedly used for this purpose. However, model parameterization and calibration remain challenging and critical.

S. Mithun
Department of Geography, Haldia Government College, Haldia, West Bengal 721657, India

S. Parveen
Department of Geography, Aligarh Muslim University, Aligarh, Uttar Pradesh 202001, India

M. Sahana (✉)
Department of Geography, The University of Manchester, Manchester, UK
e-mail: mehebub.sahana@manchester.ac.uk

S. Chattopadhyay
Department of Architecture and Regional Planning, Indian Institute of Technology, Kharagpur, West Bengal 721302, India

2.1   Introduction

Presently, understanding urban growth and its dynamics in rapidly changing cities are critical to city planners and resource managers (Knox 1993; Turner et al. 1993). Hence, the importance of research on urban growth and urban sprawl has been felt strongly throughout the world (Bhatta et al. 2010a). Ensuring planned urban growth and sustainable urban planning in the future as prescribed in the Goal 11 of the Sustainable Development Goals (United Nations 2018) requires such urban physical expansion to be studied, understood, and modeled adequately (Mithun et al. 2016).

Urban growth is a wide-ranging concept defined in many ways by different scholars. Generally, urban growth is recognized as physical and functional changes in the urban landscape driven by social, economic, and political transformations (Kivell 1993; Black and Henderson 2003; Hall and Tewdwr-Jones 2010; Duwal 2013). It leads to conversion in land use and land covers (LULCs) of rural landscapes into urban forms driven by the interaction between different biophysical and socioeconomic factors. The studies of urban growth and sprawl can be attributed to various contexts, and characterizing urban sprawl has been a contentious issue (Sudhira 2008). The existing literature on urban growth and urban sprawl is voluminous. According to Galster et al. (2001), the concept of sprawl suffers from difficulty in definition, and the literature on sprawl is 'lost in a semantic wilderness.' Given the above, it seems pertinent here to review the past literature related to the scope under study.

In the current chapter, an extensive review of concurrent and relevant research works has been conducted to briefly document the important aspects of urban growth and urban sprawl under the scope of the present study. Particularly, the present research pertains to the nature and dimensions of studies on urban growth and issues associated with rapid built-up growth, particularly in developing countries like India. The present research reviews the role of remote sensing (RS) and geographic information system (GIS) in urban growth studies, preprocessing, classification, and accuracy assessment of the used satellite images, techniques of measuring and monitoring urban growth, and modeling urban growth dynamics. It also highlights similar studies conducted in the Indian context. Finally, it describes the proposed research and significance of the study based on the findings of the review study.

2.2   The Concept of Urban Growth and Urban Sprawl

As discussed previously, urban growth is recognized as physical and functional changes in the landscape (Kivell 1993; Black and Henderson 2003; Hall and Tewdwr-Jones 2010; Duwal 2013), leading to the conversion of LULCs into urban forms driven by the interaction between different factors. Urban growth can occur in several ways like compact or sprawling, clustered or scattered, and planned or organic (Cheng 2003; Duwal 2013). Urban sprawl is a complex (Frenkel and Ashkenazi 2008), dynamic (Harvey and Clark 1965; Ewing 1997; Sudhira 2008), multi-dimensional and multifaceted phenomenon (Galster et al. 2001; Ewing et al. 2002; Wolman et al. 2005; Frenkel and Ashkenazi 2008; Torrens 2008; Cabral et al. 2013), hence suffers from difficulties in definition (Johnson 2001; Barnes et al. 2001; Wilson et al. 2003; Roca et al. 2004; Angel et al. 2007).

While urbanization is a global phenomenon, it is very dynamic in developing countries like India. In India, the urban population has expanded more than five times significantly from 62 million (i.e., 17.29%) in 1951 to 377 million (i.e., 31.16%) in 2011 and is expected to be 600 million by 2031. In India, the physical expansion of the cities remained mostly confined within municipal boundaries during the first half of the twentieth century (Shaw 2005). However, the tremendous increase in urban population during the last few decades has led to the unprecedented peripheral expansion of the Class-I cities (Shaw

2005). This rapid peripheral growth is featured by uncontrolled, low-density, fragmented, and haphazard patchwork of development popularly known as urban sprawl (Barnes et al. 2001; Sudhira et al. 2003; Shaw, 2005; Kumar et al. 2007; Rahman et al. 2011). Such faster peripheral growth, in turn, transforms natural land covers into urban impervious surfaces and consequently induces enormous environmental and social impacts.

Moreover, the impacts that transcend far beyond a city's physical boundary (Grimm et al. 2008; Wu 2014; Wu et al. 2016) are more threatening in developing countries like India, where urban expansion occurs mostly in unplanned and haphazard fashion (Mohan et al. 2011; Attua and Fisher 2011; Haregeweyn et al. 2012). As such, the coming decades are likely to face a significant challenge to ensure human welfare and a viable global environment (Redman and Jones 2005). Hence, understanding urban growth and its dynamics in these rapidly changing environments are critical to city planners and resource managers (Knox 1993; Turner et al. 1993). Thus, the importance of research on urban growth and urban sprawl has been felt strongly throughout the world (Bhatta et al. 2010a).

2.3   Methodology

2.3.1   Bibliometric Analysis of Urban Growth Modeling Using Scopus Database

The present study selected the Scopus database to analyze data and create a bibliometric map using VOSviewer software. The data mining was performed with the help of the Scopas database searched on April 17, 2022. The Scopas data was chosen due to its worldwide application in the research community. The title, abstract, and keyword option added the main theme of 'Urban Growth Modeling' and the key search of this study included mainly research articles. The output of the search revealed old to recent year publications from 1982 to 2022, and the search string query was

TITLE-ABS-KEY (urban AND growth AND modeling)

The search results showed 6298 documents from the previous search string query, and after the option limit to Article and Journal, it gave 1559 documents. The second search string query was

TITLE-ABS-KEY (urban AND growth AND modeling) AND (LIMIT-TO (OA, "all")) AND (LIMIT -TO (DOCTYPE, "ar")) AND (LIMIT—TO (SRCTYPE, "j"))

This study will mainly focus on the selected 20 best-published articles and their distribution in different countries from 1982 to April 17, 2022. It will also analyze the year-wise published documents since 1982, the bibliometric map of co-authorship, author keywords co-occurrence, and co-authorship countries applied to the main theme of 'urban growth modeling.'

2.4   Results and Discussion

2.4.1   Results of the Bibliometric Analysis

The graph (Fig. 2.1) displayed below shows the total published documents from 1982 to April 17, 2022. From the beginning of few years, it has been seen that the number of published documents was significantly less. But after the year 2000, it changed with increasing and decreasing manner. The year 2021 published maximum documents with 261 out of 1559, but again in 2022, it sharply declined and reached only 74 articles.

The map below (Fig. 2.2) depicts the distribution of published articles in different countries from 1982 to April 17, 2022. It has been seen that out of total 1559 published articles, USA contributes 482 articles alone followed by China (282), UK (208), Australia (94), Germany (90), France (84), Netherlands (75), Italy (74), Canada (62), Spain (59), Japan (50), Switzerland (50), India (49), Brazil (45), Iran (41), South Korea (30), Belgium (29), Portugal (29), Sweden (29), Malaysia (24), Austria (23), Finland (23), South Africa (23), Poland (21), Russian Federation
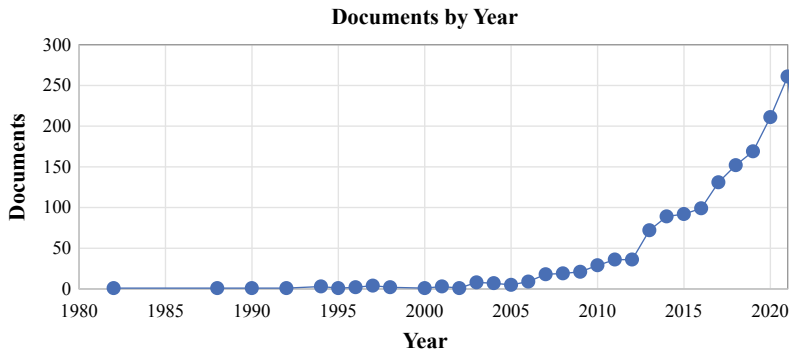
Fig. 2.1 Documents on urban growth modeling from 1982 to April 17, 2022. *Source* Scopas Database (https://www.scopus.com)
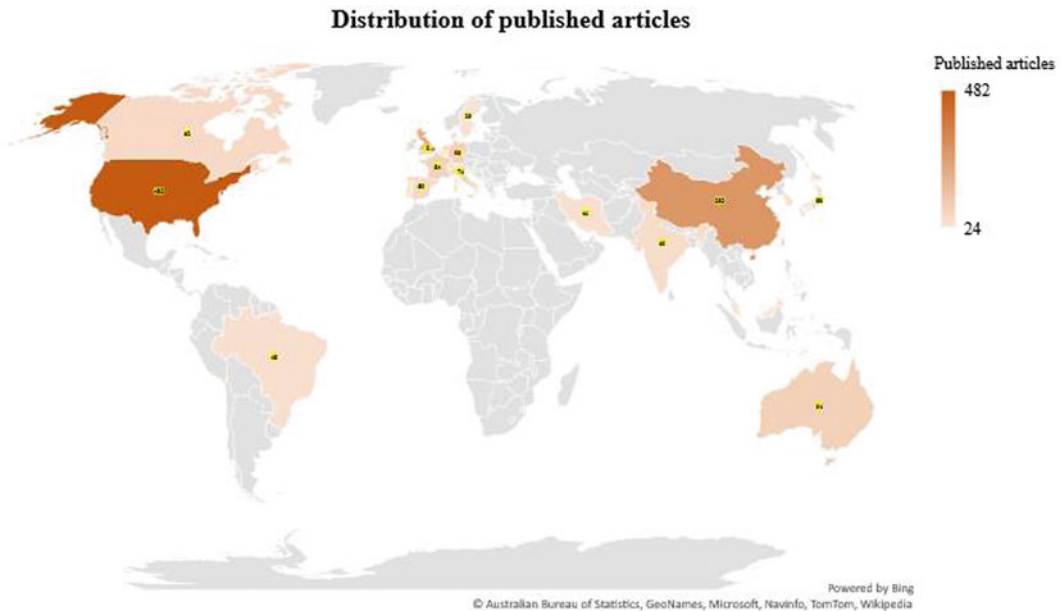
Fig. 2.2 Top 20 countries with the distribution of published articles. *Source* Scopas Database (https://www.scopus.com)

(20), and so on. The other countries such as Iraq, Nepal, Pakistan, Oman, Ukraine, Slovakia, Estonia, Fiji, Iceland, Senegal, Sudan, Myanmar, Moldova, etc., published a minimum number of articles like 4, 3, 2, or 1 document of each.

The map (Fig. 2.3) elucidated the co-authorship with a network diagram where the total co-authors were 5800; out of all these co-authors, 663 met the threshold. A minimum number of documents and citations of an author selection were 2. After applying all the filters, the final author selection number was 663; these selection criteria were software generated. Among all the authors, Liu y. published maximum documents of 21 with 342 and 50 citations and total strength links, respectively. Another author named Clarke k.c. published only nine papers but has recorded maximum citations with 2091 and 9 total strength links. Other recognizable authors in this theme were Wang j., Liu y.,

Fig. 2.3 Bibliometric map
based on co-authorship with
network visualization
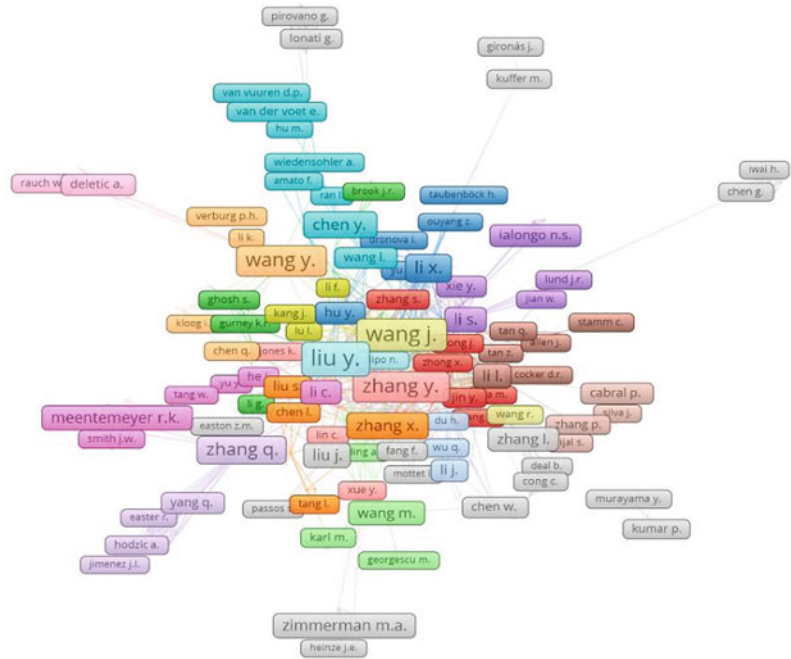
Zhang y., Zhang x., Wang y., Zimmerman m.a., Meentemeyer r.k., and so on. Different colors, the thickness of lines, and proximity to each other indicate different clusters and authors with similar interests in topics.

The map represented (Fig. 2.4) shows the total number of author keywords as 12,892, where the minimum number of occurrence keywords was 5, with a 1221 meeting the threshold level. The final selected keywords were 1000. All the criteria were selected by default from the software. Among all the keywords, 'urban growth' occurred maximum with 734 and 9824 total link strength. The other keywords are as follows: urban area, human, humans, land use, united states, urbanization, priority journal, numerical model, controlled study, urban development, female, climate change, China, land-use change, remote sensing, GIS, etc. Different colors indicate different clusters with a similar study of interest. There are a few dry areas of keywords that researchers are recently studying with a huge research work potential in the future such as analytical hierarchical process, simulation platform, swmm, total suspended solids, flood, flow of water, heat flux, Covid-19, pm 2.5, atmospheric boundary layer, climate models, precipitation intensity, water pollutant, gas emission, machine learning, smart cities, structural equation modeling, ecosystem services, watershed, groundwater resources, water quality, storm water, absorption, etc. The big circle indicates maximum occurrence, whereas a small circle indicates dry areas and the areas attracted by researchers in recent times.

The above bibliometric map (Fig. 2.5) was created based on documents availability. A total of 132 countries met 85 threshold levels beside a minimum number of documents of a country, and citations were selected of 2. At last, 85 countries were selected after applying all of the limitations. These 85 countries calculated the greatest total link strength of the co-authorship links with other countries, and all of these selections were based on the software. In this case, the USA has 481 documents with 17,099 citations and 331 total strength links, followed by the UK, China, Australia, France, Canada, Germany, Sweden, South Africa, India, Brazil, etc. The bigger circle size, the thickness of the line, and the proximity between two countries represent maximum documents and stronger network

Fig. 2.4 Bibliometric map of author keywords co-occurrence with network visualization

links. Few emerging countries such as Ukraine, Poland, Egypt, Cyprus, Oman, Pakistan, Kazakhstan, Montenegro, Ethiopia, Jordan, Estonia, etc. are recently focusing on the main theme of the 'urban growth model.'

2.4.2 Urban Sprawl and Growth Study

Measuring urban sprawl and urban growth with their temporal dynamics are crucial research topics in contemporary urban studies (Schneider and Woodcock 2008; Feng 2009; Bhatta 2012). Detecting and quantifying patterns and forms of urban physical expansion are common practices in such studies (Forman 1995; Galster et al. 2001; Heimlich and Anderson 2001; Wilson et al. 2003; Sudhira et al. 2003, 2004; Jat et al. 2008; Besussi et al. 2010; Bhatta et al. 2010a, b; Ramachandra et al. 2012). Based on the study by Galster et al. (2001), Angel et al.

(2007) argued that a study on urban sprawl could be a *pattern* of the spatial configuration of urban growth at a particular point in time, and a *process* signifying a change in such configuration over time, which need to be distinguished from the *cause* that is responsible for such pattern and *consequence* of patterns and processes of sprawl. Researchers advocate for different indices to measure urban sprawl. Some of these indices are GIS-based, while others are based on descriptive statistics, covering population, employment, traffic, living standard, resource consumption, architectural aesthetics, etc. (Nelson 1999; Torrens and Alberti 2000; Galster et al. 2001). Moreover, commonly deployed indices include population growth, built-up growth rate, residential and employment density, a spatial configuration such as fragmentation, accessibility, and proximity, and others like per-capita consumption of land use, etc. (Jiang et al. 2007; Bhatta 2012).

Fig. 2.5 Bibliometric map shows the co-authorship countries (maximum documents) with network visualization mode

Jiang et al. (2007) advocated for 13 attributes as geospatial indices for measuring sprawl in Beijing, China, and, finally, proposed an integrated urban sprawl index combining all the 13 indices. However, such an approach needs wide multi-temporal socioeconomic and geospatial data; therefore, appears to be challenging to derive mainly for cities in developing countries, where availability of such data is a major issue. Moreover, such an approach fails to ascertain any threshold for a city whether sprawling, instead helps to determine if a city is sprawling more in a relative sense. According to Torrens (2008), urban sprawl needs to be measured at multiple scales. The study proposed the city-scale or metropolitan-scale and intraurban or local-scale analysis, in which measurement of descriptive characteristics is translated into quantitative form. Finally, it devised 42 measures of sprawl. However, the methodology lacks the use of

geospatial data. Moreover, the methodology seems to be complex and confusing owing to the use of many scales and indices. Thus, studies of urban sprawl can be attributed to various contexts, and characterizing urban sprawl has been a contentious issue (Sudhira 2008). Hence, Galster et al. (2001) pointed out that sprawl literature is 'lost in a semantic wilderness.'

2.4.3 Forms, Patterns, and Temporal Dynamics of Urban Growth

Wilson and Chakraborty (2013) believed that studying physical characteristics as a pattern of development is one of the most common approaches to defining urban sprawl. Detecting and quantifying the pattern and form of urban physical expansion, i.e., *pattern* with its temporal

dynamics (i.e., the *process*) of urban expansion, are standard practices in sprawl studies (Forman 1995; Wasserman 2000; Galster et al. 2001; Heimlich and Anderson 2001; Wilson et al. 2003; Sudhira et al. 2003, 2004; Jat et al. 2008; Besussi et al. 2010; Bhatta et al. 2010a, b; Ramachandra et al. 2012). The common consensus on the physical form and pattern of urban sprawl includes the ribbon (Harvey and Clark 1965; Angel et al. 2007) and leapfrog development (Harvey and Clark 1965; Gordon and Richardson 1997; Ewing 1997; Tsai 2005), scattered (Ewing 1997; Benfield et al. 1999; Tsai 2005; Angel et al. 2007) and fragmented morphology of urban development (Benfield et al. 1999), low-density urbanization (Ewing 1997; Gordon and Richardson 1997; Pendall 1999; Fulton et al. 2001; Tsai 2005), uncontrolled, uncoordinated, unplanned (Batty et al. 2003; Sudhira and Ramachandra 2007) and dispersed urban growth (Angel et al. 2005; Kumar et al. 2007; Sudhira and Ramachandra 2007), and disjointed pattern of land development (Wu 2006). Urban built-up consisting of all human-made structures and impervious surfaces is employed as an efficient and straightforward parameter or indicator for quantifying urban physical expansion and urban sprawl (Torrens and Alberti 2000; Barnes et al. 2001; Sudhira et al. 2003, 2004; Cabral et al. 2006; Kumar et al. 2007; Jat et al. 2008; Feng 2009; Bhatta 2009b; Bhatta et al. 2010a, b; Rahman et al. 2011; Punia and Singh 2012; Pandey et al. 2013).

Wilson et al. (2003) distinguished five types of physical urban growth: infill, expansion, isolated, linear branch, and clustered branch, whereas Berling-Wolff and Wu (2004) identified four types of urban growths, namely spontaneous, diffusive, organic, and road influenced. Herold et al. (2005) presented a schema of the process of urban growth that starts with an initial core, then grows and disperses to new development. As such, three common types of urban growth, namely infill, expansion, and scattered, are emphasized by many researchers (e.g., Wilson et al. 2003; Duwal 2013). Infill refers conversion of non-built-up areas into built-up cover when the former is surrounded by the latter. This type of urban growth is common in the core of a city (Xu et al. 2007). Expansion occurs adjacent to the urban fringe, where newly developed areas spread outward in adjacency to existing urban areas. This type of urban growth is also called fringe development (Xu et al. 2007), and linear urban growth along road corridors that stimulates new development is included in the expansion category (Berling-Wolff and Wu 2004). A scattered type of urban growth occurs in the formation of new isolated urban patches without having direct spatial linkage with the existing urban areas (Berling-Wolff and Wu 2004).

2.4.4 Geospatial Application in Urban Growth Studies

The conventional surveying and mapping techniques are time-consuming and expensive; therefore, require a great deal of time, effort, and money to meet the demand for mapping and monitoring of fast-growing urban centers (Sudhira et al. 2004; Jat et al. 2008; Punia and Singh 2012). The advent of RS and GIS has made it comfortable. It offers spatially consistent multi-spectral, multi-temporal, and multi-spatial resolution data that can play a significant role in analyzing and modeling land-cover changes and dynamics (Yuan et al. 2005; Herold et al. 2003, 2005; Araya and Cabral 2010). Thus, satellite RS (SRS) imagery can present a synoptic view of a landscape at the frequent interval, provide images of areas inaccessible to conventional surveying, and reveal explicitly land-use and land-cover patterns (Jensen and Cowen 1999; Schneider and Woodcock 2008), which is widely used as an input database to extract urban built-up areas. The technology of RS coupled with GIS is a cost-effective, technologically sound, and powerful tool, which can effectively be deployed to detect, map, monitor, and analyze urban growth dynamics (Jensen and Cowen 1999; Yeh and Li 2001b; Sudhira et al. 2003, 2004; Herold et al. 2003; Yang 2003, 2005; Li and Yeh 2004; Li et al. 2005; Yang and Liu 2005; Kumar et al. 2007; Weng and Quattrochi 2006; Jat et al. 2008; Schneider and Woodcock

2008; Rahman et al. 2011; Thapa and Murayama 2009; Besussi et al. 2010; Pandey et al. 2013). Since its inception, the RS-GIS tool is extensively applied by many geographers, planners, and spatial scientists for analyzing and modeling spatial phenomena geographically.

Moreover, the required socioeconomic data for essential variables for modeling urban growth is limited in terms of availability, temporal accuracy, and consistency, specifically in case of the developing countries. Longley and Mesev (2000) claimed that understanding urban modeling is limited by the availability of datasets. Accordingly, several studies are concerned with exploring the alternative source of data for modeling urban growth. Since, SRS data, as discussed, provides a spatially consistent time series dataset over large areas with great spatial detail and temporal frequency (Batty and Howes 2001), it indirectly offers a variety of socioeconomic information such as spatial extent and pattern of land use, urban infrastructures, etc. (Clarke et al. 2002; Herold et al. 2005). However, the potentiality of the combination of RS tool and urban modeling is yet to be fully explored (Longley and Mesev 2000; Batty and Howes 2001; Herold et al. 2005).

2.4.5 Preprocessing of SRS Data

Preprocessing of the collected SRS data needs to be undertaken before classification. It includes detection and restoration of bad lines, image registration or geometric rectification, radiometric calibration and atmospheric correction, and topographic correction (Jensen 1996; Bhatta 2009; Richards 2013; Lillesand et al. 2015). Many textbooks and articles deal extensively with image preprocessing, such as Jensen (1996) and Richards (2013). Accurate geometric rectification is a prerequisite for a combination of different data in a classification process. Also, atmospheric calibration is mandatory in cases when multi-temporal or multi-sensor data is used together (Lu and Weng 2007). Different methods are devised for radiometric calibration and atmospheric normalization and correction, such

as relative calibration, dark object subtraction, and other sophisticated calibration approaches (Lu and Weng 2007). Among the sophisticated techniques, the quick atmospheric correction (QUAC), fast line-of-sight atmospheric analysis of hypercubes (FLAASH), atmospheric correction (ATCOR), and second simulation of the satellite signal in the solar spectrum (6S) are notable and frequently used (Nazeer et al. 2014; Zhang et al. 2012; Wang et al. 2019). Since the FLAASH is one of the sophisticated and popularly used atmospheric correction tools, many researchers use it for calibrating multi-spectral and hyper-spectral images such as Landsat (Perkins et al. 2005; Nazeer et al. 2014; Wang et al. 2019), Hyperion (Felde et al. 2003; Perkins et al. 2005; Yuan and Niu 2008; Vibhute et al. 2015), AVIRIS (Kruse 2004; Perkins et al. 2012), ALI (Yuan and Niu 2008), HSI (Cooley et al. 2002) data. Many studies find the FLAASH radiometric calibration as more consistent and better than some other techniques (e.g., Yuan and Niu 2008; Vibhute et al. 2015). Besides, the ENVI (Exelis 2015) is a popularly used software for implementing FLAASH correction (Cooley et al. 2002; Yuan and Niu 2008; Perkins et al. 2012; Vibhute et al. 2015).

2.4.6 Satellite Image Classification

Ideally, preprocessing of SRS data is followed by image classification, referring to the groping of image pixels based on different rules and algorithms (Jensen 1996; Lillesand et al. 2015) that produce the predefined land-cover classes (Araya and Cabral 2010). There are many factors, such as types of input images, classification methods, algorithms, etc. that affect the result of image classification. Many studies in urban studies extensively focus on image classification (e.g., Lu and Weng 2007; Araya and Cabral 2010; Belal and Shafizadeh-Moghanm 2011; Bhatta 2013; Estoque et al. 2015). Researchers have employed a large number of approaches in the classification of satellite images (e.g., Lu and Weng 2007; Li et al. 2013, 2014) even in urban studies (e.g., Estoque et al. 2015). The parametric

maximum likelihood classifier (MLC)-based per-pixel supervised classification is one of the widely and popularly used approaches in this regard (Maktav and Erbek 2005; Yuan et al. 2005; Oluseyi 2006; Xiao et al. 2006; Lu and Weng 2007; Shafizadeh-Moghadam and Helbich 2013; Estoque et al. 2015; Mondal et al. 2017; Aburas et al. 2017). However, the assumption of normal distribution in such parametric classification often violates actual spectral distribution, especially in a complicated landscape like the Kolkata metropolitan area (KMA). Insufficient, non-representative, and multi-modal training samples add further uncertainty to classification (Lu and Weng 2006). As a result, nonparametric classifiers, such as neural networks, decision trees, and knowledge-based classifiers, are increasingly recruited in image classification. But, the variation in characteristics of training and testing data and dimensionality of a dataset may affect classification accuracy. For moderate-resolution satellite imagery like Landsat thematic mapper (TM) and Landsat operational land imager (OLI) (30 m), per-pixel LULC classification may not be useful as mixed pixels are common in such data (Fisher 1997; Cracknell 1998; Lu and Weng 2006).

The domain experts have made a great effort in improving classification accuracy by developing advanced classification approaches. Sub-pixel image classification approaches provide a more appropriate representation and estimation of land covers of an area (Foody and Cox 1994; Woodcook and Gopal 2000; Lu and Weng 2006). Object-based image analysis is also used occasionally over pixel-based image classification even for medium resolution satellite images (Platt and Rapoza 2008; Estoque et al. 2015). The advent of machine learning approaches offers opportunities to implement the per-pixel, sub-pixel, and object-based satellite image classification with greater accuracy for medium resolution satellite images like Landsat TM and OLI (Watanachaturaporn et al. 2006; Li et al. 2014; Estoque et al. 2015).

The support vector machine (SVM) classifier is a powerful nonlinear, nonparametric, and supervised classification technique (Rimal et al. 2018), which is commonly used by the research community. The SVM is a flexible supervised classifier that produces high classification accuracy (e.g., Schneider 2012; Rimal et al. 2018). Ibrahim Mahmoud et al. (2016) used the SVM classifier for monitoring urbanization, and the study by Schneider (2012) found the SVM and decision tree (DT) as better classifiers than MLC in a study of LULC change applying Landsat data over urban and peri-urban areas. Waske and Benediktsson (2007) concluded that SVM achieves the highest accuracy while classifying multi-spectral data. It suits well for segmented raster; however, it can also be used for any standard raster. The use of SVM is advantageous over the conventional MLC classifier as the former is less susceptible to noise, correlated bands, and an unbalanced number or size of training sites within each class (Mountrakis et al. 2011; ESRI 2017).

2.4.7 Quantifying Urban Growth

With the advancement in research, researchers have used various indices and models integrated with RS-GIS for quantifying patterns of growth in a city. Thus, there are ample numbers of metrics, indicators, and statistics proposed by many researchers that are employed to detect, measure, and quantify patterns of urban expansion. The measures include sprawl dimensions and quantitative indices (Galster et al. 2001; Tsai 2005; Wolman et al. 2005; Jiang et al. 2007; Torrens 2008; Jaeger et al. 2010a, b; Jaeger and Schwick 2014; Tian et al. 2017), landscape metrics (McGarigal and Marks 1994; Turner et al. 2001; Herold et al. 2002, 2003, 2005; Cabral et al. 2006; Hardin et al. 2007; Thapa and Murayama 2009; Wang et al. 2009; Aguilera et al. 2011; Zhao and Murayama 2011; Lü et al. 2013; Zeng et al. 2014), Shannon's and relative entropy index (Yeh and Li 2001b, 2004; Lata et al. 2001; Sudhira et al. 2003; Tsai 2005; Kumar et al. 2007), etc. The measures can be in both absolute and relative scales; absolute measures are able to quantify sprawl with a black-and-white distinction between sprawled and non-

sprawled cities, whereas, in contrast, relative measures are applied to quantify the degree of sprawl without a black-and-white distinction that can be applied for comparative study among cities, among the sub-zones within a particular city, or explicitly for temporal study (Bhatta et al. 2010b; Bhatta 2012).

2.4.7.1 Change Detection Analysis

Change detection refers to the process of determining an areal change in land covers based on co-registered multi-temporal SRS data. Different researchers use different change detection techniques, such as image differencing, image rationing, vegetation index differencing, principal component analysis (PCA), and post-classification comparison (PCC). However, the PCC is probably the most widely and popularly employed change detection technique (Singh 1989; Yuan et al. 2005; Belal & Shafizadeh-Moghanm 2011; Zaki et al. 2011; Abd El-Kawy et al. 2011). It renders a 'from-to' change information and the kind of land-cover transformations that occurs over some time and can easily be derived and mapped (Yuan et al. 2005). Many studies have implemented the post-classification change detection technique in quantifying urban growth dynamics, such as Herold et al. (2002, 2003, 2005), Sudhira et al. (2003, 2004), Jat et al. (2008), Punia and Singh (2012), Tewolde and Cabral (2011), Tavares et al. (2012), Bhatta (2009, 2012), Mitra et al. (2012), Ramachandra et al. (2012), Duwal (2013), Al-Sharif & Pradhan (2014), Wu et al. (2015), Aithal & Ramachandra (2016), Islam et al. (2018), Sahana et al. (2018), Mithun et al. (2021), etc.

2.4.7.2 Landscape Metrics

Landscape metrics are defined as the quantitative indices or measures that are used to quantify the structure and pattern of a landscape (O'Neill et al. 1988; McGarigal and Marks 1994; Herold et al. 2002). The metrics that came initially in the field of Landscape Ecology in the late 1980s incorporate measures based on information-theory measures and fractal geometry (McGarigal and Marks 1994; Herold et al. 2002, 2003, 2005). Landscape metrics can be applied to quantify spatial heterogeneity at the three different levels, viz. patch, class, and landscape (Herold et al. 2002, 2003, 2005). A patch is a homogeneous unit of a particular class or category under the study; a class is a collection of all patches belonging to a specific category; and a landscape refers to the collection of all patches belonging to all classes in a landscape (McGarigal and Marks 1994). The metrics which are even spatially non-explicit, still reflect spatial properties. On the other hand, spatially explicit metrics can be as patch-based and pixel-based indices (Gustafson 1998; Herold et al. 2002, 2005). Based on the study by O'Neill et al. (1988), several groups of landscape metrics were developed, modified, and tested (Hargis et al. 1998; McGarigal et al. 2002; Ritters et al. 1995; Rahaman et al. 2019). Herold et al. (2003, 2005) argued that landscape metrics, while applied outside the discipline of landscape ecology, should be referred to as spatial metrics as they deal with spatial structures and patterns of a geographical phenomenon.

Although landscape metrics are commonly used to quantify spatial heterogeneity of vegetation cover (O'Neill et al. 1988; Hargis et al. 1998; Gustafson 1998; McGarigal et al. 2002), the use of the metrics in analyzing urban environment is a recent practice (Herold et al. 2003, 2005). Parker et al. (2001) explored the effectiveness of spatial metrics for socioeconomic application. Alberti and Waddell (2000) substantiated the importance of such metrics and proposed specific metrics for urban modeling. Herold et al. (2005) urged for the coupling of RS and spatial metrics to facilitate more consistent and detailed information on urban structure, analysis, and dynamics. Recently, there has been increasing interest in the application of spatial metrics to quantify the heterogeneity, change, and dynamics of the urban landscape. The RS-GIS integrated studies dealing with the application of spatial metrics, such as Geoghegan et al. (1997), Alberti and Waddell (2000), Parker et al. (2001), Herold et al. (2002, 2003, 2005), Cabral et al. (2005, 2006, 2011), Zhao and Murayama (2006, 2011), Huang et al. (2007), Hardin et al. (2007), Taubenböck et al. (2009, 2012), Sudhira (2008), Thapa and

Murayama (2009), Zhang (2009), Araya & Cabral (2010), Jaeger et al. (2010b), Peng et al. (2010), Pham et al. (2011), Tian et al. (2011), Aguilera et al. (2011), Ramachandra et al. (2012), Liu and Feng (2012), Kong et al. (2012), Lü et al. (2013), Ramachandra et al. (2015), Megahed et al. (2015), Wu et al. (2015). Aithal and Ramachandra (2016), and Mithun et al. (2021) have applied and suggested some specific metrics to quantify structures and patterns of urban growth with their effectiveness and scaling effects. Most of the studies demonstrate the importance of the metrics and argue for further systematic investigation of urban analysis (Parker et al. 2001; Herold et al. 2005).

Even though spatial metrics have essential applications in quantifying urban growth and urban sprawl (Hardin et al. 2007), there are some challenges related to the application of spatial metrics. Some of the metrics are correlated, and thereby contain redundant information (Cushman et al. 2008; Bhatta 2012). According to Parker et al. (2001), there is no standard set of metrics best suited for urban studies, since the significance of metrics varies with the objective under investigation. Therefore, selecting independent metrics for a particular study has been a challenging task for the researchers. Besides, spatial accuracy or spatial resolution and classification or thematic accuracy of remote sensing data also matter while applying spatial metrics (Herold et al. 2005; Bhatta 2012). Therefore, while using metrics, it is required to evaluate and interpret their ability to capture the information of interest.

2.4.7.3 Shannon's Entropy Approach

The index of Shannon's entropy is one of the widely used metrics in measuring urban growth and sprawl. It is a significant and reliable measure for calculating the degree of compactness and dispersion of urban growth and urban sprawl (Thomas 1981; Yeh and Li 2001b; Lata et al. 2001; Li and Yeh 2004; Sudhira et al. 2004; Kumar et al. 2007; Bhatta 2010b, 2012; Araya and Cabral 2010; Tewolde and Cabral 2011; Punia and Singh 2012; Cabral et al. 2013; Zeng et al. 2015; Bagheri and Tousi 2018; Mithun

et al. 2021). The measure of entropy is a superior measure over other measures of spatial dispersal statistics, like Gini's and Moran's coefficients, which depend on the shape, size, and a number of regions under study (Smith 1975; Thomas 1981; Yeh and Li 2001b; Tsai 2005). According to Bhatta (2012), this is a robust measure as it can identify sprawl in a black-and-white categorization. The measure of relative entropy that is based on Shannon's entropy is also used for the purpose (Thomas 1981; Bhatta 2009, 2012; Bhatta et al. 2010b; Tewolde and Cabral 2011; Cabral et al. 2013). In relative entropy, the value of Shannon's entropy can be rescaled between 0 and 1. However, relative entropy is sensitive to variation in the shape and size of units under consideration (Bhatta 2012). Yeh and Li (2001b) argued that entropy values for different years could be used to show the difference in entropy between t_1 and t_2 to indicate the magnitude of change in entropy as a result of a change in spatial phenomena during a specific period. The magnitude of change in entropy signifies whether a city is becoming more dispersed with time (Dhali et al. 2019).

2.4.7.4 Pearson's Chi-Square Statistic and Degree of Goodness

Almeida et al. (2005) used Pearson's chi-square measure and degree of freedom to investigate the discrepancy between expected and observed urban growth over time. The measure may be specifically useful for cities in developing counties where cities lack planned and predicted growth, unlike most of the cities in developed countries where actual growth usually meets planned growth. Hence, it necessitates evaluating the discrepancy between observed and expected growth in the cities of developing countries over time. Subsequently, several studies have used the technique and found the same useful (e.g., Cabral et al. 2006; Cabral and Zamyatin 2009; Bhatta et al. 2010b; Bhatta 2012). The degree of goodness (Bhatta 2009, 2012; Bhatta et al. 2010a) is a measure that combines entropy and chi-square statistic. It refers to the extent to which observed growth relates to the expected growth and the magnitude of compactness in a region over a specific period.

2.4.8 Artificial Intelligence in Urban Growth Modeling

Understanding the dynamics of urban growth remains critical to city planners and resource managers, especially in rapidly changing urban environments (Knox 1993; Turner et al. 1993). Besides, modeling urban growth is an essential tool for geographers, city planners, ecologists, and resource managers (Herold et al. 2005). Understanding the dynamics of a complex urban system and investigating the impacts of such dynamics on the environment involves modeling spatiotemporal urban growth. Modeling urban dynamics has a long history dating back to the 1950s, featured by many periodical reviews (Batty 1979; Berling-Wolff and Wu 2004). Many analytical and static modeling approaches have been devised that are based on diverse theories, such as urban geometry, rank–size relationship, economic activities, and social pattern and city structures. However, such models primarily deal with historical evolution, growth, and expansion at the spatiotemporal dimension, but cannot be used to simulate future urban growth. Besides, many of the latter approaches are quantitative (Berling-Wolff and Wu 2004), which are developed by neoclassical economists based on 'friction of space' borrowed from Physics (He et al. 2008). Hence, such models are insufficient to capture and simulate the complexity of an urban system (Batty 1979); moreover, the models do not consider spatiality to a large extent (He et al. 2008). Thus, several modeling approaches have been developed to simulate and forecast urban dynamics (Berling-Wolff and Wu, 2004). According to Hu and Lo (2007), Zeng et al. (2008), and Duwal (2013), these models are broadly grouped into four types, namely empirical estimation, optimization, stochastic, and rule-based dynamic simulation models featured by some advantages and disadvantages, as in Table 2.1.

A dynamic modeling system is preferred to simulate urban growth and to understand the spatial consequences of such growth (Batty and Longley 1994). Considerable efforts have been made for developing and improving dynamic urban modeling (Batty and Xie 1994a, b, c, 1997; Landis 1995; Veldkamp and Fresco 1996; White and Engelen 1997; Clarke and Gaydos 1998; Batty et al. 1999; Wu and Webster 1998, 2000; Li and Yeh 2000; Yeh and Li 2002; Sui and Zeng 2001; Pijanowski et al. 2002; Batty 2005). Significant improvement in the spatiality of urban growth modeling came only with the use of cellular automata (CA) models by the end of the 1980s. Since then, the CA models are widely used for modeling urban growth dynamics (Xie 1996; Batty and Xie 1997; Batty et al. 1999; Clarke et al. 1998; Coucelis 1997; White and Engelen 1997; Ward et al. 2000; Clarke and Gaydos 1998; Wu and Webster 1998; Li and Yeh 2000, 2002; Wu 2002; Barredo et al. 2003; Liu and Phinn, 2003; Almeida et al. 2005; Fang et al. 2005; Yeh and Li 2006; Al-Ahmadi et al. 2009; Gong et al. 2009; Feng et al. 2011; Stanilov and Batty 2011; White et al. 2012; Chowdhury and Maithani 2014; Lin et al. 2014; Munshi et al. 2014; Aithal and Ramachandra 2016; Aburas et al. 2017; Devendran and Lakshmanan 2019; Mondal et al. 2017, 2019). The domain experts, specifically in the field of modeling urban growth, use the CA model coupled with other techniques and models known as hybrid models that yield better performance. Among them, the neural network CA (Li and Yeh 2002; Devendran and Lakshmanan 2019), Fuzzy-CA (e.g., Liu 2008, 2012; Al-Ahmadi et al. 2009), logistic-CA (e.g., Hu and Lo 2007; Liu and Feng 2012; Munshi et al. 2014), CA and partial swarm optimization (e.g., Feng et al. 2011), multi-agent CA (e.g., Arsanjani et al. 2013), variable grid CA (e.g., Van Vliet et al. 2009), gravitational field model with CA (e.g., He et al. 2013), CA and system dynamics (e.g., Haase et al. 2012), CA-Markov (e.g., Liu 2008; Araya and Cabral 2010; Guan et al. 2011; Mitsova et al. 2011; Sang et al. 2011; Shafizadeh-Moghadam and Helbich 2013; Rimal et al. 2018; Siddiqui et al. 2018; Mondal et al. 2017, 2019; Eastman and Toledano 2018; Mithun et al. 2022) are notable.

Over the years, researchers have developed and used different other sophisticated models to simulate and analyze urban growth, such as the

Table 2.1 Categorization of the commonly used models for urban growth and LULC dynamics studies

Model	Characteristics/theme/principles	Advantages	Disadvantages	Examples
Empirical statistical models	Explicitly identify the causes of land-use changes using multivariate analysis and their contribution to land-use change	An analytical tool to test the dependency of land-use change on driving factors; requires relatively less data	Not suitable for wide extrapolation, does not incorporate the temporal dynamics, intrinsically not spatial, lack of understanding on simulation process that influences land-use process	Multiple linear regression, logistic linear regression
Optimization models	Econometric approach, any parcel of land given its attributes and location, is modeled as being used in the way that yields the highest rent	The agents whose behavior is modeled can make informed predictions and plans	Several assumptions are taken into consideration	Von Thunen's model, agent-based model
Stochastic models	Land-use change is a first-order process, which is condition probability of land-use change, and future change depends on present, not past	Mathematical and operational simplicity can be used where no information on driving factors and mechanisms of land-use change is available	Does not consider the factor of spatiality and temporal dynamics; not suitable for modeling of long term and large area	Stochastic Markov, cellular automata
Process-based dynamic simulation models	Rule-based system dynamic models within a GIS framework, understanding complex phenomenon through dynamic simulation, different branches of methods in an integrative model	Well suited for representing non-stationary process; highly adaptable; inherently spatial and dynamic	Does interpret the spatiotemporal process of land-use change; many individual processes of decision making cannot be modeled	CA-SLEUTH, CA-MARKOV, MCE, Fuzzy-CA, ANN-CA

Source Based on (Lambin 2004; Zhang 2009; Bhatta 2013; Duwal 2013)

artificial neural network (ANN) (e.g., Pijanowski et al. 2005; Lin et al. 2011; Almeida et al. 2008; Maithani 2009; Abiden et al. 2010), agent-based model (e.g., Jjumba and Dragićević 2012; Arsanjani et al. 2013), genetic algorithm (GA) (Tang et al. 2007), geographically weighted regression (e.g., Mondal et al. 2015), SLEUTH model (e.g., Clarke 2008, 2018; Herold et al. 2003, 2005; Jat et al. 2017; Mondal et al. 2019), analytic hierarchy process (AHP) (e.g., Park et al. 2012; Devendran and Lakshmanan 2019), bivariate or step-wise multiple regression (e.g., Sudhira et al. 2004; Jat et al. 2008; Al-Sharif and Pradhan 2014), logistic regression (LR) (e.g., Hu and Lo 2007; Nong and Du 2011; Arsanjani et al. 2013; Munshi et al.

2014; Shafizadeh-Moghadam and Helbich 2015), Markov chain (MC) (e.g., Tang et al. 2007; Takada et al. 2010; Wilson and Weng 2011; Ahmed and Ahmed 2012; Arsanjani et al. 2013), fuzzy logic (e.g., Liu 2012). Therefore, plenty of models have been devoted based on different theories and rules to predict future LULCs of urban areas.

The multi-layer perceptron (MLP) is one of the widely applied ANN approaches in modeling and forecasting urban growth (Hu and Weng 2009; Ahmed and Ahmed 2012; Megahed et al. 2015; Mishra and Rai 2016; Mondal et al. 2019; Mithun et al. 2022). In addition, the transition potential used in the MLP model is reported to be the best performer as compared to other

modeling techniques (Eastman et al. 2005). Hybrid modeling approaches that combine ANN and other techniques are reportedly more robust than the ANN while applied in isolation. Pijanowski et al. (2002) used neural networks and GIS together to predict LULC change in Michigan Grand Traverse Bay Watershed. Yeh and Li (2001a, 2002) integrated neural networks, CA, and GIS for simulating alternative development patterns based on different land-use planning. Some studies have used the MC in combination with ANN for modeling urban growth dynamics (Mithun et al. 2022).

The MC is a stochastic process depicting the possibility of changes from one state to another state with respect to time defined by the transition probability matrix (Zhang et al. 2011; Arsanjani et al. 2013). The MC is believed to be a useful tool for modeling LULC change when the process of land-cover change in an area is complex and challenging to describe. Hence, the ANN modeling, in combination with the Markov chain, is capable of effective simulation of urban dynamics as ANN can fit complicated nonlinear relationships between urban land-use dynamics and the drivers behind such dynamics (Tewolde and Cabral 2011; Ahmed and Ahmed 2012; Eastman and Toledano 2018). However, the quality of modeling depends on the quality of data used, model parameterization and calibration, and validation of results. Noteworthy to mention is that the TerrSet software (Eastman 2015) provides a suitable platform for robust implementation of the modeling approaches integrated with RS-GIS.

During the last couple of decades, RS and GIS integrated dynamic modeling of urban growth has rapidly gained popularity among geographers, urban planners, and policymakers. This development has been possible owing to the increased availability and usability of multiple SRS datasets at different spatiotemporal scales and the development of computer hardware and software tools for processing a wide variety of data as per requirement. Considerable efforts have been made in exploring the modeling approaches integrated with RS-GIS for simulating urban growth and its dynamics (Turner 1987;

Meaille and Wald 1990; Batty and Xie 1994a, b; Landis 1995; Veldkamp and Fresco 1996; Pijanowski et al. 1997; White and Engelen 1997; Clarke and Gaydos 1998; Wu and Webster 1998, 2000; Li and Yeh 2000; Sui and Zeng 2001; Wang and Zhang 2001).

2.4.9 Model Validation and Accuracy Assessment

An accuracy assessment of classified images follows the process of image classification. The term accuracy assessment typically implies expressing the degree of 'correctness' in image classification. Congalton (1991, 2001), Congalton and Green (1993), and Foody (2002) meant accuracy assessment as the agreement between classified and reference data. Congalton (1994) and Congalton and Green (2019) identified four major stages or epochs related to accuracy assessment research. According to them, the fourth and the latest type of accuracy assessment consider more meaningful use of the information on the correspondence of the classified image to those observed on the ground based on reference data, ground truth verification data, etc. A confusion or an error matrix is generated to describe the pattern of the class allocation made relative to the reference data.

Presently, the confusion or error matrix lies at the core of the accuracy assessment of classified or thematic data; hence, the present age of accuracy assessment could be called the age of the error matrix (Congalton 1994; Foody 2002; Congalton and Green 2019). In addition to the commission and omission errors, an error matrix can also be deployed to compute overall accuracy (OA), producer's accuracy (PA), and user's accuracy (UA), as introduced by Story and Congalton (1986). The measure of OA is found to be the most commonly reported technique of accuracy assessment. However, PA and UA are ways of representing individual class accuracies instead of just the OA. A PA is said to be how accurately an analyst classifies an image by class or category, while a UA is defined as how well the classification performs in the field by class

(Story & Congalton 1986; Ahmed and Ahmed 2012; Latifovic et al. 2017; Yang et al. 2017). The sample size is another vital aspect in assessing the accuracy of classified images. An accuracy assessment requires an adequate number of samples per map class to be gathered so that the assessment performed is valid statistically. The researches by Congalton (1988, 1991) and Congalton and Green (2019) suggest a general guideline or rule of thumb to acquire a minimum of 50 samples per category of classified image for images having less than one million acres in size and fewer than 12 classes or categories. Several studies, such as Maktav and Erbek (2005); Yuan et al. (2005); Oluseyi (2006); Xu et al. (2007); Belal and Shafizadeh-Moghanm (2011); Zaki et al. (2011), achieved the accuracy level of the classified images with 3–7 land-cover classes ranging between 85 and 95% for multi-spectral and temporal Landsat imageries. The choice of sampling technique in the determination of sites is also an essential part of the process of accuracy assessment. Many studies, such as Hord and Brooner (1976), Ginevan (1979), Rhode (1978), and Fitzpatrick-Lins (1981), suggested that a proper sampling scheme requires to be deployed while assessing accuracy. The frequently applied schemes include simple random, stratified, and systematic random sampling schemes.

Building an error matrix is the first step in the objective comparison of maps (Pontius 2000; Congalton and Green 2019), and the measures so derived are straightforward. However, it is tricky to interpret as a surprisingly high number of samples can be classified correctly due to the chance factor. Hence, it requires incorporating the expected proportion of correct classification that is due to the chance factor while assessing accuracy (Pontius 2000). The Kappa is a discrete multivariate technique that is used in accuracy assessment to statistically determine if one error matrix is significantly different from another. The KHAT statistic ($\widehat{K}$) is a maximum likelihood estimate of Kappa from multinomial distribution and is a measure of actual agreement minus chance agreement (Cohen 1960; Congalton

1991). Initially, the technique was introduced by Congalton et al. (1983) to the RS community. Now, the Kappa analysis seems to be a standard component of accuracy assessment (Congalton et al. 1983; Rosenfield and Fitzpatrick-Lins 1986; Hudson and Ramm 1987; Congalton 1991). Landis and Koch (1977) described the relative strength of agreement associated with Kappa statistics into six categories, and they further characterized the $\widehat{K}$ into the three groups, viz. a value higher than 0.80 that represents a strong agreement, a value between 0.40 and 0.80 that constitutes a moderate agreement, and a value below 0.40 representing a weak agreement.

2.4.9.1 Urban Grown Modeling in Indian Cities

Though studies on urban growth based on SRS data started in the early 1970s following the advent of Landsat multi-spectral scanner (MSS) data, similar research in developing countries, particularly in India, was initiated much later. In the late 1980s, the two studies, particularly Sokhi et al. (1989) and Uttarwar and Sokhi (1989), were conducted on urban growth, applying SRS data, in which the former dealt with mapping and monitoring of urban sprawl of the Delhi urban agglomeration. They emphasized the potentialities of SRS data in such studies for effective and efficient urban planning. The study used Landsat MSS and Landsat TM images of 1975, 1981, 1985, and 1987, which were manually mapped and visually interpreted. The latter pointed out the usefulness of aerial photography in studying the urban fringe dynamics of Delhi, following a similar approach as adopted in the previous study. Pathan et al. (1989) analyzed the physical urban growth of the Bombay metropolitan region (BMR) for the period between 1968 and 1989, applying multi-temporal RS data and population growth. It also estimated the additional requirement of areas for further urban development in 2001 by identifying suitable land through land suitability analysis. The study found that particularly after 1975, a distinct outgrowth was associated along railway corridors toward the periphery. Another study by Pathan

et al. (1991) deployed SRS data, like MSS, TM, SPOT, and IRS LISS-II for urban sprawl mapping of Ahmedabad city applying both visual and digital analysis techniques. Taragi and Pundir (1997) mapped and analyzed the urban sprawl of Lucknow city with the application of SRS data, like IRS-1B, LISS-II, SPOT-HRV-I, Landsat MSS, and SOI toposheets. The study concluded about the potentiality of SRS data in the demarcation of urban spread and monitoring of urban growth at the spatiotemporal dimension. The studies discussed above are concerned with mere spatiotemporal change detection analysis of land covers along with built-up cover dynamics.

With the advancement of research, several studies aimed at quantification of spatiotemporal dynamics of different cities in India applying different techniques, frequently landscape metrics, and entropy approach. Lata et al. (2001) measured and analyzed the urban sprawl of Hyderabad, using an entropy approach integrated with RS and GIS. The authors concluded that the entropy approach is a good indicator for identifying spatial processes of land development, and the analysis can easily be implemented within a GIS framework to facilitate urban sprawl measurement. Sudhira et al. (2003) examined spatiotemporal urban growth and urban sprawl along the Bangalore–Mysore highway with a 4 km buffer using RS and GIS for over three decades (i.e., 1972–1998). They advocated for built-up cover as a good indicator for measuring urban sprawl. According to them, the use of RS and GIS, coupled with Shannon's entropy, could help immensely in a spatiotemporal analysis of urban growth. The study by Sudhira et al. (2004) was concerned with the identification, measurement, modeling, and prediction of urban sprawl over the same study area, as in Sudhira et al. (2003). The study used Shannon's entropy along with several other landscape metrics for analyzing urban sprawl. Furthermore, the study used stepwise multiple regression to model the future urban sprawl with some chosen causal factors, such as population growth, population density, and distance from the city center. However, the rationality behind the selection of sprawl metrics and explanatory variables for regression

modeling seems to be not evident in the study concerned. Moreover, several researchers argue that simple techniques like multiple regression cannot adequately capture the complexity of urban sprawl. Another study by Sudhira and Ramachandra (2007) was analytically similar to the kind of research performed by Sudhira et al. (2004). It also suffers from a similar type of shortcomings, as in Sudhira et al. (2004). Besides, Sudhira and Ramachandra (2009) addressed the issue of urban sprawl in the Indian context with a focus on Bangalore. They advocated for an integrated spatial planning support system (SPSS) with policy analysis to mitigate the challenges posed by the evils of urban sprawl. The study by Kumar et al. (2007) dealt with monitoring the spatiotemporal urban growth of Indore city using Shannon's entropy integrated with RS and GIS. The study concluded that the concentric zone approach is a useful one in identifying patterns of urban growth in different directions around a city. Jat et al. (2008) carried out another similar kind of research on monitoring and modeling the urban sprawl in Ajmer city over 25 years (1977–2005). As the study by Sudhira et al. (2004), employed landscape metrics to quantify the spatiotemporal pattern of sprawl and a step-wise regression to predict the future status of urban sprawl.

Several similar kinds of literature are also available in Indian context dealing with analysis and quantification of urban growth. Among them, Aligarh city (Farooq and Ahmad 2008), Hyderabad–Secunderabad or Hyderabad urban agglomeration (Rahaman et al. 2010; Wakode et al. 2014), Delhi megacity (Mohan et al. 2011; Chakraborty et al. 2021), Mumbai megacity (Sahana et al. 2019), Lucknow city (Dutta 2012), Jaipur city (Punia and Singh 2012), Ranchi (Pandey et al. 2013), Hawalbagh block in Almora district of Uttarakhand (Rawat & Kumar, 2015), Pune metropolis (Kantakumar et al. 2016), Chennai (Aithal and Ramachandra 2016), Dehradun city (Bhat et al. 2017), selected administrative units in Goa (Vaz et al. 2017), Dhanbad urban agglomeration (DUA) (Lal et al. 2017), Guwahati metropolitan area (GMA) (Pawe and Saikia 2018), and Kolkata megacity

(Sahana et al. 2018; Mithun 2020) are notable. They often employed landscape metrics and Shannon's entropy approach for characterizing urban growth. However, some other techniques are also in practice to extract and analyze built-up growth. Sharma and Joshi (2013) investigated the urban dynamics over the national capital region (NCR) of Delhi. They applied the normalized difference built-up index (NDBI) and urban landscape analysis tool (ULAT) to extract and analyze urban expansion.

Along with change detection, landscape metrics, and entropy measures, several studies applied different zoning approaches, and other techniques and approaches to quantify urban growth in India. The study by Ramachandra et al. (2012) aimed at quantifying the urban dynamics of Bangalore city by employing concentric zone and gradient analysis along with landscape metrics to understand the local-level change in extent and pattern of urban growth and sprawl. Moreover, a PCA was employed to prioritize the applied metrics. Ramachandra et al. (2015) quantified the urbanization and associated growth pattern in Delhi, in which the region was divided into four zones and circles of 1 km incrementing radius to understand and quantify the local spatial changes. Jain and Sharma (2019) have extracted the built-up areas in some selected small, medium, and large cities in India, employing a two-stage object-based nearest neighbor classification approach with hierarchical segmentation.

A few numbers of studies have attempted to model and predict urban growth in India. As discussed earlier, the studies by Sudhira et al. (2004) and Jat et al. (2008) employed step-wise regression to model and predict urban growth. Shafizadeh-Moghadam and Helbich (2013) conducted examined the urban growth of Mumbai, in which the Markov chain-cellular automata (MC-CA) urban growth model was implemented to predict the city's future expansion in 2020 and 2030. The MC-CA model was connected to a multi-criteria evaluation to generate transition probability maps considering the factors affecting urban growth (Malick et al., 2021). Chowdhury and Maithani (2014) implemented a CA model for simulating urban growth in the Indo-Gangetic plain using operational linescan system (OLS) data-derived maps. Munshi et al. (2014) aimed to the simulation of urban growth and urban development in Ahmedabad city, applying a hybrid simulation-based modeling approach combining LR and CA. LR was used to estimate a probability surface of development transition, while a CA-based spatial interaction model was employed to simulate urban growth. Deep and Saklani (2014) implemented a CA–Markov model to investigate urban dynamics in Dehradun city. Shafizadeh-Moghadama and Helbich (2015) employed a regression-based LULC change model, namely non-spatial LR and auto-LR models (ALR), for understanding urban LULC dynamics to determine the underlying driving forces behind the spatiotemporal urban expansion in Mumbai. Aithal and Ramachandra (2016) applied a CA model to predict the urban growth scenario in Chennai. Mishra and Rai (2016) attempted to appraise the ability of the MLP and Markov chain analysis (MLP-MCA) modeling approach to monitor and predict the future LULC change scenario in the Patna district of Bihar. Siddiqui et al. (2018) engaged an LR-based CA-Markov analysis to simulate urban growth in Dehradun, undertaking certain biophysical and proximity factors. Jat et al. (2017) evaluated the performance of the CA-based SLEUTH modeling approach to simulate the urban growth of Ajmer city. Devendran and Lakshmanan (2019) have studied the urban growth of Sriperumbudur Taluk in Tamil Nadu using three types of CA models, namely traditional CA (TCA), agents-based CA (ACA), and neural network coupled agent-based CA (NNACA) models. The AHP technique was adopted to estimate the weights of the agents for the preparation of the suitability map. The study found the NNACA model as a better-performed model as compared to the TCA and ACA models. Mondal et al. (2019) have simulated the urban growth of Udaipur city for 2021, applying three spatial modeling approaches, namely CA-Markov, multi-criteria cellular automata-Markov chain (MCCA-MC), multi-layer perceptron Markov chain (MLP-MC) and SLEUTH models. The study has pointed out that the three models are embodied with their own merits and demerits while serving specific purposes.

2.5 Findings and Conclusions

The findings based on the present review study are listed as follows,

- The bibliometric analysis finds that USA tops urban growth research followed by China, while India ranks 54th position.
- Over the last couple of decades, most of the studies on urban growth and modeling have been implemented with the application of the RS-GIS tool.
- Most of the studies conclude that RS-GIS is a very efficient and powerful tool for mapping, measuring, analyzing, monitoring, and modeling spatiotemporal urban growth dynamics.
- Open-source SRS data, such as Landsat TM, ETM+, and OLI, IRS LISS III, are extensively applied in urban growth studies. However, some commercial SRS data, like IKONOS LISS IV, Cartosat, etc. are also used for the purpose.
- Preprocessing of SRS data appears to be crucial, and the FLAASH atmospheric correction is one of the popularly applied methods for radiometric calibration and atmospheric correction of satellite images.
- The MLC algorithm is the most popularly applied classifier for classifying SRS data to extract land-cover classes. However, recently, some machine learning algorithms, like SVM, decision tree, and random forest classifiers, are increasingly been used.
- Urban sprawl is largely explored as a *pattern* and *process* of urban growth compared to *cause* and *consequence*, and the urban built-up cover is often employed as an efficient and straightforward parameter or indicator for quantifying urban sprawl and urban expansion.
- Parameters and indices for measuring urban growth and sprawl are large in number and diverse in nature. However, the entropy approach and landscape metrics are frequently used in quantifying urban growth and sprawl.
- Most of the studies relating to the spatiotemporal analysis of urban growth and sprawl intend to analyze at the level of administrative units, such as ward, borough, municipality, etc. and with gradient zoning, i.e., concentric circles of specific width from the urban center toward periphery.
- Modeling approaches, like MC, CA, SLEUTH, and LR, are frequently deployed modeling approaches often integrated with RS-GIS. Furthermore, very recently, some machine learning approaches (e.g., MLP) are reportedly used for this purpose. However, model parameterization and calibration remain challenging and critical.

References

Abd El-Kawy OR, Rød JK, Ismail HA, Suliman AS (2011) Land use and land cover change detection in the western Nile delta of Egypt using remote sensing data. Appl Geogr 31(2):483–494

Abiden MZZ, Abidin SZ, Jamaluddin MNF (2010) Pixel based urban growth model for predicting future pattern. In: 2010 6th international colloquium on signal processing & its applications, pp. 1–5. IEEE

Aburas MM, Ho YM, Ramli MF, Ash'aari ZH (2017) Improving the capability of an integrated CA-Markov model to simulate spatio-temporal urban growth trends using an analytical hierarchy process and frequency ratio. Int J Appl Earth Obs Geoinformation 59:65–78

Aguilera F, Valenzuela LM, Botequilha-Leitão A (2011) Landscape metrics in the analysis of urban land use patterns: a case study in a Spanish metropolitan area. Landscape Urban Plan 99(3–4):226–238

Ahmed B, Ahmed R (2012) Modeling urban land cover growth dynamics using multi-temporal satellite images: A case study of Dhaka, Bangladesh. ISPRS Int J Geo-Inf 1(1):3–31

Aithal BH, Ramachandra TV (2016) Visualization of urban growth pattern in Chennai using geoinformatics and spatial metrics. J Indian Soc Remote Sens 44 (4):617–633

Al-Ahmadi K, See L, Heppenstall A, Hogg J (2009) Calibration of a fuzzy cellular automata model of urban dynamics in Saudi Arabia. Ecol Complex 6 (2):80–101

Alberti M, Waddell P (2000) An integrated urban development and ecological simulation model. Integr Assess 1(3):215–227

Almeida CMD, Monteiro AMV, Câmara G, Soares-Filho BS, Cerqueira GC, Pennachin CL, Batty M (2005) GIS and remote sensing as tools for the simulation of urban land-use change. Int J Remote Sens 26(4):759–774

Almeida CD, Gleriani JM, Castejon EF, Soares-Filho BS (2008) Using neural networks and cellular automata for modelling intra-urban land-use dynamics. Int J Geogr Inf Sci 22(9):943–963

Al-Sharif AA, Pradhan B (2014) Urban sprawl analysis of Tripoli Metropolitan city (Libya) using remote sensing data and multivariate logistic regression model. J Indian Soc Remote Sens 42(1):149–163

Angel S, Sheppard S, Civco DL, Buckley R, Chabaeva A, Gitlin L., … Perlin M (2005) The dynamics of global urban expansion. Washington, DC: World Bank, Transport and Urban Development Department

Angel S, Parent J, Civco D (2007) Urban sprawl metrics: an analysis of global urban expansion using GIS. In: Proceedings of ASPRS 2007 annual conference, Tampa, Florida May 7–11

Araya YH, Cabral P (2010) Analysis and modeling of urban land cover change in Setúbal and Sesimbra Portugal. Remote Sens 2(6):1549–1563

Arsanjani JJ, Helbich M, de Noronha Vaz E (2013) Spatiotemporal simulation of urban growth patterns using agent-based modeling: the case of Tehran. Cities 32:33–42

Attua EM, Fisher JB (2011) Historical and future land-cover change in a municipality of Ghana. Earth Interact 15(9):1–26

Bagheri B, Tousi SN (2018) An explanation of urban sprawl phenomenon in Shiraz Metropolitan Area (SMA). Cities 73:71–90

Barnes KB, Morgan III, JM, Roberge MC, Lowe S (2001) Sprawl development: Its patterns, consequences, and measurement. Retrieved from Towson University, Towson, pp 1–24

Barredo JI, Kasanko M, McCormick N, Lavalle C (2003) Modelling dynamic spatial processes: simulation of urban future scenarios through cellular automata. Landsc Urban Plan 64(3):145–160

Batty M (1979) Progress, success, and failure in urban modelling. Environ Plan A 11(8):863–878

Batty M, Howes D (2001) Predicting temporal patterns in urban development from remote imagery

Batty M, Longley PA (1994) Fractal cities: a geometry of form and function. Academic press

Batty M, Xie Y (1994a) From cells to cities. Environ Plann B: Plann Des 21(Celebration Issue):531–548

Batty M, Xie Y (1994b) Modelling inside GIS: Part 2. Selecting and calibrating urban models using ARC-INFO. Int J Geogr Inf Syst 8(5):451–470

Batty M, Xie Y (1994c) From cells to cities. Environ Plann B: Plann Des 21(7):S31–S48

Batty M, Xie Y (1997) Possible urban automata. Environ Plann B: Plann Des 24(2):175–192

Batty M, Besussi E, Chin N (2003) Traffic, urban growth and suburban sprawl. CASA Working Papers. London: Centre for Advanced Spatial Analysis (UCL)

Batty M, Xie Y, Sun Z (1999) Modeling urban dynamics through GIS-based cellular automata. Comput Environ Urban Syst 23(3):205–233

Belal AA, Moghanm FS (2011) Detecting urban growth using remote sensing and GIS techniques in Al

Gharbiya governorate Egypt. Egypt J Remote Sens Space Sci 14(2):73–79

Benfield EK, Raimi M, Chen D (1999) Once there were greenfields: how urban sprawl is undermining America's environment, economy and social fabric. Natural Resources Defense Council, Washington, DC

Berling-Wolff S, Wu J (2004) Modeling urban landscape dynamics: a case study in Phoenix, USA. Urban Ecosyst 7(3):215–240

Besussi E, Chin N, Batty M, Longley P (2010) The structure and form of urban settlements. In: Remote sensing of urban and suburban areas. Springer, Dordrecht, pp 13–31

Bhat PA, Shafiq Mul, Mir AA, Ahmed P (2017) Urban sprawl and its impact on landuse/land cover dynamics of Dehradun City, India. Int J Sustain Built Environ 6 (2):513–521

Bhatta B (2009) Analysis of urban growth pattern using remote sensing and GIS: a case study of Kolkata, India. Int J Remote Sens 30(18):4733–4746

Bhatta B (2013) Research methods in remote sensing. Springer

Bhatta B, Saraswati S, Bandyopadhyay D (2010a) Quantifying the degree-of-freedom, degree-of-sprawl, and degree-of-goodness of urban growth from remote sensing data. Appl Geogr 30(1):96–111

Bhatta B, Saraswati S, Bandyopadhyay D (2010b) Urban sprawl measurement from remote sensing data. Appl Geogr 30(4):731–740

Bhatta B (2012) Urban growth analysis and remote sensing: a case study of Kolkata, India 1980–2010. Springer Science & Business Media

Black D, Henderson V (2003) Urban evolution in the USA. J Econ Geogr 3(4):343–372

Cabral P, Zamyatin A (2009) Markov processes in modeling land use and land cover changes in Sintra-Cascais, Portugal. Dyna 76(158):191–198

Cabral P, Santos JA, Augusto G (2011) Monitoring urban sprawl and the national ecological reserve in Sintra-Cascais, Portugal: Multiple OLS linear regression model evaluation. J Urban Plann Develop 137(3):346–353

Cabral P, Augusto G, Tewolde M, Araya Y (2013) Entropy in urban systems. Entropy 15 (12):5223–5236

Cabral P, Gilg JP, Painho M (2005) Monitoring urban growth using remote sensing, GIS, and spatial metrics. In: Remote sensing and modeling of ecosystems for sustainability II, vol 5884, p 588404. International Society for Optics and Photonics

Cabral P, Geroyannis H, Gilg JP, Painho M (2006) Analysis and modeling of land-use and land-cover change in Sintra-Cascais area. In: The 8th AGILE international conference on geographic information science, AGILE 2005

Chakraborty S, Pramanik S, Follmann A, Giri B, Mondal B, Patel PP, Sahana M (2021) Dominant urban form and its relation to nighttime land surface temperature in the rapidly urbanizing National Capital Region of India. Urban Clim 40, 101002

Cheng J (2003) Modelling spatial & temporal urban growth. Retrieved from https://webapps.itc.utwente.nl/librarywww/Papers_2003/phd_theses/cheng_jianquan.pdf

Chowdhury PKR, Maithani S (2014) Modelling urban growth in the Indo-Gangetic plain using nighttime OLS data and cellular automata. Int J Appl Earth Obs Geoinf 33(1):155–165

Clarke KC, Gaydos LJ (1998) Loose-coupling a cellular automaton model and GIS: Long-term urban growth prediction for San Francisco and Washington/Baltimore. Int J Geogr Inf Sci 12(7):699–714

Clarke KC, Hoppen S, Gaydos L (1997) A self-modifying cellular automaton model of historical urbanization in the San Francisco bay area. Environ Plann B: Plann Des 24:247–261

Clarke KC, Parks BO, Crane MP (2002) Geographic information systems and environmental modeling. Prentice Hall, New Jersey

Clarke KC (2008) Mapping and modelling land use change: an application of the SLEUTH model. In: Landscape analysis and visualisation. Springer, Berlin, Heidelberg, pp 353–366

Clarke KC (2018) A Short Presentation of SLEUTH. In: Geomatic approaches for modeling land change scenarios. Springer, Cham, pp 521–525

Cohen J (1960) A coefficient of agreement for nominal scales. Educ Psychol Measur 20(1):37–46

Congalton RG (1988) A comparison of sampling schemes used in generating error matrices for assessing the accuracy of maps generated from remotely sensed data. Photogramm Eng Remote Sens 54(5):593–600

Congalton RG (1991) A review of assessing the accuracy of classifications of remotely sensed data. Remote Sens Environ 37(1):35–46

Congalton RG (2001) Accuracy assessment and validation of remotely sensed and other spatial information. Int J Wildland Fire 10(4):321–328

Congalton RG, Green K (1993) Practical look at the sources of confusion in error matrix generation. Photogramm Eng Remote Sens 59(5):641–644

Congalton RG, Green K (2019) Assessing the accuracy of remotely sensed data: principles and practices, 3rd edn. CRC Press. Taylor & Francis, Boca Ratón

Congalton RG, Mead RA (1983) A quantitative method to test for consistency and correctness in photointerpretation. Photogramm Eng Remote Sens 49(1):69–74

Congalton RG (1994) Accuracy assessment of remotely sensed data: Future needs and directions. In: Proceedings of Pecora, vol 12, pp 383–388

Cooley T, Anderson GP, Felde GW, Hoke ML, Ratkowski AJ, Chetwynd JH, … Bernstein LS (2002) FLAASH, a MODTRAN4-based atmospheric correction algorithm, its application and validation. In: IEEE international geoscience and remote sensing symposium, vol 3. IEEE, pp 1414–1418

Cracknell AP (1998) Review article synergy in remote sensing-what's in a pixel? Int J Remote Sens 19(11):2025–2047

Cushman SA, McGarigal K, Neel MC (2008) Parsimony in landscape metrics: Strength, universality, and consistency. Ecol Ind 8(5):691–703

Deep S, Saklani A (2014) Urban sprawl modeling using cellular automata. Egypt J Remote Sens Space Sci 17(2):179–187

Devendran AA, Lakshmanan G (2019) Analysis and prediction of urban growth using neural-network-coupled agent-based cellular automata model for Chennai metropolitan area, Tamil Nadu, India. J Indian Soc Remote Sens 47(9):1515–1526

Dhali MK, Chakraborty M, Sahana M (2019) Assessing spatio-temporal growth of urban sub-centre using Shannon's entropy model and principle component analysis: A case from North 24 Parganas, lower Ganga River Basin, India. The Egypt J Remote Sens Space Sci, 22(1):25–35.

Dutta V (2012) Land use dynamics and peri-urban growth characteristics: reflections on master plan and urban suitability from a sprawling north Indian city. Environ Urban Asia 3(2):277–301

Duwal S (2013) Modeling urban growth in Kathmandu Valley. Retrieved from http://www.itc.nl/library/papers_2013/msc/upm/duwal.pdf

Eastman JR (2015) TerrSet: geospatial monitoring and modeling system. Clark University, Worcester, MA, USA

Eastman JR, Van Fossen ME, Solarzano LA (2005) Transition potential modeling for land cover change. In: Maguire DJ, Goodchild MF, Batty M (eds) GIS. ESRI Press, Spatial analysis and modeling, pp 357–386

Eastman JR, Toledano J (2018) A short presentation of CA_MARKOV. In Geomatic approaches for modeling land change scenarios. Springer, Cham, pp 481–484

ESRI (2017) ArcGIS Desktop Release 10.6. Environmental Systems Research Institute, Redlands, CA, USA

Estoque RC, Murayama Y, Akiyama CM (2015) Pixel-based and object-based classifications using high- and medium-spatial-resolution imageries in the urban and suburban landscapes. Geocarto Int 30(10):1113–1129

Ewing RH (1997) Is Los Angeles-style sprawl desirable? J Am Plann Assoc 63(1):107–126

Ewing RH, Pendall R, Chen DD (2002) Measuring sprawl and its impact. Smart Growth America, Washington, DC

Exelis VIS (2015) ENVI 5.3. Exelis VIS: Boulder, CO, USA

Fang S, Gertner GZ, Sun Z, Anderson AA (2005) The impact of interactions in spatial simulation of the dynamics of urban sprawl. Landsc Urban Plan 73:294–306

Farooq S, Ahmad S (2008) Urban sprawl development around Aligarh city: A study aided by satellite remote sensing and GIS. J Indian Soc Remote Sens 36(1):77–88

Felde GW, Anderson GP, Cooley TW, Matthew MW, Berk A, Lee J (2003) Analysis of Hyperion data with

the FLAASH atmospheric correction algorithm. In: Proceedings of IEEE international geoscience and remote sensing symposium. (IEEE Cat. No. 03CH37477), vol 1. IEEE, pp 90–92

Feng L (2009) Applying remote sensing and GIS on monitoring and measuring urban sprawl. A case study of China. Revista Internacional Sostenibilidad, Tecnología y Humanismo 4:47–56

Feng YJ, Liu Y, Tong XH, Liu ML, Deng S (2011) Modeling dynamic urban growth using cellular automata and particle swarm optimization rules. Landsc Urban Plan 102:188–196

Fisher P (1997) The pixel: a snare and a delusion. Int J Remote Sens 18(3):679–685

Fitzpatrick-Lins K (1981) Comparison of sampling procedures and data analysis for a land-use and land-cover map. Photogramm Eng Remote Sens 47(3):343–351

Foody GM (2002) Status of land cover classification accuracy assessment. Remote Sens Environ 80 (1):185–201

Foody GM, Cox DP (1994) Sub-pixel land cover composition estimation using a linear mixture model and fuzzy membership functions. Int J Remote Sens 15(3):619–631

Forman RTT (1995) Land mosaics: the ecology of landscapes and regions. Cambridge University Press

Frenkel A, Ashkenazi M (2008) Measuring urban sprawl: how can we deal with it? Environ Plann B Plann Des 35(1):56–79

Fulton WB, Pendall R, Nguyễn, M., & Harrison, A. (2001) Who sprawls most? How growth patterns differ across the US. Brookings Institution, Center on Urban and Metropolitan Policy, Washington, DC

Galster G, Hanson R, Ratcliffe MR, Wolman H, Coleman S, Freihage J (2001) Wrestling sprawl to the ground: defining and measuring an elusive concept. Hous Policy Debate 12(4):681–717

Geoghegan J, Wainger LA, Bockstael NE (1997) Spatial landscape indices in a hedonic framework: an ecological economics analysis using GIS. Ecol Econ 23 (3):251–264

Ginevan ME (1979) Testing land-use map accuracy: another look. Photogramm Eng Remote Sens 45 (10):1371–1377

Gong JZ, Liu YS, Xia BC, Zhao GW (2009) Urban ecological security assessment and forecasting, based on a cellular automata model: a case study of Guangzhou China. Ecol Modell 220(24):3612–3620

Gordon P, Richardson HW (1997) Are compact cities a desirable planning goal? J Am Plann Assoc 63(1):95–106

Grimm NB, Faeth SH, Golubiewski NE, Redman CL, Wu J, Bai X, Briggs JM (2008) Global change and the ecology of cities. Science 319(5864):756–760

Guan D, Li H, Inohae T, Su W, Nagaie T, Hokao K (2011) Modeling urban land use change by the integration of cellular automaton and Markov model. Ecol Model 222(20–22):3761–3772

Gustafson EJ (1998) Quantifying landscape spatial pattern: what is the state of the art? Ecosystems 1(2):143–156

Haase D, Haase A, Kabisch N, Kabisch S, Rink D (2012) Actors and factors in land-use simulation: the challenge of urban shrinkage. Environ Model Softw 35:92–103

Hall P, Tewdwr-Jones M (2010) Urban and regional planning. Routledge

Hardin PJ, Jackson MW, Otterstrom SM (2007) Mapping, measuring, and modeling urban growth. In: Geo-Spatial technologies in urban environments. Springer, pp 165–166

Haregeweyn N, Fikadu G, Tsunekawa A, Tsubo M, Meshesha DT (2012) The dynamics of urban expansion and its impacts on land use/land cover change and small-scale farmers living near the urban fringe: a case study of Bahir Dar Ethiopia. Landsc Urban Plann 106 (2):149–157

Hargis CD, Bissonette JA, David JL (1998) The behavior of landscape metrics commonly used in the study of habitat fragmentation. Landscape Ecol 13(3):167–186

Harvey RO, Clark WA (1965) The nature and economics of urban sprawl. Land Econ 41(1):1–9

He C, Okada N, Zhang Q, Shi P, Li J (2008) Modelling dynamic urban expansion processes incorporating a potential model with cellular automata. Landsc Urban Plan 86(1):79–91

He J, Liu Y, Yu Y, Tang W, Xiang W, Liu D (2013) A counterfactual scenario simulation approach for assessing the impact of farmland preservation policies on urban sprawl and food security in a major grain-producing area of China. Appl Geogr 37:127–138

Heimlich RE, Anderson WD (2001) Development at the urban fringe and beyond: impacts on agriculture and rural land. In: Agricultural economic report no. 803, (803), pp 1–88

Herold M, Scepan J, Clarke KC (2002) The use of remote sensing and landscape metrics to describe structures and changes in urban land uses. Environ Plan A 34 (8):1443–1458

Herold M, Goldstein NC, Clarke KC (2003) The spatiotemporal form of urban growth: measurement, analysis and modeling. Remote Sens Environ 86 (3):286–302

Herold M, Couclelis H, Clarke KC (2005) The role of spatial metrics in the analysis and modeling of urban land use change. Comput Environ Urban Syst 29 (4):369–399

Hord RM, Brooner W (1976) Land-use map accuracy criteria. Photogramm Eng Remote Sens 42(5):671–677

Hu Z, Lo CP (2007) Modeling urban growth in Atlanta using logistic regression. Comput Environ Urban Syst 31(6):667–688

Hu X, Weng Q (2009) Estimating impervious surfaces from medium spatial resolution imagery using the self-organizing map and multi-layer perceptron neural networks. Remote Sens Environ 113(10):2089–2102

Huang J, Lu XX, Sellers JM (2007) A global comparative analysis of urban form: Applying spatial metrics and remote sensing. Landsc Urban Plan 82(4):184–197

Hudson WD, Ramm CW (1987) Correct formulation of the Kappa coefficient of agreement. Photogramm Eng Remote Sens 53(4):421–422

Ibrahim Mahmoud M, Duker A, Conrad C, Thiel M, Shaba Ahmad H (2016) Analysis of settlement expansion and urban growth modelling using geoinformation for assessing potential impacts of urbanization on climate in Abuja City Nigeria. Remote Sensing 8(3):220

Islam K, Jashimuddin M, Nath B, Nath TK (2018) Land use classification and change detection by using multi-temporal remotely sensed imagery: the case of Chunati wildlife sanctuary, Bangladesh. Egypt J Remote Sens Space Sci 21(1):37–47

Jaeger JaGG, Bertiller R, Schwick C, Kienast F (2010a) Suitability criteria for measures of urban sprawl. Ecol Indic 10(2):397–406

Jaeger JAG, Schwick C (2014) Improving the measurement of urban sprawl: weighted urban proliferation (WUP) and its application to Switzerland. Ecol Ind 38:294–308

Jaeger JA, Bertiller R, Schwick C, Cavens D, Kienast F (2010b) Urban permeation of landscapes and sprawl per capita: new measures of urban sprawl. Ecol Indic 10(2):427–441

Jain GV, Sharma SA (2019) Spatio-temporal analysis of urban growth in selected small, medium and large Indian cities. Geocarto Int 34(8):887–908

Jat MK, Garg PK, Khare D (2008) Modelling of urban growth using spatial analysis techniques: a case study of Ajmer city (India). Int J Remote Sens 29(2):543–567

Jat MK, Choudhary M, Saxena A (2017) Urban growth assessment and prediction using RS, GIS and SLEUTH model for a heterogeneous urban fringe. Egypt J Remote Sens Space Sci 10(3):1–19

Jensen JR (1996) Introductory digital image processing. Prentice Hall, Englewood Cliffs, NJ

Jensen JR, Cowen DC (1999) Remote sensing of urban/suburban infrastructure and socio-economic attributes. Photogramm Eng Remote Sens 65:611–622

Jiang F, Liu S, Yuan H, Zhang Q (2007) Measuring urban sprawl in Beijing with geo-spatial indices. J Geog Sci 17(4):469–478

Jjumba A, Dragićević S (2012) High resolution urban land-use change modeling: Agent iCity approach. Appl Spat Anal Policy 5(4):291–315

Johnson MP (2001) Environmental impacts of urban sprawl: a survey of the literature and proposed research agenda. Environ Plan A 33(4):717–735

Kantakumar LN, Kumar S, Schneider K (2016) Spatiotemporal urban expansion in Pune metropolis, India using remote sensing. Habitat Int 51:11–22

Kivell P (1993) Land and the city: patterns and processes of urban change. Routledge and Kegan Paul, London

Knox PL (1993) The restless urban landscape. Prentice Hall, Englewood Cliffs, NJ

Kong F, Yin H, Nakagoshi N, James P (2012) Simulating urban growth processes incorporating a potential model with spatial metrics. Ecol Ind 20:82–91

Kruse Fa (2004) Comparison of ATREM, ACORN, and FLAASH Atmospheric Corrections Using Low-Altitude AVIRIS Data of Boulder, CO. In: 13th JPL airborne geoscience workshop, (May), pp 1–10

Kumar JAV, Pathan SK, Bhanderi RJ (2007) Spatio-temporal analysis for monitoring urban growth–a case study of Indore city. J Indian Soc Remote Sens 35 (1):11–20

Lal K, Kumar D, Kumar A (2017) Spatio-temporal landscape modeling of urban growth patterns in Dhanbad Urban Agglomeration, India using geoinformatics techniques. Egypt J Remote Sens Space Sci 20 (1):91–102

Lambin EF (2004) Modelling land-use change. In: Wainwright J, Mulligan M (eds) Environmental modeling: finding simplicity in complexity. Wiley, Chichester, UK, pp 245–254

Landis JD (1995) Imagining land use futures: applying the California urban futures model. J Am Plann Assoc 61(4):438–457

Landis JR, Koch GG (1977) An application of hierarchical Kappa-type statistics in the assessment of majority agreement among multiple observers. Biometrics, 363–374

Lata KM, Rao CS, Prasad VK, Badarianth KVS, Rahgavasamy V (2001) Measuring urban sprawl: a case study of Hyderabad. GIS Development 5(12):26–29

Latifovic R, Pouliot D, Olthof I (2017) Circa 2010 land cover of Canada: local optimization methodology and product development. Remote Sens 9(11):1098

Li X, Yeh AGO (2000) Modelling sustainable urban development by the integration of constrained cellular automata and GIS. Int J Geogr Inf Sci 14(2):131–152

Li X, Yeh AGO (2004) Analyzing spatial restructuring of land use patterns in a fast growing region using remote sensing and GIS. Landscape Urban Plan 69(4):335–354

Li X, He HS, Bu R, Wen Q, Chang Y, Hu Y, Li Y (2005) The adequacy of different landscape metrics for various landscape patterns. Pattern Recogn 38 (12):2626–2638

Li X, Meng Q, Gu X, Jancso T, Yu T, Wang K, Mavromatis S (2013) A hybrid method combining pixel-based and object-oriented methods and its application in Hungary using Chinese HJ-1 satellite images. Int J Remote Sens 34(13):4655–4668

Li M, Zang S, Zhang B, Li S, Wu C (2014) A review of remote sensing image classification techniques: The role of spatio-contextual information. Eur J Remote Sens 47(1):389–411

Lillesand T, Kiefer RW, Chipman J (2015) Remote sensing and image interpretation. Wiley

Lin YP, Chu HJ, Wu CF, Verburg PH (2011) Predictive ability of logistic regression, auto-logistic regression and neural network models in empirical land-use change modeling–a case study. Int J Geogr Inf Sci 25 (1):65–87

Lin J, Huang B, Chen M, Huang Z (2014) Modeling urban vertical growth using cellular automata—Guangzhou as a case study. Appl Geogr 53:172–186

Liu Y (2008) Modelling urban development with geographical information systems and cellular automata. CRC Press, New York

Liu Y (2012) Modelling sustainable urban growth in a rapidly urbanising region using a fuzzy-constrained cellular automata approach. Int J Geogr Inf Sci 26 (1):151–167

Liu Y, Phinn SR (2003) Modelling urban development with cellular automata incorporating fuzzy-set approaches. Comput Environ Urban Syst 27(6):637–658

Liu Y, Feng Y (2012) A logistic based cellular automata model for continuous urban growth simulation: a case study of the Gold Coast City, Australia. In: Agent-based Models of Geographical Systems. Springer, Dordrecht, pp 643–662

Longley PA, Mesev V (2000) On the measurement and generalisation of urban form. Environ Plan A 32 (3):473–488

Lü Y, Feng X, Chen L, Fu B (2013) Scaling effects of landscape metrics: a comparison of two methods. Phys Geogr 34(1):40–49

Lu D, Weng Q (2006) Use of impervious surface in urban land-use classification. Remote Sens Environ 102(1–2):146–160

Lu D, Weng Q (2007) A survey of image classification methods and techniques for improving classification performance. Int J Remote Sens 28(5):823–870

Maithani S (2009) A neural network based urban growth model of an Indian city. J Indian Soc Remote Sens 37 (3):363–376

Maktav D, Erbek FS (2005) Analysis of urban growth using multi-temporal satellite data in Istanbul Turkey. Int J Remote Sens 26(4):797–810

Mallick SK, Das P, Maity B, Rudra S, Pramanik M, Pradhan B, Sahana M (2021) Understanding future urban growth, urban resilience and sustainable development of small cities using prediction-adaptation-resilience (PAR) approach. Sustain Cities Soc 74, 103196.

McGarigal K, Cushman SA, Neel MC, Ene E (2002) Spatial pattern analysis program for categorical maps. Computer software program produced by the authors at the University of Massachusetts, Amherst.–2002. Available at the following web site: http://www. umass.edu/landeco/research/fragstats/fragstats.html

McGarigal K, Marks BJ (1994) FRAGSTATS–Spatial pattern analysis program for quantifying landscape structure. Oregon State University, Forest Science Department, Portland, OR

Meaille R, Wald L (1990) Using geographical information systems and satellite imagery within a numerical simulation of regional urban growth. Int J Geogr Inf Syst 4:445–456

Megahed Y, Cabral P, Silva J, Caetano M (2015) Land cover mapping analysis and urban growth modelling using remote sensing techniques in greater Cairo region-Egypt. ISPRS Int J Geo Inf 4(3):1750–1769

Mishra VN, Rai PK (2016) A remote sensing aided multi-layer perceptron-Markov chain analysis for land use and land cover change prediction in Patna district (Bihar), India. Arab J Geosci 9(4)

Mithun S, Chattopadhyay S, Bhatta B (2016) Analyzing urban dynamics of metropolitan Kolkata, India by using landscape metrics. Pap Appl Geogr 2(3):284–297

Mithun S (2020) Quantifying and modeling metropolitan growth dynamics: a case study on Kolkata Metropolitan Area (Doctoral dissertation, IIT Kharagpur)

Mithun S, Sahana M, Chattopadhyay S, Johnson BA, Khedher KM, Avtar R (2021) Monitoring metropolitan growth dynamics for achieving sustainable urbanization (SDG 11.3) in Kolkata Metropolitan Area, India. Remote Sens 13(21):4423

Mithun Sk, Sahana M, Chattopadhyay S, Chatterjee S, Islam J, Costache R (2022) Comparative framework for spatially explicit urban growth modeling for monitoring urban land-use efficiency and sustainable urban development (SDG 11.3.1): a study on Kolkata metropolitan area India. Geocarto Int 1–38. https://doi.org/10.1080/10106049.2022.2136259

Mitra C, Marshall Shepherd J, Jordan TR (2012) Assessment and dynamics of urban growth in the City of Kolkata. In: Facets of social geography: facets of social geography international and Indian perspectives, pp 541–555

Mitsova D, Shuster W, Wang X (2011) A cellular automata model of land cover change to integrate urban growth with open space conservation. Landsc Urban Plan 99(2):141–153

Mohan M, Pathan SK, Narendrareddy K, Kandya A, Pandey S (2011) Dynamics of urbanization and its impact on land-use/land-cover: a case study of megacity Delhi. J Environ Prot 2(09):1274

Mondal B, Das DN, Dolui G (2015) Modeling spatial variation of explanatory factors of urban expansion of Kolkata: a geographically weighted regression approach. Model Earth Syst Environ 1(4):29

Mondal B, Das DN, Bhatta B (2017) Integrating cellular automata and Markov techniques to generate urban development potential surface: a study on Kolkata agglomeration. Geocarto Int 32(4):401–419

Mondal B, Chakraborti S, Das DN, Joshi PK, Maity S, Pramanik MK, Chatterjee S (2019) Comparison of spatial modelling approaches to simulate urban growth: a case study on Udaipur city, India. Geocarto Int:1–23

Mountrakis G, Im J, Ogole C (2011) Support vector machines in remote sensing: a review. ISPRS J Photogramm Remote Sens 66(3):247–259

Munshi T, Zuidgeest M, Brussel M, van Maarseveen M (2014) Logistic regression and cellular automata-based modelling of retail, commercial and residential development in the city of Ahmedabad, India. Cities 39:68–86

Nazeer M, Nichol JE, Yung YK (2014) Evaluation of atmospheric correction models and Landsat surface reflectance product in an urban coastal environment. Int J Remote Sens 35(16):6271–6291

Nelson AC (1999) Comparing states with and without growth management analysis based on indicators with policy implications. Land Use Policy 16(2):121–127

Nong Y, Du Q (2011) Urban growth pattern modeling using logistic regression. Geo-Spatial Inf Sci 14(1):62–67

Oluseyi OF (2006) Urban land use change analysis of a traditional city from remote sensing data: The case built-up area assessment of Ranchi Township using Cartosat-I stereopairs satellite images of Ibadan metropolitan area Nigeria. Humanity Soc Sci J 1(1):42–64

O'Neill RV, Krummel JR, Gardner REA, Sugihara G, Jackson B, De Angelis DL, ... Dale VH (1988) Indices of landscape pattern. Landscape Ecol 1(3):153–162

Pandey AC, Kumar A, Jeyaseelan AT (2013) Urban. J Indian Soc Remote Sens 41(1):141–155

Park S, Jeon S, Choi C (2012) Mapping urban growth probability in South Korea: comparison of frequency ratio, analytic hierarchy process, and logistic regression models and use of the environmental conservation value assessment. Landsc Ecol Eng 8(1):17–31

Parker DC, Evans T, Meretsky V (2001) Measuring emergent properties of agent-based landcover/landuse models using spatial metrics. In: Proceedings of 7th annual conference of the international society for computational economics. http://php.indiana.edu/dawparke/parker.pdf.

Pathan SK, Jothimahi P, Kumar DS, Pendharkar SP (1989) Urban land use mapping and zoning of Bombay metropolitan region using remote sensing data. J Indian Soc Remote Sens 17(3):11–22

Pathan SK, Shukla VK, Patel RG, Patel BR, Mehta KS (1991) Urban land use mapping: a case study of Ahmedabad city and its environs. J Indian Soc Remote Sens 19(2):95–112

Pawe CK, Saikia A (2018) Unplanned urban growth: land use/land cover change in the Guwahati Metropolitan Area, India. Geografisk Tidsskrift - Danish J Geo 118(1):88–100

Pendall R (1999) Do land-use controls cause sprawl? Environ Plann B 26(4):555–571

Peng J, Wang Y, Zhang Y, Wu J, Li W, Li Y (2010) Evaluating the effectiveness of landscape metrics in quantifying spatial patterns. Ecol Ind 10(2):217–223

Perkins T, Adler-Golden SM, Matthew MW, Berk A, Bernstein LS, Lee J, Fox M (2012) Speed and accuracy improvements in FLAASH atmospheric correction of hyperspectral imagery. Opt Eng 51(11):111–707

Perkins T, Adler-Golden S, Matthew M, Berk A, Anderson G, Gardner J, Felde G (2005) Retrieval of atmospheric properties from hyper and multispectral imagery with the FLAASH atmospheric correction algorithm. In: Remote sensing of clouds and the atmosphere X, vol 5979, pp 59790E

Pijanowski BC, Brown DG, Shellito BA, Manik GA (2002) Using neural networks and GIS to forecast land use changes: a land transformation model. Comput Environ Urban Syst 26(6):553–575

Pijanowski BC, Pithadia S, Shellito BA, Alexandridis K (2005) Calibrating a neural network-based urban change model for two metropolitan areas of the Upper Midwest of the United States. Int J Geogr Inf Sci 19(2):197–215

Pijanowski BC, Long DT, Gage SH, Cooper WE (1997) A land transformation model: conceptual elements, spatial object class hierarchies, GIS command syntax and an application for Michigan's Saginaw Bay Watershed. NCGIA at http://www.ncgia.ucsb.edu/conf/landuse97/papers/pijanowski_bryan/paper.html.Pond

Platt RV, Rapoza L (2008) An evaluation of an object-oriented paradigm for land use/land cover classification. Prof Geogr 60(1):87–100

Pontius RG (2000) Quantification error versus location error in comparison of categorical maps. Photogramm Eng Remote Sens 66(8):1011–1016

Punia M, Singh L (2012) Entropy approach for assessment of urban growth: a case study of Jaipur, India. J Indian Soc Remote Sens 40(2):231–244

Rahaman M, Dutta S, Sahana M, Das DN (2019) Analysing urban sprawl and spatial expansion of Kolkata urban agglomeration using geospatial approach. In Appl challenges of geospatial tech (pp. 205–221). Springer, Cham

Rahman A, Aggarwal SP, Netzband M, Fazal S (2011) Monitoring urban sprawl using remote sensing and GIS techniques of a fast growing urban centre, India. IEEE J Sel Top Appl Earth Observations Remote Sens 4(1):56–64

Ramachandra TV, Aithal BH, Sanna DD (2012) Insights to urban dynamics through landscape spatial pattern analysis. Int J Appl Earth Obs Geoinf 18:329–343

Ramachandra TV, Bharath AH, Sowmyashree MV (2015) Monitoring urbanization and its implications in a mega city from space: Spatiotemporal patterns and its indicators. J Environ Manage 148:67–81

Rawat JS, Kumar M (2015) Monitoring land use/cover change using remote sensing and GIS techniques: A case study of Hawalbagh block, district Almora, Uttarakhand, India. Egypt J Remote Sens Space Sci 18(1):77–84

Redman CL, Jones NS (2005) The environmental, social, and health dimensions of urban expansion. Popul Environ 26(6):505–520

Rhode WG (1978) Digital image analysis techniques required for natural resource inventories. In: Proceedings of national computer conference, IEEE, pp 43–106

Richards JA (2013) Remote sensing digital image analysis: an introduction, 5th edn. Springer, New York

Rimal B, Zhang L, Keshtkar H, Haack B, Rijal S, Zhang P (2018) Land use/land cover dynamics and modeling of urban land expansion by the integration

of cellular automata and Markov chain. ISPRS Int J Geo Inf 7(4):154

Ritters KH, O'neill RV, Hunsaker CT, Wickham JD, Yankee DH, Timmins SP, Jackson BL (1995) A factor analysis of landscape pattern and structure metrics. Landsc Ecol 10(1):23–39

Roca J, Burns MC, Carreras JM (2004) Monitoring urban sprawl around Barcelona's metropolitan area with the aid of satellite imagery. In: XXth ISPRS congress. Istanbul, Turkey, pp 12–23

Rosenfield GH, Fitzpatrick-Lins K (1986) A coefficient of agreement as a measure of thematic classification accuracy. Photogramm Eng Remote Sens 52(2):223–227

Sahana M, Hong H, Sajjad H (2018) Analyzing urban spatial patterns and trend of urban growth using urban sprawl matrix: a study on Kolkata urban agglomeration, India. Sci Total Environ 628–629:1557–1566

Sahana M, Dutta S, Sajjad H (2019) Assessing land transformation and its relation with land surface temperature in Mumbai city, India using geospatial techniques. Inter J Urban Sci 23(2):205–225

Sang L, Zhang C, Yang J, Zhu D, Yun W (2011) Simulation of land use spatial pattern of towns and villages based on CA–Markov model. Math Comput Model 54(3–4):938–943

Schneider A (2012) Monitoring land cover change in urban and peri-urban areas using dense time stacks of Landsat satellite data and a data mining approach. Remote Sens Environ 124:689–704

Schneider A, Woodcock CE (2008) Compact, dispersed, fragmented, extensive? A comparison of urban growth in twenty-five global cities using remotely sensed data, pattern metrics and census information. Urban Stud 45(3):659–692

Shafizadeh-Moghadam H, Helbich M (2013) Spatiotemporal urbanization processes in the megacity of Mumbai, India: a Markov chains-cellular automata urban growth model. Appl Geogr 40:140–149

Shafizadeh-Moghadam H, Helbich M (2015) Spatiotemporal variability of urban growth factors: A global and local perspective on the megacity of Mumbai. Int J Appl Earth Obs Geoinf 35:187–198

Shaw A (2005) Peri-Urban Interface of Indian Cities. Econ Polit Weekly:129–136

Siddiqui A, Maithani S, Jha AK, Kumar P, Srivastav SK (2018) Urban growth dynamics of an Indian metropolitan using CA-Markov and Logistic Regression. Egypt J Remote Sens Space Sci 21(3):229–236

Singh A (1989) Review article digital change detection techniques using remotely-sensed data. Int J Remote Sens 10(6):989–1003

Smith DM (1975) Patterns in human geography. David & Charles, Newton Abbot

Sokhi BS, Sharma ND, Uttarwar PS (1989) Satellite remote sensing in urban sprawl mapping & monitoring: A case study of Delhi. J Indian Soc Remote Sens 17(3):57–69

Stanilov K, Batty M (2011) Exploring the historical determinants of urban growth patterns through cellular automata. Trans GIS 15(3):253–271

Story M, Congalton RG (1986) Accuracy assessment: a user's perspective. Photogramm Eng Remote Sens 52(3):397–399

Sudhira HS, Ramachandra TV (2009) Planning support systems best practice and new methods. In: Geertman S, Stillwell J (eds) Planning support systems best practice and new methods. Springer, Dordrecht, pp 175–190

Sudhira HS, Ramachandra TV, Raj KS, Jagadish KS (2003) Urban growth analysis using spatial and temporal data. J Indian Soc Remote Sens 31(4):299–311

Sudhira HS, Ramachandra TV, Jagadish KS (2004) Urban sprawl: metrics, dynamics and modelling using GIS. Int J Appl Earth Obs Geoinf 5:29–39

Sudhira HS, Ramachandra TV (2007) Characterising urban sprawl from remote sensing data and using landscape metrics. In: Proceedings of 10th international conference on computers in urban planning and urban management, pp 11–13

Sudhira HS (2008) Studies on urban sprawl and spatial planning support system for Bangalore, India (Doctoral dissertation, Indian Institute of Science, Bangalore)

Sui DZ, Zeng H (2001) Modeling the dynamics of landscape structure in Asia's emerging desakota regions: a case study in Shenzhen. Landsc Urban Plan 53(1–4):37–52

Takada T, Miyamoto A, Hasegawa SF (2010) Derivation of a yearly transition probability matrix for land-use dynamics and its applications. Landscape Ecol 25(4):561–572

Tang J, Wang L, Yao Z (2007) Spatio-temporal urban landscape change analysis using the Markov chain model and a modified genetic algorithm. Int J Remote Sens 28(15):3255–3271

Taragi RCS, Pundir PPS (1997) Use of satellite data in urban sprawl and land use studies - a case of lucknow city. J Indian Soc Remote Sens 25(2):113–118

Taubenböck H, Wegmann M, Roth A, Mehl H, Dech S (2009) Urbanization in India-Spatiotemporal analysis using remote sensing data. Comput Environ Urban Syst 33(3):179–188

Taubenböck H, Esch T, Felbier A, Wiesner M, Roth A, Dech S (2012) Monitoring urbanization in mega cities from space. Remote Sens Environ 117:162–176

Tavares AO, Pato RL, Magalhães MC (2012) Spatial and temporal land use change and occupation over the last half century in a peri-urban area. Appl Geogr 34:432–444

Tewolde MG, Cabral P (2011) Urban sprawl analysis and modeling in Asmara Eritrea. Remote Sens 3(10):2148–2165

Thapa RB, Murayama Y (2009) Urban mapping, accuracy, & image classification: a comparison of multiple approaches in Tsukuba City Japan. Appl Geogr 29(1):135–144

Thomas RW (1981) Information statistics in geography. United Kingdom, Norwich: Geo Abstracts

Tian G, Jiang J, Yang Z, Zhang Y (2011) The urban growth, size distribution and spatio-temporal dynamic pattern of the Yangtze River delta megalopolitan region China. Ecol Model 222(3):865–878

Tian L, Li Y, Yan Y, Wang B (2017) Measuring urban sprawl and exploring the role planning plays: a shanghai case study. Land Use Policy 67(Sept 2016):426–435

Torrens PM (2008) A toolkit for measuring sprawl. Appl Spat Anal Policy 1(1):5–36

Torrens PM, Alberti M (2000) Measuring sprawl. (CASA Working Papers 27). Centre for Advanced Spatial Analysis (UCL): London, UK

Tsai Y (2005) Quantifying urban form: compactness versus "sprawl." Urban Stud 42(1):141–161

Turner MG (1987) Spatial simulation of landscape changes in Georgia: a comparison of 3 transition models. Landscape Ecol 1(1):29–36

Turner MG, Gardner RH, O'neill RV, O'Neill RV (2001) Landscape Ecology in Theory and Practice, vol 401. New York: Springer

Turner BL, Moss RH, Skole DL (1993) Relating land use and global land- cover change: a proposal for an IGBP-HDP core project. International Geosphere Biosphere Programme, IGBP Report No. 24, HDP Report No. 5

United Nations (2018) Goal 11: Make cities inclusive, safe, resilient and sustainable

Uttarwar PS, Sokhi BS (1989) Remote sensing application in urban fringe study: a case study-Delhi. J Indian Soc Remote Sens 17(3):43–56

Vaz E, Taubenböck H, Kotha M, Arsanjani JJ (2017) Urban change in Goa, India. Habitat Int 68:24–29

Veldkamp A, Fresco LO (1996) CLUE: A conceptual model to study the conversion of land use and its effects. Ecol Model 85(2–3):253–270

Vibhute AD, Kale KV, Dhumal RK, Mehrotra SC (2015) Hyperspectral imaging data atmospheric correction challenges and solutions using QUAC and FLAASH algorithms. In: Proceedings of 2015 international conference on man and machine interfacing (MAMI). IEEE, pp 1–6

Vliet JV, White R, Dragicevic S (2009) Modeling urban growth using a variable grid cellular automaton. Comput Environ Urban Syst 33(1):35–43

Wakode HB, Baier K, Jha R, Azzam R (2014) Analysis of urban growth using Landsat TM/ETM data and GIS— a case study of Hyderabad India. Arab J Geosci 7(1):109–121

Wang L, Ma L, Song F, Zuo D (2009) Dynamics analysis of crop-landscape of agri-grazing-ecotone in Hobq desert. Res Agric Modernization 30(5):595–598

Wang D, Ma R, Xue K, Loiselle SA (2019) The assessment of landsat-8 OLI atmospheric correction algorithms for inland waters. Remote Sens 11(2)

Ward DP, Murray AT, Phinn SR (2000) A stochastically constrained cellular model of urban growth. Comput, Environ Urban Syst 24:539–558

Waske B, Benediktsson JA (2007) Fusion of support vector machines for classification of multisensor data. IEEE Trans Geosci Remote Sens 45(12):3858–3866

Wasserman M (2000) Confronting urban sprawl. Regional Review of the Federal Reserve Bank of Boston

Watanachaturaporn P, Arora MK, Varshney PK (2006) Sub-pixel land cover classification using support vector machines. In: Proceedings of ASPRS 2006 annual conference Reno, vol 1, no 5

Weng Q, Quattrochi DA (2006) Thermal remote sensing of urban areas: an introduction to the special issue. Remote Sens Environ 2(104):119–122

White RW, Engelen G (1997) Cellular automaton as the basis of integrated dynamic regional modelling. Environ Plann B Plann Des 24:235–246

White R, Uljee I, Engelen G (2012) Integrated modelling of population, employment and land-use change with a multiple activity-based variable grid cellular automaton. Int J Geogr Inf Sci 26(7):1251–1280

Wilson B, Chakraborty A (2013) The environmental impacts of sprawl: emergent themes from the past decade of planning research. Sustainability 5(8):3302–3327

Wilson CO, Weng Q (2011) Simulating the impacts of future land use and climate changes on surface water quality in the Des Plaines River watershed, Chicago metropolitan statistical area Illinois. Sci Total Environ 409(20):4387–4405

Wilson EH, Hurd JD, Civco DL, Prisloe S, Arnold C (2003) Development of a geospatial model to quantify, describe and map urban growth. Remote Sens Environ 86(3):275–285

Wolman H, Galster G, Hanson R, Ratcliffe M, Furdell K, Sarzynski A (2005) The fundamental challenge in measuring sprawl: Which land should be considered? Prof Geogr 57(1):94–105

Woodcock CE, Gopal S (2000) Fuzzy set theory and thematic maps: accuracy assessment and area estimation. Int J Geogr Inf Sci 14(2):153–172

Wu F (2002) Calibration of stochastic cellular automata: the application to rural-urban land conversions. Int J Geogr Inf Sci 16(8):795–818

Wu J (2006) Environmental amenities, urban sprawl, and community characteristics. J Environ Econ Manag 52(2):527–547

Wu J (2014) Urban ecology and sustainability: the state-of-the-science and future directions. Landscape Urban Plann 125:209–221

Wu F, Webster CJ (1998) Simulation of land development through the integration of cellular automata and multicriteria evaluation. Environ Plann B Plann Des 25(1):103–126

Wu F, Webster CJ (2000) Simulating artificial cities in a GIS environment: urban growth under alternative regulation regimes. Int J Geogr Inf Sci 14(7):625–648

Wu W, Zhao S, Zhu C, Jiang J (2015) A comparative study of urban expansion in Beijing, Tianjin and Shijiazhuang over the past three decades. Landsc Urban Plan 134:93–106

Wu Y, Li S, Yu S (2016) Monitoring urban expansion and its effects on land use and land cover changes in Guangzhou city, China. Environ Monit Assess 188 (1):54

Xiao J, Shen Y, Ge J, Tateishi R, Tang C, Liang Y, Huang Z (2006) Evaluating urban expansion and land use change in Shijiazhuang, China, by using GIS and remote sensing. Landsc Urban Plan 75(1–2):69–80

Xie Y (1996) A generalized model for cellular urban dynamics. Geogr Anal 28(4):350–373

Xu C, Liu M, Zhang C, An S, Yu W, Chen JM (2007) The spatiotemporal dynamics of rapid urban growth in the Nanjing metropolitan region of China. Landscape Ecol 22(6):925–937

Yang X (2003) Remote sensing and GIS for urban analysis: an introduction. Photogramm Eng Remote Sens 69(9):593–598

Yang X, Liu Z (2005) Use of satellite-derived landscape imperviousness index to characterize urban spatial growth. Comput Environ Urban Syst 29(5):524–540

Yang Y, Xiao P, Feng X, Li H (2017) Accuracy assessment of seven global land cover datasets over China. ISPRS J Photogramm Remote Sens 125:156–173

Yang J (2005) The spatial and temporal dynamics of commuting: examining the impacts of urban growth patterns, 1980–2000 (Doctoral dissertation, Massachusetts Institute of Technology)

Yeh AGO, Li X (2001a) A constrained CA model for the simulation and planning of sustainable urban forms by using GIS. Environ Plann B Plann Des 28(5):733–753

Yeh AGO, Li X (2001b) Measurement and monitoring of urban sprawl in a rapidly growing region using entropy. Photogram Eng Remote Sens 67:83–90

Yeh AGO, Li X (2002) A cellular automata model to simulate development density for urban planning. Environ Plann B Plann Des 29(3):431–450

Yeh AGO, Li X (2006) Errors and uncertainties in urban cellular automata. Comput Environ Urban Syst 30 (1):10–28

Yuan F, Sawaya KE, Loeffelholz BC, Bauer ME (2005) Land cover classification and change analysis of the Twin Cities (Minnesota) Metropolitan Area by multitemporal Landsat remote sensing. Remote Sens Environ 98(2–3):317–328

Yuan J, Niu Z (2008) Evaluation of atmospheric correction using FLAASH. In: 2008 International workshop on earth observation and remote sensing applications. IEEE, pp 1–6

Zaki R, Zaki A, Ahmed S (2011) Land use and land cover changes in arid region: the case new urbanized zone, northeast Cairo Egypt. J Geogr Inf Syst 3(03):173

Zeng YN, Wu GP, Zhan FB, Zhang HH (2008) Modeling spatial land use pattern using autologistic regression. Int Arch Photogramm Remote Sens Spat Inf Sci 37:115–118

Zeng C, He S, Cui J (2014) A multi-level and multi-dimensional measuring on urban sprawl: a case study in Wuhan metropolitan area, central China. Sustainability 6(6):3571–3598

Zeng C, Liub Y, Steind A, Jiao L (2015) Characterization and spatial modeling of urban sprawl in the Wuhan metropolitan area, China. Int J Appl Earth Obs Geoinf 34(1):10–24

Zhang Q, Ban Y, Liu J, Hu Y (2011) Simulation and analysis of urban growth scenarios for the Greater Shanghai Area, China. Comput Environ Urban Syst 35(2):126–139

Zhang Y, Wang X, Chen Y (2012) An improved 6S code for atmospheric correction based on water vapor content. Adv Remote Sens 01(01):14–18

Zhang Q (2009) Spatial-temporal patterns of urban growth in Shanghai, China: Monitoring, analysis, and simulation (Doctoral dissertation, KTH Royal Institute of Technology)

Zhao Y, Murayama Y (2011) Urban dynamics analysis using spatial metrics geosimulation. In: Spatial analysis and modeling in geographical transformation process. Springer, Dordrecht, pp 153–167

Zhao Y, Murayama Y (2006) Effect of spatial scale on urban land-use pattern analysis in different classification systems. Theory Appl GIS 14(1):29–42

Urban Expansion Monitoring Using Machine Learning Algorithms on Google Earth Engine Platform and Cellular Automata Model: A Case Study of Raiganj Municipality, West Bengal, India

3

Sunil Saha, Debabrata Sarkar, and Prolay Mondal

Abstract

Since producing a reliable land use land cover map is complex and time-consuming, the introduction of Google Earth Engine (GEE) and the availability of enormous volumes of Geosciences and Remote Sensing information provide a possibility for spatiotemporal monitoring of changing earth surface. The aim of this study is to utilise machine learning (random forest) on the Google Earth Engine framework with earth observation data to analyse land use land cover change in the Raiganj municipality. The research also uses a logistic regression-cellular automata model to evaluate the potential land use land cover changes by 2025. The findings of the study demonstrate that between 1990 and 2000, the study area experienced 1.87 km^2 of urban expansion at an annual rate of 8.68%. The five-year land use land cover change study revealed that urban expan-

sion was recorded at 59.88% from 1990 to 1995, followed by 2010–2015 (28.26%). With an average annual growth rate of 1.8% (0.41 sq. km), the lowest urban expansion was seen between 2005 and 2010. In Raiganj municipality, the majority of urban expansion and growth occurs in the southwest direction. According to the predicted land use land cover map for 2025, about 5.06% of the study area will be urbanised in the upcoming five years and urbanisation will spread in the northeastern part of the study region. The results highlight the requirement of monitoring land use land cover change and assisting policymakers in implementing policies to limit haphazard urbanisation and avoid human–environment conflict in the study region.

3.1 Introduction

According to the UN report (2018), urbanisation is a worldwide trend, and the world's population and city areas increase, resulting in the alteration of present land use (Xu et al. 2019a, b; Shao et al. 2021). Rapid urban expansion is frequently linked

S. Saha · D. Sarkar · P. Mondal (✉)
Department of Geography, Raiganj University, Raiganj, West Bengal 733134, India
e-mail: mon.prolay@gmail.com

S. Saha
e-mail: sahasunil2507@gmail.com

D. Sarkar
e-mail: debabratas077@gmail.com

to and driven by population density in a given location. As per the UNEP report (2005), over half of the world's population lived in cities in 2005. According to the United Nations, by 2050, more than half of the world's population lives in cities, with that number expected to rise to more than 65% in the present scenario. Odindi and Mhangara (2012) mentioned that, based on the current population growth rate, by 2030, it is expected that over 60% of the world's population will be living in cities. According to Fenta et al. (2017), this massive population growth will result in an additional 2.5 billion people living in urban areas throughout the world, with 90% of urban growth taking place in less-developed countries. The UN report (2016) mentioned that Africa and Asia are experiencing rapid urbanisation, and by 2050, these areas will have seen around 90% urbanisation. According to the United Nations (2014), due to the faster population growth rate, Asian countries like India, Bangladesh, Pakistan, Sri Lanka, and Singapore have evidence of rapid urbanisation. By 2050, the urban population in Asia will increase from 42.5% (2010) to 64.6%. In terms of urbanisation and population expansion, India has followed a similar trend. Between 1981 and 2011, India's population grew dramatically, rising from 68.33 million to 121.01 million. Now it is estimated that, by 2028, India is expected to have the world's highest population, but in recent times, a declining trend of population growth has been observed (Seto et al. 2012; Bakr and Bahnassy 2019).

According to Tewolde and Cabral (2011), the urban territory is expanding at a faster pace than the urban population. Rafiee et al. (2009) mentioned that cities are putting a lot of strain on existing lands and commodities as a result of their fast expansion. The physical loss of agricultural land, as well as natural or cultural landscapes, is a direct adverse result of urban growth, but it also has indirect repercussions. Some of the indirect effects of urbanisation include fragmentation of the landscape, soil erosion, increased run-off, surface hardening, and loss of biodiversity (Ceccarelli et al. 2014). Cities in rising urban and suburban regions are interested in precise data on the extent, magnitude, and level of urban expansion for a variety of reasons, including

urban planning, drainage systems, resource management, infrastructure development, allocating services, product positioning, and so on.

Regrettably, traditional survey and mapping approach for estimating urban sprawl are costly and effort-intensive, and such data is not accessible for most metropolitan sites, particularly in emerging nations. As a result, researchers are increasingly interested in employing remote sensing (RS) and geographic information system (GIS) techniques (Epstein et al. 2002) to map and track urban growth and sprawl. There seem to be several methods for studying land use change and urban expansion/sprawl (Arsanjanj et al. 2013). With the advancement of technologies, different kinds of models have been developed for land use change detection and urban sprawl modelling, including the logistic regression (LR) model (Arsanjanj et al. 2013; Alsharif and Pradhan 2014; Aiddiqui et al. 2018), CA Markov model (Arsanjanj et al. 2013; Moghadam and Helbich 2013), cellular automation model (Arsanjanj et al. 2013; Deep and Saklani 2014), machine learning models like ANN, SVM (Huang et al. 2010; Kamusoko and Gamba 2015; Shafizadeh-Moghadam et al. 2017; Karimi et al. 2019; Ou et al. 2019; Xu et al. 2019a, b; Khan and Sudheer 2022), Google Earth Engine (Feizizadeh et al. 2021; Xue et al. 2021), etc. Because remote sensing and GIS are both cost-effective and technically competent, these techniques have been frequently utilised for urban sprawl studies. For over three decades, researchers have been working on detecting urban change and modelling urban sprawl using remotely sensed satellite images (Gomarasca et al. 1993; Yeh and Li 2001; Hack and Rafter 2006).

Google Earth Engine (GEE) has recently gained popularity in the scientific community for land use and land cover analysis since this platform provides the simplest approach to classify land use land cover utilising spatio-temporal earth surface data. The Google Earth Engines platform and machine learning algorithms were widely used by academics and researchers to monitor changes in land usage, e.g. measuring urban city growth and boundaries in India using Google Earth Engine (Goldblatt et al. 2016),

Google Earth Engine-based land use land cover change detection in Singapore (Sidhu et al. 2018), detecting urban growth of Ankara city using Google Earth Engine platform (Celik 2018), mapping the urbanisation in Greenville county in Southern United States using Google Earth Engine platform (Zurqani et al. 2019), Mugiraneza et al. (2020) used the Google Earth Engine platform along with Landsat satellite data for monitoring the urban land use land cover of Kigali city of Rwanda, land use land cover dynamics using Google Earth Engine along with snic, glcm and machine learning approach in central Italy (Tassi and Vizzari 2020), land use land cover change detection in Northern Iran using machine learning along with Google Earth Engine (Feizizadeh et al. 2021), land use land cover change and prediction using Google Earth Engine and Markov-CA for Rondonia state (Floreano and de Moraes 2021), detection of urban growth in Datong city of China using Google Earth Engine (Xue et al. 2021).

Geographic information system (GIS) science and spatial analysis are effective tools for investigating and monitoring changes in land use patterns, as well as generating predictions for possible eventualities, and are an important tool for land use planning, urban sprawl modelling, and decision-making process (Bakr et al. 2010). Remote sensing satellite imagery can effectively record the current LULC distribution geographically as well as temporally (Rai et al. 2018), allowing for the derivation, analysis, and prediction of LULC changes (Liping et al. 2018). Furthermore, machine learning techniques are a typical subset of artificial intelligence. Machine learning algorithms may be used to prepare data for forecast assessment, resulting in more accurate outcomes (Liping et al. 2018; Rai et al. 2018; Sarker et al. 2021). Machine learning techniques are much more effective in image classification activities, including land use classifications, modelling, and prediction (Han et al. 2011).

The main objective of this present study is to measure the land use land cover change in the last three decades; by doing this, the author trying to assess the urban growth modelling using machine learning on the Google Earth Engine platform. Another objective of the study is to project the land use land cover using a logistic regression-based cellular automata model. The study area is one of the most important urban centres of the district as well as in North Bengal. In the last three to four decades, massive influx of people from the surrounding areas forced to urbanise this area very rapidly and make changes in the land use land cover quite significantly. Surprisingly, except for a comparative study between cities, no significant research work was previously done by any researcher on this topic in the selected study area. In the surrounding region, conventional method-based land use land cover change studies were conducted, but the Google Earth Engine platform with machine learning and cellular automata model-based urban growth analysis in the study region will make a significant contribution in the field of changing earth surface by human activities. This type of LULC change monitoring and prediction is a challenging task to do since it requires a great deal of effort and precise modelling capacity. This work will assist urban planners in the implementation of new sustainable urbanisation projects and help to demarcate suitable sites for future urban growth in the study region.

3.2   Database and Methods

3.2.1   Study Area

Raiganj municipality is located in the Uttar Dinajpur district of West Bengal, India (Fig. 3.1). On 19 July 1951, the town officially became a municipality. With a huge rural hinterland, Raiganj has long been a regional hub for employment and economic progress. The Raiganj municipality is governed by the Raiganj metropolitan region authority. The municipality and its surrounding region have seen enormous population expansion in recent decades. According to the 2011 Census, Raiganj has a total population of 199,758 people, with 52.49% of men and 47.51% of women. The study region
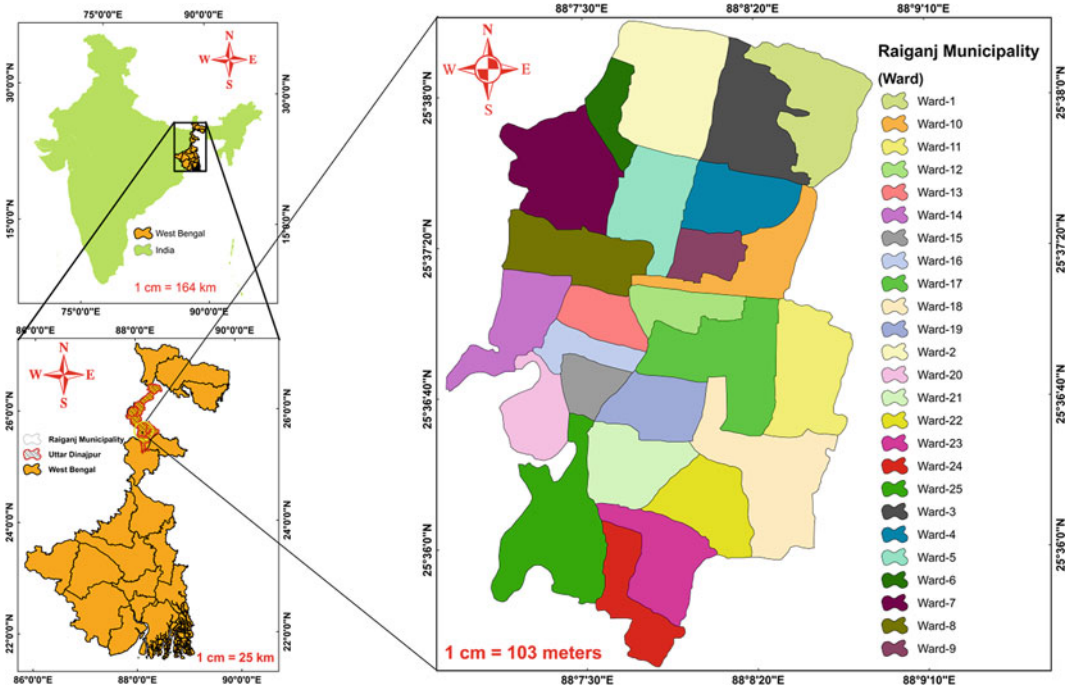
Fig. 3.1 Geographical location of the study area

has a total area of 10.76 square kilometres. The Raiganj municipality has a population density of 18,378 people per square kilometre. Kasba, Nachhratpur, Katabari, and Raiganj are the primary metropolitan areas of Raiganj Municipality. The current trend of urbanisation in the Raiganj municipality is particularly striking. A similar pattern may be seen throughout the agglomeration area. Maraikura, Karnojora, Bahin, Maharaja Hat, and Birghai are experiencing a similar population boom to Raiganj municipality town, with the majority of the people working in Raiganj municipality town. The main highways connecting Siliguri city in the north to Kolkata, the state capital, in the south are NH 12 and SH 10A, which connect Balurghat town. With over a lakh people travelling each working day, the Raiganj municipality has emerged as West Bengal's most significant commerce hub. Agriculture in the surrounding region has a significant impact on the city's economy. The municipality has seen substantial urban growth during the previous two decades.

3.2.2 Data Source

The LULC maps for individual years were generated on the Google Earth Engine platform using a classifier tool with true colour combinations. Landsat 5, Landsat 7, and Landsat 8 satellite images with 30 resolutions were used in this exploration. A detailed account of data sources is given in Table 3.1.

3.2.3 Methods

3.2.3.1 LULC Classification

The pre-processing phase is performed to get corrected pixel and radiometric values from multiple recording times in order to produce a clear image of the cloud cover. LULC classification utilises the random column (RC) approach of machine learning by collecting training data for each land cover type in GEE. GEE is a sophisticated cloud-based platform for processing satellite imagery and generating global

Table 3.1 Details of the Landsat satellite imageries

Satellite data	Collection	Row/path	Calibrate	Data availability	Numbers of band	Sun-synchronous	Cloud cover (%)	Resolution (m)
Landsat 5	1	Row: 42	TOA[a]	1984-03-16T16:20:00Z —2012-05-05T00:00:00	7	Altitude: 705 km	Less than 10	30
Landsat 7	1	Path: 139	TOA	1999-05-28T01:02:17Z —2021-12-31T00:00:00	8	Inclined at 98.2°		30
Landsat 8	1		TOA	2013-03-18T15:59:02Z —2022-01-02T00:00:00	11			30

[a] top-of-atmosphere (TOA) reflectance. *Source* Acknowledgement or credit of the USGS

geospatial data. The random column method was used to split the single sample set into the training set and the test set (Yang et al. 2021). In order to extract land cover types in the monitoring area, the LULC classification method utilising RF was executed.

These LULC maps are classified into four categories: water bodies; urban regions; vegetation; and agricultural and open land. The results of the RC classification of each Landsat image provide LULC data for each year, which will be used for the analysis of LULC change and LULC maps. The whole process of LULC output generation is classified into the following steps:

Step I Importing Shapefile and Landsat imageries and Filtering the shape file

At the very first step, the study area shape file (shp., prj., shx., dbf.) is imported into the Earth Engine platform and selected Landsat data from the earth engine catalogue.

$$var\, selection\, =\, L5/L7/L8.filterBounds(AOI)$$
$$.filterDate\,('start\,year','End\,year')$$
$$.filterMetadata$$
$$('CLOUD\_COVER','less\_than',1)$$
$$.mean()$$
$$.clip(AOI)$$

$$var\text{viz}\, =\{bands:\,[L5:'B3','B2','B1';$$
$$L7/L8:'B4','B3','B2'],\,min:0,$$
$$max:0.4,\,gamma:1.2\};Map.add$$
$$Layer(selection,\text{viz},'landsat5/7/8');$$

Step II Create training data and merging it for LULC

In this step, the training samples were identified (50 samples for each class), and all collected geometry samples were merged using the merge algorithm in the Earth Engine platform. In this process, the property label was 'LULC' with 0 to 3 value codes.

$$var\quad training = alternative1.merge$$
$$(alternative2).merge(alternative3)$$
$$.merge(alternative4);$$
$$var\,label = \text{“LULC”}$$
$$var\quad bands = ['B1','B2',\quad 'B3',$$
$$'B4','B5',\,'B7'];$$
$$var\qquad input = selection.select$$
$$(bands);$$

Step III Make a training dataset and overlay the points

In this step, the sampled training was linked with the raster data using the function 'sampleRegions'. The pixel size was 30 m. Here, the

'input' is the variable name of Landsat imagery for a specific year. In this step, the Landsat bands were extracted by training data points.

$$var\ trainimage = input.sampleRegions(\{$$
$$collection : training,$$
$$properties : [label],$$
$$scale : 30\});$$

Step IV Separate the Training data and Test data.

The random fields were used to generate the training validation data. The random column function was used to separate the training data and the test data set.

$var\ trainingdata = trainimage.randomColumn();$

$var\ trainSet = trainingdata.filter(ee.Filter.lessThan('random', 0.8));$

$var\ testSet = trainingdata.filter(ee.Filter.greaterThanOrEquals('random', 0.8));$

Step V Organise run and the Classification model

The random forest classifier has been used to generate the LULC of the selected years. The training set was run with the classifier function. Leo Breiman's Random Forest (Breiman 2001) is a set of unpruned classification or regression trees made from a random selection of training data samples. During the process of induction, random features are chosen. To make a prediction, all of the assumptions made by the ensemble are added up (majority vote for classification or average for regression).

$$var\ classifier = ee.Classifier.smileRandom$$
$$Forest(100).train(trainSet, label, bands)$$

Step VI Link the classifier model with the Landsat bands

In this step, the classify function has been used to link up the Landsat bands with the classification model. This function generates major classified images for interpretation.

$var\ classified = input.classify(classifier);$

Step VII Define colour palette of the alternatives for classification

To define the colour of the LULC pattern classes, the 'HTML colour codes' have been used.

$$var\ lulcpalette = ['33FFF8','DB0A2F',$$
$$'0ADB31','DACE1E'];$$
$$Map.addLayer(classified.clip(AOI),$$
$$\{palette : lulcpalette,$$
$$min : 0,\ max : 4\}),'CARTlassification'$$

Step VIII Measuring the overall accuracy of the outputs

The ee.confusion Matix function has been used on test set and classifier to classify the confusion matrix. The overall accuracy results have been generated using the 'print' function.

```
var confusionMatrix = ee.ConfusionMatrix(testSet.classify(classifier)
.errorMatrix({
        actual :' LULC',
        predicted :' classification'}));

print('confusion Matrix :', confusionMatrix);
print('Overall Accuracy :', confusionMatrix.accuracy());
```

Step IX Exporting the LULC maps

In this step, the generated LULC maps have been exported with a 30 m cell size. The 'Export.image' function has been used to export the maps.

$$Export.image.toDrive(\{$$
$$image : classified,$$
$$description :' Y2020/2015/$$
$$2010/2005/2000/1995/1990',$$
$$scale : 30,$$
$$region : AOI\})$$

3.2.3.2 LULC Simulation for 2025 Using Logistic Regression Transition Potential Modelling-Cellular Automata Approach

Regression is a technique for determining the empirical relationships between a binary dependent and independent categorical and continuous variable (Xie et al. 2005). Logistic regression is a function to uses statistics to predict a yes or no

answer based on what has been seen in a data set before. Logistic regression uses the relationship between predictor variables and the presence or absence of landslides within a geographic cell to make a map that shows the likelihood of future landslides given the slopes and geologic units in the area. The area change coefficient matrix has been generated using the logistic regression transition potential model, and thereafter, the cellular automata approach has been used to stimulate the LULC pattern of 2025 using the Modules for Land Use Change Evaluation (MLUSCE) plug-in in QGIS. The cellular automata model is a well-known simulation model in which space and time are discrete and only local interactions happen. In actuality, in cellular automata (CA), space is divided into regular cells, and the state of each cell is based on how it and the cells around it was at a certain point in time in the past. This is done through a set of transition rules. But the state of each cell can be changed at the same time. Numerous CA models have been used to simulate urban systems, such as sprawl (Wu 1996). Cellular automata models are used more and more in environmental studies because they are dynamic, have a clear sense of space, and can work with the raster format that is commonly used in GIS. Figure 3.2 shows the detailed methodology of the present work.

3.2.3.3 Estimation of the Rate of Urban Expansion

The Urban Expansion Rate

Urban expansion appears to mean that the built-up area of a city or group of cities is getting bigger. This often happens when the number of people living in cities grows. The following equation has been used to estimate the urban expansion rate:

$$\text{Expansion}^{\text{rate}} = \left\{ \frac{(\text{Present year area} - \text{Previous year area})}{\text{Previous year area}} \right\} \times 100$$
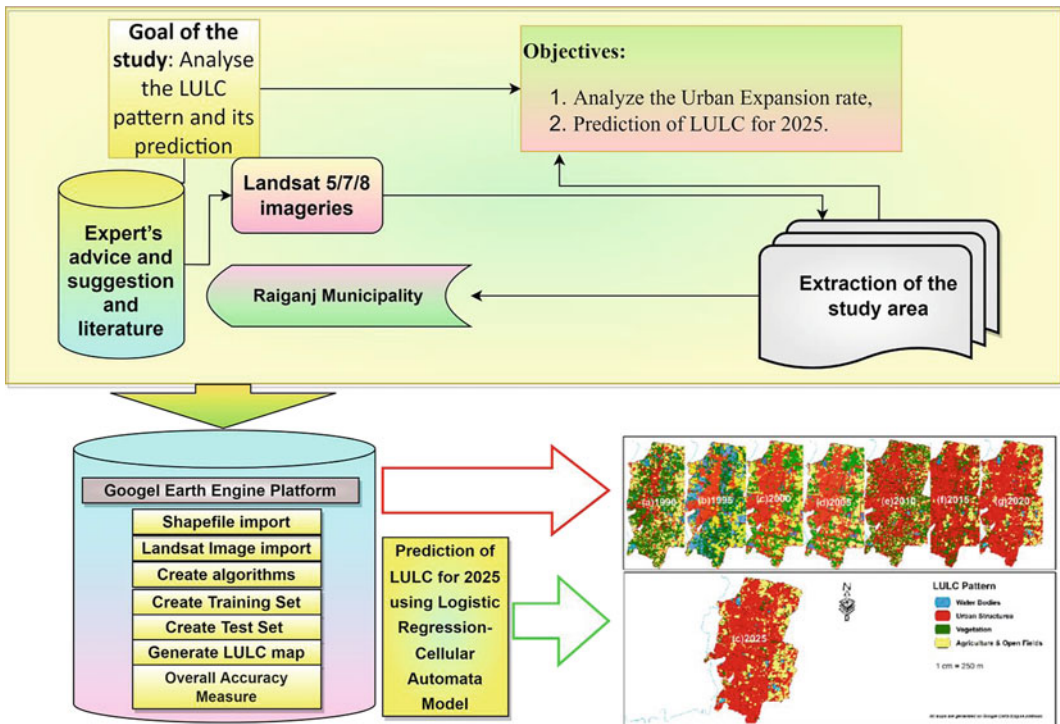
Fig. 3.2 Flow diagram of the whole study

3.3   Results and Discussion

3.3.1   LULC Change Analysis

The LULC map of 1990 was generated using Landsat 5 data and the spatial distribution of that map was classified into four potential classes, i.e.

water bodies (9.44%), urban structure (20.02%), vegetation (29.29%), agriculture and open fields (36.94%). About 65% (about 7.13 km^2) (Table 3.2) of land was covered with vegetation, agriculture, and open fields (Fig. 3.3) were mostly found in eastern, north-eastern and south-eastern parts of the study area.

Table 3.2 Area distribution of LULC types for different years

Year	Value	Area (%)	Area (km^2)	Overall accuracy
1990	Water bodies	9.44	1.02	0.801
	Urban structures	20.02	2.15	
	Vegetation	29.29	3.15	
	Agriculture and open fields	36.94	3.98	
1995	Water bodies	15.11	1.29	0.881
	Urban structures	31.98	3.44	
	Vegetation	26.47	2.85	
	Agriculture and open fields	41.55	4.47	
2000	Water bodies	2.99	0.32	0.814
	Urban structures	37.41	4.03	
	Vegetation	27.39	2.95	
	Agriculture and open fields	32.22	3.47	
2005	Water bodies	2.75	0.3	0.879
	Urban structures	42.28	4.55	
	Vegetation	24.84	2.67	
	Agriculture and open fields	29.71	3.2	
2010	Water bodies	1.29	0.14	0.834
	Urban structures	46.05	4.95	
	Vegetation	24.15	2.6	
	Agriculture and open fields	19.94	2.15	
2015	Water bodies	1.27	0.14	0.843
	Urban structures	59.06	6.35	
	Vegetation	23.82	2.56	
	Agriculture and open fields	15.81	1.7	
2020	Water bodies	1.06	0.11	0.81
	Urban structures	66.07	7.11	
	Vegetation	10.55	1.14	
	Agriculture and open fields	21.35	2.3	
2025	Water bodies	0.88	0.09	
(Predicted)	Urban structures	69.37	7.46	
	Vegetation	9.05	0.97	
	Agriculture and open fields	17.65	1.9	

In the year 1995, the urban sarea drastically increased by +11.96% (1.29 km^2) of the total geographical area. This increment happened just after the division of the West Dinajpur into North and South Dinajpur on 1 April 1992. Water bodies rose by + 5.67% and vegetation areas fell by −2.82% from the previous year, according to the findings. Remarkably, the water bodies shifted in a positive mood from 9.44% to 15.11% during this time. It is likely because of the flooding in the region in 1992.

The total urban area increased by +5.46% from 1995 to 2000. In the year 1995, about 31.98% area was urbanised, whereas it is about 37.41%, respectively. Between 1995 and 2000, the percentage of water bodies decreased from 15.11% to 2.99%, and the agricultural area also decreased by −9.33% from 41.55% to 32.22%. On the other side, between 2000 and 2005, urban areas grew by 4.87 per cent. The vegetation-covered area, water bodies, and agriculture decreased by −2.14%, −024%, and −2.51% respectively, over the same duration of time. In 2010, like the previous year, urban expansion took place. The urban area increased by about +3.77% from 2005 to 2010. The water bodies were decreased by −1.46% due to urban expansion. The agricultural field drastically decreased by −9.77% in the same period. In 2015, there was about a +13.01% jump in the urban area from the previous year, and the agricultural area decreased by −4.13%. The water bodies (−0.02%) and vegetation area (−0.33%) negatively deviated from 2010 to 2015. In 2020, the urban area was 66.07%, whereas it was 59.06% in 2015. The water bodies and vegetation decreased by −0.21% and −13.27%, respectively. The other patterns of the LULC decreased from the previous year.

3.3.2 Prediction of LULC for 2025

The logistic regression-cellular automata approach was used to predict the LULC pattern of 2025 in the QGIS environment. The spatial distribution of the LULC map of 2025 was also categorised as water bodies with 0.88%, urban
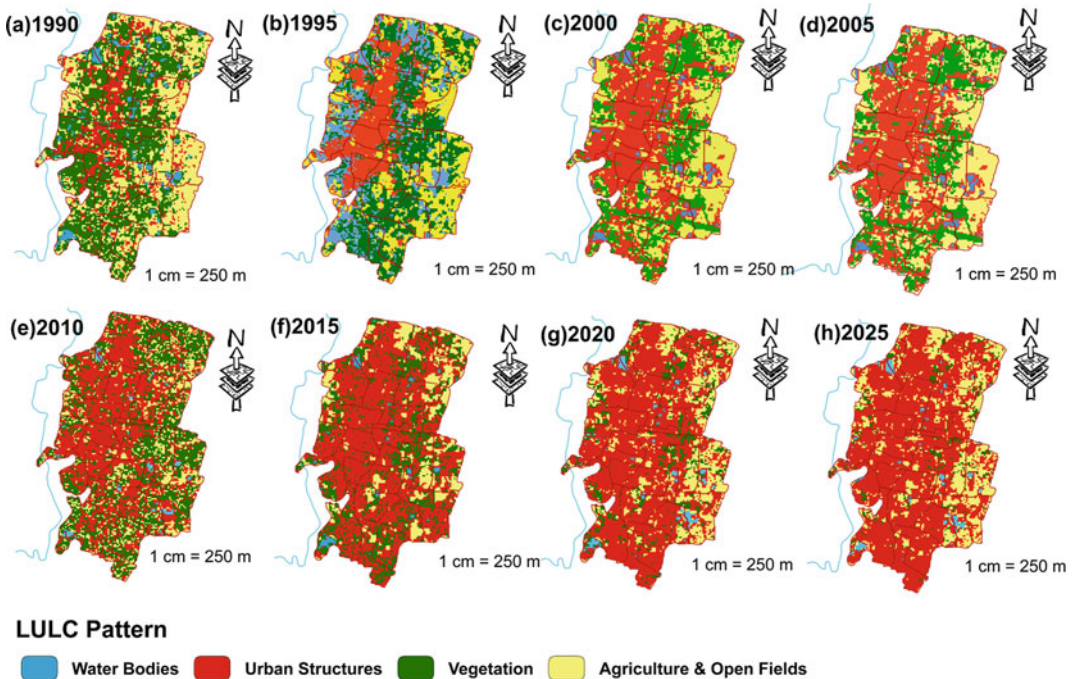

LULC Pattern

Water Bodies   Urban Structures   Vegetation   Agriculture & Open Fields

Fig. 3.3 LULC pattern of the study area **a-h**: **a** 1990, **b** 1995, **c** 2000, **d** 2005, **e** 2010, **f** 2015, **g** 2020, **h** 2025

Table 3.3 Areal deviation of LULC between the selected years

Year	LULC pattern	Area deviation (%)	Year	LULC pattern	Area deviation (%)
1990–1995	Water bodies	−4.79	1995–2000	Water bodies	−5.97
	Urban structures	11.96		Urban structures	5.43
	Vegetation	−2.81		Vegetation	0.91
	Agriculture and open fields	4.6		Agriculture and open fields	−9.33
2000–2005	Water bodies	−0.23	2005–2010	Water bodies	−1.47
	Urban structures	4.87		Urban structures	3.77
	Vegetation	−2.13		Vegetation	7.47
	Agriculture and open fields	−2.51		Agriculture and open fields	−9.77
2010–2015	Water bodies	−0.01	2015–2020	Water bodies	−0.21
	Urban structures	13.01		Urban structures	7.01
	Vegetation	−8.9		Vegetation	−13.26
	Agriculture and open fields	−4.13		Agriculture and open fields	5.54
2020–2025	Water bodies	−0.19			
	Urban structures	3.3			
	Vegetation	−1.5			
	Agriculture and open fields	−3.71			

structure with 69.97%, vegetation with 9.05%, and agriculture and open fields with 17.65%, respectively. The prediction result indicates that the urban areas increased by +3.3%, whereas the other forms were decreased (Fig. 3.3). Another side, water bodies decreased by −0.18%, vegetation by −1.5%, and agricultural fields by −3.7%, respectively (Table 3.3).

3.3.3 Urban Expansion Rate (1990–2025)

The urban expansion rate from 1990 to 1995 was 59.88%, whereas it is about 16.85% from 1995 to 2000 (Table 3.4). The increments in service sectors were the reason behind it. There are service industries that make it easier to move, sell, and distribute goods made in the secondary sector. Production, consumption, and gradually building capital are all connected. When the amount of goods and services produced goes up, the amount of money spent and saved also goes

up. A lot of non-Muslim people were forced to leave Bangladesh and move to the Uttar Dinajpur district because of religious conflicts. People of the Muslim faith also moved to the Uttar Dinajpur district because it was a better place to live.

The urban growth from 1900 to 2000 was about 86.83%. From 2000 to 2005, the rate of urban growth was about 12.92%. Due to frequent recurrent floods in the state of Bihar, people migrated from those areas to Raiganj, as Raiganj is situated just adjacent to Bihar. Some of those migrated people started to live in slums, as they were called 'urban villagers' (the people lived in urban areas but their lifestyle and occupation were still in rural regions). Some of the people migrated permanently from Western Indian states for business purposes, as Raiganj is a 'Business Hotspot'.

From 2005 to 2010, the urban growth rate was only 9.01%. Between 2000 and 2010, the urbanisation rate was 23.09%. During this period, the service sectors rapidly gear up, such as the establishment of wholesale and retail malls;

Table 3.4 Rate of urban areal changes

Year	Changes (%)	Changes (km^2)	Year	Changes (%)	Changes (km^2)
	5 years span			10 years span	
1990–1995	59.88	1.29	1990–2000	86.83	1.87
1995–2000	16.85	0.58			
2000–2005	12.92	0.52	2000–2010	23.09	0.93
2005–2010	9.01	0.41			
2010–2015	28.26	1.4	2010–2020	43.48	2.15
2015–2020	11.8	0.75			
2020–2025	5.06	0.36			

Fig. 3.4 Urban expansion rate and its deviation from the previous year
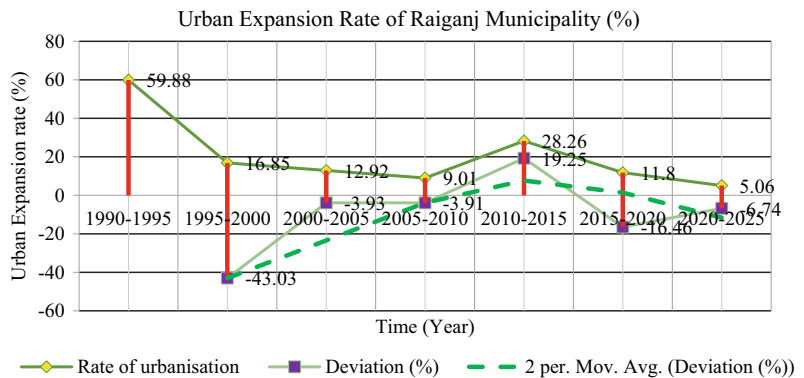
markets are expanded, and the education sectors also improve during this period. From 2010 to 2015, the urban growth rate was 28.26%. During this period, the education sector drastically grew, and several shopping malls and markets were established in the Raiganj municipality region. From 2015 to 2020, the urban growth rate was 11.80, whereas it was about 43.48% from 2010 to 2020. The main causes of this increment most probably were the establishment of Raiganj University, Raiganj Super Specialty Hospital, and Raiganj Medical College. A large number of professors, teachers, and scholars have permanently or non-permanently migrated to this city region. Several shopping malls and Bazar malls were also established during this period.

It is predicted that the urban growth rate of this city from 2020 to 2025 will be 5.06% (Fig. 3.4). Improvement in the service sector, expansion in the business sector, and expansion in the education sector will be the main causes behind future urbanisation.

3.3.4   Accuracy Analysis of the Outputs

The overall accuracy of the LULC maps was measured in the Earth Engine Environment. It is found that the accuracy of LULC in 1990 is 80.12%, whereas it is 88.10% for LULC in 1995. The overall accuracy of LULC 2000 is 81.36%, LULC 2005 is 87.91%, LULC 2010 is 83.39%, LULC 2015 is 84.25%, and LULC 2020 is 80.95%. These accuracies imply that the training data set and test data test for LULC calculation were accurately estimated.

3.4   Conclusion

The study analyses the land use land cover change and predicts urban expansion of Raiganj municipality. As a consequence of rapid urban expansion and urban expansion, the Raiganj municipality has seen rapid urban expansion from

1990 to 2020. The urban built-up area has increased by 46.05% from 2.15 km^2 in 1990 to 7.11 km^2 in 2020. All other land use classes, on the other hand, have decreased over time, resulting in urbanisation. Vegetation and water bodies both dropped by 20.24% and 8.56%, respectively, between 1990 and 2020. Due to the abundance of marsh and agricultural land, urban expansion is concentrated towards the city's northeast boundary. The predicted LULC map for the year 2025 indicates that the present pattern of urban growth will prevail. In 2025, the area under urbanisation will be 7.46 km^2, which is 69.37% of the total area, compared to 2.15 km^2 in 1990. The outcomes of the study revealed that alterations in land use land cover had an impact on the urban environment. To guarantee sustainable development, the urban planner and the city planning department must supervise the pace and scale of urban growth. To mitigate the adverse consequences of haphazard and uncontrolled urban expansion, policymakers might examine urban growth variables under various LULC scenarios. In addition, additional study is needed to assess the consequences of urban growth on the urban environment so that effective mitigation techniques can be implemented.

References

Alsharif AA, Pradhan B (2014) Urban sprawl analysis of Tripoli Metropolitan city (Libya) using remote sensing data and multivariate logistic regression model. J Indian Soc Remote Sens 42(1):149–163

Arsanjani JJ, Helbich M, Kainz W, Boloorani AD (2013) Integration of logistic regression, Markov chain and cellular automata models to simulate urban expansion. Int J Appl Earth Obs Geoinf 21:265–275

Bakr N, Bahnassy MH (2019) Egyptian natural resources. In: The soils of Egypt. Springer, Cham, pp 33–49

Bakr N, Weindorf DC, Bahnassy MH, Marei SM, El-Badawi MM (2010) Monitoring land cover changes in a newly reclaimed area of Egypt using multi-temporal Landsat data. Appl Geogr 30(4):592–605

Breiman L (2001) Random Forests. Mach Learn 45(1): 5–32

Ceccarelli T, Bajocco S, LUIGI PL, Luca SL (2014) Urbanisation and land take of high quality agricultural soils-exploring long-term land use changes and land capability in Northern Italy

Celik N (2018) Change detection of urban areas in Ankara through Google Earth engine. In: 2018 41st international conference on telecommunications and signal processing (TSP). IEEE, pp 1–5

Deep S, Saklani A (2014) Urban sprawl modeling using cellular automata. Egypt J Remote Sens Space Sci 17 (2):179–187

Epstein J, Payne K, Kramer E (2002) Techniques for mapping suburban sprawl. Photogramm Eng Remote Sens 68(9):913–918

Feizizadeh B, Omarzadeh D, Kazemi Garajeh M, Lakes T, Blaschke T (2021) Machine learning data-driven approaches for land use/cover mapping and trend analysis using Google Earth Engine. J Environ Plann Manage:1–33

Fenta AA, Yasuda H, Haregeweyn N, Belay AS, Hadush Z, Gebremedhin MA, Mekonnen G (2017) The dynamics of urban expansion and land use/land cover changes using remote sensing and spatial metrics: the case of Mekelle City of northern Ethiopia. Int J Remote Sens 38(14):4107–4129

Floreano IX, de Moraes LAF (2021) Land use/land cover (LULC) analysis (2009–2019) with Google Earth Engine and 2030 prediction using Markov-CA in the Rondônia State Brazil. Environ Monit Assess 193 (4):1–17

Goldblatt R, You W, Hanson G, Khandelwal AK (2016) Detecting the boundaries of urban areas in India: a dataset for pixel-based image classification in google earth engine. Remote Sens 8(8):634

Gomarasca MA, Brivio PA, Pagnoni F, Galli A (1993) One century of land-use changes in the metropolitan area of Milan (Italy). Int J Remote Sens 14(2):211–223

Haack BN, Rafter A (2006) Urban growth analysis and modeling in the Kathmandu Valley Nepal. Habitat Int 30(4):1056–1065

Han J, Pei J, Kamber M (2011) Data mining: concepts and techniques. Elsevier

Huang B, Xie C, Tay R (2010) Support vector machines for urban growth modeling. GeoInformatica 14(1):83–99

Kamusoko C, Gamba J (2015) Simulating urban growth using a random forest-cellular automata (RF-CA) model. ISPRS Int J Geo Inf 4(2):447–470

Karimi F, Sultana S, Babakan AS, Suthaharan S (2019) An enhanced support vector machine model for urban expansion prediction. Comput Environ Urban Syst 75:61–75

Khan A, Sudheer M (2022) Machine learning-based monitoring and modeling for spatio-temporal urban growth of Islamabad. Egypt J Remote Sens Space Sci 25(2):541–550

Liping C, Yujun S, Saeed S (2018) Monitoring and predicting land use and land cover changes using remote sensing and GIS techniques—a case study of a hilly area, Jiangle China. PLoS ONE 13(7):e0200493

Moghadam HS, Helbich M (2013) Spatiotemporal urbanisation processes in the megacity of Mumbai, India: a

Markov chains-cellular automata urban growth model. Appl Geogr 40:140–149

Mugiraneza T, Nascetti A, Ban Y (2020) Continuous monitoring of urban land cover change trajectories with landsat time series and landtrendr-google earth engine cloud computing. Remote Sens 12(18):2883

Nations U (2014) World urbanization prospects. United Nations: San Francisco, CA, USA

Odindi JO, Mhangara P (2012) Green spaces trends in the city of Port Elizabeth from 1990–2000 using remote sensing

Ou C, Yang J, Du Z, Zhang X, Zhu D (2019) Integrating cellular automata with unsupervised deep-learning algorithms: a case study of urban-sprawl simulation in the Jingjintang urban agglomeration China. Sustainability 11(9):2464

Rafiee R, Mahiny AS, Khorasani N, Darvishsefat AA, Danekar A (2009) Simulating urban growth in Mashad City, Iran through the SLEUTH model (UGM). Cities 26(1):19–26

Rai R, Zhang Y, Paudel B, Acharya BK, Basnet L (2018) Land use and land cover dynamics and assessing the ecosystem service values in the trans-boundary Gandaki River Basin Central Himalayas. Sustainability 10 (9):3052

Sarker IH, Hoque MM, Uddin M, Alsanoosy T (2021) Mobile data science and intelligent apps: concepts, AI-based modeling and research directions. Mob Networks Appl 26(1):285–303

Seto KC, Güneralp B, Hutyra LR (2012) Global forecasts of urban expansion to 2030 and direct impacts on biodiversity and carbon pools. Proc Natl Acad Sci 109 (40):16083–16088

Shafizadeh-Moghadam H, Tayyebi A, Ahmadlou M, Delavar MR, Hasanlou M (2017) Integration of genetic algorithm and multiple kernel support vector regression for modeling urban growth. Comput Environ Urban Syst 65:28–40

Shao Z, Sumari NS, Portnov A, Ujoh F, Musakwa W, Mandela PJ (2021) Urban sprawl and its impact on sustainable urban development: a combination of remote sensing and social media data. Geo-Spatial Inf Sci 24(2):241–255

Sidhu N, Pebesma E, Câmara G (2018) Using Google Earth Engine to detect land cover change: Singapore as a use case. Eur J Remote Sens 51(1):486–500

Tassi A, Vizzari M (2020) Object-oriented LULC classification in google earth engine combining snic, glcm, and machine learning algorithms. Remote Sens 12(22):3776

Tewolde MG, Cabral P (2011) Urban sprawl analysis and modeling in Asmara Eritrea. Remote Sens 3(10): 2148–2165

UN (2016) The World's Cities in 2016—Data Booklet (ST/ESA/SER. A/392)

UNEP (2005) United Nations environmental program. Key facts about cities: issues for the urban millennium. United Nations Environmental Program, New York

United Nations Department of Economic and Social Affairs (2018) Revision of world urbanization prospects

Wu F (1996) A linguistic cellular automata simulation approach for sustainable land development in a fast-growing region. Comput Environ Urban Syst 20 (6):367–387

Xie C, Huang B, Claramunt C, Chandramouli C (2005) Spatial logistic regression and GIS to model rural-urban land conversion. In: Proceedings of PROCESSUS second international colloquium on the behavioural foundations of integrated land-use and transportation models: frameworks, models and applications. University of Toronto, pp 12–15

Xu G, Dong T, Cobbinah PB, Jiao L, Sumari NS, Chai B, Liu Y (2019a) Urban expansion and form changes across African cities with a global outlook: spatiotemporal analysis of urban land densities. J Clean Prod 224:802–810

Xu T, Gao J, Coco G (2019b) Simulation of urban expansion via integrating artificial neural network with Markov chain–cellular automata. Int J Geogr Inf Sci 33(10):1960–1983

Xue M, Zhang X, Sun X, Sun T, Yang Y (2021) Expansion and evolution of a typical resource-based mining city in transition using the google earth engine: a case study of datong China. Remote Sens 13 (20):4045

Yang Y, Yang D, Wang X, Zhang Z, Nawaz Z (2021) Testing accuracy of land cover classification algorithms in the qilian mountains based on gee cloud platform. Remote Sens 13(24):5064

Yeh AGO, Li X (2001) Measurement and monitoring of urban sprawl in a rapidly growing region using entropy. Photogramm Eng Remote Sens 67(1):83–90

Zurqani HA, Post CJ, Mikhailova EA, Allen JS (2019) Mapping urbanization trends in a forested landscape using Google Earth Engine. Remote Sens Earth Syst Sci 2(4):173–182

Multi-temporal Dynamics of Land Use Land Cover Change and Urban Expansion in the Tropical Coastal District of Kozhikode

4

Aakriti Grover and Ashique Vadakkuveettil

Abstract

Man is more dependent on the environment than any other species, but his relentless pursuit of development, comfort, and security has exacerbated environmental stress, resulting in changes in land use and land cover over time. Urbanization is one of the leading causes of this phenomenon. By 2030, 60% of the world's population is projected to reside in urban areas, with one in three people residing in cities with populations of at least 500,000. Understanding the significant urbanization trends anticipated to emerge in the coming years is essential for implementing the 2030 Agenda for Sustainable Development and advancing efforts to develop a new urban planning framework. This study examines the change in land use and land cover in the Kozhikode district between 1993 and 2018. A supervised approach with a maximum likelihood algorithm has been utilized for classification purposes. Afterward, change detection analysis is carried out. In addition, the overall spatiotemporal characteristics of city growth in the Kozhikode Urban Area (KUA) are computed using a combination of remotely sensed data and GIS-based buffer gradient analyses. The findings indicate that extensive areas of vegetation have been transformed into urban areas. Moreover, the concentration of built-up area was primarily confined within 2 km of the city center and decreased as one moved away from the city center, indicating that the concentration of urbanization in 1993 was in the vicinity of the urban core. On the other hand, as one moves away from the city center in 2018, a growing trend of urbanized areas is observed. In addition, numerous census towns were developed and merged with the primary urban area, resulting in the rapid growth of the city. This study advocates for appropriate stakeholder action in this matter, given that this growth and merger is occurring without prior planning.

4.1 Introduction

Rapid changes in land use and land cover as a result of urbanization have a substantial impact on biodiversity and ecosystem function, as well as local and regional climate (Choudhury et al. 2019; Luck and Wu 2002; Vadakkuveettil and

A. Grover · A. Vadakkuveettil (✉)
Department of Geography, Central University of Tamil Nadu, Thiruvarur, India
e-mail: ashique.vv@outlook.com

Grover 2022). Changes in land cover caused by land use do not necessarily indicate land degradation. Nonetheless, many shifting land use patterns driven by a variety of social causes result in land cover changes that impact biodiversity, water and radiation budgets, trace gas emissions, and other processes that collectively affect climate and biosphere (Riebsame et al. 1994). Population growth and the ongoing demand for housing and other amenities are inextricably linked to human responses to environmental and sociocultural stimuli which is one cause for the increase in urbanized land (Antrop 2004; Kulkarni and Ramachandra 2006; Viana et al. 2019). This process has led to the spontaneous or unplanned development of typically dispersed and inefficient urban areas (Ewing and Hamidi 2015; Hasse and Lathrop 2003).

The strategies of smart growth and sustainable development of urban regions will depend upon improvements in our knowledge of the causes, chronology, and impacts of the process of urbanization and its driving forces (McKinney 2006; Paul and Meyer 2001; Potter and Unwin 1995; Swenson and Franklin 2000; Weng 2007). Hence, land use/land cover (LULC) information and the morphology and evolution of cities due to urban sprawl have long been hot topics in geographic research and urban planning to understand, represent, and model the complex urban system (Antrop 2004; Bryant 2006; Douglass 1998; Gaubatz 1999; Li et al. 2010; Sudhira et al. 2004). Continual, historical, and precise information about the LULC changes of the Earth's surface is extremely important for any kind of sustainable development program, in which LULC serves as one of the major input criteria. Thus, analyzing and mapping both the present LULC situation as well as the changes in LULC over time is recognized as important to better understand and provide solutions for social, economic, and environmental problems (Das 2009; Lu et al. 2004; Pelorosso et al. 2009). Also, such studies are essential for the selection, planning, and implementation of management strategies to meet the increasing demands for basic human needs and welfare of the ever-growing population.

Remote sensing and GIS are effective tools for deriving accurate and timely data on the spatial distribution of land use and land cover. GIS offers a versatile environment for collecting, storing, displaying, and analyzing the digital data required for LULC detection (Anji Reddy 2001). With the development of remote sensing and GIS techniques, land use/land cover mapping has become a useful and comprehensive tool for enhancing the selection of agricultural, urban, and industrial areas within a region (Selçuk et al. 2003). Since the end of the twentieth century, advances in GIS and information technologies have contributed to a substantial increase in research studies focusing on patterns of urban growth and its effects on human life and natural resources (Terzi and Bolen 2009). These studies facilitate comprehensive monitoring of physical changes over time. Although extensive study has been conducted on LULC, comparatively little has been conducted on Kozhikode, despite the fact that it is one of India's fastest-growing cities (Navaneeth et al. 2021; Nishara et al. 2021; Wihbey 2016). According to a research by UN Environment and the Lincoln Institute of Land Policy, Kozhikode is the urban habitat with the highest rate of growth. In a study of 200 cities from around the world, 17 were from India, and Kozhikode topped the list (www.zinfog.com). However, there have been relatively few substantial research conducted on this topic, which calls for attention. Consequently, this article will throw light on these concerns.

4.2   Study Area

Kozhikode is one of the coastal districts of Kerala (Fig. 4.1). Kozhikode district is bordered on the north by Kannur district, on the east by Wayanad district, on the south by Malappuram district, and on the west by Lakshadweep Sea. It is located between north latitudes 11° 08′ and 11° 50′ and east longitudes 75° 30′ and 76° 8′. It is precipitating on sections of Survey of India Toposheets 58 A and 49 M (T&CP Department Kozhikode 2015).
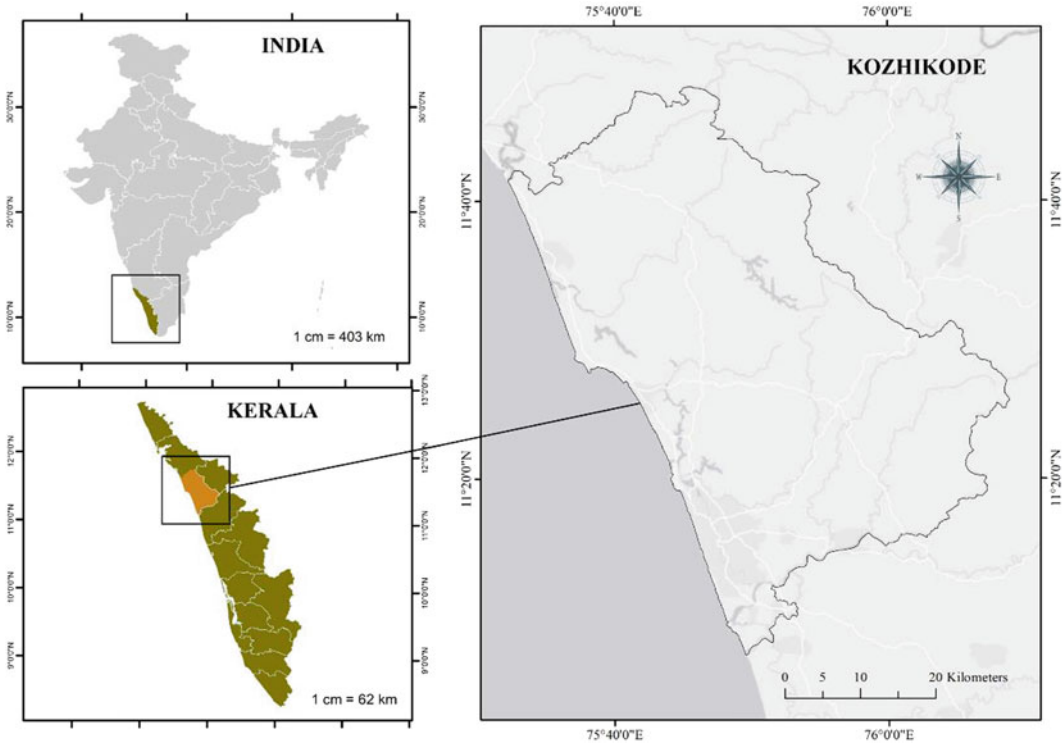
Fig. 4.1 Study area map

The district has an area of 2344 km^2 and is accessible by road, rail, and air (Vadakkuveettil et al. 2022). The district is traversed by NH-17, which connects Cochin and Mangalore. Kozhikode, the district capital, is well connected by road to the rest of the state. The Trivandrum–Mangalore–Mumbai railway runs through the district. The Kozhikode airport, which operates several international flights to Gulf countries, is located at Karipur in Malappuram district, very close to Kozhikode city. Kozhikode city in the Kozhikode district is currently one of the world's fastest-growing cities (Navaneeth et al. 2021; Nishara et al. 2021).

4.3 Data Sources and Methodology

The methodology used in this study to create land cover maps from satellite images consists of the following phases: Acquisition of the satellite imageries, pre-processing of satellite images, creation of the training dataset, classification of satellite images, accuracy assessment, change detection analysis, and urban expansion map (Fig. 4.2).

This study utilized Landsat 5 Thematic Mapper I and Landsat 8 Operational Land Imager (OLI) multi-spectral digital satellite data obtained from the United States Geological Survey (USGS) website (https://earthexplorer.usgs.gov/). Landsat 5 images were acquired on January 23, 1993, and January 2, 1997, while Landsat 8 images were acquired on February 2, 2014, and November 28, 2018. Landsat 7 Enhanced Thematic Mappers (ETM+) have been discarded because the Scan-Line corrector has been malfunctioning since 2003, resulting in approximately 22% scene loss (Viana et al. 2019). The quality of the image and the absence of cloud cover influenced the selection of available Landsat satellite images (All images have less
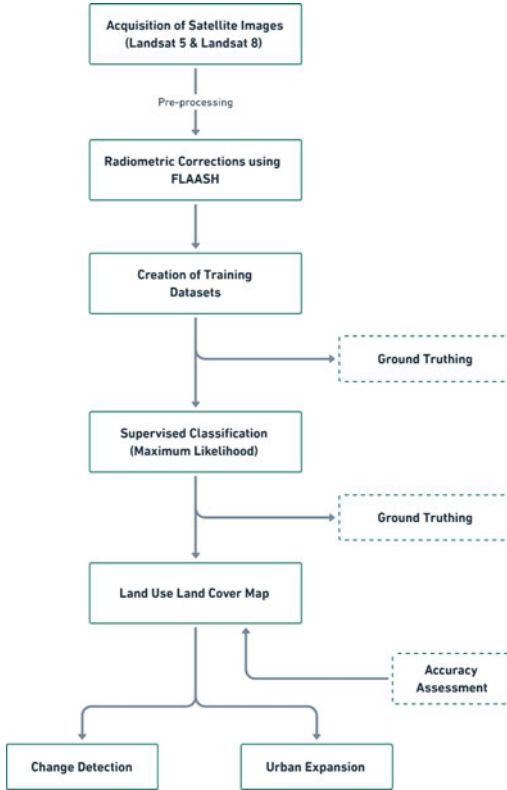
Fig. 4.2 Methodology flow chart

than 2% land cloud cover). When using multi-date images from different sources, different atmospheric and terrain conditions may cause data variations. Because the images initially reported top of atmosphere (TOA) reflectance, radiometric corrections, including atmospheric correction, were used in this study to convert their values to bottom of atmosphere reflectance. The Environment for Visualizing Images (ENVI) software package's Fast Line-of-Sight Atmospheric Analysis of Spectral Hypercubes (FLAASH) module was used to make this correction (Nazeer et al. 2014).

The study area is classified into five major land cover classes as per the NRSC and ISRO's level 1 land use/land cover classification (Arveti et al. 2016), i.e., vegetation, built-up area, agricultural land, waterbodies, and waste land, using a supervised technique combined with the

maximum likelihood classification method in ArcGIS 10.8. For supervised classification, well-distributed regions of visually homogeneous spectral response (30–40 training samples per class) were selected. These features are also known as area of interest (AOI). In addition, these AOI are added to the editor for spectral signatures. Using Google Earth, pre-classification ground truth was utilized to aid in the selection of training samples. The land use and land cover classes derived from digital image classification were validated using data from post-classification limited ground verification and high-resolution Google Earth images. Finally, an evaluation of accuracy has been conducted. Microsoft Office Excel 2019, IBM SPSS Statistics 20, and OriginPro 2021 were used to create all statistical calculations and graphs.

The accuracy of the classified images was evaluated using a random sample of 330 points for each year. For the years 1993, 1997, 1998, and 2018, the overall accuracy of the classified maps is 0.92, 0.94, 0.97, and 0.95, respectively. The year-specific Kappa coefficients are 0.88, 0.92, 0.95, and 0.93. The value of Kappa is always less than or equal to 1. A high Kappa value indicates more accurate information. According to the classification provided by Monserud and Leemans (1992), the accuracy of the classified land use is in excellent accord with the real world.

Following this, change detection analysis is performed. Utilizing at least two period data sets is required to detect changes in land use/land cover. In this study, four independently classified photos for the years 1993, 1997, 2014, and 2018 were compared post-classification to provide a change detection analysis. In addition, this study employed a GIS-based buffer analysis that incorporated circular buffer zones encircling the city center to study the urban expansion. Each buffer zone was used as a fundamental spatial unit to characterize distance-dependent urban growth behavior with their constructed area values over a specified time period.

4.4   Results and Discussion

4.4.1   Land Use Land Cover Classification

Land use maps were extracted for four years in accordance with classification criteria using the corrected remote sensing image. Land use was classified into five types. The LULC classification of KUA for the years 1993 and 2018

indicates significant differences in land use and land cover patterns (Figs. 4.3, 4.4 and 4.5, Tables 4.1 and 4.2). Out of the total area in 1993, vegetation accounted for the largest proportion (75.58%), followed by agricultural land (15.75%). Built-up, waste land, and waterbodies covered a small area, accounting for only 3.85%, 2.86% and 1.95% of the total, respectively. In 1997, the pattern remained almost similar; however, there was a slight decrease in
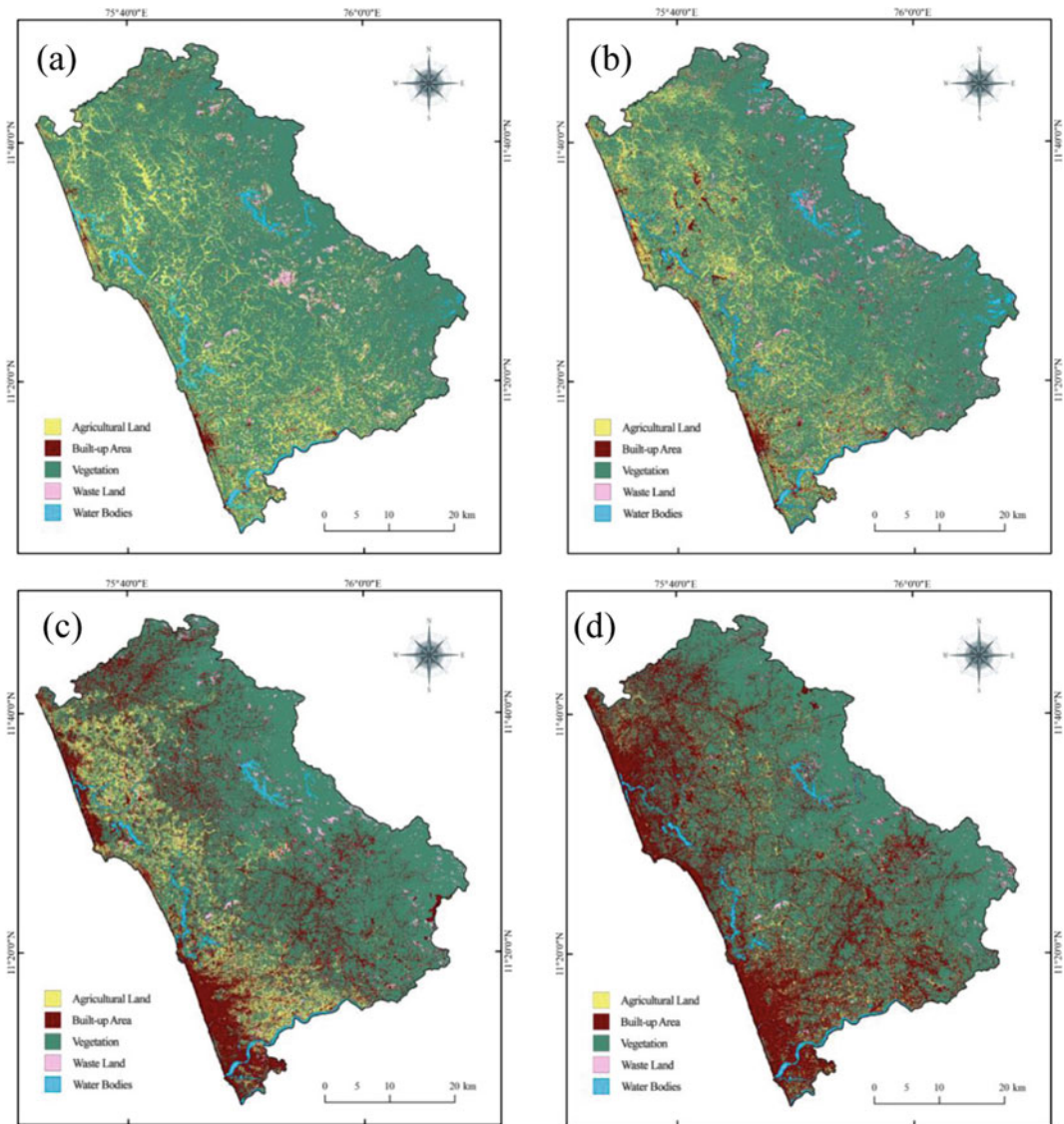

Fig. 4.3 LULC map of the Kozhikode District for the years **a** 1993, **b** 1997, **c** 2014, and **d** 2018
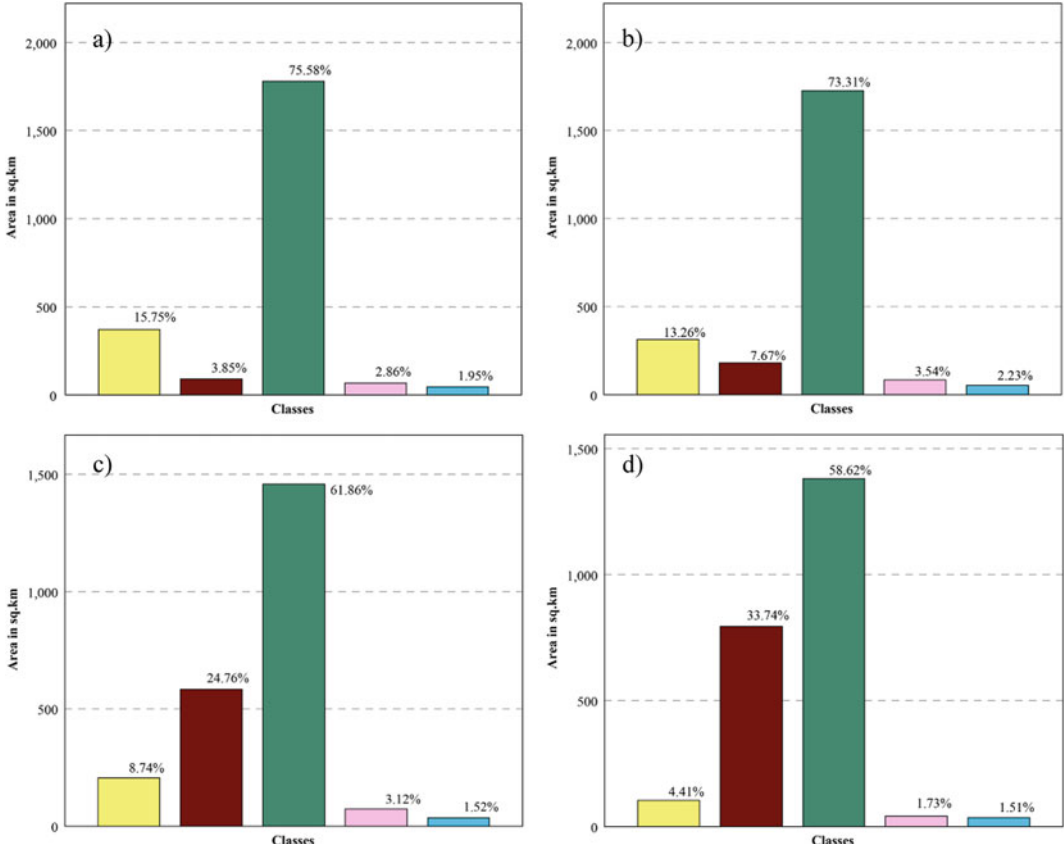
Fig. 4.4 Percentage of area under different LULC classes for the years **a** 1993, **b** 1997, **c** 2014, and **d** 2018

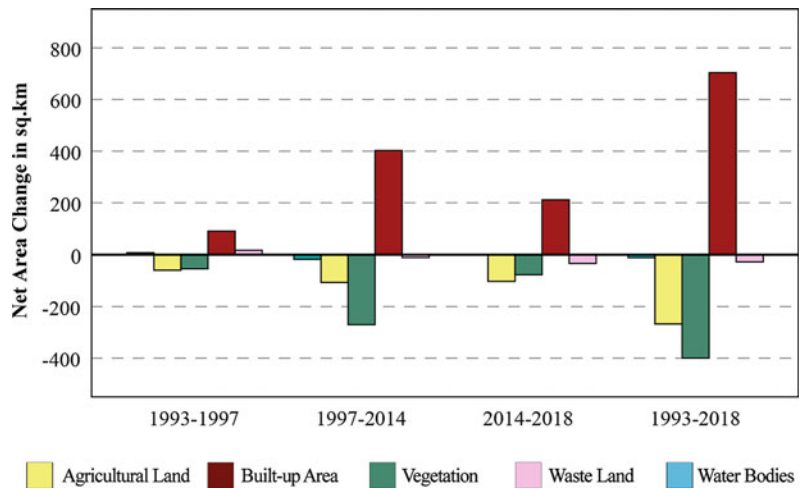**Fig. 4.5** Net area change of LULC classes in different time intervals

Table 4.1 Area under different LULC classes for the years 1993, 1997, 2014, and 2018

Land cover classes	Area (in km^2) 1993	Area (in km^2) 1997	Area (in km^2) 2014	Area (in km^2) 2018
• Water bodies	46.04	52.51	35.92	35.51
• Agricultural land	371.17	312.39	205.88	103.83
• Vegetation	1780.70	1727.30	1457.48	1381.16
• Built-up area	90.77	180.60	583.38	794.90
• Waste land	67.43	83.31	73.44	40.71
Total area	2356.11	2356.11	2356.11	2356.11

Table 4.2 Net area changes of LULC classes in different time intervals

Land cover classes	Net area change (in km^2)			
	1993–1997	1997–2014	2014–2018	1993–2018
Water bodies	6.47	−16.58	−0.41	−10.53
Agricultural land	−58.78	−106.51	−102.05	−267.34
Vegetation	−53.41	−269.81	−76.32	−399.54
Built-up area	89.83	402.78	211.52	704.13
Waste land	15.88	−9.87	−32.73	−26.72

vegetation area (73.21%) while an increase in built-up area (7.67%). Compared with 1993 and 1997, evident changes in the land use types had occurred by 2014 and 2018. The greatest increase in area is found in built-up area, i.e., 180.60 km^2 of area in 1997 increased to 583.38 km^2 (24.76%) in 2014, which augmented to 794.90 (33.74%) in 2018. The total built-up area increased by 704.13 km^2 during the 25-year period. Immigrants from the Middle East spurred an economic boom in Kozhikode, which is one of the major reasons for the increase in built area (Veettil and Grondona 2018; Zachariah and Rajan 2015). However, the area of vegetation and agriculture has decreased by 399.54 km^2 and 267.34 km^2, respectively, in this time span. To varying degrees, water bodies and waste lands also decreased.

The results of the change detection analysis clearly demonstrate that the majority of agricultural lands and vegetated regions have vanished as urban settlements have expanded (Figs. 4.6 and 4.7). Change detection is highly effective for analyzing urban landscape pattern changes (Batisani Yarnal 2009; Chen et al. 2009; Dewan and Yamaguchi 2009; El-kawy et al. 2011).

4.4.2 Urban Expansion

To gain a better understanding of the city's growth, a buffer analysis is performed by constructing seven concentric rings, each with a 2 km radius (Fig. 4.8). The Valiyangadi market is regarded as the city center for the purposes of this buffer analysis. In 1993 and 1997, the concentration of built-up area was largely confined within 2 km of the city center, with a total area of 5.35 km^2 and 6.72 km^2, respectively; this concentration decreased as one moved away from the city center (Figs. 4.8, 4.9 and Table 4.3). In the 1990s, most urban activities were confined to the vicinity of the Valiyangadi market, making the 2 km radius highly packed, which indicates that the urbanization intensity in 1993 and 1997 was concentrated in the immediate locality of urban centers. Beyond 2 km, there is a consistent decline in the density of built-up. Contrary to that, in 2014 and 2018, there can be seen an increasing trend of built-up areas while moving away from the city center. As the inner core of the city highly saturated with built-ups, the outlying buffers began to expand. The maximum increment of the built-up
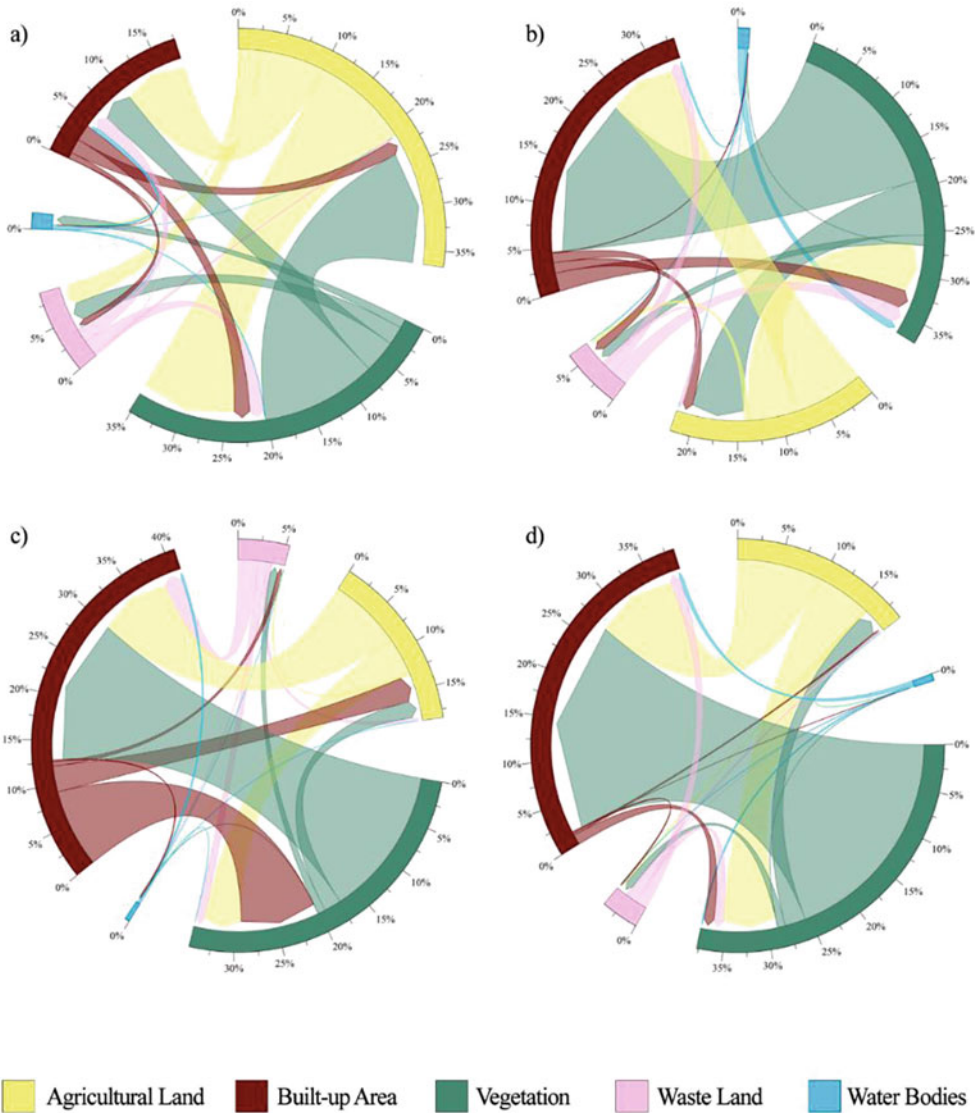
Fig. 4.6 Percentage of LULC transition between **a** 1993–1997, **b** 1997–2014, **c** 2014–2018, **d** 1993–2018

area can be observed within 6 and 8 km radius. However, after 8 km, there can be seen a decreasing trend in the built-up area. The least urban expansion occurred within a 2 km radius, which may be attributed to the scarcity of available space, the high cost of land, and the presence of diverse economic activities within the old city region. In summary, the emergence of various census towns that amalgamated with the city and expanded its size is a key factor in Kozhikode city's expansion. This quick development of Kozhikode was fueled by the real estate and gulf booms (Zachariah and Rajan 2015).
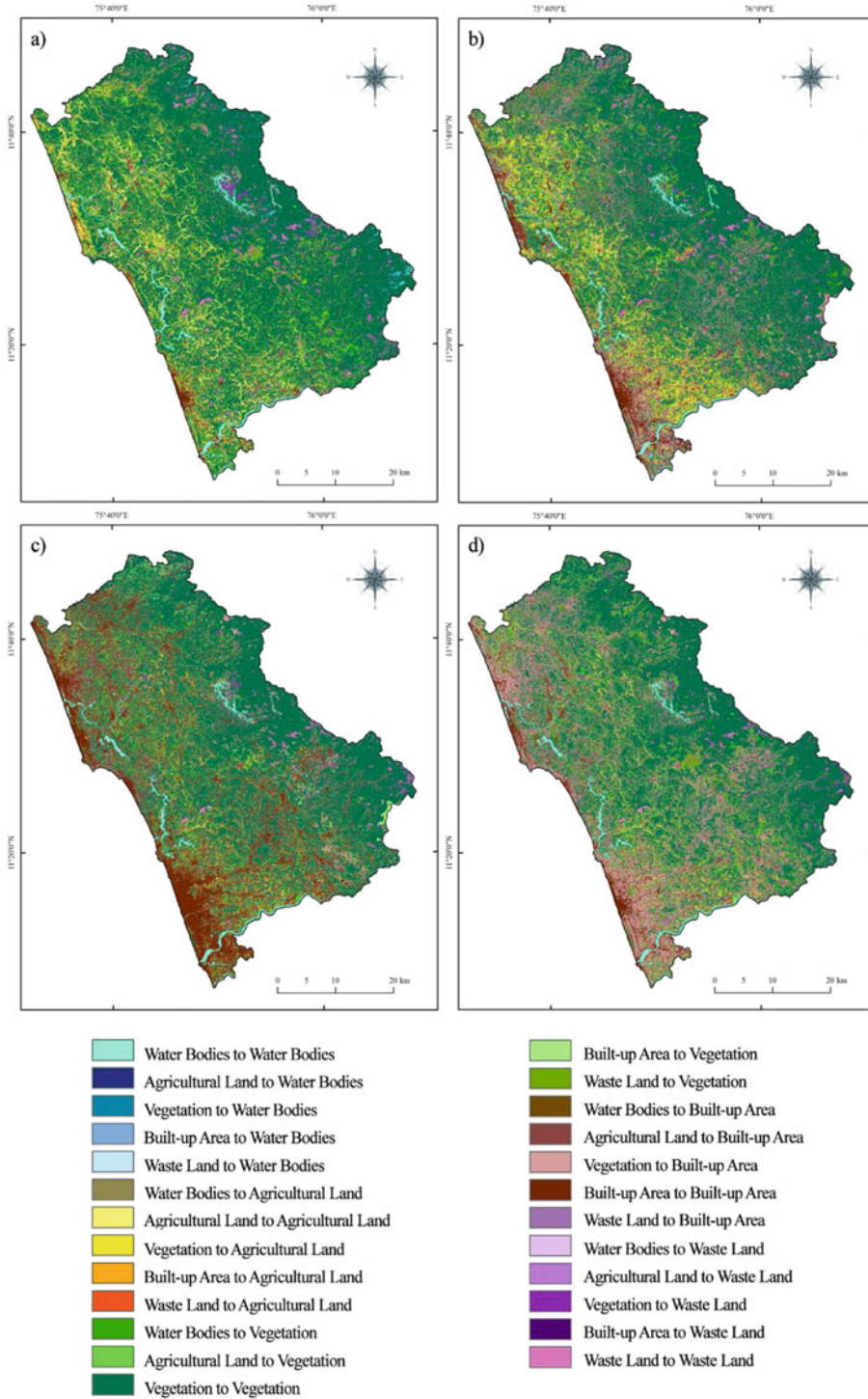
Fig. 4.7 Change detection map
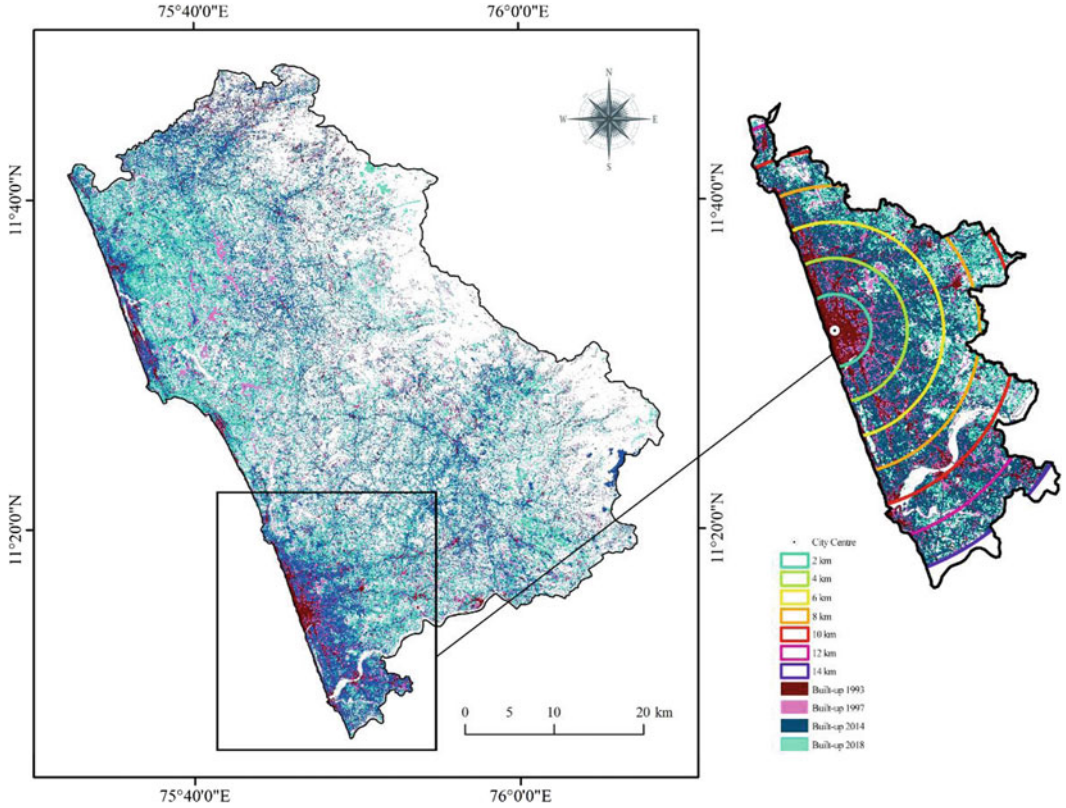
Fig. 4.8 Zone-wise urban expansion map of Kozhikode district

Fig. 4.9 Zone-wise urban expansion graph of Kozhikode district
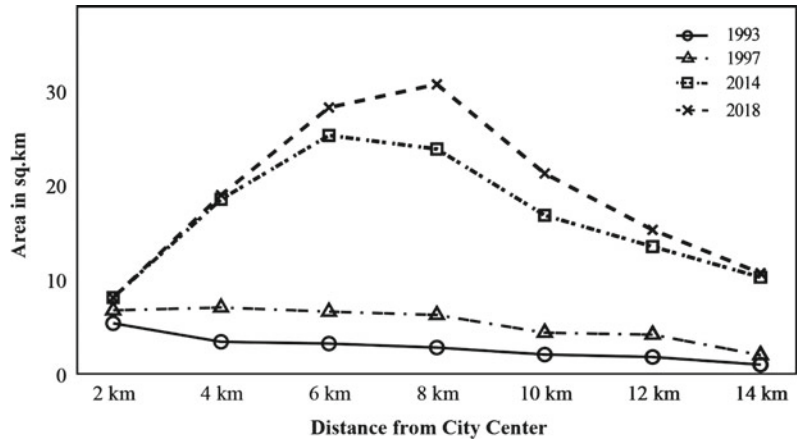
Table 4.3 Net area change of urbanization in different time intervals

Distance from city center	Urban area in km^2				Net area change in km^2			
	1993	1997	2014	2018	1993–1997	1997–2014	2014–2018	1993–2018
2	5.35	6.72	8.07	8.06	1.37	1.35	0.00	2.71
4	3.39	7.02	18.48	18.93	3.64	11.46	0.45	15.55
6	3.20	6.58	25.24	28.19	3.38	18.65	2.95	24.99
8	2.78	6.23	23.80	30.65	3.44	17.57	6.85	27.87
10	2.04	4.35	16.78	21.21	2.32	12.43	4.43	19.18
12	1.78	4.14	13.47	15.24	2.35	9.33	1.77	13.45
14	0.97	1.98	10.23	10.66	1.01	8.25	0.43	9.69

4.5   Conclusion

In this study, the land use and land cover of the Kozhikode district have been analyzed using Landsat 5 and Landsat 8 satellite images for the years 1993, 1997, 2014, and 2018. According to the findings, huge amounts of vegetation in the district have been converted to built-up areas. Urban areas are rapidly developing at the expense of vegetated and agricultural areas. As stated in this study, built-up areas were confined to a restricted level, i.e., within the vicinity of the city, which later on unbind to the larger vegetated and agricultural area. Consequently, city and town planners, as well as government officials, who seek a more thorough understanding of the urban environment in order to plan for sustainable growth, can rely on these kinds of studies. The importance of urban planning in the city of Kozhikode was highlighted in this study, as vegetative areas are being converted to built-up areas at an alarming rate without planning. The results of this research work have the potential to provide some insight on the critical significance of immediate planning intervention that is required in Kozhikode.

References

Anji Reddy M (2001) Textbook of remote sensing and geographical information systems. S. Publications, Hyderabad

Antrop M (2004) Landscape change and the urbanization process in Europe. Landscape Urban Plann 67(1):9–26. https://doi.org/10.1016/S0169-2046(03)00026-4

Arveti N, Etikala B, Dash P (2016) Land use/land cover analysis based on various comprehensive geospatial data sets: a case study from Tirupati Area South India. Adv Remote Senss 05(02):73–82. https://doi.org/10.4236/ars.2016.52006

Batisani N, Yarnal B (2009) Urban expansion in Centre County, Pennsylvania: spatial dynamics and landscape transformations. Appl Geogr 29(2):235–249

Bryant MM (2006) Urban landscape conservation and the role of ecological greenways at local and metropolitan scales. Landsc Urban Plan 76(1–4):23–44

Chen LQ, Wang L, Yuan LS (2009) Analysis of urban landscape pattern change in Yanzhou city based on TM/ETM+ images. Proc Earth Planet Sci 1(1):1191–1197. https://doi.org/10.1016/J.PROEPS.2009.09.183

Choudhury D, Das K, Das A (2019) Assessment of land use land cover changes and its impact on variations of land surface temperature in Asansol-Durgapur Development Region. Egypt J Remote Sens Space Sci 22(2):203–218. https://doi.org/10.1016/j.ejrs.2018.05.004

Das T (2009) Land use/land cover change detection: an object oriented approach. Münster, Germany

Dewan AM, Yamaguchi Y (2009) Land use and land cover change in Greater Dhaka, Bangladesh: using remote sensing to promote sustainable urbanization. Appl Geogr 29(3):390–401. https://doi.org/10.1016/J.APGEOG.2008.12.005

Douglass M (1998) A regional network strategy for reciprocal rural-urban linkages: an agenda for policy research with reference to Indonesia. Third World Plann Rev 20:1–34

El-kawy ORA, Rød JK, Ismail HA, Suliman AS (2011) Land use and land cover change detection in the western Nile delta of Egypt using remote sensing data. Appl Geogr 31(2):483–494. https://doi.org/10.1016/j.apgeog.2010.10.012

Ewing R, Hamidi S (2015) Compactness versus Sprawl: a review of recent evidence from the United States. J Plan Lit 30(4):413–432. https://doi.org/10.1177/0885412215595439

Gaubatz P (1999) China's urban transformation: patterns and processes of morphological change in Beijing Shanghai and Guangzhou. Urban Stud 36(9):1495–1521

Hasse JE, Lathrop RG (2003) Land resource impact indicators of urban sprawl. Appl Geogr 23(2):159–175. https://doi.org/10.1016/j.apgeog.2003.08.002

Kozhikode—The Fastest Growing Metropolis|Website development Company. (n.d.). Retrieved June 21, 2022, from https://zinfog.com/blog/kozhikode_-_the_fastest_growing_metropolis.html

Kulkarni V, Ramachandra TV (2006) Environmental management. The Energy and Resources Institute (TERI)

Li X, Zhang L, Liang C (2010) A GIS-based buffer gradient analysis on spatiotemporal dynamics of urban expansion in Shanghai and its major satellite cities. Procedia Environ Sci 2:1139–1156. https://doi.org/10.1016/j.proenv.2010.10.123

Lu D, Mausel P, Brondizio E, Moran E (2004) Change detection techniques. Int J Remote Sens 25(12):2365–2401

Luck M, Wu J (2002) A gradient analysis of urban landscape pattern: a case study from the Phoenix metropolitan region, Arizona, USA. Landscape Ecol 17(4):327–339. https://doi.org/10.1023/A:1020512723753

McKinney ML (2006) Urbanization as a major cause of biotic homogenization. Biol Conserv 127(3):247–260. https://doi.org/10.1016/j.biocon.2005.09.005

Monserud RA, Leemans R (1992) Comparing global vegetation maps with the Kappa statistic. Ecolog Modell 62(4):275–293. https://doi.org/10.1016/0304-3800(92)90003-W

Navaneeth A, Sreeda P, Vishnu Maya TM, Sanusree PS, Harikumar PS (2021) Evaluation of the challenges in water governance through citizen's perception and Water Quality Index: a case study of a fast-growing city in India. H2Open J 4(1):336–351. https://doi.org/10.2166/h2oj.2021.106

Nazeer M, Nichol JE, Yung YK (2014) Evaluation of atmospheric correction models and Landsat surface reflectance product in an urban coastal environment. Int J Remote Sens 35(16):6271–6291. https://doi.org/10.1080/01431161.2014.951742

Nishara VP, Sruthi Krishnan V, Firoz CM (2021) Geo-intelligence-based approach for sustainable development of peri-urban areas: a case study of Kozhikode City, Kerala (India). In: Geo-intelligence for sustainable development. Springer, pp 35–52

Paul MJ, Meyer JL (2001) Streams in the urban landscape. Annu Rev Ecol Syst 32(1):333–365

Pelorosso R, Leone A, Boccia L (2009) Land cover and land use change in the Italian central Apennines: a comparison of assessment methods. Appl Geogr 29(1):35–48

Potter RB, Unwin T (1995) Urban-rural interaction: physical form and political process in the Third World. Cities 12(1):67–73. https://doi.org/10.1016/0264-2751(95)91866-E

Riebsame WE, Meyer WB, Turner BL (1994) Modeling land use and cover as part of global environmental change. Clim Change 28(1):45–64. https://doi.org/10.1007/BF01094100

Selçuk R, Nisanci R, Uzun B, Yalcin A, Inan H, Yomralioglu T (2003) Monitoring land-use changes by GIS and remote sensing techniques: case study of Trabzon. Proceedings of 2nd FIG regional conference, Morocco, pp 1–11

Sudhira HS, Ramachandra TV, Jagadish KS (2004) Urban sprawl: metrics, dynamics and modelling using GIS. Int J Appl Earth Obs Geoinf 5(1):29–39

Swenson JJ, Franklin J (2000) The effects of future urban development on habitat fragmentation in the Santa Monica Mountains. Landscape Ecol 15(8):713–730. https://doi.org/10.1023/A:1008153522122

T&CP Department Kozhikode (2015) Master plan for Kozhikode urban area—2035, pp 1–400

Terzi F, Bolen F (2009) Urban sprawl measurement of Istanbul. Eur Plan Stud 17(10):1559–1570

Vadakkuveettil A, Grover A (2022) Assessing the intensity of land surface temperature in Thiruvarur district (India). Evaluación de la intensidad de la temperatura de la superficie terrestre en el distrito de Thiruvarur (India). Sustainability, Agri, Food and Environmental Research, 12

Vadakkuveettil A, Grover A, Menon R (2022) Expeditious response to epidemics: the chronicle of Nipah in Kerala. J Global Resour 08(07):127–132. https://doi.org/10.46587/jgr.2022.v08i01.015

Veettil BK, Grondona AEB (2018) Vegetation changes and formation of small-scale urban heat islands in three populated districts of Kerala State India. Acta Geophys 66(5):1063–1072. https://doi.org/10.1007/s11600-018-0189-z

Viana CM, Oliveira S, Oliveira SC, Rocha J (2019) Land use/land cover change detection and urban sprawl analysis. Spat Model GIS R Earth Environ Sci. https://doi.org/10.1016/b978-0-12-815226-3.00029-6

Weng YC (2007) Spatiotemporal changes of landscape pattern in response to urbanization. Landscape Urban Plann 81(4):341–353. https://doi.org/10.1016/j.landurbplan.2007.01.009

Wihbey J (2016) Boundary issues: the 2016 atlas of urban expansion indicates global dedensification. Land Lines 19(Special):19–25. https://www.lincolninst.edu/publications/articles/boundary-issues

Zachariah KC, Rajan SI (2015) Dynamics of emigration and remittances in Kerala: results from the Kerala migration survey 2014. Center Develop Studs Working Paper 4:631–102. http://cds.edu/wp-content/uploads/2015/10/WP463.pdf

Land Use Land Cover Change Modeling and Future Simulation in Mumbai City by Integrating Cellular Automata and Artificial Neural Network

5

Mohd Waseem Naikoo, Shahfahad,
Swapan Talukdar, Tanmoy Das,
Mansoor Ahmad, Asif, Mohammad Ishtiaque,
and Atiqur Rahman

Abstract

The rapid urbanization driven by population growth and economic development has led to a drastic transformation of urban landscape in the cities of developing countries. As a result, large-scale changes in the urban land use land cover (LULC) pattern have been noted in recent decades. The present study is intended to study the LULC changes in the financial capital of India that is Mumbai city from 1991 to 2018 as well as forecast LULC changes for 2030. The Landsat datasets has been used for the LULC mapping of 1991, 2001, 2011 and 2018. For the LULC classification, unsupervised classification has been used employing K means clustering technique. The kappa coefficient has been applied for examining the accuracy of classified LULC maps. The LULC changes have been forecasted for 2030 by integrating artificial neural networks (ANN) and cellular automata (CA). The results of the study show large-scale changes in all LULC categories. The built-up area of the Mumbai city has increased from 28 to 57% of the total area of the city from 1991 to 2018. The vegetation, crop land and open land have witnessed considerable decline in the coverage area from 1991 to 2018. The results of LULC forecasting shows that the built-up will increase from 55 to 66% of the total area in Mumbai by 2030. At the same time, the area under open land and vegetation will reduce from 10.26 to 3.79% and 23.33 to 21.19%, respectively, by 2030. The finding of this study may be utilized in the urban planning of Mumbai city and its adjacent areas.

M. W. Naikoo · Shahfahad · S. Talukdar · T. Das · Asif · M. Ishtiaque · A. Rahman (✉)
Department of Geography, Faculty of Natural Sciences, Jamia Millia Islamia, New Delhi 110025, India
e-mail: arahman2@jmi.ac.in

M. Ahmad
Department of Geography, University of Jammu, Jammu, Jammu and Kashmir 180006, India

5.1 Introduction

The process of urbanization is rapidly changing the landscape in the developing countries with higher concentration of population settling in the urban areas (Zhongming et al. 2020). This urbanization is mainly driven by the economic development, increased employment opportunities and

higher standards of living (Sarkar 2020; Crankshaw and Borel-Saladin 2019). The increasing concentration of population in the in urban centers results in large-scale changes in land uses in these cities (Hussain et al. 2020; Zope et al. 2016; Naikoo et al. 2022). The emerging land use patterns are characterized by the predominance of impervious surfaces and declining concentration of vegetation and crop land (Naikoo et al. 2020). The increased proportion of impervious surfaces has resulted in various environmental problems like urban heat island (Mallick et al. 2013), decline in urban landscape quality (Kumari et al. 2019), water logging (Zhang et al. 2016), decline in groundwater quality and quantity (Roy et al. 2020; Lorenzen et al. 2012), increase in urban crime (Patil and Sharma 2020), etc. Thus, mapping and monitoring of urban land use land cover (LULC) changes and urban growth are highly required in the developing cities of the world.

Remote sensing and geographical information system (GIS) have been successfully used in mapping the features as well as processes taking place on the surface of earth (Wentz et al. 2014; Chaminé et al. 2021). One of the most important and frequently used application of remote sensing and GIS is the mapping of changes taking place in LULC over the surface of earth (Dewan and Yamaguchi 2009). Different methodologies have been used for classification of LULC including maximum likelihood classification, K means clustering as well as machine learning algorithms (Talukdar et al. 2020; Wang and Maduako 2018). In the present study, K means clustering technique has been used for the LULC classification. The K means clustering has been commonly used to classify LULC in the Indian cities. Naikoo et al. (2020) used K means clustering for LULC classification of Delhi NCR and reported an accuracy level of more than 85%. Similarly, Viana et al. (2019) used K means clustering in Portugal for LULC classification with an overall accuracy level in excess of 80%. Several methodologies have also been developed and applied for the LULC probabilities as well as forecasting (Das et al. 2022; Singh et al. 2015). Important methodologies for LULC forecasting include cellular automata, SLEUTH model,

artificial neural networking, random forest model, Markov chain, agent-based models, etc. (Aburas et al. 2017). The application of these methodologies depends upon the availability of data and the objective of the study (Tripathy and Kumar 2019).

The Indian cities are witnessing large-scale changes in the redistribution of population due to rapid urbanization in last few decades with more population concentrating in the urban areas (Ahluwalia et al. 2014). As a result, the Indian cities are subjected to fast built-up expansion resulting in various issues like urban sprawl, congestion, environmental issues like UHI, pollution, loss of ecosystem services, etc., leading to unsustainable urban development (Gumma et al. 2017; Shahfahad et al. 2022; Das and Das 2019). Therefore, monitoring the LULC changes and built-up expansion is essential for sustainable growth of Indian cities. Studies have been done to monitor the LULC changes in the metropolitan cities of Indian including Delhi (Naikoo et al. 2020), Mumbai (Shahfahad et al. 2021), Chennai (Mathan and Krishnaveni 2020) and Kolkata (Mondal et al. 2016). In the context of Mumbai city, studies have been done to quantify the LULC changes (Shahfahad et al. 2021; Jain et al. 2021; Rahaman et al. 2021) however, none of these studies have analyzed sub-district-wise changes in LULC patterns and forecasted LULC patterns. Therefore, the present study is intended to assess the LULC changes in Mumbai city as well as forecast the same for 2030 using ANN based cellular automata.

5.2 Materials and Methods

5.2.1 Study Area

Mumbai is located at the western coast of India and is the largest metropolitan city in India in terms of population. Mumbai lies between 72° to 72°59′ E longitude and 18°53′ to 19°16′ N latitude spreading over 603 km^2 (Fig. 5.1). The city has a tropical moist type climate with mean annual rainfall above 250 cm (1901–2015) with higher concentration in the months of June to August
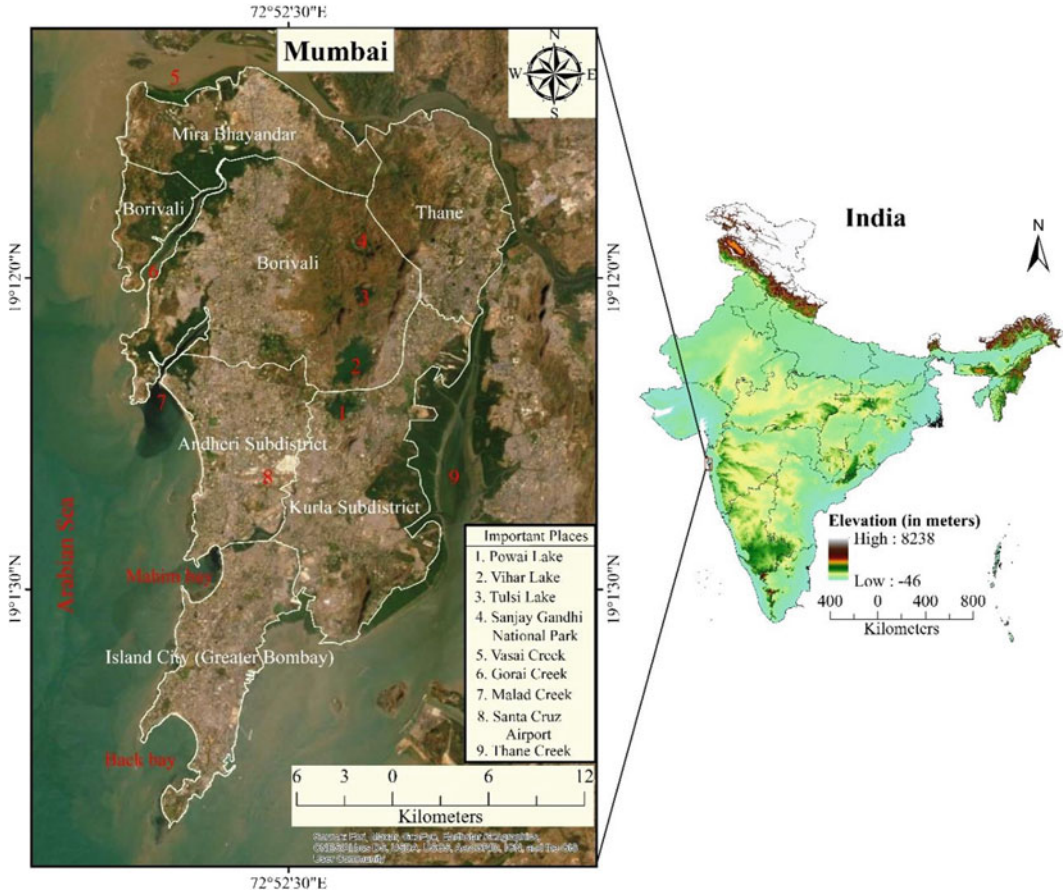
Fig. 5.1 Location of the study area

(Roy and Balling 2005). Mumbai city has an average relative humidity ranging from 54.5 to 85.5% (Rahaman et al. 2021). The Mumbai city has experienced rapid growth in population in recent decades due to higher financial prospects of the city. Mumbai city has witnessed rapid growth of population which has resulted in the degradation of environment leading to several eco-environmental problems in the city (Sarkar et al. 2020). According to the Mumbai Metropolitan Region Development Authority (MMRDA) report, nearly 5 million new housing units will be required to accommodate the increasing population of the city by 2022 (MMRDA 2016). Thus, the built-up area is expected to increase manifolds in coming decades.

5.2.2   Materials Used

The study is based on Landsat data downloaded from USA geological survey (USGS) website. Landsat (TM, ETM and OLI) data has been used for the year 1991, 2001, 2011 and 2018 to get the LULC classified images as well as for forecasting. The shapefile for Mumbai has been obtained from survey of India toposheet at a scale of 1:25,000. For LULC forecasting, eight conditioning variables have been used including elevation, slope, aspect, distance from built-up area, distance from water bodies, distance from vegetation, distance from transport network and population. The details of these conditioning variables have been presented in Table 5.1.

Table 5.1 Details of the satellite datasets used

Data	Criteria	LULC simulation	Description	Source	Year
DEM	Elevation	Conditioning parameters	SRTM DEM, 30-m resolution	https://earthexplorer.usgs.gov/	2014
	Slope	Conditioning parameters	SRTM DEM, 30-m resolution	https://earthexplorer.usgs.gov/	2014
	Aspect	Conditioning parameters	SRTM DEM, 30-m resolution	https://earthexplorer.usgs.gov/	2014
LULC	LULC	Input data	Landsat (TM, ETM+ & OLI)	https://earthexplorer.usgs.gov/	1991, 2001, 2011 & 2018
	Distance from built-up area	Conditioning parameters	Landsat (TM, & OLI)	https://earthexplorer.usgs.gov/	2011 & 2018
	Distance from vegetation	Conditioning parameters	Landsat (TM, & OLI)	https://earthexplorer.usgs.gov/	2011 & 2018
	Distance from water bodies	Conditioning parameters	Landsat (TM, & OLI)	https://earthexplorer.usgs.gov/	2011 & 2018
Transport network	Distance from Transport Network	Conditioning parameters	Major and minor roads	http://www.diva-gis.org/gdata	2011
Population	Population	Conditioning parameters	Grid-wise Population data	–	2011
City shapefile	City boundary	Input data	City boundary of Mumbai city	Survey of India Toposheet	2005

5.2.3 Methods

The present study is intended to study the LULC changes in Mumbai city as well as forecast its changes for 2030. For this purpose, satellite data has been used for LULC classification using unsupervised method. Further, with the help conditioning variables and ANN-based cellular automata, LULC changes have been simulated for 2030. The details of the methodology are presented in Fig. 5.2.

5.2.3.1 Satellite Data Pre-processing
The satellite data was downloaded from the Earth Explorer website of USGS, and then atmospheric and radiometric corrections were done to increase the image quality for easy interpretation and analysis. Various image correction and enhancement techniques available include haze and noise reduction, histogram equalization, filtering, image fusion, etc. (Lu and Weng 2007). In the present study, the layer staked images were subjected to atmospheric and radiometric correction including image fusion, haze and noise reduction as well as histogram equalization. Besides all the condition variables were resampled to fit the scale of the input parameters to that of LULC images.

5.2.3.2 LULC Classification and Accuracy Assessment
There are several methods for carrying out LULC classification including Iterative Self-Organizing Data Analysis Technique (ISODATA), K means clustering, etc. (Goncalves et al. 2008). In this study, LULC classification has been carried out

Fig. 5.2 Flowchart of the methodology
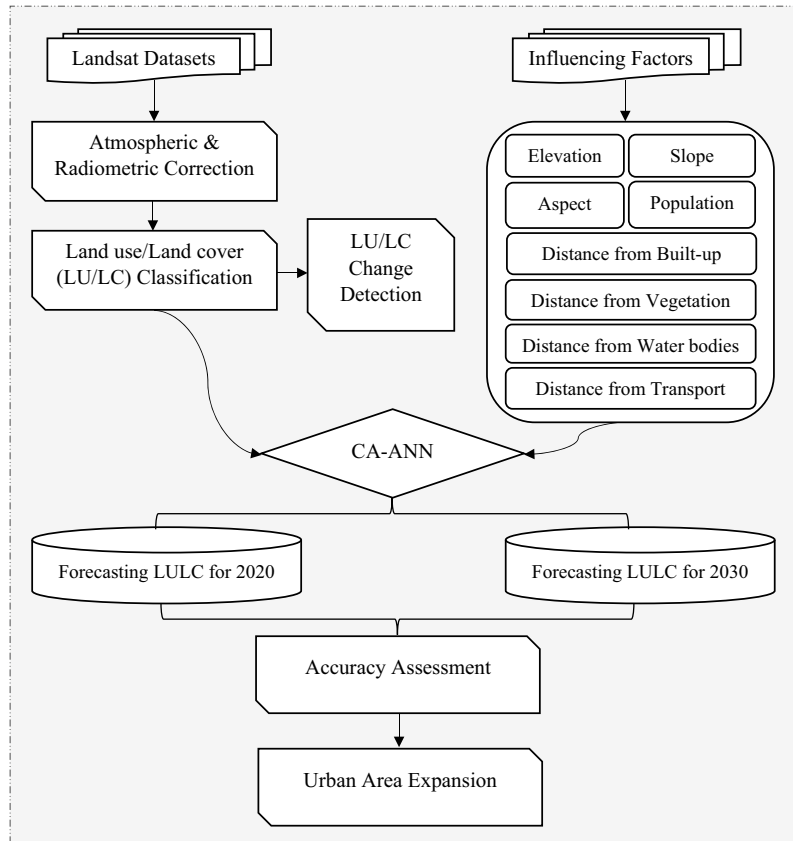
using K means clustering method in ERDAS Imagine software. K means clustering divides *m* number of observations on a m dimensional surface into k clusters (Gupta and Venkatesan 2020). A total of six major LULC classes have been identified in Mumbai, i.e., built-up, cropland, open land, water body, dense vegetation (forest) and sparse vegetation (scrubland) based on NRSC level I classification scheme. The identified classes were validated by field visits and the using GPS. Finally, LULC change was estimated using multi-temporal raster layers for 1991, 2001, 2011 and 2018 and comparing their corresponding statistics.

5.2.3.3 Preparation of the Conditioning Parameters for Future LULC Simulation

For simulation of LULC, some independent parameter needs to be identified that can explain the growth of LULC changes over time. Hence, in

this study, eight conditioning parameters have been identified namely elevation, slope, aspect, distance to waterbody, distance to built-up area, population and distance to transportation network (Fig. 5.3). Physical factors, i.e., elevation, slope and aspects, are considered as important factors that determine the LULC change (Birhane et al. 2019). Elevation, slope and aspect have been derived from Advanced Land Observing Satellite (ALOS) Polarimetric Phased Array L-band Synthetic Aperture Radar (PALSAR) digital elevation model. The population data has been taken from gridded population data taken from Socioeconomic Data and Applications Center (SEDAC) website hosted by Center for International Earth Science Information Network (CIESIN) at Columbia University. Population growth is the primary cause leading to the changes in LULC changes. Euclidian distance has been used to obtain the distance to built-up area, vegetation and water bodies from LULC images.
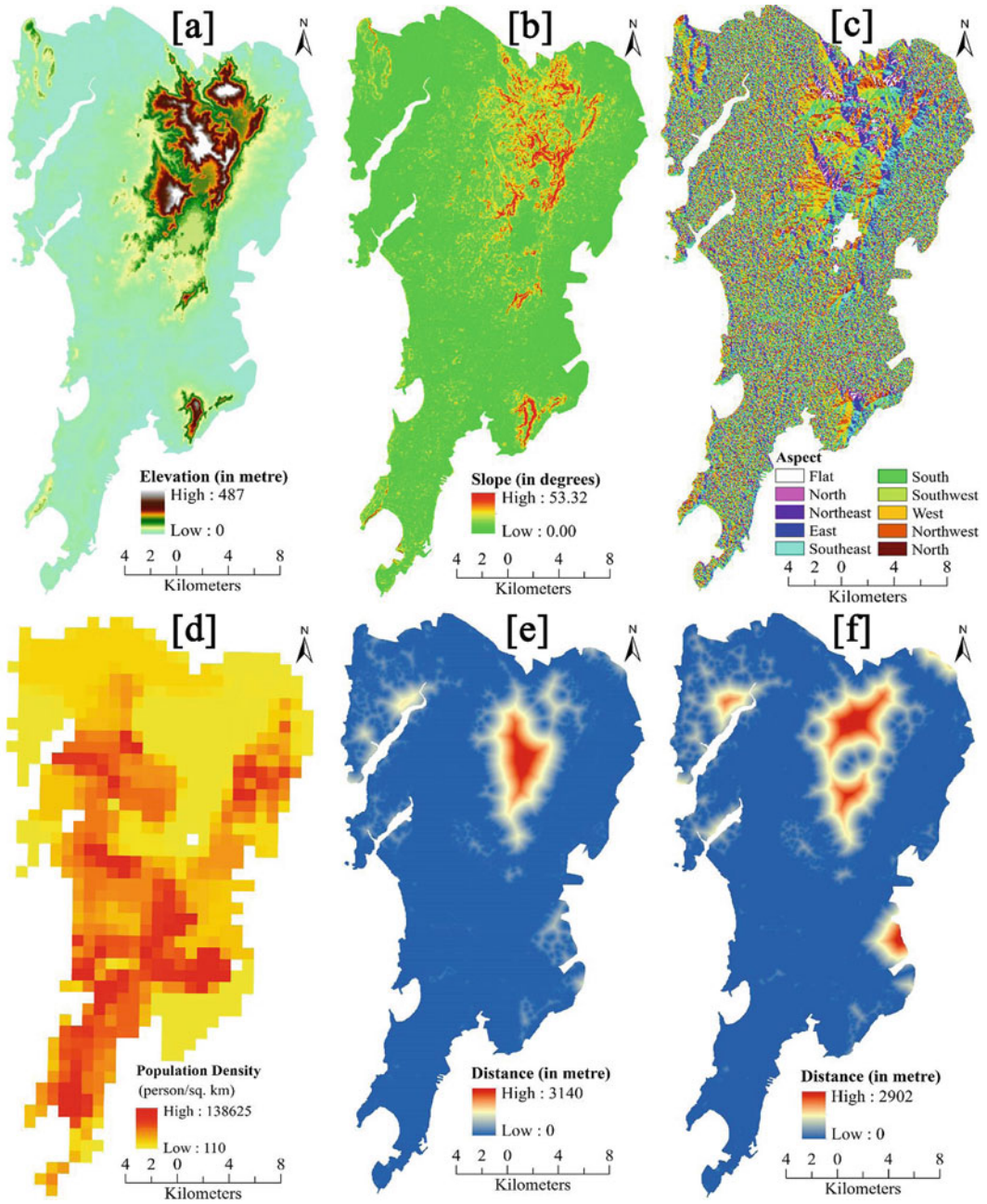
Fig. 5.3 LU/LC simulation conditioning parameters **a** elevation, **b** slope, **c** aspect, **d** population, **e** distance from built-up area 2011, **f** distance from built-up area 2018, **g** distance from transport network, **h** distance from vegetation 2011, **i** distance from vegetation 2018, **j** distance from water bodies 2011 and **k** distance from water bodies 2018
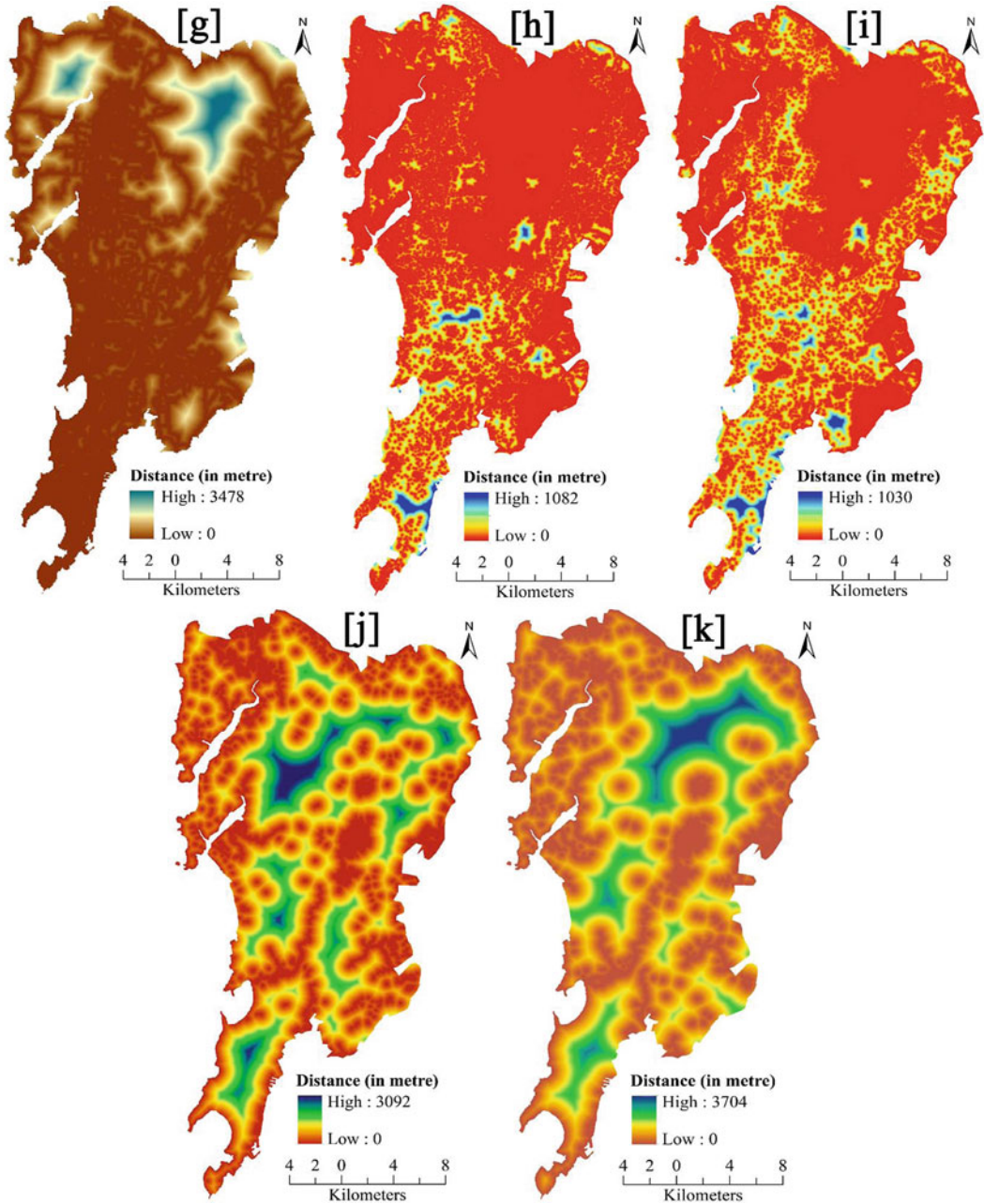
Fig. 5.3 (continued)

5.2.3.4 Simulation of Future LULC Pattern

The LULC changes have been simulated for 2030 using artificial neural network (ANN)-based cellular automata (CA). ANN estimates LULC transformation probabilities using multiple output neurons by simulating several LULC changes. The transition probabilities learnt from ANN learning process are used by the CA to simulate LULC changes (Saputra and Lee 2019). The CA-ANN model was applied in six steps using QGIS open-source software version 3.22.

In the first step, the input layers of neural network are defined to simulate the future LULC changes. The simulation process executes at pixel level, in which each pixel in the neural network gets input from n-attributes. The attributes in the neural network can be estimated using Eq. 5.1.

$$X = [x_1, x_2, x_3, \ldots\ldots\ldots, x_n]^{\mathrm{T}} \quad (5.1)$$

where x_1, x_2, x_3 are attributes, and T represents the transposition. In this step, the LULC maps of 1991, 2001, 2011 and 2018 along with all conditioning variables are used as input layers. These conditioning variables were resampled at 30 m resolution in raster format to match the resolution with the LULC images and for obtaining the attributes. In the second step, correlation between the conditioning variables was ascertained by two-way raster comparison, in which first raster is selected from one variable, while second raster is selected from different variables. Further, in this step, the change in area from starting raster to final raster is calculated, and transition matrix for the proportion of changed pixels was calculated.

In third step, transition probabilities were modeled using ANN. The structure of neural network is made up of three layers input layer, hidden layer and output layer. The input layer involves the resampling of each variable into 0 and 1, and each variable gets associated with a neuron. In hidden layer, the signal received by any neuron from input layer at any time is given by Eq. 5.2.

$$\mathrm{net}_j(k, t) = \sum_i w_{i,k} x'_i(k, t) \quad (5.2)$$

where $w_{i,k}$ describes the weight between the input and hidden layers; x'_i refers to the i scaled attribute which is associated with the neuron i in the input layer related to the k-th cell at time t. A total of 12 neurons have been used to get perfect fit of a continuous function in the neural networks. The output layer has 6 neurons which corresponds to the 6 LULC classes. Further, the neuron m in the output layer generates a value

which represents the transition probabilities from original LULC type m. The transition probability is calculated as per the output function in the neural network given by Eq. 5.3.

$$P(k, t, m) = \sum_j w_{j,m} \frac{1}{i + e - \mathrm{net}_j(k, t)'} \quad (5.3)$$

where $P(t, k, m)$ represents the possibility of conversion to m-class LULC at time t for the cell k, while $w_{j,1}$ refers to the refers to the weight between hidden layer and output layers.

The fourth step involves applying the CA model to simulate LULC change. The CA is made up of regular spatial grids of cells that can be used in any number of states, depending on the states of surrounding cells. It evaluates the structure of cell connections in the vicinity of a single cell. The validation of simulated LULC maps was completed in next step, followed by a comparison of the simulated and original LULC maps from 2018. Finally, following confirmation, the LULC projection for 2018 was made based on the assumption that the current LULC change pattern will continue.

5.3 Results and Discussion

5.3.1 LULC Pattern During 1991–2018

The LULC pattern for Mumbai city from 1991 to 2018 has been divided into six categories including built-up area, crop land, dense vegetation, sparse vegetation, water bodies and open land (Fig. 5.4). For LULC classification, K means clustering has been used which is simple and easy to execute and has been successfully used by several studies as well (Naikoo et al. 2020; Viana et al. 2019). In Mumbai city, the built-up area is mostly concentrated in the southern peninsular parts of the city in 1991. The prominence of built-up area increases in the subsequent time periods toward the western and eastern parts of the city. In 2018, with the exception of the central region of city and small
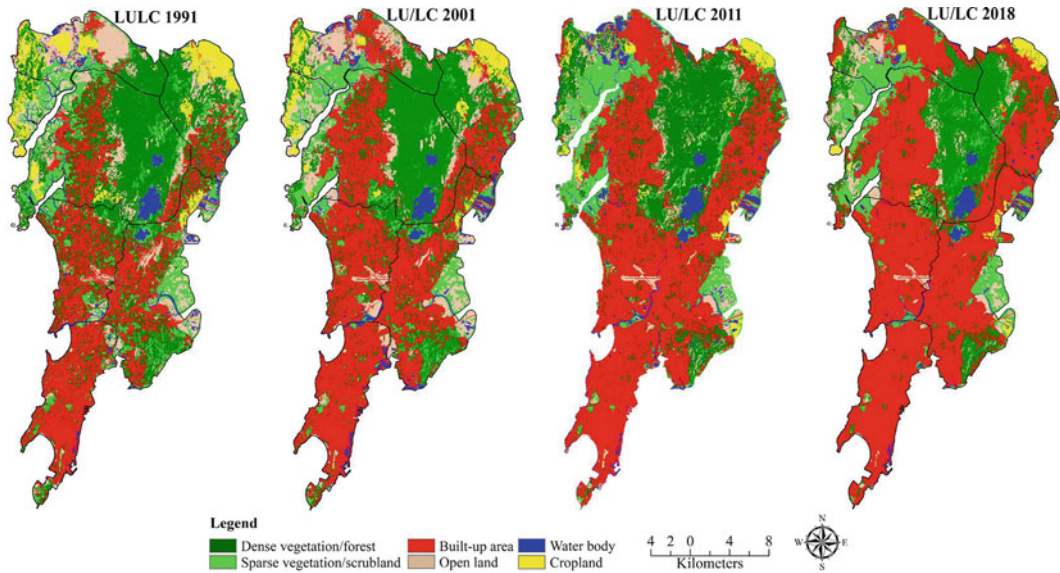
Fig. 5.4 Land use/land cover (LU/LC) pattern of Mumbai city during 1991–2018

portions in NW and SE, entire landscape is covered by built-up area. Thus, in Mumbai, the built-up area increased both in core (peninsular part) and other peripheral parts. Previously, studies have shown the infilling in the core due to continues migration and population growth in cities (Yang et al. 2018). Further, the expansion of built-up area into the peripheries of core is occurring due to congestion in the core region (Güneralp et al. 2020). Dense vegetation is present in the central region of the city and in patches in the eastern and western stretches of the city. Over time, there is little change in the homogeneity of the dense vegetation in the central region but its presence in other parts of the city diminishes considerably. Cropland is present on the extreme NW and NE of the Mumbai city in 1991, and over time, the agricultural land on the NE declined considerably, while on the NW, it disappeared in 2018.

In 1991, the maximum area of Mumbai city was under vegetation (215 km^2), and minimum was under water bodies (27.19 km^2), while the area under built-up area was only 173 km^2 (Table 5.2). Over all, the maximum percentage area was under vegetation (35%) followed by

built-up area (28%) and minimum area was under water bodies (4.50%) and crop land (5.82%) in 1991. In 2001, the percentage area under built-up was 40% which increased up to 49% in 2011 and 57% in 2018. Similarly, the percentage area under crop land was about 3% in 2001, 2.46% in 2011 and 1.71% in 2018. The percentage area under scrubland was about 11.93% in 1991, 9.45% in 2001, 11.08% in 2011 and 10.61% in 2018. In 1991, open land occupied 13.34% area in 1991, 11.69% in 2001, 6.58% in 2011 and 5.59% in 2018. In 2018, the area was maximum under built-up (346 km^2) followed by vegetation (21%), while the area was minimum under crop land (10.32 km^2). In terms of percentage, the maximum area was under built-up area (about 57%) followed by vegetation cover (21%) and scrubland (10.61%), while open land (5.59%) and water bodies (3.36%) had very low percent of area under it.

The city of Mumbai is divided into six sub-districts namely Greater Mumbai, Andheri, Borivali, Kurla, Thane and Mira Bhayandar. Among the sub-districts, the built-up area is maximum in greater Bombay with value ranging from 71km^2 in 1991 to 91km^2 2018 (Fig. 5.5).

Table 5.2 Land use land cover (LULC) change in Mumbai city during 1991–2018

LU/LC class	1991		2001		2011		2018	
	Area in km^2	Area in percent	Area in km^2	Area in percent	Area in km^2	Area in percent	Area in km^2	Area in percent
Built-up area	173.09	28.67	247.09	40.90	296.79	49.16	346.02	57.31
Open land	80.57	13.34	70.16	11.69	39.74	6.58	33.78	5.59
Vegetation	215.8	35.74	179.48	29.71	159.05	26.34	129.27	21.41
Scrubland	71.96	11.93	57.18	9.46	66.87	11.08	64.08	10.61
Cropland	35.17	5.82	23.47	3.88	14.86	2.46	10.32	1.71
Water bodies	27.19	4.50	26.40	4.36	26.47	4.38	20.31	3.36
Total	603.78	100	603.78	100	603.78	100.00	603.78	100.00

The built-up area is minimum in Mira Bhayandar in 1991 (6.59%), while in 2018, it is minimum in Borivali (37.11km^2). The area under open land is maximum in Mira Bhayandar which constitutes about 32.1% in 1991 and 12% of the total open area of the city in 2018. The open area is minimum in greater Bombay constituting about 4% in 1991 and 1.82% of the total open area of the city in 2018. Dense vegetation is maximum in Borivali making up to 34% of the total area under dense vegetation in 2018. Similarly, Borivali has the maximum area under scrubland constituting to about 12% in 1991 and 15% of the total area under scrubland in 2018. In 1991, the area of crop land is maximum under Mira Bhayandar (15.5%), while in 2018, it is maximum in Kurla (2.22%). The area under water bodies is maximum in Borivali throughout the study time. Thus, maximum area under dense vegetation, scrubland and water bodies is found in Borivali sub-district of Mumbai city.

5.3.2 LU/LC Change During 1991–2018

The transformation of one LULC class into another in Mumbai city has been presented in Fig. 5.6 and Table 5.3. The built-up area expansion of about 350 km^2 has come mostly at the cost of vegetation (96.6 km^2), open land (41 km^2), scrubland (22 km^2) and crop land

(12.35 km^2). The expansion of built-up area at the expense of vegetation, open land and scrubland has been reported in several parts of the globe (Nong et al. 2018; Spyra et al. 2021; Naikoo et al. 2023). Vegetation has witnessed a maximum decline up to 129 km^2 and has been transformed mostly into scrubland (13.18 km^2), open land (7.86 km^2), crop land (7.1 km^2) and built-up area (2.47 km^2). However, the area under scrubland has declined marginally by 7 km^2. The scrubland got converted into in to built-up area (22.25 km^2), vegetation (13.18 km^2) and open land (3.06 km^2). At the same time, the scrubland increased it area from open land (16.21 km^2) and water body (5.1 km^2). In Mumbai city, the open land has been converted into built-up (41 km^2), scrubland (16.21 km^2) and vegetation (7.86 km^2). Crop land was converted into built-up area (12.35 km^2) and open land (7.45 km^2).

5.3.3 Sub-district-Wise Change in LU/LC Pattern

The heat-map prepared using R Studio software package shows LULC changes in the sub-district of Mumbai city during 1991–2018 (Fig. 5.7). The analysis of figure shows that the built-up area has increased in the all the sub-districts of Mumbai city. At the same time, the scrublands, open land and vegetation cover had experienced

Fig. 5.5 Sub-district-wise variation in LU/LC pattern in Mumbai city during 1991–2018
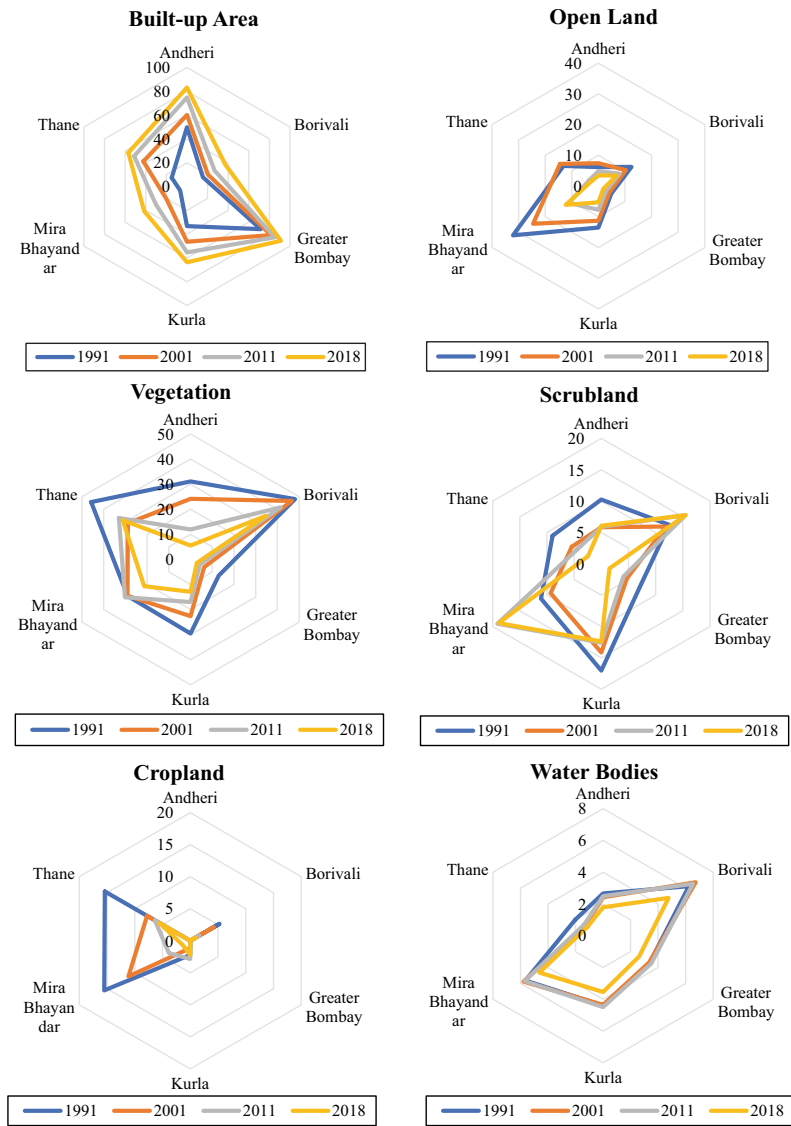
consistent decline. Overall, the maximum change has been noticed from the vegetation cover, open land and built-up area. Studies shows that in the process of urbanization, the built-up areas expand mostly at the expense of vegetation cover, cropland and open land (Borrelli et al. 2020). However, in Mumbai city, the cropland was present in very low proportion in 1991 which has been declined to almost half of its total area during 1991–2018. Contrary to this, the vegetation cover had the maximum areal coverage in 1991 with 215.18 km^2 area under it which had declined to 129.27 km^2 in 2018. Shahfahad et al. (2021) reported a similar result for LULC changes in Mumbai city. During 1991–2018, while open land has seen the greatest reduction in Andheri and Kurla sub-districts, the greatest decline in vegetation cover was seen in Andheri and Mira Bhayandar sub-districts. However, the built-up area had increased in all the sub-districts with a consistent rate during 1991–2018.
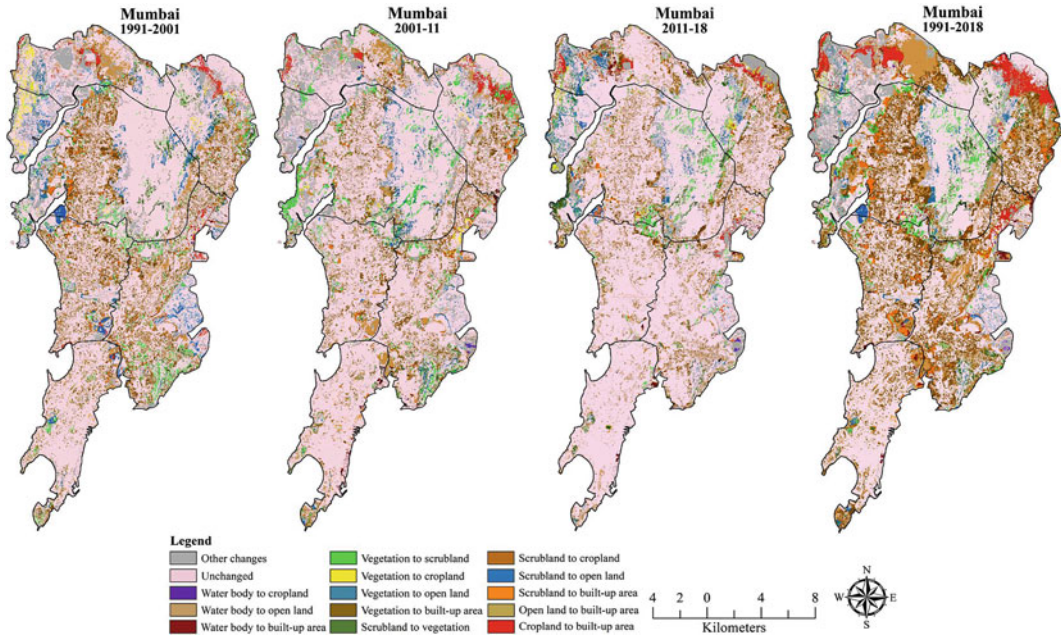
Fig. 5.6 LU/LC change in Mumbai city during 1991–2018

5.3.4 Analysis of Classification Accuracy

The accuracy assessment is a critical exercise in post classification analysis of LULC mapping. The accuracy assessment of the LULC has been assessed with the help of Kappa coefficient employing users' accuracy, producer accuracy and overall accuracy. User's accuracy for all the classified maps is over 78% with highest user's accuracy in case of 2018 (93.17%) and 2011 (93.02%). Similarly, the producer's accuracy ranges from 75% (2030) to 93.49% (2018). The overall accuracy of the LULC maps is maximum in 2018 with a value of 93% followed by 2011 with 92.80% accuracy. The overall accuracy is minimum in 2030 with a value of 76.63% (Table 5.4).

5.3.5 Analysis of Simulated LU/LC for 2020 and 2030

The LULC simulation has been done in two steps. The conditioning variables of 2011 have

been used to simulate LULC change for 2020 in the first step. This simulated LULC was cross checked with the actual LULC of 2018. Once the similarity was established between simulated LULC for 2020 and actual 2018 through visualization, the second step was proceeded. In this step, the conditioning variables of 2020 have been used to forecast LULC changes for 2030 using ANN-based cellular automata. The cellular automata has been preferred for LULC furcating because it not only predicts the futuristic changes in LULC but also takes into account the influence of each conditioning factors (Wu et al. 2022). The forecasted LULC of 2030 shows a further expansion of built-up area especially in the NW and SE of the study area (Fig. 5.8).

The area under different LULC categories for simulated 2020 and forecasted 2030 has been presented in Table 5.5. Table 5.5 shows that maximum area of 332 km^2 is under built-up in 2020, while minimum area is under crop land (24.61 km^2). Similarly in forecasted 2030, built-up area further increases to 400 km^2 while crop land is reduced to only 2.86 km^2. With the exception of built-up area, all other LULC

Table 5.3 LU/LC transition matrix

LU/LC classes	Water body	Cropland	Scrubland	Vegetation	Built-up area	Open land
1991–2001 (in km^2)						
Water body	17.94	0.06	3.29	0.41	1.5	2.47
Crop land	0.12	18.18	1.25	5.63	2.52	9.45
Scrubland	2.22	0.31	36.73	15.79	10.1	8.2
Vegetation	0.5	2.62	8.02	137.56	54.27	12.69
Built-up area	1.86	0.08	1.22	9.93	159.22	1.67
Open land	3.46	2.21	6.5	10.12	20.43	39.62
2001–2011 (in km^2)						
Water body	18.37	0.39	2.08	0.39	3	1.06
Crop land	0.11	9.45	1.53	7.14	3.57	1.64
Scrubland	1.9	0.69	37.11	8.61	6.21	2.05
Vegetation	0.84	1.31	11.97	115.21	40.07	9.98
Built-up area	1.51	0.81	3.07	14.78	225.68	2.13
Open land	3.62	2.2	12.12	14.92	18.27	22.86
2011–2018 (in km^2)						
Water body	16.04	0.22	2.85	0.67	4.08	2.52
Crop land	0.18	8.17	0.94	1.16	2.81	1.58
Scrubland	0.64	0.28	46.66	10.48	7.39	2.43
Vegetation	0.34	1.43	6.79	103.04	38.16	11.29
Built-up area	1.76	0.19	2.7	7	283.96	1.16
Open land	0.8	0.02	5.65	6.85	9.36	17.06
1991–2018 (in km^2)						
Water body	13.51	0.19	5.1	0.56	4.91	1.37
Crop land	0.31	7.48	2.45	7.1	12.35	7.45
Scrubland	1.76	0.5	32.48	13.18	22.25	3.06
Vegetation	0.73	0.63	8.8	98.1	96.6	10.81
Built-up area	1.24	0.09	1.02	2.47	168.56	0.61
Open land	2.72	1.43	16.21	7.86	41.34	12.81

categories are expected to witness a decline in coverage area in 2030. The maximum decline is expected in open land whose coverage area is reduced from 61 to 22.91 km^2 only from 2020 to 2030.

5.4   Conclusion

The study has been done to analyze and forecast the spatio-temporal LULC pattern in Mumbai city using Landsat datasets. For forecasting of LULC changes for 2030, ANN integrated with CA has been used. The study's findings indicate that the built-up area has grown from 28% to the 57% of the total area of the city from 1991 to 2018. While, the vegetation, open land and crop land have declined from 35, 13.34 and 5.582% in 1991 to corresponding values of 21.41, 5.59 and 1.71% in 2018. Further, built-up area is expected to increase up to 66% of the total area of the city by 2030 as shown by the LULC simulations. The built-up area in Mumbai has expanded mostly on vegetation and open land. Among the sub-
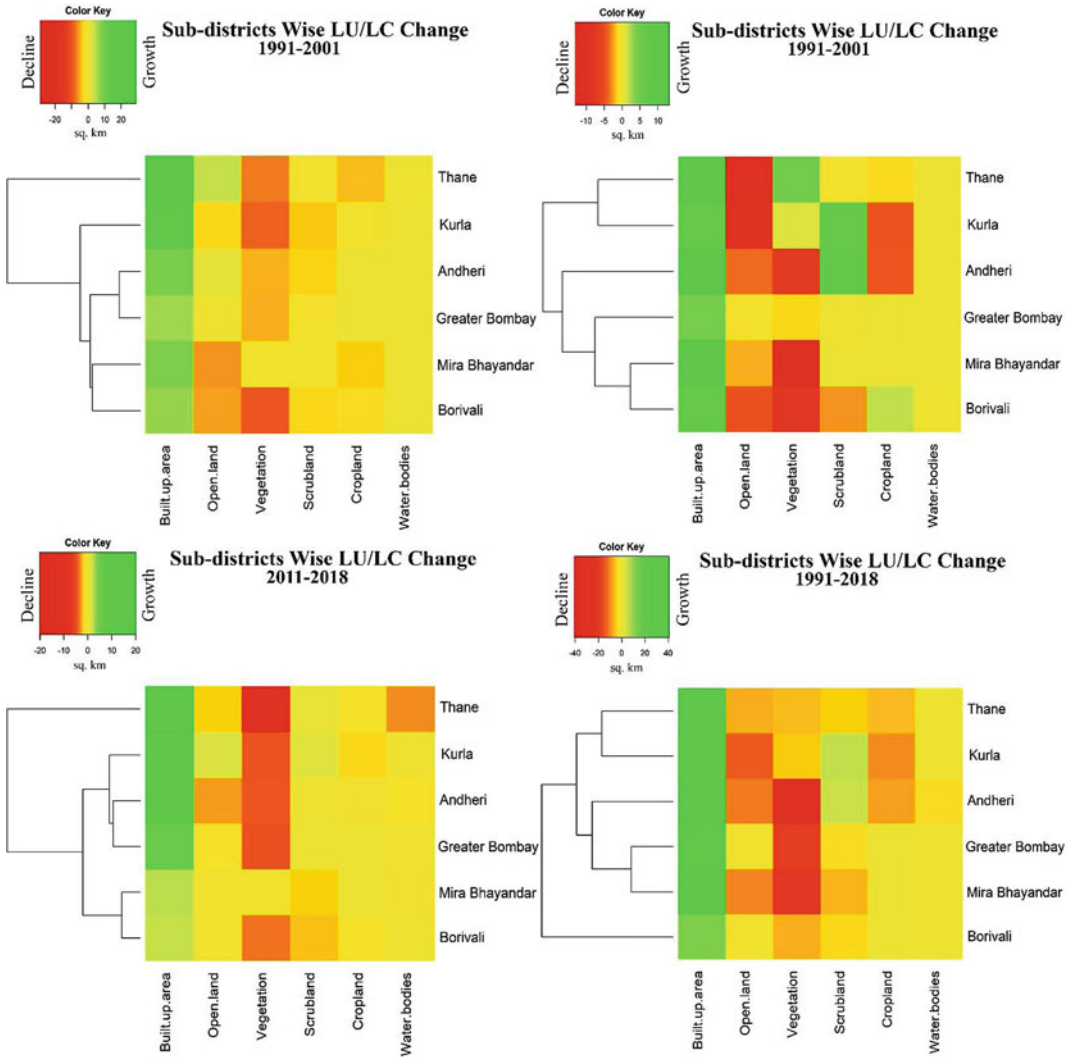
Fig. 5.7 Sub-district-wise LU/LC change in Mumbai city during 1991–2018

Table 5.4 Accuracy assessment of LU/LC maps using Kappa coefficient

Year	User's accuracy (%)	Producer's accuracy (%)	Overall accuracy (%)	Kappa coefficient
1991	88.23	88.71	87.20	0.883
2001	87.42	87.08	85.80	0.879
2011	93.02	93.05	92.80	0.941
2018	93.17	93.49	93.01	0.957
2020	86.32	85.18	85.12	0.824
2030	78.52	75.25	76.63	0.754

Fig. 5.8 Simulated LU/LC pattern of Mumbai for the year 2020 and 2030
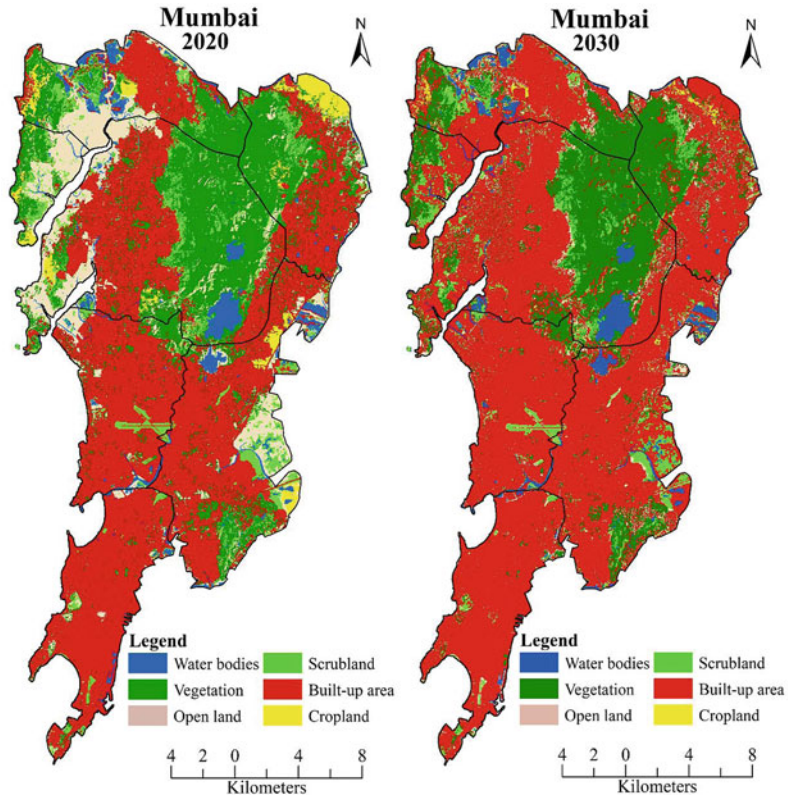
Table 5.5 Area under simulated LU/LC types in Mumbai for 2020 and 2030

Class	2020		2030	
	Are in km^2	Area in percent	Are in km^2	Area in percent (%)
Water bodies	24.61	4.08	20.88	3.46
Vegetation	140.88	23.33	127.95	21.19
Open land	61.96	10.26	22.91	3.79
Scrubland	29.28	4.85	28.72	4.76
Built-up area	332.93	55.14	400.46	66.33
Crop land	14.12	2.34	2.86	0.47
Total	603.78	100.00	603.78	100.00

districts, the built-up area has increased in all the sub-districts. However, Andheri and Mira Bhayandar sub-district has seen the maximum reduction in vegetation cover, while open land had witnessed maximum decline in Andheri and Kurla sub-districts. Moreover, the vegetation cover, scrubland and open land are expected to decline significantly, mostly in the northern sub-districts like Mira Bhayandar and Thane.

However, water bodies did not show a significant change in near future because most of the water bodies in Mumbai city is either protected or in the form of rivers and bays. The finding of the study that the process of urbanization leading to LULC changes has been taking place at a rapid pace and is expected to increase further in near future. Thus, there is an urgent need for the regulation and planning of the LULC changes

taking place in Mumbai city. Further research in this direction can be directed toward finding the local underlying factors leading to LULC changes as well as simulation can be done for longer time period using other methodologies like CA Markov and CA integrated machine learning algorithms.

References

Aburas MM, Ho YM, Ramli MF, Ash'aari ZH (2017) Improving the capability of an integrated CA-Markov model to simulate spatio-temporal urban growth trends using an Analytical Hierarchy Process and Frequency Ratio. Int J Appl Earth Obs Geoinf 59:65–78

Ahluwalia IJ, Kanbur R, Mohanty PK (eds) (2014) Urbanisation in India: challenges, opportunities and the way forward. SAGE Publications India

Birhane E, Ashfare H, Fenta AA, Hishe H, Gebremedhin MA, Solomon N (2019) Land use land cover changes along topographic gradients in Hugumburda national forest priority area, Northern Ethiopia. Remote Sens Appl Soc Environ 13:61–68

Borrelli P, Robinson DA, Panagos P, Lugato E, Yang JE, Alewell C, Wuepper D, Montanarella L, Ballabio C (2020) Land use and climate change impacts on global soil erosion by water (2015–2070). Proc Natl Acad Sci 117(36):21994–22001

Census of India (2011) Mumbai (Greater Mumbai) City Census 2011 data. https://www.census2011.co.in/census/city/365-mumbai.html#:∼:text=Aspercent20 perpercent20provisionalpercent20reportspercent20of, malespercent20andpercent208percent2C522percent2 C641percent20arepercent20females. Accessed on 06/05/2022

Chaminé HI, Pereira AJ, Teodoro AC, Teixeira J (2021) Remote sensing and GIS applications in earth and environmental systems sciences. SN Appl Sci 3(12):1–3

Crankshaw O, Borel-Saladin J (2019) Causes of urbanisation and counter-urbanisation in Zambia: natural population increase or migration? Urban Stud 56(10):2005–2020

Das M, Das A (2019) Dynamics of urbanization and its impact on urban ecosystem services (UESs): a study of a medium size town of West Bengal, Eastern India. J Urban Manag 8(3):420–434

Das T, Naikoo MW, Talukdar S, Parvez A, Rahman A, Pal S, Asgher MS, Islam ARMT, Mosavi A (2022) Analysing process and probability of built-up expansion using machine learning and fuzzy logic in English bazar, West Bengal. Remote Sens 14(10):2349

Dewan AM, Yamaguchi Y (2009) Land use and land cover change in Greater Dhaka, Bangladesh: using remote sensing to promote sustainable urbanization. Appl Geogr 29(3):390–401

Gebeyehu MN (2019) Remote sensing and GIS application in agriculture and natural resource management. Int J Environ Sci Nat Resourc 19(2):45–49

Goncalves ML, Netto MLA, Costa JAF, Zullo Junior J (2008) An unsupervised method of classifying remotely sensed images using Kohonen self-organizing maps and agglomerative hierarchical clustering methods. Int J Remote Sens 29(11):3171–3207

Gupta P, Venkatesan M (2020) Mineral identification using unsupervised classification from hyperspectral data. In: Emerging research in data engineering systems and computer communications. Springer, Singapore, pp 259–268

Gumma MK, Mohammad I, Nedumaran S, Whitbread A, Lagerkvist CJ (2017) Urban sprawl and adverse impacts on agricultural land: a case study on Hyderabad, India. Remote Sens 9(11):1136

Güneralp B, Reba M, Hales BU, Wentz EA, Seto KC (2020) Trends in urban land expansion, density, and land transitions from 1970 to 2010: a global synthesis. Environ Res Lett 15(4):044015

Hussain S, Mubeen M, Ahmad A, Akram W, Hammad HM, Ali M, Masood N, Amin A, Farid HU, Sultana SR, Nasim W (2020) Using GIS tools to detect the land use/land cover changes during forty years in Lodhran district of Pakistan. Environ Sci Pollut Res 27(32):39676–39692

Jain S, Roy SB, Panda J, Rath SS (2021) Modeling of land-use and land-cover change impact on summertime near-surface temperature variability over the Delhi-Mumbai Industrial Corridor. Model Earth Syst Environ 7(2):1309–1319

Kumari B, Tayyab M, Hang HT, Khan MF, Rahman A (2019) Assessment of public open spaces (POS) and landscape quality based on per capita POS index in Delhi India. SN Appl Sci 1(4):1–13

Lambin EF, Helmut GJ, Lepers E (2003) Dynamics of land-use and land-cover change in tropical regions. Annu Rev Environ Resour 28(1):205–241

Lorenzen G, Sprenger C, Baudron P, Gupta D, Pekdeger A (2012) Origin and dynamics of groundwater salinity in the alluvial plains of western Delhi and adjacent territories of Haryana State India. Hydrol Process 26(15):2333–2345

Lu D, Weng Q (2007) A survey of image classification methods and techniques for improving classification performance. Int J Remote Sens 28(5):823–870

Mallick J, Rahman A, Singh CK (2013) Modeling urban heat islands in heterogeneous land surface and its correlation with impervious surface area by using night-time ASTER satellite data in highly urbanizing city Delhi-India. Adv Space Res 52(4):639–655

Mathan M, Krishnaveni M (2020) Monitoring spatio-temporal dynamics of urban and peri-urban land transitions using ensemble of remote sensing spectral indices—a case study of Chennai Metropolitan Area, India. Environ Monitor Assessm 192(1)

Mondal MS, Sharma N, Garg PK, Kappas M (2016) Statistical independence test and validation of CA Markov land use land cover (LULC) prediction results. Egypt J Remote Sens Space Sci 19(2):259–272

MMRDA (2016) Mumbai Metropolitan regional plan; MMRDA: Mumbai, India

Naikoo MW, Rihan M, Ishtiaque M (2020) Analyses of land use land cover (LULC) change and built-up expansion in the suburb of a metropolitan city: spatio-temporal analysis of Delhi NCR using landsat datasets. J Urban Manag 9(3):347–359

Naikoo MW, Rihan M, Peer AH, Talukdar S, Mallick J, Ishtiaq M, Rahman A (2022) Analysis of peri-urban land use/land cover change and its drivers using geospatial techniques and geographically weighted regression. Environ Sci Pollut Res, 1–19

Naikoo MW, Shahfahad, Talukdar S, Ishtiaq M, Rahman A (2023) Modelling built-up land expansion probability using the integrated fuzzy logic and coupling coordination degree model. J Environ Manage 325:116441. https://doi.org/10.1016/j.jenvman.2022.116441

Nong DH, Lepczyk CA, Miura T, Fox JM (2018) Quantifying urban growth patterns in Hanoi using landscape expansion modes and time series spatial metrics. PLOS ONE 13(5):e0196940. https://doi.org/10.1371/journal.pone.0196940

Patil GR, Sharma G (2020) Urban quality of life: an assessment and ranking for Indian cities. Transp Policy

Rahaman S, Jahangir S, Haque MS, Chen R, Kumar P (2021) Spatio-temporal changes of green spaces and their impact on urban environment of Mumbai, India. Environ Dev Sustain 23(4):6481–6501

Roy SS, Balling Jr RC (2005) Analysis of trends in maximum and minimum temperature, diurnal temperature range, and cloud cover over India. Geophys Res Lett 32(12)

Roy SS, Rahman A, Ahmed S, Ahmad IA (2020) Alarming groundwater depletion in the Delhi Metropolitan Region: a long-term assessment. Environ Monit Assess 192(10):1–14

Saputra MH, Lee HS (2019) Prediction of land use and land cover changes for north sumatra, Indonesia, using an artificial-neural-network-based cellular automaton. Sustainability 11(11):3024

Sarkar R (2020) Association of urbanisation with demographic dynamics in India. GeoJournal 85(3):779–803

Sarkar T, Kannaujiya S, Taloor AK, Ray PKC, Chauhan P (2020) Integrated study of GRACE data derived interannual groundwater storage variability over water stressed Indian regions. Groundw Sustain Dev 10:100376

Shahfahad, Naikoo MW, Islam ARMT, Mallick J, Rahman A (2022) Land use/land cover change and its impact on surface urban heat island and urban thermal comfort in a metropolitan city. Urban Clim 41:101052

Shahfahad, Rihan M, Naikoo MW, Ali MA, Usmani TM, Rahman A (2021) Urban Heat island dynamics in response to land-use/land-cover change in the coastal city of Mumbai. J Indian Soc Remote Sens 49(9):2227–2247

Singh SK, Mustak S, Srivastava PK, Szabó S, Islam T (2015) Predicting spatial and decadal LULC changes through cellular automata Markov chain models using earth observation datasets and geo-information. Environ Process 2(1):61–78

Spyra M, Kleemann J, Calò NC, Schürmann A, Fürst C (2021) Protection of peri-urban open spaces at the level of regional policy-making: examples from six European regions. Land Use Policy 107:105480. https://doi.org/10.1016/j.landusepol.2021.105480

Talukdar S, Singha P, Mahato S, Pal S, Liou YA, Rahman A (2020) Land-use land-cover classification by machine learning classifiers for satellite observations—a review. Remote Sens 12(7):1135

Tripathy P, Kumar A (2019) Monitoring and modelling spatio-temporal urban growth of Delhi using cellular automata and geoinformatics. Cities 90:52–63

Viana CM, Girão I, Rocha J (2019) Long-term satellite image time-series for land use/land cover change detection using refined open source data in a rural region. Remote Sens 11(9):1104

Wang J, Maduako IN (2018) Spatio-temporal urban growth dynamics of Lagos metropolitan region of Nigeria based on hybrid methods for LULC modeling and prediction. Eur J Remote Sens 51(1):251–265

Wentz EA, Anderson S, Fragkias M, Netzband M, Mesev V, Myint SW, Quattrochi D, Rahman A, Seto KC (2014) Supporting global environmental change research: a review of trends and knowledge gaps in urban remote sensing. Remote Sens 6(5):3879–3905

Wu X, Liu X, Zhang D, Zhang J, He J, Xu X (2022) Simulating mixed land-use change under multi-label concept by integrating a convolutional neural network and cellular automata: a case study of Huizhou China. Gisci Remote Sens 59(1):609–632

Yang Y, Liu Y, Li Y, Du G (2018) Quantifying spatio-temporal patterns of urban expansion in Beijing during 1985–2013 with rural-urban development transformation. Land Use Policy 74:220–230

Zhang N, Chen H, Chen J, Chen X (2016) Social media meets big urban data: a case study of urban waterlogging analysis. Comput Intell Neurosci

Zhongming Z, Linong L, Xiaona Y, Wangqiang Z, Wei L (2020) World cities report 2020: the value of sustainable urbanization

Zope PE, Eldho TI, Jothiprakash V (2016) Impacts of land use–land cover change and urbanization on flooding: a case study of Oshiwara River Basin in Mumbai, India. CATENA 145:142–154

Monitoring Urban Sprawl Using Geo-Spatial Technology: A Case Study of Kanpur City, India

6

Aruna Paarcha, Sandeep Maithani, Mujahid Husain, Nisa Suhanee, and Rohit Kumar Azad

Abstract

In India, cities have been experiencing rapid urbanization from the last decade. Rapid land transformation activities have been taking place in and around the city areas. This type of anthropogenic activity disrupts the ecological equilibrium. The present study has used remotely sensed data Landsat 5 TM and Landsat 8 OLI for the land use and land cover (LULC) classification and to analyze urban expansions that are the result of the dynamic processes related to landscape modification. The main objective of this work was analysis and identification of urban sprawl in Kanpur city, India. The built-up classification has been the quantification using satellite imageries of 2004, 2011 and 2021 data over a period of 17 years. To evaluate the trend and extent of urban growth, multi-ring buffer (MRB) method has been applied, and Shannon's entropy estimation has been performed

with MRB. The spatial analysis has been done by dividing study region into nine concentric circles of 2 km each, with increasing order of outward. The Shannon's entropy values for the three-time period data of 2004, 2011 and 2021 are found to be 1.70, 1.80 and 1.84, respectively. High coalesced settlement core with sparse growth extent to outskirts has been replicating by the higher values of entropy index. This study is depicting built-up area and vegetation increased up to 33.7 km^2 and 10.5 km^2, respectively. To evaluate the density of urban growth for the present work, the density index was calculated. The results of the study depicting the first three zones are from compact to moderately compact, and further consecutive zones built-up area expansion has been highly dispersing in nature.

Keywords

Shannon's entropy · Density index · Multi-ring buffer (MRB) · Urban sprawl · Built-up index

A. Paarcha (✉) · M. Husain · N. Suhanee · R. K. Azad
Department of Geography, Faculty of Natural Sciences, Jamia Millia Islamia, New Delhi 110025, India
e-mail: apaarcha@jmi.ac.in

S. Maithani
Urban and Regional Studies Department, Indian Institute of Remote Sensing, Dehradun, India
e-mail: maithani@iirs.gov.in

6.1 Introduction

The main concerns of the late twentieth and early twenty-first centuries are the unparalleled urban expansion and its effects (Redman and Jones 2005; Taubenbock et al. 2009). The process of

urbanization has been a global phenomenon, but it is more of a concern to a developing country like India. India has seen dynamic growth in population, from 62 million in 1951 to 377 million in 2011, which is expected to grow by 600 million in 2031 (Census of India 2011; JNNURM 2011). The uncontrolled physical expansion of cities is known as urban sprawl and is characterized by low density, fragmented random growth patterns. Urban sprawl brings into its ambit villages, forest areas, agricultural land, vacant land and other low-density areas of various land use and land (Sudhira et al. 2003; Shaw 2005; Kumar et al. 2007; Rahman 2011) to accommodate the escalating urban population. Sustainable land use planning focuses on planning of urban development, to ensure a lower level of entropy within the city limits to sustain the ecological functions of the land and ensure a healthy and balanced land ecosystem. Sustainable land use planning focuses on planning at various spatial and temporal scales and analysis of its impact (Xu et al. 2013). The man-made impervious surfaces are used as an indicator for quantification of urban sprawl (Torrens and Alberti 2000; Sudhira et al. 2003; Sudhira et al. 2004; Kumar et al. 2007; Jat et al. 2008).

The method of Shannon's entropy and other landscape matrices is used to quantify the phenomena of urban sprawl at the various administrative and spatial scales (Harvey, 2008). Previous studies have considered total city as a unit for the system analysis (Jat et al. 2008). While some studies focused on the smaller urban administrative units for study, i.e., ward boundary of the city (Herold et al. 2003; Punia and Singh 2012) and the arbitrarily created sub-zones in the city (Bhatta 2009; Bhatta et al. 2010) like the concentric circles encircling the city centers with specific widths (Ramachandra et al. 2012; Ramachandra et al. 2015). Shannon's entropy helps to achieve extracting quantitative details on spatial ground and analyzing the Shannon's entropy and spatiotemporal gradient for the change in land use and land cover (Shukla and Jain 2019). Some others define as it is degree of dispersion or spatial concentration in specific zone can be very easily noticed in the GIS and remote sensing environment using Shannon's entropy (Krishnaveni and Anilkumar 2020). Shannon's entropy's results showed relatively more variations under two separate zoning methods applied, but in Batty's spatial entropy yielded robust measurements (Cho et al. 2021).

In present article, the Kanpur Metropolitan City which is the *largest urban agglomeration in Uttar Pradesh and* the *11th most populous urban city in India* has been taken as the study area for t quantifying the pattern of urban sprawl using Entropy approach. The study will help in the effective urban land use planning of the Kanpur Metropolitan City for ensuring sustainable urban development.

6.2   Study Area

Kanpur city is one of the significant cities of Uttar Pradesh. It is geographically located on the Ganga River's right bank. This city has been recording changes in human and natural setup after the industrial revolution in India since the last decades of the twentieth century. Kanpur has been also considered as the financial capital of Uttar Pradesh given that it is the principal financial and industrial hub of North India and that it is India's ninth largest economy. It is renowned for its good quality leather items that are primarily supplied to western nations, as well as its colonial architecture, gardens and parks. The city is India's twelfth most populous city and has the eleventh most populous urban agglomeration due to its famed leather and textile industries. The 2011 Census shows Kanpur Metropolitan City (KMC) having a population of more than 27 lakhs. The projected population as per Census 2021 is more than 3,153,000 (Fig. 6.1).

6.3   Data Sources and Methods

6.3.1   Data sources

The input database for the current study consists of multispectral and multitemporal Landsat
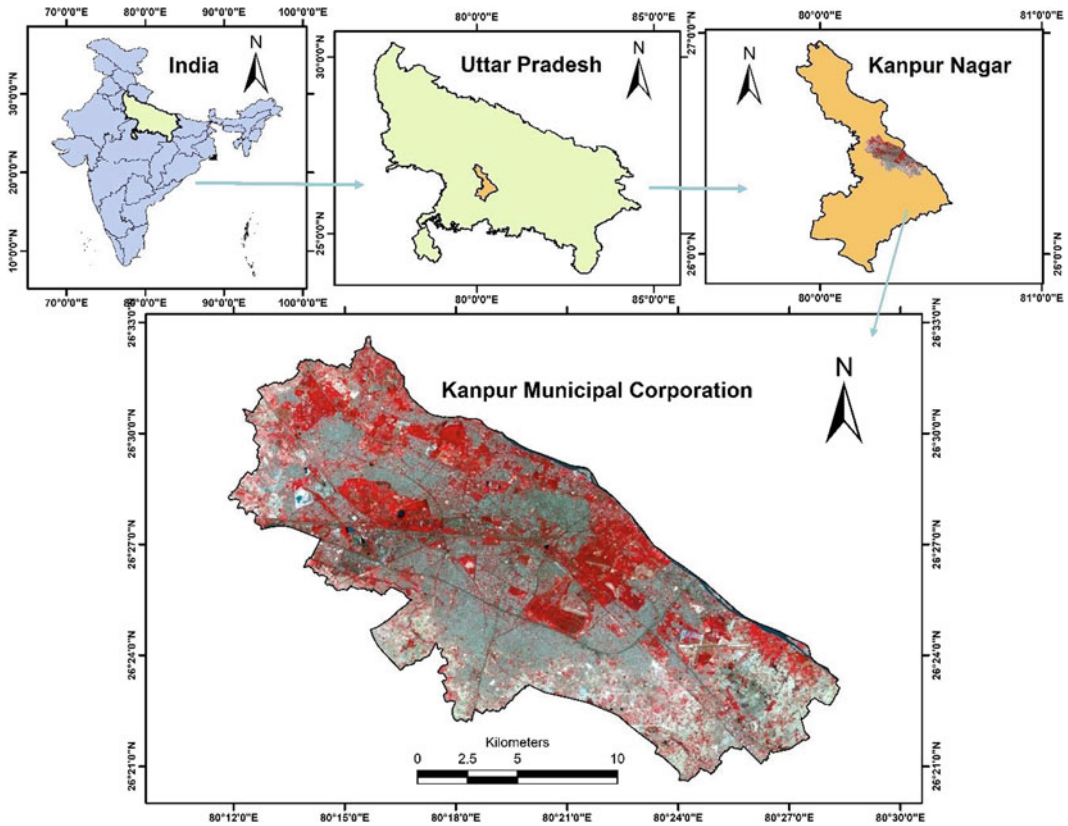
Fig. 6.1 Locational aspect and false color composite of Kanpur Metropolitan City

satellite imageries. The imageries were acquired from the official website of the US Geological Survey (USGS) Earth Explorer. Kanpur city boundary was digitized from Kanpur Municipal Corporation (KMC) portal (Table 6.1).

6.3.2 Methodology

Remotely sensed data were classified into different land cover classes using the maximum likelihood classifier which belongs to the family of supervised classification. These classified maps were subsequently used for analysis of built-up growth. Shannon's entropy was computed to calculate built-up area compactness and dispersion in the study area. Further concentric buffer zones of two (2) km interval were created around city center, viz., "Thana Bajaria" area built-up growth with respect to the city center was analyzed during the period 2004–2021 (Fig. 6.2).

Table 6.1 Detailed specification of the used satellite images

Images	Date of acquisition	Selected bands (RGB)	Spatial resolution (m)	Reference system
Landsat 5	06May 2004	4,3,2	30	UTM & WGS84
Landsat 5	10May 2011	4,3,2	30	UTM & WGS84
Landsat 8 OLI	06 June 2021	4,3,2	30	UTM & WGS84
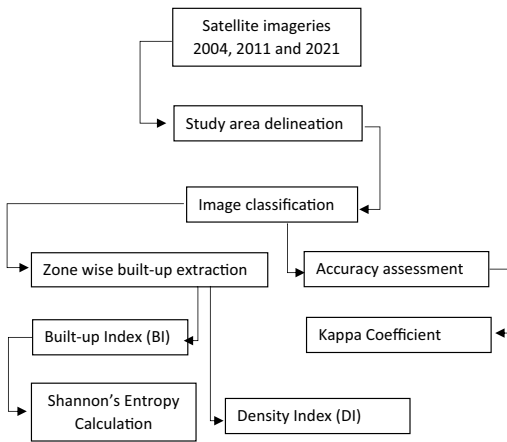
Fig. 6.2 Methodology flow chart

6.3.2.1 Urban Compactness and Dispersion Analysis

Shannon's Entropy

One of the crucial and reliable methods for assessing the level of uncertainty in the given random variables is Shannon's entropy (Cabral et al. 2013). The integration of spatial variables with Shannon's entropy was performed to calculate urban growth. This technique is very efficient in quantifying the compactness and dispersion of built-up growth patterns.

The formula for Shannon Entropy is,

$$H_n = -\sum n_i = 1 P_i \log(P_i) \qquad (6.1)$$

$$P_i = \frac{B_i}{\text{Total area}}$$

where

H_n is the value of Shannon's entropy, $P_i =$ is the ratio of built-up area to the total area in a particular zone, $B_i =$ is the built-up area and $n =$ total number of zones,

According to Shannon's entropy, if the entropy value results in low, i.e., 0, it depicts built-up growth is concentrated in one zone. On contrary to this, if the entropy value is of order "log n," it shows that the built-up growth is evenly distributed among all zones, n. In present study, for entropy computation, the study area was divided into nine concentric zones of 2 km

intervals defined with respect to the city center. An outward extension of the city from city center is limited to a radius of 18 km. Further, the built-up class was extracted from the land cover map generated by supervised classification.

Density Index (DI)

The Polsby–Popper test was used to assess the compactness of urban expansion (Polsby and Popper 1991). The built-up class to the area of a multiple ring buffer (MRB) with the same perimeter is compared using the Polsby–Popper test (McDonald 2010).

$$DI = (4\pi * B_i)/\text{Perimeter}^2 \qquad (6.2)$$

where Perimeter = area of MRB zone. DI = density index shows the complexity of built-up structures and its morphology. The value of DI ranges between 0 and 1, where value of 0 indicates low density and 1 depicts high density.

6.4 Results and Discussion

6.4.1 Urban Structure and Complexity Analysis

6.4.1.1 Land Use and Land Cover (2004)

LULC of any region reflects the scenario of available facilities and resources. Using the maximum likelihood classifier, five classes were identified in this investigation. Namely, the fallow land class has highest areal coverage (110.9 km^2), followed by, built-up class (65 km^2), vegetation class (49.4 km^2), agriculture class (33.7 km^2) and water body (5.6 km) (refer Table 6.2). In the given study, 94.70% overall accuracy was achieved, and the kappa value achieved was 0.932, which is more than the minimum accuracy criteria of 85% specified by Anderson 1976. The built-up area is visible in the center of the study area and spreads outward of the city extent. The agricultural fields are present along the water bodies in north direction, south and south-west part of study area. Vegetation is mostly concentrated in some restricted

Table 6.2 Land use and land cover area in km^2

Classes	Year 2004	Year 2011	Year 2021	Change 2004–2021 (in km^2)
	Area (km^2)	(Area (km^2)	Area (km^2)	
Built-up	65	87.44	98.7	33.7
Fellow land	110.9	88.7	72.5	−38.4
Agriculture	33.7	29.9	28.2	−5.5
Water	5.6	5.5	5.4	−0.2
Vegetation	49.4	53.1	59.9	10.5
Total	264.7	264.7	264.7	
Overall accuracy	94.7	93.87	94.89	
Kappa	0.932	0.923	0.934	

and reserved areas, i.e., cantonment, Armapur Estate, COD and Railway Colony (Fig. 6.3).

6.4.1.2 Land Use and Land Cover (2011)

The imagery of year 2011 was also classified into five classes. Fallow land had the maximum areal coverage (88.7 km^2), followed by built-up (87.44 km^2), vegetation (53.1 km^2), agriculture (29.9 km^2) and water body (5.5 km^2) as mentioned in Table 6.2. The classified imagery had overall accuracy of 93.87% and t kappa value of 0.923 which was more than the Anderson Criteria. The built-up area is visible in the study area and it is spreading outward of the city extent. The agricultural fields are along water body lies in the north direction, south and south-west of the study area. Vegetation is concentrated in some restricted and reserved compounds. Green space has increased in the, i.e., Armapur Estate, COD and Railway Colony (Fig. 6.3).

6.4.1.3 Land Use and Land Cover (2021)

Third time period LULC classification shows the drastic change in areal coverage of different classes, with built-up class (98.7 km^2) having the maximum coverage followed by fallow land (72.5 km^2), vegetation (59.9 km^2), and agriculture (28.2 km^2) and water body (5.4 km^2) (Table 6.2). The overall accuracy achieved is 94.89% achieved, and kappa value is 0.934. The built-up area is expanding in all directions, with

the east direction showing the least built-up area growth. However, the vegetation class is increasing in restricted areas like that of the Kanpur Cantonment, COD, Arampur Estate and Railway Colony sing. Fallow land area recorded a decrease of 38.4 km^2 area (Table 6.2).

6.4.2 Shannon's Entropy Analysis

KMC has experienced considerable urban growth during the period 2004–2011–2021. Analysis with the LULC (Fig. 6.3) maps depicted an increment of built-up class by 22.92 km^2 during 2004–2011. During period 2011–2021, the increase in built-up class was calculated as 11.26 km^2. While during period 2004–2021, the built-up area increased by 34.18 km^2. Nine concentric zones were generated having a radial distance 2 km for calculating the Shannon's entropy for Kanpur city (Fig. 6.5). The number of zones is represented n, where the area having number of zones nine would be 2.1972 (Ln (9) = 2.1972). These nine zones were considered for the temporal study of Kanpur city for period 2004–2011–2021. During 2004–2011, urban area increased from 7.52 to 7.69 km^2; this slight increment was observed in first buffer zone(0–2 km), second buffer zone (2–4 km) recorded growth from 14.38 to 14.41 km^2, third buffer zone (4–6 km) noticed minimum urban expansion, i.e., 16.47 to 16.73 km^2, in fourth buffer zone (6–8 km), there was abrupt increment of

Fig. 6.3 Land use and land cover classified image 2004, 2011, 2021
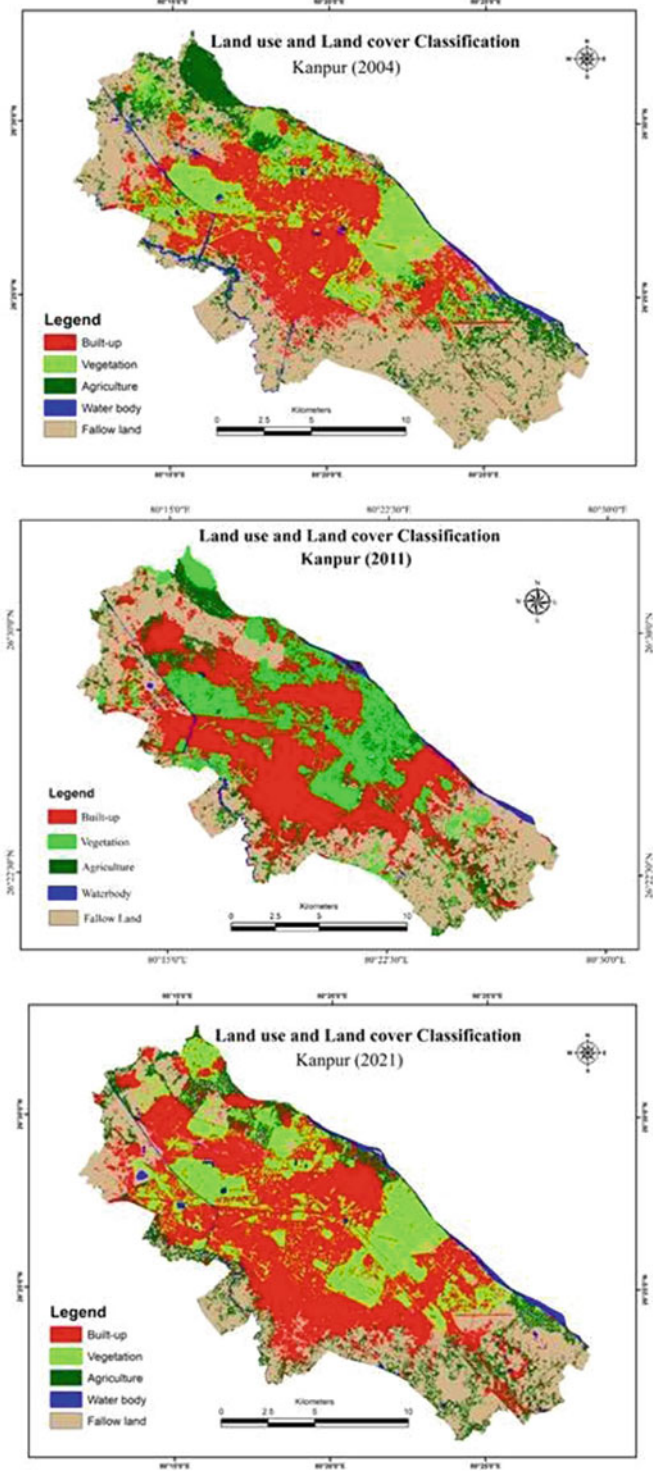
built-up area from 14.08 to 17.21 km^2, in fifth buffer zone (8–10 km), urban area increased from 9.46 to 22.42 km^2, sixth buffer zone (10–12 km), built-up area increased more than three times, i.e., 2.21 to 7.09 km^2, in seventh buffer zone (12–14 km), built-up area increased from 0.29 to 0.82 km^2, buffer zone eighth (14–16 km) had growth from 0.07 to 0.96 km^2 and the last buffer zone that is ninth zone (16–18 km), the urban area increased from 0.04 to 0.11 km^2. While during 2011–2021, 7.69–8.02 km^2 urban area increased in zone 1. In zone 2, very slight increment observed in built-up area 14.41–14.47 km^2. Third buffer zone also experienced substantial change in built-up area, i.e., 16.73–16.90 km^2. Fourth buffer zone experienced highest increase in built-up that is 17.21–

22.82 km^2. Further buffer zones also experienced increase in built-up but at a decreasing rate (Table 6.3).

Shannon's entropy values of the inner core buffer (zone 1) of the base years are 0.25, 0.21 and 0.20 for the years 2004, 2011 and 2021, respectively, showing the city core was moderately compact in 2004, but now in 2021, city is more compact. Scenario of zone 2 and zone 3 shows that not much changes has taken place. Analysis of the computed Shannon's entropy values represented that the urban growth from city center up to 6 km was compact to moderately compact. The peripheral area of had low values of Shannon's entropy (Table 6.4). All nine zones have been evaluated in all years' images. All zones observed increment of built-up class,

Table 6.3 Zone-wise Shannon's entropy of built-up area extent

Zones	Built-up (km^2) 2004	Shannon's entropy (2004)	Built-up (km^2) (2011)	Shannon's entropy (2011)	Built-up (km^2) (2021)	Shannon's entropy (2021)
1	7.52	0.251	7.69	0.214	8.02	0.204
2	14.38	0.335	14.41	0.297	14.47	0.282
3	16.47	0.349	16.73	0.316	16.9	0.302
4	14.08	0.332	17.21	0.32	22.82	0.339
5	9.46	0.282	22.42	0.349	24.66	0.346
6	2.21	0.116	7.09	0.204	8.26	0.208
7	0.29	0.024	0.82	0.044	1.56	0.066
8	0.07	0.007	0.96	0.05	1.63	0.068
9	0.04	0.004	0.11	0.008	0.39	0.022

Table 6.4 Computation of ratio of built-up to total area

MRB zones	P_i		
	2004	2011	2021
1	0.1166	0.0879	0.0812
2	0.2229	0.1647	0.1466
3	0.2552	0.1913	0.1712
4	0.2183	0.1968	0.2312
5	0.1466	0.2564	0.2498
6	0.0343	0.0810	0.0837
7	0.0045	0.0093	0.0158
8	0.0010	0.0109	0.0165
9	0.0006	0.0012	0.0040

Urban growth
2004–2021
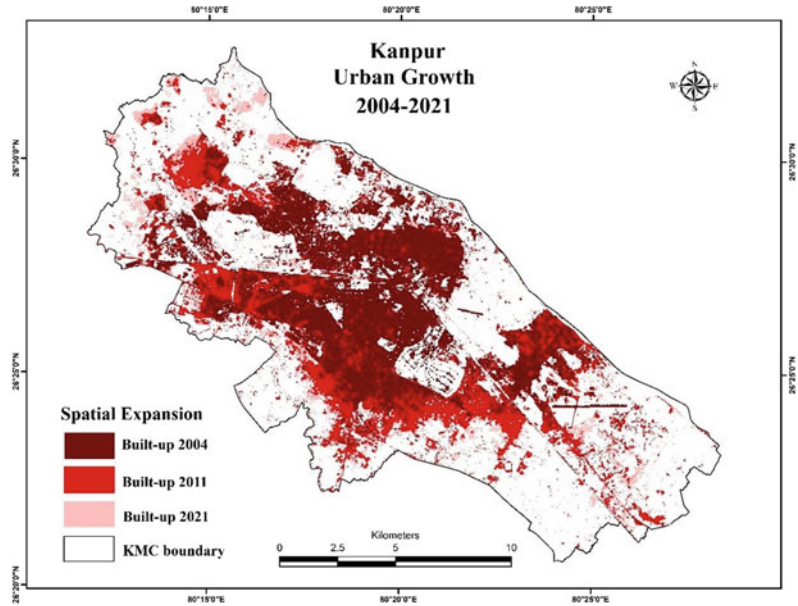
with an overall increment of 33.7 km^2 area during this period 2004–2021 (Table 6.2).

Table 6.4 shows the spatial extent of urban sprawl, broken down by year, away from the city core. The tremendous growth of built-up class has been noticed from 2004 to 2021 as shown in (Fig. 6.5). The computation of P_i is represented in the (Table 6.4) for both years in every zone (Fig. 6.4).

P_i is computed using (Table 6.4) for three years 2004, 2011 and 2021 for Shannon's entropy (H_n) is shown in the (Table 6.5); the entropy value has been obtained by Eq. (6.1) as 2.1972. It shows the compactness and dispersion of urban sprawl during the study period.

Shannon's entropy values of all years calculated using Eq. (6.1) are 1.70, 1.80 and 1.84 for 2004, 2011 and 2021, respectively. In contrast to high values which show a dispersive growth of the city toward the city's periphery, low values of Shannon's entropy show a built-up structure that is compact.

6.4.3 Density Index Analysis

For the years 2004, 2011 and 2021, the density index (DI) analysis was performed in order to

track the complexity of the Kanpur city. The DI has been calculated for the nine zones; zone 1 starts from Thana Bajaria city center with an outward stretch with a radius of 2 km. It can be observed from (Table 6.6) that high values were obtained as 0.59, 0.61 and 0.63 for the years 2004, 2011 and 2021, respectively, in zone 1, i.e., the city center. The remaining zones all show a declining index. According to this pattern in the successive buffer zones, the urban nature of the city center is compact and displays a loss of compactness as it approaches the city boundary. Hence, the city center is highly dense, and the outer areas are dispersed for the built-up area expansion.

6.4.4 Urban Sprawl Multiple Ring Buffer (MRB) Analysis

Buffer rings have been created around the city center in donuts shape. It was generated for the analysis of urban expansion pattern; 9 MRB was developed with the interval of 2 km from the origin center of the study area (Fig. 6.5). In this study, each ring buffer was incorporated to calculate urban expansion for distinctive year of study. Built-up feature gradually increasing from

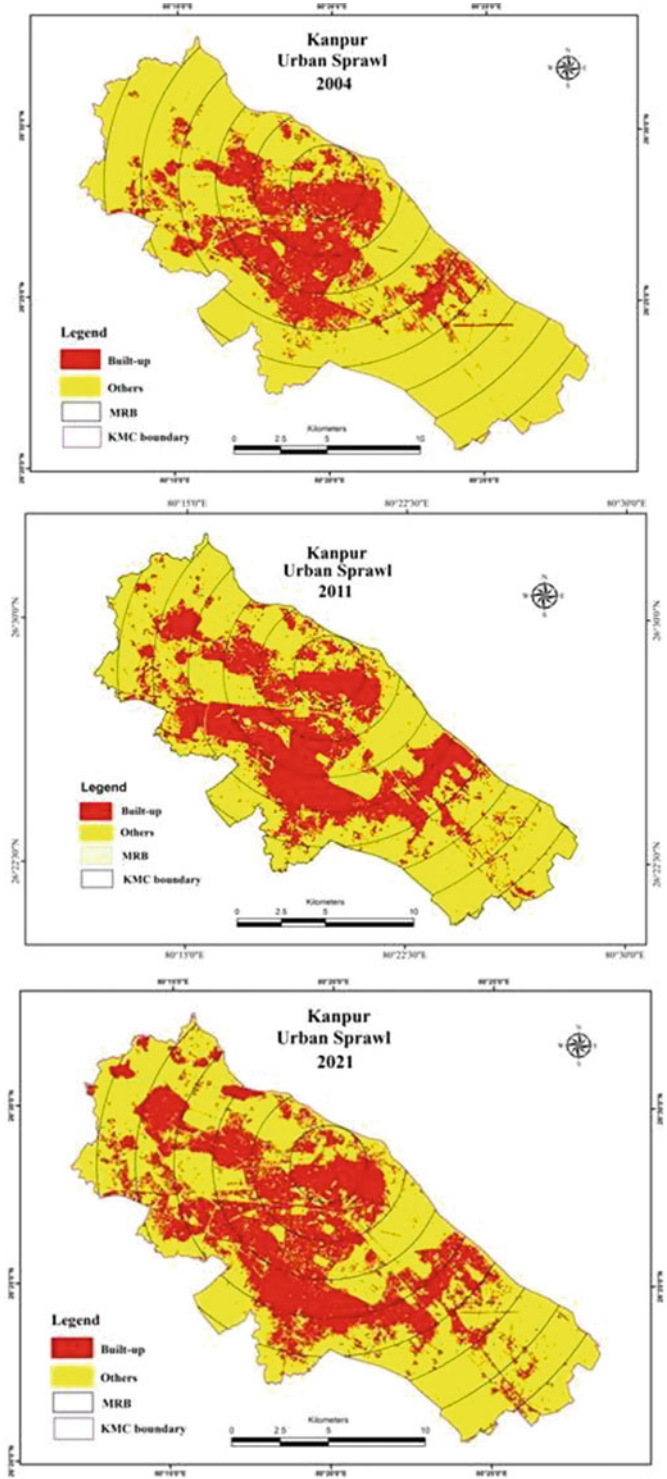**Fig. 6.5** Urban Sprawl map
2004, 2011 and 2021

Table 6.5 Shannon's entropy of Kanpur city in 2004 and 2021

Study Area	Year	Shannon's entropy (H)	Ln(9)
Kanpur	2004	1.7	2.1972
	2011	1.80	2.1972
	2021	1.84	2.1972

Table 6.6 Density index for 2004, 2011 and 2021

MRB Zones	Bi (2004)	Bi (2011)	Bi (2021)	Perimeter	DI (2004)	DI (2011)	DI (2021)
1	7.52	7.69	8.02	12.57	0.59	0.61	0.63
2	14.38	14.41	14.47	28.28	0.22	0.22	0.23
3	16.47	16.73	16.90	37.42	0.15	0.15	0.15
4	14.08	17.21	22.82	47.74	0.08	0.09	0.12
5	9.46	22.42	24.66	56.30	0.04	0.09	0.10
6	2.21	7.09	8.26	38.77	0.02	0.06	0.07
7	0.29	0.82	1.56	20.59	0.01	0.02	0.05
8	0.07	0.96	1.63	16.75	0.003	0.04	0.07
9	0.04	0.11	0.39	6.31	0.01	0.03	0.12

the city center toward outward in such way; till zone 3, it is depicting built-up development, and after this zone, it tends to decline (Fig. 6.6).

6.5 Conclusion

A critical evaluation has been done in this spatio-temporal study of Kanpur city urban structure, to study and comprehend the city's dispersion and compactness. A modest to dispersion growth was seen in Kanpur city in the base year (2004), a compact to dispersion growth was seen in the second time period (2011) and a dispersion growth was also shown in the third time period (2021). The Shannon's entropy values for the three-time period data of 2004, 2011 and 2021 are found to be 1.70, 1.80 and 1.84, respectively. These values are much close to the upper limit of Ln (9), i.e., 2.1972. This explains the high degree of built-up area dispersion in Kanpur city. DI value indicates core part of the city is a densely built-up plot, while the scattered built-up arrangement is toward the outer extent. MRB results reveals built-up feature gradually increasing from the city center toward outward in such way; till zone 3, it is depicting built-up development, and after this zone, it tends to decline (Fig. 6.6). Same trend found in every map of MRB (Fig. 6.5). The LULC classification had high accuracy 94.7% for the year 2004, 93.87% for the year 2011 and 94.89% for the year 2021. Analysis of the classified images depicting built-up area increased to 33.7 km^2, and vegetation also increased to 10.5 km^2 in restricted areas like the Kanpur cantonment, Armapur Estate and Railway Colony. The fallow land of the Kanpur city is decreasing at a very high rate.

The goals of obtaining quantitative data from the built-up area and using Shannon's entropy analysis to determine how the LULC alteration will affect the environment were successfully met by this work. Every method used in this study offers a quantitative analysis of the spatial pattern of urban growth. The current investigation exemplified the value of remote sensing information in urbanization. The results of this study will help to the planners and decision-makers comprehend the spatiotemporal evolution of urban sections for sustainable urban area planning to stop urban sprawl and other associated problems (Krishnaveni and Anilkumar 2020).
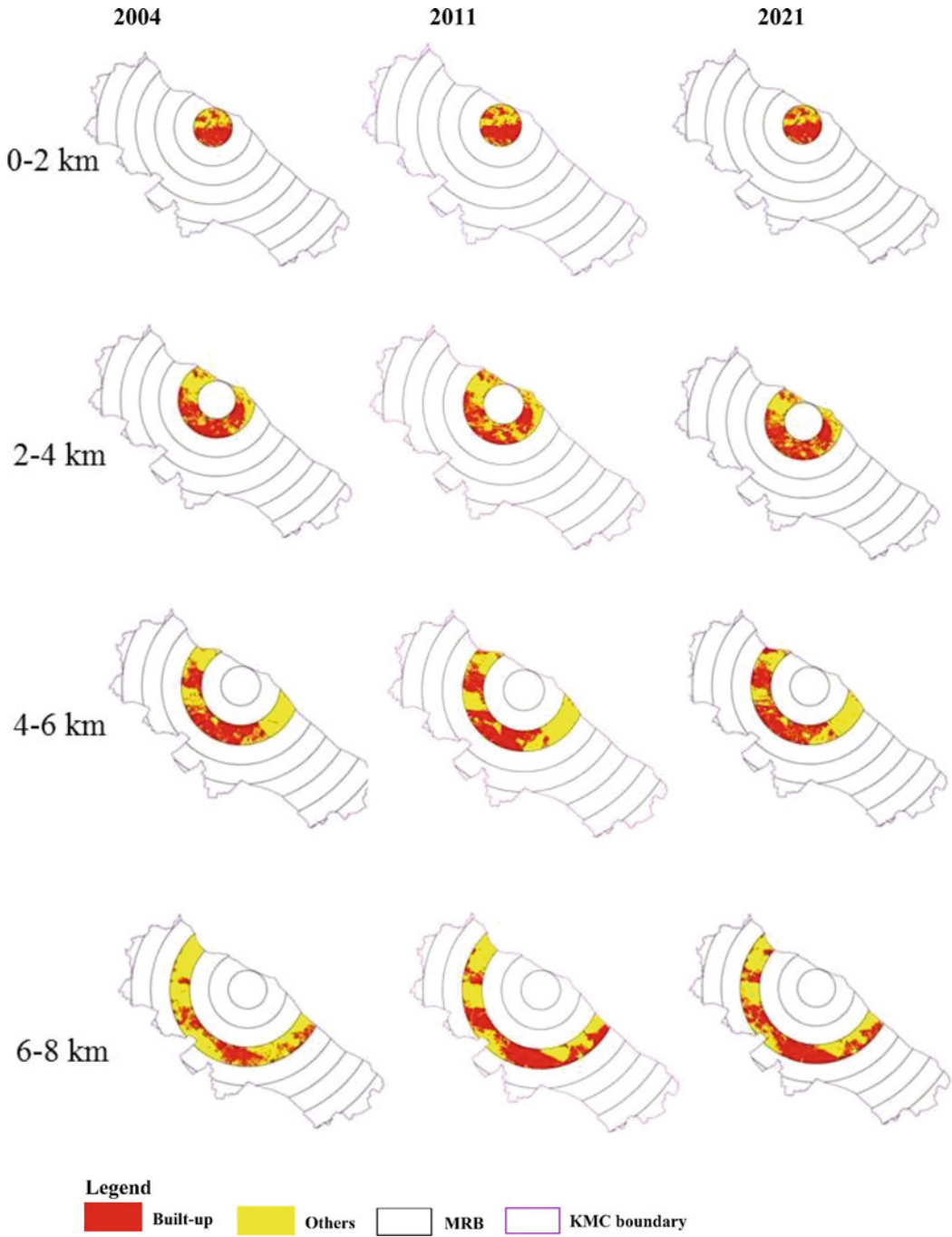
Fig. 6.6 Multiple ring buffer maps for built-up area of years 2004, 2011 and 2021
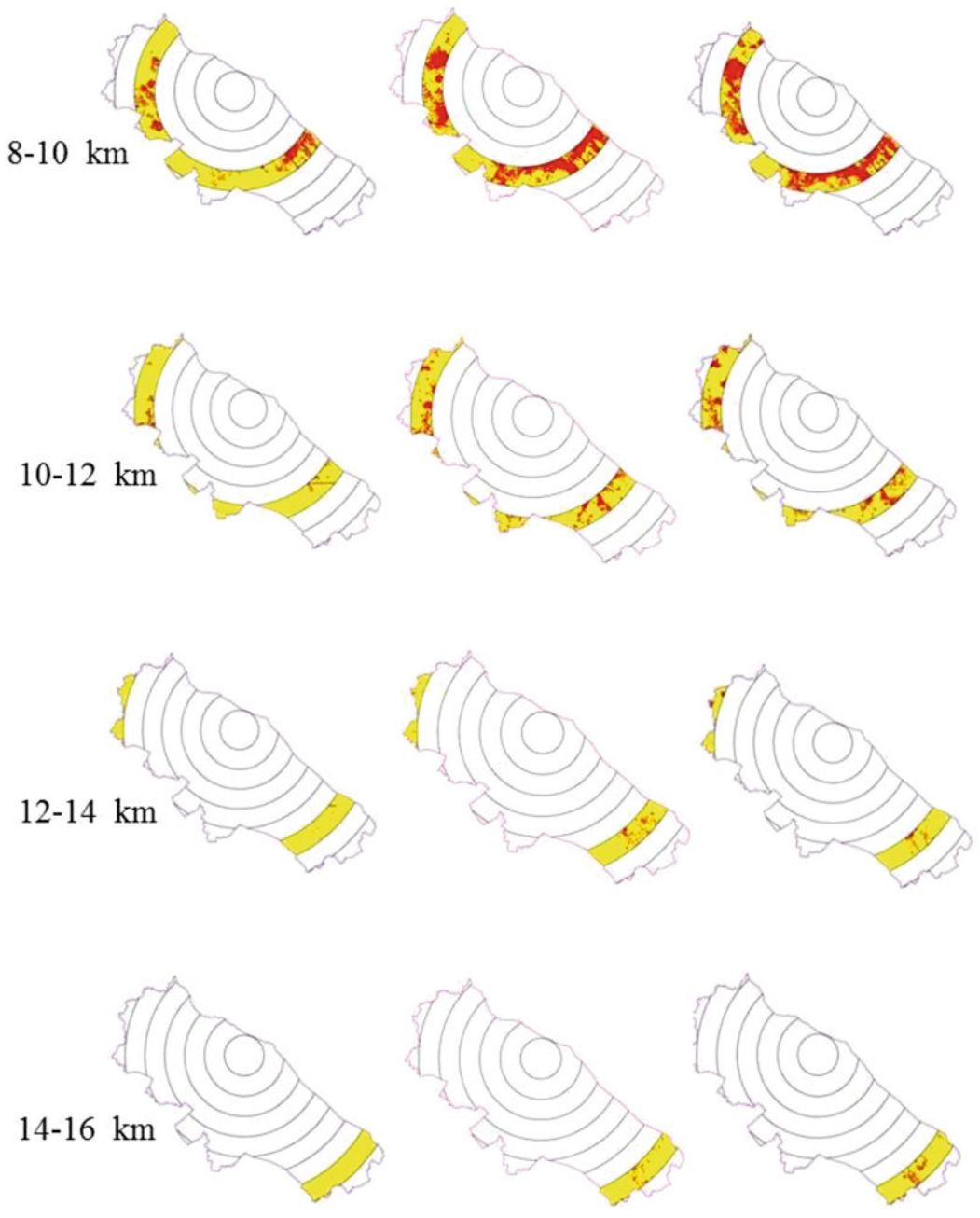
Fig. 6.6 (continued)

References

Anderson JR, Hardy EE, Roach JT, Witmer RE (1976) A land use and land cover classification system for use with remote sensor data. USGS professional paper 964. A revision of the land use classification system as presented in the USGS Circular 671

Bhatta B (2009) Analysis of urban growth patter using remote sensing and GIS: a case study of Kolkata, India. Int J Remote Sens 30:4733–4746

Bhatta B, Saraswati S, Bondyopadhyay D (2010) Urban sprawl measurement from remote sensing data. Appl Geogr 30:731–740

Cabral P, Augusto G, Tewolde M, Araya Y (2013) Entropy in urban systems. J Multidisc Digital Publ Inst 15:5223–5236

Census of India (2011) https://censusindia.gov.in/2011-common/censusdata2011

Cho KH, Lee DH, Jang GS (2021) Measurement of 30-years urban expansion using spatial entropy in Changwon and Gimhae, Korea. Sustainability 13:632

Harvey D (2008) The right to the city. New Left Rev 53:23–40

Herold M, Liu XH, Clarke CK (2003) Spatial metrics and image texture for mapping urban land use. Photogram Eng Remote Sens, 992–1001

Jawaharlal Nehru National Urban Renewal Mission (2011) https://mohua.gov.in

Jat MK, Garg PK, Khare D (2008) Monitoring and modelling of urban sprawl using remote sensing and GIS techniques. Int J Appl Earth Obs Geoinf 10 (1):26–43

Krishnaveni KS, Anilkumar PP (2019) Managing urban sprawl using remote sensing and GIS. Int Arch Photogramm Remote Sens Spatial Inf Sci XLII/W11

Kumar JAV, Pathan SK, Bhanderi RJ (2007) Spatio-temporal analysis for monitoring urban growth—a case study of Indore City. J Indian Soc Remote Sens 35(1):11–20

McDonald M (2010) Midwest mapping project. George Mason University. In: Department of Public and International Affairs

Polsby DD, Popper RD (1991) The third criterion: compactness as a procedural safeguard against partisan gerrymandering. Yale Law Policy Rev 9 (2):301–353

Punia M, Singh L (2012) Entropy approach for assessment of urban growth: a case study of Jaipur, India. J India Soc Remote Sens 40:231–244

Rahman A, Aggarwal SP, Netzband M, Fazal S (2011) Monitoring urban sprawl using remote sensing and gis techniques of a fast growing urban center, India. IEEE J Sel Top Appl Earth Obs Remote Sens 4(1):56–64

Ramachandra TV, Aithal BH, Sanna DD (2012) Insights to urban dynamics through landscape spatial pattern analysis. Int J Appl Earth Obs Geoinf 18:329–343

Ramachandra TV, Bharath AH, Sowmyashree MV (2014) Monitoring urbanization and its implications in a mega city from space: spatiotemporal patterns and its indicators. J Environ Manag, 1–15

Redman CL, Jones NS (2005) The environmental, social, and health dimensions of urban expansion. Popul Environ 26(6):505–520

Shaw A (2005) Peri-urban interface of Indian cities: growth, governance and local initiatives. Econ Pol Wkly 40:129–136

Sudhira HS, Ramachandra TV, Raj KS, Jagadish KS (2003) Urban growth analysis using spatial and temporal data. J Indian Soc Remote Sens 31:299–311

Sudhira HS, Ramachandra TV, Jagadish KS (2004) Urban sprawl: metrics, dynamics and modeling using GIS. Int J Appl Earth Obs Geoinf 5(1):29–39

Shukla A, Jain K (2019) Critical analysis of spatial-temporal morphological characteristic of urban landscape. Arab J Geosci 12:112

Taubenbock H, Wegmannb M, Roth A, Mehl H, Dech S (2009) Urbanization in India—spatiotemporal analysis using remote sensing data. J Comput Environ Urban Syst 33:179–188

Torrens PM, Alberti M (2000) Measuring sprawl. CASA working paper 27, University College London, Centre for Advanced Spatial Analysis, London. Accessed 27 Sept 2021

Xu L, Li Z, Song H, Yin H (2013) Land-use planning for urban sprawl based on the CLUE-S model: a case study of Guangzhou, China. J Multidisc Digital Publ Inst 15:3490–3506

Studying Urban Growth Dynamics in Indo-Gangetic Plain

7

Sandeep Maithani and Hamde Narayan Shankar

Abstract

The spatio-temporal characteristics of urban growth in the Indian-Gangetic planes (IGP) using night-time light (NTL) data sets have been studied in the present chapter. The study proposes to use Mann–Kendall's (MK) test and Principal Component Analysis (PCA) (S-Mode) for urban area extraction from NTL data sets in place of traditional thresholding techniques. The urban areas extracted using MK test and PCA (S-Mode) had 0.92 accuracy when evaluated using area under curve (AUC–ROC) method. Subsequently, urban areas of year 2000 and 2018 were extracted using the MK test and PCA (S-Mode). Using NTL extracted urban areas of year 2000 and 2018 and other thematic layers as input variables, three machine learning algorithms (i.e. artificial neural network, decision tree, and logistic regression)-based cellular automata models were executed for predicting the urban growth in year 2028. The model calibration results were evaluated using spatial metrics and it was found that artificial neural networks-based CA model gave the best simulation result. Thus, the present study provides a methodology for understanding spatio-temporal characteristics of urban areas at the regional scale using of NTL data (which is freely available in public domain).

Keywords

Night-time light · Principal component analysis · Indian-Gangetic plane · Mann–Kendall's test · Cellular automata · Artificial neural networks · Decision tree

7.1 Introduction

The finest and worst of urbanization can be seen in the present century. Urban centres have dramatically multiplied as a result of large-scale economic activity agglomeration brought by rapid industrialization. This has ushered in better services, businesses, jobs, and infrastructure all intertwined columns of increasing urbanization. Nevertheless, the unstructured, haphazard expansion of urban settlements has irreparably damaged adjacent agricultural regions and affected a number of ecological and hydrological cycles.

Depending on the level of development and population density, urbanization process differs significantly in various parts of the world. Urbanization has typically progressed more quickly in developing nations than it has in developed nations. In year 1950, developed

S. Maithani (✉) · H. N. Shankar
Urban and Regional Studies Department, Indian Institute of Remote Sensing, Dehradun, Uttarakhand, India
e-mail: maithanis99@gmail.com;
maithani@iirs.gov.in

nations had higher urban population compared to the developing nations. However, in beginning of 1970, the population in developing nations began to increase rapidly, while in the developed nations it is almost saturated, which is reflected in the slower urban population growth rates of developed nations (UNDESA 2019). India has rapidly urbanized over the past few decades, and population increase has been a primary driver of urban expansion in Indian cities. Since 1980s, the Indian economy has become more service and market driven. Rapid urbanization brought about by the new, emerging industries has resulted in unregulated expansion of urban areas. Although urbanization negatively affects the environment, however it is one of the root causes for expanding a nation's economy.

The present research aims to study the applicability of night-time light (NTL) data sets in monitoring and modelling the process of urban expansion in the Indian part of the Indo-Gangetic Plain (hereafter referred as IGP). The IGP predominantly covers states of Punjab, Haryana, Uttar Pradesh, Bihar, Jharkhand, West Bengal, Delhi, and Union territory of Chandigarh.

NTL is a time series data set available for 27 years (1992–2018) acquired by the Defence Meteorological Satellite Programme's Operational Linescan System (DMSP/OLS) and Suomi National Polar-orbiting Partnership satellite's Visible Infrared Imaging Radiometer Suite (NPP-VIIRS) at global scale. DMSP/OLS sensor provides NTL data from year 1992 till 2013, whereas NPP-VIIRS sensor provides the NTL data from year 2013 till 2018. DMSP data is a 6-bit data at spatial resolution of 30 arc-seconds (nearly 1000 m) while VIIRS data is a 12-bit data at spatial resolution of 15 arc-seconds (nearly 500 m). As the spatial and radiometric resolution of both data are different, an integrated and consistent NTL data set at spatial resolution of 1 km was generated by Xuecao et al. 2020, where they harmonized the inter-calibrated NTL observations from DMSP and VIIRS. This harmonized NTL data set was used in the present study.

NTL data has been an essential part of urban studies (Sánchez de Miguel et al. 2014; Doll and Pachauri 2010; Elvidge et al. 1997), socio-economic activities (Chen and Nordhaus 2011), light pollution (Falchi et al. 2016; Cinzano et al. 2001), urban environments (Bennie et al. 2015), urban mapping (Ritchie et al. 2018; Jiang et al. 2021; Xu et al. 2016; Xuecao Li and Zhou 2020; Miller et al. 2012). For delineating built-up areas in NTL data sets, most of the studies used image thresholding method where intensity values below a particular threshold were masked out. However, the process of image thresholding is a trade-off between determination of the threshold value that fits well for the study area and attenuates much information. To reduce this subjectivity, the present study proposes to use a nonparametric technique Contextual Mann–Kendall's (CMK) test and Principal Component Analysis (PCA) to extract built-up areas from NTL data sets.

Cellular automata (CA)-based models have been widely used in the field of urban growth modelling (Aarthi and Gnanappazham 2018) as CA can model spatial process which are complex and nonlinear in behaviour. CA-based models operate on pre-defined transition rules which decide whether a cell (grid) changes its state (for example from non-urban to urban). Definition of these transition rules in the CA model and their calibration is a time taking and subjective process. The present study proposes to use different machine learning algorithms for transition rule definition and model calibration, which in leads to reduction in model calibration time and makes the CA model more objective in nature. The present study evaluates the following machine learning-based CA models: artificial neural network (ANN)-based CA model, decision tree (DT)-based CA model, and logistic regression (LR)-based CA model.

Machine learning techniques such as ANN, DT, and LR make no pre-assumptions about the data distribution are nonparametric in nature and can capture the nonlinearity inherent in the data set (Li and Yeh 2002; Judge et al. 2016; Arsanjani et al. 2012; Rastogi and Sharma 2020; Maithani et al. 2007; Aarthi and Gnanappazham 2018).

The major research objectives of the present study are

1. To reduce subjectivity in delineation of built-up areas in night-time light (NTL) data sets using a Contextual Mann–Kendall's (CMK) test and Principal Component Analysis (PCA) approach.
2. To carry out a comparative study of different machine learning algorithms for simulating urban growth in the IGP region, using built-up areas classified using NTL data sets.

7.2   Study Area

IGP occupies most of the northern part of India and is one of the most densely populated regions of the world. Three major rivers Ganges, Indus, and Brahmaputra and their tributaries have formed the IGP. The portion of IGP falling in India extends from north central up to Thar Desert in the west, to Assam in the East, to Bay of Bengal in down south. Region's east part is blessed with tremendous amount of rainfall in rainy season and decreases towards west. Major portion of IGP region is occupied by states: Punjab, Haryana, Uttar Pradesh, Bihar, Jharkhand, West Bengal, Delhi, and Union territory of Chandigarh. These states are taken as study area for the current study. Figure 7.1 shows the study area and its location in the country.

The entire IGP region shows varying urbanization pattern across its span, to the North-West, are highly urbanized regions such as Punjab, Haryana, and NCT of Delhi, to the extreme South-East, is West Bengal also having high urban growth and, in the middle, less urbanized states such as Uttar Pradesh, Bihar, and Jharkhand are situated. The urban area in Indian IGP (hereafter referred as IGP) region increased from 6257 km^2 in 1975 to 14,902 km^2 in 2015, thus registering a 2.3 times increase in urban areas over a span of four decades.
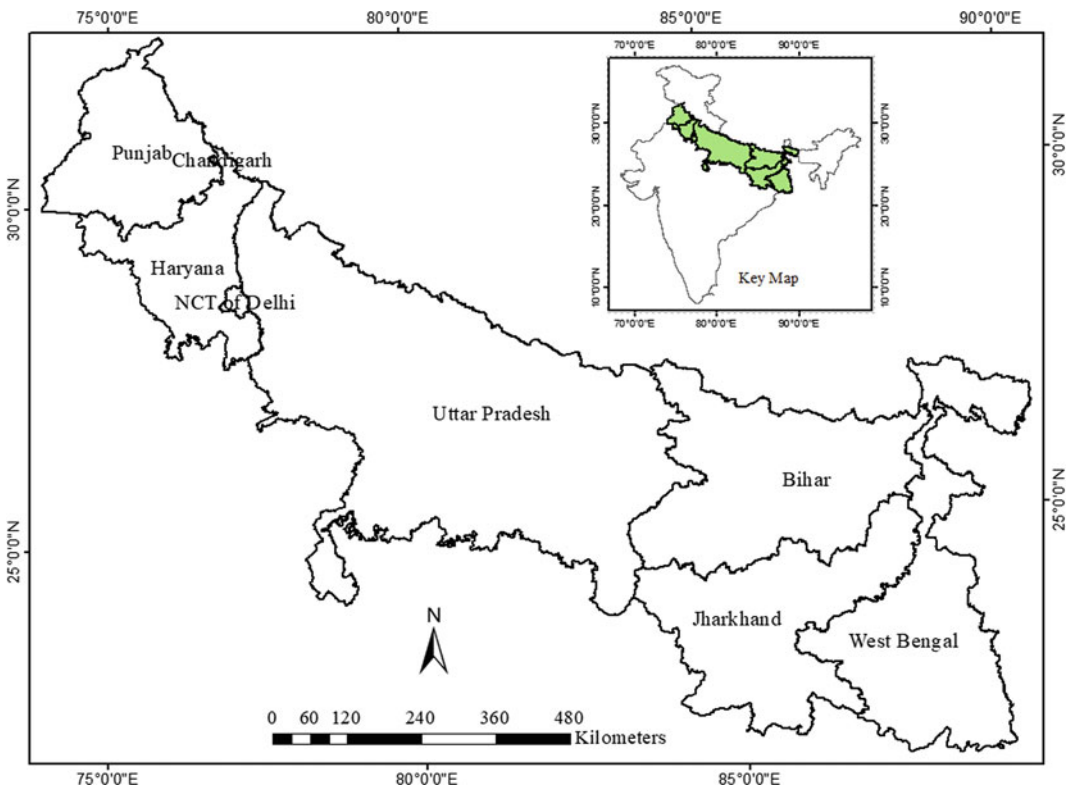

Fig. 7.1 Location of study area

7.3 Data Sources and Methodology

Detecting trend and its strength in any time series is an important step to extract meaningful information from the data. Linear regression is one of the conventional methods for trend analysis and is dependent of assumption that the data is a sample from a population that can modelled by a probability distribution, also called as parametric test. Parametric tests often give similar importance to outliers and majority of the data distribution. On the other hand, nonparametric tests do not depend on the pre-assumptions of the data and emphasizes on the majority distribution of data (Sulaiman et al. 2015). Thus, the present study uses a nonparametric test for the trend analysis of NTL called as Mann–Kendall's test (Kendall 1975; Mann 1945). The test gives two outputs, viz. significance values and strength of trend at each location (grids). The significance values were calculated from the probability distribution curve of the strength of trend at the given grids. When the trend is significant, the MK test signifies the presence of monotonic trend at that significance level. MK test calculates the slopes all pair-wise combinations of the observations or samples. Equation (7.1) defines Kendall's S:

$$S = \sum_{i=1}^{n-1} \sum_{j=i+1}^{n} \text{sign}(x_i - x_j) \qquad (7.1)$$

where n is the length of the data set and x_i and x_j are observations at times i and j. The slope between two observations comes to be positive, negative, or zero; the value of sign function in above equation becomes 1, −1, or 0, respectively. According to Kendall (1975) and Mann (1945), statistics S is almost normally distributed when $n \geq 8$. In such cases, mean and variance of distribution are given in Eq. (7.2) and (7.3):

$$E(S) = 0 \qquad (7.2)$$

$$\text{Var}(S) = \frac{n(n-1)(2n+5)}{18} = \sigma^2 \qquad (7.3)$$

where σ is the standard deviation. Z statistics can be calculated as shown in Eq. 7.4

$$Z = \begin{cases} \dfrac{S-1}{\sqrt{\text{Var}(S)}} & \text{for } S > 0 \\ 0 & \text{for } S = 0 \\ \dfrac{S-1}{\sqrt{\text{Var}(S)}} & \text{for } S < 0 \end{cases} \qquad (7.4)$$

The Z statistics follows normal distribution under the null hypothesis of no trend. Z results a positive value if the trend is upward and negative when trend is downward. The probability of no trend is then calculated as given in Eq. (7.5):

$$p = 2[1 - \phi(|Z|)] \qquad (7.5)$$

where ϕ () is the normal cumulative distribution function. These p values are used for significance of the trend.

When the data of a large area is given, it is highly possible that a lot of singular grids exhibit significant increasing trend. However, the grid should be considered as urban area if the surrounding grids also exhibit similar trend as the urban area grows in a cluster form. Contextual Mann–Kendall's (CMK) provides significance levels at each grid considering the presence or absence of similar trends at neighbouring grids proving that trends at such isolated grids are not just occurring by chance. Thus, the CMK significance values are used for the extraction of urban areas which is based on regionally averaged Mann–Kendall (RAMK) test (Douglas et al. 2000) and evaluates the trend at a regional scale using a 3 by 3 neighbourhood around each pixel. Regional average Kendall's S (S_m) is calculated as shown in Eq. (7.6):

$$S_m = \frac{1}{m} \sum_{k=1}^{m} S_k \qquad (7.6)$$

where S_k is the Kendall's S for kth grid in the neighbourhood with m grids. Similarly, mean and variance can be given as shown in Eqs. (7.7) and (7.8).

$$E(S_m) = 0 \qquad (7.7)$$

$$\text{Var}(S_m) = \frac{n(n-1)(2n+5)}{18m} = \frac{\sigma^2}{m} \qquad (7.8)$$

For the S_m distribution, Z_m can be described as given in Eq. (7.9).

$$Zm = \frac{S_m - E(S_m)}{\frac{\sigma}{\sqrt{m}}} \qquad (7.9)$$

Thus, p value is calculated for Zm which is used for detecting the significant contextual night light trend. When $p < 0.05$, significant trend exists with 95% confidence. Thus, the CMK significance values ($p < 0.05$) were used for the extraction of grids with significant monotonous trend of NTL increase.

PCA has a utility of transforming a set of inter-correlated data into a set of uncorrelated components, first one containing maximum of the information from the data. Mostly, PCA is used, when the data is of high dimension, to reduce the dimensionality along with the preservation of maximum information in the data. There are two modes of PCA, viz. Time (T) and Space (S). Generally, T mode is used due to its property that it considers raster bands of a data set as variables (dimensions) representing time slices and space (grids) as observations, it finds recurrent patterns across space in time and outputs images with clusters of pixels as principles components. First few components contain maximum of the information from the imagery. On the other hand, S-Mode considers temporal profiles of each grid as its variables and interprets recurrent pattern across time in space (Compagnucci et al. 2001; Compagnucci and Salles 2001; Ehrendorfer 1987; Manatsa et al. 2008). There are two basic outputs of PCA namely loadings and components. Loadings are correlation values of the principle components with each variable in respective modes of PCA. In T mode, loadings are graphs depicting correlations of the components with each data set raster, whereas in S-Mode loadings are images depicting correlation of each grid with its temporal profile from the data set (Neeti and Ronald Eastman 2014).

For carrying out the MK test and PCA (S-Mode), TerrSet Geospatial Monitoring and Modelling System computer program is used. Both the tests are carried out on two subsets of the NTL data, viz. 1992–2000 and 1992–2018. Using the outputs of CMK test, which is the significant strength of NTL trend and PCA, which is represented by the reduced dimensionality version of NTL data, urban areas were extracted from the subsets for the years 2000 and 2018. The built-up extracted for year 2000 is validated using the Global Human Settlement Layer (GHSL) of year 2000 using AUC–ROC (receiver operating curve) (Florczyk et al. 2019). It is a two-dimensional graph showing true positive rate on Y axis and false positive rate on X axis. This value varies between 0 and 1 and requires to be above 0.5 for acceptable results. Higher the area under curve (AUC), higher is the true positives. The AUC value for the extracted urban built-up was 0.92 (Fig. 7.2).
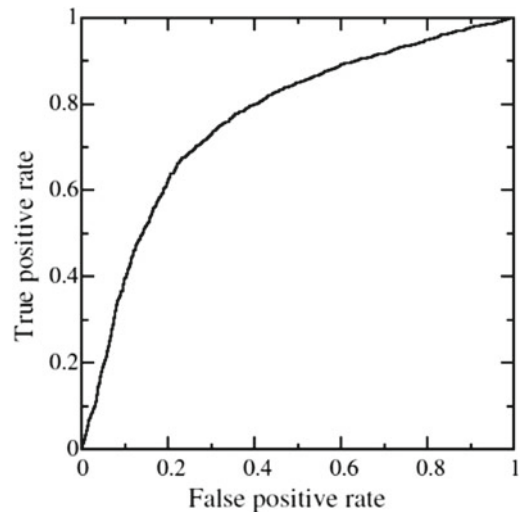
Fig. 7.2 AUC–ROC curve

7.4   Simulation of Urban Growth

The urban growth in the IGP was simulated using city proximity and travel time as driving variables of built-up area growth. City proximity layer was generated using GIS and travel time to the major urban cities was taken from Cattaneo et al. (2021). Three CA urban growth models based on ANN, DT, and logistic regression algorithms were executed in GeoSOS tool (Xia and Li 2010) to predict the built-up area for year 2018 using built-up area of year 2000 as baseline data.

The ANN-CA requires to tune the hyper-parameters of the model, viz. number of neurons, number of iterations, window size, disturbance factor, and dispersion factor. Using trial and error method, the number of neurons was set to be 3 and window size was kept at 5. Number of iterations were set at 90 and dispersion factor at 10. Number of iterations decide how many times the model should be trained on the training data. Figures 7.3, 7.4 and 7.5 show parameter setting of the models which are to be decided by the user.

In LR algorithm, the hyper parameter to be tuned is the dispersion factor, as it decides the distance decay gradient. Higher the dispersion, deeper is the distance–decay gradient (Fig. 7.6). While in DT algorithm, the depth of tree was kept to be ten (10) as large trees tend to result in over training of the data.

After fixing the hyper-parameters in the three algorithms, all the three models were executed and the built-up area in year 2018 was simulated. The simulated built-up maps of year 2018 were compared with the actual built-up map of 2018

Fig. 7.4   Accuracy of model (changing window size)
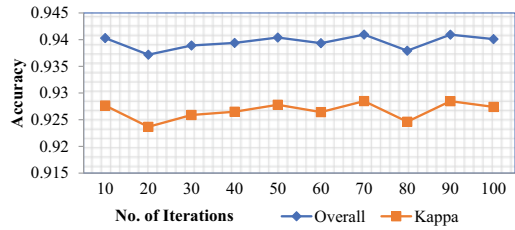
Fig. 7.5   Accuracy of model (changing no. of iterations)
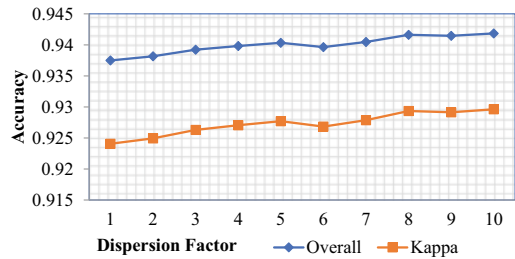
Fig. 7.6   Accuracy of model (changing dispersion factor)
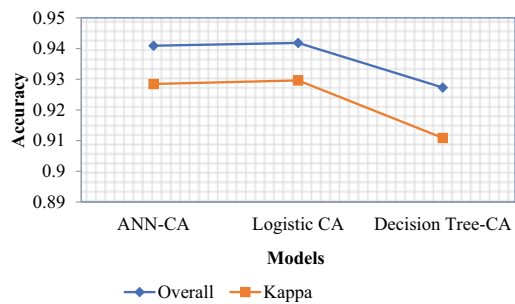
Fig. 7.7   Accuracy comparison between growth models

extracted from NTL data (Fig. 7.7). It can be observed from Fig. 7.7 that ANN-CA and Logistic CA gave results with higher accuracies compared to DT-CA.

Fig. 7.3   Accuracy of model (changing no. of neurons)

Using the calibrated models, the urban built-up area was subsequently predicted for year 2028. Results of the simulation are shown in Figs. 7.8, 7.9 and 7.10.

The simulated built-up area in year 2028 by the three models was analysed using the spatial metrics (Table 7.1).

It can be observed from Table 7.1 that ANN-CA and logistic CA simulations produced similar results in all the metrics, whereas DT-CA simulation showed comparatively high number of urban patches, which indicates that DT-CA was predicting a more sprawled growth compared to the ANN-CA and logistic CA models.

7.5 Discussion

Studies on urban growth dynamics play important role in land resource policy making. Therefore, within the context of remote sensing and its applications in urban growth, overall aim of the study is to map urban expansion using night-time light data and model urban growth dynamics at a regional scale. Robust attributes of urban growth are studied for the Indo-Gangetic Plains in India and future scenario building techniques are explored. The study includes six Indian States in IGP which are Punjab, Haryana, Uttar Pradesh, Bihar, Jharkhand, West Bengal, two Union Territories of Chandigarh, and NCT of Delhi.

Mann–Kendall's test on NTL time series, viz. 1992–2000 and 1992–2018 was applied, which resulted in locations where NTL increasing trend was significant. PCA was used due to its ability to generate data with high variance from the highly correlated data. In this study, S-Mode of PCA was used to preserve temporal information. Using the results from two analyses, urban area was extracted for year 2000 and 2018. The urban area extracted for the year 2000 was validated with GHSL 2000 data using ROC curve and the
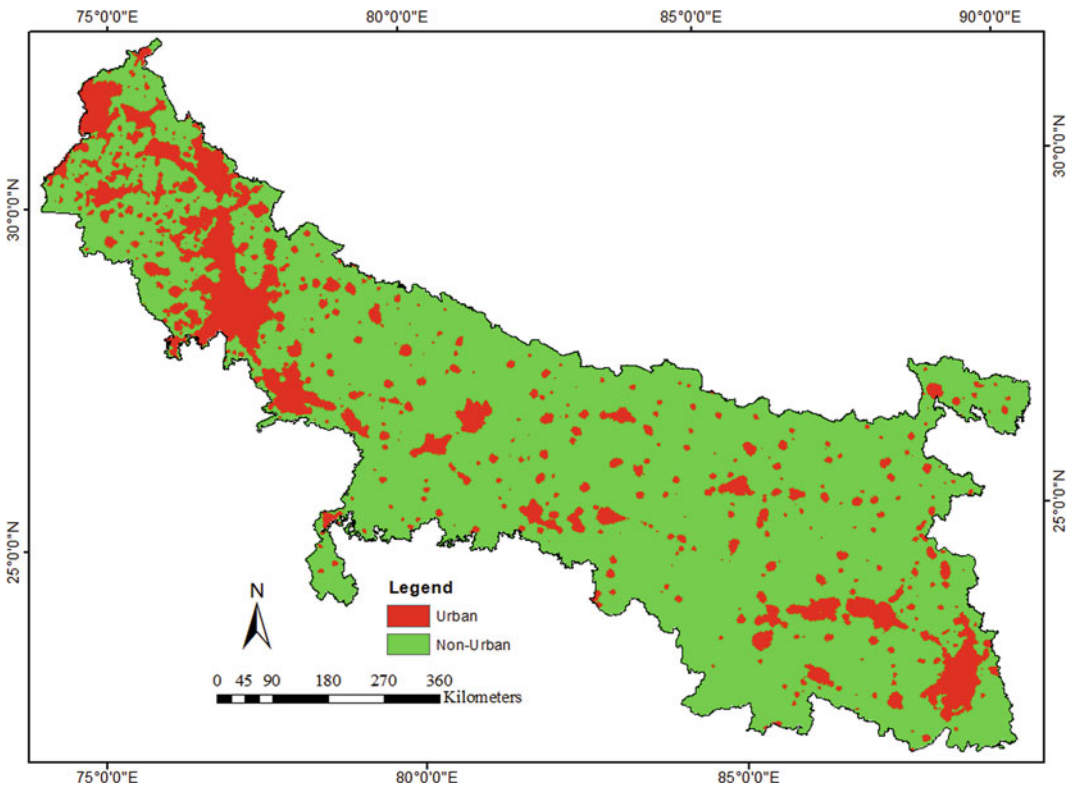
Fig. 7.8 Predicted urban area for 2028 (ANN-CA)
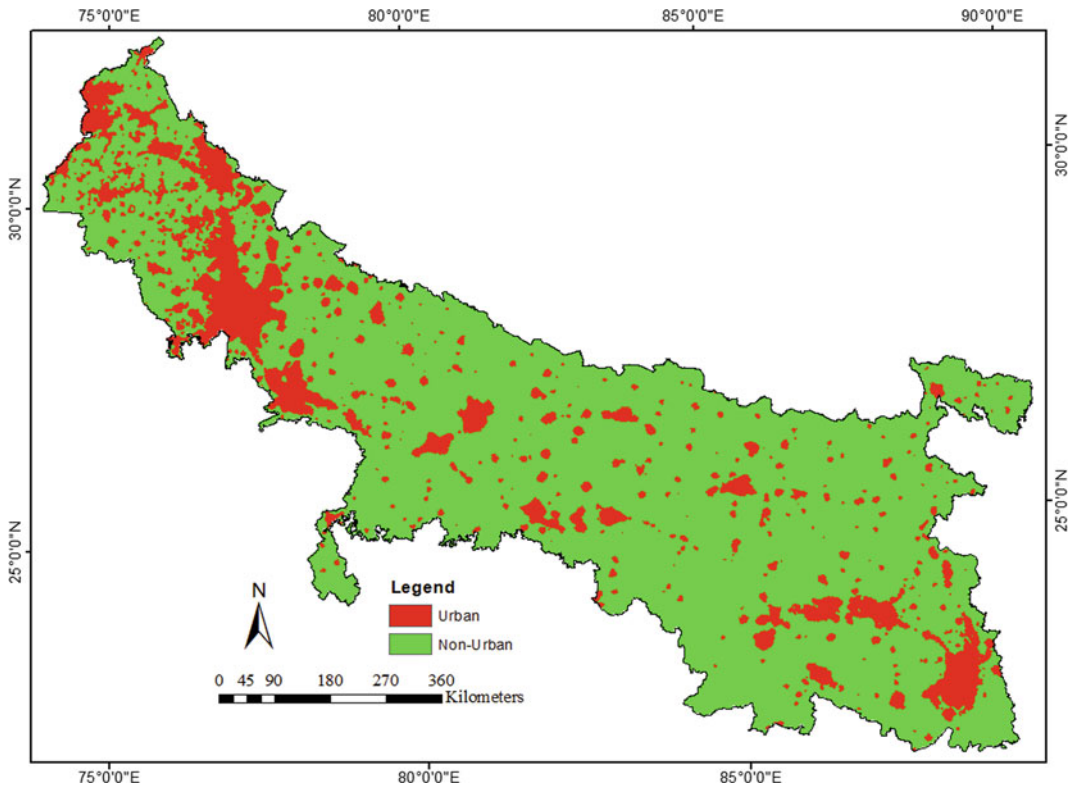
Fig. 7.9 Predicted urban area for 2028 (logistic-CA)

accuracy achieved was 0.92. Thus, it can inferred that NTL data is useful in extracting urban areas without involving direct subjectivity using proposed methodology.

The three urban growth models (ANN-CA, DT-CA, and logistic regression-CA) were executed to simulate the urban area in year 2018, a comparative analysis of the simulated results showed that ANN-CA and logistic CA gave better results compared to the DT-CA. The three trained models were then run for predicting the urban built-up in year 2028, and the simulated results were compared based on spatial metrics. ANN-CA and logistic CA simulated built-up growth for year 2028 which had higher consistency compared to DT-CA. The study showed that model performances can be enhanced through the regulation of the hyper-parameters of the models.

Overall, the present study tries to formulate a methodology for analysis of built-up area

extracted from NTL data set at a regional scale. Land use planning strategies have two major goals: to manage urban area growth and to make built-up areas more integrated for intense usage throughout urban expansion. With the help of studies of urban growth dynamics, specific policies can be formulated in order to lead to planned and sustainable urban growth.

7.6 Conclusion

The present study is based on NTL derived urban maps of year 2000 and 2018, however in future studies more data sets can be added to the study. For urban growth simulation, the urban area built-up maps along with two causative variables driving urban growth were used; however, more variables can be included to further improve the model performance. For finding relationship between the urban growth and causative
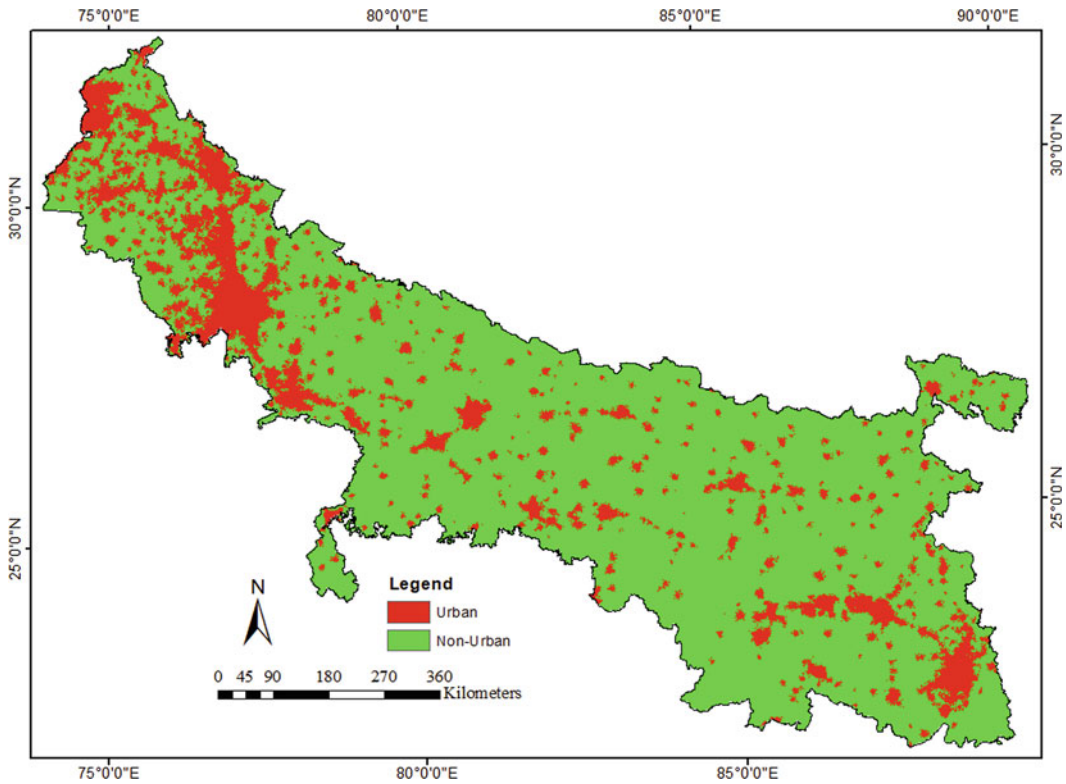
Fig. 7.10 Predicted urban area for 2028 (decision tree-CA)

Table 7.1 Spatial metrics calculated for built-up area simulated for year 2028

Simulation	NP	LSI	MPS	AI
ANN-CA	504	24.6	20,170	92
DT-CA	2555	52.39	3963	83.7
Logistic CA	505	22.91	19,756	93.03

where NP = No. of patches, LSI = Landscape shape index, MPS = Mean patch size, and AI = Aggregation index

variables, more advanced machine learning algorithms namely convolution neural network (CNN) can be employed.

The machine learning-based urban growth models provide a "what-if" kind of tool to the urban planners and city administrators. Various future urban growth scenarios in response to various policy measures can be generated which serve as input to the master plan formulation and other planning activities. The models thus provide a better understanding of the urban growth dynamics and the responses to various policy measures.

References

Aarthi AD, Gnanappazham L (2018) Urban growth prediction using neural network coupled agents-based cellular automata model for Sriperumbudur Taluk, Tamil Nadu, India. Egypt J Remote Sens Space Sci 21(3):353–362. https://doi.org/10.1016/j.ejrs.2017.12.004

Arsanjani JJ, Helbich M, Kainz W, Boloorani AD (2012) Integration of logistic regression, Markov chain and cellular automata models to simulate urban expansion. Int J Appl Earth Obs Geoinf 21(1):265–275. https://doi.org/10.1016/j.jag.2011.12.014

Bennie J, Duffy JP, Davies TW, Correa-Cano ME, Gaston KJ (2015) Global trends in exposure to light

pollution in natural terrestrial ecosystems. Remote Sens 7(3):2715–2730. https://doi.org/10.3390/rs70302715

Cattaneo A, Nelson A, McMenomy T (2021) Global mapping of urban-rural catchment areas reveals unequal access to services. Proc Natl Acad Sci 118(2): e2011990118. https://doi.org/10.1073/pnas.2011990118

Chen X, Nordhaus WD (2011) Using luminosity data as a proxy for economic statistics. Proc Natl Acad Sci United States Am 108(21):8589–8594. https://doi.org/10.1073/pnas.1017031108

Cinzano P, Falchi F, Elvidge CD (2001) The first world atlas of the artificial night sky brightness. Mon Not R Astron Soc 328(3):689–707. https://doi.org/10.1046/j.1365-8711.2001.04882.x

Compagnucci RH, Alejandra Salles M, Canziani PO (2001) The spatial and temporal behaviour of the lower stratospheric temperature over the southern hemisphere: the MSU view. Part II: spatial behaviour. Int J Climatol 21(4):439–454. https://doi.org/10.1002/joc.607

de Miguel S, Alejandro JZ, Castaño JG, Pascual S (2014) Evolution of the energy consumed by street lighting in Spain estimated with DMSP-OLS data. J Quant Spectrosc Radiat Transfer 139:109–117. https://doi.org/10.1016/j.jqsrt.2013.11.017

Doll CNH, Pachauri S (2010) Estimating rural populations without access to electricity in developing countries through night-time light satellite imagery. Energy Policy 38(10):5661–5670. https://doi.org/10.1016/j.enpol.2010.05.014

Douglas EM, Vogel RM, Kroll CN (2000) Trends in floods and low flows in the United States: impact of spatial correlation. J Hydrol 240(1–2):90–105. https://doi.org/10.1016/S0022-1694(00)00336-X

Ehrendorfer M (1987) A regionalization of austria's precipitation climate using principal component analysis. J Climatol 7(1):71–89. https://doi.org/10.1002/joc.3370070107

Elvidge CD, Baugh KE, Kihn EA, Kroehl HW, Davis ER, Davis CW (1997) Relation between satellite observed visible-near infrared emissions, population, economic activity and electric power consumption. Int J Remote Sens 18(6):1373–1379. https://doi.org/10.1080/014311697218485

Falchi F, Cinzano P, Duriscoe D, Kyba CCM, Elvidge CD, Baugh K, Portnov BA, Rybnikova NA, Furgoni R (2016) The new world atlas of artificial night sky brightness. Sci Adv 2(6):1–26. https://doi.org/10.1126/sciadv.1600377

Florczyk AJ, Daniele C, Christina E, Sergio F, Luca K, Thomas M, Martino M, Michele P, Marcello P, Panagiotis S, Filip S, Luigi Z (2019) GHSL data package 2019. doi:10.2760/0726

Jiang S, Wei G, Zhang Z, Wang Y, Xu M, Wang Q, Das P, Liu B (2021) Detecting the dynamics of urban growth in Africa using DMSP/OLS night time light data. Land 10(1):1–19 https://doi.org/10.3390/land10010013

Judge V, Omrani H, Antoni JP, Klein O (2016) Analysing urban development with decision tree based cellular automata. Toward an automatic transition rules creation process. Cellular Automata Modeling for Urban and Spatial Systems (CAMUSS), no. February 2017. https://www.researchgate.net/profile/Jean-Philippe_Antoni/publication/313889981_Analysing_urban_development_with_decision_tree_based_cellular_automata_Toward_an_automatic_transition_rules_creation_process/links/58adc22592851cf7ae85ac2a/Analysing-urban-dev.

Kendall MG (1975) Rank Correlation Methods. Griffin, London

Li X, Dan L (2010) GeoSOS for ArcGIS. http://www.geosimulation.cn/GeoSOS/

Li X, Yeh AGO (2002) Neural-network-based cellular automata for simulating multiple land use changes using GIS. Int J Geogr Inf Sci 16(4):323–343. https://doi.org/10.1080/13658810210137004

Li X, Zhou Y, Zhao M, Zhao X (2020) A harmonized global night time light dataset 1992–2018. Sci Data 7 (1):1–9

Li X, Gong, et al. (2020). Mapping global urban boundaries from the global artificial impervious area (GAIA) data. Environmental Research Letters. 15. https://doi.org/10.1088/1748-9326/ab9be3

Maithani S, Jain RK, Arora MK (2007) An artificial neural network based approach for modelling urban spatial growth. ITPI J 4(2):43–51. www.itpi.org.in

Manatsa D, Chingombe W, Matarira CH (2008) The impact of the positive Indian ocean dipole on Zimbabwe droughts tropical climate is understood to be dominated by. Int J Climatol 2029: 2011–2029. https://doi.org/10.1002/joc

Mann HB (1945) Non-parametric test against trend. Econometrica 13(3):245–259. http://www.economist.com/node/18330371?story%7B_%7Did=18330371

Miller SD, Mills SP, Elvidge CD, Lindsey DT, Lee TF, Hawkins JD (2012) Suomi satellite brings to light a unique frontier of nighttime environmental sensing capabilities. Proc Natl Acad Sci USA 109(39):15706–15711. https://doi.org/10.1073/pnas.1207034109

Neeti N, Ronald Eastman J (2014) Novel approaches in extended principal component analysis to compare spatio-temporal patterns among multiple image time series. Remote Sens Environ 148:84–96. https://doi.org/10.1016/j.rse.2014.03.015

Rastogi K, Sharma SA (2020) Integration of cellular automata-Markov chain and artificial neural network model for urban growth simulation 14 (1)

Ritchie H (2018) Urbanization. Our world in data. https://ourworldindata.org/urbanization

Sulaiman NH, Kamarudin MKA, Mustafa AD, Amran MA, Azaman F, Abidin IZ, Hairoma N (2015) Trend analysis of Pahang river using non-parametric analysis: Mann Kendall's trend test. Malays J Anal Sci 19(6):1327–1334

United Nations, Department of Economic and Social Affairs, Population Division (2019). World

Urbanization Prospects: The 2018 Revision (ST/ESA/SER.A/420). New York: United Nations

Xu P, Jin P, Yang Y, Wang Q (2016) Evaluating urbanization and spatial-temporal pattern using the DMSP/OLS nighttime light data: a case study in Zhejiang Province. Math Probl Eng 2016 https://doi.org/10.1155/2016/9850890

Monitoring and Prediction of Spatiotemporal Land-Use/ Land-Cover Change Using Markov Chain Cellular Automata Model in Barisal, Bangladesh

8

Md. Naimur Rahman, Md. Mushfiqus Saleheen, Sajjad Hossain Shozib, and Abu Reza Md. Towfiqul Islam

Abstract

Land use and land cover (LULC) is the dominant approach to evaluating urban expansion and estimating proper urban planning and management. LULC changes reflect the economic and structural development of specific areas. These types of drivers of land use and land cover (LULC) are accountable for a slew of issues, including road congestion, flooding, sanitation facilities, and agricultural land depletion. This chapter utilized an integrated Markov chain cellular automata method to simulate LULC and prediction in the Barisal district to analyze these issues. Firstly, visualization of spatiotemporal changes was extracted for two different periods of 2002 and 2021 from satellite images. Then the combined technique of GIS, RS (Remote Sensing), and the Markov chain cellular automata method was employed to predict LULC in the 2031 period. The results of this study, the maximum area of water bodies increased from 4.47 to 9.93% between 2002 and 2021, while bare land decreased from 20.93 to 16.63%. The increase in water bodies may be the consequence of sea level rise and flooding as well. As a coastal location, the expected changes show that agricultural land might decline from 57.45 to 49.23% between 2021 and 2031 due to the water body's dominance (9.94–10.03%). So, the future model could help with planning and building cities in a way that protects the environment and is sustainable.

Keywords

Land use land cover · Cellular automata · Markov Chain · Urban change and prediction · Remote sensing

8.1 Introduction

Globally, increasing human activity is modifying the Earth's land surface on a vast scale, having a dramatic influence on the operation of global ecosystems (Lambin et al. 2001). This is what has caused soil deterioration, biodiversity loss, uncontrolled urban sprawl, plus overall land degradation due to agricultural growth and the

Md. Naimur Rahman · Md. Mushfiqus Saleheen
Department of Geography and Environmental Science, Begum Rokeya University, Rangpur 5400, Bangladesh
e-mail: naimurbrur@gmail.com

S. H. Shozib
Department Environmental Engineering, Nanjing Forestry University, Nanjing 2130007, China
e-mail: shozib@njfu.edu.cn

A. R. Md. Towfiqul Islam (✉)
Department of Disaster Management, Begum Rokeya University, Rangpur 5400, Bangladesh
e-mail: towfiq_dm@brur.ac.bd

tourism sector and pollution from nonpoint sources and a progressive reduction in ecological processes (Mundia and Aniya 2006; Ojima et al. 1994; Quétier et al. 2007; Shalaby and Tateishi 2007; Xian et al. 2007; Yu and Ng 2007). Although environmental disruption by anthropogenic behaviors started in the late Pleistocene, it accelerated with the advent of agriculture and urbanization (Stephens et al. 2019). Among the various aspects of the man-environment connection, land usage is the most prevalent. Land cover refers to the observed (bio) physical layer on the surface of the planet (Di Gregorio 2005). Multiple variables acting on local, continental, and global stages are responsible for the land use changes, which are dynamic in essence (Hassan et al. 2016; Rahman et al. 2012). Rapid and unchecked population increase, coupled with industrialization and economic expansion, has continuously altered the LULC pattern (Dutta et al. 2019). Additionally, variations in LULC caused by humans have an impact on the global carbon cycle and lead to increases in atmospheric CO_2 (Alves and Skole 1996; Dixon et al. 1994). These changes have a profound and, in some cases, permanent effect on the natural global ecosystem (Abdullah and Nakagoshi 2006). Urban change refers to any transformation in the urban landscape linked with the expansion or contraction of a city. Some transformations are beneficial to people, while others are detrimental. During the late 1700s and early 1800s, the Industrial Change saw the industrialization of agricultural and textile production, as well as a transition in power, notably steam ships and railroads. This led to the rapid urbanization of Europe. A distinct set of processes are happening in HICs today, with urban locations deteriorating as newer manufacturers and service sectors eschew them in favor of bordering city sites, culminating in urban deterioration (CoolGeography 2022).

Geospatial approaches such as remote sensing (RS) and geographic information systems (GIS) have long been acknowledged as critical and efficient tools for identifying variations in LULC at various geographical scales. Numerous image analysis and change detection algorithms have been applied to remote sensing-based data

to extract information (Lu et al. 2011). On the other hand, GIS enables the incorporation of RS data into the explicit knowledge and modeling of LULC (Mesev and Walrath 2007). In 1995, the International Geosphere-Biosphere Project (IGBP) and the International Human Dimensions Programme (IHDP) introduced the "Land Use/Cover Change (LUCC)" strategy to address the different facets of global change (Guan et al. 2011). Since then, using hyperspectral and multitemporal remote sensing data with GIS (Jat et al. 2008a, b; Long et al. 2007; Mundia and Aniya 2006; Muttitanon and Tripathi 2005; Shalaby and Tateishi 2007; Xiao and Weng 2007, (Long et al. 2007; Mundia and Aniya 2006; Muttitanon and Tripathi 2005; Shalaby and Tateishi 2007; Yin et al. 2005).

Because of its high population density and low purchasing capacity, Bangladesh is one of the world's poorest countries. For the first time since 1970, the service sector has overtaken the agriculture sector as the largest contributor to GDP, accounting for 62% of total GDP. Contrary to this, industrial growth is fairly flat and barely accounts for 18% of GDP (Baker 2007; BBS 2011). Bangladesh has lost huge areas of agricultural land and put a tremendous strain on its conventional energy sources because of uncertain changes in the economy. Each year, Bangladesh converts over 800 km^2 of agricultural land into urban areas, roadways, and infrastructure (BBS 1996). For example, the 2008 agrarian census revealed a 0.3% annual loss in cultivated lands (BBS 2010). Additionally, the percentage of the nation protected by forests has been gradually declining in places with a larger population (Giri and Shrestha 1996). Simultaneously, urbanization has accelerated, with an increase of the country's urban population from 14.1 million in 1981 to 33.6 million in 2011 (BBS 2001, 2003, 2012). However, the depletion of land, which was formerly the economic driver of the country, has a variety of economic and social consequences. Increased landlessness creates social turmoil and discontent in a typically agrarian culture. Additionally, the decrease in crop production represents a risk to the food security of Bangladesh, with the likelihood that the country

would be even less capable of meeting the demands for food of its ever-growing demographic in the future.

The Barishal district is strategically significant for farming land diversification, barren land protection, and rapid urbanization. Unfortunately, rapid and unplanned urbanization is a significant feature in the growth of the economy, social advancement, and societal change since the urban sector generates 64% of the overall gross domestic product (GDP) (Nazem et al. 2011; UPPR 2011). Furthermore, the city occupies a unique position in the country as the artistic, commercial, industrial, educational, technological, recreational, and political center of the whole country (Islam and Ahmed 2011). According to empirical evidence, agricultural deterioration, urbanization, and land cover have grown increasingly diversified in pattern, fractured in structure, and complicated in shape, resulting in a range of negative implications for biotic and abiotic resources (Qi et al. 2014). Thus, periodical urban growth and its changing pattern must be studied and characterized, as well as its impact on the land, environment, and environment in relation to specific and temporal circumstances.

However, inadequate research has been conducted in the study area to monitor and predict certain types of LULC change. Moreover, Abdullah et al. (2019) studied the entire coastal region, which includes Barisal as a part, Rahman et al. (2022), and Salman et al. (2021) only studied LULC changes with a variety of time series. From this perspective, it is critical to evaluate LULC over time and predict future changes for sustainable development and urban planning. There are several approaches for discovering and analyzing LULC categorization. Remote sensing and GIS methods are frequently used by researchers in the field of LULC categorization studies (Dewan and Yamaguchi 2009a, b; Mallick et al. 2008; Mamun et al. 2013; Nemani 1997; Wang et al. 2009; Zhan et al. 2002). Thus, the primary aims of this work are to (1) analyze the temporal evolution of LULC over the last 20 years (2002–2021) [The reason for selecting this time span was that

considerable changes, vegetation loss, and urbanization in land use activities happened on a larger scale during this period than during the prior time period] and (2) predict LULC map for 2031 utilizing spatial modeling (Markov Chain and Cellular Automata) in LULC Modeller.

8.2   Materials and Methods

8.2.1   Study Area

Barishal, located between 22°48′0″N and 90°30′0″E, is a district in southern Bangladesh with a tropical wet and dry climate. It is the largest city in the district and the administrative center of the Barishal division. Barishal is a major city in south-central Bangladesh located on the banks of the Kirtankhola River (Fig. 8.1). The district has a land area of 2784.52 km^2 and is surrounded by several waterbodies, including the Meghna, Arial Khan, Kirtankhola, Tentulia, Nayabhanga, Jayanti, Swarupkati, Hatra, and Amtali (Salman et al. 2021). According to Rony and Jannat (2021), Rahman et al. (2022), Rahman and Azim (2021), the annual average temperature is around 26.04 °C, the annual average rainfall is 2084.9 mm, and the elevation ranges from 0 to 4 (m).

8.2.2   Data Acquisition and Preparation

For this study, we have collected data from secondary sources. We used satellite images of 2002 and 2020. The images were downloaded from the United States Geological Survey (USGS), Google Earth Engine (GEE). Since this research has one study area and needs to analyze images of two different years, several satellite images were required. Images from Landsat 7 and Landsat 8 were acquired in the spring and early summer of 2002 and 2021, respectively. Each Landsat image was enhanced using statistical indexation to facilitate locating ground control sites for rectification. Each pair of images was classified using at least 75 ground control points (GCPs) taken from 1990 topographic
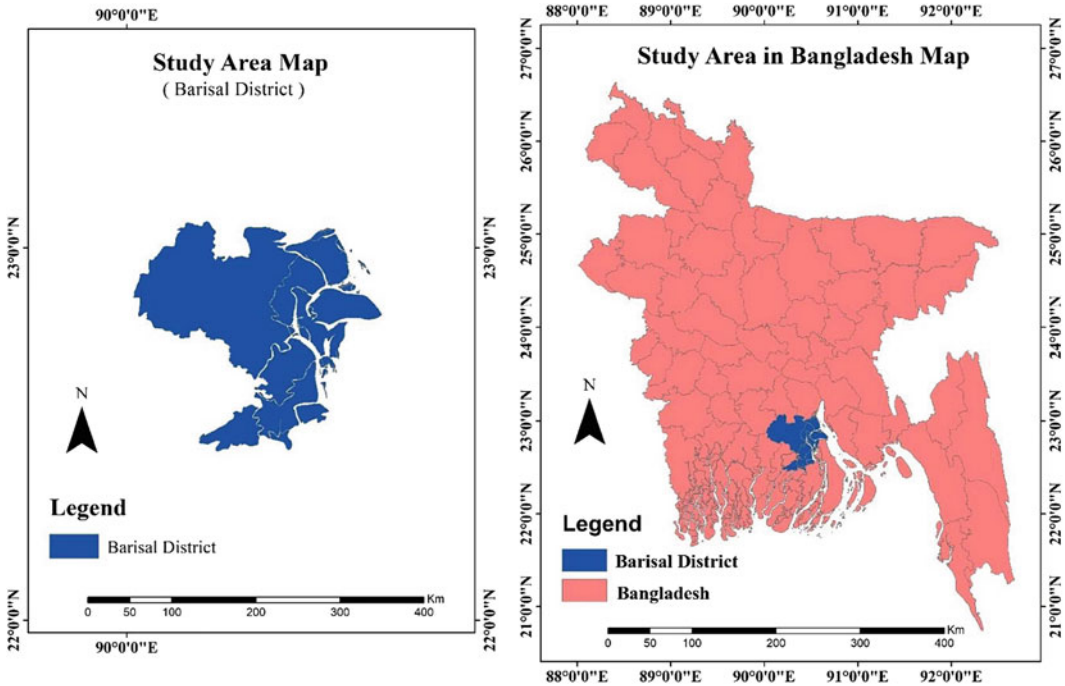
Fig. 8.1 Study area (Barishal District)

maps to the Bangladesh Transverse Mercator (BTM) system. The BTM method is a Bangladesh-specific UTM projection system. The GCPs were spread uniformly across the scenery, resulting in an RMS error of 0.5 pixels. First, a quadratic fit was used, and then the nearest neighbor method was used to change the size of each pixel to 30 m (Table 8.1).

After correcting the pairings of Landsat images, they were mosaicked. Due to the fact that the data is historical and quasi-period, the three resulting preprocessed pictures were subjected to radiometric correction to account for variations in solar angle and surface absorption (Balistreri and Ullrich 1996). An image-based radiometric correction was utilized to minimize radiometric variations in the Landsat data. Finally, every

Landsat image was clipped using an area of interest (AOI) file created from a vector dataset representing the study region's boundaries (Chavez 1996).

8.2.3 Image Analysis

In this research of LULC change, a revised version of the Anderson Level I Scheme was used. Though it was initially devised for the United States, the method is now widely utilized worldwide (Anderson 1976; Mundia and Aniya 2006; Shalaby and Tateishi 2007; Weng 2002; Yuan et al. 2005). It is a hierarchical LULC classification, featuring Level I classes mappable using Landsat or other satellite imagery and

Table 8.1 Landsat images

Satellite image	Date of acquisition	Sensor	Path/row	Spectral resolution	Projection
Landsat 8	2021-03-17	OLI/TIRS	137/44	30 m	UTM/WGS 84
Landsat 7	2002-03-05	ETM+			

Levels II, III, and IV requiring the use of high-, medium-, or low-altitude aerial pictures, respectively. This research identifies four distinct LULC types: waterbodies, built-up areas, vegetation, and bare soil or land (Table 5.1). To digitally classify each Landsat image, a composite classification algorithm was used, as this method has been demonstrated to perform better when dealing with the optical variability of distinct cover categories (Mas 1999). Numerous studies have shown that hierarchical clustering improves pixel-based supervised or unsupervised classification alone (Garcia and Alvarez 1994; Xiao and Weng 2007). Every image was previously defined using the intermittent self-organizing data analysis (ISODATA) method, and 200 spectral signatures were obtained for each image. Each of these groups was then tested for specificity using histogram plots and transformed divergence (TD) approaches (Balistreri and Ullrich 1996). To assure the unimodality of histograms and TD values, signatures were revised, eliminated, renamed, and combined. Finally, each image was classified using a supervised maximum likelihood classification (MLC) algorithm. Bolstad and Lillesand (1991) have consistently been shown to produce improved results when used with remotely sensed data, assuming that the pixels in each category have a Gaussian distribution (Bolstad and Lillesand 1991).

A post-classification comparison method of change detection was utilized to evaluate the differences in LULC between various years. While this methodology has several drawbacks, it is the most often used method for comparing data from different periods. The advantage of post-classification comparison is that it avoids the problems inherent in analyzing photos obtained at various seasons of the year and/or using various sensors (Balistreri and Ullrich 1996; Coppin et al. 2004; Lu et al. 2004, 2011; Singh 1989). The advantage of post-classification comparison is that it avoids the problems inherent in analyzing images obtained at various seasons of the year and/or using various sensors (Alphan 2003; Coppin et al. 2004; Lu and Weng 2005; Yuan et al. 2005). Additionally, the

approach of post-classification quickly provides data on the intensity, location, and kind of change (Howarth and Wickware 1981). However, a significant disadvantage is that the accuracy of the change maps is contingent upon the quality of individual classifications, hence sensitive to error propagation (Zhang et al. 2002). After that, Jensen et al. (1987) said that the classified maps were looked at pixel by pixel.

8.2.4   Markov Chain Cellular Automata Model

The fusion of CA-Markov modeling is deemed beneficial for modeling land use changes and is capable of simulating and forecasting changes (Amini et al. 2016; Singh et al. 2015). The CA–Markov model is a hybrid of cellular automata with a matrix of transition probabilities formed by cross-tabulating two distinct pictures (Singh et al. 2015). This hybrid CA–Markov model enables a comprehensive approach to spatiotemporal dynamic simulation (Singh et al. 2015; Wang and Zhang 2001). Additionally, CA is utilized with Markov chains to infuse the model with spatial dimension. In other words, the CA-Markov chain can simulate and anticipate two-way transformations between any variety of segments (Pontius and Malanson 2005; Ye and Bai 2007). It is worth noting that cellular automata is a dynamic process model that is used to simulate land use change. This type of model is quite prevalent in the research on land use modeling. Each cell, with its unique properties, can symbolize tracts of land and self-growth relationships due to its dynamic and reduplicate nature (Brown et al. 2012). Additionally, the land use changes for every location (unit) can be defined by the current state and changes in surrounding cells, simulating two-directional expansion. This model is extensively used in spatial models for the purpose of forecasting future land use (Amini Parsa et al. 2016; Ye and Bai 2007). The essential features of CA are that they depict spatial and dynamic processes, which explains why they are often utilized in land use modeling (Ye and Bai 2007). Also, Reddy et al.

(2017) found that the state of each cell depends on the temporal and spatial states of the cells around it.

Equation (8.1) denotes the equation of CA modelling

$$S(t, t + 1) = f(S(t), N) \qquad (8.1)$$

where $S(t + 1)$ denotes the system's situation at $(t, t + 1)$ and is regulated by the situation of probability at any time (N).

On suitability imagery, the typical contiguous filter of 5×5 pixels has been used to identify neighborhoods for each cell of land cover class. To exert a significant effect on the cellular center, each cellular center is surrounded by a matrix space made of 5×5 cells.

The 5×5 spatial filter allows a category's increase to occur close to where the category previously existed. Additionally, this type of CA contiguity filter eliminates the possibility of arbitrarily changing land use (Ahmed 2011).

8.3 Results

8.3.1 Accuracy Assessment

A classified image or change detection map must be differentiated with reference data (Foody 2002). Consequently, producer accuracy, user accuracy, and overall accuracy assessment report must be included in the complete accuracy, validated using the Kappa coefficient. The accuracy evaluation depicts the fundamental differences between classified and the reference map or data (Disperati and Virdis 2015; Lillesand et al. 2015; Pouliot et al. 2014; Tsutsumida and Comber 2015). Whereas, if the reference dataset is inaccurate, the evaluation may show the results of classification are weak (Table 8.2).

8.3.2 Pattern of LULC Change

Figure 8.2 depicts the regional patterns of LULC change in the research area from 2002 to 2021. Between 2002 and 2021, collectively referred to as vegetation and bare land, decreased, while the extent of built-up area and waterbodies increased. From 2002 to 2021, vegetation and bare land declined in some areas and increased in others. Still, the decreased amount was more than doubled, while the water body increased continually, and the built-up area increased slightly. Given that the 2011 data is from late spring and early summer, the rise in the vegetative category could just represent seasonal fluctuations. During the same time period, significant expansion in the category of bare soil was recorded, along with an increase in built-up regions. The trend of LULC changes up to 2021 indicated that Barisal is expanding in waterbody and built-up directions, primarily through urbanization. It is notable that the rate of built-up area is encroaching significantly following the development of a new master plan for a number of new infrastructural projects (Islam 2005; Siddiqui 2000). The distribution pattern of the bare land, as depicted on the maps, demonstrates precisely how urban areas have encroached into waterbodies on Barisal (Figs. 8.1 and 8.2). Field observation reveals that most of the suburban growth occurs as a result of people's speculative land-use changes. It must be mentioned that the process of urbanization is now a highly complex process which involves a variety of parameters.

Table 8.2 Accuracy assessment table

Period	User accuracy				Producer accuracy				Classification accuracy (%)	Kappa statistics
	Water body	Bare land	Vegetation	Built-up area	Water body	Bare land	Vegetation	Built-up area		
2002	85	100	95	91	88	96	85	100	91	0.89
2020	88	99	96	89	90	91	100	89	89	0.97
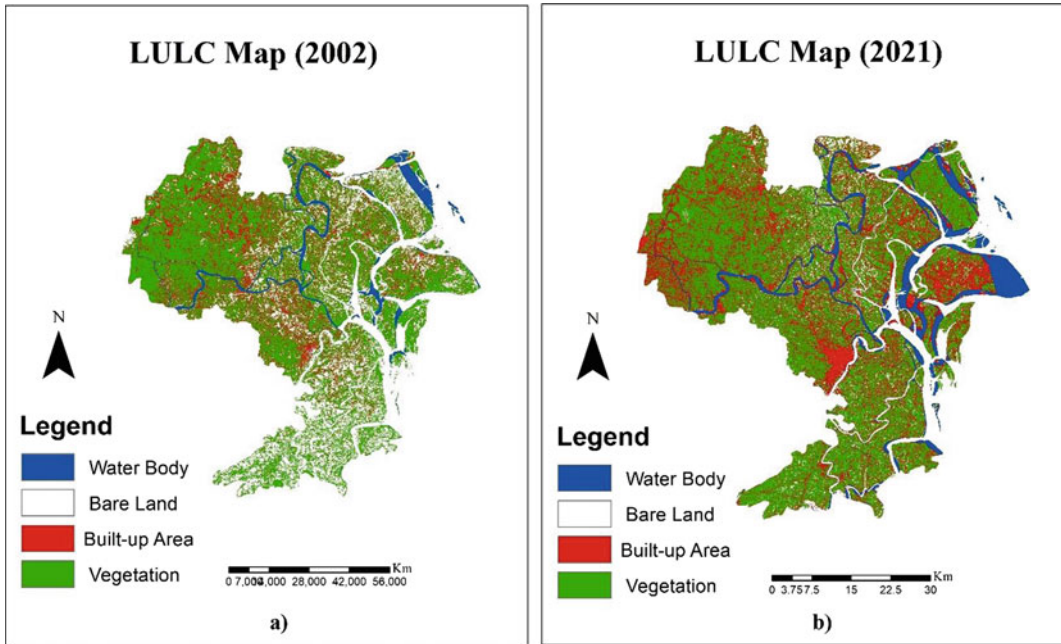
Fig. 8.2 **a** Observed LULC status of 2002. **b** Observed LULC status of 2021

Two of these, speculation and property value, may not properly describe the pattern of suburbanization in the studied area. As a result, additional research is required to substantiate the factors affecting suburban growth in Barisal. Additionally, ineffective cooperation among government executive departments is to blame for the study area's environmental degradation.

Estimated increases in LULC indicate that both built-up areas and waterbody categories have increased significantly (Table 8.3). In 2002, waterbodies covered 100.1 km^2 (4.47%) of the total study area (3742.81 km^2), which increased to 222.29 km^2, indicating 100% growth (from 4.47 to 9.93%) in a 20-year interval. Table 8.3 also shows a slight increase in built-up area by this 20-year interval, from 349.94 to 356.74 km^2. On the other hand, bare land and vegetation have decreased by this time by 5% and 1%, respectively (Table 8.3).

To handle its population increase, the city has significantly expanded, and yet this growth has been seriously impacted by a number of physical constraints. As a result, the majority of the growth has occurred in the depletion of natural resources. Barisal's growth has been noted to be significantly faster than some other districts in Bangladesh. The fundamental difference would be that some districts expanded gradually, allowing them to efficiently create the required infrastructure and governance facilities for citizens, whereas for Barisal, which is a little bit different due to intense population pressure. As a result, local governments face a variety of obstacles in pursuing sustainable development, which will grow more serious in the years ahead if development restrictions are not strictly implemented.

The 2002–2021 time period was tabulated to provide the LULC transition probabilities (TPs) shown in Table 8.3. Built-up areas had the highest probability of conversion to vegetated land. Land conversion to urbanization happened at a high rate in agriculture, which means that this land cover type has a greater chance of becoming developed.

Table 8.3 Changes from 2002 to 2021

LULC classification	Area (km^2)	%
2002		
Water body	100.10	4.47
Bare land	468.15	20.93
Vegetation	1318.90	58.96
Built-up	349.94	15.64
Total	2237.19	100
2021		
Water body	222.29	9.936217
Bare land	372.97	16.67133
Vegetation	1285.19	57.44646
Built-up	356.74	15.946
	2237.19	100

8.3.3 Analysis of Future LULC Simulation

A comparison of the 2011 land-use classifications shown in Fig. 8.2 was used to verify that the MCA-CA model correctly predicted land-use patterns. The bare land LULC group was found to be the most difficult to model, followed by the built-up area category. The waterbody and vegetation categories had the best agreement. The actual waterbody category was 9.94% in real life, while its equivalent simulation category would be 10.03%. Similarly, 57.45% of the total area was detected as vegetation, whereas 49.23% of the whole area was forecasted to be decreased by 8%. For bare land and built-up areas, they will also decrease by nearly 4% and 2.5%, respectively (Fig. 8.3; Table 8.5). It is possible that the proximity of existing LULC categories to each other may have a detrimental effect on the poor modeling of LULC categories using the Markov-cellular automata technique (Pontius and Malanson 2005). Also, a few close pixels can change how LULC development is modeled by making a certain category less important (Kamusoko et al. 2009).

Graphical representations of LULC change over time has historically been accomplished by clarifying the overall number (Table 8.4), types, and places of transition Using Markov chains, we demonstrate how LULC and potential land use
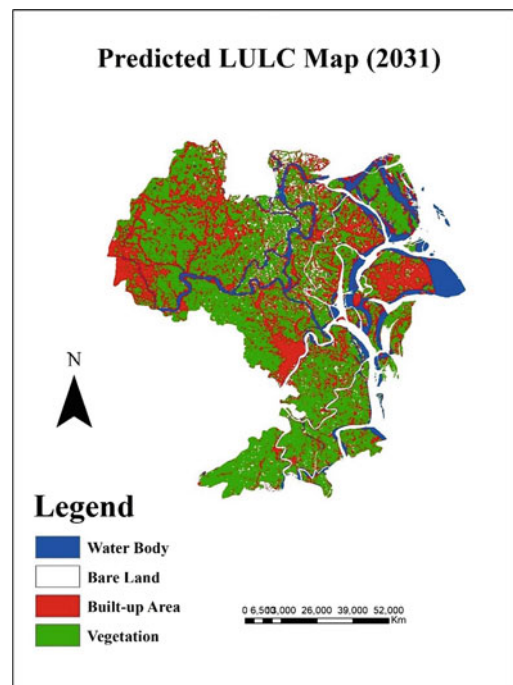
Fig. 8.3 Predicted LULC map of 2031

pattern may be described and predicted using stochastic processes. GIS-based tools are also used to create and query update mechanisms in a spatial context, and an application for this purpose is presented here. Using data of Barishal, this dynamic spatial query program is used to investigate the influence of city development management policies (Table 8.5).

Table 8.4 Probability of changing

Vegetation	LULC	Period	To		
			Water body	Bare land	Built-up area
From	Water body 0.0669	02–21	0.7102	0.0385	0.1844
		21–31	0.9789	0.0000	0.0211
	0.0000 Bare land 0.7071	02–21	0.0728	0.1331	0.0870
		21–31	0.0172	0.6668	0.0060
	0.3100 Built-up area 0.5453	02–21	0.0226	0.0201	0.4120
	0.2593 Vegetation 0.6331	02–21	0.0563	0.0467	0.2639
		21–31	0.0260	0.0132	0.1515
	0.8092				

Table 8.5 LULC transition between 2002 and 31

2002	2031			
	Water body	Bare land	Vegetation	Built-up
Water body	0.1140	0.6930	0.1930	0.0000
Bare land	0.1070	0.0779	0.4080	0.4071
Vegetation	0.7238	0.0179	0.1390	0.1193
Built-up	0.7412	0.0555	0.0894	0.1139

8.4 Conclusion

This chapter describes multi-temporal LULC classifications based on Landsat data. The Dhaka Megacity's future LULC changes were then simulated using the Markov-CA method, utilizing data from the obtained datasets. Barisal is undergoing rapid urban growth, which is resulting in a rapid depletion of rural and agricultural land, according to the findings. The encroachment of urban areas on natural land cover is causing a decline in the ecosystem. Between 2002 and 2021, built-up areas grew from 303.65 to 310.45 km^2, mainly due to river bank erosion in some parts and increasing waterbodies. This has resulted in a severe reduction in the amount of land available for agriculture, wildlife habitat, and wetlands/lowlands. According to observations gathered on the ground, there have been few or no attempts to control the environmental

deterioration risk in the district's informal settlements. Efforts must be made to reduce the negative environmental impacts of urban expansion by enforcing planning restrictions and coordinating government entities in order to conserve the earth's diminishing natural resources. Waterways and vegetation, as well as cultivated fields, should be protected from urban sprawl. This could prevent the degradation of productive, rich soils while also helping to maintain the ecological balance. In order to effectively manage urban land use and the environment, it is becoming increasingly important to employ an integrated strategy. In addition, it is also necessary to review regional and local land-use management policies and to begin interdisciplinary integrated research in order to establish a sustainable urban development plan in the year 2031. The Markov-CA modeling method was used to investigate how LULC would alter over time. If current practices continue, the LULC

categories for vegetated land and bare land will be drastically decreased by 2031. Rural settlements, on the other hand, would grow in size. It is possible that the findings from this study may help local authorities devise effective responses to protect valuable natural resources that are threatened by LULC change in urban environments. Due to a lack of available data in the study area, this study did not include other socioeconomic elements in the simulation of a LULC shift. Biophysical, socioeconomic, and policy-related factors could be used in more research to simulate how LULC will change in Dhaka Megacity in the future and give better information for making decisions.

References

Abdullah SA, Nakagoshi N (2006) Changes in landscape spatial pattern in the highly developing state of Selangor, peninsular Malaysia. Landsc Urban Plan 77(3):263–275

Abdullah AYM, Masrur A, Adnan MSG, Baky MAA, Hassan QK, Dewan A (2019) Spatio-temporal patterns of land use/land cover change in the heterogeneous coastal region of Bangladesh between 1990 and 2017. Remote Sens 11(7):790

Ahmed B (2011) Land cover change prediction of Dhaka City: a Markov Cellular Automata Approach

Alphan H (2003) Land-use change and urbanization of Adana Turkey. Land Degrad Dev 14(6):575–586

Alves DS, L Skole D (1996) Characterizing land cover dynamics using multi-temporal imagery. Int J Remote Sens 17(4):835–839

Amini Parsa V, Yavari A, Nejadi A (2016) Spatio-temporal analysis of land use/land cover pattern changes in Arasbaran biosphere reserve: Iran. Model Earth Syst Environ 2(4):1–13

Anderson JR (1976) A land use and land cover classification system for use with remote sensor data, vol 964. US Government Printing Office

Baker J (2007) Dhaka: improving living conditions for the urban poor. Bangladesh development series, 17

Balistreri Q, Ullrich Jr F B (1996) Introductory digital image processing: a remote sensing perspective

BBS (1996) Agricultural census of Bangladesh. Bangladesh Bureau of Statistics. Ministry of Planning, Dhaka

BBS (2001) Population census 2001. In: Statistics BBo (ed) Ministry of Planning, Dhaka

BBS (2003) Population census *community series*. Ministry of Planning, Dhaka

BBS (2010) Census of Agriculture 2008: structure of agricultural holdings and livestock population. In Statistics BBo (ed), vol 1. Ministry of Planning, Dhaka

BBS (2011) Bangladesh Bureau of Statistics (BBS), Statistics and Informatics Division (Sid) Ministry of Planning, Government of the People's Republic of Bangladesh, Parishankhan Bhaban: E-27/A, Agargaon, Dhaka-1207. www. bbs. gov. bd

BBS (2012) Population and housing census 2011. Ministry of Planning, Dhaka

Bolstad P, Lillesand T (1991) Rapid maximum likelihood classification. Photogramm Eng Remote Sens 57(1):67–74

Brown DG, Walker R, Manson S, Seto K (2012) Modeling land use and land cover change. In: Land change science. Springer, pp 395–409

Chavez PS (1996) Image-based atmospheric corrections-revisited and improved. Photogramm Eng Remote Sens 62(9):1025–1035

Coppin P, Jonckheere I, Nackaerts K, Muys B, Lambin E (2004) Review article digital change detection methods in ecosystem monitoring: a review. Int J Remote Sens 25(9):1565–1596

CoolGeography (2022) Urban change. Retrieved 28 June 2022, from https://www.coolgeography.co.uk/advanced/Urban_change.php#:~:text=Urban%20Change%20involves%20any%20change,decline%20of%20an%20urban%20area

Di Gregorio A (2005) Land cover classification system: classification concepts and user manual: LCCS (Vol. 2): Food & Agriculture Org.

Dewan AM, Yamaguchi Y (2009a) Using remote sensing and GIS to detect and monitor land use and land cover change in Dhaka Metropolitan of Bangladesh during 1960–2005. Environ Monit Assess 150(1–4):237–249. https://doi.org/10.1007/s10661-008-0226-5

Dewan AM, Yamaguchi Y (2009b) Land use and land cover change in Greater Dhaka, Bangladesh: using remote sensing to promote sustainable urbanization. Appl Geogr 29:390–401. https://doi.org/10.1016/j.apgeog.2008.12.005

Dixon RK, Solomon A, Brown S, Houghton R, Trexier M, Wisniewski J (1994) Carbon pools and flux of global forest ecosystems. Science 263(5144):185–190

Dutta D, Rahman A, Paul S, Kundu A (2019) Changing pattern of urban landscape and its effect on land surface temperature in and around Delhi. Environ Monit Assess 191(9):1–15

Garcia M, Alvarez R (1994) TM digital processing of a tropical forest region in southeastern Mexico. Int J Remote Sens 15(8):1611–1632

Giri C, Shrestha S (1996) Land cover mapping and monitoring from NOAA AVHRR data in Bangladesh. Int J Remote Sens 17(14):2749–2759

Guan D, Li H, Inohae T, Su W, Nagaie T, Hokao K (2011) Modeling urban land use change by the integration of cellular automaton and Markov model. Ecol Model 222(20–22):3761–3772

Hassan Z, Shabbir R, Ahmad SS, Malik AH, Aziz N, Butt A, Erum S (2016) Dynamics of land use and land cover change (LULCC) using geospatial techniques: a case study of Islamabad Pakistan. Springerplus 5(1):1–11

Howarth PJ, Wickware GM (1981) Procedures for change detection using Landsat digital data. Int J Remote Sens 2(3):277–291

Islam N (2005) Dhaka now: contemporary urban development. Bangladesh Geographical Society

Islam MS, Ahmed R (2011) Land use change prediction in Dhaka city using GIS aided Markov chain modeling. Journal of Life and Earth Science 6:81–89

Jat M, Garg P, Khare D (2008a) Modelling of urban growth using spatial analysis techniques: a case study of Ajmer city (India). Int J Remote Sens 29(2):543–567

Jat MK, Garg PK, Khare D (2008b) Monitoring and modelling of urban sprawl using remote sensing and GIS techniques. Int J Appl Earth Obs Geoinf 10 (1):26–43

Jensen JR, Ramsey EW, Mackey Jr H, Christensen E, Sharitz R (1987) Inland wetland change detection using aircraft MSS data. Photogrammetric engineering and remote sensing (USA)

Kamusoko C, Aniya M, Adi B, Manjoro M (2009) Rural sustainability under threat in Zimbabwe–simulation of future land use/cover changes in the Bindura district based on the Markov-cellular automata model. Appl Geogr 29(3):435–447

Lambin EF, Turner BL, Geist HJ, Agbola SB, Angelsen A, Bruce JW, Coomes OT, Dirzo R, Fischer G, Folke C (2001) The causes of land-use and land-cover change: moving beyond the myths. Glob Environ Chang 11(4):261–269

Long H, Tang G, Li X, Heilig GK (2007) Socio-economic driving forces of land-use change in Kunshan, the Yangtze River Delta economic area of China. J Environ Manage 83(3):351–364

Lu D, Weng Q (2005) Urban classification using full spectral information of Landsat ETM+ imagery in Marion County Indiana. Photogram Eng Remote Sens 71(11):1275–1284

Lu D, Mausel P, Brondizio E, Moran E (2004) Change detection techniques. Int J Remote Sens 25(12):2365–2401

Lu D, Moran E, Hetrick S, Li G (2011) Land-use and land-cover change detection. Advances in environmental remote sensing sensors, algorithms, and applications. CRC Press Taylor & Francis Group, New York, pp 273–290

Mallick J, Kant Y, Bharath B (2008) Estimation of land surface temperature over Delhi using Landsat-7 ETM +. J Ind Geophys Union 12(3):131–140

Mamun AA, Mahmood A, Rahman M (2013) Identification and monitoring the change of land use pattern using remote sensing and GIS: a case study of Dhaka City. IOSR J Mech Civil Eng 6(2):20–28

Mas J-F (1999) Monitoring land-cover changes: a comparison of change detection techniques. Int J Remote Sens 20(1):139–152

Mesev V, Walrath A (2007) GIS and remote sensing integration: in search of a definition. Wiley, Chichester

Mundia CN, Aniya M (2006) Dynamics of landuse/cover changes and degradation of Nairobi City Kenya. Land Degrad Dev 17(1):97–108

Muttitanon W, Tripathi N (2005) Land use/land cover changes in the coastal zone of Ban Don Bay, Thailand using Landsat 5 TM data. Int J Remote Sens 26 (11):2311–2323

Nazem N, Chowdhury A, Mahbub A (2011) Economic geography of urbanization and development. Paper presented at the Bangladesh Urban Forum edited by Sarwar Jahan and Nurul Islam Nazem

Nemani R, Running S (1997) Land cover characterization using multi temporal red, near-ir, and thermal-ir data from NOAA/AVHRR. Ecol Appl https://doi.org/10.1890/1051-0761(1997)

Ojima D, Galvin K, Turner B (1994) The global impact of land-use change. Bioscience 44(5):300–304

Pontius GR, Malanson J (2005) Comparison of the structure and accuracy of two land change models. Int J Geogr Inf Sci 19(2):243–265

Qi Z-F, Ye X-Y, Zhang H, Yu Z-L (2014) Land fragmentation and variation of ecosystem services in the context of rapid urbanization: the case of Taizhou city, China. Stoch Env Res Risk Assess 28(4):843–855

Quétier F, Lavorel S, Thuiller W, Davies I (2007) Plant-trait-based modeling assessment of ecosystem-service sensitivity to land-use change. Ecol Appl 17(8):2377–2386

Rahman MN, Azim SA (2021) Spatiotemporal evaluation of rainfall trend during 1979–2019 in seven climatic zones of Bangladesh. Geol Ecol Landscapes, pp 1–16. https://doi.org/10.1080/24749508.2021.2022425

Rahman A, Kumar S, Fazal S, Siddiqui MA (2012) Assessment of land use/land cover change in the North-West District of Delhi using remote sensing and GIS techniques. J Indian Soc Remote Sens 40(4):689–697

Rahman MN, Rony MRH, Jannat FA, Chandra Pal S, Islam MS, Alam E, Islam ARMT (2022) Impact of urbanization on urban heat island intensity in major districts of Bangladesh using remote sensing and geospatial tools. Climate 10(1):3

Reddy CS, Singh S, Dadhwal V, Jha C, Rao NR, Diwakar P (2017) Predictive modelling of the spatial pattern of past and future forest cover changes in India. J Earth Syst Sci 126(1):1–16

Salman MA, Nomaan MSS, Sayed S, Saha A, Rafiq MR (2021) Land use and land cover change detection by using remote sensing and gis technology in Barishal District, Bangladesh

Shalaby A, Tateishi R (2007) Remote sensing and GIS for mapping and monitoring land cover and land-use changes in the Northwestern coastal zone of Egypt. Appl Geogr 27(1):28–41

Siddiqui K (2000) Overcoming the governance crisis in Dhaka City. University Press

Singh A (1989) Review article digital change detection techniques using remotely-sensed data. Int J Remote Sens 10(6):989–1003

Singh SK, Mustak S, Srivastava PK, Szabó S, Islam T (2015) Predicting spatial and decadal LULC changes through cellular automata Markov chain models using

earth observation datasets and geo-information. Environ Process 2(1):61–78

Stephens L, Fuller D, Boivin N, Rick T, Gauthier N, Kay A, Marwick B, Armstrong CG, Barton CM, Denham T (2019) Archaeological assessment reveals Earth's early transformation through land use. Science 365(6456):897–902

UPPR (2011) Poor settlement in Bangladesh, urban partnership for poverty reduction. Local Government Engineering Department

Wang L, Chen J, Gong P, Shimazaki H, Tamura M (2009) Land cover change detection with a cross-correlogram spectral matching algorithm. Int J Remote Sens 30 (12):3259–3273

Wang Y, Zhang X (2001) A dynamic modeling approach to simulating socioeconomic effects on landscape changes. Ecol Model 140(1–2):141–162

Weng Q (2002) Land use change analysis in the Zhujiang Delta of China using satellite remote sensing, GIS and stochastic modelling. J Environ Manage 64(3):273–284

Xian G, Crane M, Su J (2007) An analysis of urban development and its environmental impact on the Tampa Bay watershed. J Environ Manage 85(4):965–976

Xiao H, Weng Q (2007) The impact of land use and land cover changes on land surface temperature in a karst area of China. J Environ Manage 85(1):245–257

Ye B, Bai Z (2007) Simulating land use/cover changes of Nenjiang County based on CA-Markov model. Paper presented at the International conference on computer and computing technologies in agriculture

Yin Z-Y, Stewart DJ, Bullard S, MacLachlan JT (2005) Changes in urban built-up surface and population distribution patterns during 1986–1999: a case study of Cairo Egypt. Comput Environ Urban Syst 29 (5):595–616

Yu XJ, Ng CN (2007) Spatial and temporal dynamics of urban sprawl along two urban–rural transects: a case study of Guangzhou China. Landscape Urban Plann 79(1):96–109

Yuan F, Sawaya KE, Loeffelholz BC, Bauer ME (2005) Land cover classification and change analysis of the twin cities (Minnesota) metropolitan area by multi-temporal landsat remote sensing. Remote Sens Environ 98(2–3):317–328

Zhan X, Sohlberg R, Townshend J, DiMiceli C, Carroll M, Eastman J, Hansen MC, DeFries R (2002) Detection of land cover changes using MODIS 250 m data. Remote Sens Environ 83(1–2):336–350

Zhang Q, Wang J, Peng X, Gong P, Shi P (2002) Urban built-up land change detection with road density and spectral information from multi-temporal Landsat TM data. Int J Remote Sens 23(15):3057–3078

Urban Change Detection Analysis Using Big Data and Machine Learning: A Review

9

Bushra Praveen, Shaghla Parveen, and Vaseem Akram

Abstract

Globally, urbanization is ongoing, and its effects on the environment and the built environment are becoming more and more serious. Due to the increased demand for fewer resources and harm to the biophysical environment, it is particularly difficult in developing societies. Traditional analytical approaches to analysing the dynamics of urban land use are constant and frequently depend on top-down strategies which includes mathematical as well as linear modelling. The nonlinear characteristics of land use change are not captured by these conventional methods. It is now feasible to recount and anticipate nonlinear elements related to urban land dynamics with the introduction of new technologies like artificial intelligence (AI) and machine learning (ML). Implementation of AI and ML techniques enhances quick and accurate identify patterns, make predictions and carry out actions. The study aims to highlight the various machine learning (ML) algorithms and conventional representations used to study various facets of LULC. It aims to evaluate their functionality, interoperability needs, and performance, as well as the best research issues to which they might be put. According to the literature research, the methods used for categorization and pattern anatomization of earth observation-based datasets are random forest (RF), deep learning techniques including convolutional neural network (CNN) as well as support vector machine (SVM). Urban expansion, land use change, and settlement pattern analysis have all been studied using algorithms of cellular automata, spatial logistic regression, and agent-based modelling. The majority of the publications examined used machine learning (ML) techniques to classify EO data and explore urbanization and land use change. In terms of accuracy, efficiency, and computing cost, it has been found that hybrid techniques perform better.

B. Praveen (✉)
Department of Economics, IIT Indore, Indore, Madhya Pradesh, India
e-mail: bushraparvn@gmail.com

S. Parveen
National Institute of Urban Affairs, New Delhi, India

V. Akram
Economics and Business Environment Area, Indian Institute of Management Jammu, Jammu, Jammu and Kashmir 180016, India
e-mail: vakram@iimj.ac.in

Keywords

Urban change detection · Land use land cover · Artificial intelligence · Machine learning · Conventional techniques

9.1 Introduction

Perceptibility of LULC is widely regarded as a purposive debate on sustainability. Subsequently, the world has seen substantial changes in recent decades (Arnell et al. 2016) repeatedly been linked to increased deforestation, desertification, and land degradation in vast regions, necessitating continual monitoring and management (Borrelli et al. 2017). The LULC approach, which is supported by scientists and policymakers in tackling the issues of ecological and environmental changes, is currently poorly supported. Remote sensing provides efficacious multispectral and multi-temporal detailing for the functional perusal of the results and monitoring of land use models.

However, GIS dispenses a multifaceted environment for data storage, analysing, and viewing of digital statistics, which is critical for spotting changes in databases (Ennouri et al. 2020a, b, c). Urban expansion is a broad classification of LULC, which has severe environmental effects, such as water and air quality damage (). It also has social consequences, such as income disparities, community fragmentation, and increased infrastructure costs (Keola et al. 2015). Urban transformations provide the required knowledge to validate remote sensing statistics. Researchers and planners used to construct land exploitation strategies based on visual aerial picture analysis (Barrientos et al. 2011). Nonetheless, remote sensing devices with high-resolution digital technology, and land use maps may be created that are suitable, affordable, and accurate (Ottaviani et al. 2020). The unparalleled urban expansion (Hegazy et al. 2015) has negative

consequences for the loss of biodiversity, erosion of soil, hydrological disruptions, water pollution, solid waste, as well as temperature thawing globally. Environmental sustainability, in addition to regional planning, examination, and modelling is critical (Weng 2012) (Table 9.1).

The process of recognizing alterations in land cover by monitoring them over time is known as the recognition of changes (Kuenzer et al. 2011). Various techniques of change detection are frequently compared to the most significant outcomes (Rawat et al. 2015). For example, image distinction, post-categorizing, the transfiguration of vector assessment, and principal component analysis (PCA) were the often-used approaches for change detection (Peiman et al. 2011). These approaches may accurately detect variations in several land cover types using multi-temporal satellite pictures to bring forth a heterogeneity of purposes (Tewkesbury et al. 2015). In addition, this chapter studies the approaches to detect a functional change in the context of urban and environmental development (Hu et al. 2013). This chapter encapsulates an objective to analyse city transformation using big data and machine learning. We have analysed both conventional and machine learning methods for change detection in order to assess changes in LULC and, in particular, growth in urban regions. The research will aid decision-makers in formulating better LULC regulations to protect ecosystems and sustainability. In relation to the objectives and requirements of urban land use planning and decision-making connected to land use planning and urban change detection, the objective of this chapter finds a relative investigation of the conventional and ML algorithms. Based on

Table 9.1 Machine learning algorithms and their advantages

Machine learning algorithms	Advantages, usefulness, appropriations for related applications
Super vector machines (SVMs)	SVM performs well in hyperplane conditions
Markov random field (MRF)	Compares regions and pixel information
A convolutional neural network (CNN)	CNN with local spatial coherence performs feature extraction
Random forest (RF)	It incorporates spectral bands like soil index, water index, NDVI and textural features like entropy, variance, morphology, line feature, etc., and rejects over-fitting

Source Chaturvedi and Vries (2021)

the reviewed publications, it has been noted that the machine learning algorithms produce the best outcomes in computing costs and precisions.

We begin the chapter with a conceptual framework for the methods utilized in conventional or machine-learning algorithms for detecting urban change. Finally, the results are concluded after examining the functions, applications, and benefits of the approach used to analyse the various ML algorithms for urban transformation and LULC planning.

9.2   Land Use and Land Cover (LULC) Change Detection Analysis

Alterations in the LULC are significant contributors to global change and have significant international policy initiatives. A shift from grassland to agricultural and residential areas has occurred in the last several years as an outturn of population increase as well as urbanization (Zope et al. 2016). In comparison to conventional research and statements conducted over vast spaces, the satellite remote sensing dataset offers important facts and knowledge about the phenomenal arrangements of LULC (Camilleri et al. 2017). Additionally, remote sensing datasets may give details regarding temporal and geographical distributions of urbanized areas that are important for planning resources, and development. The technique determines changes in its status with the help of frequent data collection and analysis (Table 9.2).

9.3   Urban Change Detection Using Conventional Techniques

LULC is considered a significant component of environmental variation, affecting natural characteristics and functioning of ecosystems. Agricultural growth and production escalation, deforestation, and urbanization have shown its impact over the unfrozen land area during the last several decades. LULC have reportedly brought major consequences for biodiversity, water quality, climate, soil, food security as well as human well-being (Lynch et al. 2013). Urbanization is often regarded as the most intense form of LULC (Lynch et al. 2013). It is also noticeable that urban regions account for a small percent of the forest and other natural land alterations.

Changes in cover may be related to improper land management and preparation. The deteriorating quality of water and air, disappearance of agricultural land and forests, as well as social and economic constraints, financial inequities, social segregation, etc., are only a few examples of how these factors may have a big impact on the climate and ecosystems. (Yin et al. 2011). Furthermore, metropolitan areas absorb more solar radiation, have a larger thermal capacity, and have a higher conductivity rate. As a result, metropolitan regions typically experience greater temperatures than agricultural ones. Strong strategies and methodologies are required for monitoring and presenting urban development. Traditional research and mapping techniques lack the ability to deliver the required data quickly and affordably. Studies conducted in the last several decades have demonstrated the ability of remote sensing alteration detection methods to deliver precise and fast information on urbanized land change (Akbar et al. 2019). Mas (1999) discovered that post-classification, which includes data on multiple soil moisture and vegetation phenology situations, is the most effective approach to detecting urban change. Furthermore, Li and Yeh (1998) came to the conclusion that multi-date PCA and classification could be successfully used to assess fast urbanized growth into one of the Chinese rivers. PCA serves as a footing base for multivariate data exploration. The most important use of principal component analysis is the building of a multivariate record board as a condensed collection of variables with the aim of analysing trends, borders, groupings, and outliers (Yang et al. 2020). Examining datasets that may include faulty data as well as multi-collinearity, incorrect values, and categorical records is part of the principal component analysis process, which is a very

Table 9.2 Categorization of the commonly used models for urban growth and LULC dynamics studies

Model	Qualities, a theme, and guiding principles	Advantages	Disadvantages	Examples
Empirical statistical models	Using multivariate analysis, specifically identify the drivers of land use changes and their impact on land-use change	An analytical technique that takes comparatively less data to examine how dependent land use change is on influencing variables	Does not include the temporal dynamics, making it unsuitable for broad extension; lacking a spatial foundation and lacking comprehension of the simulation process that influences land use process	Logistic linear regression, multiple linear regression
Optimization models	According to the econometric method, each piece of land is represented as being used in the manner that generates the highest rent, given its characteristics and location	The modelled agents are capable of making well-informed forecasts and strategies	Several assumptions are taken into consideration	Von-Thunen's model, agent-based model
Stochastic models	Land use change is a first-order process, meaning that the present determines future change rather than the past	Mathematical and operational simplicity can be used where no information on driving factors and mechanisms of land use change is available	Does not take into account spatiality and temporal dynamics; unsuitable for long-term and extensive area modelling	Stochastic Markov, cellular automata
Process-based dynamic simulation models	Rule-based system dynamic models within a GIS framework, understanding complex phenomenon through dynamic simulation, different branches of methods in an integrative model	Inherently spatial and dynamic; excellent for expressing non-stationary processes; very flexible	Does interpret the spatiotemporal process of land use change; many Individual processes of decision making cannot be modelled	Fuzzy-CA, CA-MARKANN-CAOV, MCE, CA-SLEUTH

(*Source* Based on Lambin 2004; Zhang 2009; Bhatta 2013; Duwal 2013)

flexible technique (Ennouri et al. 2020). The aim is to find and express pertinent data records as a collection of key indices or defining characteristics is the aim. Geographic information systems (GIS) change detection and remote sensing were integrated to track the spatial dynamics of urban land modifications (Anees et al. 2020).

Accurately determining the proportionate contribution of reflection from a variety of materials in an urbanized setting is the fundamental problem for classifying urban land cover. Additionally, consideration must be given to changes such as seasonal vegetation fluctuations that are unrelated to changes in urbanized land cover. Additionally, several studies have looked into how to use contextual (Sun et al. 2019) and textural (Mishra et al. 2019) information to enhance per-pixel compartmentalization and get around the sub-pixel mixing issue.

9.4 Urban Change Detection Using Machine Learning

The difficulty in identifying the kind and scope of transformation amongst the two photos that depict the same site or location but were taken at various times is typically referred to as the

discernment of variation in computer view. Depending on the goals of each work, certain changes are significant and need more modelling and analysis, while others are only surface-level or inadequate and ought to be disregarded. Change can be difficult to detect because it changes a number of variables, including temporal, spectral, spatial, restraint, radiometric resolution, and atmospheric circumstances (Wu et al. 2017). A variety of adjustments to detecting skills have been created in an effort to get around the problems and deliver real change in the detection of outcomes. Pre-classification or post-classification approaches (Xiao et al. 2016) and pixel-form or object-form techniques are two ways that authors have categorized change detection methods established on the ground of perceptible points of opinion. The fundamental section of image perusal and change, according to pixel-based change detection algorithms, is the image pixel. These approaches were incorporated in the scientific studies on change detection techniques and may also be thought of as pre-classification methods given that they are applied to raw data. To increase the precision of change detection, a number of pixel-based change detection techniques are created, examining the benefits and drawbacks of each.

Image distinction, image rationing, picture regression, background removal, principal component analysis, and change vector analysis are well-studied pixel-based change detection techniques (CVA). Two similar scenes that were generated at separate periods will have spectral differences that may be recognized via change vector analysis. For each picture, variations in vector analysis are only possible in two bands. Every pixel has an estimated change vector for the spectral dual-dimensional space. It describes how one-character changes as a vector inside the space of indicators amongst two different limits of time across its range of occurrences (variables) (Landmann et al. 2013). Unfortunately, the local brightness variations found in photos make it challenging to establish exact regression functions. The background removal method (Shen et al. 2018) looks for background details in the photographs being contrasted (Shah et al. 2020).

In order to remove superfluity in the data achieved amongst the multispectral bands and punctuate several theoretical and data details, the PCA uses dimensionality reduction. The Bayes principle applied in order to categorize pixels into a couple of classifications, "change" and "no change," PCA was employed as a means of distance or interspace measure (Almutari and Warner 2010) to assess the degree of change in the value of the pixel. The difficulty in understanding and labelling the findings of the principal component analysis, as well as the dearth of extracted data on the nature of the changes, are drawbacks of the principal component analysis change detection techniques (Sahu and Parsai 2012). The drawbacks of PCA towards the understanding of change detection methods is the comprehension and labelling of the results. Traditional research and mapping techniques lack the ability to deliver the required data quickly and affordably. Studies conducted in the last several decades have demonstrated the ability of remote sensing alteration detection methods to deliver precise and fast information on urbanized land change (Akbar et al. 2019). Mas (1999) discovered that post-classification, which includes data on multiple soil moisture and vegetation phenology situations, is the most effective approach to detecting urban change. Furthermore, Li and Yeh (1998) came to the conclusion that multi-date PCA and classification could be successfully used to assess fast urbanized growth in the Chinese river. The assessment of multivariate data using projection/estimation methods is built on PCA. Construction of a multivariate dossier panel as a condensed collection of factors in order to observe trends and pattern, boundaries, groupings, and outliers is one of the pronounced uses of principal component analysis (Ennouri et al. 2020). A very versatile tool, principal component analysis enables the examination of datasets that may contain inaccurate data as well as multi-collinearity, misplaced values, and unambiguous datas (Yang et al. 2020). Finding and the goal of expressing relevant statistical dossiers to collect indexes and components (Ennouri et al. 2018). While plotting the mechanism of city space alterations, Anees et al. (2020) combined remote sensing techniques

with geographic information systems (GIS) for change detection addressals. Based on evaluation concerning similarity metrics between the windows being compared, these algorithms' change detection solutions are determined. There are various texture analyses supporting change detection techniques with the help of correlation as a common similarity metric. This correlation can be applied in the time domain using normalized cross-correlation (NCC) (Debella-Gilo and Kaab 2011) or in the frequency dominion employing Fourier to transform images, analysing index spectrum (phase correlation (PC)) (Sarvaiya et al. 2012). NCC is a key mathematical tool in character matching, correspondence analysis, signal tracking, and object recognition in signal and image processing (Jawak et al. 2018; Cai et al. 2017). In accordance with high computational complexity, the digital standardized cross-correlation is executed through several quick algorithms and hardware structures in order to increase real-time and effective performance.

The object-based change detection approaches revolve around picture partition, and several supervised and unsupervised partition algorithms were applied to variable degrees of success. The majority of object-based change detection approaches plunge into such three categorizations: field-based (pixel similarity), boundary-based (pixel discontinuity), or edge-based (Ennouri et al. 2020). The support vector machine (SVM) classifiers (Ennouri 2020; Aptoula 2013), expectation–maximization (EM) algorithms (Lv et al. 2018), and artificial neural networks (ANNs) (Sahin 2012) were all image partition techniques often utilized in object-based change detection technical studies.

Reading through the literature, it is identified that EM algorithm-based change detection approaches are more accurate than previous procedures, however, prior apprehensions are requisite for joint probability class. (Şahin 2012) The artificial neural network technique can yield considerable findings of change identification, especially when classifications may not ordinarily be allotted throughout, and a longer time is required to produce training data. Artificial neural networks are nonlinear statistical data modelling tools that are used to create or discover complicated correlations between inputs and outputs. Because artificial neural networks vary based on input and output, data passing through the network has an impact on its structure. Artificial neural networks are deep learning frameworks that may construct machine learning and identification.

Finally, support vector machine classifiers have the benefit of avoiding making presumptions concerning the aforesaid data distribution, treating change detection as a dual classification issue. With the goal of categorizing pixels into the "no change" or "change" categories, the support vector apparatus classifier comprehends from the training dossier and the optimum threshold is established (Thanh et al. 2018) from the spectral properties. Fuzzy logic (Pradhan et al. 2010), random forest, and genetic programming are examples of machine learning algorithms employed in monitor categorization, classification, and change detection. Fuzzy logic is a genre of valued logic where the variable values can be any real integer between 0 and 1. After taking a test, the fuzzy logic method makes it simpler to answer problems.

The random forest method has recently gained popularity in the area of remote sensing, which is quite fast in comparison to machine learning techniques (Izquierdo et al. 2020). Rather than using a single decision tree's forecast, the algorithm generates numbers of decision trees. The "random" word derives from "bootstrap aggregating," sometimes known as "bagging." It implies that all the trees in the forest may learn to train on a subset of the whole training data. For accuracy evaluation, training data elements for each tree left concealed, thought to be "out-of-bag." Un-reliability aids in making decisions about which variables to use (Chen et al. 2020).

For heuristic unsupervised categorization, genetic algorithms (GA) are the best alternative. This relies on the building of mathematical conjectures and the subsequent refinement of a predetermined variable to mechanically controlled cluster detailing and centroids (Al-Fugara et al. 2020). Heuristic optimization processes have reliability, accuracy, and time-saving approach to categorize the remote sensing

pictures frequently. Moreover, the genetic algorithms are certified for image processing (Celik et al. 2010) and picture identification for specialized applications like therapeutic treatment (Reddy et al. 2020).

Object-based techniques that rely on image segmentation are plagued by over or under segmentation issues (Grigillo et al. 2012). To make present objects more practical, over-segmentation produces finer components of real-life things that must be combined (Wang et al. 2010). Unfortunately, the final change map includes errors from the photo classification technique that was used, which reduces the precision of the most recent change detection findings (SiA et al. 2010). To improve the results of change detection, individual picture classification must be as precise as is practical.

9.5 Conclusion

- The study illustrates how remote sensing, GIS, and LCM combined with multi-temporal data may be used to investigate and evaluate the dynamics of LULC and potential urban growth patterns.
- The studies have demonstrated that a variety of factors put obstacles to the creation of sustainable cities in the future. In order to prevent negative repercussions, urban simulation studies can aid in understanding the implications of upcoming changes as well as the shortcomings of present planning practices.
- The outcomes of the predictions show that the model has a lot of promise and accuracy in influencing future trends. In order to balance demand and lessen the effects of changing land use patterns, such a database is highly helpful for multi-criteria decision-making, ecologically responsible management, and future urban planning.
- These reports also provides planners and policymakers with a multidisciplinary framework for creating new master plans and improving existing ones.

- The studies have pointed towards the needs to implement short-term action plans with a long-term outlook in order to attain an urban green–blue network due to the disparity between the existing state and expected changes in urban expansion.
- Most of the studies conclude that RS-GIS is a very efficient and powerful tool for mapping, measuring, analysing, monitoring, and modelling spatiotemporal urban change detection analysis.
- The MLC algorithm is the most popularly applied classifier for classifying SRS data to extract land cover classes in terms of urban change studies. However, recently, some machine learning algorithms, like SVM, decision tree, and random forest classifiers are increasingly been used.
- Most of the studies relating to the urban change detection analysis of urban growth and sprawl intend to analyse traditional techniques such as statistical and PCA however recent techniques are good for better detection such as artificial intelligence and machine learning.
- Modelling approaches, like CVA, and PCA, are frequently conventional modelling approaches, often integrated with RS-GIS. Furthermore, very recently, some machine learning approaches (e.g., ANN, SVM, and MLP) are reportedly used for this purpose and give high accuracy results.

References

Akbar TA, Hassan QK, Ishaq S, Batool M, Butt HJ, Jabbar H (2019) Investigative spatial distribution and modelling of existing and future urban land changes and its impact on urbanization and economy. Remote Sens 11(2):105

Al-Fugara AK, Ahmadlou M, Al-Shabeeb AR, AlAyyash S, Al-Amoush H, Al-Adamat R (2020) Spatial mapping of groundwater springs potentiality using grid search-based and genetic algorithm-based support vector regression. Geocarto Int:1–2

Almutairi A, Warner TA (2010) Change detection accuracy and image properties: a study using simulated data. Remote Sens 2(6):1508–1529

Anees MM, Mann D, Sharma M, Banzhaf E, Joshi PK (2020) Assessment of urban dynamics to understand spatiotemporal differentiation at various scales using remote sensing and geospatial tools. Remote Sens 12 (8):1306

Aptoula E (2013) Remote sensing image retrieval with global morphological texture descriptors. IEEE Trans Geosci Remote Sens 52(5):3023–3034

Arnell NW, Brown S, Gosling SN, Gottschalk P, Hinkel J, Huntingford C, Lloyd-Hughes B, Lowe JA, Nicholls RJ, Osborn TJ, Osborne TM, Rose GA, Smith P, Wheeler TR, Zelazowski P (2016) The impacts of climate change across the globe: a multi-sectoral assessment. Clim Change

Barrientos A, Colorado J, Cerro JD, Martinez A, Rossi C, Sanz D, Valente J (2011) Aerial remote sensing in agriculture: a practical approach to area coverage and path planning for fleets of mini aerial robots. J Field Robot 28(5):667–689

Bhatta B (2013) Research methods in remote sensing. Springer

Cai J, Wang C, Mao X, Wang Q (2017) An adaptive offset tracking method with SAR images for landslide displacement monitoring. Remote Sens 9(8):830

Camilleri S, De Giglio M, Stecchi F, Pérez-Hurtado A (2017) Land use and land cover change analysis in predominantly man-made coastal wetlands: towards a methodological framework. Wetl Ecol Manag 25 (1):23–43

Celik T (2010) Change detection in satellite images using a genetic algorithm approach. IEEE Geosci Remote Sens Lett 7(2):386–390

Chen Q, Miao F, Wang H, Xu ZX, Tang Z, Yang L, Qi S (2020) Downscaling of satellite remote sensing soil moisture products over the Tibetan Plateau based on the random forest algorithm: preliminary results. Earth Space Sci 7(6):e2020EA001265

Debella-Gilo M, Kääb A (2011) Sub-pixel precision image matching for measuring surface displacements on mass movements using normalized cross-correlation. Remote Sens Environ 115(1):130–142

Ennouri K, Ayed RB, Smaoui S (2018) Opportunities for computational biology uses in enhancement of bio-product quality: lessons from olive oil. Emir J Food Agr, 532–538

Ennouri K, Ben Ayed R, Ben Hlima H et al (2020a) Analysis of variability in Pistacia vera L. fruit genotypes based on morphological attributes and biometric techniques. Acta Physiol Plant 42:70

Ennouri K, Ottaviani E, Smaoui S, Triki MA (2020b) Use of remote sensing technology and geographic information system for agriculture and environmental observation. In: Ennouri K (ed) Emerging technologies in agriculture and food science. Bentham Science Publishers, pp 108–138 (31)

Ennouri K, Triki MA, Kallel A (2020c) Applications of remote sensing in pest monitoring and crop management. In: Keswani C (ed) Bioeconomy for sustainable development. Springer, Singapore

Grigillo D, Kanjir U (2012) Urban object extraction from digital surface model and digital aerial images. ISPRS Ann Photogram Remote Sens Spat Inf Sci 3:215–220

Hegazy IR, Kaloop MR (2015) Monitoring urban growth and land use change detection with GIS and remote sensing techniques in Daqahlia governorate Egypt. Int J Sustain Built Environ 4(1):117–124

Hu S, Wang L (2013) Automated urban land-use classification with remote sensing. Int J Remote Sens 34(3):790–803

Izquierdo-Verdiguier E, Zurita-Milla R (2020) An evaluation of guided regularized random forest for classification and regression tasks in remote sensing. Int J Appl Earth Obs Geoinf 88:102051

Jawak SD, Kumar S, Luis AJ, Bartanwala M, Tummala S, Pandey AC (2018) Evaluation of geospatial tools for generating accurate glacier velocity maps from optical remote sensing data. In: Multidisciplinary Digital Publishing Institute Proceedings, vol 2, No. 7, p 341.

Keola S, Andersson M, Hall O (2015) Monitoring economic development from space: using nighttime light and land cover data to measure economic growth. World Dev 66:322–334

Kuenzer C, Bluemel A, Gebhardt S, Quoc TV, Dech S (2011) Remote sensing of mangrove ecosystems: a review. Remote Sens 3(5):878–928

Landmann T, Schramm M, Huettich C, Dech S (2013) MODIS-based change vector analysis for assessing wetland dynamics in Southern Africa. Remote Sens Lett 4(2):104–113

Li X, Yeh AGO (1998) Principal component analysis of stacked multi-temporal images for the monitoring of rapid urban expansion in the Pearl River Delta. Int J Remote Sens 19(8):1501–1518

Lv Z, Liu T, Atli Benediktsson J, Lei T, Wan Y (2018) Multi-scale object histogram distance for LCCD using bi-temporal very-high-resolution remote sensing images. Remote Sens 10(11):1809

Lynch J, Maslin M, Balzter H, Sweeting M (2013) Choose satellites to monitor deforestation. Nature 496:293–294

Mas JF (1999) Monitoring land-cover changes: a comparison of change detection techniques. Int J Remote Sens 20(1):139–152

Mishra VN, Prasad R, Rai PK, Vishwakarma AK, Arora A (2019) Performance evaluation of textural features in improving land use/land cover classification accuracy of heterogeneous landscape using multi-sensor remote sensing data. Earth Sci Inform 12(1):71–86

Ottaviani E, Barelli E, Ennouri K (2020) Machine learning for precision agriculture: methods and applications. In: Ennouri K (ed) Emerging technologies in agriculture and food science. Bentham Science Publishers, pp 91–107

Peiman R (2011) Pre-classification and post-classification change-detection techniques to monitor land-cover and land-use change using multi-temporal Landsat imagery: a case study on Pisa Province in Italy. Int J Remote Sens 32(15):4365–4381

Pradhan B (2010) Application of an advanced fuzzy logic model for landslide susceptibility analysis. Int J Comput Intell Syst 3(3):370–381

Rawat JS, Kumar M (2015) Monitoring land use/cover change using remote sensing and GIS techniques: a case study of Hawalbagh block, district Almora, Uttarakhand, India. Egypt J Remote Sens Space Sci 18(1):77–84

Reddy GT, Reddy MPK, Lakshmanna K, Rajput DS, Kaluri R, Srivastava G (2020) Hybrid genetic algorithm and a fuzzy logic classifier for heart disease diagnosis. Evol Intell 13(2):185–196

Şahin M (2012) Modelling of air temperature using remote sensing and artificial neural network in Turkey. Adv Space Res 50(7):973–985

Sahu DK, Parsai MP (2012) Different image fusion techniques–a critical review. Int J Mod Eng Res (IJMER) 2(5):4298–4301

Sarvaiya JN, Patnaik S, Kothari K (2012) Image registration using log polar transform and phase correlation to recover higher scale. J Pattern Recognit Res 7 (1):90–105

Services for conservation of forest and environmental resources. https://www.kkc.co.jp/english/service/env_energy/k_green_solar.html

Shah M, Cave V, Dos Reis M (2020) Automatically localising ROIs in hyperspectral images using background subtraction techniques. In: 2020 35th international conference on image and vision computing New Zealand (IVCNZ). IEEE, pp 1–6

Shen W, Lin Y, Yu L, Xue F, Hong W (2018) Single channel circular SAR moving target detection based on logarithm background subtraction algorithm. Remote Sens 10(5):742

Sun Y, Xin Q, Huang J, Huang B, Zhang H (2019) Characterizing tree species of a tropical wetland in southern China at the individual tree level based on convolutional neural network. IEEE J Sel Top Appl Earth Obs Remote Sens 12(11):4415–4425

Tewkesbury AP, Comber AJ, Tate NJ, Lamb A, Fisher PF (2015) A critical synthesis of remotely sensed optical image change detection techniques. Remote Sens Environ 160:1–14

Thanh Noi P, Kappas M (2018) Comparison of random forest, k-nearest neighbor, and support vector machine classifiers for land cover classification using Sentinel-2 imagery. Sensors 18(1):18

Wang Z, Jensen JR, Im J (2010) An automatic region-based image segmentation algorithm for remote sensing applications. Environ Model Softw 25(10):1149–1165

Wu C, Du B, Cui X, Zhang L (2017) A post-classification change detection method based on iterative slow feature analysis and Bayesian soft fusion. Remote Sens Environ 199:241–255

Xiao P, Zhang X, Wang D, Yuan M, Feng X, Kelly M (2016) Change detection of built-up land: a framework of combining pixel-based detection and object-based recognition. ISPRS J Photogramm Remote Sens 119:402–414

Yang JH, Zhao XL, Ji TY, Ma TH, Huang TZ (2020) Low-rank tensor train for tensor robust principal component analysis. Appl Math Comput 367:124783

Yin J, Yin Z, Zhong H, Xu S, Hu X, Wang J, Wu J (2011) Monitoring urban expansion and land use/land cover changes of Shanghai metropolitan area during the transitional economy (1979–2009) in China. Environ Monit Assess 177:609–621

Zope PE, Eldho TI, Jothiprakash V (2016) Impacts of land use–land cover change and urbanization on flooding: a case study of Oshiwara River Basin in Mumbai, India. CATENA 145:142–154

Part II

Urban Green and Blue Spaces

Urban Green and Blue Spaces Dynamics—A Geospatial Analysis Using Remote Sensing, Machine Learning and Landscape Metrics in Rajshahi Metropolitan City, Bangladesh

10

Md. Rejaur Rahman and Atiqur Rahman

Abstract

As important biophysical considerations of the urban ecosystem, vegetation and water dynamics are crucial to understanding the process of urban ecosystem functions, biodiversity, and ecological sustainability. The expansion of urban areas hurts vegetation and water bodies within the city area. Therefore, the main objective of this chapter was to quantify the green and blue spaces within the city area of Rajshahi Metropolitan, Bangladesh, and find out the geospatial pattern of green and blue spaces dynamics during 1990–2021. Landsat TM, ETM+ and OLI satellite data, geographic information system, and support vector machine were used to extract land use/land cover, urban green space, and blue space. Landscape matrices were followed to calculate the landscape structure of green and blue spaces. The changes in green and blue spaces were measured using the green space index (GSI) and blue space index (BSI), respec-
tively. The zonal and directional analysis was performed to measure the magnitude and direction of urban green space change. Spatial trend and hotspots analysis were executed to find out the nature and hotspots of the green space change. The findings revealed that the green and blue spaces of the city decreased remarkably over time. The green space became fragmented, unevenly distributed, and less physically connected due to the rapid urban growth. The highest decline in green space was noticed in the north-west-west (NWW), north–north-west (NNW), north–north-east (NNE), and north-east-east (NEE) directions. The transformation of green space to built-up was started from the central parts and spread out towards the western, northern, and south-eastern parts. The hotspots of green space change gradually moved towards the fringe area of the city, resulting in a large threat to urban green space. Thus, the outcomes can help the urban planners and policymakers in formulating a comprehensive management plan to control the urban green and blue spaces shrinking, and to conserve the existing green and blue spaces for ensuring the safety of urban life and the urban environment in the city area.

Md.Rejaur Rahman (✉)
Department of Geography and Environmental Studies, University of Rajshahi, Rajshahi 6205, Bangladesh
e-mail: rejaur@ru.ac.bd; rejaur2001@yahoo.com

A. Rahman
Department of Geography, Faculty of Natural Sciences, Jamia Millia Islamia, New Delhi 110025, India
e-mail: arahman2@jmi.ac.in

10.1 Introduction

The pattern of land use/land cover and changes over time in urban area play a vital role in controlling the total environment of the area. Notably, green and blue spaces and their changes affect the urban ecological functions. These two important components of the urban environment also contribute in balancing human biophysical interconnections and maintaining good environmental quality. Through photosynthesis, green space releases sufficient oxygen to the air and absorb carbon dioxide from the air and on the other hand, also reduce air temperature and enhances aesthetic quality. Urban green spaces (UGS) are the areas that comprise a significant amount of vegetation in the urban area. On the other hand, urban blue spaces (UBS) represent the surface water bodies in the area. However, greatest environmental consequences of urban growth are related with the green and blue spaces. Due to rapid urbanization, growth of population and commercial evolution in the city areas, the spatial pattern of urban land-use changes dramatically and it was found that mainly vegetation and water bodies declined considerably not only in the cities of developing countries but also globally (Muhamad Nor et al. 2021). In the last two decades, due to the industrialization and economic development, urbanization has taken place significantly in the South and Southeast Asia (Sharifi et al. 2014). In these regions, the urban growth rate is about 2.4% per year, which is relatively high compare to the developed regions of the world (UNDESA 2012). Rapid urban growth intensely converts vegetation and water areas to built-up in the city and causes noteworthy drop of green and blue spaces (Ward et al. 2010). The shrinking of green and blue spaces may reduce the connectivity, biodiversity, and quality of life of the urban inhabitants (Tian et al. 2011). Lack of sufficient vegetation and water spaces gear up the pollution, soil erosion, and other critical environmental outbreaks, and all of these need to be addressed in formulating sustainable urban planning and development. The extensive and rapid urban development and continuous transformation of land use make a key challenge to the policy maker for the management of green and blue spaces (Sperandelli et al. 2013; Wu et al. 2018). For proper management of vegetation and water bodies, the inventories of the areas, monitoring of the changing pattern, trajectories, landscape pattern, hotspots of change and trends of change are essential since these can provide adequate guidelines for the development of sustainable management strategies (Östberg et al. 2018; Huerta et al. 2021).

Existing literature supports that several studies have been done on vegetation and water bodies dynamics and their importance in different cities of the world focusing urban growth and social values of green and blue spaces instead of considering landscape pattern (Yang et al. 2013, 2019; Li et al. 2017). Several studies highlighted that in the tropical region, loss of green and blue spaces was highest and these losses are mostly due to the absence of proper land use and urban planning, weak management strategy and sustainable urban development and expansion (Zhou and Wang 2011; Muhamad Nor et al. 2021; Siddique and Uddin 2022). Studies on green and blue spaces condition, extent and form and, integration of these information into the local urban planning and policy are crucial. Moreover, observing these two important components of the urban ecosystem is essential to know the variations of these components and how the variations are exaggerated by various controlling forces and ambient conditions (Msofe et al. 2019; Liu et al. 2021). In contrast, modern technologies like remote sensing and GIS helps to detect and manage the changes of earth phenomena in the right way. By classifying multi-temporal satellite images and information extraction through GIS, monitoring and changes can be observed in quantitative form (Shekinah et al. 2004; Rahman and Saha 2008; Rahman et al. 2009, 2014, 2018; Rahman 2013; Di et al. 2014; Huerta et al. 2021). Because of the technological advancement and the integration of mathematical models like machine learning algorithms-based decision tree (DT), random forest (RF), and support vector

machine (SVM) into GIS supports to detect and monitor earth phenomena with very high accuracy and effectively (Kopecká et al. 2017; Sharifi and Hosseingholizadeh 2019). Among the methods, SVM can produced higher accuracy of classifications with minimum efforts (Kranjcic et al. 2019). With quantitative analysis and modelling support, nowadays RS and GIS have become important tools for analysing changes in green and blue spaces (Di et al. 2014; Li et al. 2018, 2019). Also, some other scholars used transformation matrix to obtain information on changes and trajectories of green space, and landscape indices to identify the structure and changing pattern of green space landscape, combined with *Fragstats* software (Byomkesh et al. 2012; Li et al. 2016; Nor et al. 2017; Zhao et al. 2020). Nevertheless, few studies were available on the changing nature of green space and spatial analysis for the cities of South Asia, particularly, for the middle-sized cities. In recent decades, these cities are developing firstly and the combination of land use and unrestrained rapid growth are the key reasons of urban growth (Sharifi and Hosseingholizadeh 2019; Klopp and Petretta 2017). On the other hand, detailed geometric information on UGSs is not available and updated regularly; therefore, the changes of green space that have taken place because of the urban growth are not properly addressed. To create safe, protected, more comprehensive, robust eco-friendly cities, and geospatial data of UGS is needed and it is also recognized by the UN Sustainable Development Agenda (Klopp and Petretta 2017). Also, the generation of UGS geospatial data can helps to fulfil and obtain the Sustainable Development Goal 11.7 (SDG 11.7) i.e. "provide universal access to safe, inclusive and accessible, green and public spaces" (Huerta et al. 2021).

Therefore, considering the above facts, this chapter focuses on quantify the green and blue spaces within the Rajshahi Metropolitan City area, Bangladesh, and find out the geospatial pattern of green and blue spaces dynamics over the periods 1990–2021. Specifically, this chapter addressed the questions, (i) how much areas were there under green and blue spaces, and how have these spaces changed in the last 32 years?;

(ii) was there any spatial pattern of green and blue spaces change in the city area?; (iii) was there any zonal and directional pattern of green and blue spaces change?; (iv) was there any spatial trend in the change of green space?; and (v) where were the significant locations of hotspots of the changes of UGS?

10.2 Materials and Methods

10.2.1 Study Area

The Rajshahi Metropolitan City, one of the largest cities in Bangladesh, with about 1.0 million inhabitants and an administrative area of 48 km^2 (BBS 2020), was chosen as study area to analyse the green and blue spaces dynamic during the period 1990–2021. The city is situated in the north-western part of Bangladesh and geographically extend in between latitude 24° 12′ to 24° 42′ N and longitude 88° 15′ to 88° 50′ E (Fig. 10.1). The city is well networked with capital city and others through road, rail and air. The city enjoys tropical monsoon climate with an average temperature 24.5 °C and average annual rainfall of 1448 mm. However, maximum temperature varies from 30 to 40 °C, and April and May are the hottest months in the area (BBS 2013; Kafy et al. 2020). Since this city act as divisional headquarter, during the last few decades rapid urbanization has taken place in the city. The increase in the size of the population observed from about 0.52 million to 1.0 million (annual growth rate 2.88%) during the period 1990 to 2022 (BBS 2020). Currently, the city is divided into 30 Wards under four Police Stations namely *Boalia*, *Rajpara*, *Matihar* and *Shah Makhdum*. From the city centre, distance of the city boundary to the north, west, and east is 5.75, 5.90, and 7.00 km, respectively. The city boundary distance is only 0.65 km from the city centre to the south. The southern part of the city is bounded by the mighty river Padma. Therefore, the city is mainly expanded to the north, west, and east directions over the periods. The enormous growth and unrestricted development of different built-up areas, growth zones and

other urban structures, which amplify the significant drop of green spaces, water area, barren land, cropland etc., and therefore, the overall condition, competence and environmental safety of the city were affected harmfully thereof. It was found that the share and dynamics of green and blue spaces associated with different land uses are not well studied, and for the proper urban planning and development, details information of green and blue spaces dynamics are important. This chapter is therefore, designed to analyse the green and blue spaces dynamics over the period 1990–2021 in Rajshahi Metropolitan City of Bangladesh.
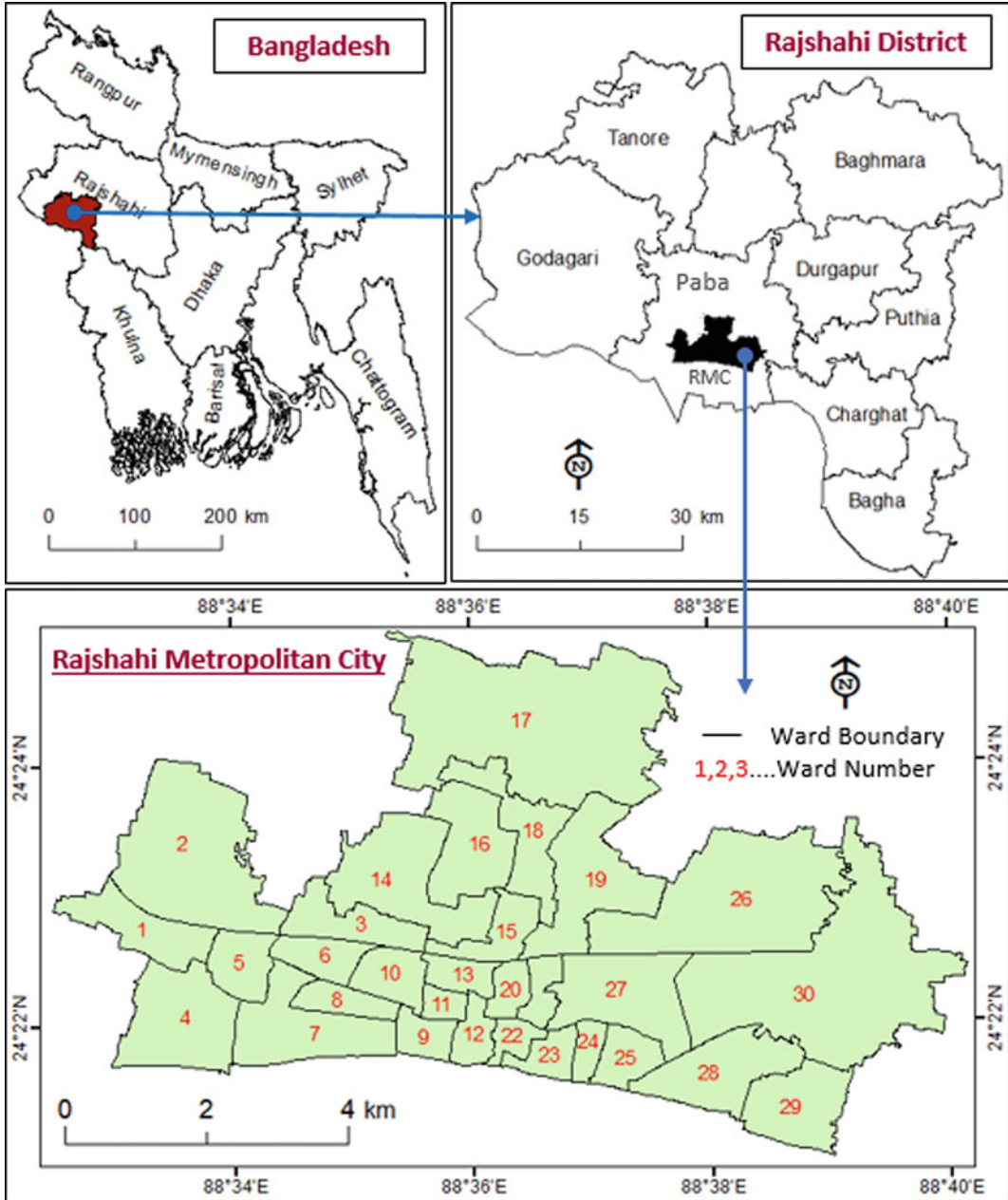

Fig. 10.1 Study area-Rajshahi Metropolitan City

10.2.2   Data Used

Primarily, satellite remote sensing data were used to extract and analyse the vegetation and water area dynamics. Landsat TM, ETM+, and OLI satellite data were acquired for the years 1990, 2000, 2010, and 2021. All multispectral data were downloaded from the United States Geological Survey (USGS) website using GLOVIS download portal (http://glovis.usgs.gov) to fulfil the coverage of the entire study period. The detailed pertinent information of the obtained Landsat data is given in Table 10.1. To select the images, the data for the month of November of the respective year was considered to avoid cloud cover, since all images were optical remote sensing-based. Moreover, during the November, it was considered more likely to have a similar condition of vegetation cover and other ground conditions from year to year, ensuring consistency in seasonal vegetation. Besides, some other data, e.g., city boundary, ward boundary geospatial data and field data (obtained using global positioning system, observation technique) were used.

10.2.3   Methods

This chapter analyses the dynamics of green and blue spaces in Rajshahi Metropolitan City of Bangladesh by extracting land use/land cover information from the Landsat satellite data. The overall methodology involved for the work is shown in Fig. 10.2. To extract the information from the satellite data, digital image classification procedure was followed. In this process, first, images were first corrected geometrically using well distributed sufficient ground control points (GCPs), accepting a root mean square error (RMSE) less than 0.15. Then, all images were resampled following Universal Transverse Mercator projection (UTM), nearest neighbour algorithm, and polynomial transformation, with corresponding sensor pixel size. To classify the image, support vector machine (SVM) technique was used since it is an advance technique, provides high classification accuracies and have good generalization capabilities (Brown et al. 2003; Hong et al. 2016; Kranjcic et al. 2019). Satellite image can be classified using SVM which is based on supervised machine learning algorithm, allows the computer to work in a self-learning mode without being explicitly programmed. Training cases on the edge of SVM class distribution, focuses on support vectors, tries to find the best classification hyperplane within the class, and effectively eliminates other training cases (Brown et al. 2003). Following the SVM classification procedure, both training and testing sites were developed. A classification scheme with four types of land use/land cover, viz. vegetation, water bodies, built-up, and bare land was followed to generate training and testing sites, and ground truth information was

Table 10.1 Description of obtained Landsat satellite data

Satellite	Sensor	Date of acquisition	Spatial resolution (m)	Bands used	Wavelength (μm)	Source
Landsat 5	TM	14 Nov 1990	30	Green Red NIR	0.52–0.60 0.63–0.69 0.76–0.90	USGS
Landsat 7	ETM+	17 Nov 2000	30	Green Red NIR	0.52–0.60 0.63–0.69 0.77–0.90	USGS
Landsat 5	TM	05 Nov 2010	30	Green Red NIR	0.52–0.60 0.63–0.69 0.76–0.90	USGS
Landsat 8	OLI	03 Nov 2021	30	Green Red NIR	0.53–0.59 0.64–0.67 0.85–0.88	USGS

incorporated into the training and testing site selection. The SVM classifier seeks to find a best separation hyperplane that can distinguish two classes (Hong et al. 2016). In SVM, selection of Kernel is important and can be treated as key parameter since it retains the accuracy of the training and classification effectively (Wang et al. (2020). Among the used kernels, radial basis function (RBF) kernel has shown high performance for data modelling (Kia et al. 2012). Thus, the SVM model with RBF kernel was used here to classify the satellite images. Details of SVM and RBF kernel mathematical algorithms can be found in He et al. (2021), Wang et al. (2020) and Kalantar et al. (2018). In this study, to train the

SVM for assessing land use/land cover and build each scenario, training data-set and the "Train Support Vector Machine Classifier" of ArcGIS 10.6 was used and then classified. Furthermore, for the validation of classified maps, testing data set was crossed and error matrix was generated to find out the accuracy level.

To analyse the spatial dynamics of urban green and blue spaces, first vegetation and water bodies were extracted from the classified map of the respective year, and then ward level urban green space index (UGSI) and urban blue space index (UBSI) were calculated using Eqs. 10.1 and 10.2, respectively (Shekhar and Aryal 2019). The UGSI and UBSI provides the indication of
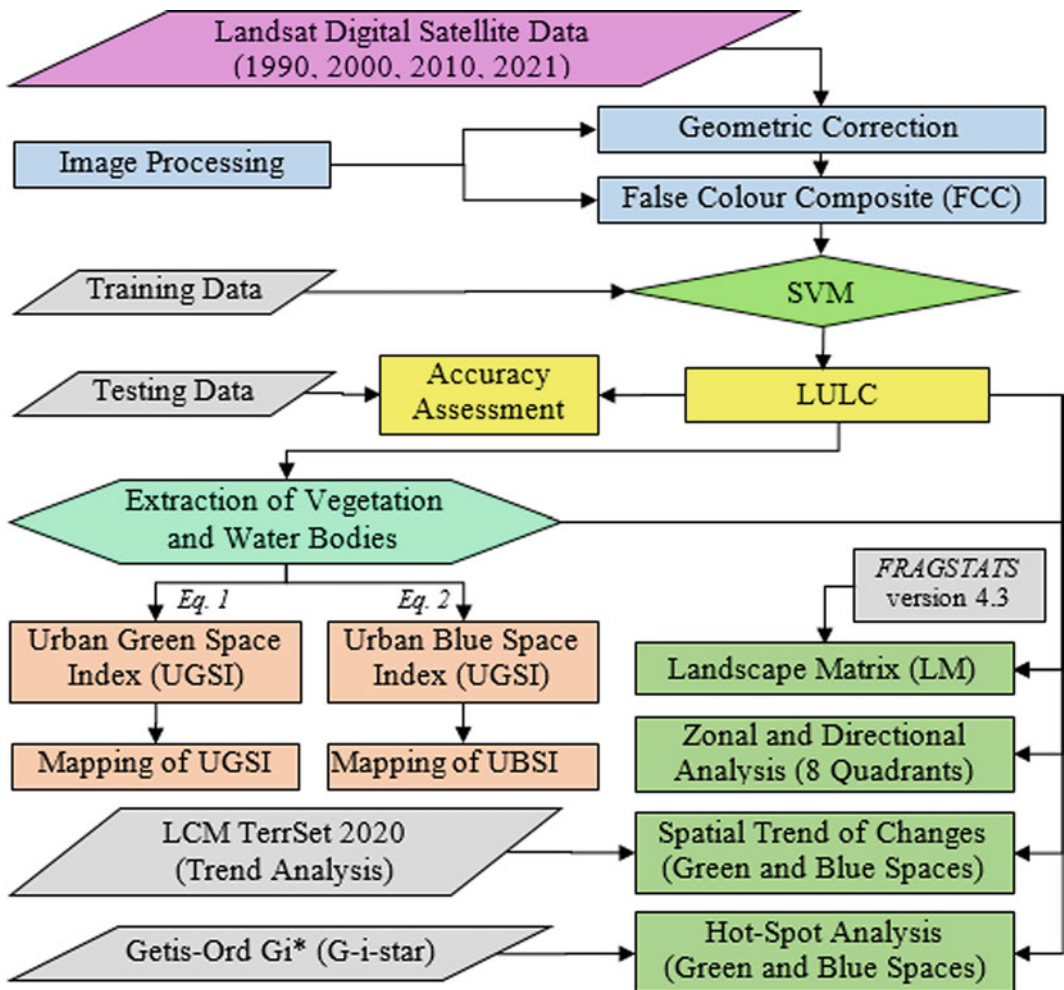

Fig. 10.2 Overall methodology of the study

the quality of eco-environment and the amount of UGS and UBS in relation to other urban land uses. High index value means high proportion of UGS or UBS, low green index means low proportion of the UGS and UBS in the study area. Later, using the water level index value, spatial pattern was identified through GIS.

$$\text{UGSI} = \frac{A_\text{G}}{A_\text{T}}, \qquad (10.1)$$

$$\text{UBSI} = \frac{A_\text{B}}{A_\text{T}}, \qquad (10.2)$$

where UGSI and UBSI represent urban green space index and urban blue space index, respectively. A_G is area under vegetation, A_B is area under water bodies, and A_T is the total area.

To examine the landscape structure for the years 1990, 2000, 2010, and 2021 at landscape, class and patch levels, six metrics were selected, viz. number of patches (NP), patch density (PD), mean patch area (AREA_MN), largest patch index (LPI), landscape shape index (LSI), and Euclidean nearest neighbour distance (ENN_MN) (Table 10.2). FRAGSTATS (Version 4.3) software was used to figure out the selected matrices (McGarigal et al. 2002). Detailed information for the metrics are available in McGarigal et al. (2012). Selected indices were computed to detect the temporal dynamics in all categories of land use/land cover spaces composition and landscape configuration. However, emphasis has been given on green, blue and built-up spaces.

One of the objectives was to find out the zonal and directional changes of green and blue spaces with the context of built-up expansion. Thus, a combined directional and zonal study of green, blue and built-up areas was performed considering eight quadrants at an angle 45° from the city centre (as a centre for directional analysis) for measuring variations of urban expansion and UGS change in the study area, as shown in Fig. 10.3. The eight quadrants were "North-West-West (NWW), North–North-West (NNW), North–North-East (NNE), North-East-East (NEE), South-East-East (SEE), South-South-East (SSE), South-South-West (SSW) and South-West-West (SWW)" (Fig. 10.2).

Moreover, the spatial trend analysis of changes of green, blue and built-up areas was accomplished to know the spatial pattern and locations of changes during the periods. Land change modeller (LCM) of TerrSet 2020 geospatial monitoring and modelling system was used to spatial trend analysis and mapping.

Table 10.2 Description of landscape metrics

Matrix	Class/group	Description	Indicator of
Number of patches (NP)	Area/density/edge	Provides total number of patches of a landscape class	Fragmentation
Patch density (PD) in Number per 100 ha	Area/density/edge	Number of patches/the total landscape area (m^2) * 1,000,000	Fragmentation
Mean patch area (AREA_MN) in ha	Area/density/edge	Provides the average area of patches	Dominance
Largest patch index (LPI) in %	Area/density/edge	Largest patch area (m^2)/total landscape area (m^2) * 100	Dominance
Landscape shape index (LSI) in m/ha	Area/density/edge	Total length of edge/minimum length of class edge	Shape complexity; boundary sharing with other patch types
Euclidean nearest neighbour distance (ENN_MN) in m	Isolation/proximity/ aggregation	Provides the distance of the nearest neighbouring patch (m) based on the distance from edge to edge	Quantifies patch isolation
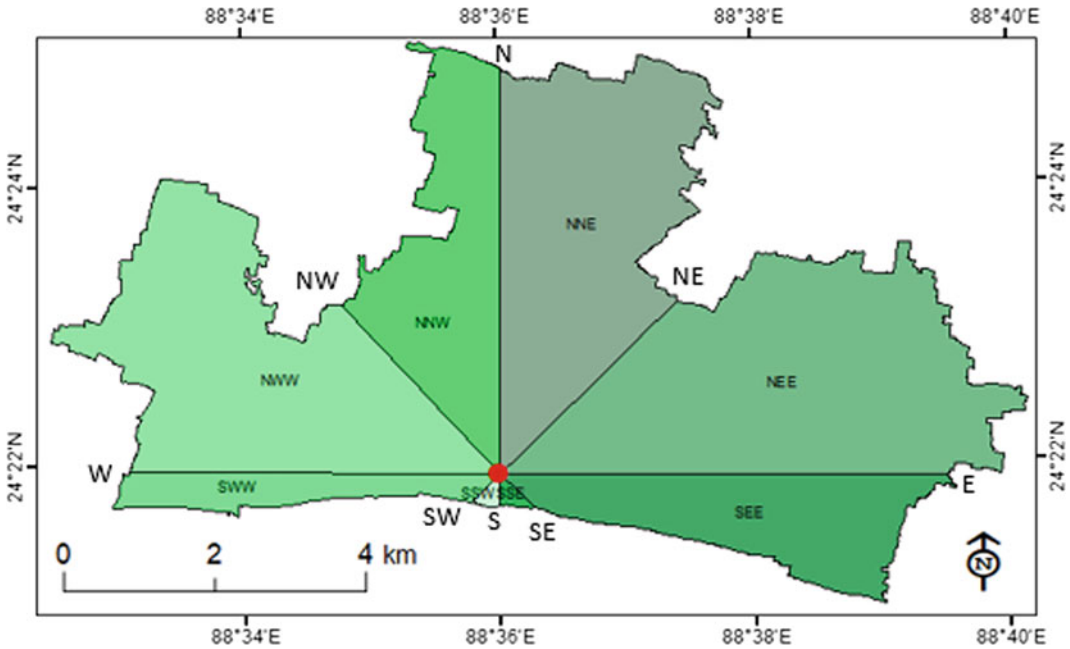
Fig. 10.3 Eight quadrants for zonal and directional change analysis. Red circle indicates city centre

In LCM, the trend analysis creates surface as change and no change areas and assign as 1 and 0, respectively, for quantitative representation. In the pattern of change between two spaces (change and no change), LCM produced a best-fit polynomial trend surface (Rahman and Saha 2009). Here, the spatial trend of change was generated following a 7rd-order surface trend between 'green space to built-up' and 'blue space to built-up', and analysed.

In addition to spatial trends, a hotspot analysis of changes between the classes was also done. Spatial Getis-Ord Gi* (G-i-star) technique was used to find out the significant hot-spots of the changes (Getis and Ord 1992). The results of spatial G-i-star based on z-scors and p-values highlighted the high and low values cluster. Thus, high value spatial clustering which is assigned by high z and low p values representing hotspots of the changes and vice versa (Rahman et al. 2021). The G-i-star statistics expressed as Eq. 10.3. ArcGIS (version 10.6; Environmental Systems Research Institute, Inc.) was used to identify, analyse data spatially and hotspot area mapping.

$$G_i^* = \frac{\sum_{j=1}^{n} w_{i,j} x_j - \overline{X} \sum_{j=1}^{n} w_{i,j}}{S \sqrt{\frac{\left[n \sum_{j=1}^{n} w_{i,j}^2 - \left(\sum_{j=1}^{n} w_{i,j} \right)^2 \right]}{n-1}}}, \quad (10.3)$$

$$\overline{X} = \frac{\sum_{j=1}^{n} x_j}{n}, \quad (10.3.1)$$

$$S = \sqrt{\frac{\sum_{j=1}^{n} x_j^2}{n} - \left(\overline{X} \right)^2}, \quad (10.3.2)$$

where x_j represents attribute value of feature j, $w_{i,j}$ is the spatial weight between feature i and j, n is the total number of features.

10.3 Results and Discussion

10.3.1 General Land Use/Land Cover

Land use/land cover (LULC) classification was conducted using the SVM model with RBF kernel basis function. Figure 10.3 executed the classification result of LULC in four major classes, including vegetation, water bodies, built-

up and bare land. Using the testing site, an assessment of the accuracy of the classified was done and achieved the overall accuracy ranges from 90 to 93% and the Kappa coefficient ranges from 0.87to 0.89 for the four classified images., i.e. 1990, 2000, 2010, and 2021. Table 10.3 presents the evolution of the surface of each class from 1990 to 2021 with their proportion in the total surface area of the city, the surface area of each type of land use change and the proportion of each type in the total surface area. Table depicts that the vegetation cover was the dominant in the city area in the years 1990, 2000, and 2010, however, in 2021 built-up became leading coverage in the city area. Figure 10.4 further portraits that vegetation area decreased in all the observed years and during the period 1990–2021, total decreased area of vegetation was about 26% of the total area of the city. In contrast, built-up area increased in all the years and total increased area of built-up was about 27.62% of the area between 1990 and 2021 (Fig. 10.4; Table 10.3). The area under water bodies also decreased and from 1990 to 2021, it was decreased from 10 to 7% (net decreased 3%) of the total area, respectively (Table 10.3; Fig. 10.4) The urban growth, i.e. increase of built-up area was highest in the period of 2010–2021 compared to the previous periods, denoting urbanization intensified in this period. The highest increase of built-up areas and highest decrease of vegetation areas illustrate that area under vegetation mainly converted to built-up areas, and this indicates rapid urban expansion in the area during the periods.

The spatial pattern of LULC of Rajshahi Metropolitan city in 1990, 2000, 2010, and 2021 illustrated in Fig. 10.5. Figure depicts that rapid urbanization was taken place in the city during the period particularly, since 2010 and mainly due to the urbanization i.e. expansion of built-up areas vegetation cover has decreased remarkably. Notably, urban expansion was more in the central, eastern and western part of the city. During the period, the area under built-up has increased and occupied highest proportion of the area, and as a consequence of increased built-up, vegetation areas were converted to built-up. However,

Table 10.3 Dynamics of land use/land cover of Rajshahi Metropolitan City

LULC	1990		2000		2010		2021		Change (% of total area)			
	km⁻²	% of the total area	km⁻²	% of the total area	km⁻²	% of the total area	km⁻²	% of the total area	1990–2000	2000–2010	2010–2021	1990–2021
Built-up	9.73	20.27	11.79	24.56	15.22	31.70	22.99	47.89	4.29	7.14	16.19	27.62
Vegetation	30.72	64.00	26.88	56.00	24.00	50.00	18.24	38.00	−8.00	−6.00	−12.00	−26.00
Water bodies	4.80	10.00	4.80	10.00	4.32	9.00	3.36	7.00	0.00	−1.00	−2.00	−3.00
Bare land	2.75	5.73	4.53	9.44	4.46	9.30	3.41	7.11	3.71	−0.14	−2.19	1.38
Total	48.00	100.00	48.00	100.00	48.00	100.00	48.00	100.00	–	–	–	–
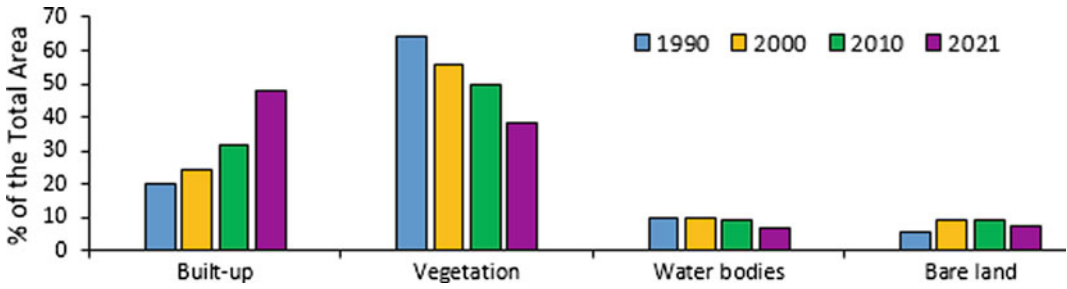
Fig. 10.4 Temporal pattern of land use/land cover of RMC
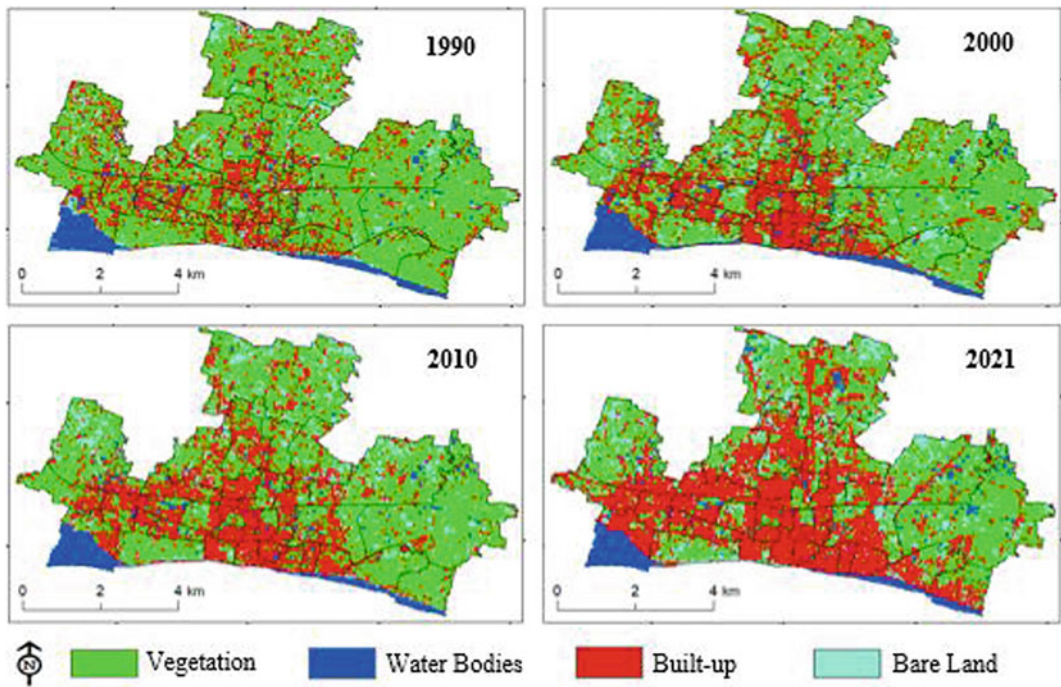
Fig. 10.5 Land use/land cover, Rajshahi Metropolitan City produced by SVM

the growth of built-up area was not entirely from the vegetation conversion, it was the combined transformation of other land uses, urban growth, road development, human settlements, economic development, and gradual development to a rationalized city. Thus, the observed spatial pattern of LULC can be considered as an indication of urban expansion and mainly reducing of green space during the analysed years, which has taken place within different parts of the city.

10.3.2 Dynamics of Urban Green and Blue Spaces

10.3.2.1 Urban Green Space Index (UGSI)

It was mentioned that due to urban expansion, a general declined trend was observed in the green space of metropolitan area, Rajshahi. As shown in Table 10.4, in the study area, the UGS was 64% in 1990 and this proportion declined to 56%

in 2000 and further reduced to 50% in 2010. Finally, it reduced to only 38% of the total area in 2010, perceiving rapid reduction of the UGS (total of 26% of the total area). For detailed analysis of green space dynamics, Ward wise distribution of green space was analysed using urban green space index (UGSI). UGSI indicates that there was a variation in Ward wise green area distribution during the periods and found declined trend in all the wards during 1990–2021 (Table 10.4). Based on the area occupied by green space, Wards 30, 27, 29, 18, and 1 were

Table 10.4 Ward wise green space and blue space indices

Ward number	Urban green space index (UGSI)					Urban blue space index (UBSI)				
	Period				Change	Period				Change
	1990	2000	2010	2021	1990–2021	1990	2000	2010	2021	1990–2021
1	0.72	0.65	0.61	0.31	−0.41	0.02	0.02	0.01	0.01	−0.01
2	0.58	0.57	0.54	0.47	−0.11	0.06	0.05	0.05	0.04	−0.02
3	0.59	0.49	0.33	0.09	−0.50	0.04	0.04	0.02	0.00	−0.04
4	0.19	0.18	0.16	0.03	−0.16	0.58	0.56	0.55	0.53	−0.05
5	0.58	0.41	0.35	0.15	−0.43	0.06	0.06	0.04	0.03	−0.03
6	0.44	0.31	0.27	0.15	−0.29	0.13	0.12	0.12	0.10	−0.03
7	0.68	0.61	0.60	0.49	−0.19	0.09	0.09	0.06	0.06	−0.03
8	0.52	0.33	0.31	0.20	−0.32	0.11	0.06	0.06	0.04	−0.07
9	0.53	0.23	0.19	0.12	−0.41	0.07	0.06	0.03	0.02	−0.05
10	0.60	0.48	0.47	0.29	−0.31	0.02	0.02	0.02	0.01	−0.01
11	0.45	0.27	0.14	0.10	−0.35	0.06	0.06	0.03	0.02	−0.04
12	0.31	0.12	0.09	0.04	−0.27	0.10	0.09	0.03	0.00	−0.10
13	0.42	0.24	0.24	0.16	−0.26	0.08	0.08	0.07	0.06	−0.02
14	0.60	0.54	0.42	0.27	−0.33	0.02	0.02	0.02	0.01	−0.01
15	0.52	0.39	0.36	0.30	−0.22	0.12	0.12	0.10	0.07	−0.05
16	0.64	0.50	0.45	0.25	−0.39	0.04	0.04	0.04	0.02	−0.02
17	0.68	0.64	0.58	0.52	−0.16	0.04	0.04	0.03	0.03	−0.01
18	0.72	0.66	0.61	0.34	−0.38	0.02	0.02	0.01	0.00	−0.02
19	0.61	0.60	0.49	0.36	−0.25	0.02	0.02	0.02	0.01	−0.01
20	0.45	0.34	0.33	0.24	−0.21	0.04	0.04	0.03	0.02	−0.02
21	0.57	0.38	0.24	0.09	−0.48	0.07	0.06	0.05	0.02	−0.05
22	0.47	0.20	0.13	0.06	−0.41	0.09	0.06	0.05	0.03	−0.06
23	0.44	0.30	0.27	0.04	−0.40	0.15	0.12	0.10	0.07	−0.08
24	0.53	0.23	0.20	0.04	−0.49	0.18	0.18	0.11	0.07	−0.11
25	0.56	0.38	0.32	0.04	−0.52	0.11	0.14	0.06	0.07	−0.04
26	0.71	0.64	0.54	0.50	−0.21	0.15	0.12	0.11	0.08	−0.08
27	0.76	0.63	0.53	0.34	−0.42	0.12	0.11	0.10	0.03	−0.09
28	0.68	0.57	0.54	0.30	−0.38	0.17	0.16	0.14	0.12	−0.05
29	0.74	0.66	0.61	0.36	−0.38	0.17	0.16	0.16	0.16	−0.01
30	0.78	0.72	0.70	0.65	−0.13	0.11	0.11	0.10	0.07	−0.04
Total	0.64	0.56	0.50	0.38	−0.26	0.10	0.10	0.09	0.07	−0.03

the top 5 greenery Wards in 1990 (having 78–72% green space), Wards 30, 29, 18, 1, and 26 in 2000 (having 72–64% green space) and Wards 30, 29, 18, 1, and 7 in 2010 (having 70–60% green space). However, in 2021, top 5 greenery Wards were 30, 17, 26, 7, and 2 (having 65–47% green space). Thus, these statistics indicate variation in the changing pattern of green space in the area. UGSI further shows that highest decrease of green space was found in Wards 25 and 3 (52 and 50%, respectively) which was followed by Wards 24, 21, 5, and 27 (49, 48, 43, and 42%, respectively).

In the spatial context, significant changes occurred in the distribution of UGS in city area. As shown in Fig. 10.6, Ward wise distribution of green space (as UGSI) highlighted that in the central part of the city area contains lowest percentage of green space in all the observed years and found basically steady. In 1990 and 2000, the northern, eastern, and south eastern parts of the city cover highest percentage of green space (60–80%), however, in 2010 and 2021, the percentage of green space was sharply declined in these part of the city (40–60%, somewhere 20–40%), reporting faster shrinkage of the UGS over the period 2010–2021 in these particular areas. The alarming situation is that in 2021, only one Ward which located in the eastern part occupied 60–80% green space whereas in 1990 total thirteen Wards occupied 60–80% green space. Remarkable change in the percentage of green space in these parts demonstrating UGS destruction due to uncontrolled and unplanned urban growth. Because of the limited urban space, the urban expansion unavoidably extended and progressed outer part from the city centre, which resultant continual decrease of green space in the urban fringe area. Hence, the proper planning in city structure and the implementation of greening policy need to be incorporated in management planning to increase green area or remains relatively steady.
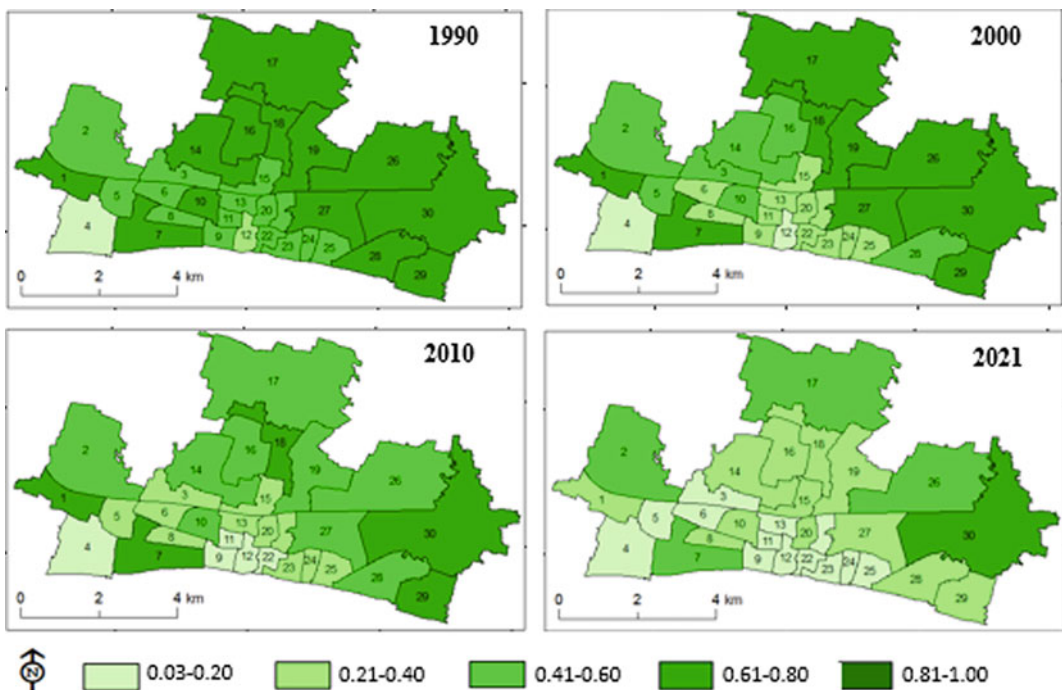

Fig. 10.6 Ward wise spatial distribution of UGSI

10.3.2.2 Urban Blue Surface Index (UBSI)

The dynamics of blue space was analysed using urban blue surface index (UBSI). Ward wise UBSI is shown in Table 10.4. As shown in Table, the UBS was 10% of the total area in both the years 1990 and 2000. In 2010 this proportion declined to 9% and further reduced to 7% in 2021. Thus, the total losses of blue space was 3% over the past 32 years i.e. 1990–2021. UBSI also indicates that there was a variation in Ward wise blue area distribution during the periods and found declined trend in all the wards during 1990–2021 (Table 10.4). In 1990 and 2000, in terms of blue space top 5 ranked Wards were 4, 24, 28, 29, and 26 (having 58–12% blue space). In contrast, Wards 4, 30, 29, 6, and 26/24 were in the top 5 ranked in 2010 (having 55–11% blue space). Finally, in 2021, top 5 ranked Wards were 4, 29, 28, 6, and 26 (having 53–8% blue space) considering blue space occupied area. It should be noted here that the Padma River passes through the Wards 4, 28 and 29. That's why the proportion of blue space is higher in these wards.

UBSI further shows that highest decrease of blue space was found in Wards 24 and 12 (11 and 10%, respectively) which was followed by Wards 27, 26, and 23 (9, 8 and 8%, respectively).

The spatial pattern of UBSI illustrates how blue spaces are changing in the study area over the time-lapse (Fig. 10.7). Ward wise distribution of blue space (as UBSI) highlighted that in the northern part of the city area contains lowest percentage of blue space in all the observed years and found mostly steady. In 1990 and 2000, the eastern, south eastern, southern and western parts of the city cover highest percentage of blue space (14–18%), however, in 2010 and 2021, the percentage of blue space was sharply declined in these part of the city (5–13%, somewhere <5%), reporting faster decline of the UBS over the period 2010–2021 in these particular areas. Alarmingly, the blue space in the central and north-western parts of the city declined rapidly and only occupied <5% of the total area in 2021. The remarkable change in the percentage of blue space in these parts demonstrates UBS shrinking and mainly due to the uncontrolled urban growth
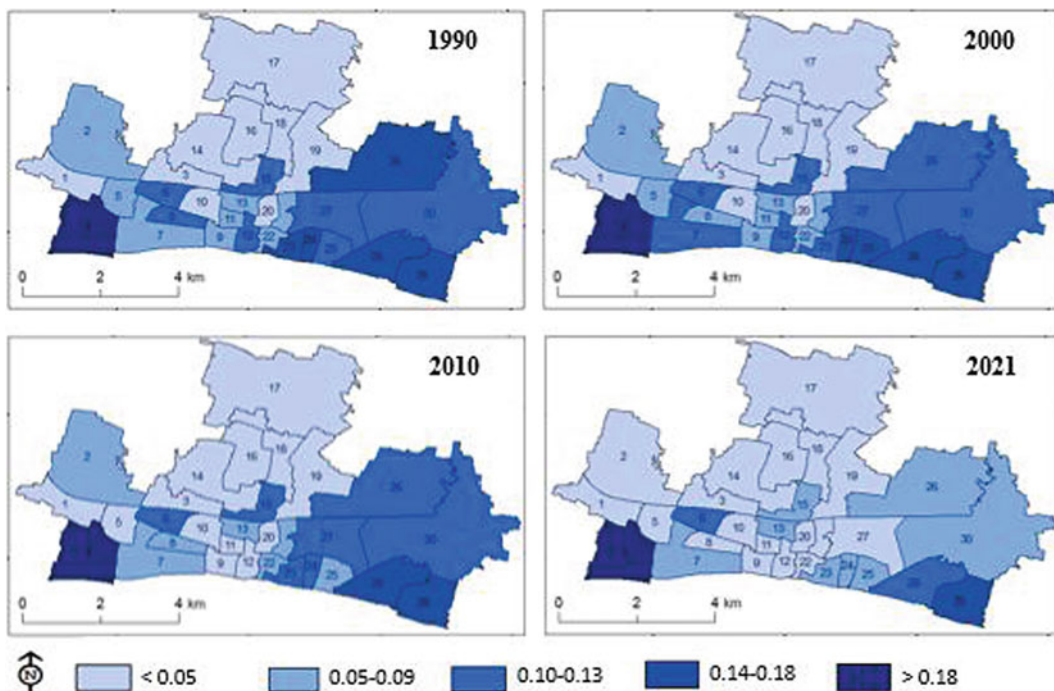

Fig. 10.7 Ward wise spatial distribution of UBSI

since the land price is much higher in these parts of the city. However, to maintain the eco-friendly environment of the city, the availability of blue space is essential, and therefore, in urban planning, initiatives should be taken to preserve the blue space, increase the blue space and remains blue space stable.

10.3.2.3 Landscape Structure Analysis by Landscape Matrices (LM)

Landscape structure of the city for the periods 1990, 2000, 2010 and 2021 was analysed using six landscape matrices. Landscape matrices were calculated to measure the spatial structure of green space, blue space, built-up, and bare land. As shown in Table 10.5 and Fig. 10.8, the number of patches (NP) and patch density (PD) were observed to increase and decrease for green space, blue space and bare land during the period 1990–2021, indicating that the fragmentation degree of the classes was both higher and lower between the years. Increasing in number denotes more fragmentation and more isolation and vice versa. In built up class, a decreasing trend was observed for NP and PD, denoting lower fragmentation, less isolation, and a lower percentage of edge area in patches. In case of LPI, a sharp decreasing trend (from 53.41to 13.43%) in green space and an increasing trend (from 1.39 to 31.73%) in built-up were observed during the period 1990–2021, meaning that there were fewer large patches of green space (i.e. more fragmentation), and in contrast, more large patches of built-up showing less fragmentation and less separation. The decreasing trend of LPI for green space and increasing trend of LPI for built-up over the time also indicate that the green space was converted to built-up area gradually and this conversion was the main cause of green space loss. Landscape shape Index (LSI) is an indicator of shape complexity. The LSI for green space in 2010 and 2021 was lower than in 2000, however, the there was no decreasing of LSI between 2010 and 2021. On the other hand, the LSI for built-up gradually decreased from 1990 to 2021 (Table 10.5 and Fig. 10.8), meaning the patch size became smaller and makes shape

complexity and dispersedly other land was converted to built-up. In case of mean patch area (MPA), a decreasing trend for the green space and in contrast, increasing trend for the built up were observed during the period. Decreasing trends of MPA signifying the disappearance or loss of green spaces and on the other hand, increasing trend of MPA representing gain of built-up during the period. The average distance between two patches in a landscape represents Euclidean nearest neighbour distance (ENN); the greater ENN means more fragmented patches of that landscape. Table 10.5 depicts that the ENN has slightly increased for both the green space and built up during 2010–2021 (Fig. 10.8), indicating that the green inter-patch distance increased and also the built-up inter-patch distance increased. This increased ENN also highlight the more fragmented of the patches and the conversion form green space to built-up was taken place in a scattered way during this period. Besides, there was no remarkable changes in selected matrices for the blue space during the period (Fig. 10.8). Thus, overall, landscape metrics analysis showed significant changes in the structure and pattern of green space and built-up area, as revealed by the changes in selected six matrices. Over the time green areas gradually became fragmented, more unevenly distributed and decreased physical extent with less physical connectivity due to the increasing human activities and unban expansion.

10.3.3 Zonal and Directional Analysis

Table 10.6 portraits statistics of the zonal and directional changes of green space, blue space, and built-up area. Zonal and directional analysis was executed to measure the directional change of urban expansion and green space. The directional analysis can help establish spatial relationships between land use/land cover changes and dynamics from a city centre (Zhang et al. 2019). Thus, in this study combined directional and zonal analysis was followed for the eight different directions from the city centre, as shown in Fig. 10.9. Over the last 32 years, the highest

Table 10.5 Landscape structure by landscape matrices

| Type	Year	Landscape matrix					
		NP (number)	PD (patches/100 ha)	LPI (%)	LSI (m/ha)	MPA (ha)	ENN_MN
Green space	1990	547	11.38	53.41	36.18	5.58	49.47
	2000	1147	23.87	25.34	46.56	2.30	48.61
	2010	760	15.82	20.28	36.34	3.47	55.25
	2021	1032	21.48	13.43	38.09	1.85	60.10
Blue space	1990	449	9.34	2.45	16.09	0.62	139.74
	2000	537	11.18	2.38	20.46	0.65	130.56
	2010	370	7.70	0.58	18.00	0.51	141.17
	2021	430	8.95	2.24	16.78	0.69	135.29
Built-up	1990	2125	44.22	1.39	52.68	0.51	57.69
	2000	1882	39.17	5.91	44.92	0.66	58.57
	2010	1106	23.02	11.70	36.87	1.26	70.30
	2021	783	16.29	31.73	30.35	2.47	68.69
Bare land	1990	1396	29.05	0.24	38.10	0.29	78.94
	2000	1832	38.13	0.29	43.89	0.32	67.63
	2010	1591	33.11	0.27	41.72	0.37	68.41
	2021	1821	37.90	0.35	44.20	0.37	68.37
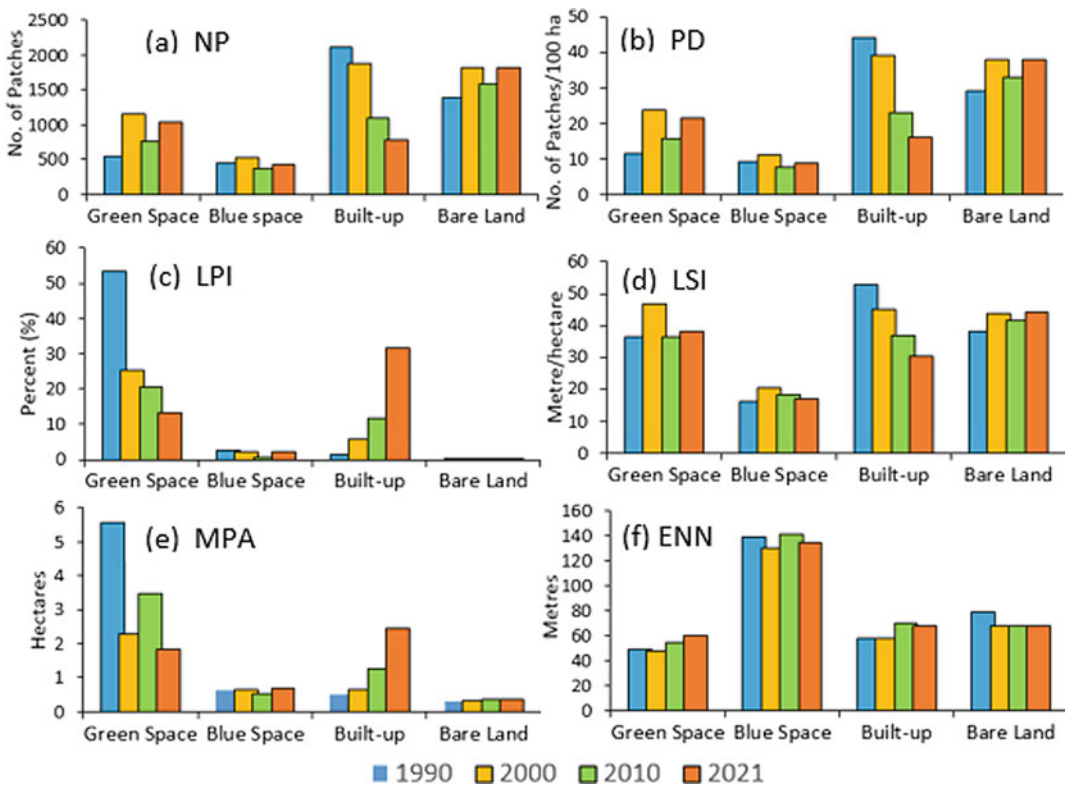
Fig. 10.8 Changes of landscape pattern index at class level

reduction of green space was observed in the NWW direction at a rate of 1014 ha y^{-1}. From 1990 to 2021, the second and third highest reductions in green space were found in the NEE and NNE directions, which were about 866 and 763 ha y^{-1}, respectively. A significant reduction in green space was also found towards SEE and NNW (Table 10.6). In contrast, the highest area increased of built-up was noticed in the NWW, NEE and NNW directions. The rate of built-up area expansion in NWW, NEE and NNW was 1027, 870 and 830 ha y^{-1}, respectively, reporting the city expanded mainly in these three directions during the study period. For blue space, highest shrinking was detected in the

NWW (116 ha y^{-1}), SEE (103 ha y^{-1}) and NEE (70 ha y^{-1}) directions during the period 1990–2021 (Table 10.6). The low level of urban expansion in the SEE and SWW direction was associated with the natural characteristics of the area. The river Padma flows in the southern part of the city and acted as barriers for urban expansion. The directional analysis further shows that the decline of green space in the NWW, NNW, NNE, and NEE directions was mainly due to rapid urban expansion in these directions over time (Fig. 10.9). Additionally, Fig. 10.9 illustrates how urban expansion gradually engulfed green space in different directions from the city centre at different times. The rapid of urban

Table 10.6 Directional change of green, blue and urban spaces in eight quadrants in RMC

| Zone	LULC	Area (km^2)				Change rate (ha/year)			
		1990	2000	2010	2021	1990–2000	2000–2010	2010–2021	1990–2021
NNE	Green space	6.410	5.998	5.177	4.045	−411.90	−821.10	−1029.55	−763.06
	Blue space	0.596	0.596	0.562	0.378	0.30	−34.20	−167.00	−70.19
	Built-up	2.179	2.387	2.940	4.344	208.10	553.00	1277.00	698.65
NEE	Green space	9.890	8.979	8.100	7.206	−911.20	−879.00	−812.55	−865.81
	Blue space	0.695	0.695	0.643	0.572	−0.40	−51.90	−65.09	−39.97
	Built-up	2.201	2.321	2.989	4.898	119.80	667.50	1735.45	869.77
SEE	Green space	3.377	2.721	2.212	1.372	−656.30	−508.90	−762.91	−646.58
	Blue space	0.988	0.884	0.804	0.668	−103.60	−80.40	−123.64	−103.23
	Built-up	0.750	1.120	1.570	2.659	369.40	450.50	989.64	615.65
SSE	Green space	0.020	0.002	0.008	0.005	−18.00	6.30	−3.27	−4.94
	Blue space	0.025	0.017	0.005	0.001	−8.30	−12.40	−3.45	−7.90
	Built-up	0.058	0.080	0.085	0.087	22.50	4.80	2.18	9.58
SSW	Green space	0.029	0.013	0.023	0.003	−16.20	9.90	−18.00	−8.42
	Blue space	0.025	0.019	0.001	0.001	−5.50	−17.80	−0.27	−7.61
	Built-up	0.049	0.068	0.078	0.064	19.80	9.20	−12.45	4.94
SWW	Green space	0.795	0.554	0.679	0.446	−240.30	124.20	−211.09	−112.35
	Blue space	0.992	0.992	0.923	0.776	0.50	−69.30	−133.45	−69.55
	Built-up	0.200	0.326	0.853	0.572	126.20	527.00	−255.27	120.13
NWW	Green space	6.310	5.292	5.082	3.166	−1017.60	−210.40	−1741.82	−1014.19
	Blue space	1.192	1.229	1.104	0.832	37.50	−125.18	−246.75	−115.84
	Built-up	2.994	3.606	4.300	6.486	612.00	693.86	1987.67	1126.55
NNW	Green space	3.890	3.319	2.716	2.001	−571.30	−602.60	−650.09	−609.35
	Blue space	0.286	0.363	0.276	0.134	76.70	−86.80	−129.27	−49.13
	Built-up	1.304	1.886	2.411	3.876	582.30	524.90	1331.64	829.68
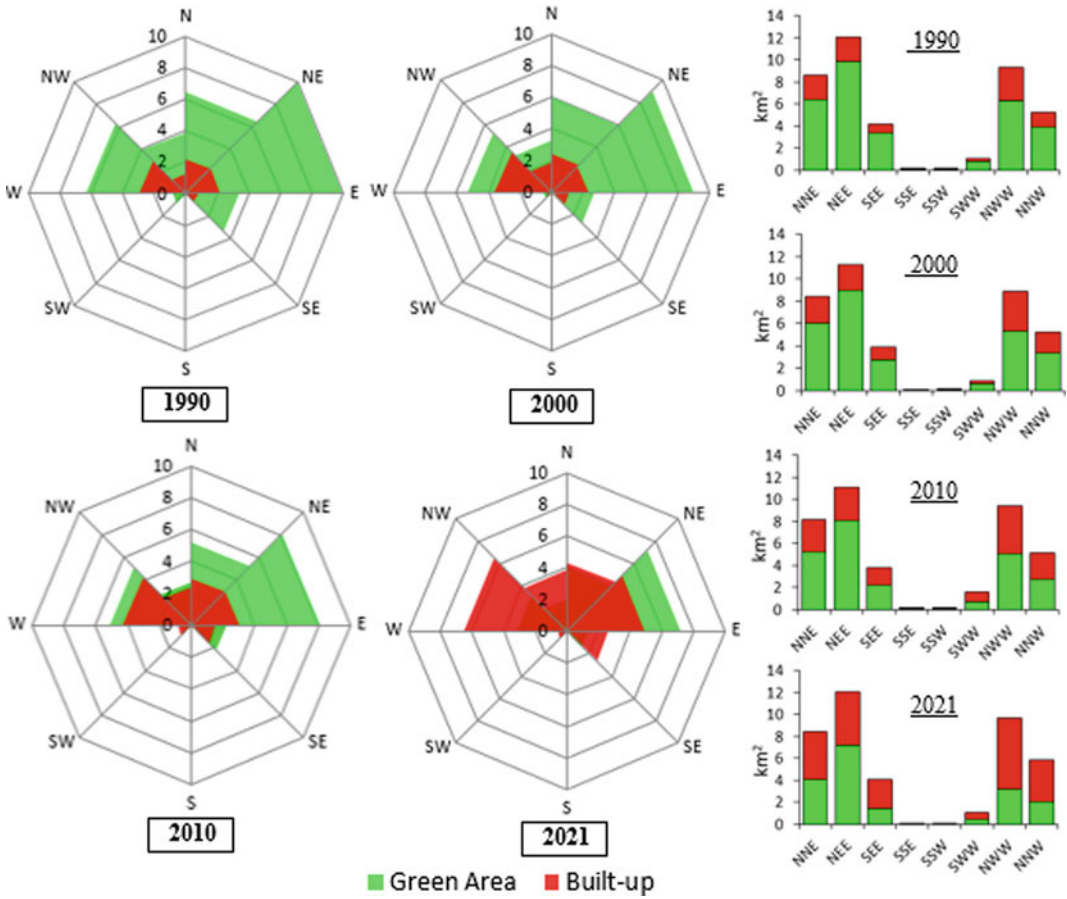
Fig. 10.9 Eight quadrants directional temporal pattern of green space and built-up, (area in km^2)

expansion in these directions may be attributed to the size of quadrant, suitability of land, increase in the road network and infrastructural development, increase land value/price and rapid population growth, i.e. tremendous pressure in the city area which facilitated mobility and urban expansion, as indicated above.

10.3.4 Spatial Trend and Hotspot Analysis

Here, the spatial trend of the change of green and blue spaces to built-up was analysed during the periods 1990–2000, 2000–2010, 2010–2021, and 1990–2021. The spatial trend analysis provides a spatial pattern of changes and simplifying the

trend of change (Eastman 2020), as shown in Figs. 10.10 and 10.11. During 1990–2000 and 2000–2010, remarkable changing trend of green space to built-up was mainly observed in the central part and some extent towards the western part of the city. However, during 2010–2021, notable trend of changing was further extent towards the northern and south eastern parts of the city. Overall, during the period 1990–2021, spatial pattern of the trend illustrated that conversion of green space to built-up was mainly taken place in the central, western, northern and south eastern parts. The conversion was started from the central parts and spread out towards the western, northern and south eastern parts (Fig. 10.10). Conversely, On the other hand, spatial trend analysis of the change of blue space
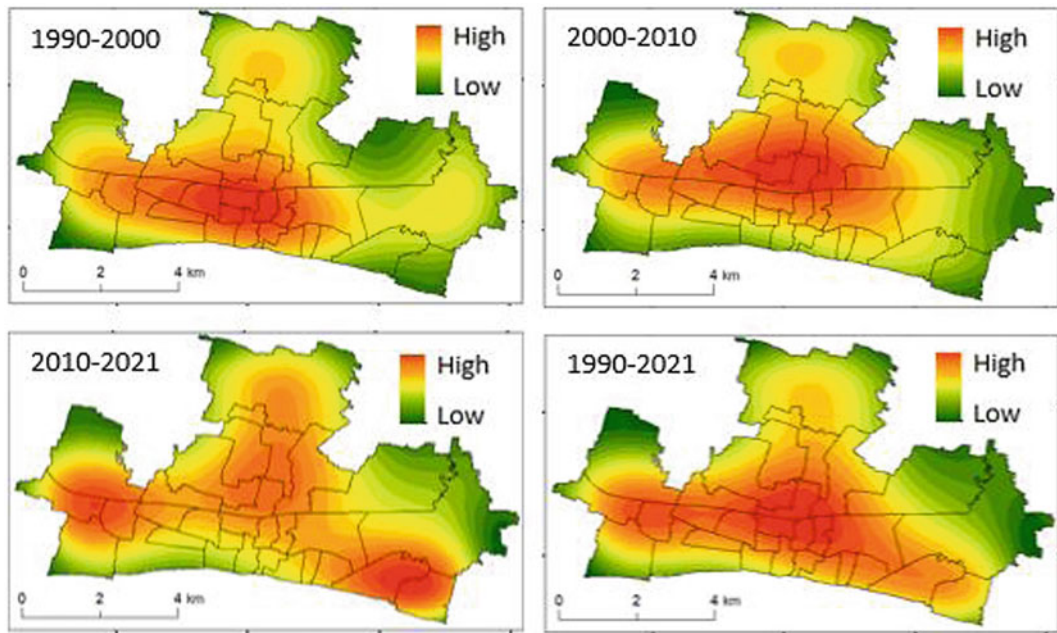
Fig. 10.10 Spatial trends of the changes of green space to built-up

to built-up denotes that there was no remarkable change of blue space to built-up during 1990–2000 and 2000–2021 except south western part (Fig. 10.11). However, during the period 2010–2021, changing trend of blue space to built-up was high in the central and central south eastern parts of the city. Overall, the changing trend of blue space during the period 1990–2021 shows that the area changed from blue space to built-up was mainly concentrated in the south western and central southern parts of the city (Fig. 10.11). From the trend analysis, it is clear that the central, northern, western and south eastern parts of the city are more unprotected in terms of eco-urban structure and eco-friendly environment. Hence, for sustainable urban development, special attention need to be taken on priority basis in these areas to restore the greenery and blue areas and also protect the existing green and blue spaces.

Apart from the trend analysis of changes of green space, here a hotspot analysis of the green space change was performed using Getis-Ord Gi* (G-i-star) statistics to find out the significant hotspot of the green space change to built-up. As shown in Fig. 10.12, during 1990–2000, green space change hotspots with 99% confidence level was in a small account, mainly distributed in the central southern part, and some few small patches in the western and northern part. During 2000–2010, only two significant patches were distributed in the north–north west and central eastern parts. During 2010–2021, due to the more area conversion from green space to built-up, hotspots were concentrated in the south eastern, some portion of northern and south western parts of the city. Overall, the hotspot analysis depicts that during 1990–2021, green space change hotspots with a 99% confidence level were most prominent and distributed in the central-eastern, south eastern, and central-western parts of the city. A similar pattern of hotspots observed for the conversion from green space to all classes (Fig. 10.13). Thus, the distribution of green space change hotspots illustrates that the conversion from green space to built-up and others, i.e. hotspots gradually moved toward the fringe area of the city. And over time, green space disappears in these locations, resulting in the large eroding of urban green space.
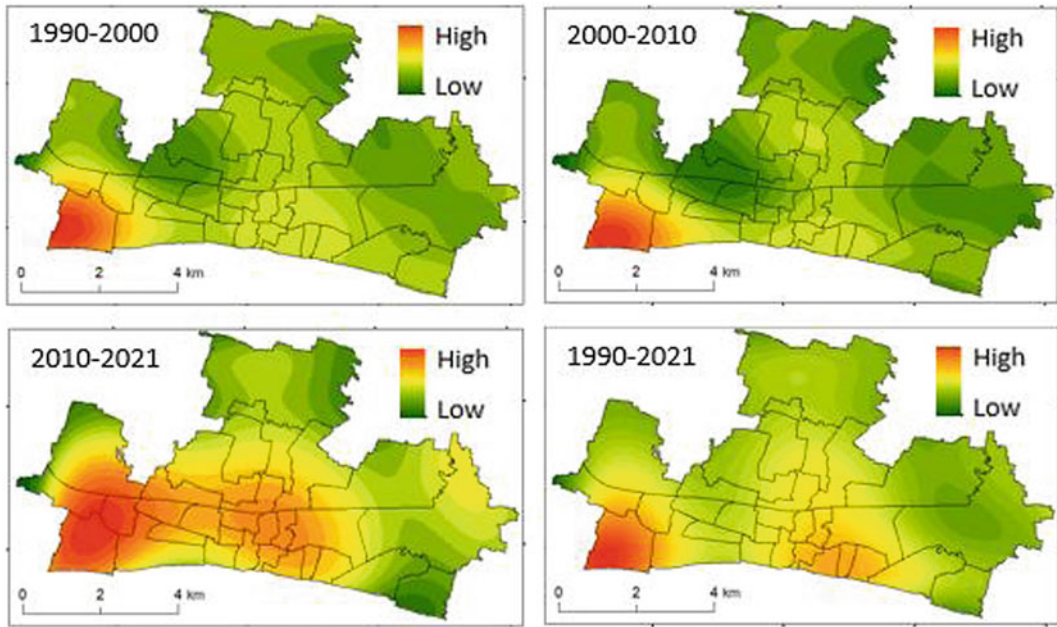
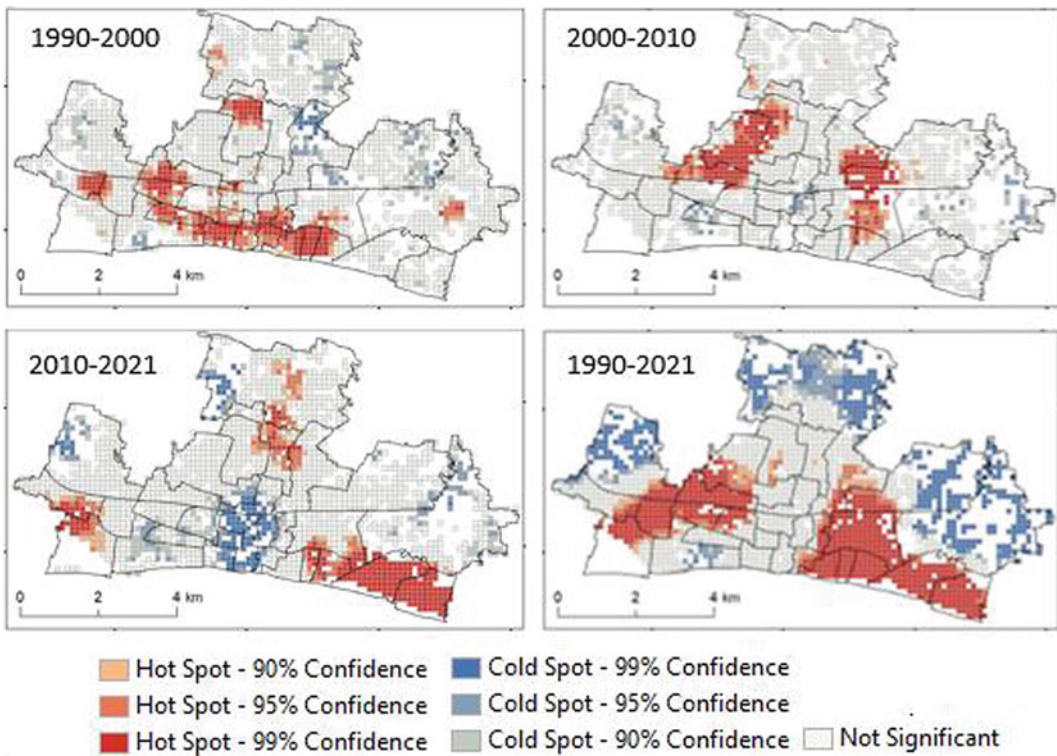**Fig. 10.11** Spatial trends of the changes of blue space to built-up

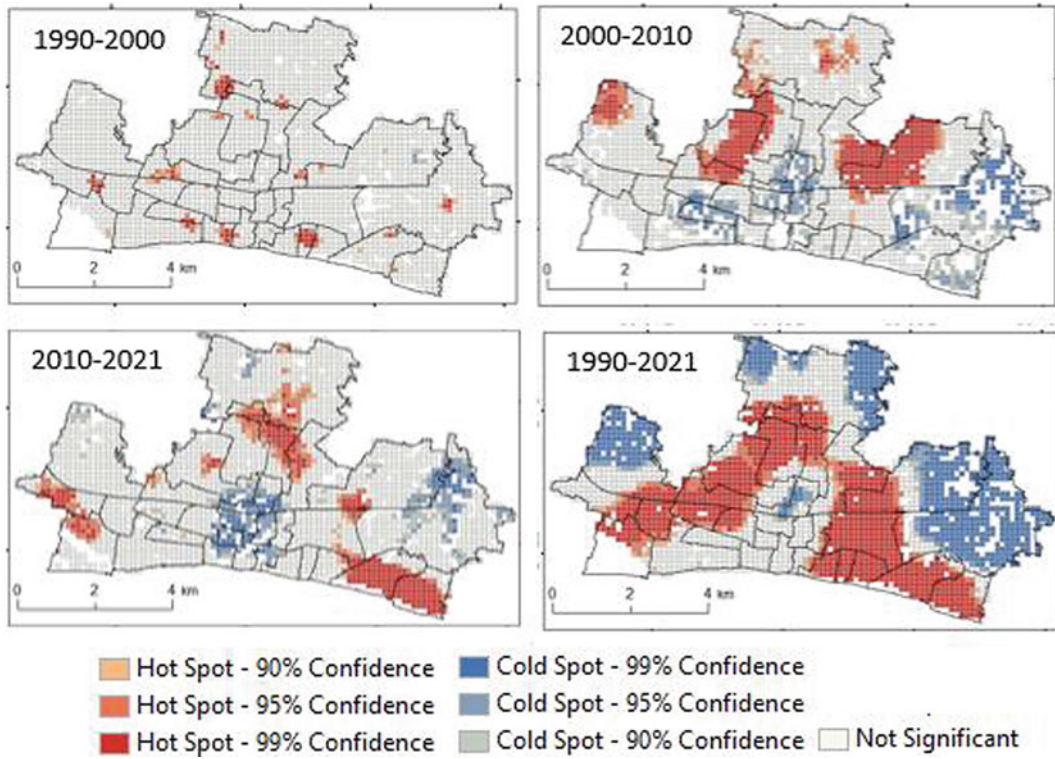**Fig. 10.12** Hotspots of the change of green space to built-up

Fig. 10.13 Hot spots of the change of green space to all other classes (water bodies, built-up and bare land)

10.4 Conclusions

The study analyses the spatial–temporal change of green and blue spaces in Rajshahi Metropolitan City, Bangladesh over the past 32 years, 1990–2021. Urban green and blue spaces dynamics were assessed in terms of spatio-temporal changes, green space index, blue space index, landscape structure, zonal and directional changes, spatial trend, and hotspot analysis. The green and blue spaces were extracted using Landsat multispectral remote sensing data, image processing and machine learning approach. The method applied in this study offered scientific evidence on spatial and temporal variation of urban growth, UGS and UBS changes in the city from 1900 to 2021. The result showed that both the urban green and blue spaces in the city reduced over the past

32 years, mainly due to rapid urban expansion. During this period, the total loss of green space was about 26% of the total area and in contrast, the total gain of the built-up area was 27.62% of the total area, proving that over time, the area under built-up was expanded mainly due to the conversion of green space. Most significantly, the study established that the study of spatial–temporal dynamics, zonal and directional analysis along with landscape structure, spatial trend and hotspot analysis can give a better understanding of urbanization dynamics and the pattern of UGS and UBS changes, which is essential information for urban planners and decision makers for better urban planning and management. Study on landscape structure based on landscape matrices highlighted notable changes in the distribution and pattern of green spaces. The structure of the green space gradually became fragmented, more

unevenly distributed and decreased physical extent with less physical connectivity. The zonal and directional analysis exposed that the highest decline of green space was taken place in the NWW, NNW, NNE, and NEE directions, and the decline was mainly due to rapid urban expansion in these directions over time. Finally, spatial trend and hot-spot analysis evinced that the conversion of green space to built-up started from the central parts of the city and spread out towards the western, northern and south-eastern parts, which indicated the significant reduction of green space gradually occurred towards the fringe area of the city.

In conclusion, the study revealed that the city expanded outward, particularly, to the western, northern and eastern directions over the period, the UGS and UBS are generally declined because of urban growth and economic development. It is true and alarming that a regular decline of the UGS and UBS will result in various environmental problems, and regular changes and destruction can result in the standard of in urban environments. More attention needs to be paid to urban green areas, especially near the fringe area of the city, and to improving ecological efficiency and quality of residential living within the urban landscape. Hence, a proper sustainable urban planning need to be formulated and implemented. Moreover, in formulating spatial planning, the national urban infrastructure standard which stipulates 30% green space, 30% transport, and 40% built up need to be executed. The limitation of this study is using 30 m resolution Landsat satellite data, so the analysis and information which are provided, based on 30 m scale. However, the application of high-resolution data can provide detailed urban information, especially for greenery in urban areas with higher fragmentation. Thus, the approaches which are applied here, it could be followed to evaluate the urban components dynamic analysis with high resolution data.

References

BBS (2013) District Statistics, Rajshahi. In: Ministry of Planning, Government of the People's Republic of Bangladesh. Bangladesh Bureau of Statistics, Dhaka, Bangladesh

BBS (2020) Statistical Yearbook Bangladesh-2019. Bangladesh Bureau of Statistics (BBS), Statistics & Informatics Division (SID), Ministry of Planning, Government of the People's Republic of Bangladesh Dhaka, Bangladesh

Brown M, Lewis HG, Gunn SR (2003) Linear spectral mixture models and support vector machines for remote sensing. IEEE Trans Geosci Remote Sens 38:2346–2360

Byomkesh T, Nakagoshi N, Dewan AM (2012) Urbanization and green space dynamics in Greater Dhaka, Bangladesh. Landsc Ecol Eng 8:45

Di X, Hou X, Wu L (2014) Land use classification system for China's coastal zone based on remote sensing. Resour Sci 36:463

Eastman JR (2020) TerrSet 2020 user's manual. Clark Labs, Clark University, Worcester, MA

Getis A, Ord JK (1992) The analysis of spatial association by use of distance statistics. Geogr Anal 24(3):189–206

He Y, Ma D, Xiong J, Cheng W, Ji H, Wang N, Guo L, Duan Y, Liu J, Yang G (2021) Flash flood vulnerability assessment of roads in China based on support vector machine. Geocarto Int. https://doi.org/10.1080/10106049.2021.1926560

Hong H, Pradhan B, Bui DT, Xu C, Youssef AM, Chen W (2016) Comparison of four kernel functions used in support vector machines for landslide susceptibility mapping: a case study at Suichuan area (China). Geomat Nat Haz Risk 1–26. https://doi.org/10.1080/19475705.2016.1250112

Huerta RE, Yépez FD, Lozano-García DF, Guerra Cobián VH, Ferriño Fierro AL, de León Gómez H, Cavazos González RA, Vargas-Martínez A (2021) Mapping urban green spaces at the Metropolitan level using very high resolution satellite imagery and deep learning techniques for semantic segmentation. Remote Sens 13:2031. https://doi.org/10.3390/rs13112031

Kafy AA, Rahman MS, Faisal AA, Hasan MM, Islam M (2020) Modelling future land use land cover changes and their impacts on land surface temperatures in Rajshahi, Bangladesh. Remote Sens Appl: Soc Environ 18:100314

Kalantar B, Pradhan B, Naghibi SA, Motevalli A, Mansor S (2018) Assessment of the effects of training data selection on the landslide susceptibility mapping: a comparison between support vector machine (SVM), logistic regression (LR) and artificial neural networks (ANN). Geomat Nat Haz Risk 9(1):49–69. https://doi.org/10.1080/19475705.2017.1407368

Kia MB, Pirasteh S, Pradhan B, Mahmud AR, Sulaiman WNA, Moradi A (2012) An artificial neural network model for flood simulation using GIS: Johor River

Basin, Malaysia. Environ Earth Sci 67:251–264. https://doi.org/10.1007/s12665-011-1504-z

Klopp JM, Petretta DL (2017) The urban sustainable development goal: Indicators, complexity and the politics of measuring cities. Cities 63:92–97

Kopecká M, Szatmári D, Rosina K (2017) Analysis of urban green spaces based on Sentinel-2A: case studies from Slovakia. Land 6:25

Kranjcic N, Medak D, Zupan R, Rezo M (2019) Machine learning methods for classification of the green infrastructure in city areas. Earth Environ Sci 362:012079

Li Y, Huang C, Zhang Y (2016) Investigating spatiotemporal patterns of landscape gradient and diversity of urban green spaces of Shanghai in response to rapid urbanization. Ecol Environ Sci 25:1115

Li F, Xie S, Li X (2018) The spatio-temporal evolution of green spaces in Central Beijing based on multi source data (1992–2016). Landsc Arch 25:46

Li Z, Zhong J, Sun Z, Yang W (2017) Spatial pattern of carbon sequestration and urban sustainability: analysis of land-use and carbon emission in Guang'an, China. Sustainability 9:1951

Li Q, Li X, Lu L, Cheng Y, Wu R (2019) Remote sensing analysis of spatiotemporal changes in Beijing's green space. Software 40:37

Liu S, Zhang X, Feng Y, Xie H, Jiang L, Lei Z (2021) Spatiotemporal dynamics of urban green space influenced by rapid urbanization and land use policies in Shanghai. Forests 476. https://doi.org/10.3390/f12040476

McGarigal K, Cushman SA, Neel MC, Ene E (2002) FRAGSTATS: spatial pattern analysis program for categorical maps. Computer Software Program Produced by the Authors at the University of Massachusetts, Amherst. Available online: http://www.umass.edu/landeco/research/fragstats/fragstats.html

McGarigal K, Cushman S, Ene E (2012) FRAGSTATS v4: spatial pattern analysis program for categorical and continuous maps [online], Available from Internet: http://www.umass.edu/landeco/research/fragstats/fragstats.html

Msofe N, Sheng L, Lyimo J (2019) Land use change trends and their driving forces in the Kilombero Valley Floodplain, Southeastern Tanzania. Sustainability 11:505

Muhamad Nor AN, Abdul Aziz H, Nawawi SA, Muhammad Jamil R, Abas MA, Hambali KA, Yusoff AH, Ibrahim N, Rafaai NH, Corstanje R et al (2021) Evolution of green space under rapid urban expansion in Southeast Asian cities. Sustainability 13:12024. https://doi.org/10.3390/su132112024

Nor ANM, Corstanjea R, Harrisa JA, Brewer T (2017) Impact of rapid urban expansion on green space structure. Ecol Ind 81:274

Östberg J, Wiström B, Randrup TB (2018) The state and use of municipal tree inventories in Swedish municipalities–Results from a national survey. Urban Ecosyst 21(2)

Rahman MR (2013) Agro-spatial diversity in Bangladesh-a special reference to climate change and crop diversification in Rajshahi Division. J Geo-Environ 10:1–15

Rahman MR, Saha SK (2008) Remote sensing, spatial multi criteria evaluation (SMCE) and analytical hierarchy process (AHP) in optimal cropping pattern planning for a flood prone area. J Spat Sci 53(2):161–177

Rahman MR, Saha SK (2009) Spatial dynamics of cropland and cropping pattern change analysis using Landsat TM and IRS P6 LISS III satellite images with GIS. Geospatial Inf Sci 12(2):123–134. https://doi.org/10.1007/s11806-009-0249-2

Rahman MR, Shi ZH, Chongfa C (2009) Soil erosion hazard evaluation-an integrated use of remote sensing, GIS and statistical approaches with biophysical parameters towards management strategies. Ecol Model 220(13–14):1724–1734

Rahman MR, Shi ZH, Chongfa C (2014) Assessing regional environmental quality by integrated use of remote sensing, GIS, and spatial multi-criteria evaluation for prioritization of environmental restoration. Environ Monit Assess 186(11):6993–7009. https://doi.org/10.1007/s10661-014-3905-4

Rahman MR, Islam AHMH, Islam MN (2021) Geospatial modelling on the spread and dynamics of 154 day outbreak of the novel coronavirus (COVID-19) pandemic in Bangladesh towards vulnerability zoning and management approaches. Model Earth Syst Environ 7:2059–2087. https://doi.org/10.1007/s40808-020-00962-z

Rahman MR, Lateh H, Islam MN (2018) Climate of Bangladesh: temperature and rainfall changes, and impact on agriculture and groundwater-A GIS-based analysis. In: Islam M, van Amstel A (eds) Bangladesh I: climate change impacts, mitigation and adaptation in developing countries. Springer Climate. Springer, Cham. https://doi.org/10.1007/978-3-319-26357-1_2

Sharifi A, Chiba Y, Okamoto K, Yokoyama S, Murayama A (2014) Can master planning control and regulate urban growth in Vientiane, Laos? Landsc Urban Plan 131:1–13

Sharifi A, Hosseingholizadeh M (2019) The effect of rapid population growth on urban expansion and destruction of green space in Tehran from 1972 to 2017. J Indian Soc Remote Sens 47(10)

Shekhar S, Aryal J (2019) Role of geospatial technology in understanding urban green space of Kalaburagi city for sustainable planning. Urban Urban Green 46

Shekinah DE, Saha SK, Rahman MR (2004) Land capability evaluation for land use planning using GIS. J Indian Soc Soil Sci 52(3)

Siddique S, Uddin MM (2022) Green space dynamics in response to rapid urbanization: Patterns, transformations and topographic influence in Chattogram city, Bangladesh. Land Use Policy 114:105974

Sperandelli DI, Dupas FA, Pons NAD (2013) Dynamics of urban sprawl, vacant land, and green spaces on the

metropolitan fringe of São Paulo, Brazil. J Urban Plan Dev 139(4)

Tian Y, Jim C, Tao Y, Shi T (2011) Landscape ecological assessment of green space fragmentation in Hong Kong. Urban For Urban Green 10:79–86

UNDESA (2012) United Nations Department of Economic and Social Affairs. World urbanization prospects: the 2011 revision; United Nations Department of Economic and Social Affairs/Population Division: New York, NY, USA

Wang Z, Liu Q, Liu Y (2020) Mapping landslide susceptibility using machine learning algorithms and GIS: a case study in Shexian County, Anhui Province, China. Symmetry. https://doi.org/10.3390/sym12121954

Ward CD, Parker CM, Shackleton C (2010) The use and appreciation of botanical gardens as urban green spaces in South Africa. Urban For Urban Green 9:49–55

Wu H, Liu L, Yu Y, Peng Z (2018) Evaluation and planning of urban green space distribution based on mobile phone data and two-step floating catchment area method. Sustainability 10:214

Yang J, Li S, Lu H (2019) Quantitative influence of land-use changes and urban expansion intensity on landscape pattern in Qingdao, China: implications for urban sustainability. Sustainability 11:6174

Yang J, Huang C, Zhang Z, Wang L (2013) The temporal trend of urban green coverage in major Chinese cities between 1990 and 2010. Urban For Urban Green 13:19–27

Zhang Y, Wang X, Balzter H, Qiu B, Cheng J (2019) Directional and zonal analysis of urban thermal environmental change in Fuzhou as an indicator of urban landscape transformation. J Remote Sens 11:2810

Zhao H, Wang S, Meng F, Niu M, Luo X (2020) Green space pattern changes and its driving mechanism: a case study of Nanjing metropolitan area. Acta Ecol Sin 40:7861

Zhou X, Wang YC (2011) Spatial–temporal dynamics of urban green space in response to rapid urbanization and greening policies. Landsc Urban Plan 100:268–277

Quantifying the Impact of Urban Green Space Pattern to Land Surface Temperature: Evidence from an Urban Agglomeration of Eastern India

11

Ipsita Dutta and Arijit Das

Abstract

Understanding the spatial pattern of urban green space is largely recommended for the mitigation of urban heat island (UHI) effect. Previous researches have examined the complex relationship between green space patterns and land surface temperature (LST) but the contribution of pattern of green space is remained less explored. Therefore, this study attempted to study the variations of green space at neighborhood level during six temporal periods and to identify the relative contribution of composition and configuration of green space patterns to LST. The study is based on English Bazar urban agglomeration and its peri-urban areas. Landsat TM and OLI images with 30 m resolution were used for the extraction of green space and LST. Landscape metrics were used for identifying different patterns of green space at neighborhood level using Fragstat 4.2. Pearson correlation, stepwise regression, and hierarchical partitioning methods were used to understand this complex relationship. The result shows that there is a loss of nearly 11 km^2 (5.17%) green space between 1990 and 2015. Green space configuration and composition directly affect LST though the magnitude of contribution of different green space patterns varies. It is observed that LST is negatively correlated with percentage of green space for all the periods. Variance partitioning indicates that percentage of green space and mean area of patches are the most powerful index in influencing LST for all the year. The result of study finally emphasizes the importance of the configuration of green space patches to mitigate UHI effect and for adaptation strategies.

I. Dutta (✉) · A. Das
Department of Geography, University of Gour Banga, Malda, West Bengal, India
e-mail: ipsitadutta25@gmail.com

11.1 Introduction

Urban green space (UGS) typically refers to the open spaces with natural vegetation cover located within any city limit (Chen et al. 2017; Sathyakumar et al. 2020). It may include park,

gardens, playing fields, and even any other vegetated space in private or public lands (Sathyakumar et al. 2019, 2020; Wang et al. 2018; Chen et al. 2017). Urban green spaces are an essential part of urban landscape. They provide many services that enhance the quality of urban areas (Wang et al. 2018; Sathyakumar et al. 2020) such as ecosystem services, preservation of biodiversity, encouraging social interaction, promoting good human well-being, and mitigation of urban heat island (UHI) effect. UGS has excellent ability to mitigate the heat island effect (Guo et al. 2019; Sathyakumar et al. 2020; Li and Zhou 2019). It can absorb heat and shortwave radiation and can cool the surrounding environment especially in summer (Guo et al. 2019; Li and Zhou 2019).

Different studies have reported rapid changes of green spaces in peri-urban areas where slightly or nearly unchanged in the urban core (Zhou et al. 2008; Hostetler et al. 2013; Ramos-González 2014). Remote sensing data are widely used to detect the changes across spatiotemporal scale (Stefanov et al. 2001; Kong and Nakagoshi 2006; Dallimer et al. 2011; Sathyakumar et al. 2020; Guo et al. 2019; Li and Zhou 2019). These studies normally discussed about the changes of green space during different periods and spatial patterns and configuration of green spaces changes using some landscape matrices (Zhou et al. 2011; Kong et al. 2014). These studies provide informations regarding the direction and factors of green space changes and the arrangement of green space (Wang et al. 2018). Certain informations are helpful for the understanding of the impacts of green spaces in ecology.

This change of green space coverage causes imbalance of green spaces in a recognized area. This type of changes is identified as global environmental issues throughout the world (Sathyakumar et al. 2020; Rigolon et al. 2018; Heynen 2006). One of the greatest issues at the present day is the emerging of urban heat island (UHI). It is normally considered as the difference of temperature between rural and urban areas (Huang et al. 2019). Nowadays, over half of the global population is living in urban area and

expected to reach nearly 70% by 2050. The populations residing in the cities are facing higher temperature than rural surroundings as a result of urban heat island effect (Li and Zhou 2019; Nastran et al. 2019; Li et al. 2017). Increasing heat island effect has direct adverse impact on atmosphere as well as human health. Urban heat island is a direct outcome of urbanization. It is expected that the impact of UHI will increase in the future with increasing rate of rapid urbanization (Li and Zhou 2019; Cao et al. 2018; Wouters et al. 2017). Therefore, mitigation of this heat island through effective strategies is highly required. Different urban land uses contribute differently to the formation of heat island due to their different thermal characteristics. In this context, green space can play an excellent role in reducing this heat island effect. Vegetation land absorbs solar radiation and converts solar heat to latent heat (Li and Zhou 2019). It also can cool the surrounding environment especially during summer daytime. Several studies have reported significant negative relationship between green space and UHI intensity using various matrices (Zhao et al. 2011; Li et al. 2012, 2013; Kong et al. 2014; Zhang et al. 2017; Connors et al. 2013). Thus, increasing green spaces is widely recommended and implemented to reduce the UHI effect.

But there are some confusions related to practical context, such as, which between spatial configuration and spatial composition of green space is more important, and in which extent landscape metric explains individual contribution of green space indices in LST (Guo et al. 2019). Many researchers have studied the spatial configuration of green space and relationship between green space and LST using some statistical measurements (Zhang et al. 2009, 2017; Cao et al. 2018; Li et al. 2011; Peng et al. 2016; Chen et al. 2014), where very few researches have studied the relationship between both spatial configuration and composition of green space and LST (Nastran et al. 2019; Li et al. 2013; Zhou et al. 2011). This study assumes that there is a complex mechanism between green space patterns and LST. This mechanism can be derived by analyzing the individual relative

contribution of each green space metrics on LST. Therefore, this study attempted to study the variations of green space at neighborhood level during six temporal periods. This study also tries to study the green space contribution on mitigation of urban heat through stepwise regression and hierarchical partitioning followed by Guo et al. (2019). Hence, the main objectives of the study are (1) to analysis the spatiotemporal variations of urban green space at neighborhood level, (2) to identify the relationship between green space and LST, (3) to identify main factors of green space patterns controlling LST, and (4) to clarify individual contributions of green space landscape matrices to LST.

11.2 Data and Methodology

11.2.1 Study Area

English Bazar urban agglomeration and its peri-urban areas are selected as the study area (Fig. 11.1). English Bazar is the head quarter of Malda District, West Bengal. This region experiences tropical humid climate. Topographically, this region falls under Diara region formed by newer alluvium. This urban agglomeration had a total population more than 5 lakhs which shares 57.91% of total urban population of the district with an area of only 28 km^2. This region is an important center for economy, employment, and resources. English Bazar municipality is the main center of this urban agglomeration. The other components of this urban agglomeration are Old Malda Municipality, Bagbari (census town), Sahapur (Census town), and Chhatianmore (census town). A small urban area with a large population size often suffered from various ecological and environmental problems. This area is experiencing rapid urbanization during last decade and affects the distribution of green space due to the higher need of land for residential use. It is expected to result in increasing in UHI thoroughly. Therefore, there is an urgent need to study the heterogeneity of the green landscape characteristics and make a comparative study with LST dynamics.

11.2.2 Data Sources

Landsat TM and Landsat OLI image with 30 m spatial resolution for the year 1990, 1995, 2000, 2005, 2010, and 2015 were obtained for the purpose of the study. Necessary geometric corrections and registration were done using ArcGIS 10.3 software. These images contain spectral reflectance in red (0.63–0.69 μm) and near infrared (0.75–0.90 μm) which are very useful for mapping of vegetation (Sathyakumar et al. 2020). The date of acquisition of the images was pre-monsoon season.

11.2.3 Extraction of Green Space

There is no exact definition for urban green space. This study adopted an approach by Taylor and Hochuli (2017) and Lo and Jim (2012), where they considered urban green space as any vegetation areas within the city boundary. So, urban green space is extracted using Normalized Difference Vegetation Index (NDVI) using the following formula:

$$NDVI = \frac{IR - R}{IR + R} \qquad (11.1)$$

where

IR—reflectance value of near infrared band
R—reflectance value of red band.

The value of NDVI ranges from −1 to +1. Negative values of NDVI represent impervious or water pixels, and higher value above zero of NDVI represents good vegetation pixels (Chen et al. 2017). The pixels with value higher than 0.2 are generally considered as vegetation pixels (Franco and Macdonald 2018; Sathyakumar et al. 2020).
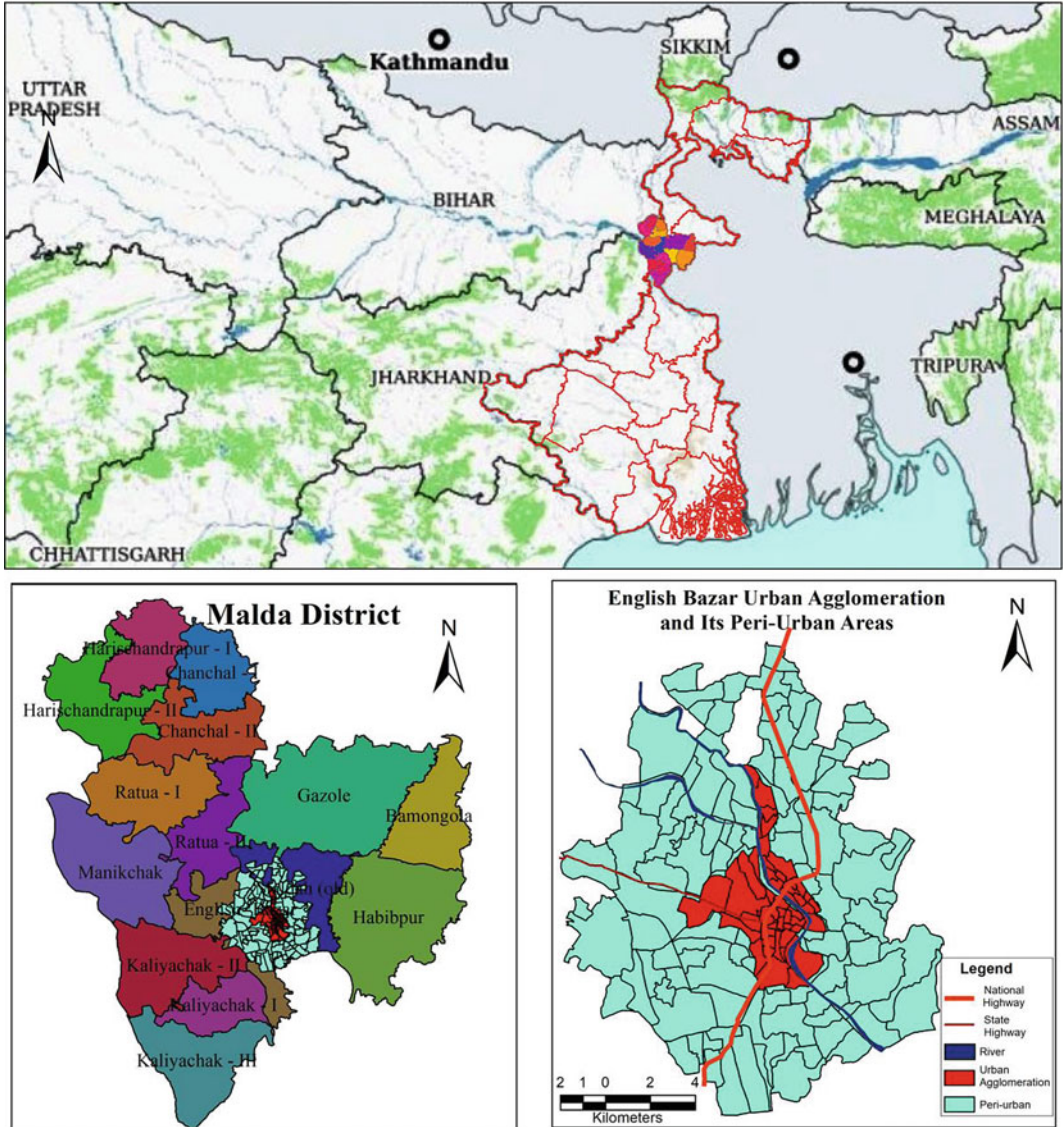
Fig. 11.1 Study area

In this study, random points were taken from the classified land use images (Table 11.1). NDVI for each point of different land uses was retrieved. Statistically, NDVI value is around 0.1–0.2 for impervious surfaces and values around 0 for water body for this study area. NDVI values for agricultural land and vegetation cover are found more than 0.2–0.23 in the area. Therefore, this analysis supports the relevance of

taking NDVI >0.23 as the threshold for designating green spaces.

11.2.4 Estimation of Green Space Changes

The change of urban green space was estimated using the following formula:

Table 11.1 Number of points on each land uses type for NDVI

	Built-up land	Water body	Agricultural land	Barren land	Vegetation
1990	19,623	6108	16,891	123,921	67,950
1995	26,155	13,759	17,262	78,606	98,716
2000	32,804	8091	24,691	88,359	80,548
2005	33,866	7760	17,965	109,553	65,354
2010	34,352	4281	28,123	97,060	70,677
2015	36,303	7043	8093	104,668	78,380

$$C = G_1 - G_0 \qquad (11.2)$$

G_0 denotes the green space area in starting year, G_1 denotes the total green space area in ending year, and C is the gross change of urban green space in the study period.

11.2.5 Computation of Green Space Indicators

Quantitative and qualitative assessment of urban green space is important for a better understanding of urban green space distribution. For this purpose, this study has used six indicators (Table 11.2)—aggregation index (AI), mean area of patches (AREA_MN), mean Euclidean distance between neighbors (ENN_MN), area weighted mean fractal dimension index (FRAC_AM), patch density (PD), and percentage of UGS area (PUGS). Among these, PUGS quantifies the green space in an area. PD, Area_MN, and ENN_MN compute the fragmentation of patches in an area. Rest two (AI and FRAC_AM) indicates the aggregation and shape complexity of patches.

These indices were computed for the mentioned six time periods using Fragstats 4.2.5 (McGarigal and Marks 1995). These metrics were computed for each administrative section for each temporal periods.

11.2.6 Retrieval of Land Surface Temperature

Landsat TM for the periods of 1990, 1995, 2000, 2005, and 2010 and Landsat OLI for the year

2015 were acquired for the utilization in study. Five Landsat scenes were used to calculate the land surface temperature of the study area (Table 11.2). Land surface temperature of each period was taken as the average of the five LST images considered in the respected five scenes (Dutta and Das 2020). The detailed process of retrieval of land surface temperature is given below.

To convert the DN values, the following formula has been used:

$$L_\lambda = \left(\frac{(L_{\text{MAX}\lambda} - L_{\text{MIN}\lambda})}{Q\text{CALMAX} - Q\text{CALMIN}} \right) \times (Q\text{CAL} - Q\text{CALMIN}) + L_{\text{MIN}\lambda} \quad (11.3)$$

where L_λ—value as radiance, QCAL—original thermal band, $L_{\text{MIN}\lambda}$—spectral radiance scales to QCALMIN, $L_{\text{MAX}\lambda}$—spectral radiance scales to QCALMAX, QCALMIN is 1 and QCAL-MAX is 255. Thermal bands were converted to satellite temperature using the following equation:

$$T = \frac{K_2}{\ln\left(\frac{K_1}{L_\lambda} + 1\right)} \qquad (11.4)$$

where T—at-satellite temperature in Kelvin (K), L_λ—radiance K_1, and K_2—thermal constant. It is then converted °C using following equation:

$$T_C = T - 273.15 \qquad (11.5)$$

Calculating emissivity is necessary for surface characterization. It was calculated using following equation:

Table 11.2 Description of indicators used in the study

Indicator	Formula	Significance
Percentage of UGS area (PUGS)	$\text{PUGS} = \frac{A_{\text{UGS}}}{A_{\text{CS}}} \times 100$ A_{UGS} = area of UGS A_{CS} = area of census section Range $0 \leq P_{\text{UGS}} \leq 100$	PUGS is 0 when there is no green space and is 100 when the whole area is covered by vegetation. High value of PUGS indicates large quantity of vegetation cover in an area
Patch density (PD)	$\text{PD} = \frac{n}{A_{\text{CS}}} \times 10^6$ n = number of green patches A_{CS} = area of census section	High value of PD refers high density of vegetation cover
Mean area of patches (Area_MN)	$\text{Area\_MN} = \frac{A_{\text{UGS}}}{n} \times 10^{-4}$ A_{UGS} = area of UGS n = number of green patches	Higher variability refers lower uniformity in pattern
Mean Euclidean nearest neighbor distance patches (ENN_MN)	$\text{ENN\_MN} = \frac{\sum_{i=1}^{n} d_i}{n}$ d_i = distance of nearest patch between an patch and i n = number of UGS patches	It refers to the minimum distance between two patches. ENN increases with increasing distance between patches
Area weighted mean fractal dimension index of patches (FRAC_AM)	$\text{FRAC\_AM} = \sum_{i=1}^{i=n} \left[\left(\frac{a_i}{A_{\text{UGS}}} \right) \left(\frac{2 \ln 0.25 p_i}{\ln a_i} \right) \right]$ a_i = area of an UGS patch i p_i = perimeter of an UGS patch i n = number of UGS patch A_{UGS} = area of UGS in a section	Value of FRAC_AM ranges from 1 to 2. Values near to 1 refers to the squared shaped of patches and value near 2 refers to complex shape of patches
Aggregation index (AI)	$AI = \left[\frac{g_{ii}}{\max g_{ii}} \right] (100)$ g_{ii} = number of like adjacencies (joins) between pixels of patch i based on the single-count method max-g_{ii} = maximum number of like adjacencies (joins) between pixels of patch type i based on the single-count method	It shows the degree of patch compactness of an urban area

$$e = 0.004 P_v + 0.986 \qquad (11.6)$$

where proportion of vegetation (P_V) can be calculated as-

$$P_V = (\text{NDVI} - \text{NDVI min} / \text{NDVI max} - \text{NDVI min})^2 \qquad (11.7)$$

Finally, LST was computed with following formula:

$$\text{Ts} = \text{BT}/1 + W \times (\text{BT}/P) \times \ln(e) \qquad (11.8)$$

BT—at-satellite brightness temperature, W—wavelength of emitted radiance in meters, P—$h * c/s$ $(1.438 \times 10^{-2}$ m K$)$ [h = Planck's constant $(6.626 \times 10^{-34}$ Js$)$, s = Boltzmann constant $(1.38 \times 10^{-23}$ J/K$)$, and c = velocity of light $(2.998 \times 10^8$ m/s$)$].

11.2.7 Statistical Analysis

To understand the relation between urban green space and LST, different statistical techniques were used.

First, Pearson's correlation was used to examine whether any relationship variability exists among the chosen periods. Correlation is simply examined between mean LST and different landscape metrics of green space for different temporal periods.

Second, stepwise linear regression model was used to overcome the multicollinearity among the landscape metrics. It helps to identify the factors that are dominant for the variation of LST during different temporal periods.

Third, hierarchical partitioning was used to identify the independent contribution of each matric by the proportion of variance explained. This process includes all the computed landscape metrics for each period. This process was conducted with the help of R software, statistical package of 'hier.part' (Guo et al. 2019; Wu et al. 2020; R Core Development Team 2008).

11.3 Results and Discussion

11.3.1 Spatiotemporal Distribution of Green Space and LST

11.3.1.1 Spatiotemporal Changes of Green Space

Figure 11.2 presents the spatial distribution of green space during different periods of time. The images from this figure revealed that within the study period, large amount of green space had disappeared. The changes of green spaces are listed in Table 11.3.

The result shown in Table 11.3 indicates that there is a loss of nearly 11 km^2 (5.17%) of its green space between 1990 and 2015. The table also shows that there was a gradual decline of green space from 1990 to 2000. Then, it increased nearly 2% in 2005. From Fig. 11.2, it is normally seen that the tendency of declining of green space is generally toward north-east and south-west direction of the study area. The main urban core had also experienced the declination of green space.

Figure 11.3 shows the gross change of green space at local level. The red circles show the decrease of green space, whereas green space refers to an increase trend of green space. The larger size of the circles represents larger difference. The maximum concentration of red circles in south-west and north-east corner of the study area for almost every year denotes a rapid loss of green space from 1990 to 2015. This figure

shows that 72 census sections have witnessed a decline of green space cover during the period 1990–2019 and 35 sections witnessed a positive growth. It is clear from Fig. 11.3 that fast urbanization rate toward these direction causes the loss of vegetation cover which transforms to impervious area. The periodical change of green space is described in Table 11.4.

11.3.1.2 Spatiotemporal Distribution of LST Changes

Figure 11.4 shows the spatial distribution of LST. The lowest temperature was recorded over the water bodies for all the periods, and highest temperature was recorded over built-up and bare lands. It is clearly reflected from the figure that the temperature has dramatically changed over the time period. The maximum temperature for the year 1990 was 30.85 °C and for 2015 it was 34.01 °C.

11.3.2 Neighborhood Level Pattern of Green Space Indices

Table 11.5 shows the descriptive statistics of different indices of green spaces for the study periods.

Figure 1S in supplementary file shows the map distribution of PUGS during different periods. The mean value of PUGS decreases from 38.26% in 1990 to 31.32% in 2015 (Table 11.5). Figure 1S shows that areas with high PUGS are located toward the suburbs and with low values are locate in the city center and north-eastern part of the region for almost all the time periods.

The AI distribution map (Fig. 2S) reveals that low clusters of AI are normally located in the center as this area has scattered green cover distributed in small patches. High AI clusters basically indicates aggregation of large green covers in the area. Area over south-eastern part shows cluster of very high AI values as these areas have dense green cover and low clusters toward north-eastern and south-western parts because of extensive clearing of green space for other purposes. Table 11.5 shows that the mean AI value decrease from 90.95 in 1990 to 87.78 in
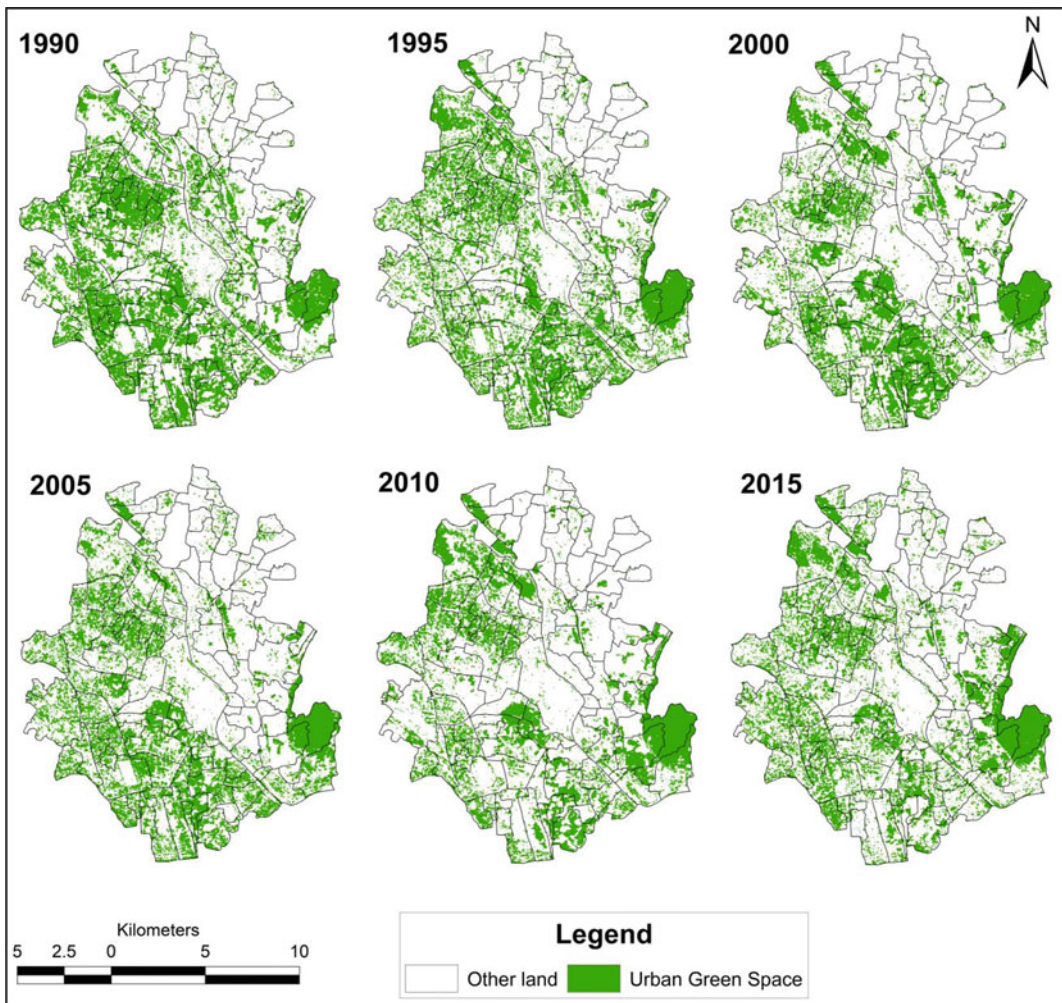
Fig. 11.2 Spatiotemporal distribution of green space

Table 11.3 Temporal changes of green space during 1990–2015

Year	Area under green space (km²)	Percentage	Change direction
1990	79.43	37.64	–
1995	75.00	35.54	↓
2000	64.67	30.64	↓
2005	67.86	32.15	↑
2010	61.36	29.08	↓
2015	68.53	32.47	↑

2015. This decrease of AI clearly depicts the fact that green space is prominently becoming disaggregated from 1990 to 2015.

Figure 3S shows the mean area of green space patches (Area_MN). This figure reveals that the study area has observed a major decrease in
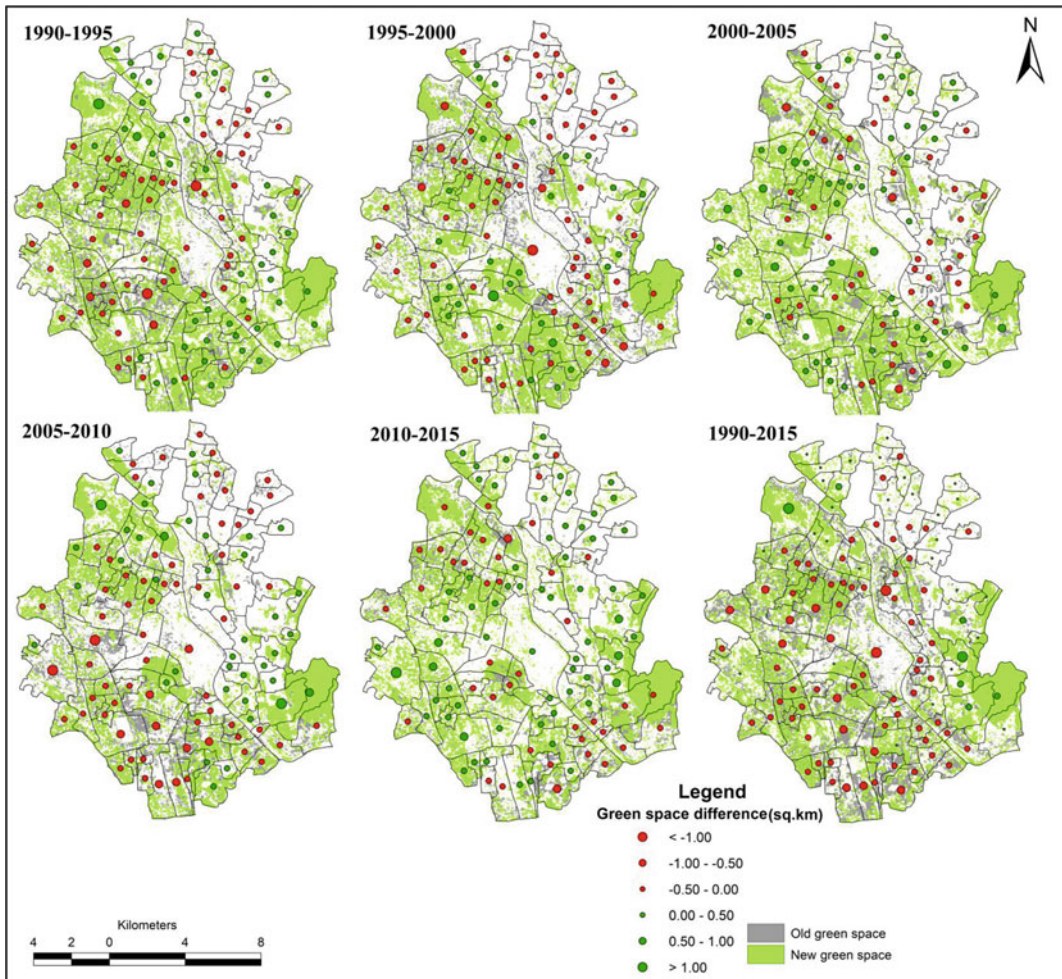
Fig. 11.3 Gross green space changes from 1990 to 2015

Table 11.4 Estimation of green space change

Period	Change in green space (km^2)	Proportion of green space change (km^2)
1990–1995	−4.43	−1.31
1995–2000	−10.33	−1.00
2000–2005	3.19	0.04
2005–2010	−6.49	−0.24
2010–2015	7.17	0.11
1990–2015	−10.90	−2.40

Area_MN from 1990 to 2015. This trend can be visualized from Table 11.5 where it is observed that mean value has decreased from 0.44 in 1990 to 0.37 in 2015. Figure 3S also shows that the areas adjoining to the main urban core have formed a cluster with low Area_MN values, whereas numbers of cluster with high values have widely decreased during the period. High

Fig. 11.4 Distribution of LST in 1990, 1995, 2000, 2005, 2010, and 2015

value cluster is found most prominently toward the south-eastern part of the study area.

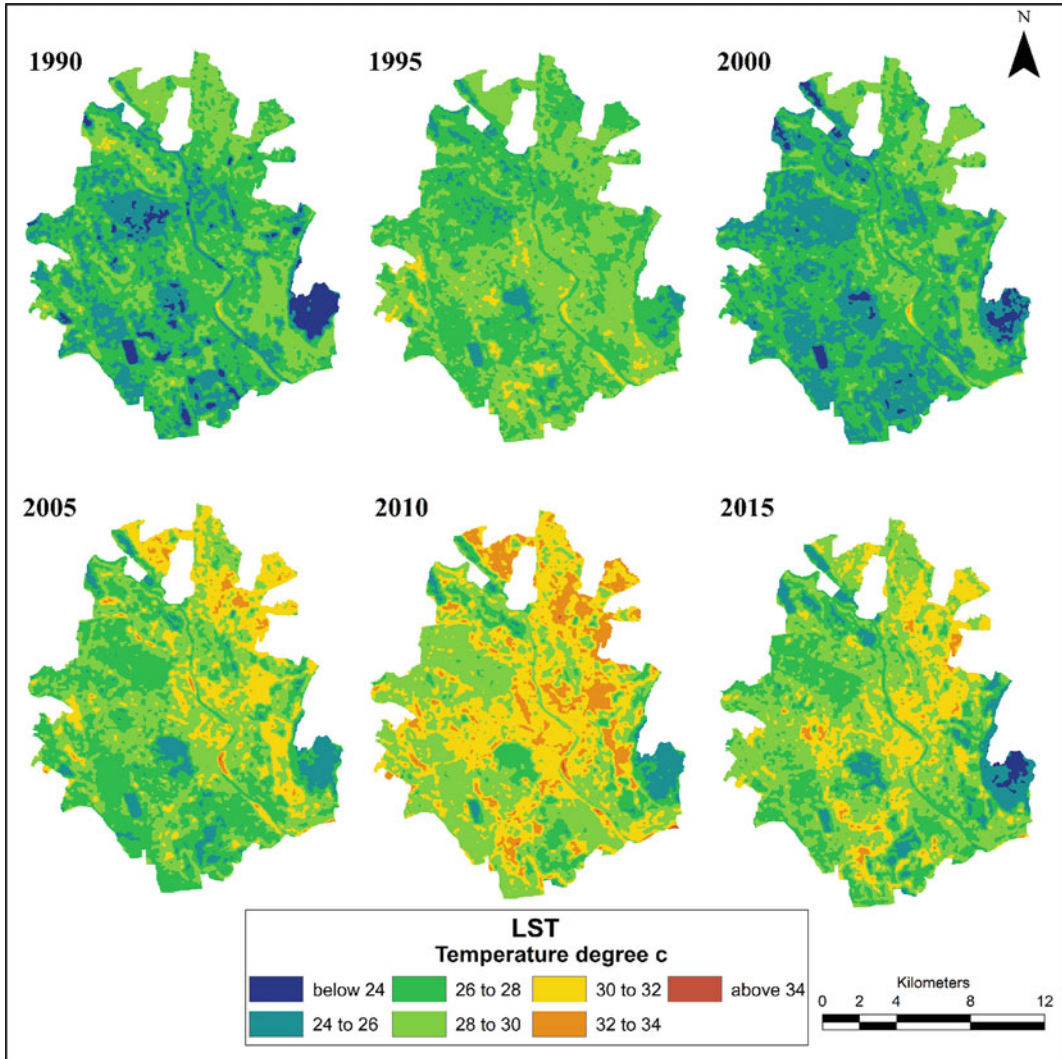The spatial distribution of ENN_MN in Fig. 4S reveals that almost all the areas have observed low ENN_MN during the study periods. Surprisingly, the ENN_MN value has increased by 0.82, but the value of S.D also increases to 2.27. The overall ENN_MN decreasing trend is mainly observed due to the loss of green patches or the fragmented green cover type.

Figure 5S shows the map of distribution of area weighted mean fractal dimension index

(FRAC_AM) of green spaces during different periods. This figure reveals that during almost each year the value of FRAC_AM is lower in north-eastern part than rest of the areas. This means the patches of green space over north-eastern part are less complex than the other parts. Further, by comparing the figure for 1990 and 2015, it is found that north-eastern and south-eastern part have lost high FRAC_AM cluster. It is simply because of the loss of green space and conversion of large patches into small fragmented patches. Though this change may not be

Table 11.5 Descriptive statistics of different indices of green space

Indicator	Year	Mean	Minimum	Maximum	S.D.
PUGS	1990	38.26	1.01	88.10	24.09
	1995	35.80	1.01	81.40	19.93
	2000	32.57	1.12	87.06	21.42
	2005	31.29	0.72	78.75	20.90
	2010	28.09	0.05	92.88	20.59
	2015	31.32	2.86	86.85	19.06
PD	1990	130.35	123.46	144.30	3.58
	1995	133.37	124.66	141.81	3.53
	2000	130.95	124.16	141.33	3.96
	2005	132.35	123.46	140.29	4.61
	2010	130.45	123.46	139.74	3.89
	2015	132.47	124.94	141.45	3.61
AREA_MN	1990	0.44	0.17	0.74	0.14
	1995	0.40	0.10	0.74	0.12
	2000	0.42	0.14	0.77	0.14
	2005	0.37	0.09	0.74	0.13
	2010	0.38	0.09	0.77	0.14
	2015	0.37	0.13	0.75	0.12
ENN_MN	1990	63.46	60.00	69.22	1.63
	1995	63.77	60.00	68.28	1.29
	2000	63.95	60.00	72.54	2.20
	2005	64.09	60.00	84.85	2.82
	2010	64.11	60.00	84.85	2.76
	2015	64.28	60.00	75.97	2.27
FRAC_AM	1990	1.02	1.01	1.03	0.00
	1995	1.02	1.00	1.04	0.01
	2000	1.02	1.00	1.03	0.01
	2005	1.02	1.00	1.04	0.01
	2010	1.02	1.00	1.03	0.01
	2015	1.02	1.00	1.03	0.01
AI	1990	90.95	81.66	100.00	3.62
	1995	87.43	67.65	98.55	4.41
	2000	90.23	81.15	98.92	4.48
	2005	88.05	75.00	100.00	4.95
	2010	89.47	0.00	100.00	9.75
	2015	87.78	73.32	98.53	4.16

visible from the mean value in Table 11.5, but Fig. 5S clearly visualize this changes.

Patch density (PD) distribution is shown in Fig. 6S. It clearly depicts the changing pattern of PD over the time periods. Increasing value of mean PD from 1990 to 2015 clearly depicts the increasing spatial heterogeneity of green spaces. Figure 6S shows the gradual shifting of low PD

clusters to high PD cluster from 1990 to 2015. It indicates huge transformation of continuous green patches to small fragmented patches.

Figure 7S shows the changing pattern of the indices during 1990–2015. The change of AI (Fig. 7S A) was in the range of −15.03 to +8.88. This map reveals that 83 census sections have experienced a decrease in AI and 24 sections have experienced an increase in AI. This decrease of AI clearly depicts that the study area has observed a disaggregated pattern of green cover during 1990–2015. The change of Area_MN is shown in Fig. 7S B. Area_MN change ranges from −0.32 to +0.37. This figure reveals that 81 census sections have witnessed a loss of Area_MN during this period. This shrinking pattern of Area_MN highlights the disaggregation of green space in the study area. Change of ENN_MN is shown in Fig. 7S C. The map of changing ENN_MN shows that 35 census sections have experienced a decrease in ENN_MN whereas 72 sections experienced increase during the period. This change of ENN_MN primarily depends on the pre-existing patches near the core or the fringe (Sathyakumar et al. 2020).

This map also shows that mainly the western parts have experienced increase in ENN_MN. Change of FRAC_AM (Fig. 7S D) ranges from −0.01 to +0.01. This map reveals that 17 census sections have a decrease in FRAC_AM value and 90s have increase value. This result reveals that green space in most of the places have become complex over the time. The map of change of PD (Fig. 7S E) ranges from −18.62 to +15.30. This map shows that 28 sections have witnessed decrease in PD value and 79 sections have experienced increase in PD value. PD is directly associated with increase or decrease of green space cover. It is observed from Fig. 7S F that among the 79 sections which have experienced an increase in PD value, 54 sections witnessed decrease in PUGS while the rest have gained green spaces. This picture clearly depicts that increase in PD value is clearly due to the fragmentation due to loss of green space.

11.3.3 Impacts of Green Spaces on LST

11.3.3.1 Relationship Between Green Space and LST

Green space cover and LST have a direct relationship between them. This section tries to examine if there is any variation existed during different periods due to the changing proportion of green space. The result shows that all the landscape metrics of green space correlated significantly with LST during all the period (Fig. 11.5).

PUGS had a consistently strong negative correlation for all the time period. Because of the increase of fragmentation and complexity of green space shapes, correlation between PD and FRAC_AM is found positive for the year 2010 and 2015. This correlation plot clearly suggests that large size of green space plays an important role in LST for all the periods. The correlation between LST and PUGS is found −0.88 in 1990 which declined to −0.78 in 2015.

11.3.3.2 Significant Green Space Landscape Metrics Affecting LST Variations

Figure 11.5 shows the relationship between different landscape metrics and green space. But it is still necessary to identify the most dominant landscape metric affecting LST variations. Stepwise regression model was used for this purpose. Table 11.6 presents the regression model result as obtained. The highest R^2 (0.86) with lowest std. error (0.37) is observed for the year 2000. In contrast, 1995 was found the lowest estimate of landscape metrics for green space ($R^2 = 0.23$). PUGS is the only surviving metric in 1995. Thus, it can be said that the year 1995, as well as 2005 were more complicated regarding landscape metrics of green space as fewer number of metrics were found significant using this model. It is also found that PUGS is a dominant metric for all the mentioned periods. The decrease in number of landscape metric indicates more complex mechanism for affecting LST, and more factors are needed to take into consideration.
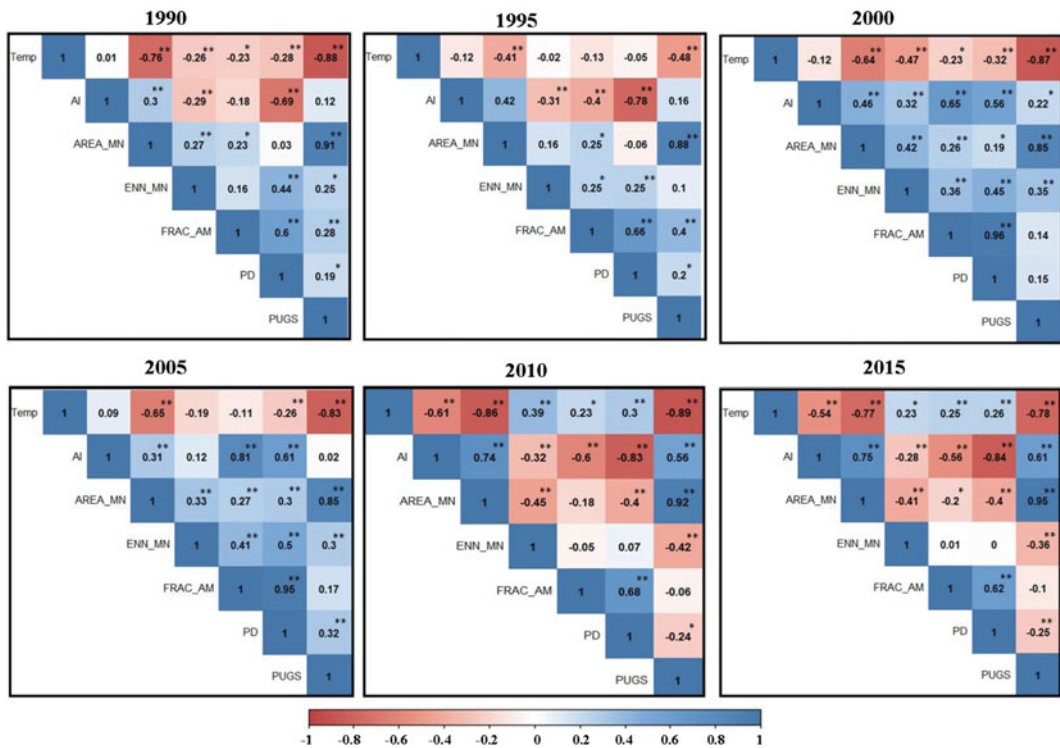
Fig. 11.5 Correlation plot for the relationship between LST and different landscape metrics

**Table 11.6** Stepwise regression model and statistics for green space landscape metrics

Year	Not entering metrics	Entered metrics	R^2	Std. error	Sig.
1990	AI, AREA_MN, ENN_MN	PUGS, PD, FRAC_AM	0.80	0.49	0.00
1995	AI, AREA_MN, ENN_MN, FRAC_AM, PD	PUGS	0.23	0.57	0.00
2000	AREA_MN, ENN_MN	PUGS, PD, FRAC_AM, AI	0.86	0.37	0.00
2005	AREA_MN, ENN_MN, FRAC_AM, PD	PUGS, AI	0.70	0.68	0.00
2010	AI, AREA_MN, ENN_MN, PD	PUGS, FRAC_AM	0.83	0.45	0.00
2015	AI, AREA_MN, ENN_MN, PD	PUGS, FRAC_AM	0.64	0.66	0.00

Dominance analysis was carried out to determine the relative contribution by the proportion of variance explained by each landscape metrics through hierarchical partitioning (Fig. 11.6). All the parameters which did not survive into stepwise regression were also taken into consideration for a better understanding. The result shows that PUGS is the most powerful index in

influencing LST for all the year. AREA_MN was also important parameters in influencing LST. AI is found dominant for the year 2010 and 2015 (Fig. 11.6).

Although the regression model (Table 11.6) for different years does not consider AREA_MN as an important parameter, but result of hierarchical partitioning considers this metric as an

Fig. 11.6 Proportion of
variance explained
independently by each
landscape metrics on LST
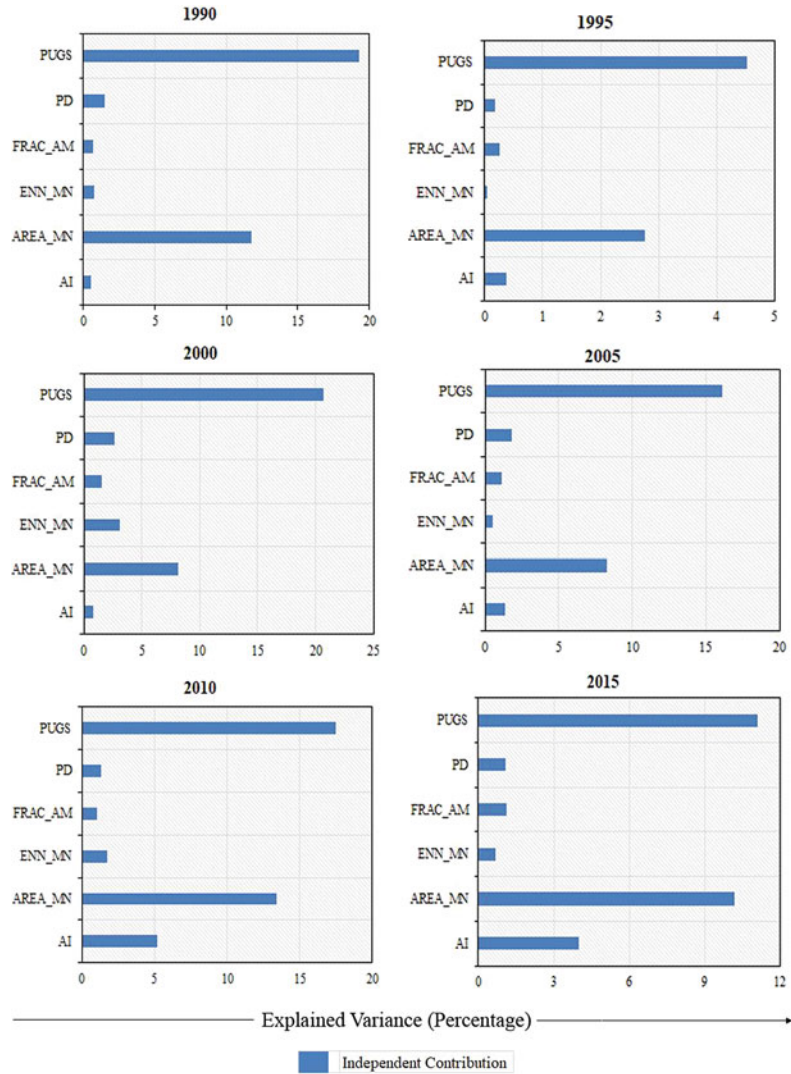
dominant contributor in influencing LST. Con-
sidering this matter, it can be said that PUGS was
the dominant factor affecting the variation of
LST. At the same time, LST is also influenced by
the shape of green space. Complex shape of
green space has a lower impact on LST because
of poor condition of green space cover. It clearly
highlights the fact that spatial configuration of
green space is a main factor for determining LST.

The spatial variation of green space shows
that there is remarkable variation of green space
during 1990–2015 (Fig. 11.2). There is a net
decline of nearly 11 km² green space cover from

1990 to 2015 (Table 11.4). During 1990–2015,
72 census sections have witnessed a decline of
green space cover and 35 sections witnessed a
positive growth. Different landscape metrics
were also applied to show the neighborhood level
distribution of green space and the relationship
between landscape metrics of green space and
LST. The result from neighborhood level analy-
sis (Sect. 3.2) indicates that the study area has
observed diminishing, fragmented, and disag-
gregated pattern of green space during 1990–
2015. The general cause for this degradation of
green space could be due to multiple causes, like,

unplanned rapid urbanization, poor planning of green space, and weak land use management policy implications. As this area is observing a high transformation of green land to built-up land, the main cause can be considered as the peri-urbanization process. The spatiotemporal analysis of neighborhood level change of green space indicators shows that the south-eastern part is gradually forming cluster of green space, whereas the un-greening process is observed in north-east and south-west direction. Furthermore, the green spaces within this neighborhood had witnessed a sharp declination of area with increasing distance among each other (Fig. 7S B and C). This suggests that these neighborhoods require more attention in order to improve their quality.

The pattern of distribution of LST (Fig. 11.4) also varied markedly during all the period. The patches of high LST values are normally observed in the areas typically characterized by dense built-up or bare land. The increasing patches of high LST can cause the formation of UHI.

Green spaces are considered as an effective mitigation strategy for UHI as vegetation cover can absorb the surface heat and radiance and can help in cooling the environment. This study upheld the direct relationship between LST and green space (Fig. 11.5). The result confirms that green space cover has a direct negative relationship with LST referring that increase in green space coverage will significantly decrease the temperature. However, different green space configuration has different impact on LST. Therefore, it is necessary to find out which configuration is more dominant in order to eliminate the effects of LST. The result of stepwise linear regression (Table 11.6) shows that percentage of green space (PUGS) is consistently dominant for all temporal periods. The second dominant metric was found FRAC_AM. But when it comes to the individual contribution to proportion of variance (Fig. 11.6), it is found that PUGS is also found as dominant indicator with highest individual contribution in determining the variation of LST. But it is surprisingly found that FRAC_AM is not considered as dominant,

whereas AREA_MN is found the second dominant indicator. AI is also found dominant for the year 2010 and 2015. Thus, it can be finally concluded that LST is also influenced by the shape of green space. Complex shape of green space has a lower impact on LST because of poor condition of green space cover. It clearly highlights the fact that spatial configuration of green space is a main factor for determining LST.

11.4   Conclusion

The complex relationship between LST and green space has been a burning topic in the field of earth science. This study conducts a multitemporal analysis of changing pattern of green space as well as LST and their relationship in and surrounding English Bazar urban agglomeration. Remotely, sensed images were used for the purpose of the study. This study provides an insightful approach to understand the complex relationship between green space and LST. This study also analyzed the neighborhood level distribution of green spaces which can help the urban planners to identify the sections which need more attention for qualitative improvement of green spaces. Normally, planners increased the coverage of green space by planting more vegetated areas for cooling the environment. But several factors like lateral expansion of urban areas toward the suburbs can cause the clustering of green spaces into fragmented patches. Therefore, this study also suggests the planners to look into this matter from a different perspective. The spatial configuration of green space can significantly influence the LST which is more suitable in mitigation UHI effect.

References

Cao Q, Yu D, Georgescu M, Wu J, Wang W (2018) Impacts of future urban expansion on summer climate and heat-related human health in eastern China. Environ Int 112:134–146

Chen A, Yao L, Sun R, Chen L (2014) How many metrics are required to identify the effects of the landscape pattern on land surface temperature? Ecol Ind 45:424–433

Chen B, Nie Z, Chen Z, Xu B (2017) Quantitative estimation of 21st-century urban greenspace changes in Chinese populous cities. Sci Total Environ 609:956–965

Connors JP, Galletti CS, ChowWT (2013) Landscape configuration and urban heat island effects: assessing the relationship between landscape characteristics and land surface temperature in Phoenix, Arizona. Landsc Ecol 28(2):271–283

Dallimer M, Tang Z, Bibby PR, Brindley P, Gaston KJ, Davies ZG (2011) Temporal changes in greenspace in a highly urbanized region. Biol Let 7(5):763–766

Dutta I, Das A (2020) Exploring the spatio-temporal pattern of regional heat island (RHI) in an urban agglomeration of secondary cities in Eastern India. Urban Clim 34:100679

Franco SF, Macdonald JL (2018) Measurement and valuation of urban greenness: remote sensing and hedonic applications to Lisbon, Portugal. Reg Sci Urban Econ 72:156–180

Guo G, Wu Z, Chen Y (2019) Complex mechanisms linking land surface temperature to greenspace spatial patterns: evidence from four southeastern Chinese cities. Sci Total Environ 674:77–87

Heynen N (2006) Green urban political ecologies: toward a better understanding of inner-city environmental change. Environ Plan A 38(3):499–516

Hostetler AE, Rogan J, Martin D, DeLauer V, O'Neil-Dunne J (2013) Characterizing tree canopy loss using multi-source GIS data in Central Massachusetts, USA. Remote Sens Lett 4(12):1137–1146

Huang Q, Huang J, Yang X, Fang C, Liang Y (2019) Quantifying the seasonal contribution of coupling urban land use types on Urban Heat Island using land contribution Index: a case study in Wuhan, China. Sustain Cities Soc 44:666–675

Kong F, Nakagoshi N (2006) Spatial-temporal gradient analysis of urban green spaces in Jinan, China. Landsc Urban Plan 78(3):147–164

Kong F, Yin H, Wang C, Cavan G, James P (2014) A satellite image-based analysis of factors contributing to the green-space cool island intensity on a city scale. Urban For Urban Green 13(4):846–853

Li X, Zhou W (2019) Optimizing urban greenspace spatial pattern to mitigate urban heat island effects: extending understanding from local to the city scale. Urban Forestry & Urban Greening 41:255–263

Li X, Zhou W, Ouyang Z (2013) Relationship between land surface temperature and spatial pattern of greenspace: what are the effects of spatial resolution? Landsc Urban Plan 114:1–8

Li X, Zhou Y, Asrar GR, Imhoff M, Li X (2017) The surface urban heat island response to urban expansion: a panel analysis for the conterminous United States. Sci Total Environ 605:426–435

Li J, Song C, Cao L, Zhu F, Meng X, Wu J (2011) Impacts of landscape structure on surface urban heat islands: a case study of Shanghai, China. Remote Sens Environ 115(12):3249–3263

Li X, Zhou W, Ouyang Z, Xu W, Zheng H (2012) Spatial pattern of greenspace affects land surface temperature: evidence from the heavily urbanized Beijing metropolitan area, China. Landsc Ecol 27(6):887–898

Lo AY, Jim CY (2012) Citizen attitude and expectation towards greenspace provision in compact urban milieu. Land Use Policy 29(3):577–586

McGarigal K, Marks BJ (1995) Spatial pattern analysis program for quantifying landscape structure. Gen. Tech. Rep. PNW-GTR-351. US Department of Agriculture, Forest Service, Pacific Northwest Research Station, 1-–22

Nastran M, Kobal M, Eler K (2019) Urban heat islands in relation to green land use in European cities. Urban for Urban Green 37:33–41

Peng J, Xie P, Liu Y, Ma J (2016) Urban thermal environment dynamics and associated landscape pattern factors: a case study in the Beijing metropolitan region. Remote Sens Environ 173:145–155

Ramos-González OM (2014) The green areas of San Juan, Puerto Rico. Ecol Soc 19(3)

Rigolon A, Browning M, Jennings V (2018) Inequities in the quality of urban park systems: an environmental justice investigation of cities in the United States. Landsc Urban Plan 178:156–169

Sathyakumar V, Ramsankaran RAAJ, Bardhan R (2020) Geospatial approach for assessing spatiotemporal dynamics of urban green space distribution among neighbourhoods: a demonstration in Mumbai. Urban for Urban Green 48:126585

Sathyakumar V, Ramsankaran RAAJ, Bardhan R (2019) Linking remotely sensed Urban Green Space (UGS) distribution patterns and Socio-Economic Status (SES)—A multi-scale probabilistic analysis based in Mumbai, India. GIScience Remote Sens 56(5):645–669

Stefanov WL, Ramsey MS, Christensen PR (2001) Monitoring urban land cover change: an expert system approach to land cover classification of semiarid to arid urban centers. Remote Sens Environ 77(2):173–185

Taylor L, Hochuli DF (2017) Defining greenspace: multiple uses across multiple disciplines. Landsc Urban Plan 158:25–38

Team RDC (2008) Team, R Development Core (2008) R: a language and environment for statistical computing. R Foundation for Statistical Computing, Vienna. Available at http://www.r-project.org

Wang J, Zhou W, Qian Y, Li W, Han L (2018) Quantifying and characterizing the dynamics of urban greenspace at the patch level: a new approach using object-based image analysis. Remote Sens Environ 204:94–108

Wouters H, De Ridder K, Poelmans L, Willems P, Brouwers J, Hosseinzadehtalaei P, Demuzere M (2017) Heat stress increase under climate change twice as large in cities as in rural areas: a study for a densely populated midlatitude maritime region. Geophys Res Lett 44(17):8997–9007

Wu Z, Yao L, Ren Y (2020) Characterizing the spatial heterogeneity and controlling factors of land surface

temperature clusters: a case study in Beijing. Build Environ 169:106598

Zhang X, Zhong T, Feng X, Wang K (2009) Estimation of the relationship between vegetation patches and urban land surface temperature with remote sensing. Int J Remote Sens 30(8):2105–2118

Zhang Y, Murray AT, Turner Ii BL (2017) Optimizing green space locations to reduce daytime and nighttime urban heat island effects in Phoenix, Arizona. Landsc Urban Plan 165:162–171

Zhao C, Fu G, Liu X, Fu F (2011) Urban planning indicators, morphology and climate indicators: a case study for a north-south transect of Beijing, China. Build Environ 46(5):1174–1183

Zhou W, Troy A, Grove M (2008) Object-based land cover classification and change analysis in the Baltimore metropolitan area using multitemporal high resolution remote sensing data. Sensors 8(3):1613–1636

Zhou W, Huang G, Cadenasso ML (2011) Does spatial configuration matter? Understanding the effects of land cover pattern on land surface temperature in urban landscapes. Landsc Urban Plan 102(1):54–63

Urban Effects on Hydrological Status and Trophic State in Peri-Urban Wetland

12

Madhurima Majumdar, Sk. Ziaul,
Swades Pal, and Sandipta Debanshi

Abstract

In spite of immense benevolent role of wetland to the urban ecosystem, natural wetland loss has become a common phenomenon nowadays. Apart from the frequently investigated reclamation of wetland and water pollution issues, the present study tried to investigate the relatively less frequent and focused issue, i.e., impact of urban activities on hydrological status and ecological responses citing examples from Chatra wetland, a peri-urban wetland of English Bazar Municipality of West Bengal, India. Satellite image-driven pixel scale hydrological data like water depth, hydro-period and consistency in water presence were used for integrated mapping of hydrological status. Trophic state index (TSI) using sample water data was applied for receiving ecological response. Before doing all these, five spectral water indices were applied for suitable water body delineation. The study revealed that Modified Normalized Water Index (MNDWI) was the best-suited method. Since, water depth, hydro-period were found gradually declining over time mainly in the peripheral part, poor hydrological status was found in this part. Due to encroachment of urban area, water storage area was squeezed, and therefore, more consistent water presence was detected even in the phase III. TSI was found increased over the phases. In 2010, 38% area was eutrophicated, and in 2020, it was increased to 44%. Untreated urban water and agricultural residue influx are the major reasons behind this. The study may be useful to mediate the urban wetland conflict and wetland sustainability. During study, due to having floating water hyacinth, patchy aquatic cultivation, the current study found some difficulties on wetland mapping and hydrological status mapping from images. However, the study would serve as a knowledge addition regarding the quantitative and qualitative degradation of wetland habitat in the peri-urban environment of a rapidly growing city. Moreover, it could be instrumental to the local authority in restoring the wetland area and its ecological health.

Keywords

Urban growth · Wetland reclamation · Wetland mapping · Spectral water indices · Wetland hydrological status and trophic state

M. Majumdar · Sk. Ziaul · S. Pal · S. Debanshi (✉)
Department of Geography, University of Gour
Banga, Malda, West Bengal, India
e-mail: debanshi.sandipta93@gmail.com

12.1 Introduction

Since 2021, a good number of literatures like Mishra et al. (2021), Wang et al. (2021), Chand et al. (2021), Islam et al. (2022) focused on the multi-faceted needs of constructed wetland for urban sustainability. A few among highlighted its benevolent role on natural treatment of wastewater (Mishra et al. 2021); management scope for mitigating urban floods (Kumar et al. 2021); cleaning of contaminated runoff and storm water (Wang et al. 2021); elimination of coliforms and wastewater nutrients using tidal water (Chand et al. 2021); removal of steroid hormones from domestic wastewater (Chen et al. 2021); treatment of sewage effluent through phytoremiation potential of constructed wetland macrophytes (Suganya et al. 2022); reduction of heavy metal contamination (Islam et al. 2022). From these studies, it was very evident that wetland provides immense ecological services, and this blue space is considered as a nature-based solution of different urban problems (Pereira and Baró 2022). It can also support fresh fish service to the urban and related livelihood to the marginal people (Ghanian et al. 2022). Like green space, it has also enough capability to build urban resilience (Beckwith 2022). Considering all these, it is very clear that wetland should have a co-habitation with urban area (Alikhani et al. 2021). The attempt toward building constructed wetland in per-urban area is also a signature for making this co-habitation.

There are so many urban areas that are having their natural wetlands; inclusive nourishment may produce more benefits than a constructed wetland can serve. The large wetlands are associated with large cites in India as well as world, for example Kolkata (East Kolkata Wetland, a Ramsar Site), Guwahati (Deepor beel, a Ramsar Site), Bhopal (Bhoj wetland, a Ramsar Site) Colombo, Amiens, Jeju, Haikou (the last four are among the 18 wetland cities). In case of small urban area, this urban wetland association is much stronger. But unfortunately, we are destroying such precious wetland and the related benefits mainly for the sake of sprawling-built land (Danso et al. 2021; Rojas et al. 2022; Sarkar and Maji 2022) and sometimes qualitative damage of wetland caused by excessive influx of urban pollutants particularly heavy metals (Lin et al. 2022; Islam et al. 2022). For instance, 41% of marsh land of Muthurajawela marsh and negombo lagoon wetland was reclaimed due to urban sprawl (Athukorala et al. 2021), more than 70% of natural wetland has been developed to other land use including agricultural, industrial and urban area since 1989 in Pudong district of Shanghai, Chaina (Wu et al. 2018), 16% of wetland and flooded area have shrunken in Bengaluru Urban district due to built-up expansion (Brinkmann et al. 2020), and there are many more concerning incidents. Since 2021, 8300 articles were written on wetland reclamation due to urban growth. So, our treatment to wetland in urban space is highly paradoxical; somewhere people are constructing wetlands and somewhere destroying the wetland. Scientist already established that vegetation and wetland are the natural means of solution. Then, the question why such natural capital is destroying, degrading? Even the costing and land issue for constructing new wetland is also very crucial. So, re-thinking on wetland reclamation, degradation is highly required.

Population pressure, high land value within main urban land, homelessness of rural to urban migrants is the root reason behind wetland reclamation. A good number of works focused on wetland reclamation. Bhat and Qayoom (2021), Kakade et al. (2021), Kończak and Huber (2022) explored the effect of urban sewage on eutrophication problems, Dar et al. (2021), Fu et al. (2021) investigated urbanization effects on aquatic ecosystem, Benassi et al. (2021) evaluated the eutrophication effects on CH_4 and CO_2, Xiao et al. (2021) explored the impact of heavy metal pollution in urban wetland, Townsend et al. (2019), Ouyang et al. (2022) explored the risk of plastic pollution in wetland ecosystem, Xue et al. (2019) revealed the cooling effects of per-urban wetland and so on. Table 12.1 also depicts some very recent literatures highlighting the different dimensions of urban wetland interactions from different parts of the world.

Table 12.1 Literatures showing the urban wetland interactions

Literatures	Focus issue	Area of interest	Main findings
Rojas et al. (2022)	Accessibility disturbances posed by the urban built environment to the wetland biodiversity	Greater Concepción area of Chile	Unsuitable spatial urbanization interacts with wetland accessibility and poses disturbances to the wetland biodiversity
Wang et al. (2022)	Habitat potentiality of urban wetlands for endangered aquatic plants	Central district of Hangzhou, China	Highlighted supporting service of urban wetlands toward endangered aquatic plant species by composing ideal habitat that in turn stabilizes urban ecological environment
Chaudhuri et al. (2022)	Ecohydrological perspective of wetland degradation in highly urbanized area	National Capital Region (NCR) of Delhi	Six lakes were identified from different parts of NCR which are on the verge of devastation caused by the intensive urban activities and the absence of immediate attention
Xu et al. (2022a, b)	Impact of intensified urbanization on river wetland bird diversity	Seven river wetland around the Chaohu lake of China	Urbanization-driven land use alteration resulted in decrease of bird species richness over the section of river
Arazmi et al. (2022)	Rapid spread of invasive species	Peninsular Malaysia	Significant positive relation of urbanization with the abundance of Javan myna invasive species
Cunillera-Montcusí et al. (2022)	Freshwater Stalinization	Available literatures mostly from America, Australia and Europe	Freshwater salinization has accelerated globally due to human activities including urbanization
Cobbinah et al. (2022)	Wetland sieging due to Urbanization	Kumasi city of Ghana	Enhanced qualitative depletion and extinction of wetland due to conversation to the residential and other areas
Das et al. (2022)	Wetland ecosystem health	Diara region of lower Gangetic plain	Geo-spatial analysis shows between 2011 and 2018 the wetlands surrounding urban areas of this region converted to sick category from healthy and sub-healthy category
Hu et al. (2022)	Perception regarding urban wetland	Jiaxing city, China	Respondents were found to have very little knowledge about the ecological services of wetland, and 57% were not ready to pay for urban wetland conservation program
Priyadarsini and Pathy (2022)	Challenges and opportunities of urban wetlands	Bhubaneswar city, India	Alongside of carbon sinking, water accumulating and cleaning the urban wetlands bind city dwellers with the nature
Xia et al. (2022)	Migration and sink of micro-plastics in urban wetlands	Huixian wetland, Guilin	Huixian wetland was able to reduce 53–60% micro-plastics in surface water
Yi et al. (2022)	Wetland soil bacterial diversity	Chang-Zhu-Tan agglomeration of Hunan province, China	In the intensive urbanized areas wetland soil bacteria phyla exhibited significantly greater divergence as compared to other areas
Xie et al. (2022)	Role of urban wetland in maintain avian species diversity	Beijing, China	Urban parks with water bodies more efficiently protect urban forest bird diversity

(continued)

Table 12.1 (continued)

Literatures	Focus issue	Area of interest	Main findings
Vymazal (2022)	Historical development of constructing wetlands	Constructed wetlands of different European cites	It clearly depicted that constructed wetlands are good fit for developing sponge cities
Pereira and Baró (2022)	Greening of the city	–	Urban blue infrastructure is essential for nature-based solution to improve urban ecosystem and biodiversity
Richardson et al. (2022)	Wetland restoration	Housing market in Arkansas	Wetland restoration increases property values up to 10%

Urban sprawl reclaiming wetland, a precious natural capital and water pollution due to urban sewerage were well studied in last few decades; however, little attention was paid on urban effects on hydrological and ecological deterioration. The present study is, therefore, focused on exploring the effect of urban on hydro-ecological condition of the wetland apart from the nature of wetland reclamation caused by urbanization.

12.2 Study Area

Present study area is Chatra wetland (24° 58′ 22″ N to 25° 0′ 18″ N and 88° 6′ 17″ E to 88° 8′ 14″ E) (Fig. 12.1) which is located adjacent to the English Bazar municipality, the administrative head quarter of the Malda district of eastern India. Geologically, this wetland belongs to Diara division, one of the three major geological divisions (Tal, Diara and Burind) of the Malda district. This is perennial wetland and considered to be old scour channel of a distributary of the River Ganga but presently not directly connected to any perennial river. It is considered as the lungs of the urban area since naturally it helps to purify wastewater. Therefore, for water source this wetland depends mainly on rainwater and eventually has to endure huge pouring of urban wastewater. In addition, draining of urban sewage, sludge and waste dumping intensify the jeopardy of the wetland sustenance. For being situated near a populous and firstly growing administrative and market town, urban expansion over the wetland bed is very evident. The seasonal spell of the rainfall (average monthly rainfall, pre-monsoon-52 mm, monsoon-250 mm, post-monsoon-70 mm and winter-8 mm) encourages agricultural practice over the wetland bed. Tying with the built-up encroachment, agricultural practice alters the land use land cover (LULC) of the wetland area very evidently. The combined effect of urban wastewater, sewage contamination and agricultural fertilizer promotes hyper-eutrophication in the wetland that results in thick water hyacinth (Eichhornia crassipes) crust over the water surface.

12.3 Materials and Methods

12.3.1 Materials

The outline of the area of interest (AOI) was delineated from the latest imagery of the Google Earth. For investigating other hydrological and physical aspect of the wetland, United State Geological Survey (USGS) provided Landsat satellite images were relied on. To fulfill these purposes, available cloud-free representative images of Landsat TM and OLI series with 30 m × 30 m spatial resolution (pixel size) of path/row-139/43 for the period of 1990–2020 were downloaded directly subscribing to the earth explorer viewer of USGS (https://earthexplorer.usgs.gov) (Table 12.2). Other information regarding hydrological status of the wetland, sewage contamination and eutrophication status was directly extracted from field.
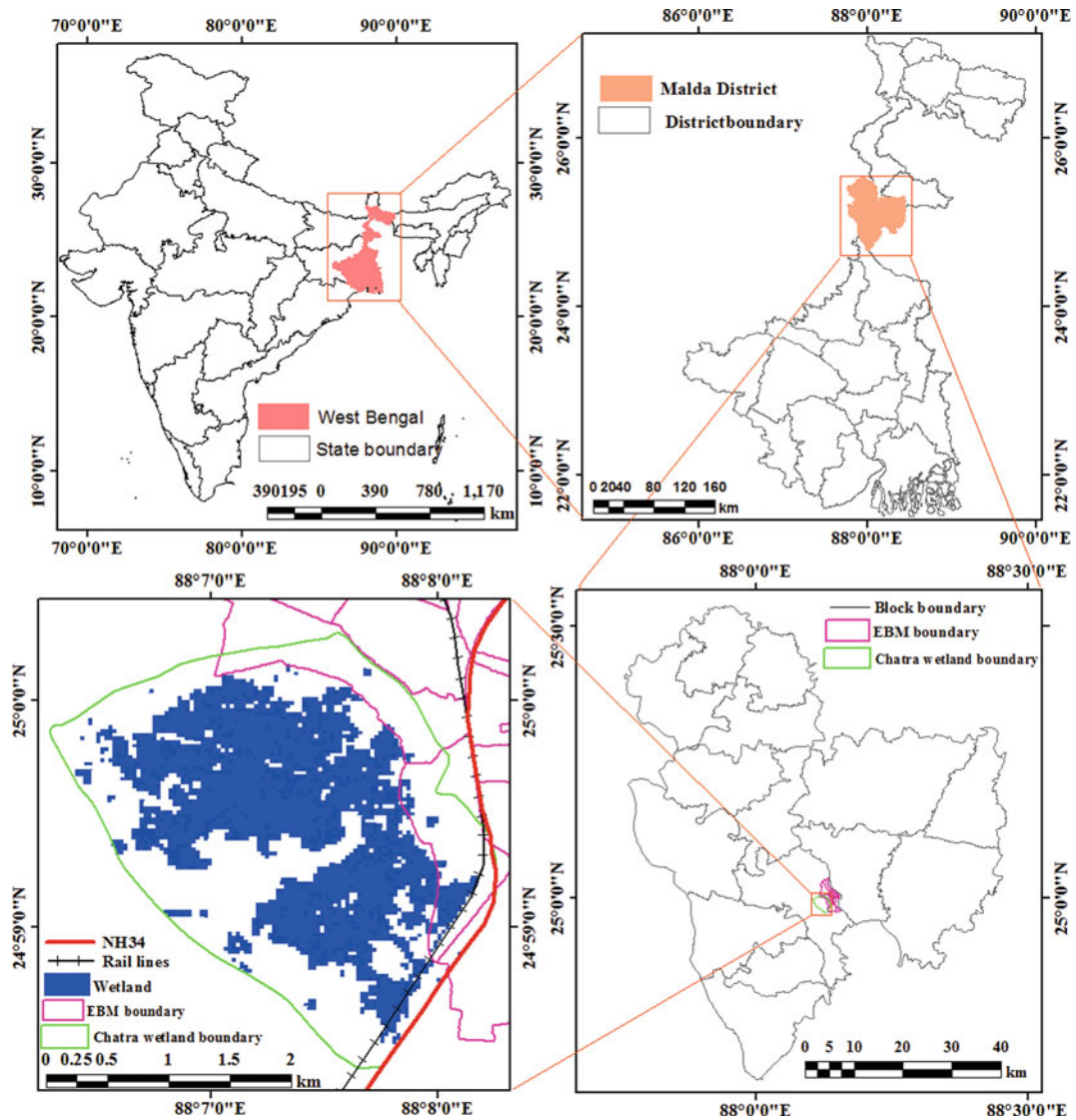
Fig. 12.1 Location of the study area showing Chatra wetland in English Bazar Municipality, major rivers, railway lines and NH-34

12.3.2   Methods

12.3.2.1   Wetland Mapping Using Water Indices and Accuracy Assessment

Differentiating water body from non-water body is very difficult. Time series satellite images and advance image classification techniques can facilitate identification water body. But this approach cannot help to analyze water depth dynamics. Spectral water index is an alternative to

resolve this issue. Normalized differences water index (NDWI) (McFeeters 1996), Modified normalized differences water index (MNDWI) (Xu 2006), Re-modified Normalized differences water index (RmNDWI) Water Ratio Index (WRI) (Shen and Li 2010), Automated Water Extraction Index (AWEI) (Feyisa et al. 2014), etc., are some good approaches for identifying water body. Aquatic vegetation, water turbidity, etc., can withstand against easy delineation of water body. If such problem poses difficulties,

Table 12.2 List of Landsat images used in this study

Phase	Year	Date of acquisition		Sensor
		Pre-monsoon	Post-monsoon	
Phase I	1990	11/04/1990	23/12/1990	TM
	1991	–	–	TM
	1992	15/03/1992	12/12/1992	TM
	1993	–	15/12/1993	TM
	1994	06/04/1994	18/12/1994	TM
	1995	24/03/1995	19/11/1995	TM
	1996	–	23/11/1996	TM
	1997	30/04/1997	08/11/1997	TM
	1998	01/04/1998	29/12/1998	TM
	1999	15/02/1999	16/12/1999	TM
	2000	–	18/12/2000	TM
Phase II	2001	25/04/2001	–	TM
	2002	29/03/2002	16/12/2002	TM
	2003	22/03/2003	25/11/2003	TM
	2004	01/04/2004	29/12/2004	TM
	2005	20/04/2005	14/11/2005	TM
	2006	18/02/2006	19/12/2006	TM
	2007	–	–	TM
	2009	26/02/2009	25/11/2009	TM
	2010	02/04/2010	14/12/2010	TM
Phase III	2011	–	15/11/2011	TM
	2013	26/04/2013	20/11/2013	OLI
	2014	–	23/11/2014	OLI
	2015	15/03/2015	26/11/2015	OLI
	2016	17/03/2016	12/11/2016	OLI
	2017	16/02/2017	01/12/2017	OLI
	2018	23/03/2018	18/11/2018	OLI
	2019	10/03/2019	5/11/2019	OLI
	2020	12/03/2020	23/11/2020	OLI

compositing all the indices can provide more reliable water body and wetland map. The present study applied NDWI, MNDWI, RmNDWI, multi-band spectral reflectance (MBSR) (Eqs. 12.1–12.4), and cumulative wetland area (CWA) of all indices for delineating the wetland area and overall accuracy and Kappa coefficient (K) (Eqs. 12.5 and 12.6) were applied for validating the wetland map. Since the water hyacinth cover area is very high, apart from the water indices, composite of all the water indices was also done.

$$NDWI = (b_G - b_{NIR})/(b_G + b_{NIR}) \quad (12.1)$$

$$MNDWI = (b_G - b_{MIR})/(b_G + b_{MIR}) \quad (12.2)$$

$$RmNDWI = (b_R - b_{MIR})/(b_R + b_{MIR}) \quad (12.3)$$

$$MBSR = (b_G + b_R) > (b_{NIR} + b_{MIR}) \quad (12.4)$$

where b_G = green band brightness value, b_R = red band brightness value, b_{NIR} = infra-red band brightness value, b_{MIR} = middle infra-red band brightness value

$$k = \frac{N \sum_{i=1}^{r} xii - \sum_{i=1}^{r}(xi+ * xi+i)}{N^2 - \sum_{i=1}^{r}(xi+ * xi+i)} \quad (12.5)$$

$$\text{Overall accuracy} = \text{Total number of correct samples}$$
$$\times 100\% \text{Total number of samples}$$
$$(12.6)$$

where N = total number of pixels; r = number of rows in the matrix; Xii = number of observations in row i and column i; $xi+$ and $x+i$ are the marginal totals for row i and column i, respectively.

12.3.2.2 Method for Exploring Hydrological Status of Wetland

Parameter Selection

Three image-driven hydrological parameters were selected for mapping hydrological status of the wetland. Water presence frequency (WPF), water depth (WD) and hydro-period (HP) derived from time series Landsat satellite imageries were taken since no ground monitoring stations were available. WPF refers that how many years a pixel recorded water appearance to total time period considered for this (1990–2020). For developing WPF layer, MNDWI maps of the respective years were converted into binary maps defining 0 to non-wetland and 1 to wetland. All these layers were added up and converted into percentage. WPF ranges from 0–100%, where the value near to 0 means inconsistent water appearance and near to 100 means consistent water appearance. This analysis is very useful for the wetlands those are highly controlled by seasonal rainfall.

Hydro-period refers to the length of time water ponds in a water body. Longer duration particularly perennial water body is ambient for ecological sustainability and pollutants removal (Khatun and Pal 2021). These data layers were developed using monthly binary MNDWI maps of the region. Binary MNDWI maps were

prepared based on the MNDWI maps, assigning 0 to non-water bodies and 1 to water bodies. Hydro-period this case ranges from 0 to 12. Value near to 1 means ephemeral type of wetland and 12 means perennial wetland.

Water depth was developed from MNDWI image calibrating it using regression coefficient generated from the MNDWI value and depth data of 35 field sites. Following Gao (2009) calibrated NDWI image for depth mapping, it was assumed that higher MNDWI value indicates greater depth and MNDWI was used for the same. The result derived from this is not highly satisfactory; however, an acceptable linear relationship was found. Since the rule-based decision tree (RBDT) was applied for integrating spatial data layers, all the data layers were classified into three sub-classes making it in categorical data.

Integration of Selected Parameters

For integrating hydrological components, rule-based decision tree (RBDT) in Arc Gis was applied. This method is very useful for compositing categorical spatial data layers. It was frequently used for various multi-parametric spatial data modeling like preparing wetland inventory (Berhane et al. 2018), suitable fish habitat (Pal and Khatun 2022), hydrological alteration (Roland and Crowley-Ornelas 2022). In this work, three hydrological parameters as mentioned earlier were applied and the rule set for combining the parameters was: The pixels are having high water depth >2.5 m., longer hydro-period (>8 months) and consistent water appearance (WPF >67%) can be treated as in good hydrological status and vice versa in case of poor hydrological status.

Validation of Model

For validating hydrological status, 42 sites from first phase were randomly selected and the same sites were monitored in consecutive phases in order to prove poor hydrological state is

susceptible to conversion. In recent phase, 57 sites were selected from classified map and verified the actual condition in ground.

12.3.2.3 Methods for Developing Trophic State Index (TSI)

Water Samples Collection

Twenty-one water samples were collected from the wetland in October 2020 for testing the nature of Cholorophyll-a (Chl-a) and Total Phosphorous (TP) in laboratory. Secchi disk depth (SDD) was directly measured from the field. The American Water Works Association (AWWA) and American Public Health Association (APHA) (APHA, AWWA, WEF 1998) endorsed standard practice were pursued for preserving and testing water sample. The sample sites were put on map based on the Garmin Global Positioning System (GPS)-driven coordinates of those sites.

Chl-a, SDD and TP Estimation from Satellite Images Using Regression Model

For pixel scale mapping of Chl-a, SDD and TP, the test result of the same on the selected sample sites was correlated with best-suited spectral water index found in this work (MNDWI). Linear regression between field-driven sample data and MNDWI value of the respective field sites was applied, and the regression slope was used for image calibration and developing pixel scale spatial data layers of the selected parameters (Chl-a, TP and SDD). TSI equation of the individual parameter was developed, and it is shown in Table 12.3. Sometimes, calibration may introduce some error in spatial data layers; however, due to scarcity of ample field data, this method was adopted.

Estimating Average TSI Based

TSI can efficiently represent the ecological responses, ecological health and water quality of the wetland (Carlson 1977). Saluja and Garg (2017), Wen et al. (2019), Li et al. (2022), Xu et al.

Table 12.3 Derived TSI equations for Chl-a, SDD and TP in 2010 and 2020

MNDWI	TSI equation developed for the parameters		
	Chl-a	SDD	TP
2010	$lnChl_a = -0.32n(MNDWI) + 0.086$	$lnSDD = -0.186ln(MNDWI) + 89.53$	$lnTP = -0.020ln(MNDWI) + 71.64$
2020	$lnChl_a = -0.26n(MNDWI) + 0.079$	$lnSDD = -0.173ln(MNDWI) + 85.31$	$lnTP = -0.018ln(MNDWI) + 69.73$

(2022a, b), Markogianni et al. (2022) estimated TSI using these parameters. In this study, Chl-a, SDD and TP were used for computing TSI.

Carlson (1977) endorsed a continuous scale from 0 to 100 compositing the mentioned parameters. TSI was classified into four classes, i.e., oligotrophic (<40), meso-trophic (40–60), eutrophic (60–80) and hyper-eutrophic (>80). Equation 12.7 was used for computing TSI averaging TSI of the constituting parameters.

$$TSI = \frac{[TSI(Chl_a) + TSI(SDD) + TSI(TP)]}{3}$$

$$(12.7)$$

where TSI = average TSI for all three parameters; TSI(TP), TSI(Chl-a) and TSI(SD) represent trophic state reference to Total Phosphorous, Chlorophyll-a Secchi Disk Depth, respectively.

12.3.2.4 Measuring Control of Hydrological State on Trophic State

For exploring the relationship between hydrological and trophic state at spatial scale, geographically weighted regression (GWR) was applied (Eqs. 12.8 and 12.9).

$$yi = \beta 0 + \beta 1 \times 1i + \beta 2 \times 2i + \cdots + \beta n \\ \times ni + \varepsilon i$$

$$(12.8)$$

With the estimators:

$$\beta'(i) = (XTW(i)X) - 1XTW(i)Y \qquad (12.9)$$

where $W(i)$ is a matrix of weights specific to location i such that observations nearer to i are given greater weight than observations further away.

12.4 Results

12.4.1 Delineated Wetland Area

Four water indices, NDWI, MNDWI, RmNDWI and MBSR, and one integrated index outputs are

presented in Fig. 12.2. Varying result was presented due to since the band selection in indexing process is different. Very minimum area was presented in NDWI since it only presented the open water. MNDWI presented the maximum area among the applied four spectral water indices. Since water hyacinth and other floating vegetation is a great challenge for wetland mapping, integration of four indices in CWA also presented larger wetland domain. From the wetland maps, no clear trend of areal extent was identified over the phases; however, water index value was declined from 1990 to 2020 (Fig. 12.3). For example, the highest MNDWI value in 1990 was 0.63 which was reduced to 0.44 signifying weakening of hydrological state. The same is true in case of NDWI and RmNDWI. This is very common trend in the wetland with high anthropogenic pressure (Chaudhuri et al. 2022). Spatial variation of wetland extent largely depends on monsoonal fluctuation of rainfall (Pal et al. 2022). In 2020, relatively greater rainfall (42% greater than average) is caused for larger wetland extent. Gradual shallowing of wetland due to sedimentation may be a reason for the same. It does not mean that area under wetland domain was increased over time; rather wider part was reclaimed due to urban encroachment. In fact, water domain area fluctuates within the deeper parts of the wetland.

12.4.2 Accuracy Assessment of Wetland Mapping

Since the areal fluctuation of wetland extent varies as per different water indices, selection of representative index is very essential. Over all accuracy and Kappa coefficient (K) applied for validating the water indices showed that NDWI is not applicable since the K value was <0.27 in all the years, RmNDWI value was <0.74 and, therefore, partially applicable. MNDWI was the best representative among the water indices since the K value was >0.83 in all the cases showing very good agreement between map and ground reality (Table 12.4). Among the water indices,
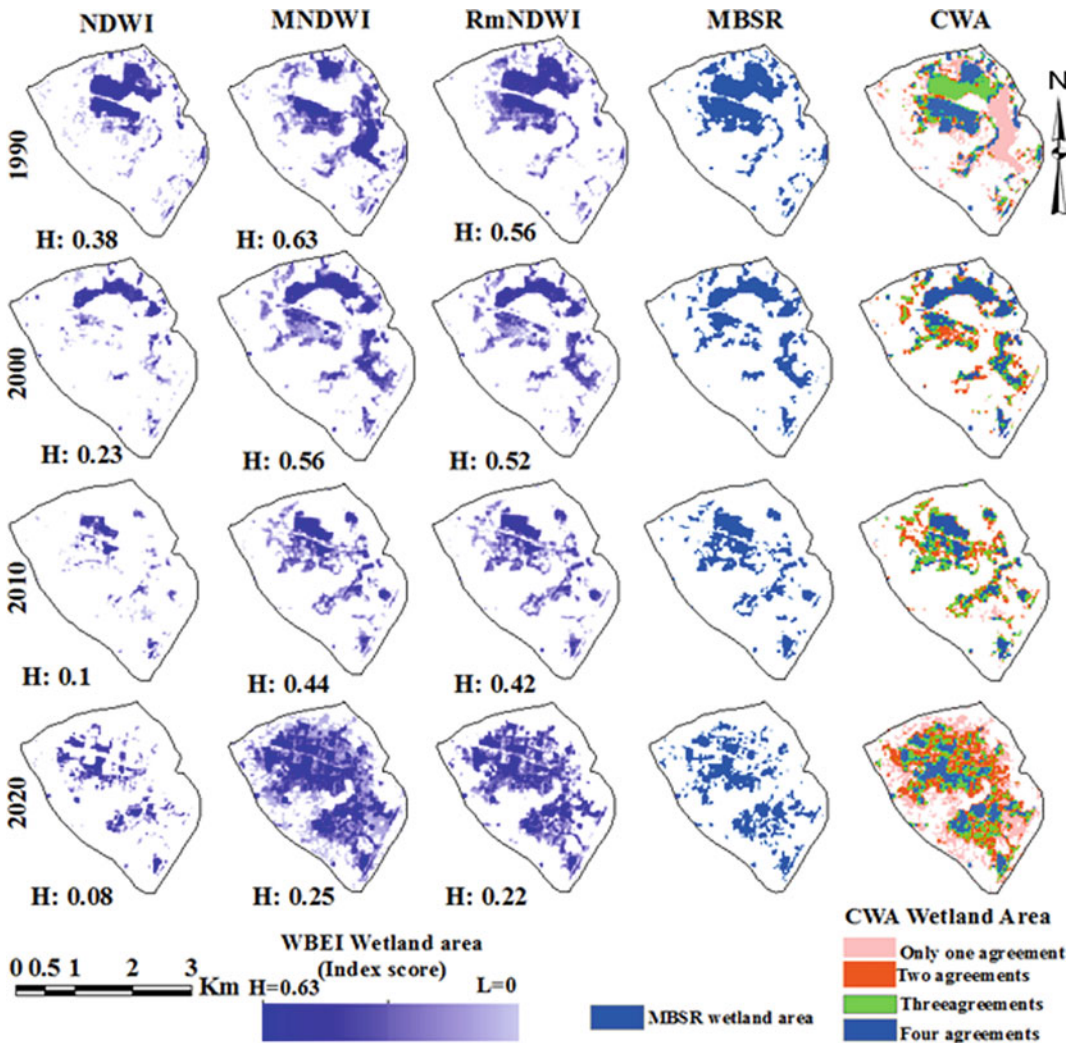
Fig. 12.2 Demarcated area of wetland recognized by different water body extraction indices

MNDWI was the best representative. Since CWA showed the integrated picture of all the applied indices, so expectedly it also more accurately represented the wetland extent. However, CWA does provide only the wetland area not the index value; it is not useful for water depth mapping. So, instead of this, MNDWI was taken for further works.

The superiority of MNDWI over NDWI in this region is not unique since previous studies like Sarp and Ozcelik (2017), Wicaksono and Wicaksono (2019), Yang et al. (2022) also reported quite similar finding from the other part of the world. Under the background of reclaiming wetland bed, hypereutrophication, sedimentation and resulted lowering of depth, the spectral distance of the reflectance of different objects trends to smear. Under such a scribble and congested LULC cover, especially at the edges of the wetland, the part of the lands that is represented by a single pixel is often shared by multiple land cover features. In this amalgamation of different land use features, the spectral reflectance of the representative feature always keep the spectral reflectance of other features from being captured by the pixel that corresponds that particular part
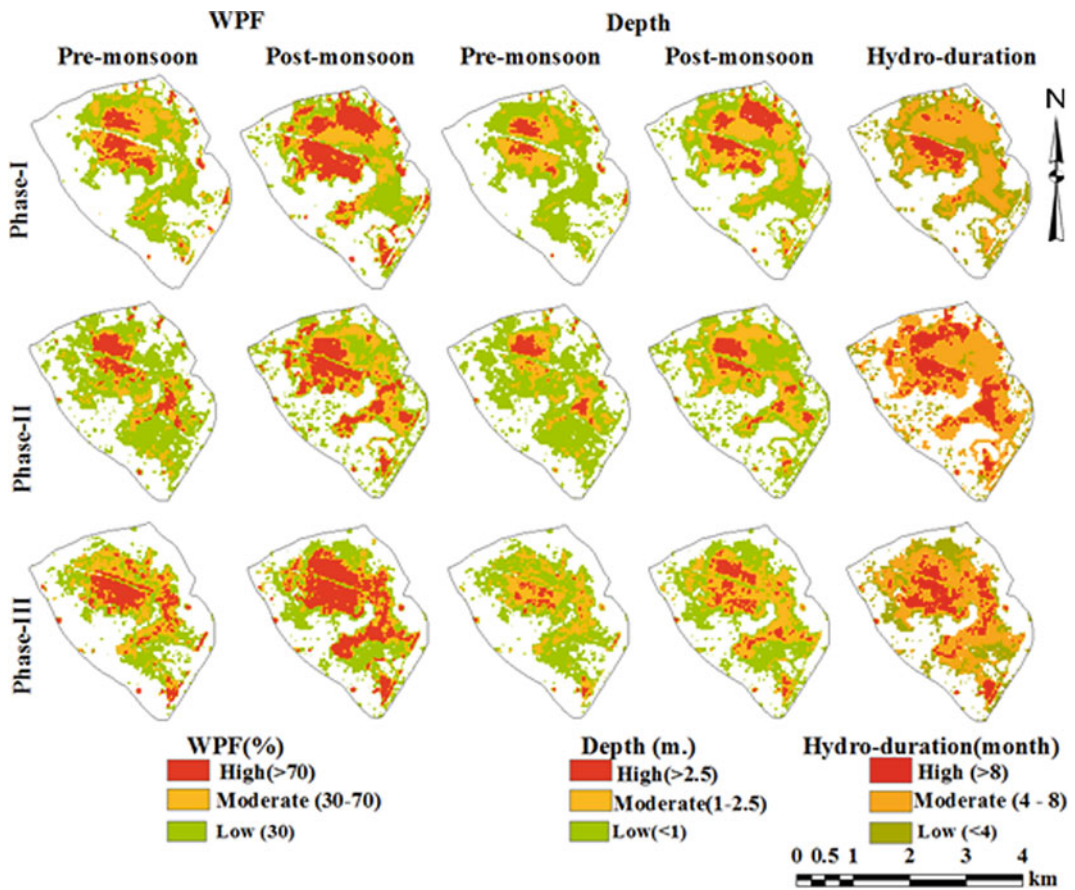
Fig. 12.3 Phase-wise spatial expression of WPF, depth and hydro-duration

of the land. The mismatches of the wetland traces extracted by different indices mostly belong the edge areas of the wetland where this kind of multiple land use congestion is very common especially in flood plain wetland (Debanshi and Pal 2020a, b). The RmNDWI has given almost similar result, but it also failed to effectively overcome the edge recognition error while mapping wetland.

12.4.3 Hydrological Status of Wetland

12.4.3.1 State of the Hydrological Components

Figure 12.3 shows three selected hydrological components; (1) water presence frequency, (2) hydro-duration and (3) water depth in three phases depicted phasal change and their spatial pattern. WPF maps of three phases were classified into high, moderate and low. Phase-wise WPF state clearly depicted quite varying picture, but it is very prominent that low WPF were found at the transitional area and it surrounds the moderate and high WPF zones. Area under high WPF zone was found quite greater in 2020, but all part of these areas were not characterized by high deep-water bodies and longer hydro-duration (Fig. 12.3). Low hydro-duration area was increased over the phases indicating enhancing seasonality effect in wetland. Season-wise comparison of water depth reflected that area under higher depth (>2.5 m.) was 0.16 km^2 in pre-monsoon and 0.48 km^2 in post-monsoon season in phase III. The same was true in case of

Table 12.4 Ground truth accuracy of different WBEI-produced wetland mapping

Years	NDWI		MNDWI		RmNDWI		MBSR		CWA	
	K coefficient	Overall accuracy (%)	K coefficient	Overall accuracy (%)	K coefficient	Overall accuracy (%)	K coefficient	Overall accuracy (%)	K coefficient	Overall accuracy (%)
2014 (pre-monsoon)	0.27	30	0.86	94	0.62	68	0.27	30	0.79	87
2016 (post-monsoon)	0.21	23	0.89	97	0.71	78	0.31	34	0.82	90
2017 (pre-monsoon)	0.24	26	0.88	96	0.74	81	0.4	44	0.8	88
2020 (post-monsoon)	0.17	19	0.83	91	0.52	57	0.37	41	0.77	84

phases I and II (Table 12.5). The fringe wetland parts with highly inconsistent water appearance, shallower depth and narrow hydro-duration are highly susceptible for wetland reclamation and transformation. This form of result was also reported by Pal et al. (2022) with higher rate of transformation in lower Atreyee flood plain area. Since eastern and northern parts are circumscribed by urban area, chance of urban encroachment and western part is surrounded by agriculture land, likelihood of agriculture encroachment is very high.

12.4.3.2 Integrated Hydrological Status and Validation

Phase-wise integrated hydrological status (Fig. 12.4) shows that some outskirt wetland area under poor hydrological state in phases I and II was declined in phase III. In phase III, some new areas were appeared under poor hydrological state which is likely to be converted into other land as the tradition proves (Paul and Pal 2020; Pal and Debanshi 2021). More than 25% (1.11 km^2) wetland area recorded poor hydrological state in phase III, and this part is susceptible to reclamation. Poor water appearance consistency, shallower water depth, small period of water stagnation, proximity to built land and agricultural land in this area may facilitate for possible conversion (Debanshi and Pal 2020a, b; Pal and Paul 2020). Although specifically this sort of work in urban wetland is quite absent, but monitoring hydrological state combining image-driven hydrological components are quite available in the flood plain agriculture proximate wetlands. Debanshi and Pal (2020a; b) and Pal and Khatun (2022) focused on this issue in Barind plain of India and Bangladesh and mature Ganges delta of India. They reported gradual degradation of hydrological state. Validation of hydrological state revealed that 71% cases poor hydrological state of the phase I was either converted into built and agriculture land or remained in the same category in phase II. In case of phase III, 74% sites reported good agreement between map and ground condition. In this sense, the hydrological status model could be treated as valid.

Table 12.5 Distribution of wetland area (km^2) under different zones of WPF, depth and hydro-duration

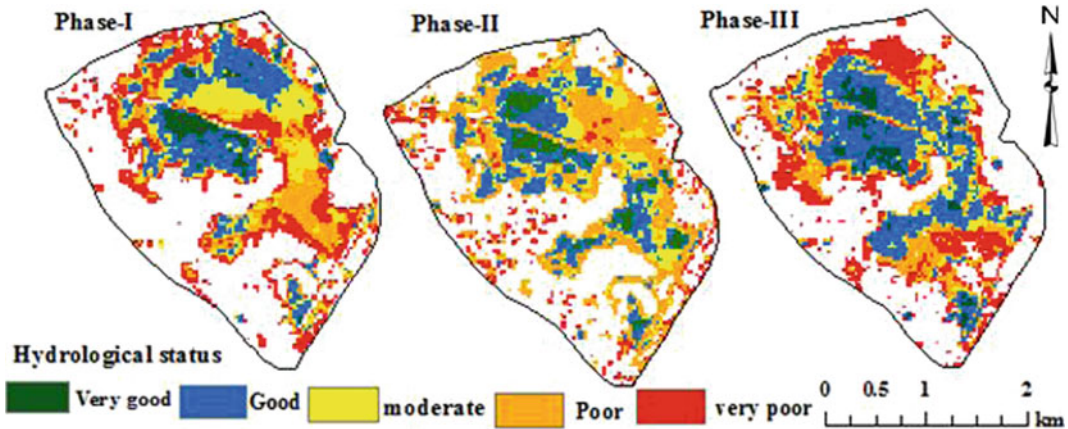| Parameters	WPF						Depth						Hydro-duration		
Seasons	Pre-monsoon			Pre-monsoon			Pre-monsoon			Pre-monsoon			I	II	III
Status/phases	I	II	III	I	II	III	I	II	III	I	II	III			
High	0.43	0.49	0.71	1.19	1.03	1.7	0.24	0.25	0.16	0.6	0.4	0.48	0.38	0.94	0.7
Moderate	0.96	0.66	1.08	1.12	1.22	0.8	0.69	0.75	1.03	1.34	1.35	1.53	2.03	2.75	2.14
Low	1.86	2.9	1.51	1.62	1.88	1.55	2.32	3.05	2.11	1.97	2.39	2.04	1.52	0.44	1.21

Fig. 12.4 Phase-wise hydrological status of the wetland

Spatial mapping of this assessment showed a strong connection between poor hydrological state and close proximity of the urban built-up environment. In the present context, urban activities like infilling, dumping, draining, promoting, sewage releasing play major role behind such lowering of hydrological viability. Such phenomenon is not at all isolated in this part of the world. Obviously, dense population plays the role of positive catalyst behind such man-environment conflict but similar findings are often reported from different parts of the world (Rojas et al. 2022; Chaudhuri et al. 2022; Arazmi et al. 2022). For being a highly populated market town, the high land values of the city area often push the decision of developing residential area toward these peri-urban parts where lowland status insists cheaper land value (Asomani-Boateng 2019). Due to the encroaching human habitation, the dumping and sewage mixing increase the sedimentation and lower the depth which in turn degrades the habitat state. Under this circumstance infilling, draining and finally encroaching become often easier (Fig. 12.10a–c). In this way, lowering of hydrological status and encroaching of urban built up go on simultaneously influencing each other reciprocally. This is quite evident from the temporal accounts of urban expansion toward the wetland bed. Since 1990, in the north-eastern verge of the wetland, urban line extended almost 350 m toward wetland in south-western direction whereas the poor hydrological status zone also expanded more than 200 m, occupying relatively better part of the wetland in the same direction toward the core of the wetland. In the under developed countries with very dense population habitation such kind of urban encroachment toward peripheral wetlands and resulted anthropogenic footprint is very evident (Cobbinah et al. 2022). Pollution influxes from the urban agglomeration and encourages eutrophication. During the lean season, local people maneuver

cleaning water hyacinth from the core parts of the wetland and for pisciculture and stack the hyacinth in the edge of the wetland. Year after year, such high accumulation of hyacinth residues makes the edge part of the wetland hydrologically poor and filled which eventually enforce quick reclamation (Fig. 12.10d).

12.4.4 Trophic State

Figure 12.5 displays the TSI of the wetland in 2010 and 2020, and real pictures can be visualize in Fig. 12.6. In 2010, the TSI value was ranged from 17 to 87, and it increased in 2020 (TSI: 34–96) indicating qualitative degradation of water quality and ecological health. In 2020, area under hyper-eutrophicated area was increased by 3%. In 2010, about 61% area under oligotrophic state and this area was reduced to about 56% in 2020. The lower limit of TSI in 2020 (TSI: 34) was reached near to eutrophicated state (TSI: 40). It does indicate in very near future, the entire wetland area will be eutrophicated. Hyper-eutrophic and eutrophic states prevail mainly in the urban fringe area where hydrological status was recorded poor. Shallower water depth and

direct influx of urban sewage may be the major reason behind this. Talukdar et al. (2020) and Khatun and Pal (2021) also reported increasing TSI near the urban wetland and agriculture-dominated wetland. Growing TSI adversely affects the ecological productivity (Tiwari and Pal, 2022) and diminishes the feasibility of producing ecological goods and services (Janssen et al. 2021; Gilby et al. 2021).

12.4.5 Control of Hydrological State on Trophic State

Figure 12.7 shows the GWR indicating the control of hydrological state on trophic state. Standard regression residual depicts high control over >58% of the total wetland area (Table 12.6). Except some patches, most part in fringe area was under this category revealing the strong influence of hydrological state on trophic state. Poor hydrological state positively instigated the poor trophic state. This control was found quite high in phase II indicating increasing control. Shallower depth of water and relatively stagnant nature of water influence the exuberant growth of water hyacinth like plants. Hyper-eutrophication may
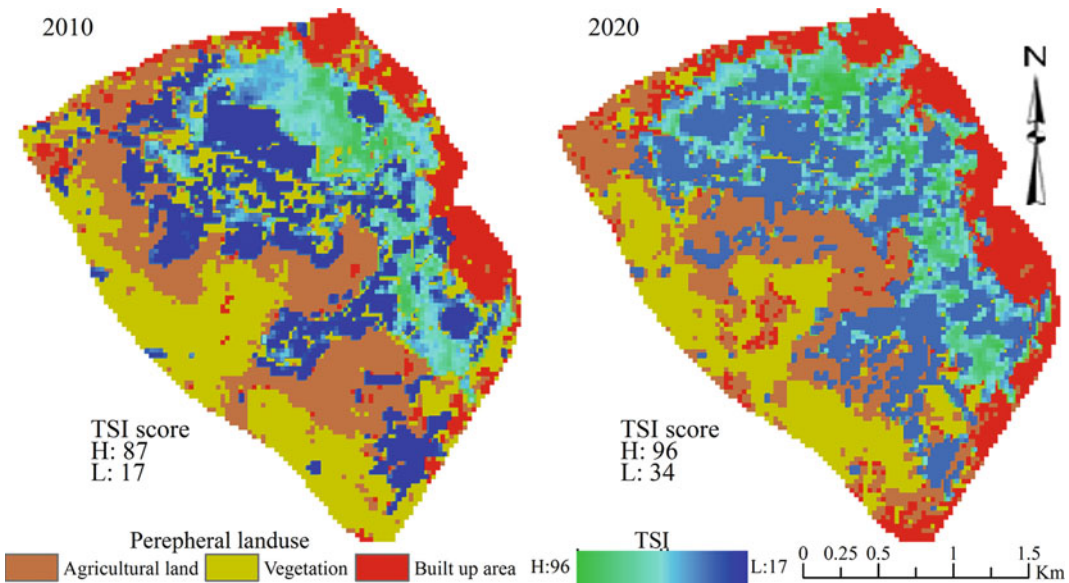

Fig. 12.5 Trophic state index of the wetland in 2010 and 2020

Fig. 12.6 Pictures of wetlands belong to different trophic states
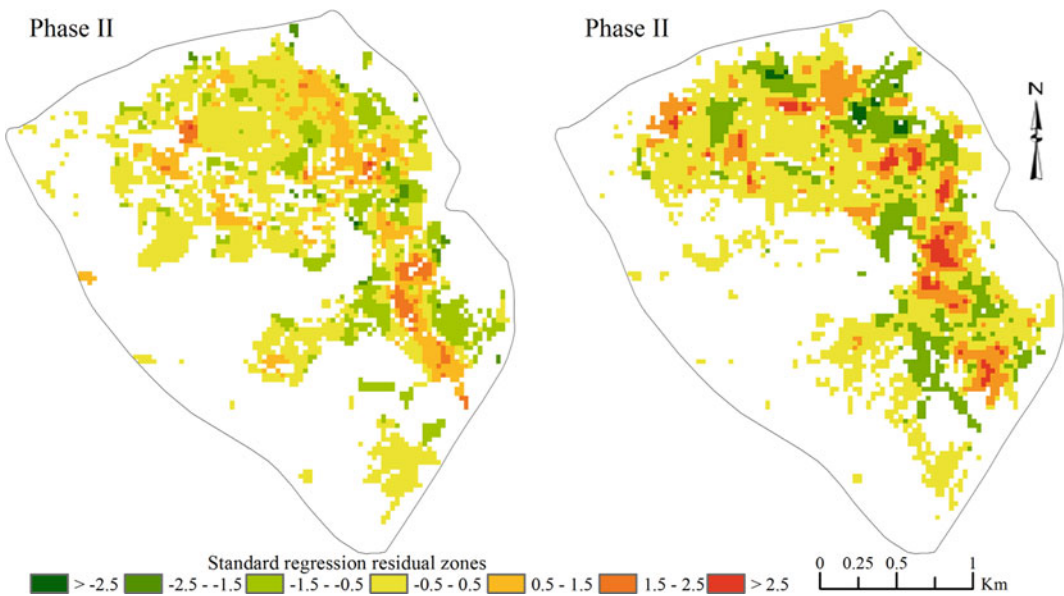

Fig. 12.7 Standard regression residual zones in reference to hydrological and trophic state

adversely impact the urban micro-climate state enhancing both CO_2 and CH_4 emissions (Benassi et al. 2021). It may also cause diminishing return of ecological goods particularly fish which the people frequently harvest from the wetland (Alprol et al. 2021; Djihouessi et al. 2021).

Table 12.6 Areal coverage under different standard regression residual zones generated using GWR between hydrological and TSI states

Standard regression residual	Phase II		Phase III	
	Area (km^2)	%	Area (km^2)	%
>−2.5	0.00	0.03	–	–
−2.5 to −1.5	0.04	1.56	0.04	1.19
−1.5 to −0.5	0.56	21.18	0.60	20.29
−0.5 to 0.5	1.53	57.57	1.76	59.88
0.5 to 1.5	0.43	16.40	0.47	15.88
1.5 to 2.5	0.08	3.19	0.08	2.75
>2.5	0.00	0.07	–	–

In the peripheral parts of the wetland a huge amount of micronutrient element influx due to contamination of urban sewage (Fig. 12.10e–g). This micronutrient increases the trophic state of the wetland and highly encourages eutrophication; such effect of urban sewage is well reported from all around the world (Oliver et al. 2019; Putt et al. 2019). It is observed in the present wetland also that the parts of the wetland approaching the urban sites mostly dominated by higher TSI values (Fig. 12.10f). As a result, with

time eutrophication dominated almost 70% water area of the wetland. The poor hydrological status of this part increases the TSI in two ways. Firstly, due to lesser water availability, the density of micronutrient in the water highly favors the growth of floating aquatic plants like water moss and hyacinth. Secondly, with the decreasing water depth of the poor hydrological parts encourages the growth of rooted plants and makes the area hyper-eutrophicated. Water hyacinth is the most common species that colonizes
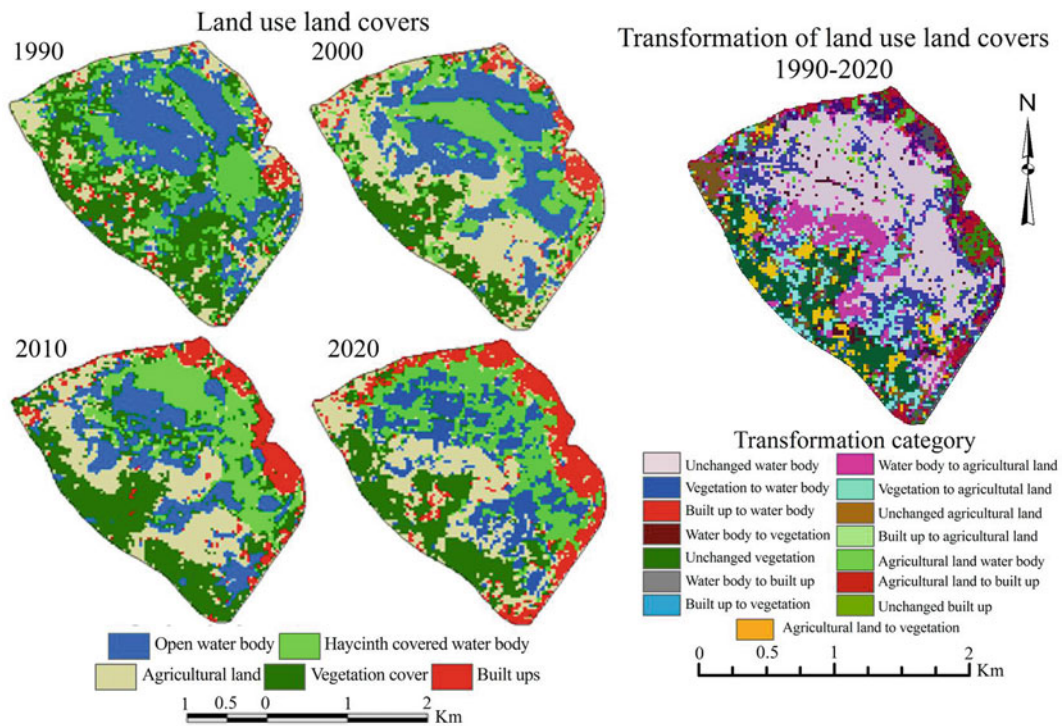

Fig. 12.8 Temporal dynamics and transformation of LULC of wetland and its adjacent area

the wetland every year and covers the water surface area under thick crust.

12.4.6 Causes of Transformation

12.4.6.1 Encroachment of Agriculture and Built-Up Area

Land use transformation particularly encroachment of built-up land from eastern and southeastern margin of the wetland is very prominent, and it was found very aggressive over the progress of time (Fig. 12.8). In 1990, only a few patches were under built-up land (only 2%), but in 2020, it was reached to more than 10% of total area. Wetland reclamation is very steady process in this area. Apart from existing built-up land, wider parts of the wetland adjacent to the built-up area were already reclaimed and ready to erect building. So, in coming days more area is likely to be turned into built land. Within urban area, land value is very high and there is very limited space within built urban area. Therefore, people frequently opt this relatively less priced land for building urban space.

Here, it is to be mentioned that supervised image classification technique in ERDAS imagine software was applied for land use/land cover mapping. Maximum likelihood classifier was used for classification. For each class, 21–30 spectral signatures were collected. Overall accuracy and Kappa coefficient (K) were applied for accuracy assessment of the LULC maps based on 57 ground control point directly from field in case of 2020, and the same number of sites was taken from Google Earth images in case of other years. Overall accuracy is greater than 83%, and K value is greater than 0.80 in all the years, signifying good agreement between map and ground condition. Change detection techniques were applied for land use transformation analysis.

12.4.6.2 Influx of Urban Sewage

English Bazar Municipality (EBM) is located at the water divide area of river Ganga and Mahananda. River Mahanada and Chatra wetland circumscribe eastern and western margin of

the study area. The urban sewage mainly influxes either into river Mahananda or Chatra wetland. At present, wider part of the wetland was reclaimed and converted into built area. So, over the progress of time the volume of wastewater influx is increased. Sixty-two number of drains (including kacha and pucca drain) directly merge into this wetland (Fig. 12.9) polluting the wetlands. Although the water quality was not measured, visual impression of the wetland is deep black and even huge amount of non-biodegradable solid waste also influxes into the wetland. Apart from pollution, huge amount of sediment load also penetrates into the wetland from some major drains (Fig. 12.8). It also causes gradual shallowing of water bodies. Ziaul and Pal (2017) also pointed out increasing water insecurity due to admixing of pollutants. Since the deposition of pollutants is quite high near to
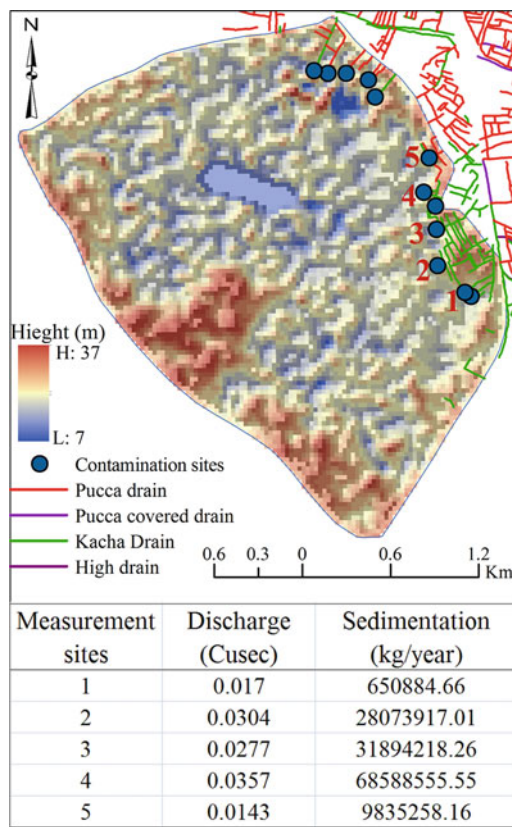

Measurement sites	Discharge (Cusec)	Sedimentation (kg/year)
1	0.017	650884.66
2	0.0304	28073917.01
3	0.0277	31894218.26
4	0.0357	68588555.55
5	0.0143	9835258.16

Fig. 12.9 Accounts of urban sewage and wastes affluence into the wetland

Fig. 12.10 Glimpses of adverse urban effect on Chatra wetland, **a–c** built-up encroachment toward wetland, **d** hyacinth stacking at the verge of wetland, **e–f** contamination of urban waste in the wetland, **g** wastewater accumulation at the periphery of the wetland, **h, i** clogged outlet of the wetland

the debouching points, the contamination rate is expected to be high in this area. Enhanced degree of TSI and consequent exuberant growth of water hyacinth in this area also proves it.

12.4.6.3 Partial Closure of Wetland Outlet

Chatra wetland actually was linked with Bhatra wetland extending toward Bangladesh. After construction Indian railway, National High Way (NH)-34, the wetland was perforated and partially blocked. Afterward, mango market was constructed just beside NH-34 reclaiming the outlet of the wetland. Major route of the outlet was closed (Fig. 12.10h, i). It has restricted the free outflow, and it causes qualitative deterioration of the water quality. Moreover, the base of the siphon constructed across the rail and high way was quite elevated than the base of the wetland (Fig. 12.10h, i). So, water partially drains only during spilling time.

12.5 Conclusion

The present study explored the role of urban growth on hydrological state of the wetland and assessed the ecological response in this regard. The study exhibited the gradual weakening of hydrological strength over the progress of time. Wide peripheral wetland with poor hydrological state was obliterated. Continuous influx of urban waste to the wetland and weakening of hydrological strength energized the ecological deterioration as reflected in growing TSI value and increasing coverage under eutrophicated area. Geographically weighted regression between hydrological and trophic state revealed a strong control over more than 56% geographical area. Apart from this, urban encroachment and wetland reclamation are also very vital issues as identified. This trend is so aggressive; in near future, more area is likely to be reclaimed. Since

the wetland is treated as the kidney of the city, quantitative loss and qualitative degradation of wetland adversely affect this precious function. Moreover, this natural capital provides a wide range of ecological goods and services, degradation can restrict this flow. Excess eutrophication problem may often cause poor carbon sinking and high methanogenesis. Hence, instead of mediating heat island effect, it can enhance the condition. Loss of storage area can also reduce the ground water recharge amount, storm storage etc. All these are against of building resilient city.

This study lacks water quality analysis. Along with the trophic state mapping, water quality data would yield a broader picture of habitat health. In addition, the wetland mapping was to some extent hampered due to highly dynamic floating hyacinth patches, but accuracy was assessed to be good enough Therefore, this study could be instrumental to the local authority to step forward in that direction. Integrated conservation and restoration of this precious resource will be a good endeavor for supporting fishes, other aquatic resources and recreational well-being of the city people as well as the outside people. Since the study clearly identified the nature of hydrological transformation, its ecological responses, causes of transformation; for the sake of ecological well-being in general and human well-being in particular, this piece of study may be very useful.

References

Alikhani S, Nummi P, Ojala A (2021) Urban wetlands: a review on ecological and cultural values. Water 13 (22):3301

Alprol AE, Heneash AM, Soliman AM, Ashour M, Alsanie WF, Gaber A, Mansour AT (2021) Assessment of water quality, eutrophication, and zooplankton community in Lake Burullus, Egypt. Diversity 13 (6):268

Arazmi FN, Ismail NA, Daud UNS, Abidin KZ, Nor SM, Mansor MS (2022) Spread of the invasive Javan myna along an urban–suburban gradient in Peninsular Malaysia. Urban Ecosyst, 1–8

Asomani-Boateng R (2019) Urban wetland planning and management in Ghana: a disappointing implementation. Wetlands 39(2):251–261

Athukorala D, Estoque RC, Murayama Y, Matsushita B (2021) Impacts of urbanization on the Muthurajawela Marsh and Negombo Lagoon, Sri Lanka: Implications for landscape planning towards a sustainable urban wetland ecosystem. Remote Sens 13(2):316

Beckwith L (2022) Cambodia's resilience agenda: understanding how local institutions and actors accept, contest and accommodate an externally driven approach. Geoforum 128:125–134

Benassi RF, de Jesus TA, Coelho LHG, Hanisch WS, Domingues MR, Taniwaki RH, Mitsch WJ (2021) Eutrophication effects on CH_4 and CO_2 fluxes in a highly urbanized tropical reservoir (Southeast, Brazil). Environ Sci Pollut Res 28(31):42261–42274

Berhane TM, Lane CR, Wu Q, Autrey BC, Anenkhonov OA, Chepinoga VV, Liu H (2018) Decision-tree, rule-based, and random forest classification of high-resolution multispectral imagery for wetland mapping and inventory. Remote Sens 10 (4):580

Bhat SU, Qayoom U (2021) Implications of sewage discharge on freshwater ecosystems. In: Sewage-recent advances, new perspectives and applications. IntechOpen

Brinkmann K, Hoffmann E, Buerkert A (2020) Spatial and temporal dynamics of urban wetlands in an Indian Megacity over the past 50 years. Remote Sens 12 (4):662

Carlson RE (1977) A trophic state index for lakes 1. Limnol Oceanogr 22(2):361–369

Chand N, Suthar S, Kumar K (2021) Wastewater nutrients and coliforms removals in tidal flow constructed wetland: effect of the plant (Typha) stand and biochar addition. J Water Process Eng 43:102292

Chaudhuri AS, Gaur N, Rana P, Verma P (2022) Ecohydrological perspective for environmental degradation of lakes and wetlands in Delhi. In: Geospatial technology for landscape and environmental management. Springer, Singapore, pp 143–163

Chen J, Liu SS, Wang YJ, Li J, Liu YS, Yang F, Ying GG (2021) Optimized constructed wetlands enhance the removal and reduce the risks of steroid hormones in domestic wastewater. Sci Total Environ 757:143773

Cobbinah PB, Korah PI, Bardoe JB, Darkwah RM, Nunbogu AM (2022) Contested urban spaces in unplanned urbanization: wetlands under siege. Cities 121:103489

Cunillera-Montcusí D, Beklioğlu M, Cañedo-Argüelles M, Jeppesen E, Ptacnik R, Amorim CA, Matias M (2022) Freshwater salinisation: a research agenda for a saltier world. Trends Ecol Evol

Danso GK, Takyi SA, Amponsah O, Yeboah AS, Owusu RO (2021) Exploring the effects of rapid urbanization on wetlands: insights from the Greater Accra Metropolitan Area, Ghana. SN Soc Sci 1(8):1–21

Dar SA, Rashid I, Bhat SU (2021) Land system transformations govern the trophic status of an urban wetland ecosystem: perspectives from remote sensing

and water quality analysis. Land Degrad Dev 32 (14):4087–4104

Das S, Bhunia GS, Bera B, Shit PK (2022) Evaluation of wetland ecosystem health using geospatial technology: evidence from the lower Gangetic flood plain in India. Environ Sci Pollut Res 29(2):1858–1874

Debanshi S, Pal S (2020a) Modelling water richness and habitat suitability of the wetlands and measuring their spatial linkages in mature Ganges delta of India. J Environ Manage 271:110956

Debanshi S, Pal S (2020b) Wetland delineation simulation and prediction in deltaic landscape. Ecol Ind 108:105757

Djihouessi MB, Tigo BA, Aina MP (2021) The use of nutrient budget approach for informing eutrophication management in urbanised shallow coastal lakes: a case study from Lake Nokoué in Benin. Ecohydrol Hydrobiol 21(2):341–353

Feyisa GL, Meilby H, Fensholt R, Proud SR (2014) Automated water extraction index: a new technique for surface water mapping using Landsat imagery. Remote Sens Environ 140:23–35

Fu H, Gaüzère P, Molinos JG, Zhang P, Zhang H, Zhang M, Xu J (2021) Mitigation of urbanization effects on aquatic ecosystems by synchronous ecological restoration. Water Res 204:117587

Gao J (2009) Bathymetric mapping by means of remote sensing: methods, accuracy and limitations. Prog Phys Geogr 33(1):103–116

Ghanian M, Ghoochani OM, Noroozi H, Cotton M (2022) Valuing wetland conservation: a contingent valuation analysis among Iranian beneficiaries. J Nat Conserv 126140

Gilby BL, Weinstein MP, Baker R, Cebrian J, Alford SB, Chelsky A, Ziegler SL (2021) Human actions alter tidal marsh seascapes and the provision of ecosystem services. Estuaries Coasts 44(6):1628–1636

Hu C, Wright AL, He S (2022) Public perception and willingness to pay for urban wetland ecosystem services: evidence from China. Wetlands 42(2):1–10

Islam N, Shaha DC, Hasan J, Asad M, Al H, Salam MA, Ahmed M (2022). Heavy metal pollution reduced the potentiality of pen culture in the wetland aquaculture in an urban area of Bangladesh. Conservation 2(1): 68–9

Janssen AB, Hilt S, Kosten S, de Klein JJ, Paerl HW, Van de Waal DB (2021) Shifting states, shifting services: Linking regime shifts to changes in ecosystem services of shallow lakes. Freshw Biol 66(1):1–12

Kakade A, Salama ES, Han H, Zheng Y, Kulshrestha S, Jalalah M, Li X (2021) World eutrophic pollution of lake and river: biotreatment potential and future perspectives. Environ Technol Innov 23:101604

Khatun R, Pal S (2021) Effects of hydrological modification on fish habitability in riparian flood plain river basin. Eco Inform 65:101398

Kończak M, Huber M (2022) Application of the engineered sewage sludge-derived biochar to minimize water eutrophication by removal of ammonium and phosphate ions from water. J Clean Prod 331:129994

Kumar S, Agarwal A, Villuri VGK, Pasupuleti S, Kumar D, Kaushal DR, Sivakumar B (2021) Constructed wetland management in urban catchments for mitigating floods. Stoch Environ Res Risk Assess 35 (10):2105–2124

Li S, Chen F, Song K, Liu G, Tao H, Xu S, Mu G (2022) Mapping the trophic state index of Eastern Lakes in China using an empirical model and Sentinel-2 imagery data. J Hydrol 127613

Lin Y, Luo K, Su Z, Wu Y, Xiao W, Qin M, Wang Y (2022) Imposed by urbanization on soil heavy metal content of lake wetland and evaluation of ecological risks in East Dongting Lake. Urban Clim 42:101117

Markogianni V, Kalivas D, Petropoulos GP, Dimitriou E (2022) Modelling of Greek Lakes water quality using Earth observation in the framework of the Water Framework Directive (WFD). Remote Sens 14(3):739

McFeeters SK (1996) The use of the Normalized Difference Water Index (NDWI) in the delineation of open water features. Int J Remote Sens 17(7):1425–1432

Mishra VK, Shukla R, Sharma NK (2021) Application of constructed wetland; a natural treatment system for environmentally sustainable domestic sewage treatment. In: Sustainable environmental clean-up. Elsevier, pp 105–129

Oliver S, Corburn J, Ribeiro H (2019) Challenges regarding water quality of eutrophic reservoirs in urban landscapes: a mapping literature review. Int J Environ Res Public Health 16(1):40

Ouyang X, Duarte CM, Cheung SG, Tam NFY, Cannicci S, Martin C, Lee SY (2022) Fate and effects of macro-and microplastics in coastal wetlands. Environ Sci Technology.

Pal S, Debanshi S (2021) Developing wetland landscape insecurity and hydrological security models and measuring their spatial linkages. Eco Inform 66:101461

Pal S, Khatun R (2022) Image driven hydrological components-based fish habitability modeling in riparian wetlands triggered by damming. Wetlands 42 (1):1–13

Pal S, Paul S (2020) Assessing wetland habitat vulnerability in moribund Ganges delta using bivariate models and machine learning algorithms. Ecol Ind 119:106866

Pal S, Sarkar R, Saha TK (2022) Exploring the forms of wetland modifications and investigating the causes in lower Atreyee river floodplain area. Eco Inform 67:101494

Paul S, Pal S (2020) Exploring wetland transformations in moribund deltaic parts of India. Geocarto Int 35 (16):1873–1894

Pereira P, Baró F (2022) Greening the city: thriving for biodiversity and sustainability. Sci Total Environ 153032

Priyadarsini P, Pathy AC (2022) Urban wetlands: opportunities and challenges in Indian cities—A case of Bhubaneswar City, Odisha. Livelihood Enhancement Through Agric, Tourism Health 305–331

Putt AE, MacIsaac EA, Herunter HE, Cooper AB, Selbie DT (2019) Eutrophication forcings on a peri-urban lake ecosystem: context for integrated watershed to airshed management. PLoS ONE 14(7):e0219241

Richardson M, Liu P, Eggleton M (2022) Valuation of wetland restoration: evidence from the housing market in Arkansas. Environ Resou Econ 1–35

Rojas C, Sepúlveda E, Jorquera F, Munizaga J, Pino J (2022) Accessibility disturbances to the biodiversity of urban wetlands due to built environment. City Environ Interact 13:100076

Roland II, VL, Crowley-Ornelas E (2022) Investigating hydrologic alteration in the Pearl and Pascagoula river basins using rule-based model trees. Environ Model Softw 105322

Saluja R, Garg JK (2017) Trophic state assessment of Bhindawas Lake, Haryana, India. Environ Monit Assess 189(1):1–15

Sarkar D, Maji N (2022) Status and threats of wetland change in land use pattern and planning: impact of land use patterns and urbanization. In: Handbook of research on monitoring and evaluating the ecological health of wetlands. IGI Global, pp 106–127

Sarp G, Ozcelik M (2017) Water body extraction and change detection using time series: a case study of Lake Burdur, Turkey. J Taibah Univ Sci 11(3):381–391

Shen L, Li C (2010) Water body extraction from Landsat ETM+ imagery using adaboost algorithm. In 2010 18th International Conference on Geoinformatics (pp. 1–4). IEEE

Suganya K, Kumar JE, Sebastian SP, Poornima R, Kannan B, Parameswari E, Kalaiselvi P (2022) Exploring the Phytoremediation potential of macrophytes for treating sewage effluent through Constructed Wetland Technology (CWT) for sustainable agriculture. In: Sustainable agriculture. Springer, Cham, pp 209–223

Talukdar S, Pal S, Chakraborty A, Mahato S (2020) Damming effects on trophic and habitat state of riparian wetlands and their spatial relationship. Ecol Ind 118:106757

Tiwari AK, Pal DB (2022) Nutrients contamination and eutrophication in the river ecosystem. In: Ecological significance of river ecosystems. Elsevier, pp 203–216

Townsend KR, Lu HC, Sharley DJ, Pettigrove V (2019) Associations between microplastic pollution and land use in urban wetland sediments. Environ Sci Pollut Res 26(22):22551–22561

Vymazal J (2022) The historical development of constructed wetlands for wastewater treatment. Land 11 (2):174

Wang J, Wang W, Xiong J, Li L, Zhao B, Sohail I, He Z (2021) A constructed wetland system with aquatic macrophytes for cleaning contaminated runoff/storm water from urban area in Florida. J Environ Manage 280:111794

Wang Y, Fukuda H, Zhang P, Wang T, Yang G, Gao W, Lu Y (2022) Urban wetlands as a potential habitat for an endangered aquatic plant, Isoetes sinensis. Glob Ecol Conserv e02012

Wen Z, Song K, Liu G, Shang Y, Fang C, Du J, Lyu L (2019) Quantifying the trophic status of lakes using total light absorption of optically active components. Environ Pollut 245:684–693

Wicaksono A, Wicaksono P (2019) Geometric accuracy assessment for shoreline derived from NDWI, MNDWI, and AWEI transformation on various coastal physical typology in Jepara Regency using Landsat 8 OLI imagery in 2018. Geoplanning J Geomat Plan 6(1):55–72

Wu W, Yang Z, Tian B, Huang Y, Zhou Y, Zhang T (2018) Impacts of coastal reclamation on wetlands: loss, resilience, and sustainable management. Estuar Coast Shelf Sci 210:153–161

Xia F, Liu H, Zhang J, Wang D (2022) Migration characteristics of microplastics based on source-sink investigation in a typical urban wetland. Water Res 118154

Xiao H, Shahab A, Xi B, Chang Q, You S, Li J, Li X (2021) Heavy metal pollution, ecological risk, spatial distribution, and source identification in sediments of the Lijiang River, China. Environ Pollut 269:11618

Xie S, Marzluff JM, Su Y, Wang Y, Meng N, Wu T, Ouyang Z (2022) The role of urban waterbodies in maintaining bird species diversity within built area of Beijing. Sci Total Environ 806:150430

Xu H (2006) Modification of normalised difference water index (NDWI) to enhance open water features in remotely sensed imagery. Int J Remote Sens 27(14): 3025–3033

Xu T, Yang T, Zheng X, Li Z, Qin Y (2022b) Growth limitation status and its role in interpreting chlorophyll a response in large and shallow lakes: a case study in Lake Okeechobee. J Environ Manage 302:114071

Xu Q, Zhou L, Xia S, Zhou J (2022a) Impact of urbanisation intensity on bird diversity in river wetlands around Chaohu Lake, China. Animals 12(4):473

Xue Z, Hou G, Zhang Z, Lyu X, Jiang M, Zou Y, Liu X (2019) Quantifying the cooling-effects of urban and peri-urban wetlands using remote sensing data: case study of cities of Northeast China. Landsc Urban Plan 182:92–100

Yang Z, Wang L, Sun W, Xu W, Tian B, Zhou Y, Chen C (2022) A new adaptive remote sensing extraction algorithm for complex muddy coast waterline. Remote Sens 14(4):861

Yi X, Ning C, Feng S, Gao H, Zhao J, Liao J, Liu S (2022) Urbanization-induced environmental changes strongly affect wetland soil bacterial community composition and diversity. Environ Res Lett 17 (1):014027

Ziaul S, Pal S (2017) Estimating wetland insecurity index for Chatra wetland adjacent English Bazar Municipality of West Bengal. Spat Inf Res 25(6):813–823

Integrated Urban Decarbonization Planning Tool for Global Cities

13

Sunil Bhaskaran, Vladimir Berg, Sanjiv Bhatia, Jayant Kumar, and Andrella Collins

Abstract

Addressing the existential threat of climate change is critical to sustain the earth and prolong human life on it. Recent spate of unprecedented increase in extreme weather events has resulted in damage to lives and property, raising fundamental questions about our level of preparedness to combat them. Urban environments are heterogenous and complex, dominated by buildings responsible for majority of carbon (CO_2) emissions. Cities consist of buildings which release CO_2 directly when they use equipment that relies on combustion. Retrofitting the buildings with carbon-free utilities and infrastructure is the key to achieving lower emissions in cities and urban environments. However, the socio-economic and structural organization of buildings in global cities may present challenges in the implementation of decarbonization plans. The age and design of buildings, electrical capacity, thermal distribution, demographic characteristics, income levels, type of dwelling, and ownership are important spatial variables that must be input and modeled in a geographic information system (GIS) environment for developing an Integrated Urban Decarbonization Planning Tool (IUDPT). Open-source datasets may be utilized to build an IUDPT that could be used in the implementation of decarbonization of cities. The City of New York has embarked on an ambitious program of decarbonizing buildings that aims to reduce CO_2 by 2050. We present a methodology to ingest, analyze, and model a wide range of open-source datasets for developing the IUDPT. The interactive model will enable practitioners and policymakers to achieve a realistic plan for implementing a holistic building decarbonization plan.

S. Bhaskaran (✉) · V. Berg · J. Kumar · A. Collins
BCC Geospatial Center of the CUNY CREST Institute, City University of New York, Bronx, USA
e-mail: Sbhaskaran@gc.cuny.edu

S. Bhatia
Department of Mathematics and Computer Science, University of Missouri-St. Louis, St. Louis, MO, USA
e-mail: sanjiv@umsl.edu

13.1 Introduction

Climate change is caused by the human use of fossil fuels which emits excess carbon and other greenhouse gases into the atmosphere increasing

global temperatures, the severity of weather events, and creating hazardous rising sea levels. Urban areas or cities account for between 71 and 76% of CO_2 emissions from global final energy use and between 67 and 76% of global energy use (IPCC 2015). In New York City, models show that increased storm surges such as the recent flash floods in 2021 will damage infrastructure and threaten the lives of millions of people living in NYC (Garner et al. 2017). Without any change to the way people consume and fuel their lives, climate change will continue to destabilize ecologies and economies in unprecedent ways (Hansen et al. 2013).

Although climate change impacts are already being felt, there are actionable steps that cities can take to reduce carbon emissions and decrease the severity of climate change impacts over time. For example, in Cincinnati, Ohio, there is a pilot program focused on providing energy efficiency upgrades to 65 low-income families to reduce emissions (City of Cincinnati 2020). The city of Copenhagen, Denmark, seeks to be the first carbon–neutral city by 2025, with 10% of CO_2 reduction coming from low energy construction and green retrofitting projects (Gerdes 2013). In a case study, retrofitting the façade of a residential building in Bari, Italy, was shown to improve energy performance indicators as an effective strategy toward mitigating the increased temperatures because of global warming in the summer (Lassandro and Di Turi 2017). In Bolzano, Italy, a smart city urban development project was created to reduce greenhouse gas (GHG) emissions, increase energy savings, and increase renewables by implementing energy efficiency retrofits, creating a smart electricity grid, and upgrading district heating and cooling systems (Hunter et al. 2018).

The New York State Energy Research and Development Authority (NYSERDA), established in 1975, is a public-benefit corporation, which is responsible for reducing carbon emissions. NYSERDA has chosen to take a decarbonization approach to addressing climate change which is a strategy to reduce carbon emissions by transitioning away from gas to electric in powering residential and commercial buildings. Additionally, retrofits need to be implemented to reduce wasteful energy usage in NYC's aging buildings and infrastructure. NYSERDA aims to have 70% of New York's electricity generated by renewable energy sources such as wind and solar by 2030 as directed by The Climate Act. They also seek to modernize the heating and cooling systems of 1–2 million buildings through retrofits such as high-performance building envelopes, smarter building energy controls, more efficient electric water heaters, high-performance windows, and energy-efficient appliances and lighting (NYSERDA 2021).

The main objective of this study is to use a GIS to build an IUPDT. New York City has set a goal to achieve carbon neutrality by 2050 by increasing renewable energy resource use, cutting emissions across building and transportation sectors, and transitioning to low carbon fuels (Mayor's Office of Sustainability, Con Edison, and National Grid 2021). As part of this effort, residential buildings were analyzed by performing a ranked suitability analysis to determine which residential buildings may be most suited for retrofitting to increase the energy efficiency and sustainability of the buildings. In the suitability analysis, we considered two primary factors: year of construction and population density within buildings. Supplementary demographic layers for race and income were also created to provide more context and informed decision-making.

Geographic Information Systems (GIS) are often used to analyze spatial patterns in cities to inform and assist decision-makers in implementing climate change adaptation strategies and reducing the role that cities have in increasing climate change. In Okutama-machi, Tokyo, Japan, GIS is being used to assess climate change threats so that local governments can take measures to target areas which are most vulnerable to climatic destabilization (Bai et al. 2014). In Oslo, Norway, the lack of environmental services within the city was geospatially analyzed to determine the best locations to prioritize for

green roofing projects (Venter et al. 2021). A Heat Exposure Indicator was developed using GIS for Athens, Greece, to measure the hottest areas within a city to assess climate change vulnerabilities since microclimates created by built-up areas can vary (Agathangelidis et al. 2019). Garguilo et al. (2020) developed a GIS decision support tool for decision-making by creating a 'Coastal Resilience Index', Urban Coastal Units, and Urban Adaptation Actions to create a continuous raster data set which can reveal the best approach for the implementation of adaptation measures for coastal communities. There are also GIS models for rainwater changes due to climate change for water management within the city of Melbourne, Australia (Kunapo et al. 2018). In Maricopa County, Arizona, GIS models were created to assess heat-related deaths to various heat factors due to microclimates within the county, so that decision-makers can mitigate future deaths by targeting the communities most vulnerable to increased extreme heat events caused by climate change (Harlan et al. 2013).

13.2 Study Area

The study area for this project is New York City, one of the largest and most ethnically diverse cities in the world. It consists of 5 boroughs (Manhattan, Bronx, Staten Island, Queens, and Brooklyn) (Fig. 13.1). In 2020, 8.8 million people were recorded as being residents of New York City in the decennial census. NYC also has some of the oldest buildings and infrastructure in the United States. 64.5% of residential buildings in NYC are built prior to 1945 (Table 13.1).

This presents many challenges to retrofitting buildings, since the infrastructure associated with the buildings is also outdated and requires changes. This is also complicated by the fact that population density in NYC is high making it difficult to implement retrofits since a large number of residents may need to be evacuated or relocated which also depends on the time for completing the retrofits. The varying income levels and income inequality in NYC pose challenges as low-income residents may have to sacrifice more during the retrofit. Higher-income

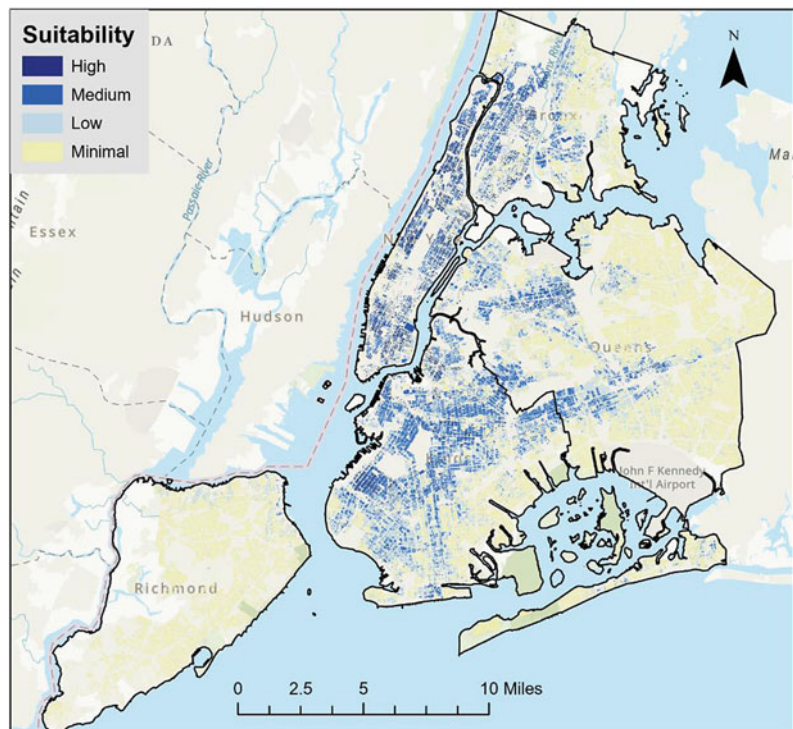**Fig. 13.1** Study area: the five New York City boroughs with the ranked suitability analysis

Table 13.1 Building age, NYC

Year built	Percentage (%)
1920 or earlier	29.18
1921 to 1945	35.31
1946 to 1980	22.06
1981 to present	13.44

Source Data extracted from Map PLUTO layer

neighborhoods tend to be in Manhattan, Queens, and Staten Island, whereas lower-income neighborhoods tend to be in Bronx and Brooklyn. New York City is racially one of the most diverse cities in the world often referred to as a melting pot, and there are historical legacies of biased policies that impact the living conditions of primarily Black and Hispanic neighborhoods. The combined influence of race, income, and population density plays a crucial role in prioritizing and planning a phase-wise approach to retrofitting buildings. A rank suitability analysis was performed by using the socio-economic variables to map the most suitable and preferred locations for retrofitting (Fig. 13.1).

13.3 Data Types and Methods

The data sources used for the project came from the New York City government open-source project website and the United States Census website (Table 13.2).

Open-source data sources were used from the City of New York's government website (NYC. GOV) and from the United States Census Bureau. The City of New York has an open-source portal for vector, raster, and continuous geospatial datasets covering different themes. The open-source project facilitates easy access to the public through an interactive spatially indexed online portal. The study used data from

the Map Pluto which represents a compilation of data from various government agencies throughout the City of New York. The underlying geography for Map Pluto is derived from the Tax Lot Polygon feature class that is part of the Department of Finance's Digital Tax Map (DTM). The tax lots have been clipped to the shoreline, as defined by NYC Map planimetric features. The attribute information is from the Department of City Planning's PLUTO data. The attribute data pertains to tax lot and building characteristics and geographic, political, and administrative information for each tax lot in New York City. The Tax Lot Polygon feature class and PLUTO are derived from different sources. As a result, some PLUTO records do not have a corresponding tax lot in the Tax Lot polygon feature class at the time of release. These records are included in a separate non-geographic PLUTO Only table, and there are data sets such as MapPLUTO which combines an assortment of data across multiple agencies and sources to form a highly detailed data layer that contains information on tax lot characteristics, building characteristics, land use, geography, and political and administrative districts. The data for MapPLUTO is drawn from the department of finance, the department of city planning, the department of parks and recreation, and the landmarks preservation commission and is often combined to form a more consolidated and comprehensive data.

Table 13.2 Data sources for the ranked suitability analysis

Data sources	Author	Data sets
NYC.gov	The City of New York	• MapPLUTO • Community Districts
Census.gov	United States Census Bureau	• Census data on race and income • Census Tiger/Line Shapefiles

The United States Census Bureau, officially the Bureau of the Census, is a principal agency of the U.S. Federal Statistical System, responsible for producing data about the American people and economy. The decennial census data is collected by a questionnaire every 10 years and is based on questions related to age, sex, race, and owner/renter status. For this project, we acquired data about race from the 2020 decennial census survey. The American Community Survey is another important source of data collection that is based on questions related to education, employment, Internet access, income, and transportation. This project utilized 2019 income data that was collected through this survey. Surveys conducted by the US Census Bureau are considered the authoritative data source for population demographics and are used by governing bodies to make decisions and allocate resources to the surveyed communities.

Open-source data has made it possible to visualize spatial and temporal patterns in urban environments, and they are used in developing informed decisions. In this project, we used NYC open-source data to visualize, analyze, and develop an integrated urban decarbonization implementation plan that is holistic and not merely driven by random action plans. However, open-source data may lack metadata which might question its accuracy and quality which may have to be cross-checked and vetted. To ensure that the data represented is viable, 15 points were randomly created across NYC (three points per borough) to assess whether the data that was being visualized and contained in the attribute tables was accurate based on third-party sources.

13.3.1 Vetting the Data for Accuracy

Points were created using the Create Random Points tool with the setting that points have to be at least 1 km apart to get points to be in different neighborhoods. Buildings were chosen that were located closest to the vetting point. Points were validated using reliable public and free-to-use private data repositories. Through cross-examining these different website sources and the data displayed in ArcGIS, all points were accurate in terms of the age of the buildings and the type of building that is located at each site. Census data was also used to validate the total population counts, race, and income level within the census data files. A degree of confidence was assigned to each point based on the availability of data and how well the data aligned with the open-source data. Finally, the data was visualized in ArcGIS (Table 13.3).

The vetting process can be used for any open-source data provided the reference data is reliable. Open-source data can be very effective after vetting because it increases the confidence level of the data sets and improves the policymaking and planning process substantially. All points assessed had a high degree of confidence in terms of the accuracy of the data.

13.3.2 Data Processing and Layer Creation Workflow

The process for building the suitability analysis model involved extraction of key variables from the MapPLUTO database. The following variables were considered important for the study: land use (40%), the age of buildings (30%), the area of the buildings, population density (20%), and other relevant data (10%). The land use variable enabled us to segregate residential use from others, the age of buildings was considered for prioritizing the implementation strategy by age while the area of buildings was used to determine the density of population for a specific building square footage (Fig. 13.2).

The residential land use consisted of one/two-family buildings, multifamily walk-up buildings, multifamily elevator buildings, and mixed residential + commercial buildings. Additionally, fields that were irrelevant to the analysis were masked off and the following fields were retained —'Borough', 'Address', 'LandUse', 'LotArea',

Table 13.3 Random points vetted for accuracy

Neighborhood	Address referenced	Land use category	Income predominance	Race predominance	Race census confirmation	Notes	Degree of confidence
Washington Heights	666 West 162 Street	Mixed residential and commercial buildings	150,000 and Greater (25.25%)	Some other (52.84%)	Some other	Rentals ranging from 1500 to 2200 in the past 3 years. Property sold for 13 million in 2015. Contains a Medical Office (Google Maps Confirmation Street maps August 2019)	9
SoHo-Cast Iron Historic District	84 Mercer Street	Multi-family elevator buildings	150,000 and Greater (59.47%)	White (76.04%)	White	Contains a luxury clothing store (Google Maps confirmation street maps Imagery from August 2021)	10
Manhattan	Park	Multi-family walk-up	25,000 to 35,000 (30.8%)	White (39.48%)	White	471 Central Park is a rental housing unit with monthly rents between $1667 and $3400 in the past year. Residential Building (Google Maps confirmation)	
Valley Pelham Pkwy	471 Central 2041 Holland Ave	Buildings multi-family elevator	45,000 to 60,000 (22.52%)	Some other (28.89%)	Some other	Street maps Imagery Building sold for 16.1 million in 2007	9.8
Riverdale	5612 Sylvan Ave	One- and two-family buildings	150,000 and Greater (37.67%)	White (40.08%)	White	There is a range of building types and values within this census block. House sold for $780,000 in 2015. (Google Maps confirmation street maps Imagery from July 2018)	9
West Farms	1932 Crotona Pkwy	Multi-family elevator buildings	15,000 to 25,000 (26.94%)	Some other (37.76%)	Some other	42 Residential Unit Building. No information on unit values found. (Google Maps confirmation street maps imagery from July 2018)	8
Sunset Park	441 52 St	One and two family	60,000 to 100,000 (25.00%)	Some other (42.26%)	Some other	2-unit residential building. No information on units found	9
East New York	911 Erskine St	Mixed residential and commercial buildings	60,000 to 100,000 (23.11%)	Black or African American (74.88%)	Black or African American	New Building Construction. Properties not as of yet for sale. Google Maps does not contain an image of the property as of January	9
Prospect		Multi-Family Walk-Up	100,000 to 150,000 (29.06%)			Rental units ranging from 2200 to 3800 in the past 3 years. (Google Maps confirmation street maps	

(continued)

Table 13.3 (continued)

Neighborhood	Address referenced	Land use category	Income predominance	Race predominance	Race census confirmation	Notes	Degree of confidence
Heights	428 Park Pl	Buildings		White (53.40%)	White	Imagery from May 2021)	10
Travis-Chelsea	157 Cannon Ave	One- and two-family buildings	45,000 to 60,000 (30.03%)	White (67.16%)	White	Purchased for $625,000 in 2017. (Google Maps confirmation street maps Imagery from October 2021)	10
		One and two family	150,000 and Greater			Purchased for $830,000 in 2021. (Google Maps confirmation street	
Tottenville	5391 Arthur Kill R	Buildings	(24.48%)	White (74.08%)	White	maps imagery from October 2019)	10
Shore Acres	4 Fingerboard Rd	One- and two-family buildings	100,000 to 150,000 (24.27%)	White (48.73%)	White	Single-family Home. Google Maps confirmation street maps Imagery from July 2018	10
Jamaica	111–50 170 St	One- and two-family buildings	15,000 to 25,000 (33.07%)	Black or African American (71.65%)	Black or African American	Single-family Home. Google Maps confirmation street maps Imagery from August 2019	10
Bay Terrace	215–49: 26 Ave	One and two family	45,000 to 60,000 (24.02%)	White (62.15%)	White	No Google Street Maps for this building	9
Glendale	78–31 73 Pl	Multi-family walk-up buildings	60,000 to 100,000 (27.43%)	White (71.08%)	White	3-family home. (Google Maps confirmation street maps imagery from July 2021)	10
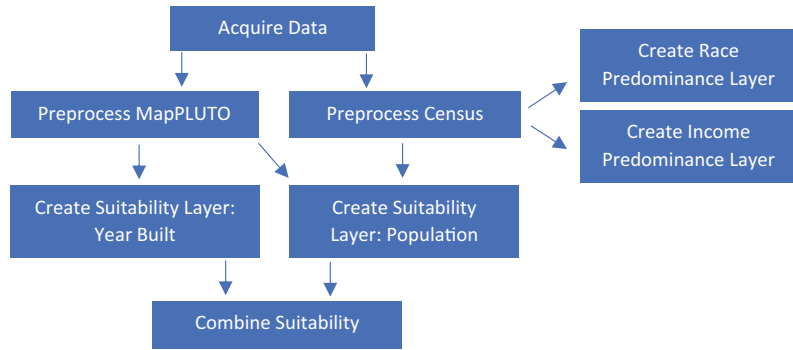
'BldgArea', 'ComArea', 'ResArea', 'OfficeArea', 'RetailArea', 'YearBuilt', and 'Landmark'. Historical buildings were not included in the suitability analysis model since they are protected and preserved by federal funding. Some of the tax lots had erroneous data that was excluded from the analysis by writing a code to eliminate buildings older than 1000 years which were unrealistic. To create the population density, the MapPLUTO layer had to be combined with the total population data extracted from census data. Population data created earlier from the race census data was joined to the 2021 Tiger/LINE shapefile. Using the 'summarize within' tool, the census data layer was combined with the Pluto residential tax lots, and these tax lots were summarized to get the sum of the building area in square feet. Square feet of the building area was used instead of the standard population per square mile because New York City is very densely populated and having a smaller unit of measure that considers the size of the buildings in an area is a much more accurate measurement.

13.3.3 Suitability Analysis Model

Prioritizing the decarbonization implementation plan must be based on a holistic plan that should include variables like age of buildings and population density since these variables correlate to higher levels of carbon emissions. Older buildings tend to have less electrical utilities and lower energy efficiency in comparison with newer

buildings. Areas with a higher population density will have more people using energy and emitting a higher concentration of CO_2 than areas with fewer people and a smaller population density. In combination, areas with high population density and old buildings will be most suitable for retrofitting projects.

The suitability analysis model (SAM) was built on the basis of these two major criteria with equal weight for the age of buildings (50%) and population density (50%). These variables were aggregated at the tax lot spatial unit. It was assumed that older buildings were not energy efficient compared to newer ones since their thermal distribution and electrical capacity were not known. Older buildings generally do not have the infrastructure for any electrical updates which will challenge the decarbonization action plan. Therefore, we assigned a maximum weight to older buildings and prioritized them for the decarbonization plan. Since older buildings emit more CO_2, it is imperative to minimize the impacts immediately.

New York City is one of the most densely populated cities in the US, with a population density of about 27,000 people per square mile. Areas that have a higher population density must be prioritized for decarbonization because the amount of carbon emissions from those locations would be higher than low-density areas. The emphasis must be placed on reducing the carbon emissions rather than prolonging it.

The SAM model ingested the relevant variables, and the ranks were determined by the count of tax lots under each rank. Ranks were

determined through an iterative process of first estimating an approximate ranking scheme, and then adjusting the values for each rank until there was a uniform distribution. This was done by creating a new field, running the calculate field tool with the ranking scheme, and then using the statistics calculated by the Summary Statistics tool within ArcGIS, which produces an output table with the sum, mean, maximum, range, standard deviation, and other statistical values. The suitability field was then calculated again until there was a more even spread of values with a standard deviation of approximately 1.0. The calculate field tool modifies a field based on an expression using Python code (Figs. 13.3 and 13.4).

The values that ensured a standard deviation near 1.0 for the 'Year Built' and 'Population Density' suitability layers were as follows (Table 13.4).

Once the suitability layers were created, they were combined using the 'Identity' Tool (Fig. 13.5).

The identity tool computes a geometric intersection of two features preserving the portions that overlap. Using this method, the Ranks for 'Year Built' and 'Population Density' are attributed to the same polygons (tax lots). After executing the identity tool, rows that had a value of 0 for any of the ranks were deleted, since these were extraneous polygons created from merging two different shaped polygon features (tax lots and census block groups). A new field was created to get the total ranked suitability and calculated by adding the two ranked fields multiplied by a weight of 0.5 to give an equal weight of 50% for each rank.
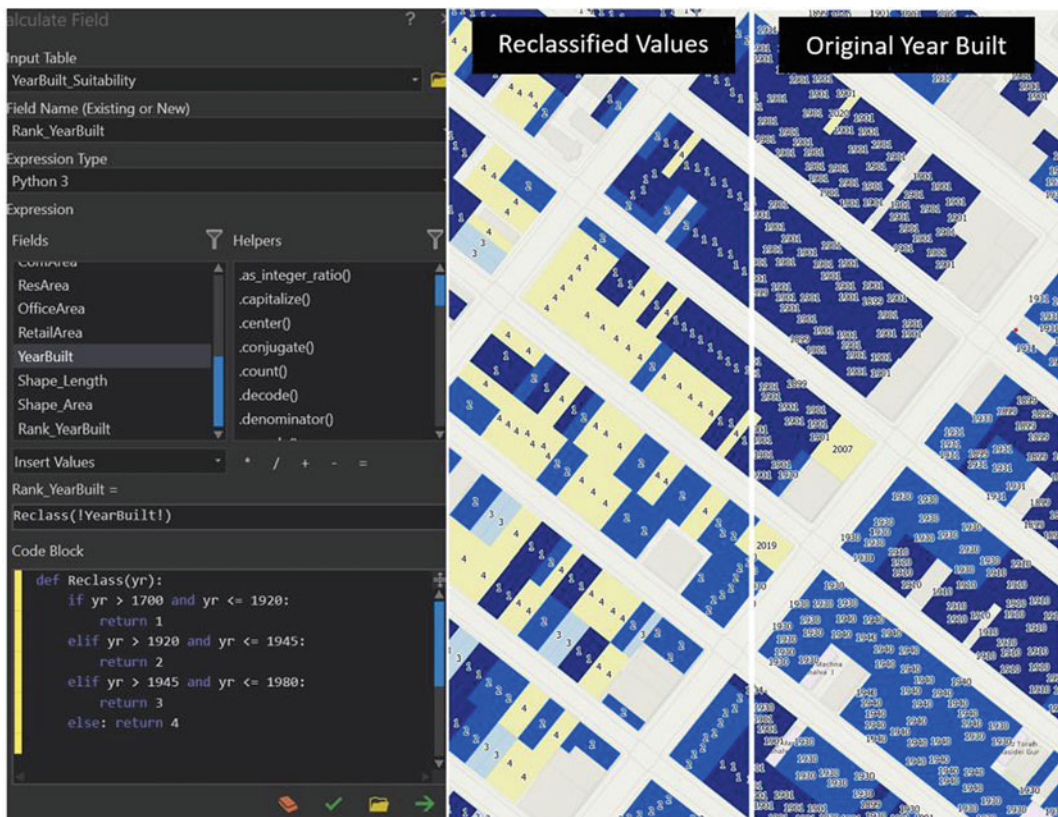

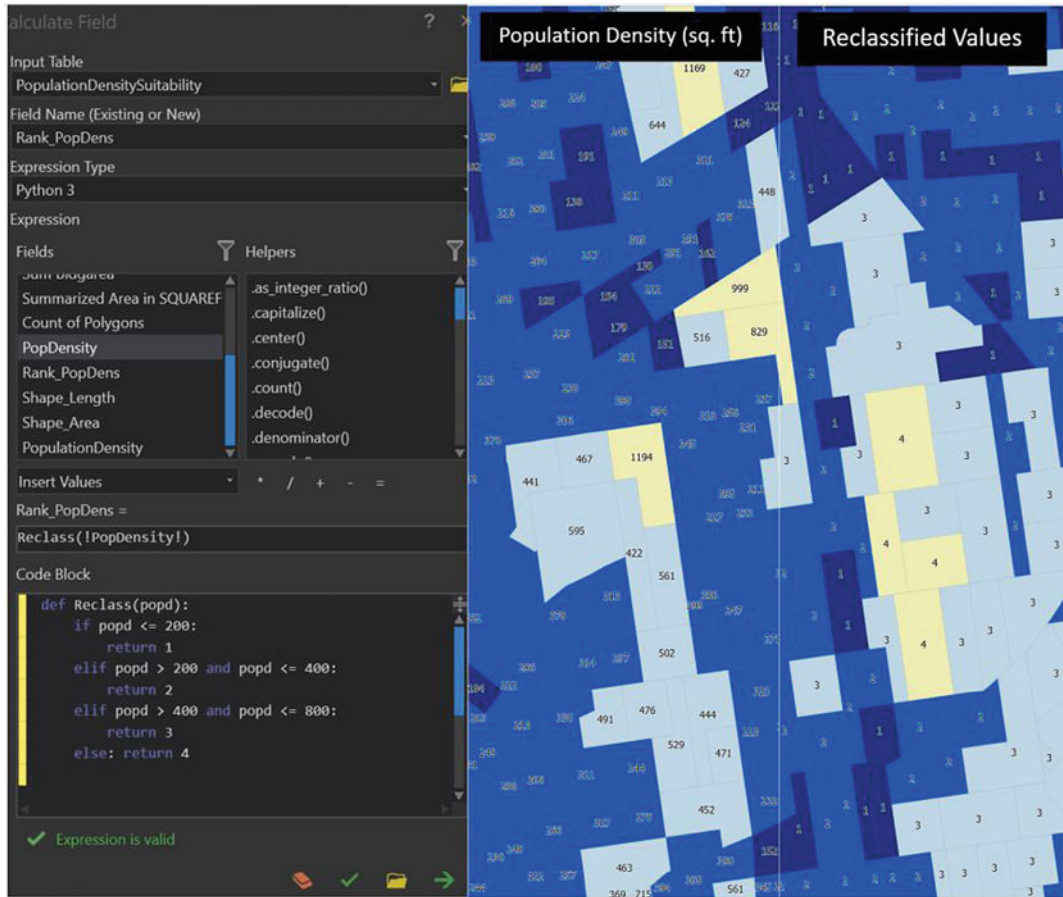**Fig. 13.3** Calculate field inputs for year-built suitability layer and reclassified values versus year-built values

Fig. 13.4 Calculate field inputs for population density suitability layer and reclassified values versus population density values

Table 13.4 Suitability ranking scheme for year built and population density

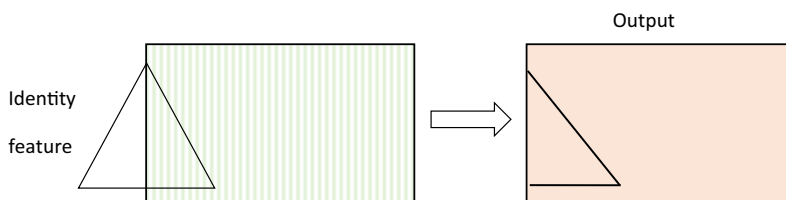| Suitability Rank	Year Built The year buildings were built in a tax lot Weight: 50% *Source: MapPLUTO*	Population Density (Building SqFt/ Person) *The population density of a census block group divided by the building area of residential buildings* Weight: 50% *Source: BldgArea (MapPLUTO) Divided by population total (Census Data)*
1—High Suitability	1920 or earlier	200 or below
2—Medium Suitability	1921 to 1945	201 to 400
3—Low Suitability	1946 to 1980	401 to 800
4—Minimal Suitability	1981 to present	801 or above

Fig. 13.5 Identity tool combines layers and attribute tables

13.3.3.1 Race and Income Supplementary Layers

The ranked suitability analysis incorporated physical features of the year that buildings were built, and the population statistics feature of population density. The qualitative features of race and income however also play an important role in the implementation of a retrofitting strategy. Race is important to consider since many minority communities historically faced discriminatory policies which led to worse economic, housing, and living conditions. Therefore, an additional layer is necessary to assess where these communities are and can be used to specifically serve certain communities.

To create the race predominance map, in ArcGIS Pro, the Race data was joined to the 2021 Tiger/Line Shapefile. This shapefile was then zipped and exported into ArcGIS Online (AGOL). AGOL offers visualization options that are built into AGOL that are not available in ArcGIS Pro. One of these visualizations is 'Predominance', a powerful visualization tool that shows which field among a selected group of fields is predominant and to what degree that field predominates. Some of the racial categories had no predominance and were removed from the final visualization. The predominance symbology was applied to the race data and then exported back into ArcGIS Pro. A few extraneous census block groups were removed that erroneously had a few people located in parks or cemeteries. The income predominance layer was created in a similar fashion. Income is very important because income inequality is a large issue in New York City and retrofitting buildings in poorer neighborhoods would require financial assistance and improve living conditions for those with lower wages. The income data was joined to the 2019 Tiger/Line Shapefile, zipped, and exported into AGOL. Predominance symbology was then applied, and the income layer was exported back into ArcGIS Pro. The predominance field was reclassified to 1–8 (1 being lowest income, 8 being highest income), and then, the symbology was changed to be a graduated symbol, since income is on a scale and not a unique value like race.

13.3.3.2 A Geospatial Design for Decarbonization

Ranked Suitability Analysis (RSA), also referred to as Multi-Criteria Suitability Analysis, is best used when the objective of the analysis is to determine what land areas are best suited based on the most essential factors relative to other land areas. It can incorporate multiple considerations whereas usually maps can only display one variable at a time for each layer. Suitability Analyses merge layers together to produce a composite vector layer. Ranked Suitability Analysis (Relative) is more dynamic than a Boolean (Absolute) analysis which chooses only areas that match all suitability criteria. RSA can show areas on a scale of suitability, showing areas that are most and least suitable rather than a simple 'yes' or 'no' in terms of suitability (Vavatsikos et al. 2020). This allows RSA to have a dynamism and nuance to evaluate each given land area based on the criteria. RSA also allows for a weighting system, to emphasize factors that are more or less important based on the authors' discretion. For this reason, RSA is the right approach for choosing residential areas that are viable candidates for retrofits to decarbonize NYC since RSA can highlight most

suited communities and allows the map end user to make the final decision based on all of the factors (Virta 2021). The end user may want to retrofit in areas that have a medium suitability or even a low suitability based on additional factors, although this project serves the purpose of highlighting and directing attention toward residential tax lots which have the highest suitability based on important factors such as the year that the building is built, the population density of the area, the vacancy percentage, and the proximity to rehousing buildings.

Additionally, income and race are added as supplementary layers which can inform the end users' decision-making process by contextualizing highly suitable areas with vital race and income data. Vector data was chosen for this analysis to target discrete buildings with certain characteristics rather than covering the entire area of New York City, allowing for a greater degree of specificity. This also allowed for data to be preserved in tax lots and has the capability to be queried for high and low suitability as well as tax lot measurements, land use types, census Geo Ids, and addresses. This makes it easy to locate and gather additional information from the dataset as opposed to a raster-based suitability

analysis which would generalize areas and would not be useable in this way. Suitability layers were chosen based on factors that implicate carbon emissions on a scale of higher and lower values, namely the age of buildings and population density. Race and income were created as supplementary layers and not incorporated into the ranked suitability analysis because there is no clear determination for whether a certain race or income bracket is more or less suitable for the decarbonization project. This data is used to contextualize the level of income and race predominance in each census block group so that decision-makers have a better basis for the approach to take in each unique demographic makeup. Race and income layers can also be used as a base layer by placing either race or income under the ranked suitability analysis (Figs. 13.6 and 13.7).

With these additional layers, decision-makers can cross reference income and race prior to deciding the highly suitable areas to prioritize based on existing socio-economic factors. This allows for a greater sensitivity to race and income issues which may be key in expediting retrofitting work since policies and funding are often predicated on race and income.

Fig. 13.6 Race predominance as a base layer for the ranked suitability analysis

Fig. 13.7 Income predominance as a base layer for the ranked suitability analysis

13.4 Results and Discussion

Based on the MapPLUTO dataset, 82.78% of tax lots contain residential buildings or mixed residential and commercial units. This suitability ranking and weighting scheme produced the following counts for each category (Table 13.5).

Ranked suitability categories were determined by the *Jenks natural breaks classification method* (Jenks, 1967) based on natural groupings inherent in the data (ESRI, 2021) (ESRI, 2022). With this RSA, we were able to identify and highlight an estimated 6.48% of residential building areas that are most suitable for a retrofitting project based on the criteria of the population density and the age of buildings. These buildings should be considered first in terms of a decarbonization retrofitting project since they are most suited for this project based on these factors. For each borough, 5 communities were identified that had

the highest numbers of medium-to-high suitability tax lots and are labeled on their respective maps. These communities are highlighted to show the location of the most suitable buildings, although suitability should still be considered at the tax lot level, and each area with high suitability should be considered as equal regardless of community in terms of this analysis (Fig. 13.8).

13.4.1 Race and Income Results

New York City is a racially diverse city made up primarily of White, Black, or African American, Hispanic or Latino, and Asian racial groupings. NYC is known for its history of immigration and celebrates diversity, while acknowledging a history of racial segregation. Observing the racial predominance map, we can see that many parts of NYC still have a high percentage of only one

Table 13.5 Tax lot polygons percentages based on ranked suitability

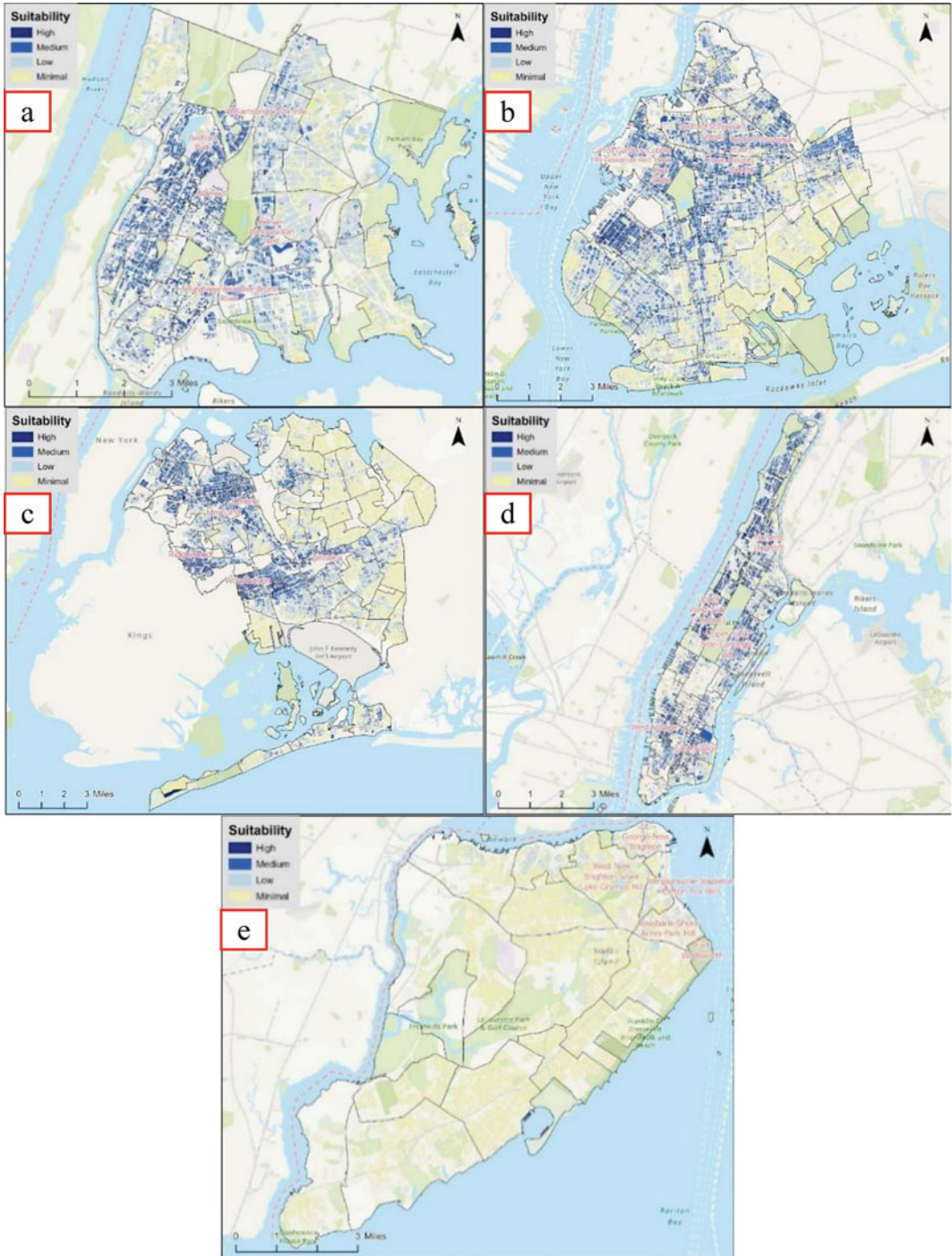| Suitability ranking	Ranked suitability	Polygon counts	Percentage (%)
High	1.00	49,561	6.48
Medium	1.01 to 1.50	134,430	17.56
Low	1.51 to 2.00	146,057	19.09
Minimal	2.01 to 4.00	435,228	56.87
Totals	–	765,276	100

Fig. 13.8 **a** Bronx, **b** Brooklyn RSA, **c** Queens RSA, **d** Manhattan RSA, **e** Staten Island RSA

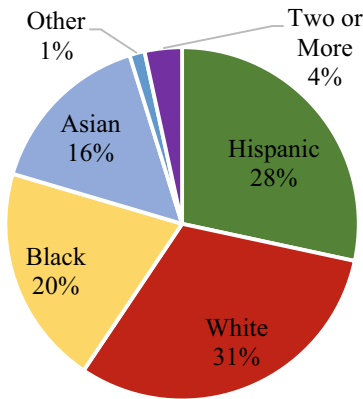## NYC Racial Composition 2020

Fig. 13.9 Racial makeup of NYC in 2020

racial group; however, there are parts of NYC that have a more complex racial makeup. From the 2020 census data, percentages of race were derived from the total population (Figs. 13.9 and 13.10).

In the race and income predominance maps, bolder colors that appear more prominent

represent the strength of the predominance. This effect was created by applying the predominance percentage to the degree of transparency for the layer. Areas without a color are census block groups where people do not reside such as airports, parks, and cemeteries. Income is another category that is vitally important to the implementation of a retrofitting project to decarbonize NYC (Fig. 13.11).

Lower-income areas would be served to receive retrofits as this would improve the quality of housing in low-income neighborhoods and reduce energy costs, directly assisting low-income households in reducing bills. Additionally, any plan to rehouse families that need to be temporarily relocated would likely receive a stipend or some form of compensation which would be much more impactful for low-income people than it would be for families in higher-income brackets. Additionally, higher-income neighborhoods may be more resistant to retrofitting projects given that the monetary benefit they would receive from it would be relatively insignificant.

Fig. 13.10 Race predominance in 2020 for each Census Block Group in New York City
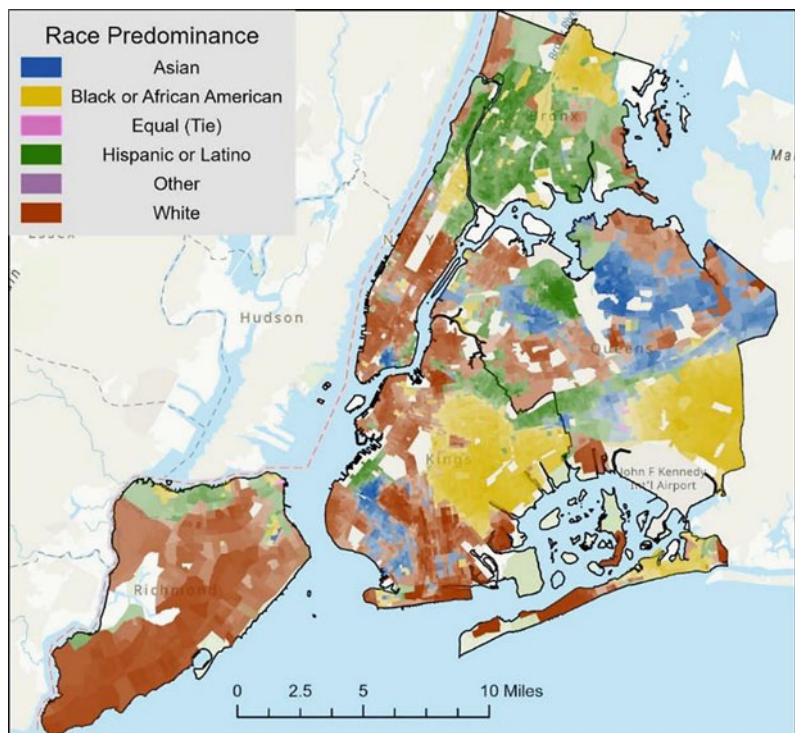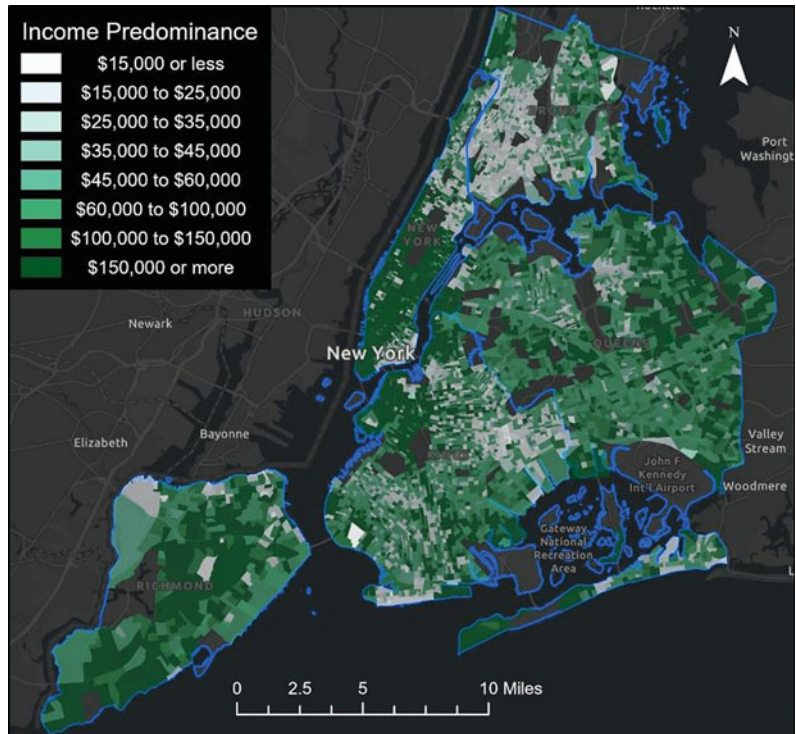
Fig. 13.11 Income predominance in 2019 for each Census Block Group in New York City

Like race, the income dynamics are complex in NYC. There are clear distinctions that can be drawn such as that residents of Manhattan and Staten Island on average have much higher incomes than those in Bronx, Queens, and Brooklyn. However, communities of varying income are much more intermixed in census block groups. This presents a challenge when choosing which areas are more suitable for a retrofit project based on income since there are many areas where the highest and lowest incomes are located within the same community. This may be in part due to gentrification in some communities such as South Bronx. Based on these factors, income is presented as a supplemental map to contextualize broader patterns of income distribution within New York City rather than being a suitability factor in the ranked suitability analysis. Supplemental demographic data should be considered when deciding what buildings will be retrofitted in conjunction to the SAM. We suggest prioritizing historically underprivileged racial groups for retrofitting improvements such as Hispanic, Black, and

Asian. We also recommend initiating retrofits in communities with lower incomes as these communities would benefit from the reduced energy use cost and home improvement features.

13.4.2 Supplemental Analysis of Existing Grant Funding Initiatives

GIS-based methods can be used to assess areas that could be eligible for existing grant funding sources. During the creation of this study, the Governor of New York Kathy Hochul announced $25 million in grants to help low- and moderate-income homeowners make critical repairs and accessibility modifications to their homes. This is in addition to a plan to achieve 2 million climate-friendly homes by 2030. The requirements for the grants include residential homes that have less than 7 floors and a *low-to-moderate* income. This initiative is important to outline and analyze because it is directly relevant to the decarbonization implementation strategy to

show existing initiatives in comparison with the decarbonization strategy delineated in this study. To visualize this funding initiative, the tax lot data from the MapPLUTO dataset was taken that had a building class of one- and two-family dwellings, and a floor number of 7 or below. Given that the income levels vary, a median household income for New York City may not be sufficient to analyze which housing locations could receive funding. The 2019 income census data was assessed to determine what the income profile appears to be in each borough. A ratio was developed to determine whether census block groups had a greater amount of people below the approximate median income bracket. Based on the income 2019 census data, Manhattan, Staten Island, and Queens had a greater percentage of households that made above $60,000, whereas Brooklyn and Bronx had a greater percentage of households that made below $60,000. This indicates that the median household income for the boroughs with higher incomes is larger than $60,000, so the next income bracket ($60,000-$100,000) is included in which census block groups could be eligible

for the grant funding. For Bronx and Brooklyn, eligible census block groups were calculated based on the sum of households that have an income below $60,000 divided by the sum of households with incomes above $60,000. For Manhattan, Queens, and Staten Island, eligible census block groups were calculated based on the sum of households that have an income below $100,000 divided by the sum of households with incomes above $100,000.

13.4.2.1 The Bronx Income Breakdown and Potential Homes Eligible for Grant Funding

The income data shows that Bronx has the highest percentage of people earning less than $15,000 a month (22.64%) (Table 13.6). 65.54% of households in the Bronx earn less than $60,000 which is the lowest of all the boroughs (Fig. 13.12).

Districts that have the highest number of potentially eligible tax lots (and homes within those tax lots) are Williamsbridge-Olinville (1814), Soundview-Bruckner-Bronx River (1129), and Soundview-Clason Point (955) (Fig. 13.13).

Table 13.6 Bronx 2019 income profile

Income category	Total	Percent of total
14,999 or less	114,051	22.64
15,000 to 25,000	64,226	12.75
25,001 to 35,000	50,954	10.11
35,001 to 45,000	45,104	8.95
45,001 to 60,000	55,869	11.09
60,001 to 100,000	91,117	18.08
100,001 to 150,000	48,914	9.71
150,001 or More	33,594	6.67
Total	503,829	100.00
Income evaluation		
$45,000 or less		54.45%
$60,000 or less		65.54%
$60,001 or more		34.46%
$100,000 or more		16.38%
Median income determination		
$60,000		
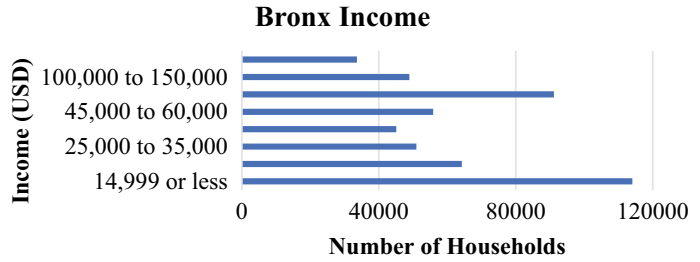
Bronx Income
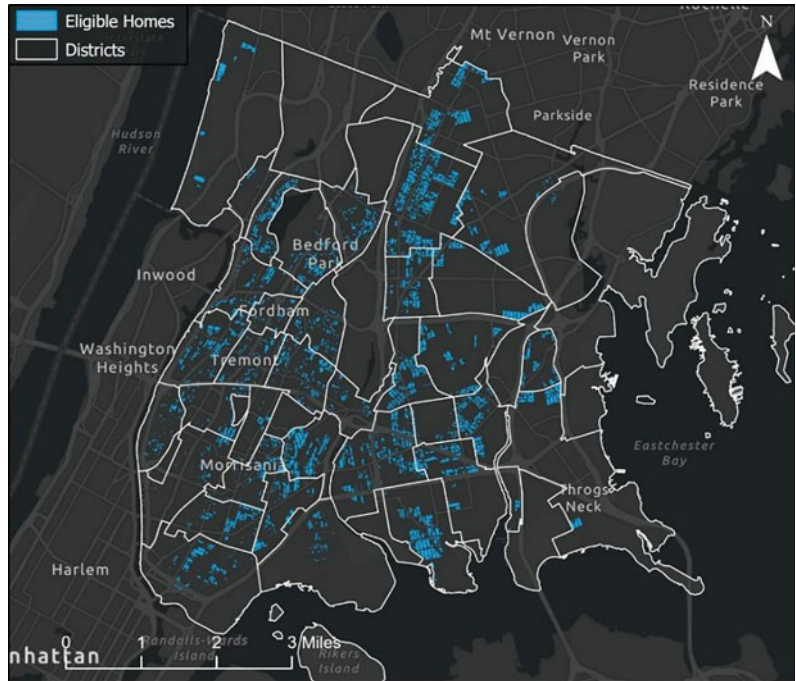
13.4.2.2 Manhattan Income Breakdown and Potential Homes Eligible for Grant Funding

Manhattan has the highest percentage of households earning $150,000 or more (31.40%). 61.59% of households in Manhattan earn more than $60,000 a year (Table 13.7). Manhattan has primarily middle- to high-income earners based on the income chart (Fig. 13.14).

Observing the map (Fig. 13.15), Manhattan clearly has the least amount of potentially eligible homes for grant funding, which aligns with the data on income. There are still some districts that could be eligible for grant funding. The

districts with the highest amount of tax lots that could be eligible are Hamilton Heights-Sugar Hill (235), Harlem North (228), and Harlem South (191). Manhattan comprised many tall buildings that are over 7 stories tall, which is another explanatory factor for why there are so few eligible areas within Manhattan.
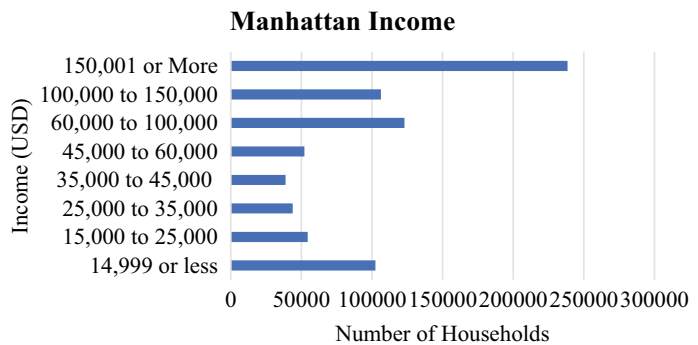
13.4.2.3 Queens Income Breakdown and Potential Homes Eligible for Grant Funding

The income bracket with the highest number of households in Queens is $60,001-$100,000 with 22.83% (Table 13.8). Based on the chart, Queens

Table 13.7 Manhattan 2019 income profile

Income category	Total	Percent of total
$14,999 or less	102,460	13.49
$15,000–$25,000	54,456	7.17
$25,001–$35,000	43,865	5.78
$35,001–$45,000	38,761	5.10
$45,001–$60,000	52,142	6.87
$60,001–$100,000	122,975	16.19
$100,001–$150,000	106,299	14.00
$150,001 or More	238,502	31.40
Total	759,460	100.00
Income evaluation		
$45,000 or less		31.54%
$60,000 or less		38.41%
$60,001 or more		61.59%
$100,000 or more		45.40%
Median income determination		
$100,000		

Fig. 13.14 Manhattan 2019 income chart

has primarily middle- to high-income earners (Fig. 13.16). The districts with the highest number of eligible taxes lots are South Ozone Park (8081), Baisley Park (6836), Queens Village (5658), and St. Albans (5551).

13.4.2.4 Brooklyn Income Breakdown and Potential Homes Eligible for Grant Funding

Although Brooklyn does not have the highest percentage of people earning below $15,000 (15.20%), it does have the highest count of households earning that amount (145,625) (Table 13.9). Brooklyn also has the highest number of households of any borough (958,336). Brooklyn has a population where nearly half (49.89%) of households earn less than $60,000 a year (Fig. 13.17).

The districts with the most potentially eligible tax lots are Bensonhurst (2443), East New York North (2379), Borough Park (2090), and East New York-New Lots (2073) (Fig. 13.18).

Fig. 13.15 Manhattan potential eligible homes for grant funding

Table 13.8 Queens 2019 income profile

Income category	Total	Percent of total
$14,999 or less	74,286	9.59
$15,000–$25,000	62,781	8.11
$25,001–$35,000	64,519	8.33
$35,001–$45,000	60,897	7.86
$45,001–$60,000	81,207	10.48
$60,001–$100,000	176,797	22.83
$100,001–$150,000	130,527	16.85
$150,001 or more	123,551	15.95
Total	774,565	100.00
Income evaluation		
$45,000 or less		33.89%
$60,000 or less		44.37%
$60,001 or more		55.63%
$100,000 or more		32.80%
Median income determination		
$100,000		

Fig. 13.16 Queens 2019 income chart
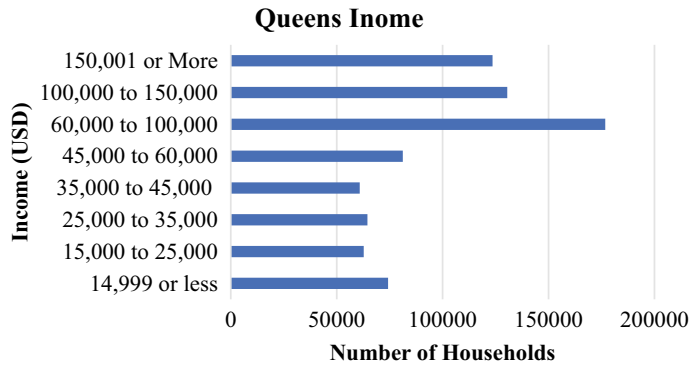
Table 13.9 Brooklyn 2019 income profile

Income category	Total	Percent of total
$14,999 or less	145,625	15.20
$15,000–$25,000	92,341	9.64
$25,001–$35,000	79,502	8.30
$35,001–$45,000	70,653	7.37
$45,001–$60,000	89,949	9.39
$60,001–$100,000	182,975	19.09
$100,001–$150,000	134,667	14.05
$150,001 or more	162,624	16.97
Total	958,336	100.00
Income evaluation		
$45,000 or less		40.50%
$60,000 or less		49.89%
$60,001 or more		50.11%
$100,000 or more		31.02%
Median income determination		
$60,000		

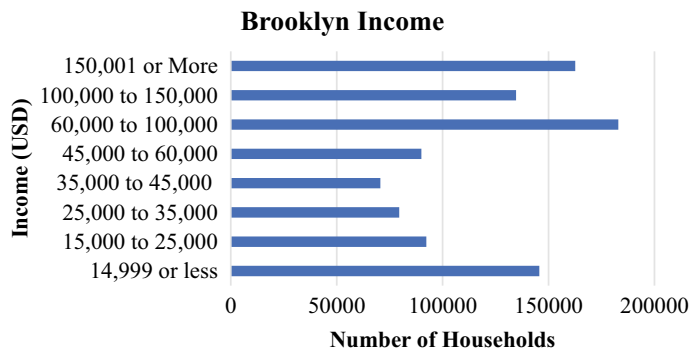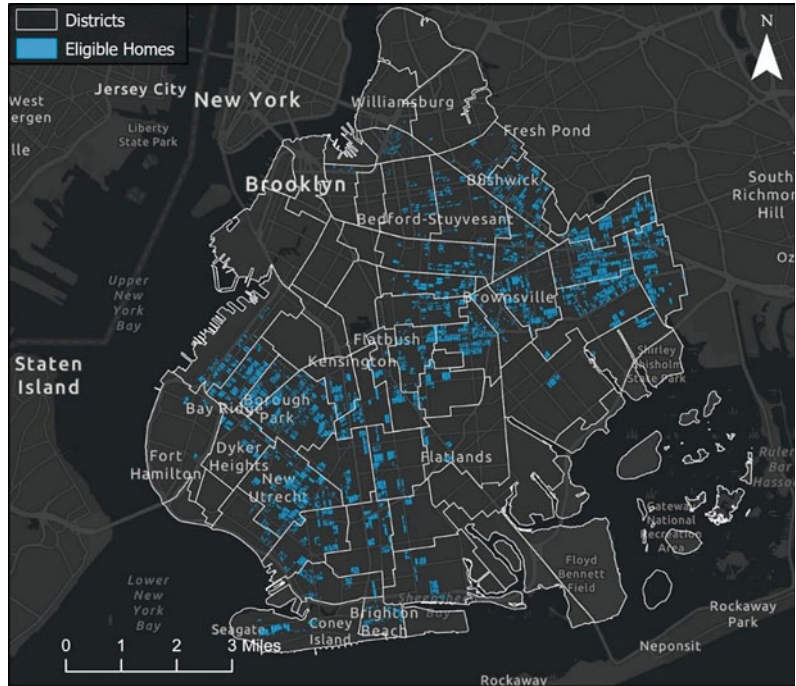**Fig. 13.17** Brooklyn 2019 income chart

Fig. 13.18 Brooklyn potential eligible homes for grant funding

13.4.2.5 Staten Island Income Breakdown and Potential Homes Eligible for Grant Funding

Staten Island has the least number of households by a large margin (166,246). They also have a high percentage of people that earn more than $60,000 a year (62.01%), and the largest income bracket for Staten Island is households that earn more than $150,001 a year (22.79%)

(Fig. 13.19). Given that the median income for Staten Island is closer to $100,000 than $60,000, there still is a large number of tax lots that could be eligible for funding (Table 13.10).

The districts with the most tax lots that are potentially eligible are Mariner's Harbour-Arlington-Graniteville (3895), New Dorp-Midland Beach (3512), and Oakwood-Richmond town (3255) (Fig. 13.20).

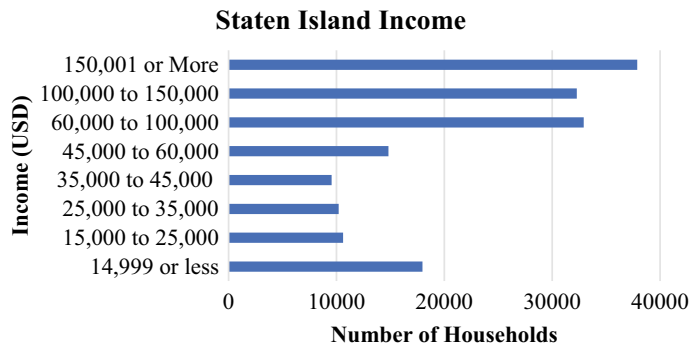**Fig. 13.19** Staten Island 2019 income chart

Table 13.10 Staten Island 2019 income profile

Income category	Total	Percent of total
$14,999 or less	17,973	10.81
$15,000–$25,000	10,610	6.38
$25,001–$35,000	10,209	6.14
$35,001–$45,000	9546	5.74
$45,001–$60,000	14,825	8.92
$60,001–$100,000	32,921	19.80
$100,001–$150,000	32,279	19.42
$150,001 or More	37,883	22.79
Total	166,246	100.00
Income evaluation		
$45,000 or less		29.08%
$60,000 or less		37.99%
$60,001 or more		62.01%
$100,000 or more		42.20%
Median income determination		
$100,000		

Fig. 13.20 Staten Island potential eligible homes for grant funding
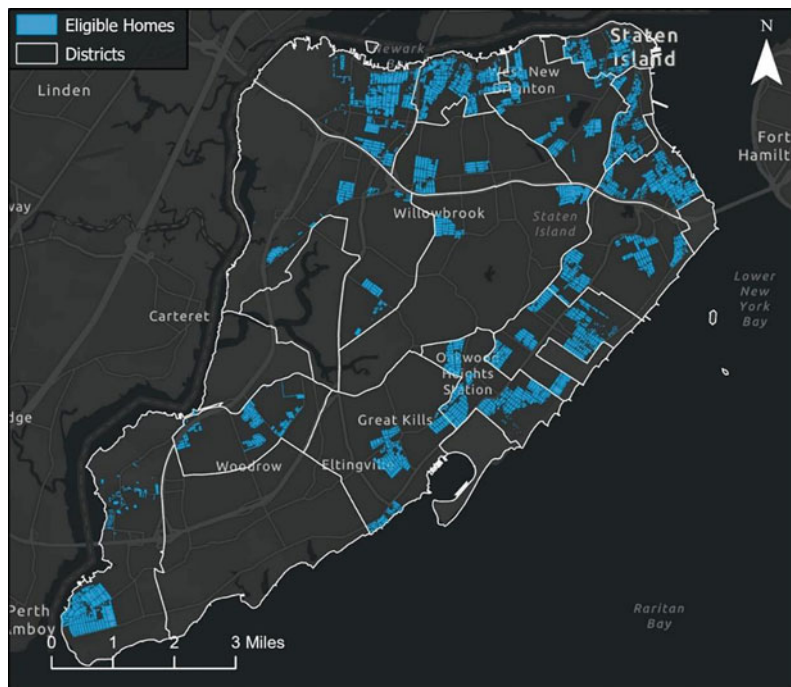
13.5   Conclusion

Through the ranked suitability analysis, highly suitable areas were emphasized as priorities at the tax lot level based on the factors of the age of buildings and population density of each area. This reduced the number of residential buildings to prioritize for retrofitting to 8.23% of buildings being highly suitable and an additional 24% having a medium suitability. Having this suitability analysis allows the decision-maker to focus on buildings within tax lot that meet the two ranked criteria. Planners can assess which medium-to-high suitable areas fit funding and logistics criteria and implement projects at a faster and more efficient rate. Additionally, the decision-makers can assess the race and income dynamics of each census block group by adding these as an underlying layer to the ranked suitability maps. In future iterations of this dataset, many more factors can be added to the suitability analysis based on additional factors such as electrical infrastructure conditions, public opinion polls, or any other dataset that may help in determining the most suitable areas to start retrofitting projects to decarbonize NYC. Relocating residents prior to retrofitting may be necessary in which case the proximity to temporary accommodation will be important. A ranked suitability analysis can be applied to other cities globally and customized to fit the priorities and limitations of those cities. Different weights can be placed on suitability factors to prioritize one variable over another making a ranked suitability analysis a dynamic and powerful tool for selecting areas within cities that could be prioritized for decarbonization.

Additional Studies

Within Bronx, variables of interest such as unit size in terms of number of bedrooms, low-income families, location of rental apartments, location of schools, infrastructure, and other historical buildings as well as vacant lands were located. Each variable has been filtered from the dataset to allow for visualization of each aspect. In mapping these features, which were chosen to

determine the groups to evacuate first, a foundation to create an evacuation plan is established.

Location of population density, i.e., number of single family and multifamily: People living in 1-, 2-, 3-, and 4-bedroom apartments are defined as single family, whereas those who live in a 5 or more-bedroom apartment are classified as multifamily. All single-family and multifamily housing in Bronx will be located. The map will show the number of families living in a one-bedroom apartment and multifamily apartment. By finding the number of families living in multifamily apartments, we can then prioritize the areas to evacuate based on population. Locating residences based on density will be integral to our implementation plan, given the assumption that the number of bedrooms directly correlates to the number of occupants. When evacuating buildings on a large borough *en masse*, it will be far too costly and time-consuming to inquire about the exact number of inhabitants in each building. The proposed strategy will instead target buildings based on their apartment size and composition. A theoretical building with 200 units and 60% of those units being 1 BR will be prioritized compared to a building with 150 units with 75% as 3 BR apartments, as the latter residency will house more people and require more infrastructure and planning to relocate the occupants. Locating the densities of each building will be part of the first phase of the implementation strategy, coupled with determining the income and rental/owner status of the units. These three factors will allow for implementing a phase that is oriented toward underserved and overlooked communities while ensuring that adequate resources will be allocated for these families and communities (Fig. 13.21).

Location of Low-Income Groups and Graphical User Interface (GUI) Showing Low-Income Groups

In a press release announcing the program, Sonal Jessel, Director of Policy at WE ACT for Environmental Justice, said: 'Low income and minority
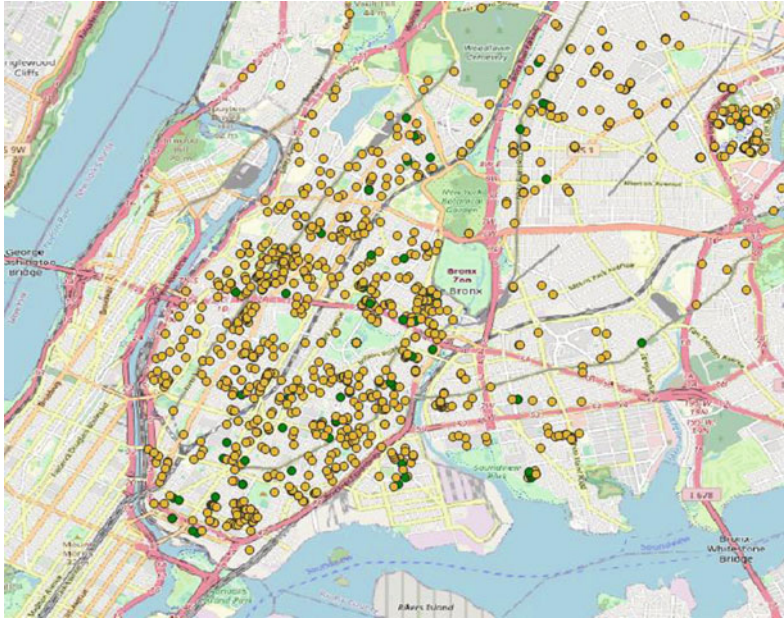
Fig. 13.21 Location of units of interest in the Bronx

populations incur disproportionately higher energy and pollution costs, as well as disproportionately higher climate change impacts' (Mayor's Office of Sustainability 2021). When implementing decarbonization policies, these high-risk communities must be prioritized. We have found the total number of low-income units in each respective zip code of Bronx area. Evacuating the low-income families who are in single-family homes should be given priority (Fig. 13.22).

Location of Rental Apartments

Using census data, families who are renters vs homeowners were mapped across Bronx. It will be easier to move the families who are renters as opposed to homeowners. Priority should be given to families having low-income single families who live in a rental unit. Type of ownership of units will be taken into consideration when determining what resources to deploy for these families. In this proposed plan, it is necessary to ensure the economic feasibility of

relocation for not only the families, but the landlords as well. While families can be relocated into an area of similar pricing or receive government subsidies to cover the cost of temporary housing, the same is needed for the recipients of the tenant's payments. When renting, it is far easier for institutions to communicate with centralized landlord associations or real estate businesses to ensure that their property is receiving the necessary funding during the building evacuation. For homeowners, this process will not be the same, as they are the sole proprietor of the unit and typically make payments on private or federal loans. Due to the differing and more complex nature of homeownership compared to renting, ensuring that loans are paid and banks agree with the proceedings of the proposed plan will be more challenging and time-consuming compared to rental units. By targeting the rental units first, we will be able to efficiently roll out the decarbonization process while simultaneously implementing the necessary bureaucratic measures for owned units (Fig. 13.23).

Fig. 13.22 Mapping of low-income apartments in the Bronx
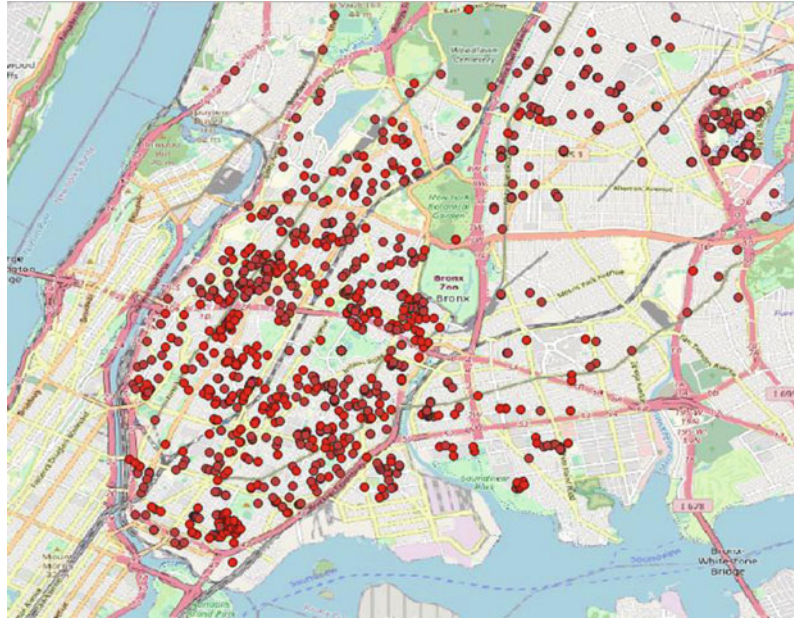
Fig. 13.23 Rental and homeowner units in the Bronx
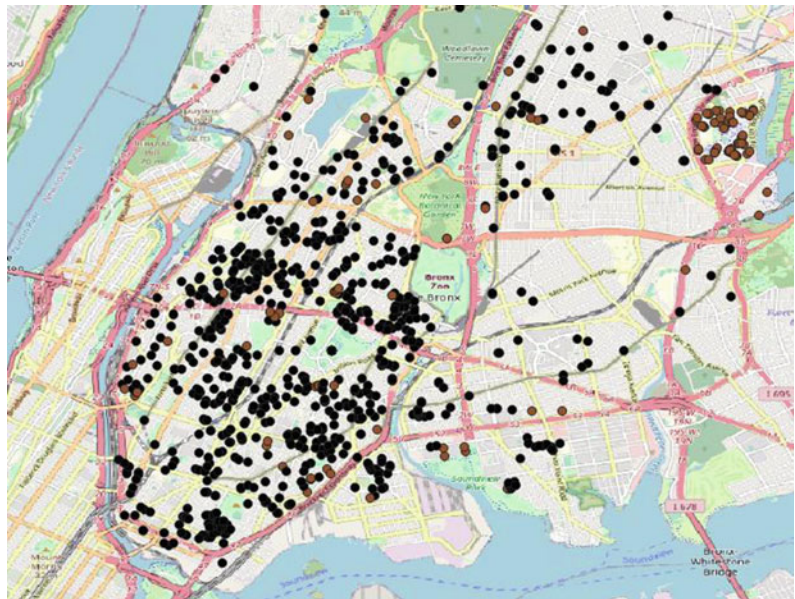
Location of Schools, Infrastructures, Historical Buildings

This study will help us to decarbonize non-residential buildings, as they are only inhabited

during certain hours as opposed to residential units. There will not be a need to evacuate these buildings, as modifications can be made during off hours. Therefore, the buildings which can be further categorized as schools, infrastructure, and historical buildings are important to map. While

residential buildings will need to be evacuated for retrofitting, commercial buildings will not require the same level of intense evacuation. As certain commercial or institutional buildings are only occupied during certain periods of the day, measures can be taken to ensure less disruption than in a residential building. Schools can be retrofitted during the summer when there are lower levels of occupancy, or larger buildings such as libraries can be worked on outside of business hours, or even in sections to create an environment where part of the building may be closed off for repairs, but the other part of the building is fully functional and operating as normal. It is important to determine the location of these buildings as although they will not require evacuation measures, each type of building will need to be assessed to determine the best course of action while meeting the needs of the community.

Location of vacant lands within New York City and beyond, including Governor Islands: An additional feature for this project is locating vacant land in New York City including Governor Island. This study helps us in finding the places where we can build temporary accommodations which can be used during evacuation.

Evacuation Plan

After extracting features of interest, we have found out that there is total 22,250 units (31.70%) of 1 Bedroom (BR), 22,828 units (32.51%) of 2BR, 10,812 units (15.40%) of 3BR, 679 units of 4BR, and 17 units of 5BR apartments available in Bronx. There are 21,329 families (32.2%) who own their units, while 44,875 (67.8%) live in rental units. When looking to implement decarbonization policies in large urban areas such as New York City, a systemic and data-backed approach is needed. Our proposed strategy is to combine GIS mapping and building infrastructure details (such as square footage, year built, building type) to determine what specific areas should be prioritized for retrofitting. Building size will be the largest factor, as this study is under the assumption that carbon emissions have a direct positive relationship with the size. Furthermore, utility usage from large buildings accounts for nearly half of total energy emissions in NYC (Virta 2021). Based on the data from the 2020 NYC Benchmarking Report, we have come up with the following categories of building sizes (Table 13.11).

As such, our policy implementation will first focus on targeting large-to-oversized buildings, as they have higher GHG emissions. When breaking down the types of buildings that retain this amount of square feet, they are typically residential, multifamily buildings. In terms of the composition of gross floor area by sector, multifamily buildings account for 65% of total square feet, with 1.388 billion square feet attributed to large multifamily homes alone, and one of the largest properties (with 5 buildings) comprising 7.7 million square feet (New York City Local Law 84 Benchmarking Report 2013; Urban Green Council 2020). Although multifamily residencies have the lowest permitted carbon emissions cap of 6.75 kg/sq^2 compared to office and hotel properties (8.46 kg/sq^2 and 9.87 kg/sq^2, respectively), the sheer number and size of multifamily properties dwarf the other types of buildings. Furthermore, not every

Table 13.11 Building classification based on square footage

Building size	Square feet (Sq^2)
Small	< 25,000
Midsize	25,000–50,000
Large	50,000–100,000
Very large	100,000–300,000
Extremely large	300,000–500,000
Oversized	500,000+

building reaches this permitted cap, with 30% of multifamily properties running over this cap, or nearly 4,200 residences (New York City Local Law 84 Benchmarking Report 2013). This is nearly 14 times greater than the number of office properties over the carbon emissions cap and 37 times greater than hotel properties. Within the first phase of the plan, categorizing and targeting buildings on the basis of size will allow for decreased GHG production in carbon-emitting giants. Based on the square footage, buildings will be prioritized in ascending order, with oversized buildings targeted first, and midsize buildings last. Small buildings will be targeted in another phase. Within these building sizes, a hierarchy of building types will be created.

Multifamily buildings will always be prioritized compared to office buildings or hotels due to their level of necessity and usage, as natural gas is the most utilized type of energy in the multifamily sector and accounts for almost half of all site energy (NYSERDA 2021). In being able to retrofit multifamily homes for cleaner energy use, the level and frequency of emissions will decrease greatly. Evacuating multifamily properties will utilize far more resources and require careful detailed planning to ensure that these groups are not inappropriately displaced, as adequate relocation and housing measures will need to be assessed. A secondary feature for evaluating the buildings to address will be the year in which they were built, and this will be implemented for all phases. According to data from the LL84 2019 filtered for data quality, emissions, energy, and property type, pre- and post-war buildings (1900–1979) in New York City consume far more fuel than homes built after 1980, and these pre/post-war structures account for 79% of all buildings (NYSERDA 2021). Newer buildings have lower fuel usage due to improvements in building materials, technology, and updated energy codes and laws. In being able to identify the year in which buildings are built, fuel-inefficient homes can be targeted, as they produce more carbon compared to their modern counterparts. The pre- and post-war structures will be given priority in retrofitting as they are the largest class of buildings and are

the least energy efficient. Modern homes, classified as those built from 1980–2011, will be targeted next, and lastly, Energy Code Era buildings built from 2012 onwards will be regarded last, as they have been built around energy-conscious efforts. There may even be a further need for analysis specifically on the Energy Code Era buildings to determine whether retrofitting for decarbonization will be appropriate due to their fuel-efficient nature. Additionally, in the first phase, there will be a subsection that will address office buildings and 'other' types of buildings such as commercial or institutional buildings. For the oversized buildings, offices will be within the second type of building structure to be retrofitted first, while the 'other' classification of buildings will go second in all other building size categories.

While this is an optimistic proposal, realistically, there may be a combination of office and 'other' buildings implemented simultaneously. As these buildings operate within certain hours, some of them may be prioritized depending on the type of operations. During the fall, it will be far easier to renovate and temporarily evacuate an office building compared to a K-12 school. Given the current environment of the workforce, an office could easily effectuate temporary work from home policies, whereas a school will find it much harder to relocate their operations during a school year. Careful consideration must be taken in this phase to target high-carbon emission buildings while retaining a similar level of operations for the affected groups. When retrofitting schools and institutions, particularly those at a K-12 level, several city agencies must be involved in the planning to minimize disruption. While decarbonization is a necessary measure, it must not be done at the expense of classroom and educational activities. Any potential adverse effects, such as delayed school hours, decreased accessibility, or hiatuses for vital after-school programs must be mitigated as much as possible. The second phase will focus on small buildings, particularly units with low-income families. This phase will be divided into two sections: first, multifamily properties, and then, single-family units. In this implementation, a hierarchy will be

determined from income, as it will be an important variable in the strategy. The levels of income will determine who gets priority in relocation measures to ensure that these communities not only reap the necessary benefits of decarbonization but receive the appropriate resources in the meantime. Multifamily units that have a high concentration of low-income residents and then single-family units will be targeted. Income is not only a number but reveals living factors that are necessary to incorporate into our plan. Those within the low-income groups are typically within the working class, which unfortunately implies less flexibility compared to the middle and upper professional class. Deloitte released findings from a survey of white-collar professionals where 70% stated that their companies offered flexible work options, such as flexible work hours, remote work, and extended leave (Deloitte Survey 2020). Those in the middle- and upper-income brackets typically have flexible jobs; this potentially means less restriction in temporarily relocating these individuals. However, our strategy implementation must account for the workforce and physical location requirements of the lower class. In being able to identify these groups, appropriate and timely measures can be taken to ensure the smoothest transition and least amount of inconvenience possible.

Low-income households will need to be identified, as well as their access to existing resources and potential needed resources defined, in the event of relocation. Levels of income have been based around a percentage of Area Median Income (AMI), and low-income levels are classified as less than 80% of AMI. City agencies should coordinate efforts with one another to support these relocated families, whether that is through childcare services, food assistance, counseling for children during a time of transition, or transportation assistance to work or school. These measures are vital to ensure that low-income families are not burdened by decarbonization efforts. This is imperative, as low-income families tend to be at greater risks for

homelessness, so appropriate policies and resources must be implemented and provided to these families (Grubman 2015). It is imperative to note that while decarbonization is essential, the proposed implementation must not disrupt families, especially at-risk low-income communities. Further measures such as rental vouchers from the Department of Housing and Urban Development to relocate families into preexisting apartment complexes that are close to their work location instead of more distant vacant housing can be introduced to decrease the strain of evacuation efforts on low-income families.

The Table 13.12 depicts each phase and subphase, such that it will be depicted as: *Phase #, Primary Feature # Secondary Feature # Secondary Feature [Letter]* following the order of Phase 1, 1.1a, Phase 1, 1.1b, and so on. For example, targeting a small multifamily property built in 1985 with residents in the low-income bracket will correspond to Phase 2a, 1.3a.

It is important to note that this chart is a representation of the proposed phases and does not account for real-life situations. For example, in Phase 1, the ordering of the chart implies that oversized multifamily properties from oldest to newest year built will be targeted first and then oversized 'other' buildings based on year will be addressed second. However, realistically, it may be more appropriate to target oversized multifamily properties built before 1980 and then extremely large multifamily properties built before 1980. A realistic implementation must account for decarbonizing buildings with the largest emissions above all else. Green Schools initiative for underserved communities (Read more about Gov Hochul's initiative from the Internet).

Schools and educational institutions: It is important to map out all the buildings which fall under the category of schools, infrastructure, and historical buildings because they are not in operation 24 h, unlike residentials units. We can decarbonize these buildings faster when they are lying dormant, and it will be faster than residential units.

Table 13.12 Breakdown of retrofitting by building size, type, and year built

Phase level	Primary feature for consideration	Secondary feature for consideration
Phase 1	Building size Oversized: 500,000 + sq^2 Extremely large: 300,000–500,000 sq^2 Very large: 100,000–300,000 sq^2 Large: 50,000–100,000 sq^2 Midsize: 25,000–50,000 sq^2	Property type Multifamily properties 'Other' building types, such as offices, institutions, and commercial buildings
		Year built 1900–1979 1980–2011 2012–Present
Phase 2a	Only multifamily properties within the category of small buildings (<25,000 sq^2)	Income level Extremely low-income: 0 to 30% AMI* Very low-income: 31–50% of AMI Low-income: 51–80% of AMI Moderate-income: 81–120% of AMI Middle-income: 121–165% of AMI
		Year built 1900–1979 1980–2011 2012–Present
Phase 2b	Only single-family units within the category of small buildings (<25,000 sq^2)	Income level Extremely low-income: 0 to 30% AMI** Very low-income: 31–50% of AMI Low-income: 51–80% of AMI Moderate-income: 81–120% of AMI Middle-income: 121–165% of AMI
		Year built 1900–1979 1980–2011 2012–Present

Rehousing During Decarbonization

The information found in this research is crucial in making a strategy for evacuation plan for successfully decarbonizing buildings in Bronx. We can strategize plans for single families who have extremely low income by providing the temporary accommodation at no additional cost to them. Regarding other groups, we can also give preference to families who can afford hotels at subsidized rate. In the future, we plan to map and locate the vacant lands in New York that can be used for temporary accommodation. Thus, overall process for evacuation plan can be as seamless as possible.

References

Agathangelidis I, Cartalis C, Santamouris M (2019) Integrating urban form, function, and energy fluxes in a heat exposure indicator in view of intra-urban heat island assessment and climate change adaptation. Climate 7(6):75. https://doi.org/10.3390/cli7060075

Bai Y, Kaneko I, Kobayashi H, Kurihara K, Takayabu I, Sasaki H, Murata A (2014) A geographic information system (GIS)-based approach to adaptation to regional climate change: a case study of Okutama-Machi, Tokyo, Japan. Mitig Adapt Strat Glob Change 19(5):589–614. https://doi.org/10.1007/s11027-013-9450-6

City of Cincinnati, Office of Environment and Sustainability (2020) City, Duke Energy Ohio Pilot energy efficiency program for income-eligible renters. https://www.cincinnati-oh.gov/oes/news/city-duke-energy-ohio-pilot-energy-efficiency-program-for-income-eligible-renters/

Deloitte Survey (2020) Most professionals take advantage of flexible work options despite perceived consequences to professional growth—press release. Deloitte United States, 20 Feb. 2020. https://www2.deloitte.com/us/en/pages/about-deloitte/articles/press-releases/deloitte-survey-most-professionals-take-advantage-of-flexible-work-options.html

ESRI Tutorial Online. (Date accessed - 4/4/2022). https://pro.arcgis.com/en/pro-app/2.7/help/mapping/layer-properties/data-classification-methods.htm

Gargiulo C, Battarra R, Tremiterra MR (2020) Coastal areas and climate change: a decision support tool for implementing adaptation measures. Land Use Policy 91:104413. https://doi.org/10.1016/j.landusepol.2019.104413

Garner AJ, Mann ME, Emanuel KA, Kopp RE, Lin N, Alley RB, Horton BP, DeConto RM, Donnelly JP, Pollard D (2017) Impact of climate change on New York City's coastal flood hazard: Increasing flood heights from the preindustrial to 2300 CE. Proc Natl Acad Sci 114(45):11861–11866. https://doi.org/10.1073/pnas.1703568114

Gerdes J (2013) Copenhagen's ambitious push to be carbon neutral by 2025. Yale Environ 360(11)

Grubman D (2015) Low-income households face greater risk of homelessness. Novogradac J Tax Credits VI (VII). https://www.novoco.com/periodicals/articles/low-income-households-face-greater-risk-homelessness

Hansen J et al (2013) Assessing 'dangerous climate change': Required reduction of carbon emissions to protect young people, future generations and nature. PLoS ONE 8(12):e81648. https://doi.org/10.1371/journal.pone.0081648

Harlan SL, Declet-Barreto JH, Stefanov WL, Petitti DB (2013) Neighborhood effects on heat deaths: Social and environmental predictors of vulnerability in Maricopa County, Arizona. Environ Health Perspect 121(2):197–204. https://doi.org/10.1289/ehp.1104625

Hunter G, Vettorato D, Sagoe G (2018) Creating smart energy cities for sustainability through project implementation: a case study of Bolzano, Italy. Sustainability 10(7):2167. https://doi.org/10.3390/su10072167

Intergovernmental Panel on Climate Change (IPCC) (2015) Climate change 2014: mitigation of climate change:

Working Group III contribution to the IPCC fifth assessment report. Cambridge University Press, Cambridge. https://doi.org/10.1017/CBO9781107415416

Jenks GF (1967) The data model concept in statistical mapping. Int Yearbook Cartography 7:186–190

Kunapo J, Fletcher TD, Ladson AR, Cunningham L, Burns MJ (2018) A spatially explicit framework for climate adaptation. Urban Water J 15(2):159–166. https://doi.org/10.1080/1573062X.2018.1424216

Lassandro P, Di Turi S (2017) Façade retrofitting: From energy efficiency to climate change mitigation. Energy Procedia 140:182–193. https://doi.org/10.1016/j.egypro.2017.11.134

Mayor's Office of Sustainability, Con Edison, and National Grid (2021) Pathways to carbon-neutral NYC: Modernize, Reimagine, Reach. https://www1.nyc.gov/assets/sustainability/downloads/pdf/publications/Carbon-Neutral-NYC.pdf

New York City Local Law 84 Benchmarking Report (2013) http://www.nyc.gov/html/planyc/downloads/pdf/publications/ll84_year_two_report.pdf.

NYSERDA (2021) Toward a clean energy future: a strategic outlook 2022 through 2025. https://www.nyserda.ny.gov/-/media/Files/About/Strategic-Plan/strategic-outlook.ashx

Urban Green Council (2020) New York City's energy and water use report. https://www.urbangreencouncil.org/sites/default/files/2020_nyc_benchmarking_report.pdf

Vavatsikos AP, Demesouka OE, Anagnostopoulos KP (2020) GIS-based suitability analysis using fuzzy PROMETHEE. J Environ Planning Manage 63 (4):604–628. https://doi.org/10.1080/09640568.2019.1599830

Venter ZS, Barton DN, Martinez-Izquierdo L, Langemeyer J, Baró F, McPhearson T (2021) Interactive spatial planning of urban green infrastructure—retrofitting green roofs where ecosystem services are most needed in Oslo. Ecosyst Serv 50:101314. https://doi.org/10.1016/j.ecoser.2021.101314

Virta (2021) What is decarbonisation, and why do we urgently need it? Available online: https://www.virta.global/blog/decarbonisation

Perception of Ecosystem Services from Urban Green Space: A Case from an Urban and a Peri-urban Green Space in English Bazar Urban Agglomeration, Eastern India

14

Manob Das, Arijit Das, and MD Tushar Ali

Abstract

Urban green space (UGS) is a significant component for urban dwellers as it provides multiple ecosystem services (ES) and enhances physical as well as mental health. It plays a significant role in regulating human health and social well-being in an urban environment. But, recently, UGS has been highly vulnerable due to rapid urban expansion and dramatic loss of green spaces (GS). Despite this, very limited focuses were attributed to the perception of ES obtained from UGS, particularly in the cities of the global south. This study aims to understand the perception of ES from UGS from an urban and a peri-urban GS in English Bazar Urban Agglomeration (EBUA), Eastern India, using a questionnaire survey and observations. The findings of the study showed that there were substantial differences in perception of ES obtained from UGS in urban and peri-urban GS. The respondents from peri-urban sites gave more importance to provisioning ES rather than other ES. On the other hand, the respondents from urban sites valued more to cultural ES and regulating ES. The observation results showed that the respondents from peri-urban sites were more dependent on GS for their livelihoods, and thus direct benefits of UGS were highly prioritized. On the other hand, in urban areas, UGS is mostly used as a place of recreation, physical activities, playing, and picnicking. Thus, two UGSs have different perspectives of perceptions on ES. The results also showed that the UGS in peri-urban sites are highly vulnerable due to rapid urban expansion, infrastructural development, and settlement expansion. Therefore, it is essential to understand the nexus between UGS and ES to improve the quality of life and make the city resilient though better urban planning.

M. Das · A. Das (✉) · M. T. Ali
Department of Geography, University of Gour Banga, Malda 732103, West Bengal, India
e-mail: arijit3333@gmail.com

14.1 Introduction

It is well documented that half of the world's population across the cities and the population in an urban environment will continue to rise (United Nations 2012). About 68% of the total

global population will live in urban areas by 2050 (Kabisch and Haase 2014). The accelerated rate of urbanization has caused a significant increase in urban land demand. Thus, the provision of new urban land for urban dwellers has become one of the great challenges to the city planner with the increase in population and expansion of urban land. These challenges are more prominent in the cities of developing countries like India (Sundaram 2011; Govindarajulu 2014). Therefore, the challenges provide opportunities to the planners and policy-makers for better management, development, and provision of urban green space (UGS). UGS has a crucial role in increasing the resilience capacity of the city to extreme weather events (such as urban heat islands and heat stress) and the effect of urban environmental pollution (Jansson 2013). The presence of UGS in the urban environment plays a significant role in contributing to human health and well-being (Ma et al. 2019; Kothencz et al. 2017). But recently, the rapid urbanization and population growth have brought serious challenges to the socio-environmental and health aspects. UGS in an urban environment not only brings environmental benefits rather it also has economic benefits (Bertram and Rehdanz 2015; Hunter et al. 2019). UGS improves air quality, reduces the UHI effect, maintains biodiversity in urban areas, promotes tourist destinations, and generates revenue (Ramaiah and Avtar 2019; Lee et al. 2015; Terkenli et al. 2020). In previous studies, it was well documented that UGS provides various direct benefits to the people, increases social cohesion, decreases mental stress, and improves mental health (Vujcic et al. 2019; Ma et al. 2019). Thus, UGS provides opportunities for physical activities and promotes physical health and mental health (Richardson et al. 2013; Lee et al. 2015).

UGS provides number environmental and social benefits to the people (Jim and Chen 2008). From UGS, environmental benefits include climate regulation, cooling effect (through the provision of urban heat island effect), noise reduction, water purification, and positive impact on the infiltration (Bowler et al. 2010; Saaroni et al. 2018; Aram et al. 2019; Xiao et al. 2018; Bolund and

Hunhammar 1999). Particularly during the hot summer season, UGS plays a significant role in reducing temperature and alleviating the negative impact of heat on health (Breuste et al. 2013). Social benefits from UGS include physical and mental health, such as mental stress reduction, physical fitness, and relaxation (Vujcic et al. 2019). UGS also provides opportunities to improve the quality of life through the provision of cultural ecosystem services (ES) (such as recreation, social relations, sense of place) (Dou et al. 2017; Bullock et al. 2018). Thus, UGS has a tremendous impact on the overall well-being of the urban residents (Nath et al. 2018; Jennings and Bamkole 2019; Ko and Son 2018). UGS provides valuable ES to the people through environmental regulation (Elmqvist et al. 2013; Ernstson et al. 2010). UGS in the urban environment provides a number of benefits to improve the quality of life in the form of ES (Sun et al. 2019; Matos et al. 2019; Du Toit et al. 2018). The Millennium Ecosystem Assessment (2005) categorized ES into four broad categories: these were provisioning ES (direct benefits from the ecosystems), regulating ES (indirect benefits from the ecosystems), cultural ES (recreational value), and supporting ES (support ecosystem functions and structure) (Costanza et al. 2017; Das and Das 2019; Anaya-Romero et al. 2016).

From the previous pieces of literature, it was well recognized that UGS has a significant impact on urban environmental regulation and enhances the quality of life. But recent studies showed that UGS is highly vulnerable due to a number of natural and anthropogenic factors such as cyclones (Nguyen et al. 2021), urban expansion (Nor et al. 2017), and transformation of vegetation cover into other land use types (Rimal et al. 2018). The increasing demand for urban land is creating huge pressure on the UGS, and it has resulted in fragmentation of UGS and loss of UGS (Roy et al. 2016; Nakagoshi et al. 2006). In developing countries, particularly in Asian countries, the degree of UGS loss is more prominent (Byomkesh et al. 2012; Wu et al. 2019). In India also, the UGS is highly vulnerable due to rapid urban expansion and transformation, as well as a dramatic loss of vegetation

cover to build up and other land uses (van Vliet 2019; Rimal et al. 2018). Therefore, it is essential to understand the perception of ES from UGS to enhance the well-being of the people and promote the management strategies.

14.2   Material and Methods

14.2.1   About Sites

In this study, English Bazar Urban Agglomeration (EBUA) located in Malda district (West Bengal, India) has been selected for the study. Malda district is located in the northern part of the state, West Bengal. English Bazar Urban Agglomeration (EBUA) is one of the rapidly growing urban agglomerations in West Bengal, consisting of two municipalities (English Bazar municipality and Old Malda municipality) and its adjacent census towns and villages. In this urban agglomeration, there are many GS (such as parks, public open spaces, and grounds) such as Bandh Road, Subhankar Sishu Uddyan, Brindabani math (field), Malda college ground, Prantapally math (Field), and Mahananda park. Most of the green spaces are public in nature and operated by municipalities. Mango orchards are one of the dominant green spaces in and around the city (Malda district is popularly known as 'Mango city'). Particularly, the peripheral area of the city is mainly surrounded by the mango orchards. The details of the sites are discussed below (Fig. 14.1).

Site 1 (Urban): This is one of the largest public GS in the city. This UGS is located on the opposite side of the University of Gour Banga and is largely covered by official use. English Bazar Municipality (EBM) operates this public green space. There is no entry fee, and this public space is covered by mainly mango trees (Mangifera indica) along with Sishu (Dalbergia sissoo), guava (Psidium guajava), Sal (Shorea robusta), and bushes. It is one of the most usable GS in the city. Many government offices are located in this GS (such as government quarters, district pollution department, land office, residence of district inspector o general of police).
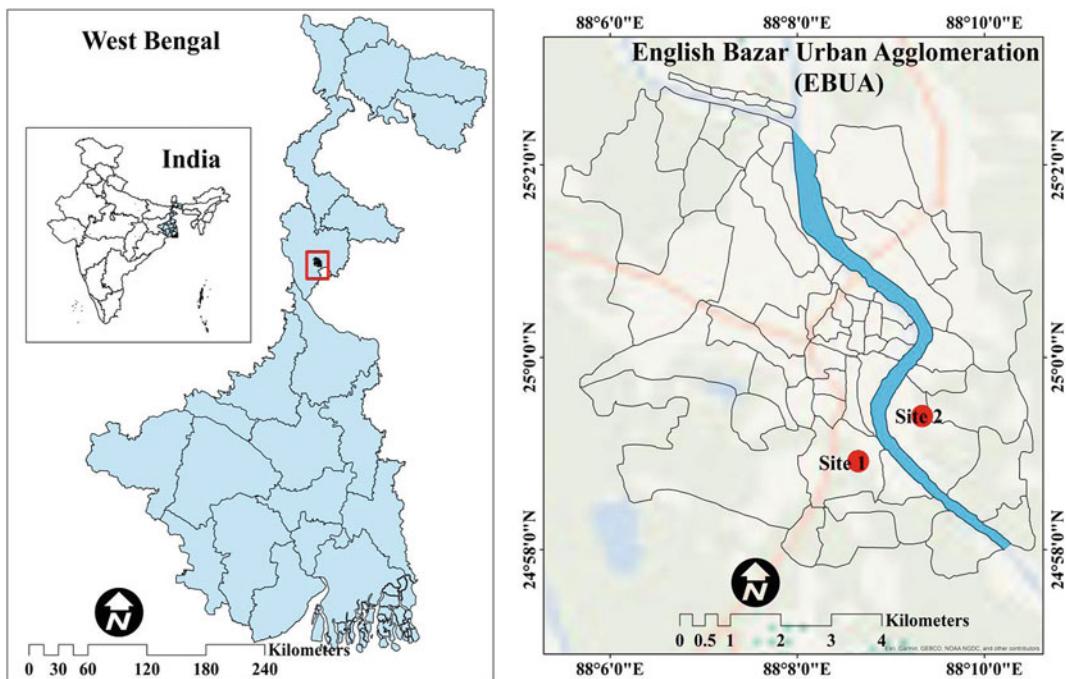

Fig. 14.1 Location of the study sites in English Bazar Urban Agglomeration (EBUA)

Site 2 (Peri-urban): In this study, the peri-urban GS were selected from the south-western part of the urban agglomeration (right side of the Mahananda River). Administratively, these GS come under Old Malda block. The mango orchard located near Setu more and Disco more were selected for the study. These GS are mainly covered by commercial uses (such as hotels, Godown restaurants, and settlements). These GS are private in nature and one of the vulnerable GS due to rapid urban expansion and infrastructural development along the road.

14.2.2 Rationale of Selection of UGS Sites

In this study, two sites were selected for the study, i.e. urban and peri-urban site. These sites are mostly characterized by mango trees (mango orchards). The UGS selected in this study is one of the largest public GS in the city and largely used by the people particularly for cultural ES. In some parts of this GS, access is restricted and effectively maintained by the government. The protection and effective conservation of this GS must be prioritized. Thus, understanding the perception to the urban GS will help to the provision of ES. In case of peri-urban GS, mango orchards are the most dominant. The mango orchards as a GS provide a number of ES to the people living in the area. Particularly, these GS provide various opportunities for livelihood to the people. Though, two sites are located in the same urban agglomeration, but these are different to some extent in terms of their location (urban and peri-urban), sociocultural, and economic conditions of the people. Therefore, it is essential to understand the perception of ES obtained from GS from two diversified sociocultural setting within the same city. For example, in English Bazar Municipality, the GS are mostly used for cultural ES, and on the other hand, the GS located in peri-urban areas (situated on the right side of the river) are mostly used for provisioning ES. But recently, these GS have experienced serious threats due to rapid urban expansion and dramatic conversion of GS for commercial

purposes. Mainly, near Setu more, Disco more, the GS are highly vulnerable due to rapid urban expansion in peri-urban GS. Therefore, these sites are ideal to understand the perception of ES obtained from GS on the basis of the respondent's subjective perception.

14.2.3 Selection of ES from GS

In this study, 15 ES were selected from two study sites under provisioning, regulating, supporting, and cultural ES. These ES were selected on the basis of the Millennium Ecosystem Assessment (2005) framework and previous literature (Costanza et al. 2017; Das and Das 2019; Anaya-Romero et al. 2016). The ES was differently identified from the two sites as these sites were located in different urban landscapes. The provisioning and regulating and supporting ES were the most prominent in site 2 (located on the right side of river), and in site 1, cultural, regulating, and supporting ES were identified. These ES were identified on the basis of the framework proposed by the Millennium Ecosystem Assessment, and then this frame was adapted for local conditions after performing comprehensive observation (Fig. 14.2, Table 14.1).

14.2.4 Data Collection and Questionnaire Survey

For the data collection from the UGS, a qualitative design was used for both sites of GS. Interviews with the individual respondent and focus group discussions were carried out as the primary method for the collection of data. The simple random sampling technique was used to collect data from the GS (Das et al. 2021). The questionnaire survey was conducted with 175 respondents (120 from urban core UGS and 155 from peri-urban UGS) from 10 to 20 December 2021. The relatively small number of samples from the study sites was selected due to the COVID-19 pandemic (third wave of COVID-19 in India). The questions were asked using stratified random
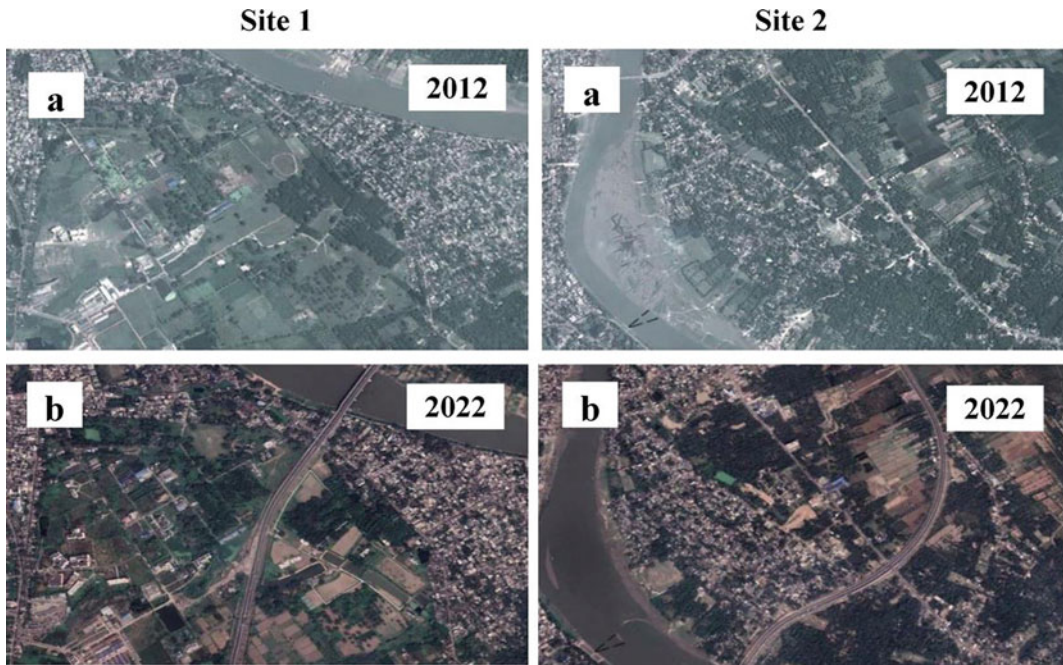
Fig. 14.2 Temporal change of GS in the study sites: **a** before the construction of bypass (National Highway 34) in 2012 and **b** after the construction of bypass (National Highway 34) in 2022

Table 14.1 Major ES identified from GS

Category	ES	References
CES	Source of inspiration (landscape that promotes new thoughts, idea, and creative expressions)	Quyen et al. (2017); Dou et al. (2017)
	Beauty and aesthetic value	Figueroa-Alfaro et al. (2017); Quyen et al. (2017)
	Sports (cricket, football)	Langemeyer et al. (2015)
	Physical and mental health benefits	Bratman et al. (2019); Tengberg et al. (2012)
PES	Fruits	Chowdhury and Behera (2020)
	Leafy vegetables	Chowdhury and Behera (2020)
	Timber	Burkhard et al. (2014)
	Fodder	Montoya-Tangarife et al. (2017); Das et al. (2021)
	Fuel wood	Lai et al. (2018); Das et al. (2021)
	Medicinal plants	Pritchard et al. (2019); Das et al. (2021, 2022)
RES	Local climate regulation	Elmqvist et al. (2015); Kremer et al. (2016)
	Hazards reduction (natural)	Quyen et al. (2017)
	Water purification	Das et al. (2021, 2022); Montoya-Tangarife et al. (2017)
	Soil erosion regulation	Olson et al. (2017); Das et al. (2021); Guerra et al. (2016)
	Air quality regulation	Das et al. (2021); Blum (2017); Manes et al. (2016)
SES	Habitat for species	Das et al. (2022); Liquete et al. (2016)
	Groundwater recharge	Chowdhury and Behera (2020)

sampling face-to-face interviews during both weekends and weekdays at different time periods of the day to record data from diversified respondents. Before the final survey, the questionnaire was pretested to validate the questions from two sites, and then a few questions were revised based on the reactions of the respondents. The questions were asked to those respondents who were interested in participating in the survey and who were well known for the GS. If any respondent disagreed with participating in the survey, then questions were asked to a new respondent.

After finishing the survey from one respondent, another respondent was asked for an interview. The entire survey was divided into two time periods, during the morning (6 am to 8 am) and evening (4 pm and onwards). The UGS located in urban areas is used during the morning and evening, and the survey was performed during two time periods. On the other hand, in the case of peri-urban UGS, the survey was carried out only in the evening (4 pm and onwards). During the face-to-face survey with respondents, the objective of this survey was explained for a better understanding of the framed questions. The interview for each respondent lasted about 15 to 20 min. During in-depth interactions and group discussion, the interview extended up to 45 min. Initially, the questionnaire was prepared in the English language, but it was asked to the respondents in 'Bengali dialect'. The entire questionnaire was framed into four sections, namely Sect. 14.3.1: socio-demographic profiles of the respondents; Sect. 14.3.2: identifications of ES from the UGS Sect. 14.3.3: valuation of ES identified from the UGS and threats towards UGS (the details of the questionnaire are given in supplementary).

14.3   Result

14.3.1   Socio-demographic Profile of the Respondents

In the case of site 1, about 63% of the respondents were male and 37% were female. The maximum percentage of respondents belonged to the age group of 20 to 30 years (36%), followed by 40 to 50 years (22%), 30 to 40 years (18%), and more than 50 years is 12%. The maximum % of respondents from this site were bachelor (37%), followed by above post-graduation (33%), high school (20%), and elementary (10%). Occupationally, the maximum % of respondents belonged to government employees (28%), followed by students (22%), businessmen (20%), daily workers (16%), and others (14%).

In the case of site 2 GS, about 86% and 14% of respondents were male and female. In the case of age groups, the maximum percentage of respondents belonged to the age group of 30–40 years (31%), followed by more than 50 years (26%), 40–50 years (24%), and 20–30 years was 19%. The maximum % of respondents from site 2 belonged to elementary (35%), followed by high school (30%), bachelor (20%), and post-graduation (15%). Most of the respondents were daily workers (31%), followed by housewives (26%), government employees (16%), businessmen (15%), and students (13%) (Supplementary Table S1).

14.3.2   Perceived ES from GS

From the field survey, it was found that there was a variation of ES from GS perceived by the respondents from site one and site 2. For example, in the case of site 1, CES, RES, and SES were highly recognized. In site 2, PES was highly prioritized, followed by SES and regulating ES.

In site 1 (Urban), among all the CES, high importance (perceived valuation) was attributed to beauty and aesthetic value (47%) followed by sports (45%) and physical and mental health benefits (40%). After CES, RES was highly valued. For example, among all the RES, very high importance was given to control of local climate regulation (45%), followed by air quality regulation (30%), soil erosion regulation (25%), and water purification (22%).

In site 2 (peri-urban), among all the ES categories, PES and RES were given more importance than CES and SES. For example, among all

the PES, relatively higher importance was given to fruits (mango mainly from mango orchards), followed by fuel wood (47%), fodder (45%), leafy vegetables (40%), and timbers (35%).

As per the results of five points Likert scale, it was observed that the respondents from site 1 (Urban) perceived high capabilities of CES (an overall score of 4.52) followed by SES (an overall score of 4.05) and RES (an overall score of 3.93). On the other hand, in site 2 (peri-urban), high capabilities of PES were perceived by the respondents (an overall score of 4.28) followed by SES (an overall score of 4.02) and RES (an overall score of 3.82). In site 1, beauty and aesthetic value had the highest score (4.88), followed by sports (4.59), physical and mental health benefits (4.41), and source of inspiration (4.19). In the case of RES, local climate regulation had the highest score (4.71), followed by water purification (4.50), hazard reduction (natural) (3.54), soil erosion regulation (2.18). In site 2 (Peri-urban), fruits (mainly from mango orchard) had the highest score (4.84), followed by fuel wood (4.75), leafy vegetables (4.19), timber (4.12), and fodder (4.02) (Figs. 14.3 and 14.4).

14.3.3 Perception Towards Management and Threats to GS

Most of the respondents from the two sites stated concerns about the deterioration of GS and various priority preferences for the management of urban and peri-urban GS. The GS (mango orchard) in peri-urban along the road (particularly from Setu more to Disco more) are highly vulnerable due to urban expansion and infrastructural development (such as hotels, restaurants, storage house, high-rise buildings). In the case of GS located in urban areas (site 1), GS are very poorly managed, and lack of cleanness is the major problem of GS as perceived by the respondents. For example, in the case of GS located in urban areas, 55% of the total respondents highly agreed that GS in urban areas are
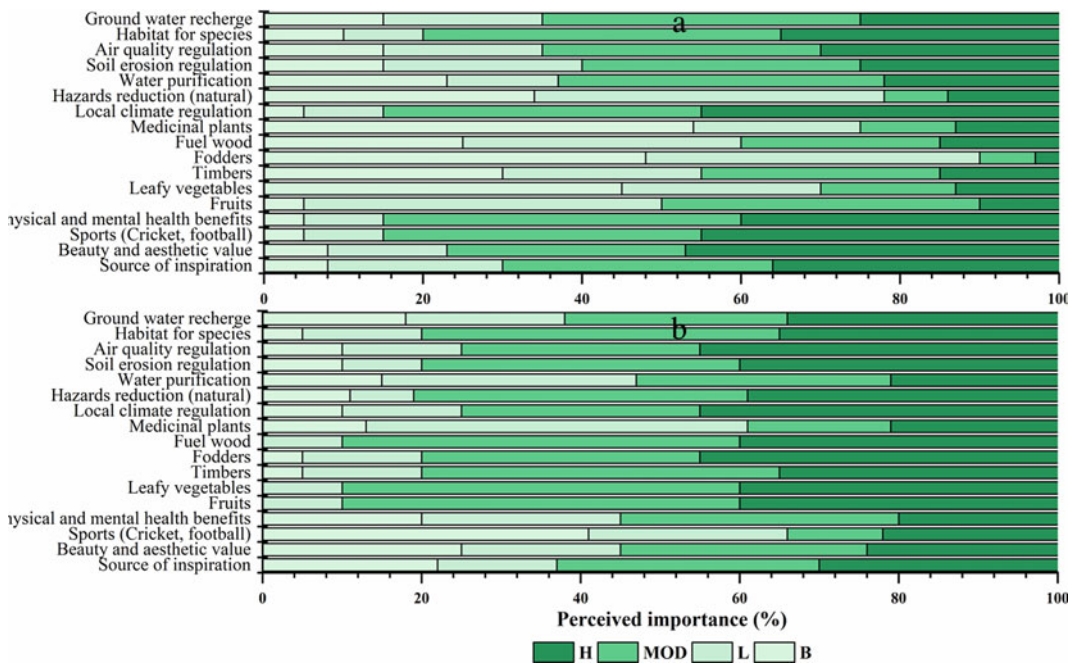

Fig. 14.3 Importance of ES from GS perceived by the respondents: **a** urban and **b** peri-urban (VL = very low, L = low, MOD = moderate, H = high, VH = very high)

Fig. 14.4 Use of GS in urban (**a** abandoned government quarters, **b** existing government quarters in GS, and **c** ground used for picnicking, plating, and gatherings) and peri-urban areas (**d** construction in progress, **e** newly constructed high-rise building, and **f** view of the GS). *Source* Field survey (2021) by the authors

very poorly managed and lack of government initiatives and infrastructural development (mainly public buildings) (42%).

In the case of peri-urban GS, 75% of the total respondents were highly agreed that GS in peri-urban areas is highly vulnerable due to urban expansion and infrastructural developments, followed by population growth (40%), lack of government initiatives (40%), lack of safety (35%), and lack of public participation (25%) (Figs. 14.5 and 14.6).

Fig. 14.5 Threats towards GS perceived by the respondents in urban areas (SD = strongly disagree; D = disagree, A = agree, HA = highly agree)
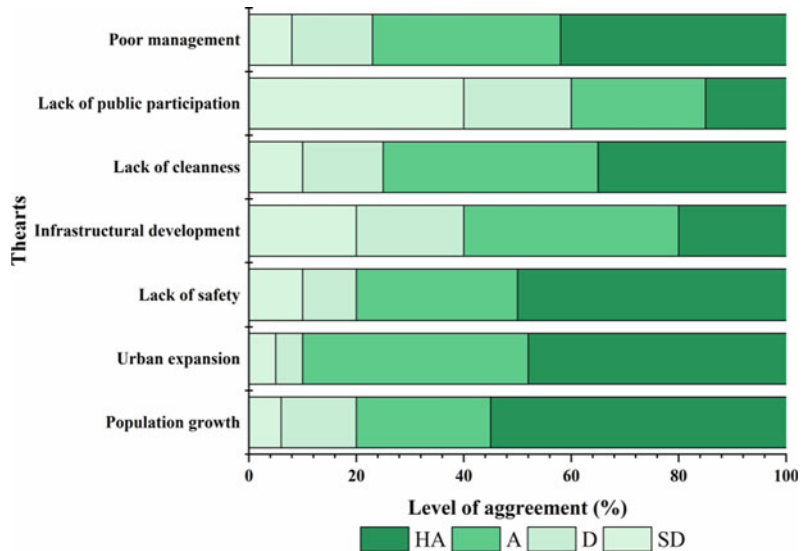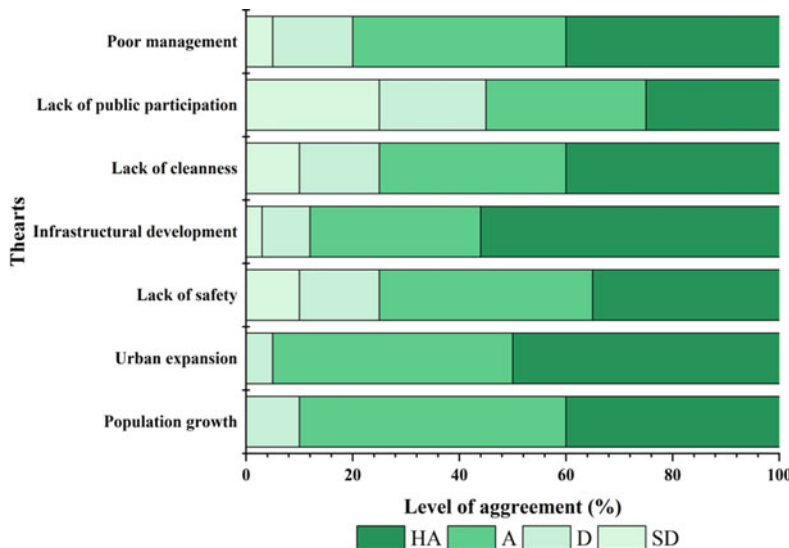
Fig. 14.6 Threats towards GS perceived by the respondents in peri-urban areas (SD = strongly disagree; D = disagree, A = agree, HA = highly agree)

14.4   Discussion

In this study, the perception to ES from GS was assessed from a secondary city in Eastern India. Two peri-urban GS were selected from a rapidly growing urban agglomeration in Easter India. From the findings, it was well documented that the ES obtained from GS were differently perceived. A clear difference in the perception of ES was found between urban and peri-urban GS. The provisioning ES were highly valued by the rural respondents, and regulating and cultural ES were highly valued by the rural respondents, respectively. In previous studies also, similar findings were reported (Hartel et al. 2014; Martín-López et al. 2012; Aguado et al. 2018). In comparison with rural areas, provisioning ES was given less importance in urban areas perceived by the respondents, and these findings were similar to other previous studies (Grimm et al. 2008). In rural areas, the people are highly dependent on provisioning ES, and their livelihoods are highly associated with the direct benefits provided by the ecosystems (Das et al. 2021; 2022). In this study, the PES such as fruits (mainly from mango orchards), fuel woods, and leafy vegetables were highly valued as these ES have a direct and daily relationship with their livelihoods. In many previous studies, it was well

documented that environmental aspects such as air quality and water quality regulations were attributed to higher importance (García-Llorente et al. 2011; Sodhi et al. 2010). The high value of these ES was attributed to the urban communities as their lifestyle is associated with the sensation of aversion to air quality and water quality, and it has an impact on human health (Kottmeier et al. 2007). Our results also showed that CES was attributed to high value by the urban people, such as recreation and aesthetics. These findings were similar to other previous studies (Martín-López et al. 2012; Dou et al. 2017). On the other hand, people living in peri-urban areas prioritized CES related to their traditional management systems and identity (López-Santiago et al. 2014). Such findings from the study revealed the fact that the experience of the people related to CES is highly variable and dependent on sociocultural factors. In many studies, this variation was reported (Martín-López et al. 2012). The study results also showed that the GS are highly vulnerable due to population growth and rapid urban expansion. Particularly, in peri-urban areas, GS are (mango orchards) highly vulnerable due to rapid urban expansion along the road. In previous studies, it was well documented that GS are under serious threats due to rapid urban expansion (Arshad et al. 2020; Haaland and van Den Bosch 2015). According to Haaland and van Den Bosch

(2015), the densification in urban areas due to infill development has posed a threat to UGS. This finding is similar to our results. Therefore, it is essential to facilitate provision of UGS in compact city through the preservation of GS, enhancement of the quality of GS, redevelopment of GS in cities, and smart allocation (Haaland and van Den Bosch 2015).

14.4.1 Policy Implication

From the findings of the study, it was well documented that UGS from both sites provides a number of benefits through the provision of ES. The well-being and livelihood of the people are highly dependent on the UGS, particularly in peri-urban UGS. The livelihood of the people largely depends on the UGS. In previous studies, the degradation of green cover across the cities in India was emphasized due to the deterioration of urban environmental quality (Sundaram 2011), and the importance of UGS in previous studies was highly prioritized (Govindarajulu 2014). In addition to this, essential to focus on the restoration as well as management must be prioritized to enhance the quality of life of the urban residents and to increase the resilience of the city. In India, a number of initiatives were implemented for the protection and management of UGS, such as The National Green Tribula Act (2010), and the National Action Plan for Climate Change (2008). Thus, the importance of UGS must be incorporated into decision-making framework and future planning strategies. From the observation, it can be stated that in English Bazar Urban Agglomeration (EBUA), very limited focuses were attributed to the provision of UGS development as well as management. Therefore, this suggests a few effective planning strategies: firstly, improvement of quality of UGS, improvement of availability (per capita increase of UGS), emphasis on the ecological planning strategies, and public participation in UGS management. These planning strategies can be taken into account during urban landscape planning. Thus, this study not only contributes the provision of UGS rather ES through which

well-being and urban environmental sustainability can be improved.

14.5 Conclusions

In this study, an attempt has been made to understand the perception of ES from a rapidly growing urban agglomeration (English Bazar Urban Agglomeration) in Eastern India. The perception of ES from an urban and a peri-urban UGS was assessed. From the results, the following conclusions were drawn: firstly, there were substantial differences in perception on ES obtained from UGS in urban and peri-urban areas. The respondents from peri-urban areas gave more emphasis on provisioning and regulating ES rather than cultural services. On the other hand, in urban areas, the respondents gave more importance to cultural and regulating ES rather than provisioning ES. Secondly, the UGS of peri-urban areas is more vulnerable due to urban expansion and infrastructural development along the road (Malda Nalagola State High Way) in comparison with UGS in urban areas. The UGS located urban areas are mostly public spaces, and these are protected by the local municipality (English Bazar Municipality or EBM). Therefore, it is essential to focus on the UGS planning strategies in compact cities like English Bazar.

References

Aguado M, González JA, López-Santiago C, Montes C (2018) Exploring subjective well-being and ecosystem services perception along a rural–urban gradient in the high Andes of Ecuador. Ecosyst Serv 34:1–10

Anaya-Romero M, Muñoz-Rojas M, Ibáñez B, Marañón T (2016) Evaluation of forest ecosystem services in Mediterranean areas. A regional case study in South Spain. Ecosyst Serv 20:82–90

Aram F, García EH, Solgi E, Mansournia S (2019) Urban green space cooling effect in cities. Heliyon 5(4): e01339

Arshad A, Ashraf M, Sundari RS, Qamar H, Wajid M, Hasan MU (2020) Vulnerability assessment of urban expansion and modelling green spaces to build heat waves risk resiliency in Karachi. Int J Disaster Risk Reduction 46:101468

Bertram C, Rehdanz K (2015) The role of urban green space for human well-being. Ecol Econ 120:139–152

Blum J (2017) Contribution of ecosystem services to air quality and climate change mitigation policies: the case of urban forests in Barcelona, Spain. In: Urban forests. Apple Academic Press, pp 21–54

Bolund P, Hunhammar S (1999) Ecosystem services in urban areas. Ecol Econ 29(2):293–301

Bowler DE, Buyung-Ali L, Knight TM, Pullin AS (2010) Urban greening to cool towns and cities: a systematic review of the empirical evidence. Landsc Urban Plan 97(3):147–155

Bratman GN, Anderson CB, Berman MG, Cochran B, De Vries S, Flanders J, Folke C, Frumkin H, Gross JJ, Hartig T, Kahn PH, Kuo M, Lawler JJ, Levin PS, Lindahl T, Meyer-Lindenberg A, Mitchell R, Ouyang Z, Roe J, Scarlett L, Smith JR, van den Bosch M, Wheeler BW, White MP, Zheng H, Daily GC (2019) Nature and mental health: an ecosystem service perspective. Sci Adv 5(7):eaax0903

Breuste J, Haase D, Elmqvist T (2013) Urban landscapes and ecosystem services. In: Ecosystem services in agricultural and urban landscapes, pp 83–104

Bullock C, Joyce D, Collier M (2018) An exploration of the relationships between cultural ecosystem services, socio-cultural values and well-being. Ecosyst Serv 31:142–152

Burkhard B, Kandziora M, Hou Y, Müller F (2014) Ecosystem service potentials, flows and demands-concepts for spatial localisation, indication and quantification. Landsc Online 34:1–32

Byomkesh T, Nakagoshi N, Dewan AM (2012) Urbanization and green space dynamics in Greater Dhaka, Bangladesh. Landsc Ecol Eng 8(1):45–58

Chowdhury K, Behera B (2020). Traditional water bodies and ecosystem services: empirical evidence from West Bengal, India. In: Natural Resources Forum, vol 44, no. 3. Blackwell Publishing Ltd., Oxford, UK, pp 219–235

Costanza R, De Groot R, Braat L, Kubiszewski I, Fioramonti L, Sutton P, Farber S, Grasso M (2017) Twenty years of ecosystem services: how far have we come and how far do we still need to go? Ecosyst Serv 28:1–16

Das M, Das A (2019) Estimation of ecosystem services (EESs) loss due to transformation of local climatic zones (LCZs) in Sriniketan-Santiniketan planning area (SSPA) West Bengal, India. Sustain Cities Soc 47:101474

Das M, Das A, Pandey R (2022) Importance-performance analysis of ecosystem services in tribal communities of the Barind region, eastern India. Ecosyst Serv 55:101431

Das M, Das A, Seikh S, Pandey R (2021) Nexus between indigenous ecological knowledge and ecosystem services: a socio-ecological analysis for sustainable ecosystem management. Environ Sci Pollut Res 1–18

Dou Y, Zhen L, De Groot R, Du B, Yu X (2017) Assessing the importance of cultural ecosystem services in urban areas of Beijing municipality. Ecosyst Serv 24:79–90

Du Toit MJ, Cilliers SS, Dallimer M, Goddard M, Guenat S, Cornelius SF (2018) Urban green infrastructure and ecosystem services in sub-Saharan Africa. Landsc Urban Plan 180:249–261

Elmqvist T, Setälä H, Handel SN, Van Der Ploeg S, Aronson J, Blignaut JN, De Groot R (2015) Benefits of restoring ecosystem services in urban areas. Current Opin Environ Sustain 14:101–108

Elmqvist T, Fragkias M, Goodness J, Güneralp B, Marcotullio PJ, McDonald RI, ... Wilkinson C (2013) Urbanization, biodiversity and ecosystem services: challenges and opportunities: a global assessment. Springer Nature, p 755

Ernstson H, Van der Leeuw SE, Redman CL, Meffert DJ, Davis G, Alfsen C, Elmqvist T (2010) Urban transitions: on urban resilience and human-dominated ecosystems. Ambio 39(8):531–545

Figueroa-Alfaro RW, Tang Z (2017) Evaluating the aesthetic value of cultural ecosystem services by mapping geo-tagged photographs from social media data on Panoramio and Flickr. J Environ Planning Manage 60(2):266–281

García-Llorente M, Martín-López B, Díaz S, Montes C (2011) Can ecosystem properties be fully translated into service values? An economic valuation of aquatic plant services. Ecol Appl 21(8):3083–3103

Govindarajulu D (2014) Urban green space planning for climate adaptation in Indian cities. Urban Climate 10:35–41

Grimm NB, Faeth SH, Golubiewski NE, Redman CL, Wu J, Bai X, Briggs JM (2008) Global change and the ecology of cities. Science 319(5864):756–760

Guerra CA, Maes J, Geijzendorffer I, Metzger MJ (2016) An assessment of soil erosion prevention by vegetation in Mediterranean Europe: current trends of ecosystem service provision. Ecol Ind 60:213–222

Haaland C, van Den Bosch CK (2015) Challenges and strategies for urban green-space planning in cities undergoing densification: a review. Urban Forestry Urban Greening 14(4):760–771

Hartel T, Fischer J, Câmpeanu C, Milcu AI, Hanspach J, Fazey I (2014) The importance of ecosystem services for rural inhabitants in a changing cultural landscape in Romania. Ecol Soc 19(2)

Hunter RF, Cleland C, Cleary A, Droomers M, Wheeler BW, Sinnett D, Braubach M (2019) Environmental, health, wellbeing, social and equity effects of urban green space interventions: a meta-narrative evidence synthesis. Environ Int 130:104923

Jansson Å (2013) Reaching for a sustainable, resilient urban future using the lens of ecosystem services. Ecol Econ 86:285–291

Jennings V, Bamkole O (2019) The relationship between social cohesion and urban green space: an avenue for health promotion. Int J Environ Res Public Health 16 (3):452

Jim CY, Chen WY (2008) Assessing the ecosystem service of air pollutant removal by urban trees in Guangzhou (China). J Environ Manage 88(4):665–676

Ko H, Son Y (2018) Perceptions of cultural ecosystem services in urban green spaces: a case study in Gwacheon, Republic of Korea. Ecol Ind 91:299–306

Kothencz G, Kolcsár R, Cabrera-Barona P, Szilassi P (2017) Urban green space perception and its contribution to well-being. Int J Environ Res Public Health 14(7):766

Kottmeier C, Biegert C, Corsmeier U (2007) Effects of urban land use on surface temperature in Berlin: case study. J Urban Plan Dev 133(2):128–137

Kremer P, Hamstead ZA, McPhearson T (2016) The value of urban ecosystem services in New York City: a spatially explicit multicriteria analysis of landscape scale valuation scenarios. Environ Sci Policy 62:57–68

Lai TY, Salminen J, Jäppinen JP, Koljonen S, Mononen L, Nieminen E, Oinonen S (2018) Bridging the gap between ecosystem service indicators and ecosystem accounting in Finland. Ecol Model 377:51–65

Langemeyer J, Baró F, Roebeling P, Gómez-Baggethun E (2015) Contrasting values of cultural ecosystem services in urban areas: the case of park Montjuïc in Barcelona. Ecosyst Serv 12:178–186

Lee ACK, Jordan HC, Horsley J (2015) Value of urban green spaces in promoting healthy living and wellbeing: prospects for planning. Risk Manage Healthc Policy 8:131

Liquete C, Cid N, Lanzanova D, Grizzetti B, Reynaud A (2016) Perspectives on the link between ecosystem services and biodiversity: the assessment of the nursery function. Ecol Ind 63:249–257

López-Santiago CA, Oteros-Rozas E, Martín-López B, Plieninger T, Martín EG, González JA (2014) Using visual stimuli to explore the social perceptions of ecosystem services in cultural landscapes: the case of transhumance in Mediterranean Spain. Ecol Soc 19(2)

Ma B, Zhou T, Lei S, Wen Y, Htun TT (2019) Effects of urban green spaces on residents' well-being. Environ Dev Sustain 21(6):2793–2809

Manes F, Marando F, Capotorti G, Blasi C, Salvatori E, Fusaro L, Munafò M (2016) Regulating ecosystem services of forests in ten Italian metropolitan cities: air quality improvement by PM10 and O_3 removal. Ecol Ind 67:425–440

Martín-López B, Iniesta-Arandia I, García-Llorente M, Palomo I, Casado-Arzuaga I, Amo DGD, Gómez-Baggethun E, Oteros-Rozas E, Palacios-Agundez I, Willaarts B, González JA, Santos-Martín F, Onaindia M, López-Santiago C, Montes C (2012). Uncovering ecosystem service bundles through social preferences. PLoS ONE 7(6):e38970

Matos P, Vieira J, Rocha B, Branquinho C, Pinho P (2019) Modeling the provision of air-quality regulation ecosystem service provided by urban green spaces using lichens as ecological indicators. Sci Total Environ 665:521–530

Montoya-Tangarife C, De La Barrera F, Salazar A, Inostroza L (2017) Monitoring the effects of land cover change on the supply of ecosystem services in an urban region: A study of Santiago-Valparaíso, Chile. PLoS ONE 12(11):e0188117

Nakagoshi N, Watanabe S, Kim JE (2006) Recovery of greenery resources in Hiroshima city after World War II. Landscape Ecol Eng 2(2):111–118

Nath TK, Han SSZ, Lechner AM (2018) Urban green space and well-being in Kuala Lumpur, Malaysia. Urban Forestry Urban Greening 36:34–41

Nguyen KA, Liou YA, Vo TH, Cham DD, Nguyen HS (2021) Evaluation of urban greenspace vulnerability to typhoon in Taiwan. Urban Forestry Urban Greening 63:127191

Nor ANM, Corstanje R, Harris JA, Brewer T (2017) Impact of rapid urban expansion on green space structure. Ecol Ind 81:274–284

Olson KR, Al-Kaisi M, Lal R, Morton LW (2017) Soil ecosystem services and intensified cropping systems. J Soil Water Conserv 72(3):64A-69A

Pritchard R, Grundy IM, van der Horst D, Ryan CM (2019) Environmental incomes sustained as provisioning ecosystem service availability declines along a woodland resource gradient in Zimbabwe. World Dev 122:325–338

Quyen NTK, Berg H, Gallardo W, Da CT (2017) Stakeholders' perceptions of ecosystem services and Pangasius catfish farming development along the Hau River in the Mekong Delta, Vietnam. Ecosyst Serv 25:2–14

Ramaiah M, Avtar R (2019) Urban green spaces and their need in cities of rapidly urbanizing India: a review. Urban Sci 3(3):94

Richardson EA, Pearce J, Mitchell R, Kingham S (2013) Role of physical activity in the relationship between urban green space and health. Public Health 127 (4):318–324

Rimal B, Zhang L, Keshtkar H, Haack BN, Rijal S, Zhang P (2018) Land use/land cover dynamics and modeling of urban land expansion by the integration of cellular automata and Markov chain. ISPRS Int J Geo Inf 7(4):154

Roy S, Dutta S, Hoque MM (2016) Urban forestry and urban greening for sustainable urban development-a case of Dhaka north city corporation area (Zone-1). J Bangladesh Agric Univ 14(2):167–176

Saaroni H, Amorim JH, Hiemstra JA, Pearlmutter D (2018) Urban Green Infrastructure as a tool for urban heat mitigation: Survey of research methodologies and findings across different climatic regions. Urban Clim 24:94–110

Sodhi NS, Lee TM, Sekercioglu CH, Webb EL, Prawiradilaga DM, Lohman DJ, Ehrlich PR (2010) Local people value environmental services provided by forested parks. Biodivers Conserv 19(4):1175–1188

Sun F, Xiang J, Tao Y, Tong C, Che Y (2019) Mapping the social values for ecosystem services in urban green spaces: integrating a visitor-employed photography method into SolVES. Urban Forestry Urban Greening 38:105–113

Sundaram MA (2011) Urban green-cover and the environmental performance of Chennai city. Environ Dev Sustain 13(1):107–119

Tengberg A, Fredholm S, Eliasson I, Knez I, Saltzman K, Wetterberg O (2012) Cultural ecosystem services provided by landscapes: assessment of heritage values and identity. Ecosyst Serv 2:14–26

Terkenli TS, Bell S, Tošković O, Dubljević-Tomićević J, Panagopoulos T, Straupe I, Živojinović I (2020) Tourist perceptions and uses of urban green infrastructure: an exploratory cross-cultural investigation. Urban Forestry Urban Greening 49:126624

United Nations (2012) World urbanization prospects, the 2011 revision (United Nations, New York). Available at: http://esa.un.org/unpd/wup/index.htm. Accessed August 12, 2022

van Vliet J (2019) Direct and indirect loss of natural area from urban expansion. Nat Sustain 2(8):755–763

Vujcic M, Tomicevic-Dubljevic J, Zivojinovic I, Toskovic O (2019) Connection between urban green areas and visitors' physical and mental well-being. Urban Forestry Urban Greening 40:299–307

Wu Z, Chen R, Meadows ME, Sengupta D, Xu D (2019) Changing urban green spaces in Shanghai: trends, drivers and policy implications. Land Use Policy 87:104080

Xiao XD, Dong L, Yan H, Yang N, Xiong Y (2018) The influence of the spatial characteristics of urban green space on the urban heat island effect in Suzhou Industrial Park. Sustain Cities Soc 40:428–439

Monitoring Spatiotemporal Reduction of an Urban Wetland Using Landsat Time Series Analysis: A Case Study of Deepor Beel, Assam, India

15

Rajib Tarani Das, Mrinalendra Narayan Dutta, and Shukla Acharjee

Abstract

Wetlands identification, monitoring, and restoration are crucial to sustaining efficient ecosystem services. Deepor Beel wetland in Assam has experienced rapid hydro-ecological alteration after huge constructional work from 1999 to 2000 that causes a major transformation of the wetland area. So, this paper intends to delineate the wetland area and monitor the transformations of the wetland triggered by the constructions in the southern parts of Deepor Beel. Water pixel frequency for each year is computed from 1988 to 2019 to estimate the total average wetted area of Deepor Beel. The water presence frequency process has also been applied for this purpose. Different landscape metrics are used to ana-lyze the fragmentation of the wetland in different temporal stages. The result shows that, in the first stage, during 1988–2000, the aerial extents of high, moderate, and low-frequency water presence areas were roughly about 4.81, 3.48, and 2.76 km^2, respectively. During the second phase from the year 2001–2018, the speedy extension of railway network has truncated the average area of wetland and has reduced the area approximately by 58, 33, and 52% in high, moderate, and low water presence frequency correspondingly. This study can be very helpful for planners to monitor future wetland loss and to draw the attention of stakeholders for its restoration.

R. T. Das (✉) · S. Acharjee
Centre for Studies in Geography, Dibruragh University, Dibrugarh, Assam, India
e-mail: rajibtaranidas@gmail.com

S. Acharjee
e-mail: sacharjee@dibru.ac.in

M. N. Dutta
Department of Applied Geology, Dibruragh University, Dibrugarh, Assam, India

Keywords

Deepor Beel · Water presence frequency · Wetland fragmentation · Wetland loss · Inconsistency of wetland

15.1 Introduction

Wetlands which are profuse in contrast to rain forests and coral reefs on our Earth's surface are loaded with rich and branched-out natural scenic panorama (Ward et al. 2002; Ramsar 2004), and as a plus point, it even provides priceless goods and essential direct or indirect assistance to the

well-being of the public at large. Despite the fact that wetlands cover only 5–6% of the Earth's surface (Mitsch 2010), it provides 40% of global ecosystem services (Zedler and Kercher 2005). In the last few decades, in spite of their vast ecological importance, wetlands have experienced thrashing loss than any other ecosystem, and it is anticipated that due to anthropogenic pressures (Marti-Cardona et al. 2013, Prasad et al. 2002), 60% of the world's wetlands have been lost since 1990 (Cutter and Finch 2008). Recouping of wetland areas by the expansion of built-up land in course of agricultural land expansion (Pal and Osoundu 2009), badly managed solid waste disposal systems, and direct untreated household sewage draining to wetlands have brought a striking transformation in the physical character of wetlands and ecological connectivity in wetland ecosystem (Pal 2015). These intensified hitches have stimulated the risk of physical nonexistence for the wetlands to face (Das and Pal 2017). With the increasing population pressure, there has been a rise in the rapid exploitation of lands for the creation of resources. While wetlands are always being regarded as a wasteland in our social order, a few tactical plans have been taken up in different wetlands area for calculating the frequency and size of man-induced pressure (Gordon et al. 2010). In the direction of preserving this prized resource, proper mapping, inventorying, and monitoring are decisive factors. Previously enormous work on wetland inventory has been prepared on ground level survey. However, in current times, the satellite imagery-based long-term time series observation has been playing an increasingly better role (Deka and Khan 2011). It has made available a constant basis for key information on the adjoining land uses, the scope of transition area, and eventually their alteration in due course of time (Chen et al. 2013), as well as provide with microscopic level, dynamic, real-time, and profitable information (Klemas 2013; Finlayson 2012).

Thus, the present study has used detailed exercise of remote sensing and GIS techniques for twofold season wetland mapping and monitoring in Deepor Beel area. It has been conceived that Deepor Beel is a permanent freshwater lake and the only Ramsar site in Assam that has a long history of degradation, and there is proof of a long-term decline over the previous two decades (Mozumder and Tripathi 2014). The unremitting wetland loss and steady water quality degradation in Deepor Beel has turned into a rising challenge in sustaining the environment in the surrounding quarters (Bhattacharyya and Kapil 2009). A few numbers of authors have asserted that more than half of the area of Deepor Beel by now has been drained out (Mozumder and Tripathi 2012). Even though significant number of laws subsists for protection, still this invaluable ecological heritage of Assam is at risk (MoEF 2008). Unrelenting unfavorable human activities, repossession of lands for cultivation, filling of wetlands for the intention of occupancy, cutting the sides of wetlands, effluences from diverse sources of waste dumping sites, pressure from unlawful over fishing, slaughter of migratory birds and animal, undue silage practice, harvesting and built-up extension, etc., incalculably shaded pressure in the ecosystem condition of the Deepor Beel area (Mozumder et al. 2014; Bhattacharyya and Kapil 2009). In last three decades, studies carried out have explained that such trend of wetland conversion in Deepor Beel is very much unambiguous. Therefore, this study attempts to analyse the trend of wetland loss, and conversion of wetland due to different natural and manmade reasons in Deepor Beel. At this moment, in time the average wetland area of Deepor Beel is 5.64 km^2 (for the period from 2001 to 2018), which is 49.14% lesser than the preceding wetland coverage (for the period from 1988 to 2000). As a result, the present study intends to build a wetland inventory model with the purpose to carry out an extensive spatiotemporal assessment on Deepor Beel wetlands. The key intention of this paper is to get ready with an effective wetland inventory with convincing approach, elucidating the trend of wetland loss, and assessment of wetland loss over the time. The study seeks to recognize intra-class wetland

transformation in two different seasons in reference to northeastern railway constructions with fragmentation of the wetland landscape in both seasons.

15.2 Study Area

Deepor Beel, a freshwater wetland to be found (Fig. 15.1) about 9 km southwest of Guwahati city, is one of the largest and vital wetlands in Assam with the longitudinal extension of 91° 35′ E to 91° 43′ E and latitudinal extension of 26° 05′ N to 26° 11′ N. This category of wetland is typically found within the biogeographic region of Burma Monsoon Forest (Das and Saikia 2011). In the year 2002, it was acknowledged as one of the most significant wetland systems in India under the Ramsar International Convention on wetlands. The wetland as understood is a discarded channel of the Brahmaputra River located in a U-shaped valley between two cliffs on the north and south (MoEF 2008; Mozumder and Tripathi 2014). The wetland stands 3–5 m deep in the monsoon time of year and up to about 1 m deep in the dry spell of the year, where the focal sources of water to the wetland are monsoon rainfall and a quantity of inflows from Bharalu and Kalman rivers contiguous to the wetland (Mozumder et al. 2014). From an ecological perspective, Deepor Beel acts as a lung of Guwahati city, and more than ten thousand of the populaces directly or indirectly are reliant on this valued wetland. This place is like a dwelling abode to different rare animal species, migratory birds, and plants.

15.3 Materials and Methods

15.3.1 Data

The Landsat satellite (Landsat TM and Landsat 8 OLI, path/row: 137/42,43; spatial resolution: 30 m) imagery data between the year 1988 and 2018 have been collected from USGS and are being used for periodic wetland change monitoring. Landsat image bands 3–5 are generally used to spot wetland aerial extent, as these bands have the potential to differentiate land–water interfaces (Dvorett et al. 2016; Baker et al. 2007; Bera et al. 2008). Topographical map from the
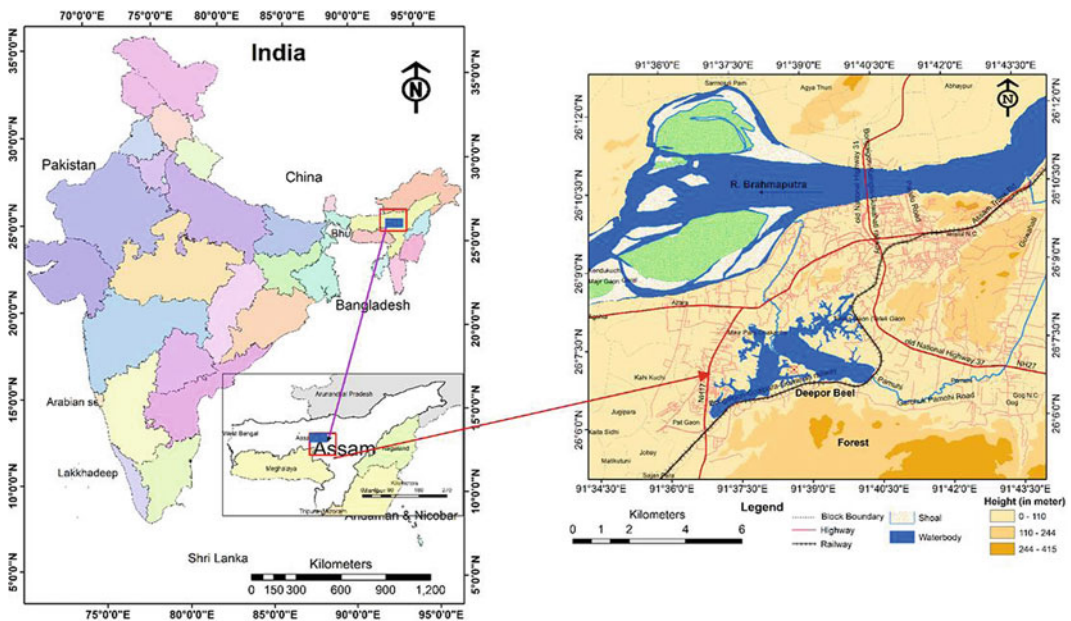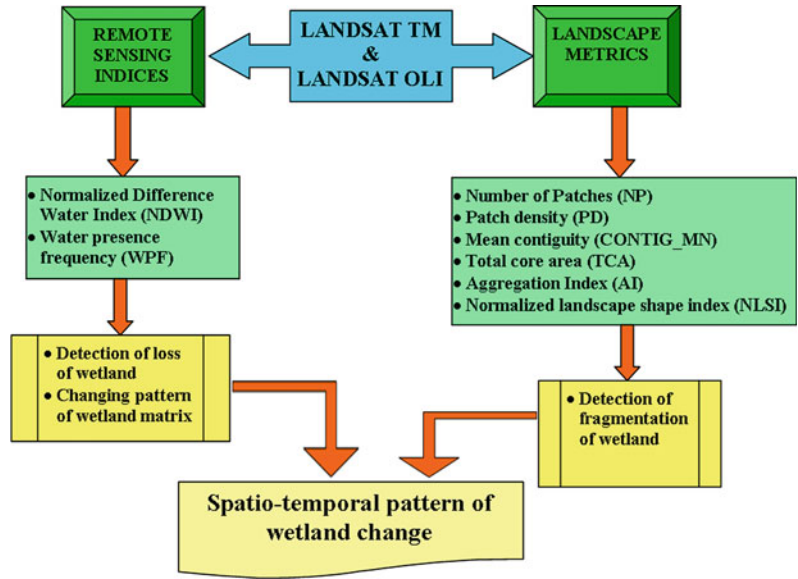

Fig. 15.1 Location of the study area

Fig. 15.2 Flowchart of the methodology of the study

Survey of India (SOI) and Google Earth imagery (2018) is used to plan the base map and make out the wetland's actual area (Fig. 15.2).

15.3.2 Identification of Wetland

Among the different prospective image base indices, normalized differences water index (NDWI) was preferred for wetland identification (McFeeters 1996) because of its maximum reflectance of a water body in the green band and that it plays down the same in the near-infrared band, and hence, water is identified from other objects. NDWI is calculated using Eq. 15.1

$$\text{NDWI} = \frac{\text{Green} - \text{NIR band}}{\text{Green} + \text{NIR band}} \qquad (15.1)$$

where a water body is detected when the value is positive (0–1).

15.3.3 Water Presence Frequency Analysis

Following the identification of wetland from imagery for each year of both pre-monsoon and post-monsoon season, a new method of water presence frequency-based counting approach (Borro et al. 2014; Pal and Saha, 2017) was applied for delineation of moderately steady wetland boundary where actual wetland area is exceedingly forceful in nature. Subsequently, a composite map was made for two different phase, i.e., Phase-I (1988–2000) and Phase-II (2001–2018) by merging all the distinct year imagery, based on extension of northeastern railway network from 1999 to 2000. Water presence frequency (WPF) of each one pixel entity was worked out from Landsat imagery by following Eq. 15.2

$$\text{WPF}_j = \frac{\sum_{i=1}^{n} I_j}{n} \times 100 \qquad (15.2)$$

WPF_j = Water presence frequency of the pixels in a particular time period;

I_j = jth pixel having water in the chosen NDWI imagery;

N = number of images. This value ranges between 0 and 100%.

Value near to 100% indicates high-frequency water body with better stability, and value near to 0 shows low-frequency water body with greater change of volatility or conversion. The derived WPF map was reclassified into three equivalent frequency class zones based on the intensity of

the WPF pixel values: high-frequency class (> 0.66), moderate frequency class (0.33–0.66), and low-frequency class (> 0.33).

15.3.4 Validation

The Kappa coefficient (k) is a commonly used measurement for validating classified satellite imageries (Congalton and Green 2009). Monserud and Leemans (1992) suggested that values lower than 0.4 embody poor or very poor result, values from 0.4 to 0.55 characterize fair result, values from 0.55 to 0.7 signify good result, values from 0.7 to 0.85 stand for very good result, and values higher than 0.85 correspond to an exceptional values. K is calculated in following Eq. 15.3

$$K = \frac{N \sum_{i=1}^{r} x_{ii} - \sum_{i=1}^{r}(x_{i+} * x_{+i})}{N^2 - \sum_{i=1}^{r}(x_{i+} * x_{+i})} \quad (15.3)$$

where N = total number of pixels in a image; r = number of rows in the matrix; X_{ii} = number of observations in row i and column i; x_{i+} and x_{+i} are the marginal totals for row i and column i, respectively.

One hundred and fifty ground control points we have selected from the field for verification of the recent phase wetland map extracted from Landsat images. Three hundred and fifty sites also randomly selected from the higher resolution Google Earth images of the same time periods and cross-checked with actual situation. From result analysis, it is found that overall accuracy is 91.23% in Phase-I, and 79.92% in Phase-II. Here, it should be mentioned that total 350 sites selected from Google Earth images are not uniformly same for all the phases because of change in wetland area and transformation over phases.

15.3.5 Inconsistency in Wetland Area

For computing of wetland loss, we have divided entire time series data for each season into two phases in reference to construction of railway network near the south of Deepor Beel in 1999–2000. For change detection, composite image of second phase is deducted from first phase. Finally, least square regression model has also applied for Phase-I and II and coefficient of determination (R^2) is calculated. Finally, inconsistency in wetland area is calculated with following Eq. 15.4 (Cuddy and Valle 1978).

$$IX = CV \times \sqrt{1 - R^2} \quad (15.4)$$

where R^2 is coefficient of determination.

CV is coefficient of variation of chosen time series water presence area. Less value of IX indicates less inconsistency and vice versa.

15.3.6 Landscape Metrics

Forest area fragmentation methods are employed here for wetland fragmentation analysis. Fragmentation procedure depends on the concept that wetlands might be alienated into parts or fragments that which are separated from each other, while still plainly might fit in the similar system (Huising 2002). For understanding the wetland landscape structure of Phase-I and II, here FRAGSTAT software is used to figure out different fragmentation indices, such as landscape shape index (LSI), landscape division index (LDI), aggregation index (AI) number of patch (NP), patch density (PD), and largest patch index (LPI). The FRAGSTAT software assists in spatial pattern analysis for categorical maps like land use change. Fine points of the chosen matrices used in this study are presented in Table 15.1.

15.4 Result and Discussion

15.4.1 Periodic Inventory of Wetland in Pre-Railway (Phase-I, 1988–2000) and Post-Railway Network (Phase-II, 2001–2018) Construction

Water body areas have been subjected to speedy changes in Deepor Beel due to modification in

Table 15.1 List of selected landscape metrics for analyzing landscape fragmentation

Indices	Symbol	Value	Description	References
Patch number	NP	$1 \leq NP \leq Nmax$	Number of patches of a specific class	Turner et al. (1989)
Patch density	PD	$0 \leq PD$	Number of patches of a specific class per unit area (standardized to 100 ha in FRAGSTATS)	McCarigal and Marks (1995)
Mean contiguity	CONTIG MIN	$1 \leq N \leq 1$	Spatial connectedness of cells within a grid to yield an index highlighting configuration of the patch outline	Johnson et al. (2007)
Total core area	TCA	$0 \leq CORE \leq 1$	Amount of area whose boundary started from patch edge to interior in specified distance	McCarigal and Marks (1995)
Aggregation index	AI	$0 \leq AI \leq 1$	Ratio between actual edge and total amount of possible edge	Bregt and Wopereis (1990)

land use change by different anthropogenic causes (Plate 1). Appraisal of multi-temporal NDWI has made known that in average, a total of 5.45 km^2 water body areas have been lost since 1988–2018 (Fig. 15.5). Wetland loss in a range of categories (high, moderate, and low water presence frequencies) for Phase-I and II has also been calculated as given in Table 15.2. There are serious hydro-ecological inferences for wetlands in Deepor Beel owing to modification in the inter-annual periodic and inter-seasonal water presence frequency changes. It has been observed that wetlands of periphery areas are fairly more conflicting than the deeper part. The hydrologic gradient of WPF zone shows that marginal parts of wetlands being inconsistent are more prone to loss (Fig. 15.4). Permanent core part and seasonal marginal wetted areas in pre- and post-railway construction periods have been calculated by using the average water pixel count, as presented in Figs. 15.3a, b and 15.4a, b, respectively. During the pre-railway period, the perennial high-frequency and low-frequency seasonal wetlands in Deepor Beel covered almost 8.30 km^2 and 2.79 km^2, respectively, while in the post-railway period, these areas were abridged to 4.31 km^2 and 1.33 km^2, respectively. Therefore, the perennial and semi-perennial wetland areas have declined by 58 and 33% subsequent to the construction of the railway

network. An additional inference puts into light that there is no notable distinction in the seasonal pattern of precipitation and temperature in the post-railway network construction phase, excluding a significant decrease in eastern shallow and marginal parts in wetlands.

Steady wetland area loss (approx. 40–50%) in Deepor Beel is recorded from Phase-I to Phase-II (Fig. 15.5). Permanent wetted area reduced significantly in both phases (Figs. 15.6 and 15.7).

From 1988 to 2018, the common trends in the wetlands area for both the seasons indicate that there was no specific trend as is evident in Phase-I and Phase-II. In pre-monsoon season of Phase-I, the rate of coefficient of determination is very meager ($r^2 = 0.556$), but it has slightly improved in Phase-II, as signified by the high coefficient ($r^2 = 0.654$). The average area in both the phases was also calculated and is shown in Fig. 15.8a, b. The average wetland area of the pre-monsoon period condensed from 7 to 6 km^2 between Phase-I and Phase-II (Fig. 15.8a, b). Conversely, in the post-monsoon season a noteworthy change in wetland area was spotted between Phase-I and Phase-II, but after construction of the railway line and extreme modification in land use change, has resulted in decline of wetland area by almost 35%. Discrepancy in the oscillation of wetland area during post-monsoon seasons has amplified (Table 15.3). These results further point out that

Table 15.2 Water presence frequency in different classes

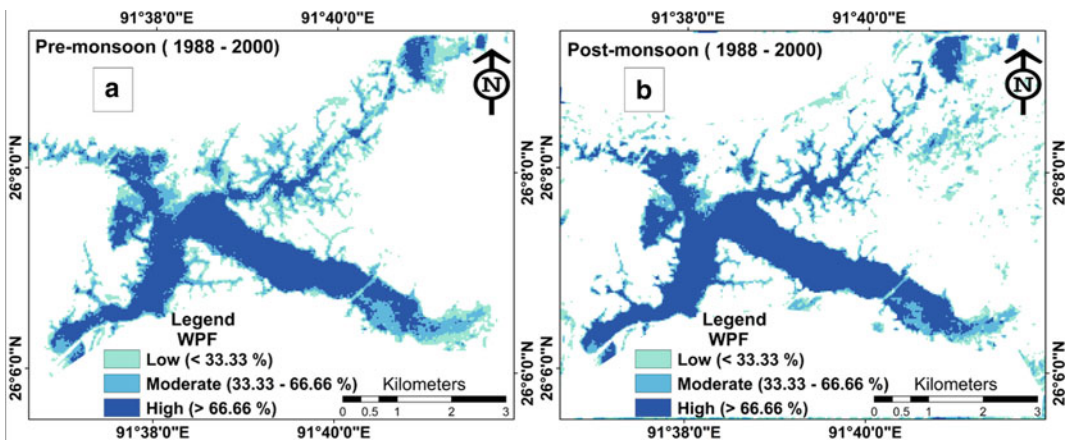|	Water presence frequency class (%)	Pre-monsoon (Area in km^2)	Post-monsoon (Area in km^2)
Phase-I	High (< 33.33)	4.8132	6.6645
	Moderate (33.33–66.66)	3.4893	4.2237
	Low (> 66.66)	2.7981	4.4064
Phase-II	High (< 33.33)	1.98	3.9195
	Moderate (33.33–66.66)	2.3355	2.0844
	Low (> 66.66)	1.3302	2.7081

Fig. 15.3 Water presence frequency distribution in Phase-I: **a** pre-monsoon and **b** post-monsoon
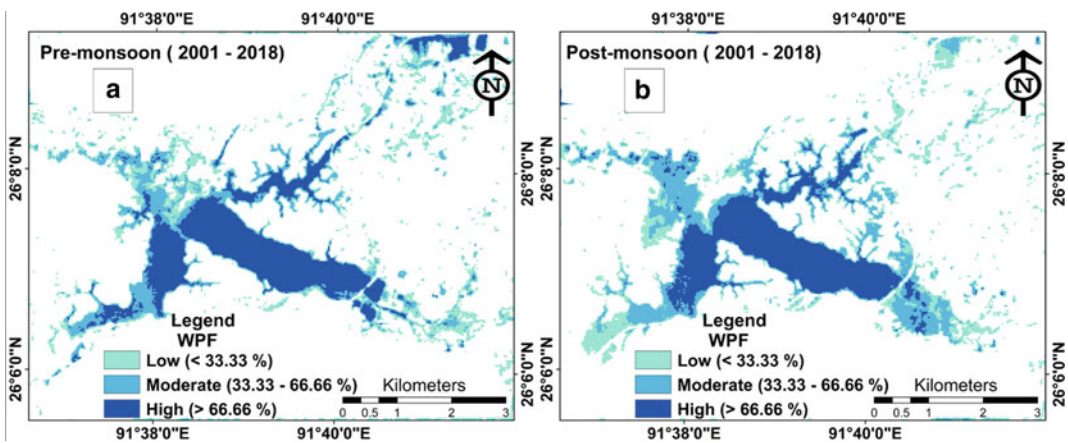

Fig. 15.4 Water presence frequency distribution in Phase-II: **a** pre-monsoon and **b** post-monsoon
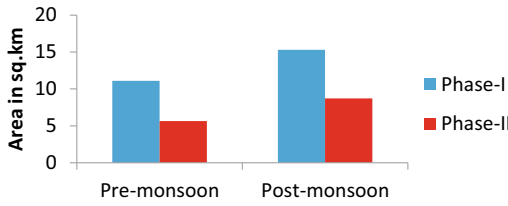
Fig. 15.5 Wetland loss in different phases

construction of railway network in the region of Deepor Beel has drastically speeded up the pace of wetland loss.

15.4.2 Change Matrix of Different Classes of Wetlands

Intra-class wetland transformation portrays the character of wetlands transformation in Deepor Beel (Fig. 15.9a, b) involving the pre- and post-railway Phase-I and II for both seasons. Table 15.4 symbolizes the percentage of area under transformation from one frequency class to another class. The assessment specifies that in the pre-monsoon season about 2.41 km^2 remains unaffected, while 5.45 km^2 of wetland area is lost
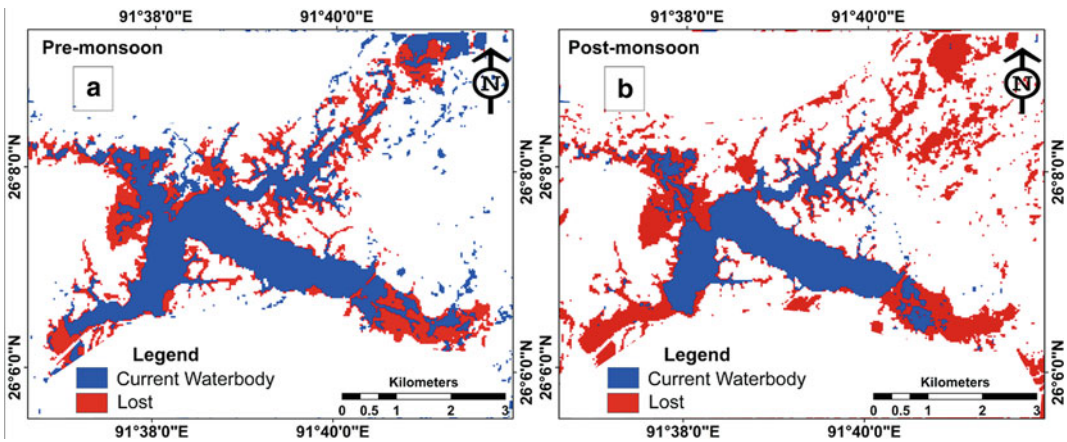

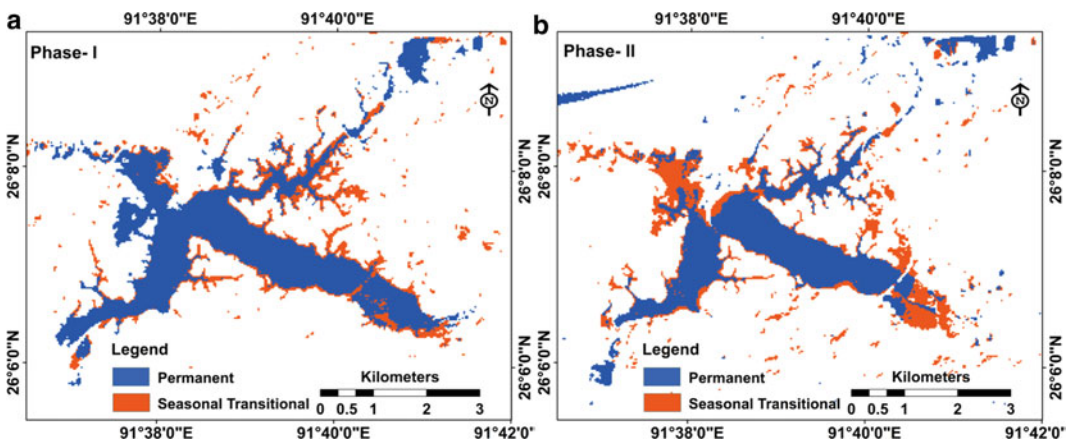**Fig. 15.6** Wetland loss: **a** pre-monsoon and **b** post-monsoon

Fig. 15.7 Actual wetland extent in different phases: **a** Phase-I and **b** Phase-II
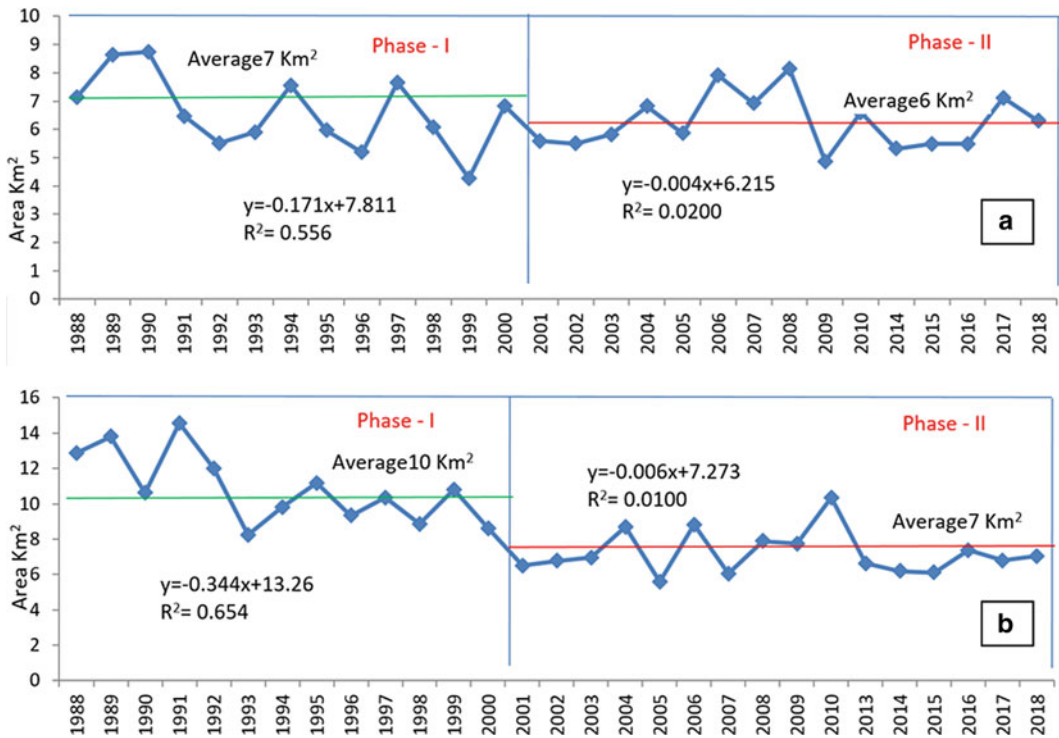
Fig. 15.8 Changing trend of wetland area: **a** pre-monsoon and **b** post-monsoon

Table 15.3 Inconsistency of wetland area in Deepor Beel

Phase	Season	$Y = a + bx$	r^2	cv	$\sqrt{1 - R^2}$	IX
I	Pre-monsoon	$y = -0.171x + 7.811$	0.556	19.91835	0.8625	17.17958
	Post-monsoon	$y = 0.004x + 6.215$	0.010	15.56635	1	15.56635
II	Pre-monsoon	$y = -0.344x + 13.26$	0.654	18.34165	0.7389	13.55264
	Post-monsoon	$y = -0.006x + 7.273$	0.020	17.0951	1	17.0951

and a total of 3.04 km^2 of area is transformed into other categories (i.e., transformation from high to medium to low-frequency classes). On the other hand, in post-monsoon season, 4.71 km^2 areas remain unchanged in various water presence frequency categories (Fig. 15.9a, b). On the whole, our study found major reductions in wetland area and greater wetland fragmentation after the construction of railways in southern part in 2001, as weighed against to the preceding decades phenomena which are definitely not exclusive of creating an impact on the local environment, fauna, and inhabitants of the area.

15.4.3   Wetland Fragmentation

In the direction of analyzing the changes in the wetland landscape, after construction of the railway network and other modification in the surrounding area of Deepor Beel, Fig. 15.10(a, b) and (c, d) demonstrates a few indices of fragmentation, for example the large core indices, small core, perforated, edge, and patch, for Phase-I & II in different seasons. Smaller size wetland patches, as well as patch density, have dwindled, large numbers of them have declined, plus low core wetland patches have clearly increased.
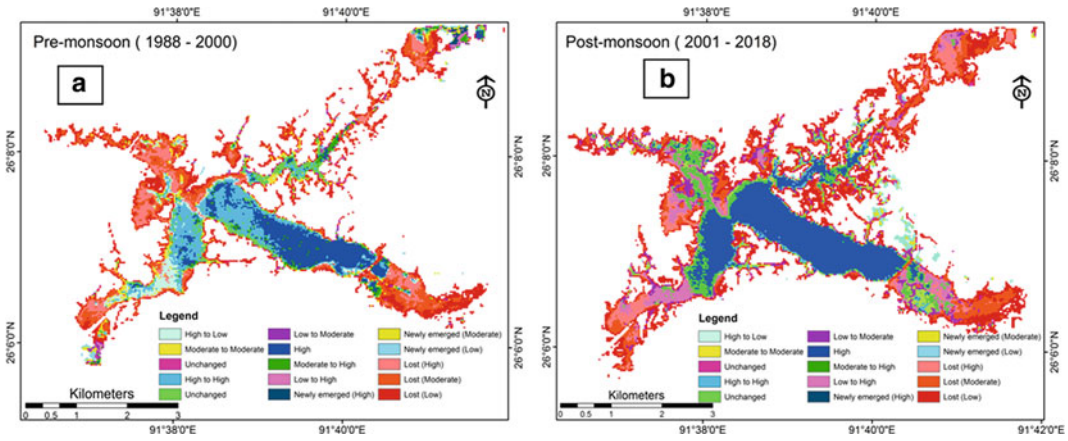
Fig. 15.9 Change matrix of water presence frequency class from Phase-I (**a**) to Phase-II (**b**)

Table 15.4 Change matrix between Phase-I and Phase-II in pre-monsoon and post-monsoon

Category	Pre-monsoon				Post-monsoon			
	Pixel	Area (km^2)	Area%	Total area	Pixel	Area (km^2)	Area%	Total area
Low to moderate	119	0.1071	0.964813	3.0402	1128	1.0152	6.637637	3.636
Low to high	67	0.0603	0.543214		1215	1.0935	7.149582	
Moderate to low	569	0.5121	4.613264		97	0.0873	0.57079	
Moderate to high	259	0.2331	2.099886		1289	1.1601	7.58503	
High to low	625	0.5625	5.067294		6	0.0054	0.035307	
High to moderate	1739	1.5651	14.09924		305	0.2745	1.794751	
Lost (Low)	2509	2.2581	20.34214	5.4549	2991	2.6919	17.60033	6.5826
Lost (Moderate)	2177	1.9593	17.6504		2893	2.6037	17.02366	
Lost (High)	1375	1.2375	11.14805		1430	1.287	8.414735	
Unchanged (Low)	184	0.1656	1.491811	2.4102	350	0.315	2.05955	4.716
Unchanged (Moderate)	672	0.6048	5.448354		856	0.7704	5.037072	
Unchanged (High)	1822	1.6398	14.77217		4034	3.6306	23.73779	
Newly emerged (Low)	90	0.081	0.72969	0.1953	86	0.0774	0.506061	0.36
Newly emerged (Moderate)	71	0.0639	0.575645		140	0.126	0.82382	
Newly emerged (High)	56	0.0504	0.45403		174	0.1566	1.023891	

Uninterrupted encroachment by agricultural field and built-up area has been areas on in the rapid shrinkage of major core area of the Beel. In post-monsoon season, there has been a considerable boost in patch number in Phase-II. Result shows that in Phase-I (1988–2000), the number of patches (NP) increased to 61 and to 91 in Phase-II (2001–2018), whereas the largest patch index (LPI) has decreased from 39.10 (1988) to 16.65 (2018). These results equally denote the fact of wetland loss in terms of fragmentation of Deepor Beel. While the mean shape index value has decreased, which means shape complexity has also decreased, but in fact a few small. Largest
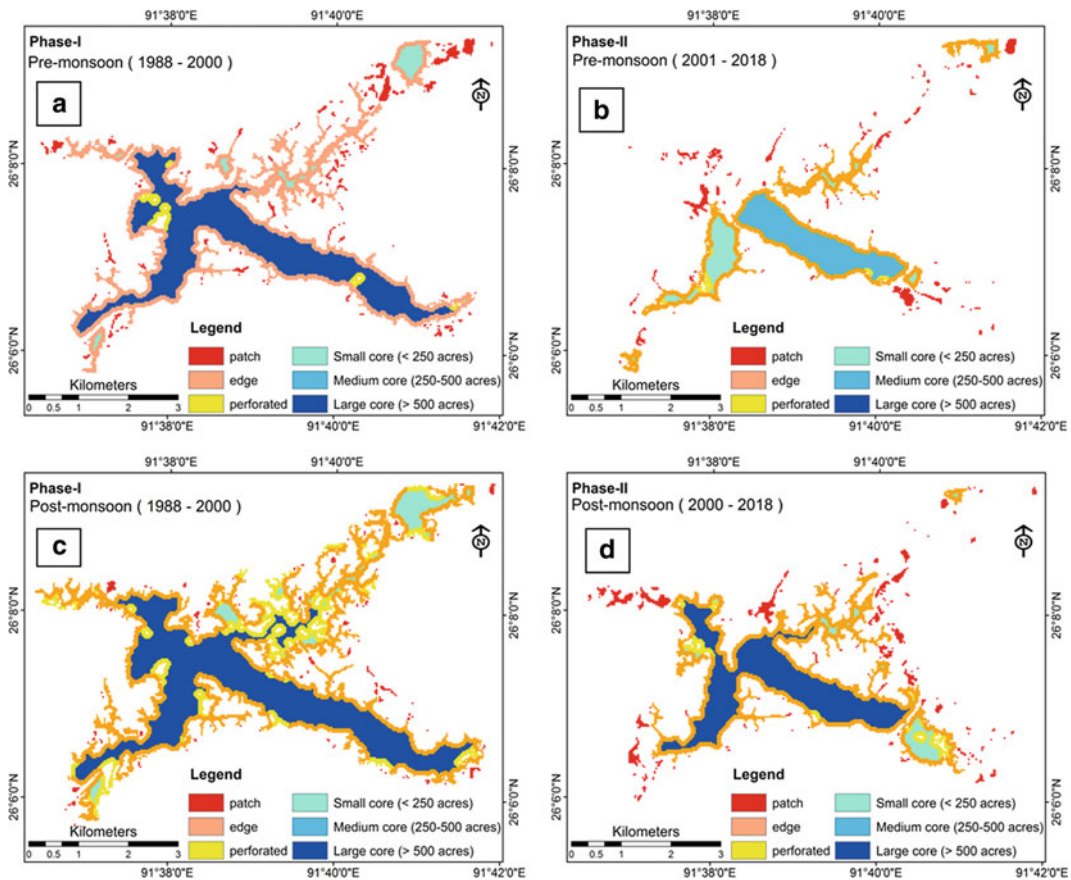
Fig. 15.10 Wetland fragmentation in Phase-I and Phase-II (for pre-monsoon (**a, b**) and post-monsoon (**c, d**))

patch index (LPI) value decreased ensuing the trends from west to east direction which bears a resemblance to the like in the trends of edge density. Numbers of patches (NP) have been identified among the 18 IDs, where important changes have been found in 30 years (Table 15.5). The high positive correlation between class area (CA) and number of patches (NP) notably specifies that the number of patches has increased in the projected area. On the whole, the ending product shows a significant decrease of aggression of water body area in last 30 years, and as in pre-monsoon season the AI value has been reduced to 90.97 in Phase-I to 89.48 in Phase-II.

15.5 Conclusion

The overall time series change detection investigation has found significant decrease in wetland area in Deepor Beel The construction of a Railroad along the Southern Boundary of the Deepor Beel in 2001 by Northeast Frontier Railway (NFR) fragmented the water body into two parts, which caused severe unfavorable consequences on the wetland ecosystem together with the local home environment, fauna, as well as on the inhabitants of the area. High embankment for the railway line has hindered the easy flow of water in the Beel which in turn has caused disturbance

Table 15.5 Wetland fragmentation in Deepor Beel

Season	Wetland fragmentation category	Phase-I (Pixel)	Area (km^2)	Phase-II (Pixel)	Area (km^2)	Change	% of change
Pre-monsoon	Patch	835	0.7515	727	0.6543	−108	−12.9341
	Edge	5568	5.0112	2828	2.5452	−2740	−49.2098
	Perforated	299	0.2691	126	0.1134	−173	−57.8595
	Small core	361	0.3249	685	0.6165	324	89.75069
	Medium core	0	0	1907	1.7163	1907	0
	Large core	5271	4.7439	0	0	−5271	−100
	NP	61	–	91	–	–	–
	LPI	39.10	–	16.65	–	–	–
	AI	90.79	–	89.48	–	–	–
Post-monsoon	Patch	318	0.2862	1009	0.9081	691	217.2956
	Edge	7076	6.3684	4243	3.8187	−2833	−40.0367
	Perforated	2140	1.926	374	0.3366	−1766	−82.5234
	Small core	689	0.6201	346	0.3114	−343	−49.7823
	Medium core	0	0	0	0	0	0
	Large core	6771	6.0939	3708	3.3372	−3063	−45.237
	NP	59	–	91	–	–	–
	LPI	61	–	31	–	–	–
	AI	91.57	–	89.87	–	–	–

to the entire ecosystem of the Beel, which in turn has led to increase in average water temperature, algae concentration, and water hyacinth condition in water. The consequences of the railway construction resulted in major cropland lost, and it was last verified by the classified maps (accuracy 88%) of Deepor Beel catchment area. It is estimated that roughly about 9.00 km^2 of croplands has by now been lost owing to the railway construction. An imperative fact to be noted is that the Guwahati Municipality waste dump yard (covering 24 ha area) located in Boragaon, which lies in the northeastern corner of Deepor Beel became functional in the year 2005, has significantly changed the projected area. Consequently, there has been steady pollution of heavy metal, oil salt content, and other toxic components that have continuously been worsening the water quality permanently. Urbanization in Guwahati city is miscellaneous and fragmented owed to the rugged nature of topography which falls out in

the modification of the natural land cover of the city. In the past there was an eco-sensitive green belt area, particularly toward the edge of Deepor Beel in the city. But as a result of the shifting of the state capital from Shillong to Dispur has built an added pressure on that area as in the upcoming days. Factors like population pressure, interchange traffic passages, and concretization in Guwahati city will increase undeniably. In view of that in the very last two decades, the city has faced lots of tribulations due to speedy and impromptu expansion of urbanization, which has hastened up environmental degradation and which may even jeopardize the biodiversity of that area. On the whole, the anthropogenic activities have turned out to be as a major cause for the wetland ecosystem modification in this area.

The present study endeavored to demarcate and observe continuing as well as seasonal hydro-physical dynamics in Deepor Beel

wetland areas by using a Landsat satellite image-based water presence frequency technique in different stages. This work aims to exhibit the practicality of this technique for creation of an effective wetland inventory model, which can be brought into play for accurate wetland delineation. The upgrading of this technique by making use of time series satellite imagery resulted in enhanced precision for delineation of wetland and even made it possible to overcome the difficulty of identification of peripheral transition zone in a dynamic wetland ecosystem. The upshot in addition reported evidence on how anthropogenic influence is accountable for wetland loss, wetland breakup, and wetland conversion. In Phase-II, results have shown that triggered by numerous factors, the wetland area during the pre-monsoon season has been abridged by 49.14%, and during the post-monsoon, it has been reduced by almost 43.03%. In the pre-monsoon season, currently, the wetland area is 5.64 km^2, out of which 76.43% is relatively stable and 23.56% is in the transitional zone, at risk to loss. Landscape metrics display results that Deepor Beel fragmentation persists at a very speedy pace owing to the extension the of railway network around the wetland, encroachment of the Guwahati city area and disposal of solid waste in northwestern part, etc., and this in due course is resulting in conversion of core wetland area to transitional low zone. Noteworthily, the wetland habitat loss which holds valued importance has augmented an increase in extinction of the rare species and further poses a threat to the lives and livelihoods of the local community. To restore Deepor Beel ecosystem for reducing future fragmentation and alteration, the following remedies may be implemented, like creation of a buffer zone by afforestation to prevent further land conversion, frequent monitoring of the wetland using remote sensing techniques, promoting environmental awareness program among stakeholders, managing alternative livelihood choices to those depending upon the lake, and at last enforcement of the Deepor Beel action plane policies strictly. This study is in progress and the other drivers of

change in the wetland ecosystem in Deepor Beel area, such as hydrological, geomorphological, topographic, and socioeconomic factors are being reflected on for future studies.

References

Baker C, Lawrence RL, Montagne C, Patten D (2007) Change detection of wetland ecosystems using Landsat imageryand change vector analysis. Wetlands 27:610–619

Bera SK, Dixit S, Basumatary SK, Gogoi R (2008) Evidence of biological degradation in sediments of Deepor Beel Ramsar Site, Assam as inferred by degraded palynomorphs and fungal remains. Curr Sci 95:178–180

Bhattacharyya KG, Kapil N (2009) Impact of urbanizationon the quality of water in a natural reservoir: a case study with the Deepor Beel in Guwahati City, India. Water Environ J 24:83–96

Borro M, Morandeira N, Salvia M, Minotti P, Perna P, Kandus P (2014) Mapping shallow lakes in a large South American floodplain: a frequency approach on multitemporal Landsat TM/ETM data. J Hydrol 512:39–52. https://doi.org/10.1016/j.jhydrol

Chen Y, Huang C, Ticehurst C, Merrin L, Thew P (2013) An evaluation of MODIS daily and 8-day composite products for floodplain and wetland inundation mapping. Wetlands 33(5):823–835. https://doi.org/10.1007/s13157-013-0439-4

Congalton RG, Green K (2009) Assessing the accuracy of remotely sensed data: principles and practices, 2nd edn. CRC Press, Boca Raton, FL

Cuddy JD, Della Valle PA (1978) Measuring the instability of time series data. Oxford Bull Econ Stat 40(1):79–85

Cutter SL, Finch C (2008) Temporal and spatial changes in social vulnerability to natural hazards. PNAS 105:2301–2306. https://doi.org/10.1073/pnas.0710375105

Das RT, Pal S (2017) Exploring geospatial changes of wetland in different hydrological paradigms using water presence frequency approach in Barind Tract of West Bengal. Spat Inf Res 1–13. https://doi.org/10.1007/s41324-017-0114-6

Das J, Saikia PK (2011) Species diversity of water birds in Deepor Beel, Assam. J Res Biol 5:363–369

Deka J, Khan L (2011) A multi-temporal remote sensing approach for monitoring changes in spatial extent of freshwater lake of Deepor Beel Ramsar site, a major wetland of Assam. J Wetl Ecol 2011:40–47

Dvorett D, Davis C, Papes M (2016) Mapping and hydrologic attribution of temporary wetlands using recurrent landsat imagery. Wetlands 36(3):431–443

Finlayson CM (2012) Forty years of wetland conservation and wise use. Aquat Conserv Mar Freshwat Ecosyst 22:139–143

Gordon LJ, Finlayson CM, Falkenmark M (2010) Managing water in agriculture for food production and other ecosystem services. Agric Water Manage 97:512–519

Huising EJ (2002) Wetland monitoring in Uganda. Int Archiv Photogram Remote Sens 34(6/W6):127–135

Klemas V (2013) Remote sensing of emergent and submerged wetlands: an overview. Int J Remote Sens 34(18):6286–6320. https://doi.org/10.1080/01431161.2013.800656

Marti-Cardona B, Dolz-Ripolle SJ, Lopez-Martinez C (2013) Wetland inundation monitoring by the synergistic use of ENVISAT/ASAR imagery and ancilliary spatial data. Remote Sens Environ 139:171–184. https://doi.org/10.1016/j.rse.2013.07.028

McFeeters SK (1996) The use of the Normalized Difference Water Index (NDWI) in the delineation of open water features. Int J Remote Sens 17(7):1425–1432. https://doi.org/10.1080/01431169608948714

Mitsch WJ (2010) Conservation, restoration and creation of wetlands: a global perspective. In: Comin F (ed) Ecological restoration: a global challenge. Cambridge University Press, Cambridge, pp 175–188

MoEF (2008) Report on visit to Deepor Beel in Assam: a wetland included under national wetland conservation management

Monserud RA, Leemans R (1992) Comparing global vegetation maps with the Kappa statistic. Ecol Model 62(4):275–293. https://doi.org/10.1016/0304-3800(92)90003-W

Mozumder C, Tripathi NK, Tipdecho T (2014) Ecosystem evaluation (1989–2012) of Ramsar wetland Deepor Beel using satellite-derived indices. Environ Monit Assess 186:7909–7927

Mozumder C, Tripathi NK (2012) Use of multiple satellite images for feature extraction and image classification: a case study of Ramsar wetland in North East India. In: Asian conference on remote sensing. Asian Association of Remote Sensing, Pattaya, Thailand, p 7

Mozumder C, Tripathi NK (2014) Geospatial scenario based modelling of urban and agricultural intrusions in

Pal S (2015) Impact of Massanjore dam on hydrogeomorphological modification of Mayurakshi River, easern India. Environ Dev Sustain 18(3):921–944. https://doi.org/10.1007/s10668-015-9679-1

Pal S, Osoundu CA (2009) Water scarcity in wetland area within Kandi Block of West Bengal: a hydro-ecological assessment. Ethiop J Environ Stud Manage 2(3):1–17

Pal S, Saha TK (2017) Identifying dam-induced wetland changes using an inundation frequency approach: the case of the Atreyee River basin of Indo-Bangladesh. Ecohydrol Hydrobiol 18(1):66–81

Prasad SN, Ramachandra TV, Ahalya N, Sengupta T, Kumar A, Tiwari AK, Vijayan VS, Vijayan L (2002) Conservation of wetlands of India—a review. Tropical Ecol 43(1):173–186

Ramsar wetland Deepor Beel in Northeast India using a multi-layer perceptron neural network. Int J Appl Earth Obs Geoinf 32:92–104

Ramsar (2004) The Ramsar convention manual: a guide to the convention on wetlands, 3rd ed. Ramsar Convention Secretariat, Gland, Switzerland. Ramsar, Iran (1971). Available at: http://www.ramsar.org/lib/lib_manual2004e.htm

Ward JV, Tockner K, Arscott DB, Claret C (2002) Riverine landscape diversity. Freshw Biol 47(5):517–539. https://doi.org/10.1046/J.1365-2427.2002.00893.X

Zedler JB, Kercher S (2005) Wetland resources: status, trends, ecosystem services, and restorability. Annu Rev Environ Resour 30:39–74

Part III

Urban Climate, Heat Island and Hazard

GIS-Based Methodology and World Urban Database and Access Portal Tools (WUDAPT) for Mapping Local Climatic Zones: A Study of Kolkata

Sk Ajim Ali, Farhana Parvin, Ateeque Ahmad, and S. Najmul Islam Hashmi

Abstract

Stewart and Oke's local climate zone (LCZ) is one of the commonly used international standards for analysing urban morphology and the resulting urban heat island phenomena. In-situ measurements, GIS-based calculations, and remote sensing image-based computations are the most common approaches for LCZ mapping. There are, however, just a few studies that address their accuracy and applicability. The objective of this study is to examine the LCZ of Kolkata Metropolitan Area (KMA) using GIS-based methodology as well as the WUDAPT. Due to its complicated urban morphology and high-density setting, KMA was chosen as the study area. Both techniques can detect LCZ categories that reflect the actual geographical pattern of land use in Kolkata, according to the study findings. When exact urban morphology data is unavailable, WUDAPT level 0 data can be utilised as input data for micro-scale weather and climate modelling. Meanwhile, the GIS-based methodology identifies more information at the district level than the WUDAPT method.

The WUDAPT technique, on the other hand, identifies land-cover types more precisely. The findings give a thorough grasp of various LCZ mapping approaches, as well as their benefits and drawbacks. The present study can also assist climatologists, modellers, and developers in selecting an effective LCZ mapping approach for their urban climate research.

16.1 Introduction

Not only has urbanisation altered the physical environment of cities, but it has also resulted in the creation of local climatic traits and features that are unique to cities (Hong et al. 2019; Rosenzweig et al. 2005; Ruocco et al. 2015; Tayanç et al. 2009; Xiao et al. 2011; Zeng et al. 2016). One of the most prominent repercussions of urbanisation and industrialisation in the twenty-first century is the urban heat island (UHI) impact (Mohan et al. 2011; Priyadarsini 2009). It is also a popular issue that has been researched using a variety of methodologies and techniques all across the world. LCZs are the world's first attempt to standardise urban climate studies. Many researches in this subject have

S. A. Ali (✉) · F. Parvin · A. Ahmad · S. Najmul Islam Hashmi
Department of Geography, Faculty of Science, Aligarh Muslim University, Aligarh, India
e-mail: skajimali.saa@gmail.com; skajimali@myamu.ac.in

used this notion and approach since then (Quan and Bansal 2021). Because of a consistent LCZ definition and categorisation hierarchy, cross-comparisons across various UHI studies around the world are conceivable (Wang et al. 2018). More importantly, because urban knowledge is key for climate change research and climatic-responsive design, the LCZ classification output data and understanding might be used for weather and climate modelling and other applications (Aslam and Rana 2022; Dissanyake and Weerasinghe 2021; Fu et al. 2022; Ren et al. 2021; Shi et al. 2018).

The phrases urban and rural are frequently used interchangeably in the urban climate literature on UHIs (Martilli et al. 2020). Stewart (2011) analysed the relevant literature and found that the lack of crucial site information detailing field site features is a serious issue in the available literature. Stewart and Oke (2012) created the LCZ categorisation system to solve the difficulty of connecting UHI presence to land-cover type. Three types of properties are included in the categorisation system: built series, land-cover series, and changeable land-cover properties. The LCZ scheme's strength resides in its thorough categorisation of urban land-use types. The LCZ scheme is a systematic and quantitative way for describing and explaining the physical features of urban morphology and their associated urban climatic qualities (Stewart and Oke 2009, 2010). Ten different construction types (LCZs 1–10) and seven different land-cover types make up the 17 different LCZ types (LCZ A–G). Some of the properties that may be separated by metadata for each LCZ class are sky view factor (SVF), building surface percentage, pervious surface fraction, height of roughness components, and terrain roughness class (Stewart and Oke 2012). Different cities can categorise and build their own LCZs based on land-use kinds and morphological traits, according to the LCZ system (Stewart and Oke 2009). The identical scheme created by LCZs aids in the investigation of the UHI phenomena in various cities (Nassar et al. 2016).

Many research on UHI have been undertaken, although the majority have concentrated on big metropolitan regions such as New York City (Bornstein 1968), Atlanta, Georgia (Bornstein and Lin 2000), Singapore (Chow and Roth 2006), and Mexico City, Mexico (Cui and de Foy 2012). These examples show how to compare and contrast well-defined urban and rural locations. Urban–rural gradients (Imhoff et al. 2010) have received less attention, although they may be more essential for describing the locations of UHIs in urban-adjacent areas (e.g. suburbs, subdivisions, and city sprawl). This was a challenging process before the LCZs were defined. The LCZ system has been used to identify and quantify UHI intensity in Singapore (Ng 2015), Nagano, Japan, Vancouver, British Columbia, Canada, Uppsala, Sweden (Stewart et al. 2014), Novi Sad, Serbia (Savic et al. 2013), and Phoenix, Arizona (Middel et al. 2014), as well as in the United States (Zhao et al. 2014).

GIS-based and remote sensing image (RSI)-based approaches are the most common LCZ methods (Ren et al. 2016). These strategies each have their own set of benefits and drawbacks (Wang et al. 2018). LCZs are frequently mapped using GIS-based methods. It employs precise GIS data on urban morphology, planning, and even building information to compute each contributing component for identifying LCZs (Chen et al. 2020). This approach was utilised by several researchers to create LCZ classification maps for their studies (Perera et al. 2012; Lelovics et al. 2014; Liu and Shi 2020). GIS-based approaches may generally achieve high accuracies since their information is drawn from genuine urban topologies. However, not all GIS data in every city is full or available to the public, particularly in developing nations and areas (Wang et al. 2018).

Another extensively used approach for classifying LCZ classes is the RSI-based method (Deur et al. 2021). The remote sensing image classification methods used to extract LCZ classes by analysing their spatial and spectral information include object-based image analysis, supervised classification, hierarchical

classification with different Normalized Difference Vegetation Indices (NDVI), and multi-source satellite images (Bechtel et al. 2016; Zhongli and Hanqiu 2016). LCZ classification uses a variety of remote sensing images (Bechtel and Daneke 2012; Feng et al. 2019; Liu and Shi 2020; Zhongli and Hanqiu 2016). WUDAPT is a global initiative and volunteer programme that employs RSI-based LCZ classification algorithms. Its goal is to provide a simple LCZ classification technique that takes use of free data sources like Landsat photographs and Google Earth training samples (Bechtel et al. 2015, 2016). As a consequence, many researchers from all around the world have adopted and implemented the WUDAPT technique in their UHI research (Brousse et al. 2016; Cai et al. 2016; Wang et al. 2019). It intends to provide three different sorts of goods: Level 0 contains primarily two-dimensional urban morphological data and a rough urban function based on their impact on local air temperature (Stewart and Oke 2012); Levels 1 and 2 contain more detailed three-dimensional urban morphological data, material composition data, and anthropogenic functions at the building level, making them suitable for various climate models (Ching et al. 2017).

Although multiple classification techniques have been developed since the LCZ scheme was announced, few cross-comparison studies have been conducted to compare the classification accuracy and application of various LCZ mapping procedures. As a result, the current study looks at the accuracy of both GIS-based and WUDAPT level 0 techniques, as well as their relevance in real-world scenarios. Because of its complex urban morphology and data availability, the Kolkata Metropolitan Area was chosen as the case study city. A performance review is also carried out to determine the applicability of both methodologies. The findings of the study can aid researchers in choosing an acceptable LCZ mapping approach, as well as developing and improving their accuracy.

16.2 Geographical Profile of the Study Area

The Kolkata Metropolitan Area (KMA) was utilised as a case study for mapping local climate zones in this study (Fig. 16.1). Kolkata is one of Eastern India's most important fast-growing million-population cities, with substantial effects from rapid urbanisation in the periphery and sprawl expansion (Sahana et al. 2018). Kolkata has a wet-dry subtropical climate (Köppen climatic classification Aw) with a monsoon season. Summers are hot and humid, with temperatures in the low 30 s, and maximum temperatures frequently approach 40 °C during dry periods in May and June (Talapatra et al. 2021). The yearly average temperature is 26.8 °C, with monthly average temperatures ranging from 15 °C to 30 °C (Fig. 16.2).

The population of the KMA has increased at an annual pace of around 2% over the previous two decades, from 9.19 million in 1981 to 13.21 million in 2001 and 14.11 million in 2011 (Mitra et al. 2012). This population increase in the suburbs has hastened peripheral urban growth in the KMA, especially in recent decades. During independence, the KMA encompassed roughly 361 km^2. However, by 1991 and 2001, it had grown to 1350 km^2 and 1851.41 km^2, respectively. KMA now covers an area of 1886.67 km^2 (Das et al. 2021). As suburbanisation has swiftly consumed agricultural land, plant cover, and water bodies around the perimeter, the metropolitan area's expansion has remained unrestrained (Fig. 16.3).

With the rate of urban growth, the pattern of urban land use and land-cover changes dramatically over time. The surface temperature of the region rises as the amount of vegetation decreases and the amount of urban or built-up area grows. The city's inner regions have a high temperature, which gradually drops as you move out to the outskirts. It has major consequences for the global ecology (Chatterjee and Majumdar 2021). It is also to blame for local climate
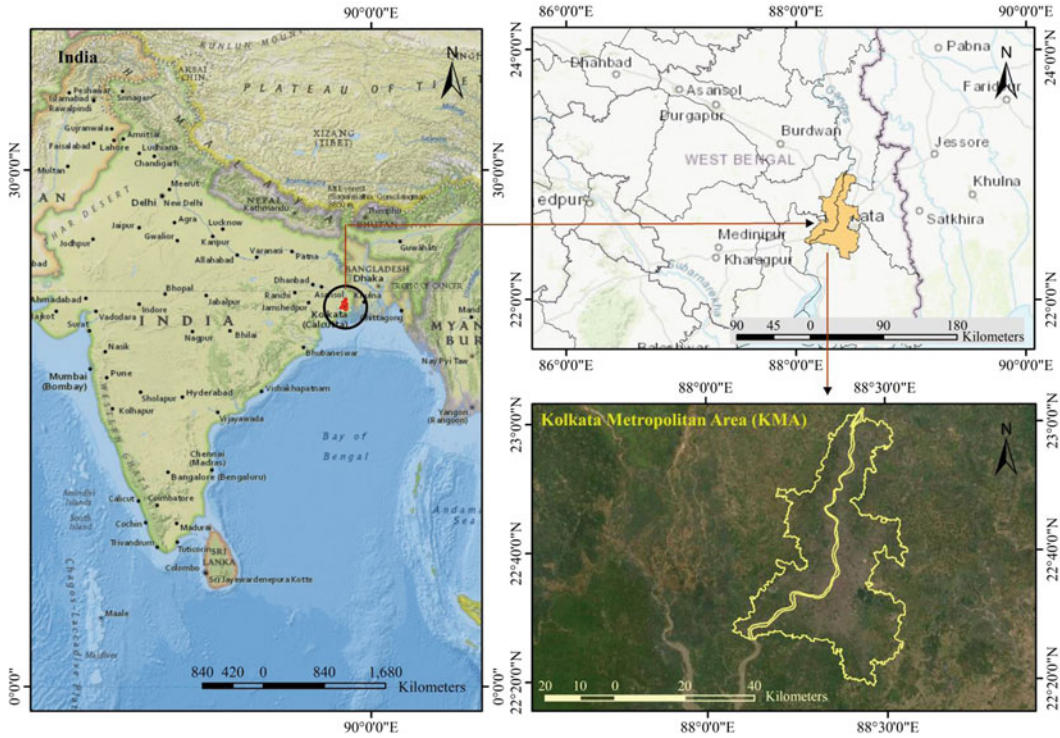
Fig. 16.1 Location of the study area. *Source* Prepared by the authors

change, habitat damage, and biodiversity loss (Skogen et al. 2018). In China, where tremendous urbanisation has occurred over the previous three decades, the extent of UHI is particularly pronounced (Zhou et al. 2016).

16.3 Objectives of the Study

The objectives of the present study regarding to GIS-based methodology and World Urban Database and Access Portal Tools (WUDAPT) for mapping local climatic zones: A study of Kolkata are given in a sequent manner:

(i) To examine the local climate zone (LCZ) of Kolkata Metropolitan Area.
(ii) To develop a GIS-based methodology for classifying LCZ by utilising built-up classification, land-cover classification, and land surface temperature as input parameters.

(iii) To assess WUDAPT methodology for examining LCZ.
(iv) To make a comparison between GIS-based and WUDAPT methodology for evaluating and validating LCZ by taking KMA as a case study area.

16.4 Materials and Method

16.4.1 GIS-Based Methodology

16.4.1.1 GIS Data

In 2020, KMA building data, build-up index, land-use data, land surface temperature, and boundary shapefile are among the input data for the GIS-based technique. KMA's building data was obtained in shapefile format from the Open Street Map (https://www.openstreetmap.org/), while the build-up index, land-use data, and land surface temperature were obtained from Landsat

Fig. 16.2 **a** Climate chart of KMA, **b** average high and low temperature in KMA. *Source* https://weatherspark.com and https://www.climatestotravel.com
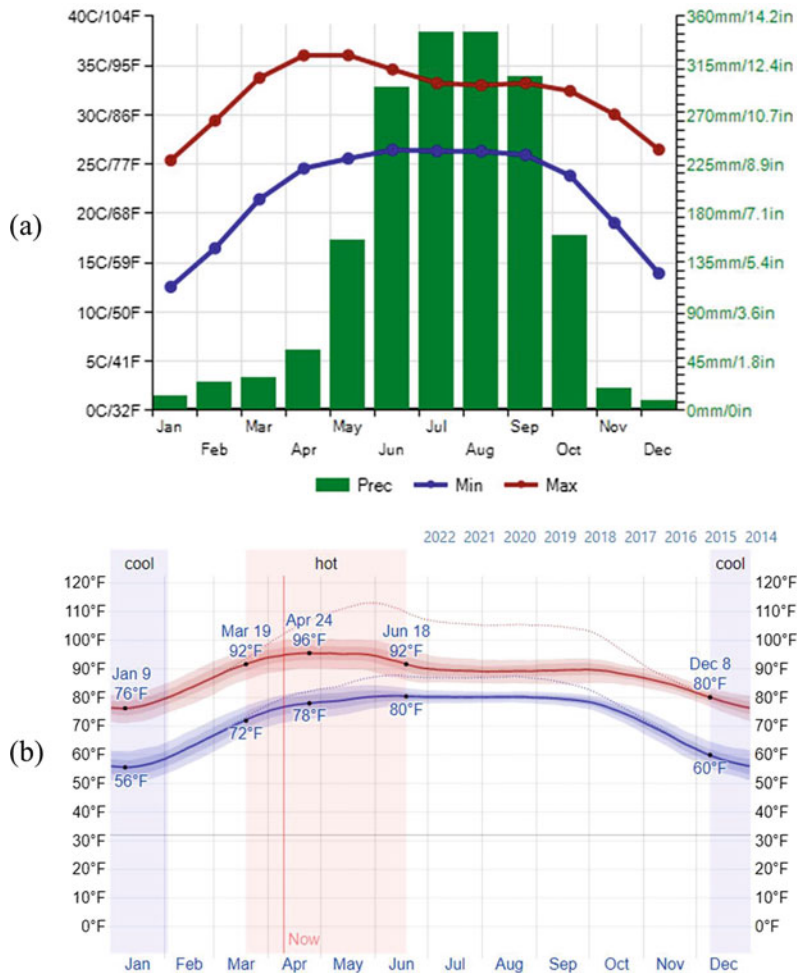
imageries, specifically Landsat-8 OLI/TIRS (https://earthexplorer.usgs.gov/).

16.4.1.2 Study Plan

Based on the LCZ classification of Stewart and Oke (2012), detailed data of Kolkata Metropolitan Area's urban morphology was utilised to undertake local climate zone (LCZ) classification. To make it easier to compare the results of the WUDAPT level 0 approaches, the resolution of all GIS datasets was adjusted to 100 m.

Built-Up Classification (LCZs 1–10): The data of contributing factors (i.e. building distribution and building surface percentage) was created in a GIS environment with a common resolution of 100 m using the input building data.

Equation 16.1 was used to produce the building surface fraction (BSF) (Fig. 16.4).

$$B_f = \frac{dT_s}{dx} \tag{16.1}$$

where B_f represents building surface fraction, dT_s is the total area of building footprint, dx is the area of the selected zone under LCZ.

Then, by adding the building height and building surface fraction, built types, i.e. LCZs 1–10, were categorised (Fig. 16.5 and Table 16.1).

Land-Cover Classification (LCZ A–G): In the KMA, a total of twelve land-cover types (Fig. 16.6a) were found, which were then grouped into six groups with LCZ A-G in mind (Fig. 16.6b). Due of a lack of knowledge on
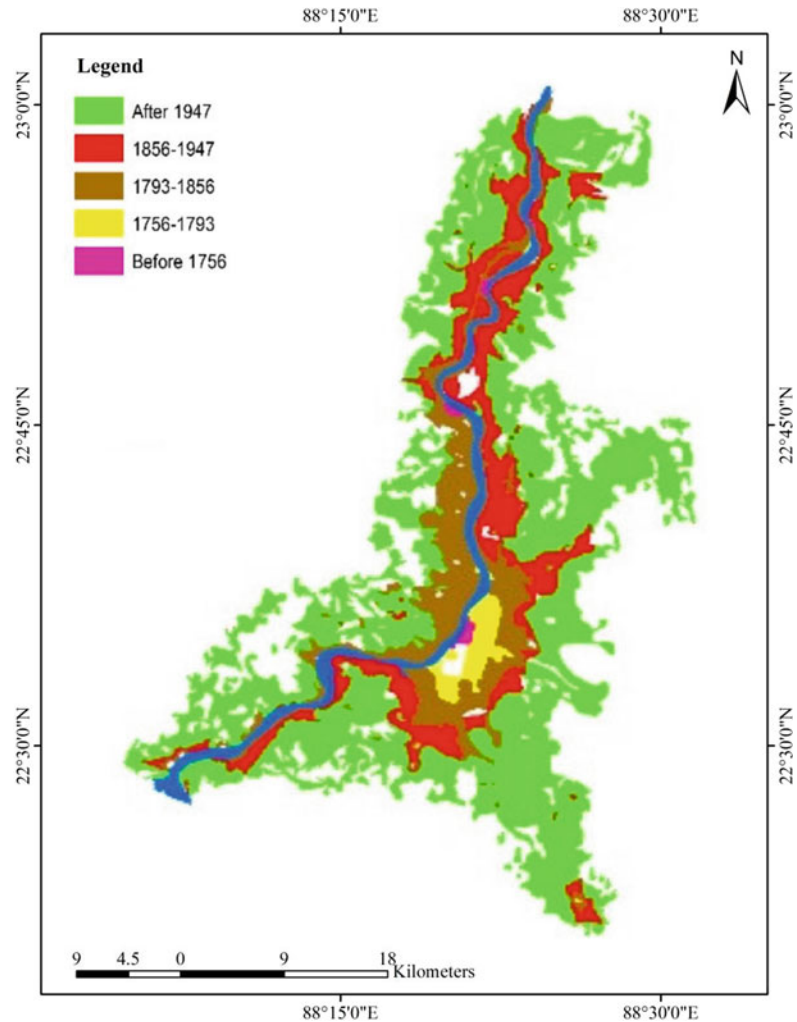
dense tree species in the metropolitan region, LCZ A and LCZ B were merged. Built types and land-cover types are included in KMA's LCZ categorisation map (LCZ A–G). To create the final LCZ map, they were mosaicked (Fig. 16.5 and Table 16.2).

Land Surface Temperature (LST): Land surface temperature refers to the land's radiative skin temperature as measured by solar radiation. LST is a measurement of thermal radiation emitted from the land surface when incoming solar energy interacts with and warms the ground or the canopy surface in vegetated regions (Hofierka et al. 2020). Roofs, roads, and buildings in urban surroundings—hard, dry

surfaces—provide less shade and moisture than natural landscapes, contributing to higher temperatures (Norton et al. 2015).

The air, surface, and soil temperatures in cities are usually always higher than those in rural regions. The urban heat island effect is the name for this phenomenon (UHI). Urban regions, where these structures are densely packed and vegetation is scarce, create temperature islands in comparison to outlying locations (Priyadarsini 2009). As a result, in order to comprehend the local urban climate, the land surface temperature was also taken into account in this study. One of the most often used methods for retrieving land surface temperature is the radiative transfer
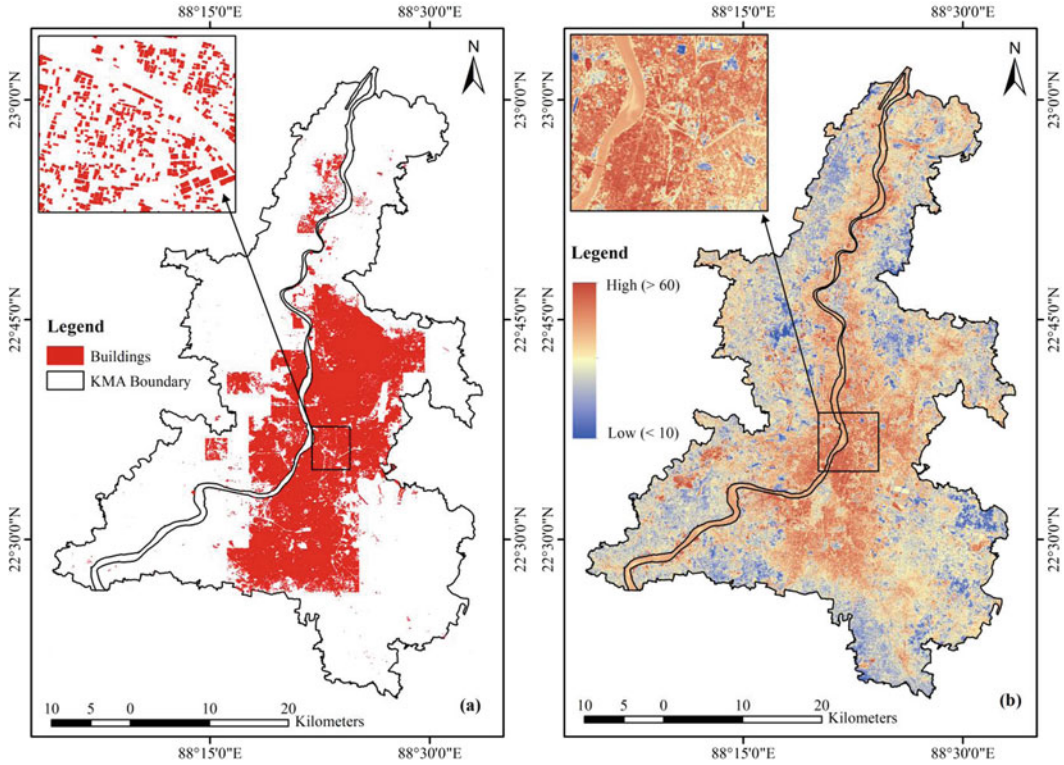
Fig. 16.4 Built-up classification. **a** Building distribution, **b** building surface fraction. *Source* Prepared by authors based on Landsat-8 data

equation (RTE). The following is a simplified radiative transfer equation (Eq. 16.2):

$$LST = (BT/(1 + (L\lambda i * BT/C_2) * Ln(\varepsilon)))$$
$$(16.2)$$

where Lλi—spectral radiance (effective band wavelength) for band *I*; C_2—$h * c/s$ (*c* is the light speed (*c* = 2.9979 × 108 m/s), *h* is the Planck's constant (*h* = 6.6261 × 10^{-34} J·s), *k* is the Boltzmann constant (*k* = 1.3806 × 10^{-23} J/K), c_2 = 1.4388*10^{-2} m K = 14,388 μm K; BT—brightness temperature; ε—emissivity.

The sensor spectral radiance and TIRS top of atmosphere brightness temperature are required to determine the LST from the preceding equation (Barsi et al. 2014). The images in the OLI and TIR sensors are analysed using 32-bit floating-point calculations, which are then transformed into 16-bit integer values in the

Level 1 final product. The following equation (Eq. 16.3) can be used to convert these DN values (Qcal) to spectral radiance:

$$L_{\lambda i} = M_L * Q_{cal} + A_L \qquad (16.3)$$

where $L_{\lambda,i}$—effective spectral radiance for band *i* (Watts/(m² * srad * μm); M_L—radiance multiplier rescaling factor (Table 16.3); Q_{cal}—L_1 pixel value in DN; A_L—radiance add rescaling factor (Table 16.3).

Now, the spectral radiance of each thermal band is utilised to convert the radiance into brightness temperature which can be expressed as (Eq. 16.4):

$$TB = \frac{K2}{\ln\left(\frac{K1}{L\lambda i} + 1\right)} \qquad (16.4)$$

where $K1$ and $K2$ = band-specific thermal conversion constants; BT = ambient brightness

Built types

Land cover types

Fig. 16.5 Local climate zone typology. *Source* The World Urban Database and Access Portal Tools

temperature (Table 16.3); $L\lambda i$ = spectral radiance of band i.

To convert brightness temperature from Kelvin (K) to Celsius (°C), subtract by 273.15 with Eq. (16.3), which can be rewritten as (Eq. 16.5):

$$TB = \frac{K2}{\ln\left(\frac{K1}{L\lambda i} + 1\right)} - 273.15 \qquad (16.5)$$

The fundamental component in LST inversion is the estimation emissivity (e). The emissivity of

Table 16.1 Classification parameters and building information by using GIS-based method

WUDAPT built code	WUDAPT built types	BSF (%)
LCZ 1	Compact high-rise	–
LCZ 2	Compact mid-rise	45–65
LCZ 3	Compact low-rise	45–65
LCZ 4	Open high-rise	25–45
LCZ 5	Open mid-rise	–
LCZ 6	Open low-rise	25–45
LCZ 7	Lightweight low-rise	–
LCZ 8	Large low-rise	20–30
LCZ 9	Sparsely built	–
LCZ 10	Heavy industry	< 10

Note—Particular type of building type which was not identified in the study area
Source Prepared by authors based on WUDAPT data and built-up classification
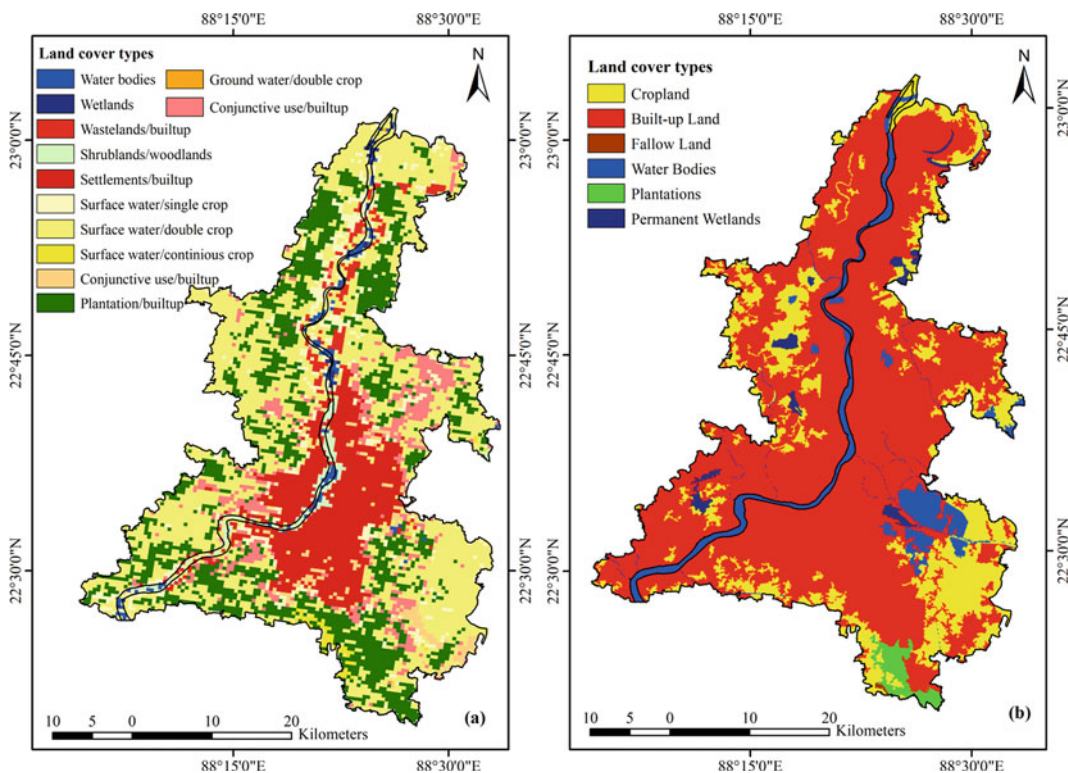
Fig. 16.6 Land-cover classification of KMA. **a** Initial classification, **b** reclassification in order to match with LCZ A–G. *Source* Prepared by authors based on Landsat-8 data

the earth's surface varies depending on factors such as soil, vegetation, roughness, and viewing angle. NDVI-based emissivity estimates, classification-based emissivity technique, and day/night temperature-independent spectral indices-based approach may all be used to estimate LSE for LST. In this study, the proportion of vegetation was calculated using the NDVI-

Table 16.2 Classification parameters and land-cover types by using GIS-based method

WUDAPT land-cover code	WUDAPT land-cover types	KMA land-cover types
LCZ A/B	Dense/scattered trees	Grassland, woodland, and fallow land
LCZ C	Bush, scrub	Plantations
LCZ D	Vegetation/low plants	Cropland
LCZ E	Bare surface or paved	Roads and all other types of built-up land
LCZ F	Bare soil or sand	Wetland
LCZ G	Water	River and all other types of water bodies

Source Prepared by authors based on WUDAPT data and land cover classification

Table 16.3 Metadata carrying constant value for thermal conversion

Thermal conversion constant	Band 10	Band 11
K1	774.89	480.89
K2	1321.08	1201.14
Radiance multiplier (ML)	0.000334	0.000334
Radiance additive (AL)	0.01	0.01

based emissivity estimation approach, which may be written as (Eq. 16.6):

$$Pv = \left(\frac{\text{NDVI} - \text{NDVImin}}{\text{NDVImax} - \text{NDVImin}} \right)^2 \quad (16.6)$$

where Pv is the proportion of vegetation; NDVI_{min} and NDVI_{max} are the minimum and maximum values of NDVI. Figure 16.7 shows the calculated LST of Kolkata Metropolitan Area.

16.4.2 World Urban Database and Access Portal Tools (WUDAPT)

16.4.2.1 Data Source

Free remote sensing data was used in the WUDAPT level 0 methods (Wang et al. 2018). Landsat-8 satellite imagery was chosen as the input image data in this work because it contains urban structural information, such as thermal information from Bands 10 and 11 that may be used to categorise and map LCZs (Fig. 16.8). They can also give 30-m-resolution images every 16 days, covering the whole globe. The pictures can be downloaded for free from the United States Geological Survey's website. The most important selection criteria for satellite photos are to prevent cloud cover, which has an impact on future processing and the overall quality of the final result. After assessing the pictures' availability and quality, the following KMA Landsat-8 imagery was chosen (Table 16.4).

16.4.2.2 Study Plan

The study strategy is detailed below and follows the stages for creating an LCZ map using WUDAPT (Bechtel et al. 2015). To begin, Landsat images was resampled from 30 to 100 m in resolution and trimmed to match the research region. Second, Google Earth was used to digitise roughly 16 training samples (polygons) for each LCZ class. When picking samples, the ruler given by Google Earth was used to measure building heights and distances between structures. According to local expertise, a total of 12 varieties of LCZs were obtained at KMA (Fig. 16.9).

Finally, the SAGA GIS programme was used (Böhner and MacCloy 2006). The random forest technique was used to classify LCZs. A random

Fig. 16.7 Land surface temperature of KMA. *Source* Prepared by authors based on Landsat-8 data
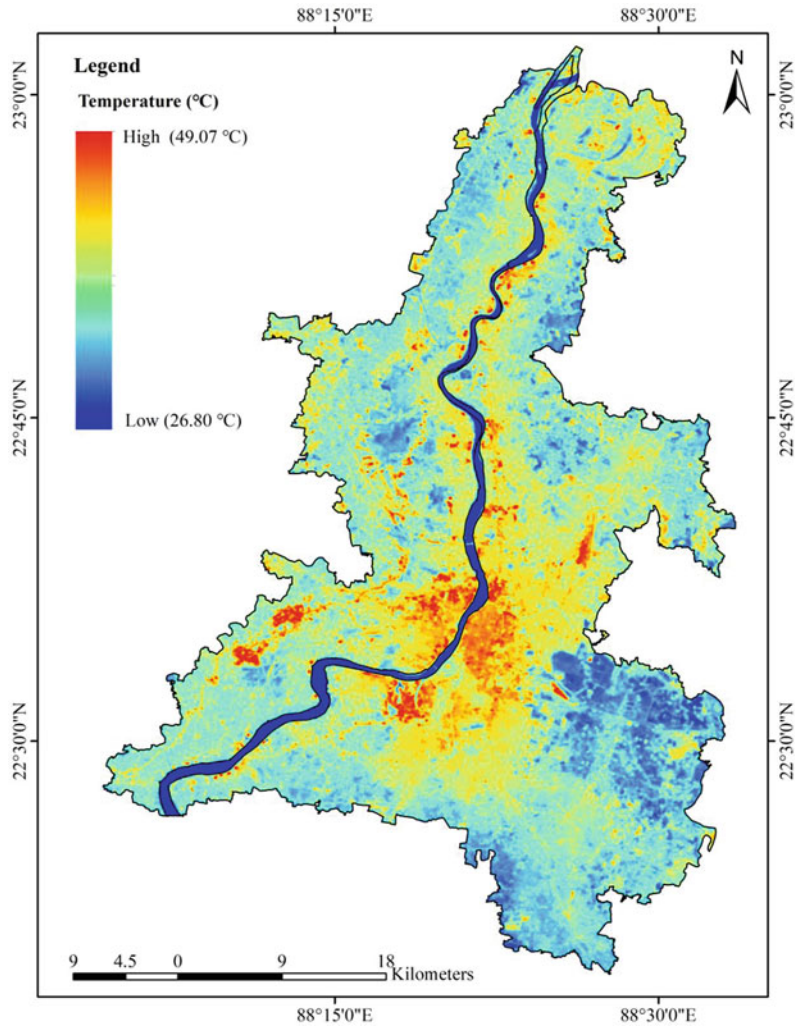
forest with a set of decision trees was built using spectral information present in training samples. The random forest classifier assigns the highest number of nodes to each output class (Ali et al. 2021). As a result, maximum ensemble is used to compute the output 'q' for an input data 'p'. Equation 16.7 may be used to express it:

$$q = (p) = \max\left[\sum_k I(t)\right] \qquad (16.7)$$

where $I(t)$ is an indicator function defined as:

$$I(t)\begin{Bmatrix} 1, & t =' \text{YES}' \\ 0, & t =' \text{NO}' \end{Bmatrix}$$

'YES' indicates successfully categorised LCZ pixels in this study's training dataset, whereas 'NO' indicates incorrectly classified LCZ pixels. A random forest is a prediction model that represents a mapping between the attributes of each LCZ class and the determined LCZ type. The input picture may be divided into various LCZ classes using the forest. Figure 16.10 depicts the complete development process.
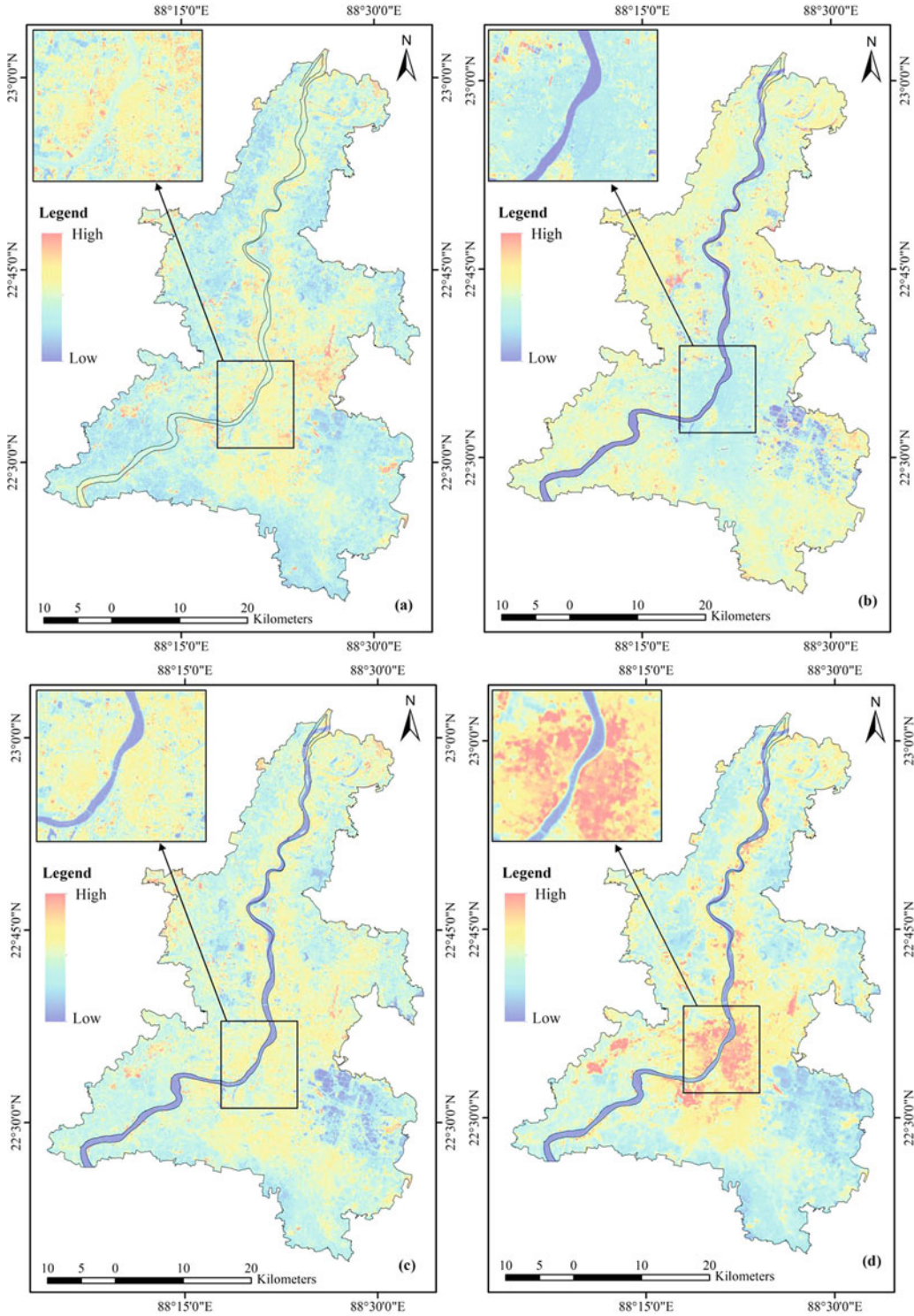
Fig. 16.8 Specific bands used in this study. **a** Band 4, **b** band 5, **c** band 7 and **d** band 10. *Source* Prepared by authors based on Landsat-8 data

Table 16.4 Input data for WUDAPT method

Path and raw number	Image data	Resolution	Cloud cover
138–044	2020–04-06	30 m	0.61%

Source MTL file of Landsat-8 satellite data

Fig. 16.9 Local climate zone training samples for KMA. *Source* Obtained by authors from Google Earth Pro

16.4.3   Accuracy Assessment

On the Google Earth platform, a manual selection of another independent group of validation samples was used to test the accuracy. For each LCZ class, around ten validation samples were discovered. To test the classification accuracy of both the GIS-based and WUDAPT techniques, confusion matrices were produced by comparing the predicted LCZ maps to those formed in the

Fig. 16.10 Flowchart of the methodological application and processing. *Source* Prepared by authors

validation samples (Tables 16.5 and 16.6). In the confusion matrix, four classification accuracy indices were used: overall accuracy (A_O), user a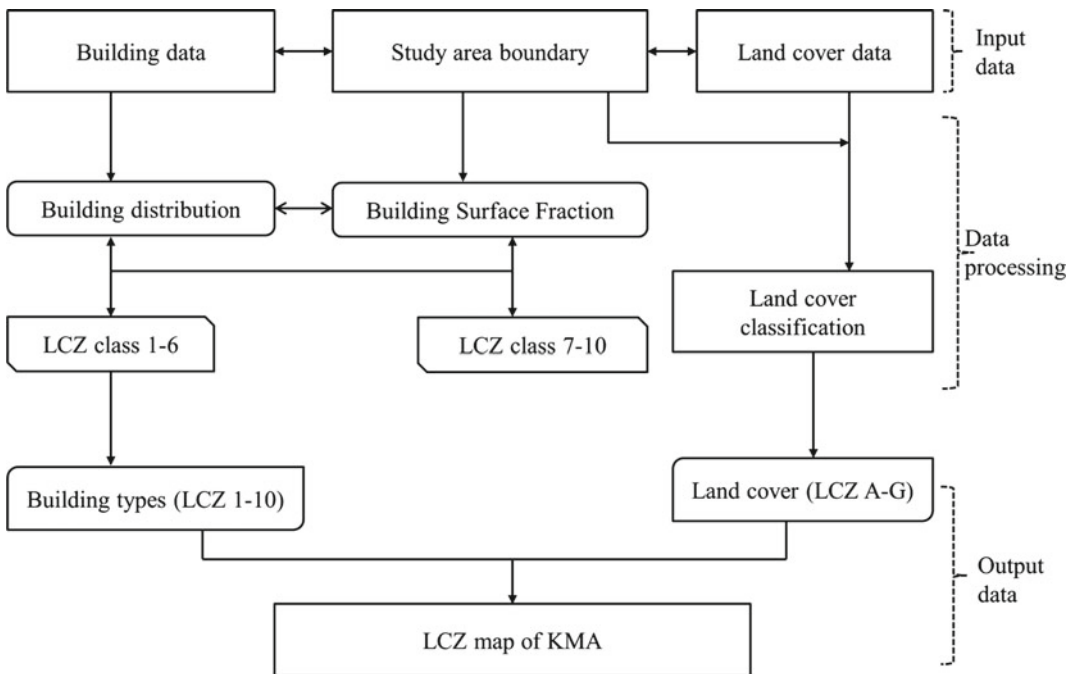ccuracy (A_U), producer accuracy (A_P), and kappa coefficient (K). Formulas are used to express these (Eqs. 16.8–16.11)

$$A_U = \frac{p_d}{P^1} \qquad (16.8)$$

$$A_P = \frac{p_d}{P^2} \qquad (16.9)$$

$$A_O = \frac{\sum p_d}{\sum P} \qquad (16.10)$$

$$K = \frac{P_d - P_e}{1 - P_e} \qquad (16.11)$$

where p_d is the no. of pixels (correctly classified pixels) of a particular LCZ class; P^1 is the total no. of pixels claimed to be in a particular LCZ class (predicted pixels); P^2 is the total no. of validation pixels of a certain LCZ class (original/actual pixels); $\sum P$ is the sum of actual/predicted pixels, equals to $\sum$ ref or

$\sum$ class; P_d and P_e are the correctly and predicted LCZ pixels, respectively.

16.5 Results

The GIS-based (Fig. 16.11a) and WUDAPT (Fig. 16.11b) approaches were used to create two LCZ maps of KMA. The WUDAPT method identified 12 LCZ classes for KMA based on local expert knowledge and chosen training samples, whereas the GIS-based method revealed 11 out of 12 LCZ classes. It should be mentioned that the WUDAPT approach discovered LCZ 8 (large low-rise). The GIS-based technique was unable to distinguish between LCZ A (dense trees) and LCZ B (scattered trees) due to a lack of precise vegetation information in the obtained datasets. When the WUDAPT and GIS-based techniques' accuracies are compared, the GIS-based method's overall accuracy is found to be greater than the WUDAPT method's.

Both local climate mapping approaches may be utilised to discern the true pattern of urban

Table 16.5 Accuracy measurement of LCZ map created by GIS-based method

LCZ	2	3	4	6	8	10	A/B	C	D	E	F	G	$\sum$ ref	A_P
2	**57**	3	5	1	0	2	3	1	4	3	0	3	82	0.70
3	1	**34**	1	2	0	2	1	3	2	4	3	1	54	0.63
4	3	3	**43**	0	1	1	2	2	2	4	1	7	69	0.62
6	2	0	9	**94**	2	1	0	3	4	2	4	1	122	0.77
8	4	3	2	1	**88**	4	3	3	2	1	1	0	112	0.79
10	1	4	3	3	3	**65**	1	0	0	2	2	3	87	0.75
A/B	0	3	0	2	3	2	**96**	4	3	3	3	1	120	0.80
C	3	2	1	3	2	3	0	**86**	1	3	0	3	107	0.80
D	0	0	2	0	4	1	3	2	**48**	1	0	0	61	0.79
E	2	0	3	2	1	7	2	0	4	**91**	2	3	117	0.78
F	1	4	6	2	0	6	3	1	2	3	**85**	4	117	0.73
G	3	3	2	3	5	2	0	4	5	9	2	**73**	111	0.66
$\sum$ class	77	59	77	113	109	96	114	109	77	126	103	99	1159	
A_U	0.74	0.58	0.56	0.83	0.81	0.68	0.84	0.79	0.62	0.72	0.83	0.74	$A_O = 0.74$	

Table 16.6 Accuracy measurement of LCZ map created by WUDAPT method

LCZ	2	3	4	6	8	10	A/B	C	D	E	F	G	$\sum$ ref	A_P
2	**65**	2	4	0	3	1	1	1	5	2	3	4	91	0.71
3	2	**37**	1	3	1	2	2	4	1	3	1	8	65	0.57
4	4	3	**54**	0	1	3	2	2	2	5	2	0	78	0.69
6	2	0	9	**56**	2	1	0	6	3	1	2	2	84	0.67
8	1	3	2	1	**67**	5	6	2	2	3	2	1	95	0.71
10	3	2	3	3	4	**61**	1	0	1	1	1	4	84	0.73
A/B	2	3	0	2	3	2	**83**	3	0	2	2	1	103	0.81
C	3	1	1	3	2	3	0	**77**	2	6	1	2	101	0.76
D	0	7	2	0	0	1	5	3	**48**	1	2	1	70	0.69
E	2	6	3	2	0	7	1	2	6	**78**	0	5	112	0.70
F	2	2	6	2	4	6	2	4	7	2	**81**	4	122	0.66
G	4	3	2	3	3	2	6	1	0	0	3	**69**	96	0.72
$\sum$ class	90	69	87	75	90	94	109	105	77	104	100	101	**1101**	
A_U	0.72	0.54	0.62	0.75	0.74	0.65	0.76	0.73	0.62	0.75	0.81	0.68	$A_O = 0.70$	

Source Prepared by authors

morphology and land use in KMA, according to the researchers. To begin, it should be remembered that vegetation covers around 36% of the entire land area in KMA (Fig. 16.12 NDVI). Both approaches can identify that roughly 70% of KMA is covered by LCZ A-E categories, which is consistent with this (Fig. 16.11a and b). These two techniques then determined that the areas of constructed kinds are mostly concentrated in the middle region of the KMA and gradually increase in the periphery (Figs. 16.3, 16.11a and b), which is consistent with the actual spatial distribution of land use in the KMA. In addition, both techniques were successful in identifying the usual high-density locations in KMA.
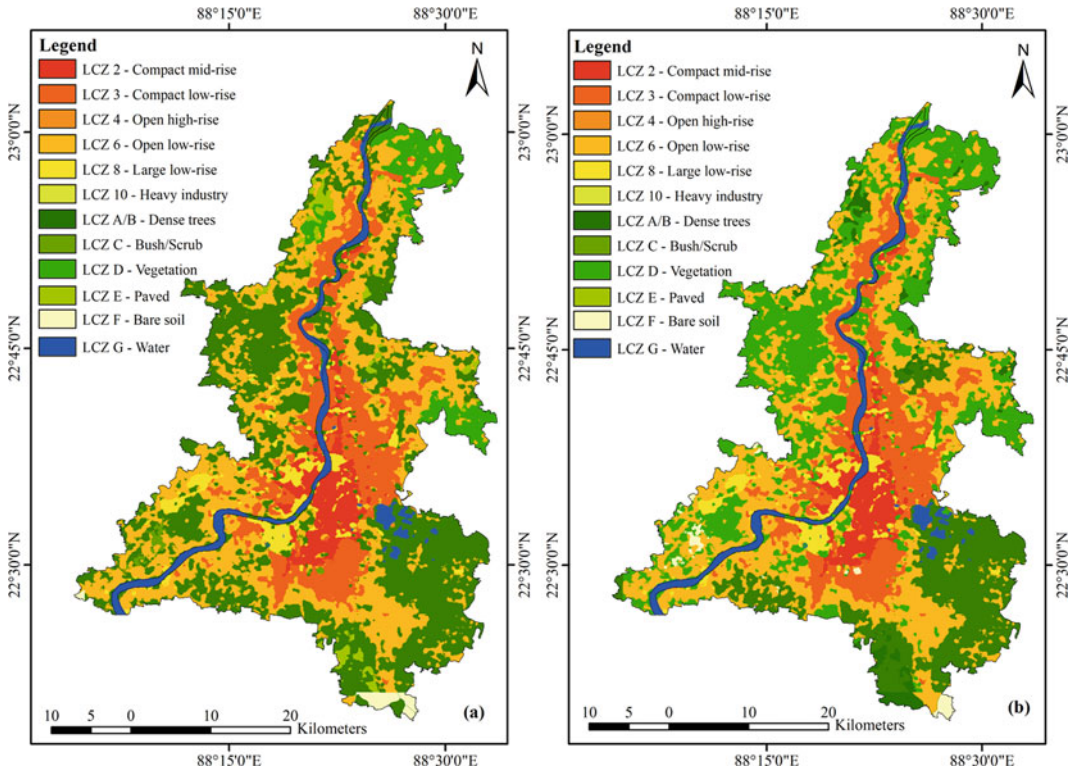
Fig. 16.11 Local climate zone map of KMA using **a** GIS-based method, **b** WUDAPT method. *Source* Prepared by authors

According to the accuracy tests, both approaches obtained an overall accuracy of greater than 70%. The GIS-based method's overall classification accuracy was 0.742 (74.2%) which is greater than the WUDAPT methods, i.e. 0.704 (70.4%). Built kinds are of special significance in this study since KMA is a typical high-density high-rise metropolis with limited land resources. The most common construction types in KMA are LCZs 2, 3, 4, and 6. The GIS-based technique outperformed WUDAPT in terms of the accuracy of LCZs 2, 3, 4, and 6, taking both A_U and A_P into account. The GIS-based technique distinguishes LCZs 2, 3, 4, and 6 with more precision than the WUDAPT method.

The poor accuracy of the WUDAPT technique, notably in LCZs 1–10, can be explained as follows. The intricate urban morphology of KMA is one of the reasons. KMA's developable land resources are limited due to its dense population. In metropolitan locations, high-density high-rise building and multiple intensive land use are widely used to optimise growth potential and developers' profits. Different forms of land use—commercial, residential, and other sorts—are combined, as are structures of various heights and coverage ratios. KMA's urban fabric is densely mixed as a result. LCZ categorisation, on the other hand, simplifies the complex and uneven urban fabric by categorising one region as a dominating LCZ type. As a result, misclassification is most common in constructed types. The GIS-based method is more accurate because it uses actual building data to accurately specify the parameters of LCZs 1–10, whereas the WUDAPT method relies heavily on the amount and quality of training samples, as well as remote sensing images and local urban morphological features. Apart from its higher overall accuracy, the GIS-based technique recognises specific LCZ classes with reasonable accuracies, according to both user and producer accuracy.

Fig. 16.12 Vegetation covers over Kolkata metropolitan area. *Source* Prepared by authors using Landsat-8 satellite data
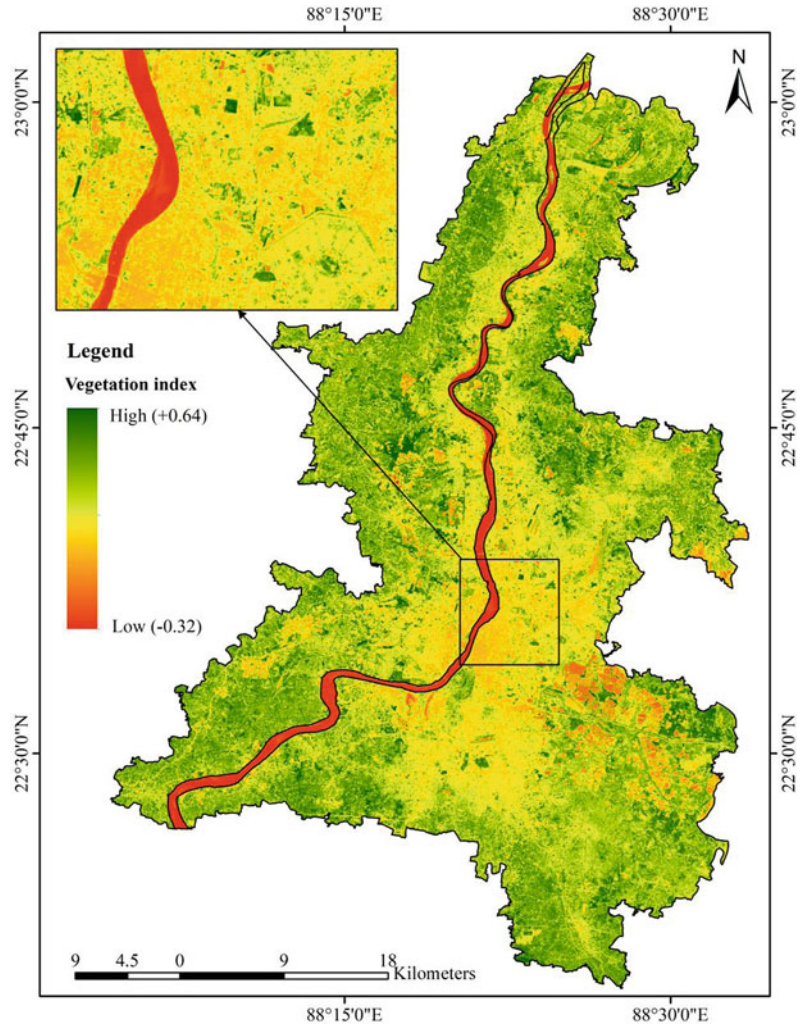
16.6 Discussion

Due to KMA's unique high-density and intricate urban geography, the WUDAPT methodology has lower overall accuracy than the GIS-based method. It is tough to represent the differences between LCZs 1–10 using WUDAPT. Furthermore, due to lack of building height information in the Landsat images, the WUDAPT technique provides less precision. Xu et al. (2017) used WUDAPT to assess the classification accuracy of the LCZ map in Guangzhou, finding that the overall accuracy of LCZs 1–10 in Guangzhou is around 60%.

The LCZ concept is based on the simplification and generalisation of built types and land-cover types in a number of locations, none of which are densely populated high-rise cities (Stewart 2011). It is based on broad information than local experience, particularly relevant when characterising the LCZ classes in locations with distinct urban morphologies, such as the Kolkata Metropolitan Area. As a result, using the generic LCZ idea for LCZ mapping in the Kolkata Metropolitan Area deprived of building information result in low accuracy. Additional explanation for the WUDAPT method's decreased accuracy might be because of this.

The WUDAPT method's present poor accuracies in LCZ constructed types match findings from prior research such as Guangzhou, Shanghai, and Hangzhou in China and San Francisco in the United States (Xu, et al. 2017; Cai et al. 2018; Wang et al. 2018). On the one hand, using high-resolution remote sensing images or conducting remote sensing image fusion can improve the quality of LCZ classification and mapping output in future; on the other hand, subclasses of built types of LCZ should be considered to capture the variation of each LCZ in high-density urban areas.

The findings of both approaches as input data for the Weather Research and Forecasting (WRF) model are discussed here in order to evaluate their use. The default input land-use data in WRF is MODIS data with a 23-category land-use type created by the US Geological Survey (USGS). Recent research, on the other hand, has attempted to analyse the roughness issue in metropolitan areas at three levels: high, medium, and low (Arnfield 2003; Ren et al. 2016). To fulfil this default land-use classification, LCZ classes were aggregated. As a result, construct types were reclassified to indicate roughness levels of high, medium, and low. The accuracy evaluation technique was carried out using the same set of validation samples as were utilised for accuracy assessment. After categorising the initial 10 construction kinds into high, mid, and low urban types, the WUDAPT approach obtains improved overall accuracy of input data over urban classes. This means that when WUDAPT level 0 data is aggregated from 100 m resolution to 1 km resolution, accuracy improves. WUDAPT level 0 data can be used as input data for the WRF model when GIS data is unavailable.

16.7 Conclusion

The use of a local climate zone to investigate urban form and its influence on local temperature is one of the commonly used international standard practises. The two most common approaches for classifying and mapping LCZs are GIS-based and WUDAPT. The current study examined the performance and accuracy of both approaches in the Kolkata Metropolitan Area's high-density complex urban regions. Although the GIS-based approach has a higher accuracy than WUDAPT, the broad geographical patterns of distinct LCZ classes in these two LCZ maps are both accurate in the Kolkata Metropolitan Area. The study's findings reveal that the LCZ system's application and technique are simple; however, there are a few restrictions to be aware of. WUDAPT's benefits of publicly available data, simple approach, and appropriate precision for application will be advantageous to researchers, especially in poor countries and regions where GIS data is either unavailable or incomplete. Researchers interested in LCZ categorisation and work for urban areas can use the findings on appropriateness and limitations of both approaches as a reference. Local planners and designers may also use the results of urban morphology analysis to gain an enhanced knowledge of urban morphological traits in highly dense urban regions. They may also be able to aid them with their new research work.

References

Ali SA, Parvin F, Vojteková J, Costache R, Linh NTT, Pham QB et al (2021) GIS-based landslide susceptibility modeling: a comparison between fuzzy multi-criteria and machine learning algorithms. Geosci Front 12(2):857–876

Arnfield AJ (2003) Two decades of urban climate research: a review of turbulence, exchanges of energy and water, and the urban heat island. Int J Climatol: J Roy Meteorol Soc 23(1):1–26

Aslam A, Rana IA (2022) The use of local climate zones in the urban environment: a systematic review of data sources, methods, and themes. Urban Climate 42:101120

Barsi JA, Schott JR, Hook SJ, Raqueno NG, Markham BL, Radocinski RG (2014) Landsat-8 thermal infrared sensor (TIRS) vicarious radiometric calibration. Remote Sens 6(11):11607–11626

Bechtel B, Daneke C (2012) Classification of local climate zones based on multiple earth observation data. IEEE J Sel Top Appl Earth Obs Remote Sens 5 (4):1191–1202

Bechtel B, Alexander PJ, Böhner J, Ching J, Conrad O, Feddema J, Stewart I (2015) Mapping local climate

zones for a worldwide database of the form and function of cities. ISPRS Int J Geo Inf 4(1):199–219

Bechtel B, See L, Mills G, Foley M (2016) Classification of local climate zones using SAR and multispectral data in an arid environment. IEEE J Sel Top Appl Earth Obs Remote Sens 9(7):3097–3105

Böhner J, MacCloy KR (2006) SAGA-analysis and modelling applications. Goltze, Göttingen

Bornstein RD (1968) Observations of the urban heat island effect in New York City. J Appl Meteorol Climatol 7(4):575–582

Bornstein R, Lin Q (2000) Urban heat islands and summertime convective thunderstorms in Atlanta: three case studies. Atmos Environ 34(3):507–516

Brousse O, Martilli A, Foley M, Mills G, Bechtel B (2016) WUDAPT, an efficient land use producing data tool for mesoscale models? Integration of urban LCZ in WRF over Madrid. Urban Clim 17:116–134

Cai M, Ren C, Xu Y, Dai W, Wang XM (2016) Local climate zone study for sustainable megacities development by using improved WUDAPT methodology–a case study in Guangzhou. Procedia Environ Sci 36:82–89

Cai M, Ren C, Xu Y, Lau KKL, Wang R (2018) Investigating the relationship between local climate zone and land surface temperature using an improved WUDAPT methodology–A case study of Yangtze River Delta, China. Urban Clim 24:485–502

Chatterjee U, Majumdar S (2021) Impact of land use change and rapid urbanization on urban heat island in Kolkata city: a remote sensing based perspective. J Urban Manage

Chen Y, Zheng B, Hu Y (2020) Mapping local climate zones using ArcGIS-based method and exploring land surface temperature characteristics in Chenzhou, China. Sustainability 12(7):2974

Ching J, See L, Ren C, Masson V, Hildalgo J, Wang X, … Feddema J (2017) The WUDAPT framework to generating urban morphology, material composition and activity data for modeling. In 13th urban environment, 97th AMS annual meeting

Chow WT, Roth M (2006) Temporal dynamics of the urban heat island of Singapore. Int J Climatol J Roy Meteorol Soc 26(15):2243–2260

Cui YY, De Foy B (2012) Seasonal variations of the urban heat island at the surface and the near-surface and reductions due to urban vegetation in Mexico City. J Appl Meteorol Climatol 51(5):855–868

Das S, Adhikary PP, Shit PK, Bera B (2021) Urban wetland fragmentation and ecosystem service assessment using integrated machine learning algorithm and spatial landscape analysis. Geocarto Int 1–19

Deur M, Gašparović M, Balenović I (2021) An evaluation of pixel-and object-based tree species classification in mixed deciduous forests using pansharpened very high spatial resolution satellite imagery. Remote Sens 13(10):1868

Dissanayake C, Weerasinghe UGD (2021) Urban microclimate and outdoor thermal comfort of public spaces in warm-humid cities: a comparative bibliometric

mapping of the literature. Am J Clim Chang 10(4):433–466

Feng P, Lin Y, Guan J, Dong Y, He G, Xia Z, Shi H (2019) Embranchment CNN based local climate zone classification using SAR and multispectral remote sensing data. In: IGARSS 2019–2019 IEEE International geoscience and remote sensing symposium. IEEE, pp 6344–6347

Fu J, Dupre K, Tavares S, King D, Banhalmi-Zakar Z (2022) Optimized greenery configuration to mitigate urban heat: a decade systematic review. Front Archit Res

Hofierka J, Gallay M, Onačillová K, Hofierka J Jr (2020) Physically-based land surface temperature modeling in urban areas using a 3-D city model and multispectral satellite data. Urban Clim 31:100566

Hong JW, Hong J, Kwon EE, Yoon D (2019) Temporal dynamics of urban heat island correlated with the socio-economic development over the past half-century in Seoul, Korea. Environ Pollut 254:112934

Imhoff ML, Zhang P, Wolfe RE, Bounoua L (2010) Remote sensing of the urban heat island effect across biomes in the continental USA. Remote Sens Environ 114(3):504–513

Lelovics E, Unger J, Gál T, Gál CV (2014) Design of an urban monitoring network based on local climate zone mapping and temperature pattern modelling. Clim Res 60(1):51–62

Liu S, Shi Q (2020) Local climate zone mapping as remote sensing scene classification using deep learning: a case study of metropolitan China. ISPRS J Photogramm Remote Sens 164:229–242

Martilli A, Krayenhoff ES, Nazarian N (2020) Is the urban heat island intensity relevant for heat mitigation studies? Urban Clim 31:100541

Middel A, Häb K, Brazel AJ, Martin CA, Guhathakurta S (2014) Impact of urban form and design on mid-afternoon microclimate in Phoenix local climate zones. Landsc Urban Plan 122:16–28

Mitra C, Shepherd JM, Jordan TR (2012) Assessment and dynamics of urban growth in the City of Kolkata. Facets of social geography: International and Indian perspectives, pp 541–555

Mohan M, Kandya A, Battiprolu A (2011) Urban heat island effect over national capital region of India: a study using the temperature trends. J Environ Prot 2(04):465

Nassar AK, Blackburn GA, Whyatt JD (2016) Dynamics and controls of urban heat sink and island phenomena in a desert city: development of a local climate zone scheme using remotely-sensed inputs. Int J Appl Earth Obs Geoinf 51:76–90

Ng YX (2015) A study of urban heat island using` local climate zones'-the case of Singapore. Br J Environ Clim Change 5(2):116–133

Norton BA, Coutts AM, Livesley SJ, Harris RJ, Hunter AM, Williams NS (2015) Planning for cooler cities: a framework to prioritise green infrastructure to mitigate high temperatures in urban landscapes. Landsc Urban Plan 134:127–138

Perera N, Emmanuel M, Mahanama P (2012) Mapping "local climate zones" and relative warming effects in Colombo, Sri Lanka. In: ICUC8–8th International conference on urban climates. Elsevier, p 576

Priyadarsini R (2009) Urban heat island and its impact on building energy consumption. Adv Build Energy Res 3(1):261–270

Quan SJ, Bansal P (2021) A systematic review of GIS-based local climate zone mapping studies. Build Environ 196:107791

Ren C, Wang K, Shi Y, Kwok YT, Morakinyo TE, Lee TC, Li Y (2021) Investigating the urban heat and cool island effects during extreme heat events in high-density cities: a case study of Hong Kong from 2000 to 2018. Int J Climatol 41(15):6736–6754

Ren C, Wang R, Cai M, Xu Y, Zheng Y, Ng E (2016) The accuracy of LCZ maps generated by the world urban database and access portal tools (WUDAPT) method: a case study of Hong Kong. In: 4th International conference on countermeasure urban heat islands, Singapore

Rosenzweig C, Solecki WD, Parshall L, Chopping M, Pope G, Goldberg R (2005) Characterizing the urban heat island in current and future climates in New Jersey. Glob Environ Change Part B: Environ Hazards 6(1):51–62

Ruocco AD, Gasparini P, Weets G (2015) Urbanisation and climate change in Africa: setting the scene. In: Urban vulnerability and climate change in Africa. Springer, Cham, pp 1–35

Sahana M, Hong H, Sajjad H (2018) Analyzing urban spatial patterns and trend of urban growth using urban sprawl matrix: a study on Kolkata urban agglomeration, India. Sci Total Environ 628:1557–1566

Savić S, Milošević D, Lazić L, Marković V, Arsenović D, Pavić D (2013) Classifying urban meteorological stations sites by 'local climate zones': preliminary results for the city of Novi Sad (Serbia). Geogr Pannon 17(3):60–68

Shi Y, Katzschner L, Ng E (2018) Modelling the fine-scale spatiotemporal pattern of urban heat island effect using land use regression approach in a megacity. Sci Total Environ 618:891–904

Skogen K, Helland H, Kaltenborn B (2018) Concern about climate change, biodiversity loss, habitat degradation and landscape change: embedded in different packages of environmental concern? J Nat Conserv 44:12–20

Stewart ID (2011) Redefining the urban heat island. Doctoral dissertation, University of British Columbia

Stewart ID, Oke TR (2009) A new classification system for urban climate sites. Bull Am Meteor Soc 90(7):922–923

Stewart ID, Oke TR (2010) Thermal differentiation of local climate zones using temperature observations from urban and rural field sites. In Ninth symposium on urban environment. Keystone, CO, pp 2–6

Stewart ID, Oke TR (2012) Local climate zones for urban temperature studies. Bull Am Meteor Soc 93(12):1879–1900

Stewart ID, Oke TR, Krayenhoff ES (2014) Evaluation of the 'local climate zone' scheme using temperature observations and model simulations. Int J Climatol 34(4):1062–1080

Talapatra A, Majumder A, Das S (2021) Geospatial analysis of the dynamics of climate in Kolkata metropolitan area. J Phys: Conf Ser 1964(4):042038

Tayanç M, İm U, Doğruel M, Karaca M (2009) Climate change in Turkey for the last half century. Clim Change 94(3):483–502

Wang R, Cai M, Ren C, Bechtel B, Xu Y, Ng E (2019) Detecting multi-temporal land cover change and land surface temperature in Pearl River Delta by adopting local climate zone. Urban Clim 28:100455

Wang R, Ren C, Xu Y, Lau KKL, Shi Y (2018) Mapping the local climate zones of urban areas by GIS-based and WUDAPT methods: a case study of Hong Kong. Urban Clim 24:567–576

Xiao L, Li X, Wang R (2011) Integrating climate change adaptation and mitigation into sustainable development planning for Lijiang City. Int J Sust Dev World 18(6):515–522

Xu Y, Ren C, Cai M, Edward NYY, Wu T (2017) Classification of local climate zones using ASTER and Landsat data for high-density cities. IEEE J Sel Top Appl Earth Obs Remote Sens 10(7):3397–3405

Zeng C, Deng X, Dong J, Hu P (2016) Urbanization and sustainability: comparison of the processes in "BIC" countries. Sustainability 8(4):400

Zhao L, Lee X, Smith RB, Oleson K (2014) Strong contributions of local background climate to urban heat islands. Nature 511(7508):216–219

Zhongli L, Hanqiu X (2016) A study of urban heat island intensity based on "local climate zones": a case study in Fuzhou, China. In 2016 4th International workshop on earth observation and remote sensing applications (EORSA). IEEE, pp 250–254

Zhou D, Zhang L, Hao L, Sun G, Liu Y, Zhu C (2016) Spatiotemporal trends of urban heat island effect along the urban development intensity gradient in China. Sci Total Environ 544, 617–626

Air Pollutants-Induced Environmental Critical Zones in Capital City of India

17

Shadman Nahid, Susanta Mahato,
Mangalasseril Mohammad Anees,
Deep Narayan Pandey,
and Pawan K. Joshi

Abstract

Changing land use/cover (LULC) is the most visible and immediate consequences of urbanization on the environment, leading to changes in temperature, microclimate, air quality, biodiversity loss, and, most crucially, diminished quality of life. The aim of the chapter is to inform about the environmental critical zones of India's capital city on the basis of Normalized Difference Vegetation Index (NDVI) and the criterion air pollutants ($PM_{2.5}$, PM_{10}, SO_2, and NO_2) during different seasons. The chapter informs the effects of urbanization on NDVI and its relationships with air quality and LST. The criterion air pollution statistics were obtained from ground-based observations, and the NDVI was taken from a Landsat satellite image. Using the interpolation technique Kriging, air quality maps were prepared to determine trends in air pollution in Delhi. Environmentally critical zones of Delhi were identified using a deductive index. The quality of the environment is quite bad during the winter (JF) season when compared with other seasons. The eastern, western, northern, and central districts of Delhi look to be under high criticality, according to this analysis. The southern district of Delhi, on the other hand, has the largest green cover and is able to maintain a high level of environmental quality, which can be ascribed to the preservation of forest areas and ongoing afforestation efforts by municipal governments. Identification of key zones based using integration of remote sensing inputs and accurate field data adds new dimensions to city planners' and decision-makers' efforts to plan for sustainable development. Such information also guides the master plan of the city and urban development policy making in the city. The demonstrated approach can be used in other cities in the tropical countries in particular and global cities as large.

Keywords

Air pollutants · Vegetation status · Deductive index · Environmental quality

S. Nahid · M. M. Anees · P. K. Joshi (✉)
School of Environmental Sciences, Jawaharlal Nehru University, New Delhi 110 067, India
e-mail: pkjoshi27@hotmail.com
pkjoshi@mail.jnu.ac.in

S. Nahid
e-mail: snahid.katras@gmail.com

M. M. Anees
e-mail: aneesssjnu@gmail.com

S. Mahato · D. N. Pandey · P. K. Joshi
Special Centre for Disaster Research (SCDR), Jawaharlal Nehru University, New Delhi 110 067, India
e-mail: susantamahato@jnu.ac.in

D. N. Pandey
e-mail: deepudai@gmail.com

17.1 Introduction

Urbanization is a spatially and temporally scaled physical and socioeconomic process that converts a rural area into an urban one (Thapa and Murayama 2010). Natural and semi-natural surfaces become impermeable during this phase (Li and Weng 2007; Taubenböck et al. 2009; Li and Weng 2007). From 224 million in 1900 to 2.9 billion in 1999, the world's urban population has grown more than tenfold in the last century (Alberti et al. 2007). According to the United Nations (UN) since 2007, more than half of the world's population has lived in cities. This urban population of the globe is predicted to grow by over 2 billion in the next 30 years. In Asia, the trend is similar, with China and India being the most concerning. The UN reports than a third of India's population now lives in cities, with that number expected to rise to more than half by 2050 (United Nations 2014). As a result, the urban population would outnumber the rural population.

The Delhi agglomeration now has a population of 26.5 million people, second only to Tokyo, and is expected to grow to 36 million by 2030 (United Nations 2018). The urbanization supports regional economic growth and improves living standards; it creates work opportunities in industries and agriculture, among other things (WHO 2010). However, the implications are reduced plant cover, air quality, water quality, soil fertility, and enhanced land use land cover (LULC) changes, land fragmentation, and other natural phenomena that contribute to major ecological and environmental deterioration (Liang and Weng 2011; Senanayake et al. 2013b; Zhou et al. 2004). It also causes environmental issues such as industrial waste dispersion, increased traffic, and pollution (Cui and Shi 2012). Health and human comfort suffer as a result of these effects (EPA 2008).

The quality of the environment has a significant impact on people's quality of life. There are direct links between the quality of life and basic environmental factors like air, water, and land surface (Banzhaf et al. 2014). Environmental quality in cities is a complicated variable that changes through time and space (Nichol and Wong 2006). It has a significant impact on quality of life, which is why it is regarded as a tried-and-true multi-dimensional indicator for urban research and planning (Moore et al. 2006). In the recent studies (Fernández and Wu 2018; Musse et al. 2018), socioeconomic data has been used to calculate urban environmental quality (UEQ) (Joseph et al. 2014), and others have employed geo-hazard potential for UEQ analysis (Liu et al. 2017). Liu et al. (2017b) have looked at the spatial patterns and factors that influence UEQ in China's hilly cities. The researchers discovered that pollution and a dense built environment have a considerable impact on the UEQ. Several studies have been carried out to assess UEQ based on factors such as air pollution, temperature, vegetation, impervious surface, population density, and accessibility to pollution-affected areas (Bonaiuto et al. 2015; Marans 2003; Joseph et al. 2014). Other indices for evaluating UEQ have been proposed, ranging from public health and energy efficiency to hazard vulnerability (Chrysoulakis et al. 2014). Physical settings as well as social and personal views are all key components of UEQ (Banzhaf et al. 2014). The study's goal was to uncover characteristics that influence the effective construction of green spaces rather than to define and characterize urban green space (Arunadeepa 2007). On the basis of urban green spaces, air quality and population density, Colombo Fort, Sri Lanka's economic hub, has the worst environmental quality, whereas residential divisions located outside of the city centre have superior environmental quality (Senanayake et al. 2013b). Similarly, the spatial extent of LST and the vegetation cover intensity revealed that LST and vegetation cover are inversely proportional when identifying crucial locations (Senanayakeet al. 2013a). With the help of geospatial dataset, the chapter focuses on UEQ in terms of environmentally sensitive zones. The most influential indicators for UEQ mapping and modelling are air quality and vegetation cover (Javanbakht et al. 2021). Urban planning projects that use

these methods effectively can take the necessary corrective actions to lessen the adverse effects of poor air quality.

The problem of air pollution in developing countries, which is exacerbated by urbanization, is complicated by interactions between regional and local sources (Kumar et al. 2016). Vehicles, coal-fired power plants, electricity generation, construction and road dust, waste burning, and household use are among the most common anthropogenic emissions, all of which have an impact on the environment's quality (Sharma et al. 2016; Cui and Shi 2012). The Delhi government attempted to control pollution in the early 2000s by introducing compressed natural gas (CNG) and closing industries (Goyal and Sidhartha 2003). According to the World Health Organization (WHO), approximately 4.2 million people have died as a result of health issues caused by air pollution (WHO 2020). Air quality data from recent years has been quite alarming, revealing that 97% of cities around the world have failed to meet WHO air quality guidelines (WHO 2018). The deterioration of air quality in urban areas is closely linked to changes in land use (Zahariet al. 2016). Due to growing human environmental intervention, the bulk of the world's landscapes have changed. There are tremendous pressures on the environment and its components as a result of rapid urbanization, with a particular emphasis on LULC. In general, land use refers to how much land is used for things like houses, industry, agriculture, plantations, and water bodies, whereas land cover refers to the rocks, vegetation, and structures that make up the surface (Lillesand et al. 2015). The LULC change analysis documents changes such as loss of vegetation, increased built-up, and open space (Ng et al. 2012), but it also affects the local environment and climate by influencing a variety of biological and physical factors. Air quality and LST are two of the most studied biophysical parameters that depict the urban environment and its health. Land-use changes have a strong association with air quality because of the impacts of the dispersion of air pollutants released from many types of sources that are reliant on land-use activities (Halim et al. 2020).

Remote sensing is crucial in the study of urban dynamics and urban greening in urban areas. Remote sensing is a method of gathering data using a space or airborne sensor without coming into physical contact with the object (Seto and Christensen 2013). The GIS is used to aid in the analysis and processing of remote sensing data and information. Because they are cost-effective while providing wide range of spatial resolutions for answering questions related to thematic disciplines, both remote sensing and GIS are used in a number of urban studies, mapping and monitoring, and change detection applications. The localities in any city can be classified as locations that support quality of life and urban sustainability by combining data from remote sensing (NDVI, LST, and others) with field measurements of environmental conditions (such as air pollution). The interpolation techniques, namely Inverse Distance Weighted, Kriging, Natural Neighbour, Spline, can be used to create map of air quality distribution using point data. Negative correlation exists between the LST and the Normalized Difference Plants Index (NDVI), which measures the health of the vegetation (Kumar et al. 2012). The environmental, social, aesthetic, economic, and resident health of humans are all regulated by vegetation cover in urban areas (Nowak et al. 1994). It can have a positive impact on the human psyche by reducing stress, increasing economic benefits, and promoting healthy living by increasing property demand and promoting tourism. Ecosystem services are the benefits provided by vegetation (Costanza et al. 1997). As a result, vegetation provides a diverse set of provisioning, regulatory, supporting, and cultural ecosystem services that are critical to maintaining urban quality and sustainability (Wolch et al. 2014).

India is an urbanizing country with a high concentration of people migrating to Delhi, the capital city, for economic and professional opportunities. Rapid urbanization has taken place due to the inflow of people at the loss of open space and forest cover. In the recent decades, such changes have aided in the maintenance of high levels of air pollution. Several studies on air quality in India's capital city have been

conducted (Kumar and Goyal 2011; Liu et al. 2018; Mohan annd Kandya 2007; Tiwari et al. 2012). However, there has been less research in combining air quality data with vegetation cover to determine criticality. Knowing these facts about Delhi, the current study realized the importance of combining data and information from other sources, such as consistent data collected on air pollution, to better understand the environmental quality associated with increased air pollution and decreased vegetation cover. This chapter emphasizes on three subcomponents: (1) understanding the spatiotemporal distribution of air quality, (2) understanding the distribution of environmental quality and implementing environmental critical zones across seasons, and (3) identifying the proximate drivers of environmental critical zones in capital city of India.

17.2 Material and Methods

17.2.1 Study Site

This study was conducted in the capital of India, Delhi, which encompasses an area of 1484 km^2. With 1.68 crore inhabitants and a high population density (11,297 persons/km^2), Delhi is the world's second largest megacity and India's largest urban agglomeration, according to the 2021 Census of India. At an altitude of 198–220 m, this megacity is located on an alluvial plain in the Indo-Gangetic area. This area has a semi-arid climate with four distinct seasons and significant wet and dry spells, as well as hot and cold spells: There are four seasons: pre-monsoon/summer (March–May), monsoon (June–September), post-monsoon (October–November), and winter (December to February) (December to February). The yearly rainfall ranges from 400 to 600 mm. The Yamuna floodplains and the Aravalli hill range terminal segment are two of Delhi's most peculiar physical characteristics. The temperature in the summer is from 42 to 48 °C, while the temperature in the winter is between 4 and 10 °C. This region has widespread fog and smog pollution during the winter, which significantly

hinders regular economic activity. Because it is considered to be both India's and the world's most polluted metropolis, the area is given priority when it comes to addressing urban air pollution. When discussing improving air quality for any occurrence, the name of this city almost immediately comes to mind. The current research region is depicted in Fig. 17.1, which contains 34 Central Pollution Control Board (CPCB) operational air quality monitoring stations from which data was collected. Delhi is the country's economic hub, attracting people from all around the country and resulting in urban sprawl. Urban sprawl alters the LULC and vegetation, as well as indirectly affecting climatic phenomena such as rainfall, temperature, wind direction, and atmospheric turbulence, affecting those who live nearby. Despite being the country's capital, the city lacks adequate urban planning and natural resource management. This is necessary for quality of life to be maintained. This research aims to document and report on the city's urbanization, vegetation, and environmental condition.

17.2.2 Data Sources and Pre-Processing

The satellite data was obtained in Geo-Tagged Image Fast Format (GeoTIFF) (level 1 product) with Universal Transverse Mercator (UTM) projection and World Geodetic System (WGS 84) datum for the year 2018 from the United States Geological Survey (USGS) website (www.usgs.gov). The criterion air pollution statistics were obtained through personal conversation and the Delhi Pollution Control Committee (DPCC) website (www.dpcc.delhigovt.nic.in). Particulate matter (PM$_{2.5}$, PM$_{10}$), sulphur dioxide (SO$_2$), and nitrogen dioxide (NO$_2$) are the most common air pollutants in urban environment. To determine the trend of air pollution in Delhi at a seasonal level, air quality maps were created for several criterion pollutants. Erdas Imagine was used for satellite data pre-processing. ArcGIS was used for other spatial database development and interpolation. For the criterion pollutants,

Fig. 17.1 Administrative unit and air quality monitoring stations of NCT Delhi

Analytic Hierarchy Process (AHP) was also used as a decision-making tool.

17.2.3 Estimation of NDVI

The red and infrared bands of Landsat data from the year 2018 were used to calculate NDVI. It is a measurement of the quantity of vegetation on the surface. It is mostly related to vegetation health, as healthy vegetation reflects very effectively in the near-infrared portion of the spectrum, whereas poor vegetation reflects more visible (red) radiation and less near-infrared radiation. Because chlorophyll plays the significant role in interaction of vegetation with these

two bands, the ratio of the NIR and red bands is employed in the computation (Bindi et al. 2009). To accommodate for changes in illumination and surface slope, the value is then normalized to −1 to +1.

$$NDVI = (NIR - Red)/(NIR + Red)$$

where Red = DN values from the red band, NIR = DN values from near-infrared band.

17.2.4 Estimation of LST

The thermal band of Landsat data was used to compute the land surface temperature. LST is

calculated in six steps, which are outlined in the following paragraphs (Table 17.1).

17.2.5 Air Quality Mapping and Statistical Analysis

Particulate matter ($PM_{2.5}$, PM_{10}), sulphur dioxide (SO_2), and nitrogen dioxide (NO_2) are the most common air pollutants in urban environments. Air quality maps for multiple criteria pollutants were created at the seasonal level to identify patterns in air pollution in Delhi. The criterion pollutants data from twenty-three Delhi monitoring stations was used for this. Four seasons (i) pre-monsoon (MAM), (ii) monsoon (JJAS), (iii) post-monsoon (OND), and (iv) winter (JF) were chosen for analysis based on the IMD classification. To create the air quality map for Delhi, the mapping was done using an interpolation technique called 'Kriging' and Gaussian model in ArcGIS software. Each pollutant had its own map, as well as one for each season.

Furthermore, using the Pearson correlation coefficient, a correlation analysis was performed among NDVI (max, mean), LST, and the criterion pollutants (NO_2, SO_2, PM_{10}, and $PM_{2.5}$) used. The Pearson correlation coefficient, which ranges from −1 to +1, is used to quantify the strength of the relationship between two variables and their affiliation with each other.

17.2.6 Environmental Critical Zones

The factors that contribute to the decline of Delhi's environmental quality were measured using a deductive indexing approach. Environmental quality is measured in terms of air quality and vegetation, with low environmental quality resulting from places with high levels of air pollution and less vegetation. Using this approach, it is feasible to conduct a quantitative investigation in Delhi and identify ecologically sensitive zones with poor environmental quality.

By dividing the NDVI mean of every season by each of the contaminants, deductive indexing was performed. Using AHP, all contaminants were combined into one map, and then all seasons were combined into annual composite map to determine environmentally critical zones (Fig. 17.2). AHP breaks down issues into their

Table 17.1 LST extraction mandatory steps

| Steps	Details
First step—Conversion of digital number of the image to spectral radiance $L_\lambda = ML \times Q_{cal} + AL$	Where L_λ = TOA spectral radiance (W/(m²/sr/μm)), ML = radiance multiplicative band (no.), AL = radiance add band (no.), Q_{cal} = quantized and calibrated standard product pixel values (DN)
Second step—Conversion of spectral radiance to top of atmosphere brightness temperature. The values of K_1 and K_2 are given $BT = K_2/\ln(K_1/(L_\lambda + 1)) - 272.15$	Where BT = top of atmosphere brightness temperature (°C), L_λ = TOA spectral radiance (Watts/(m²/sr/μm)), K_1 = K_1 constant band (no.), K_2 = K_2 constant band (no.)
Third step—Normalized Difference Vegetation Index (NDVI) calculation $NDVI = (NIR - Red)/(NIR + Red)$	Where Red = DN values from the red band, NIR = DN values from near − infrared band
Fourth step—Calculation of proportion of vegetation (PV) that contributes to increase the temperature $PV = [(NDVI - NDVI_{min})/(NDVI_{max} + NDVI_{min})]^2$	Where PV = proportion of vegetation, NDVI = DN values from NDVI image, $NDVI_{min}$ = minimum DN values from NDVI image, $NDVI_{max}$ = maximum DN values from NDVI image
Fifth step—Calculation of emissivity (E) $E = 0.004 \times PV + 0.986$	Where E = land surface emissivity, PV = proportion of vegetation
Sixth step—Calculation of land surface temperature (LST) $LST = (BT/1) + W \times (BT/14380) \times \ln(E)$	Where BT = top of atmosphere brightness temperature (°C), W = wavelength of emitted radiance, E = land surface emissivity
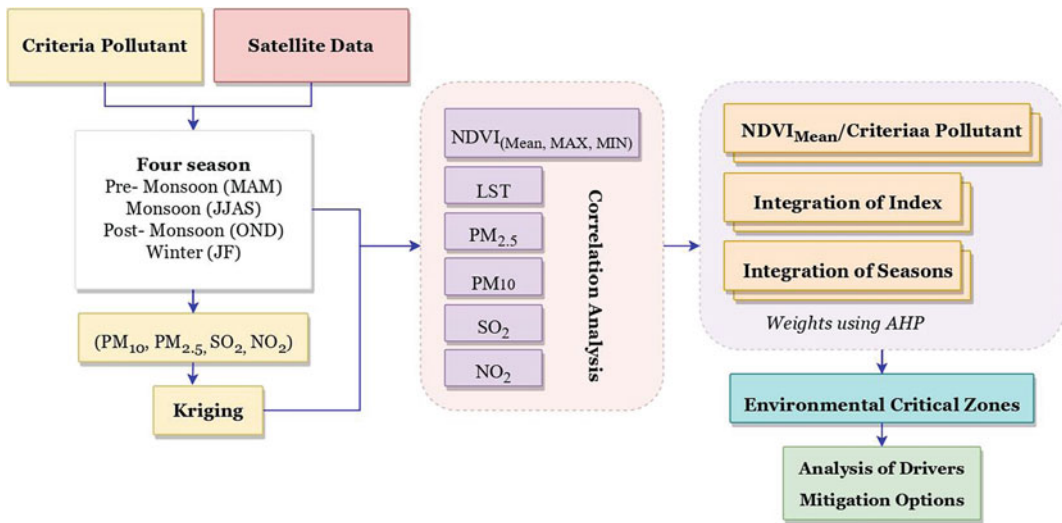
Fig. 17.2 Methodological flowchart of the study

constituent parts, identifies decision-makers' priorities based on their subjective assessments of the topic, and allows for the creation of a structure in a hierarchical manner based on these preferences (Saaty 1987). The qualifying pollutants were assigned weightage depending on their consequences using this technique, such as $SO_2 > PM2.5 > PM10 > NO_2$. These indices were calculated using raster techniques, and the outcomes were graphically represented. Low index values, as per this index method, indicate extremely critical zones with poor quality of the environment, making them less appropriate for human settlement based on air quality and vegetation. High index values, on the other hand, indicate zones with no critical issues with adequate quality of the environment that are appropriate for human settlement.

17.3 Results

17.3.1 Season Specific Spatial Concentration of Criteria Pollutants

Mapping distribution of concentration of pollutants in any city is of importance to environmental managers and city planning. For examples, for Delhi, Fig. 17.3 illustrates the spatial concentration of the criteria pollutants (PM_{10}, NO_2, $PM_{2.5}$, and SO_2) in India's capital city throughout the year. Seasonal fluctuation is readily visible in Fig. 17.3. The highest concentrations of all the criteria pollutants are seen during the post-monsoon (OND) and winter (JF) seasons. One of the main reasons for such increases in concentration in NCT Delhi is crop residue burning (Kumar et al. 2020; Laskar et al. 2020) and the atmospheric inversion process. Throughout the year, PM_{10} levels range from 88.4 to 531.7 g/m^3, with the highest concentrations in the western and northern parts of Delhi. The average concentrations are 284.06, 164.4, 344.5, and 363.1 μg/m^3 for pre-monsoon (MAM), monsoon (JJAS), post-monsoon (OND), and winter (JF), respectively (Fig. 17.3 a–d). The permissible limit of 100 μg/m^3 specified by the CPCB in 2015 has exceeded in all seasons. This permitted maximum is only 5.6% in the monsoon and 2% in the post-monsoon. Apart from that, all the seasons and every part of Delhi have reached this maximum. $PM_{2.5}$ is subjected to a similar situation, with the highest concentrations in the northwest, northeast, west, and north districts of Delhi throughout the year. The average concentration of $PM_{2.5}$ is 99.6 (pre-monsoon), 49.4 (monsoon), 195.5 (post-
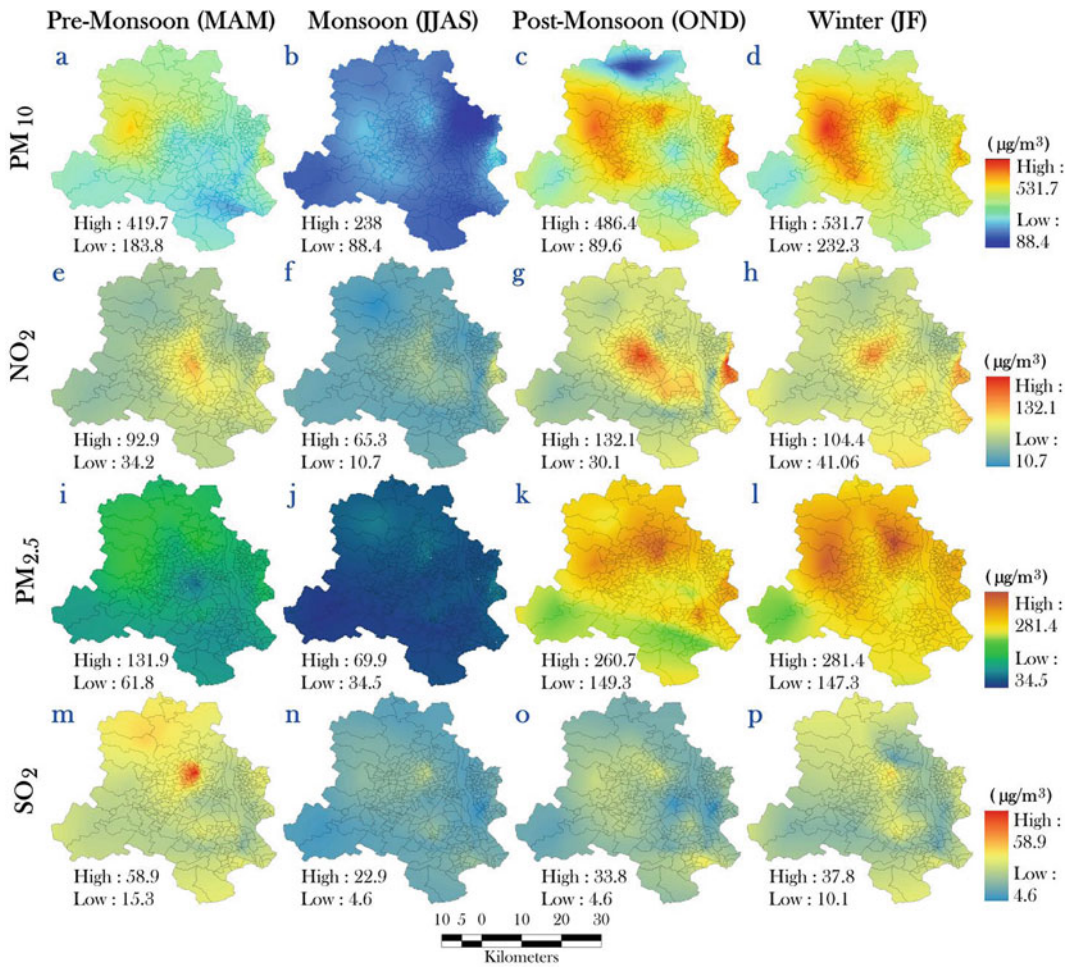
Fig. 17.3 Season-specific spatial concentration of criteria pollutants

monsoon), and 205.8 (winter) µg/m^3 (Fig. 17.3 e–h); except monsoon, all the seasons have exceeded the permissible limit (60 µg/m^3, CPCB 2015). The Delhi area is one of the India's fastest-developing cities and is known for being dusty due to construction activity. A regional climatic factor in combination with the operation of a few coal-based industries and biomass burning may also be the cause of the high PM$_{10}$ and PM$_{2.5}$ concentrations. The eastern and central areas of Delhi have the highest NO$_2$ concentrations throughout the year. NO$_2$ concentrations remained increasing throughout the year and over the permitted limit since it is mostly released by traffic, manufacturing, and power plants (80 µg/m^3, CPCB 2015). Considering Delhi is landlocked in Northern India, SO$_2$ concentrations have never exceeded the allowed permissible limit. However, shipping activities account for the majority of SO$_2$ emissions. The northwest and southwest districts of Delhi have high SO$_2$ levels during the pre-monsoon and post-monsoon seasons, whereas the southwest district experiences high SO$_2$ levels throughout the monsoon and winter seasons. According to Fig. 17.3, the concentrations and dispersion of pollution are the highest in the winter and the lowest in the monsoon.

17.3.2 Relationship Among Criteria Pollutant, NDVI, and LST

Most of the times, the distribution of pollutants is attributed to vegetation cover and the ambient temperature in the city. Figure 17.4 shows the relationship among NDVI ($_{max, mean}$), LST, and the study's criterion pollutants (NO_2, SO_2, PM_{10}, and $PM_{2.5}$). NDVI ($_{mean, max}$) and LST have a negative connection across seasons, according to the results. In the majority of seasons, there is a link between NDVI$_{mean}$ and the criterion pollutants. NDVI$_{mean}$ (0.99) and NDVI$_{max}$ (0.99) have a substantial positive association across seasons. During the winter (−0.61) and monsoon (−0.60) seasons, NDVI$_{mean}$ and NDVI$_{max}$ have a high negative correlation with LST. In the pre-monsoon (−0.53) season, LST has a substantial negative correlation with NO_2. In the pre-monsoon (−0.36) season, NO_2 is inversely
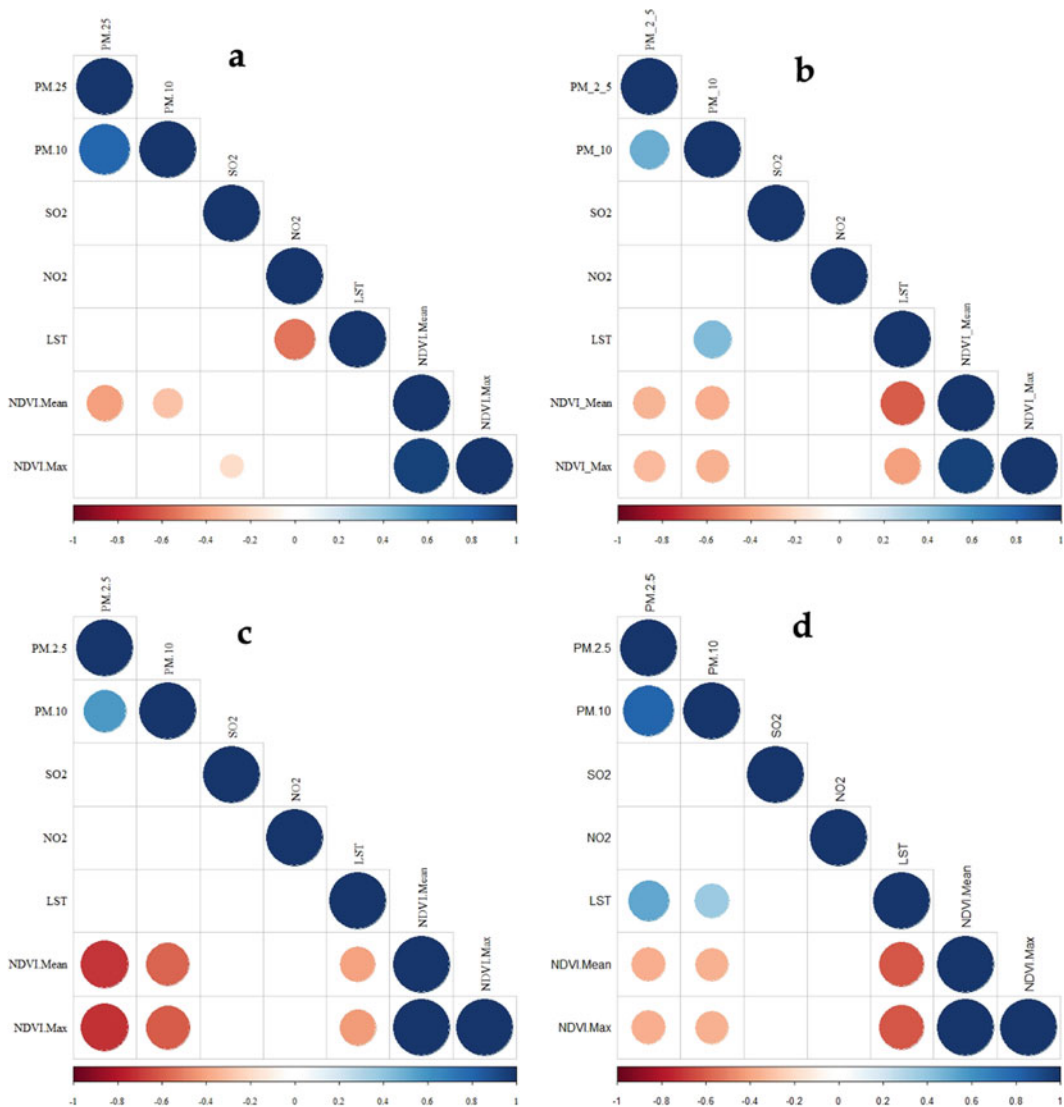
Fig. 17.4 Correlation among NDVI ($_{max, mean}$), LST, and the criteria pollutants ($PM_{2.5}$, PM_{10}, SO_2, and NO_2)—(**a**- pre-monsoon (MAM), **b**- monsoon (JJAS), **c**- post-monsoon (OND), and **d**- winter (JF))

connected with $PM_{2.5}$, whereas in the monsoon (0.46) season, it is favourably correlated with PM_{10}. In the monsoon, SO_2 is strongly associated with $PM_{2.5}$ (0.49). During the winter (0.80) and pre-monsoon (0.79) seasons, PM_{10} has a high positive connection with $PM_{2.5}$.

17.3.3 Seasonal and Annual Status of Environmental Critical Zones (ECZ)

Environmental critical zones are defined based on the decline of environmental quality. The state of the environmental quality is divided into five crucial zones: extremely high, extremely high, extremely high, extremely low, and extremely low. Figure 17.5 shows four maps of environmental quality in India's capital city for each season in 2018: pre-monsoon (MAM), monsoon (JJAS), post-monsoon (OND), and winter (JF). Since pollution levels vary seasonally, seasonal variation in environmental quality is extremely noticeable. According to the findings, environmental quality is lower in the northern, central, and eastern districts of Delhi during the pre-monsoon (MAM) season (Fig. 17.5a). The extremely high and high-critical zone categories cover around 46.86% of the land. Only 6.14% of the land has excellent environmental conditions, though. In comparison to all other seasons, the monsoon (JJAS) season has the best environmental quality (40.57% of the area in the low and very low categories), as it receives the most rainfall (80%). As a result, the particulate matter concentration is relatively low during this season. During the post-monsoon (OND) season, environmental quality is very poor in the eastern, western, and central districts of Delhi. In this season, 36.97% of the area falls under the high and very high-critical zones category. When compared to other seasons, the winter (JF) season has the worst environmental quality in the city, with the exception of rural population-dominated agricultural areas in the south and northwest districts of Delhi. About 26.33% of the area is under the very high critical zone, and 32.10% of the area is high critical, which means 58.43% of

Delhi has a critical environmental status. It is quite alarming that most parts of the city are in critical zones during this season.

Figure 17.6 depicts the annual status of environmental critical zones of India's capital city. The environmental quality status for the entire year of 2018 has been determined by combining all of the seasons. The very high and high critical zones account for 38.26% of the total, with good environmental quality accounting for 17.16% of the study area. Delhi's eastern, northern, western, and central districts appear to be quite vulnerable. The southern districts of Delhi, on the other hand, look to be in a low-crisis zone.

17.3.4 Proximate Drivers of Environmental Critical Zones

According to previous works reported in similar context, green and blue spaces have the ability to distribute mitigating effects throughout the surrounding environment, whereas grey spaces have an exacerbating influence on environmental degradation. Buffer analysis was used to determine the mitigation or exacerbation gradient with distance from green, blue, and grey zones in order to quantify this theoretical idea. OpenStreetMap (OSM) data was used to create maps of green, blue, and grey areas. From these sites, three successive buffers of 30 m, 60 m, and 90 m were established. The green, grey, and blue regions of the Delhi region are depicted in Fig. 17.7. The findings of the study to the mitigating effect of blue spaces are summarized in Table 17.2. The very high ECZ area was found to be reduced in the 30 m buffer (7.22%), growing in the 60 m buffer (22.33%), and finally increasing in the 90 m buffer (28.32%). Less-critical zone or good environmental quality, on the other hand, had the highest share (20.27%) in the nearest buffer and the lowest in the outermost buffer (14.6%). This buffer analysis clearly shows the gradient of critical status and the mitigation effect of blue areas. Similarly, the same outcome has been observed in green places
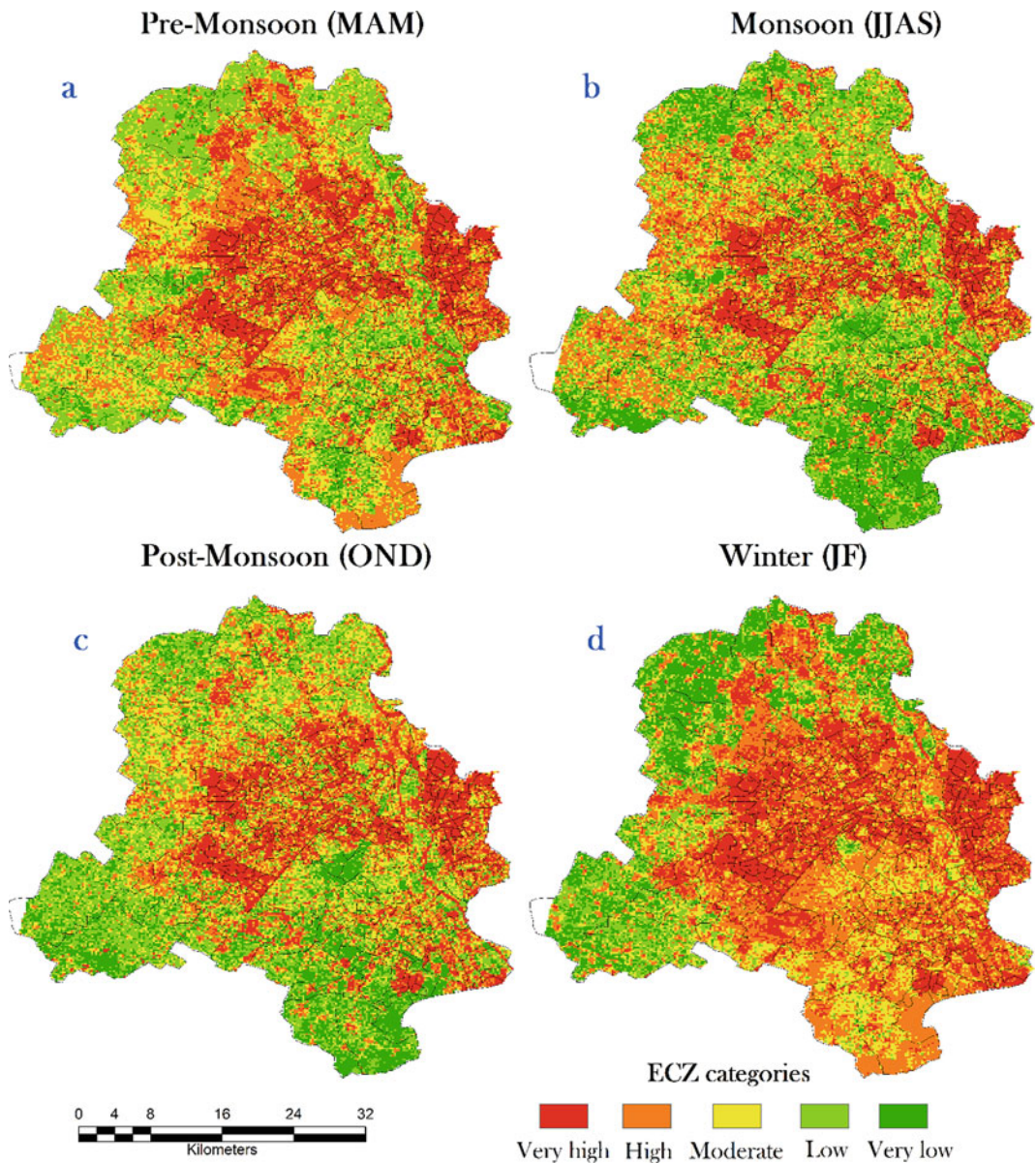
Fig. 17.5 Season-specific environmental critical zones (**a**- pre-monsoon (MAM), **b**- monsoon (JJAS), **c**- post-monsoon (OND), and **d**- winter (JF))

(Table 17.2). Extremely important zones feature 30 m, 60 m, and 90 m buffer zones of green patches with 10.36%, 22.13%, and 26.68% of area, respectively. Grey spaces have been subjected to an inverse state, which has exacerbated environmental degradation. Critical zones are higher as you go closer to grey spaces. In the presence of very high ECZ, 31.21% of the land is covered by grey space buffer zones of 30 m, with 28.11% and 21.01% shares for 60 m and 90 m, respectively. Very low critical zones, on the other hand, account for 8.24%, 14.17%, and 19% of the area beneath the 30 m, 60 m, and 90 m buffers, respectively.

Fig. 17.6 Annual scenario of environmental critical zones
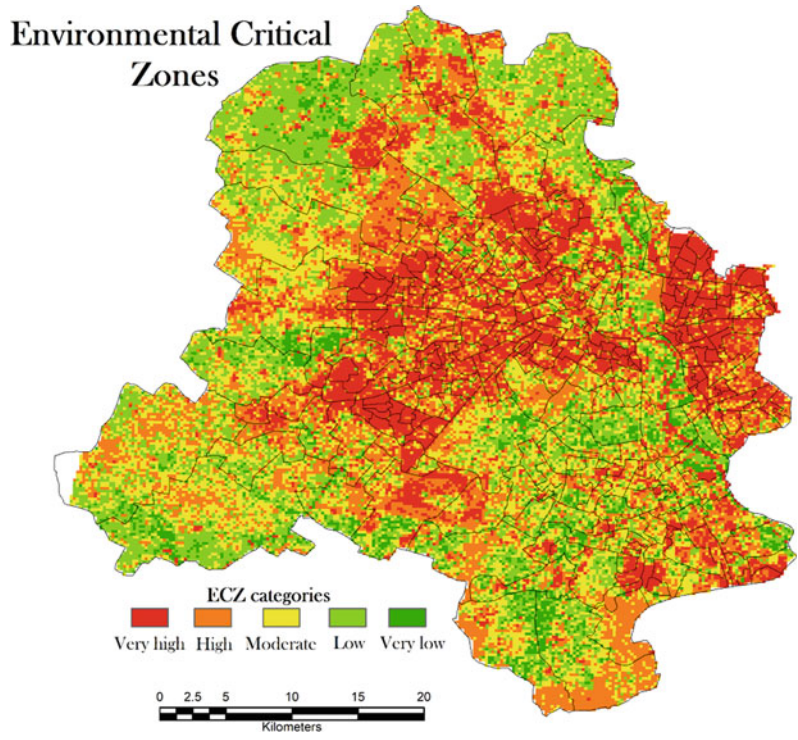
17.4 Discussion

The chapter demonstrates use of satellite remote sensing images-derived temporal NDVI and LST information and criterion air pollutants data obtained from the DPCC website. The NDVI datasets can be used as proxy metrics to identify environmental critical zones (Senanayake et al. 2013a, b). This work uses seasonal distribution of air quality in Delhi utilizing criterion pollutants (PM10, NO_2, PM2.5, and SO_2) in 2018. Pollutant concentrations and distribution were found to be extremely high during the winter season due to a decrease in mixing height, slow wind speed, and other climatic conditions (Choi and Souri 2015; İm et al. 2006). Stubble burning in agricultural areas from Punjab and Haryana during the winter season is a significant source of air pollution in Delhi (Tiwari et al. 2012). During
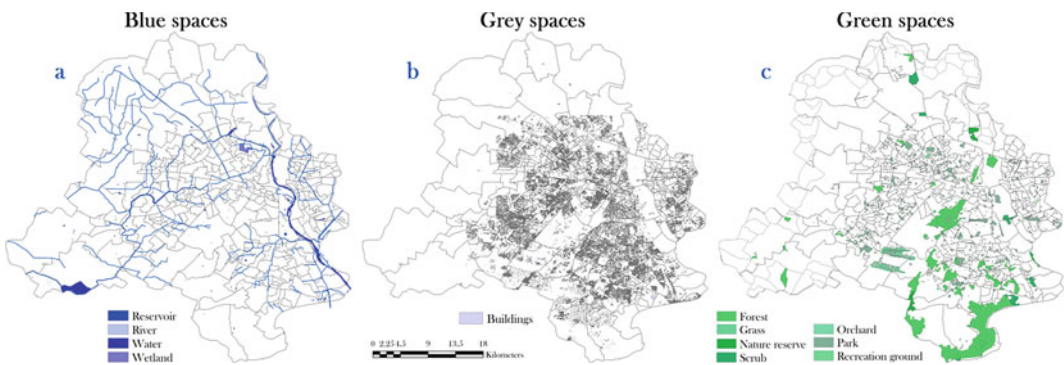

Fig. 17.7 Green, grey, and blue spaces of Delhi

Table 17.2 Statistical summary of buffer zones for blue, grey, and green spaces

ECZ categories	Different buffer zone of blue spaces					
	30 m		60 m		90 m	
	Area in km^2	Area in %	Area in km^2	Area in %	Area in km^2	Area in %
Very high	0.90	7.22	2.75	22.33	2.63	28.32
High	2.83	23.71	4.19	16.02	2.01	21.68
Moderate	2.95	24.74	5.13	25.73	1.81	19.47
Low	2.87	24.05	4.64	20.87	1.48	15.93
Very low	2.42	20.27	3.69	15.05	1.35	14.60
ECZ categories	Different buffer zone of grey spaces					
	30 m		60 m		90 m	
	Area in km^2	Area in %	Area in km^2	Area in %	Area in km^2	Area in %
Very high	68.57	31.21	33.69	28.11	16.70	21.01
High	56.18	25.57	26.47	22.08	16.62	20.91
Moderate	43.70	19.89	21.71	18.11	13.75	17.29
Low	33.16	15.09	21.01	17.53	17.32	21.79
Very low	18.10	8.24	16.99	14.17	15.10	19.00
ECZ categories	Different buffer zone of green spaces					
	30 m		60 m		90 m	
	Area in km^2	Area in %	Area in km^2	Area in %	Area in km^2	Area in %
Very high	3.82	10.36	8.95	22.13	9.77	26.68
High	8.21	22.27	10.67	26.40	8.90	24.33
Moderate	6.89	18.71	7.92	19.59	7.35	20.07
Low	9.89	26.84	7.51	18.58	5.95	16.26
Very low	8.04	21.83	5.38	13.30	4.64	12.67

the monsoon season, the concentration and dispersion of pollutants are very low because turbulence, strong winds, and a large amount of rainfall play an important role in reducing the concentration of pollutants in the atmosphere via wet deposition (Sehgal et al. 2016). The chapter demonstrates the relationship between NDVI ($_{maximum, mean}$), LST, and the pollutants under consideration (NO_2, SO_2, PM_{10}, and $PM_{2.5}$) in 2018. NDVI ($_{max, mean}$) and LST have a negative connection across seasons. Similar findings were reported by many researchers including Kumar et al. 2012, who discovered that minimum temperatures are higher in places with increased vegetation cover in Andhra Pradesh's quickly urbanized Vijayawada. LST has a strong negative correlation with NO_2 during the pre-

monsoon season because when the ground temperature rises during the pre-monsoon and midday, the vertical mixing height rises as well, reducing the concentration of NO_2 in the low-altitude atmosphere (Wang et al. 2020). The fact that SO_2 and NO_2 are positively linked with particulate matter (PM_{10}, $PM_{2.5}$) during the monsoon season could be attributed to the turbulent conditions and wind-blown dust. Because of long-distance transit and substantial biomass burning, PM_{10} is strongly positively associated with $PM_{2.5}$ throughout the winter and pre-monsoon seasons (Tiwari et al. 2012; Yadav et al. 2014).

The district-level environmental quality evaluation aided in addressing the asymmetry of urban environmental quality distributions

between seasons. Throughout the study period, the environmental quality in Delhi's northern, central, and eastern districts remained the poorest. The environmental quality of an urban region declines with greater human density, decreased vegetation cover, and increased pollutant concentration in the atmosphere, according to common understanding. During the pre-monsoon (MAM) season, environmental quality is worse in Delhi's northern, central, and eastern districts due to high human density, minimal vegetation cover, and thus poor air quality. During the monsoon (JJAS) season, the environmental quality in the northern, central, and eastern districts of Delhi is comparatively better than during the pre-monsoon season due to rainfall, as pollutants settle down to the surface (Sehgal et al. 2016; Tiwari et al. 2012) and vegetation is comparatively healthy. Due to high concentrations of pollutants from local sources, environmental quality in Delhi's eastern, western, and central districts is poor during the post-monsoon (OND) season (Liu et al. 2018; Yadav et al. 2014). When compared to other seasons, the winter (JF) season has the worst environmental quality in all parts of the city except the rural population-dominated agricultural areas in the south and northwest districts of Delhi as a result of low temperature, low wind speed, decrease in mixing height, high energy demand, and thus, the pollutant concentration is very high in the ground height (Choi and Souri 2015; İm et al. 2006). The southern districts of Delhi have good environmental quality because of low population density, planned urbanization, plantation, and forested areas such as the Delhi Ridge, the Sanjay Van, Aravalli biodiversity parks, and Asola wildlife sanctuary, which help to maintain urban environmental quality, whereas the northwest district, the largest district, contains 51% of Delhi's rural population and is occupied by agricultural land (Sharma et al. 2020). Delhi's eastern, northeastern, and central districts are densely populated, highly industrialized, and unplanned urbanized areas that ultimately deteriorate urban environmental quality. The increase of built-up territory at the expense of agricultural land has resulted in a worsening of environmental quality. The quality of life for humans is strongly influenced by environmental quality (Wolch et al. 2014).

The study of environmental critical zones aids in addressing the disproportionate distributions of urban environmental quality in Delhi in 2018. Overall, Delhi's eastern, northern, western, and central districts are considered vital. Southern districts, on the other hand, appear to be of low criticality. Our findings echoed those of Senanayake et al. 2013b, who identified environmentally essential locations in Colombo, Sri Lanka, based on population density, percentage green space, and air quality. Their findings revealed that residential areas located outside of the city centre have higher environmental quality. Senanayake et al. 2013a, identified environmental critical regions in the same region based on LST and plant cover availability. Environmental criticality is associated with metropolitan areas that have reduced vegetation cover, which contributes to an increase in LST. In densely populated places, impermeable surface increases with population density, resulting in less vegetative cover (Nowak and Greenfield 2012b). As a result, the presence of vegetative cover is seen as a measure of ecological sustainability in a city.

The results of these studies may be efficiently employed in upcoming urban planning and development initiatives, as well as a foundation for the adoption of laws and regulations by authorities for sustainable urban development with a focus on the environment. Municipalities, which frequently function on a district level, might utilize such maps to comprehend the current scope of the problem and plan their future work more efficiently. The importance of vegetation covers in preserving the quality of life and the sustainability of cities cannot be overstated. As a developing country, seeking for sensible solutions is highly recommended because resources are limited and much time might be wasted in ineffective planning without regard for the future. Using spatial analysis to develop a district-level mitigation plan and undertake afforestation programmes can be quite advantageous.

17.5   Conclusion

The National Capital Region's most populous and rapidly rising metropolitan city is Delhi. The government's recent city beautification and urban planning projects have been instrumental in strengthening Delhi's image as a world-class national capital. However, Delhi is also harmed by regional pollution, as Northern India is home to 15 of the world's 20 most polluted cities. The cities around New Delhi make up the top five of these cities. Stubble burning in agricultural areas during the winter months is a major source of air pollution in Delhi, emphasizing the significance of preserving vegetation cover. As presented in this chapter, the National Capital Region of India has poor environmental quality in terms of vegetation and air quality, but residential areas located outside of the city centre have superior environmental quality. Rapid, unplanned urbanization is the primary cause of lack of vegetation, land fragmentation, poor air quality, and a significant urban heat island. By expanding the number of factories, automobiles, transportation facilities, and road networks in metropolitan areas, rapid urbanization affects air quality. To understand the urban environmental quality distribution, ground-level pollution data from a huge network of monitoring sites, as well as satellite data can be a valuable source for interpretation. The identification of environmentally sensitive zones based on such solid and accurate data might add a new dimension to city planners' and decision-makers' efforts to plan for future development. Municipal bodies that frequently work on a district level might utilize such maps to better grasp the current scope of an issue and plan their future efforts.

References

Alberti M, Booth D, Hill K, Coburn B, Avolio C, Coe S, Spirandelli D (2007) The impact of urban patterns on aquatic ecosystems: An empirical analysis in Puget lowland sub-basins. Landsc Urban Plan 80(4):345–361

Arunadeepa KPW (2007) Factors influencing the success of urban green spaces in Sri Lanka. Doctoral Dissertation

Banzhaf E, De La Barrera F, Kindler A, Reyes-Paecke S, Schlink U, Welz J, Kabisch S (2014) A conceptual framework for integrated analysis of environmental quality and quality of life. Ecol Ind 45:664–668

Bindi M, Brandani G, Dessì A, Dibari C, Ferrise R, Moriondo M, Trombi G (2009) Impact of climate change on agricultural and natural ecosystems. Am J Environ Sci 5(5):633–638

Bonaiuto M, Fornara F, Ariccio S, Ganucci Cancellieri U, Rahimi L (2015) Perceived residential environment quality indicators (PREQIs) relevance for UN-HABITAT city prosperity index (CPI). Habitat Int 45(P1):53–63

Choi Y, Souri AH (2015) Seasonal behavior and long-term trends of tropospheric ozone, its precursors and chemical conditions over Iran: a view from space. Atmos Environ 106:232–240

Chrysoulakis N, Feigenwinter C, Triantakonstantis D, Penyevskiy I, Tal A, Parlow E, Fleishman G, Düzgün S, Esch T, Marconcini M (2014) A conceptual list of indicators for urban planning and management based on Earth Observation. ISPRS Int J Geo Inf 3(3):980–1002

Costanza R, D'Arge R, de Groot R, Farber S, Grasso M, Hannon B, Limburg K, Naeem S, O'Neill RV, Paruelo J, Raskin RG, Sutton P, van den Belt M (1997) The value of the world's ecosystem services and natural capital. LK - https://royalroads.on.worldcat.org/oclc/4592801201. Nature TA - TT -, 387(6630):253–260

CPCB (2015) Status of ambient noise level in India–2015. Central Pollution Control Board, New Delhi

Cui L, Shi J (2012) Urbanization and its environmental effects in Shanghai, China. Urban Climate 2:1–15

EPA (2008) Heat Island impacts. Heat Island Effect

Fernández IC, Wu J (2018) A GIS-based framework to identify priority areas for urban environmental inequity mitigation and its application in Santiago de Chile. Appl Geogr 94:213–222

Goyal P, Sidhartha (2003) Present scenario of air quality in Delhi: a case study of CNG implementation. Atmos Environ 37(38):5423–5431

Halim NDA, Latif MT, Mohamed AF, Maulud KNA, Idrus S, Azhari A, Othman M, Sofwan NM (2020) Spatial assessment of land use impact on air quality in mega urban regions Malaysia. Sustain Cities Soc 63:102436

İm U, Tayanç M, Yenigün O (2006) Analysis of major photochemical pollutants with meteorological factors for high ozone days in Istanbul, Turkey. Water Air Soil Pollut 175(1–4):335–359

Javanbakht M, Darvishi Boloorani A, Kiavarz M, Neisany Samany N, Zebardast L, Zangiabadi M (2021) Spatial-temporal analysis of urban environmental quality of Tehran Iran. Ecol Indicators 120:106901

Joseph M, Wang F, Wang L (2014) GIS-based assessment of urban environmental quality in Port-au-Prince, Haiti. Habitat Int 41:33–40

Kumar A, Goyal P (2011) Forecasting of daily air quality index in Delhi. Sci Total Environ 409(24):5517–5523

Kumar A, Patil RS, Dikshit AK, Islam S, Kumar R (2016) Evaluation of control strategies for industrial air pollution sources using American meteorological society/environmental protection agency regulatory model with simulated meteorology by weather research and forecasting model. J Clean Prod 116:110–117

Kumar, Bhaskar PU, Padmakumari (2012) Estimation of land surface temperature to study urban heat island effect using landsat Etm+ Image. Int J Eng Sci Technol 4(02):771–778

Kumar, R., Ghude, S.D., Biswas, M., Jena, C., Alessandrini, S., Debnath, S., Kulkarni, S., Sperati, S., Soni, V.K., Nanjundiah, R.S. and Rajeevan, M., 2020. Enhancing accuracy of air quality and temperature forecasts during paddy crop residue burning season in Delhi via chemical data assimilation. Journal of Geophysical Research: Atmospheres, 125(17), p. e2020JD033019

Laskar AH, Maurya AS, Singh V, Gurjar BR, Liang MC (2020) A new perspective of probing the level of pollution in the megacity Delhi affected by crop residue burning using the triple oxygen isotope technique in atmospheric CO_2. Environ Pollut 263:114542

Li G, Weng Q (2007) Measuring the quality of life in city of Indianapolis by integration of remote sensing and census data. Int J Remote Sens 28(2):249–267

Liang B, Weng Q (2011) Assessing urban environmental quality change of Indianapolis, United States, by the Remote Sensing and GIS Integration. IEEE J Selected Topics Appl Earth Observ Remote Sens 4(1):43–55

Lillesand T, Kiefer RW, Chipman J (2015) Remote Sensing and Image Interpretation, 7th edn, vol 736. Wiley, New York. ISBN: 978-1-118-34328-9

Liu Y, Yue W, Fan P, Zhang Z, Huang J (2017) Assessing the urban environmental quality of mountainous cities: a case study in Chongqing, China. Ecol Ind 81:132–145

Liu T, Marlier ME, DeFries RS, Westervelt DM, Xia KR, Fiore AM, Mickley LJ, Cusworth DH, Milly G (2018) Seasonal impact of regional outdoor biomass burning on air pollution in three Indian cities: Delhi, Bengaluru, and Pune. Atmos Environ 172:83–92

Marans RW (2003) Understanding environmental quality through quality of life studies: the 2001 DAS and its use of subjective and objective indicators. Landsc Urban Plan 65(1–2):73–83

Mohan M, Kandya A (2007) An analysis of the annual and seasonal trends of air quality index of Delhi. Environ Monit Assess 131(1–3):267–277

Moore G, Croxford B, Adams M, Refaee M, Cox T, Sharples S (2006) Urban environmental quality: perceptions and measures in three UK cities. WIT Trans Ecol Environ 93:785–794

Musse MA, Barona DA, Santana Rodriguez LM (2018) Urban environmental quality assessment using remote sensing and census data. Int J Appl Earth Obs Geoinf 71:95–108

Ng E, Chen L, Wang Y, Yuan C (2012) A study on the cooling effects of greening in a high-density city: an experience from Hong Kong. Build Environ 47(1):256–271

Nichol, J. E., & Wong, M. S. (2006). 12 Assessing Urban Environmental Quality with Multiple Parameters. Urban remote sensing, 253.

Nowak, D.J., McPherson, G. E., and Rowntree, R. A. (1994). Chicago's urban forest ecosystem: Results of the Chicago Urban Forest Climate Project. Gen. Tech. Rep. NE-186. Radnor, PA: US Department of Agriculture, Forest Service, Northeastern Forest Experiment Station. 201 p., 186.

Nowak DJ, Greenfield EJ (2012) Tree and impervious cover in the United States. Landsc Urban Plan 107(1):21–30

Saaty RW (1987) The analytic hierarchy process-what it is and how it is used. Math Model 9(3–5):161–176

Sehgal M, Tyagi SK, Gautam SK (2016) Air quality in Delhi: status and concerns. Int J Environ Stud 73(6):905–916

Senanayake IP, Welivitiya WDDP, Nadeeka PM (2013a) Remote sensing based analysis of urban heat islands with vegetation cover in Colombo city, Sri Lanka using Landsat-7 ETM+ data. Urban Clim 5:19–35

Senanayake IP, Welivitiya WDDP, Nadeeka PM (2013b) Urban green spaces analysis for development planning in Colombo, Sri Lanka, utilizing THEOS satellite imagery—a remote sensing and GIS approach. Urban Forestry Urban Greening 12(3):307–314

Seto KC, Christensen P (2013) Remote sensing science to inform urban climate change mitigation strategies. Urban Clim 3:1–6

Sharma S, Nahid S, Sharma M, Sannigrahi S, Mohammad M (2020) A long-term and comprehensive assessment of urbanization-induced impacts on ecosystem services in the capital city of India. City Environ Interactions 7:100047

Sharma, S. K., Mandal, T. K., Jain, S., Saraswati, Sharma, A., & Saxena, M. (2016). Source Apportionment of PM2.5 in Delhi, India Using PMF Model. Bulletin of Environmental Contamination and Toxicology, 97(2), 286–293.

Taubenböck H, Wegmann M, Roth A, Mehl H, Dech S (2009) Urbanization in India—spatiotemporal analysis using remote sensing data. Comput Environ Urban Syst 33(3):179–188

Thapa RB, Murayama Y (2010) Drivers of urban growth in the Kathmandu valley, Nepal: examining the efficacy of the analytic hierarchy process. Appl Geogr 30(1):70–83

Tiwari S, Chate DM, Pragya P, Ali K, Bisht DSF (2012) Variations in mass of the PM 10, PM 2.5 and PM 1 during the monsoon and the winter at New Delhi. Aerosol Air Qual Res 12:20–29

United Nations. (2014). World Urbanization Prospects: The 2014 Revision, Highlights (ST/ESA/SER.A/352). In *New York, United*.

United Nations. (2018). The World 's Cities in 2018. In *The World's Cities in 2018 - Data Booklet (ST/ESA/ SER.A/417)*.

Wang, L., Wang, J., Tan, X., & Fang, C. (2020). Analysis of NOx pollution characteristics in the atmospheric environment in Changchun city. *Atmosphere*, *11*(1).

Wolch JR, Byrne J, Newell JP (2014) Urban green space, public health, and environmental justice: the challenge of making cities "just green enough." Landsc Urban Plan 125:234–244

World Health Organization (2010) Urbanization and health. Bull World Health Organ 88(4):245–246. http://dx.doi.org/10.2471/BLT.10.010410

World Health Organization. (2018). *WHO global ambient air quality database* (Accessed 24 October 2019).

World Health Organization (2020) Air pollution (Accessed 28 Mar 2020)

Yadav R, Sahu LK, Jaaffrey SNA, Beig G (2014) Temporal variation of particulate matter (PM) and potential sources at an urban site of Udaipur in Western India. Aerosol Air Qual Res 14(6):1613–1629

Zahari, M., Majid, M., Ho, C., Kurata, G., Nadhirah, N., & Irina, S. (2016). Relationship between land use composition and PM concentrations in Iskandar Malaysia. *Clean Technologies & Environmental Policy*, *18*(8).

Zhou L, Dickinson RE, Tian Y, Fang J, Li Q, Kaufmann RK, Tucker CJ, Myneni RB (2004) Evidence for a significant urbanization effect on climate in China. Proc Natl Acad Sci USA 101(26):9540–9544

Rajesh Sarda and Swades Pal

Abstract

An expanding pattern of energy use, high discharge of carbon in the atmosphere, and thermal uncomfortably in the urban area is the emerging issue nowadays. Temperature change and anthropogenic heat flux (AHF) estimation were separately done by the researchers; however, very little attention was paid to exploring the nexus between AHF and urban heat islands. The present study attempted to monitor land surface temperature (LST), and AHF and explore the nexus at the spatial level by selecting the highly urbanized, industrialized, and mining-dominated Asansol Durgapur Development Area (ADDA) of Eastern India as a case. In the winter season, mean LST was increased from 18.53 °C to 22.91 °C from 1991–2000 to 2010–2019 phases. In the summer season, the mean rate of LST rise was 0.13 °C /year. Heat island was mainly identified in the mining and built areas. Mean AHF was increased from 39.59 to 98.86 W/m^2 between 2000 and 2019. Spatial least square regression analysis proved that the nexus between LST and AHF was high in the heat island-dominated areas revealing the fact that within these very little latitudinal differences solar irradiance is not the major factor, and land use composition and energy footprint are vital. The study also exhibited that green and blue space (emission sink) can vitally reduce the heat island effect and can play a multi-functional role in making a resilient urban ecosystem. Restriction in energy footprint and increase of carbon emission sink sources may reduce the AHF as well as the heat island effect.

18.1 Introduction

In the last few decades, climate change emerges as one of the most debated issues among scientists as well as researchers across the world. Since 1850, the temperature was increased each decade at an accelerated rate (IPCC 2013). The twenty-first-century accelerated urban growth was reported as one of the major factors of local climatic change. The energy footprint of the urban sector, an increase of thermally sensitive concrete building materials, and the loss of green

R. Sarda · S. Pal (✉)
Department of Geography, University of Gour Banga, Malda, West Bengal, India
e-mail: swadeshpal82@gmail.com

R. Sarda
e-mail: rajeshsarda127@gmail.com

and blue spaces within urban space have confronted urban people and urban ecology with a great challenge (Colding and Barthel 2017). The rise of the temperature and increasing discomfort ability are the direct consequences of this (Yang et al. 2017). For urban health study, air temperature, as well as land surface temperature (LST), is also be considered a bio-physical parameter (Xiao and Weng 2007), and it is one of the important indicators for monitoring urban ecological performance (Kalnay and Cai 2003). Countless investigations accentuated that time series examination of land surface temperature is exceptionally vital to evaluate regional as well as worldwide climate changes at various scales (Khandelwal et al. 2018; Meng et al. 2018; Yu et al. 2018a, b; Aithal et al. 2019). Among the studies, large numbers of studies were centered around the urban sector. Urban surface heat study is one of the focusing contents emphasized by many eminent scholars like Ranagalage et al. (2017), Santamouris et al. (2017), Son et al. (2017), Singh et al. (2017), Zhang et al. (2017), Zhou et al. (2017), Gaur et al. (2018), Mathew et al. (2018), Shi et al. (2018), Zhou et al. (2018), Sejati et al. (2019), Sultana and Satyanarayana (2020). This sort of study is not only confined to the large metropolitan cities but also focused on the medium and small cities (Pal and Ziaul 2017; Mathew et al. 2018; Dissanayake et al. 2019; Lakra and Sharma 2019). A portion of some researchers like Zhang et al. (2016), Mushore et al. (2017), Yang et al. (2017), and Arekhi (2018) also tried to explain the causes of such temperature change. Along with the change in building materials, a good number of studies condemned adverse changes in surface parameters as a major cause of rising thermal effects in the urban environment. Silva et al. (2018), Aithal et al. (2019), Dhar et al. (2019), Grigoraş and Uriţescu (2019), Tafesse and Suryabhagavan (2019), Willie et al. (2019) explained the role of land use dynamics on surface heat. Most of the mentioned scholars reported that declining vegetation cover and water cover were inversely and concrete building materials were positively related to temperature change. Zu et al. (2017), Sarangi et al. (2018), Zheng et al. (2018), and

Ziaul and Pal (2018a) tried to link temperature change with the change in aerosol concentration and energy budget. Ziaul and Pal (2018a) documented that a high concentration of aerosol in the lower atmosphere can enhance the temperature. Deficit water balance can also enhance temperature at the regional scale as explained by Mahato and Pal (2018) in the Indian context.

Anthropogenic heat implies heat delivery to the atmosphere because of human exercise. This is one of the centering themes in the situation of climate change explicitly in the urban area. Decent many quantities of researchers like Kato and Yamaguchi (2005), Zhou et al. (2012), Zhang et al. (2013), Chakraborty et al. (2015), Ogunjobi et al. (2018), Ziaul and Pal (2018b), Ayanlade and Howard (2019) in most recent twenty years highlighted in on the assessment of heat flux from satellite imageries. In a very general sense, it can be supposed that either one of the methods provides the wrong result or some of the contributing agents of heat were missed in the calculation process. However, most of the studies strongly reported that this type of heat is getting increased over the progress of time. Growing population density, high energy consumption rate, industrial emission, traffic emission, emission from the mining sector, etc., are majorly responsible for increasing heat flux. An expanding amount of heat flux can also proliferate the intensity of heat islands in the urban areas to some extent.

In India, several studies focusing on LST and urban heat islands were conducted; however, a few studies were done on anthropogenic heat flux (AHF) estimation and its effects. Chakraborty et al. (2015), and Ziaul and Pal (2018b) attempted to estimate anthropogenic heat in Delhi and a medium-sized town in West Bengal. They did not link AHF with LST in their works; however, it is essential due to its steady rise of energy footprint across the world in the general and urban areas in particular.

Therefore, continuous evaluation of anthropogenic heat is necessary since urban people are already trapped by heat island effects. The previous study discretely explored time-series changes in temperature and AHF but how far

they are spatially related was not investigated. Therefore, the present study monitored LST and AHF and linked them spatially to know whether AHF plays any role to promote urban heat islands. The highly urbanized, industry, and mining-intensive Asansol Durgapur Development Area (ADDA) in the western part of West Bengal was taken as a case for study.

18.2 Study Area

Asansol Durgapur Development Area, flanked by waterway Ajay in the northern and Damodar on the southern edge, is one of the quickest developing urban areas among the arising and arranged urban areas in Eastern India, situated in the western part of West Bengal. The study consists of eight Community Development blocks, three municipalities (Kulti, Jamuria, and Raniganj), and two municipal corporations (Asansol and Durgapur) covering an area of about 1603.17 km^2 (Fig. 18.1). The latitudinal and longitudinal extensions of this region are $23°22'20''N$ to $23°53'59''N$ and $86°46'25''E$ to $87°29'03''E$.

The climate of this region is characterized by high temperatures in summer (March–May), heavy rainfall in the monsoon season (July to mid-October), and dry winter (December–February). Maximum and minimum air temperatures during summer and winter periods are 44 °C and 5 °C, respectively.

Asansol Municipal Corporation and Durgapur Municipal Corporation are two ruled urban places inside the Asansol Durgapur Development Area (ADDA). ADDA is a chiefly developed industrial area in character for the most part because of the presence of coal mining and enormous industrial establishments. The all-out population of this area is increased from 2,552,781 in 2001 to 2,882,031 in the 2011 Census of India. The decadal development pace of the population is 12.90% somewhere in the range between 2001 and 2011 (https://censusindia.gov.in/). Over 77% of its all-out populace (2,400,000 people) live in an urban region. Strangely, around 88% urban populace of

the Paschim Bardhaman region dwells in ADDA according to the 2011 statistics.

Two major steel plants (Indian Iron and Steel Company and Steel Authority of India Limited) are excellent ventures around the ADDA region. Coal, iron, and steel are the primary sources of these endeavors. Besides the steel and coal, the locale houses other significant organizations like Durgapur Chemicals, Durgapur Thermal Power Station, Disergarh Power Supply, Damodar Valley Power Corporation, etc. The comprehensive incorporation of the metropolitan area and modern district has made the region potential for heat island influence.

18.3 Data and Methods

The ADDA area was outlined utilizing the guide gathered from the authority site of the Asansol Durgapur Development Authority. (https://ADDAonline.in/). For assessing land surface temperature (LST) and anthropogenic heat flux (AHF) from Landsat satellite imagery (1991–2019), which was downloaded from the USGS site (https://earthexplorer.usgs.gov/).

18.3.1 Methods of LST Computation from Landsat Images

Each item radiates warm electromagnetic energy as its temperature is over zero (K). Adhering to this rule, the LST of different objects was determined. For calculating land surface temperature from thermal image, step-by-step calculations are as follows:

The initial step is digital value (DN) convert to spectral radiance (Lsλ) with the help of Eq. (18.1) (USGS 2016) as follows:

$$Ls_\lambda = Ls_{\min \lambda} + \left[\frac{(Ls_{\max_\lambda} - Ls_{\min_\lambda})}{(Q_{CAL_{\max}} - Q_{CAL_{\min}})} \times Q_{CAL} \right] \tag{18.1}$$

where Lsλ is spectral reflectance (W m^{-2}sr^{-2}μm^{-2}), Ls$_{\max_\lambda}$ and Ls$_{\min_\lambda}$ is the maximum and minimum spectral radiances for the
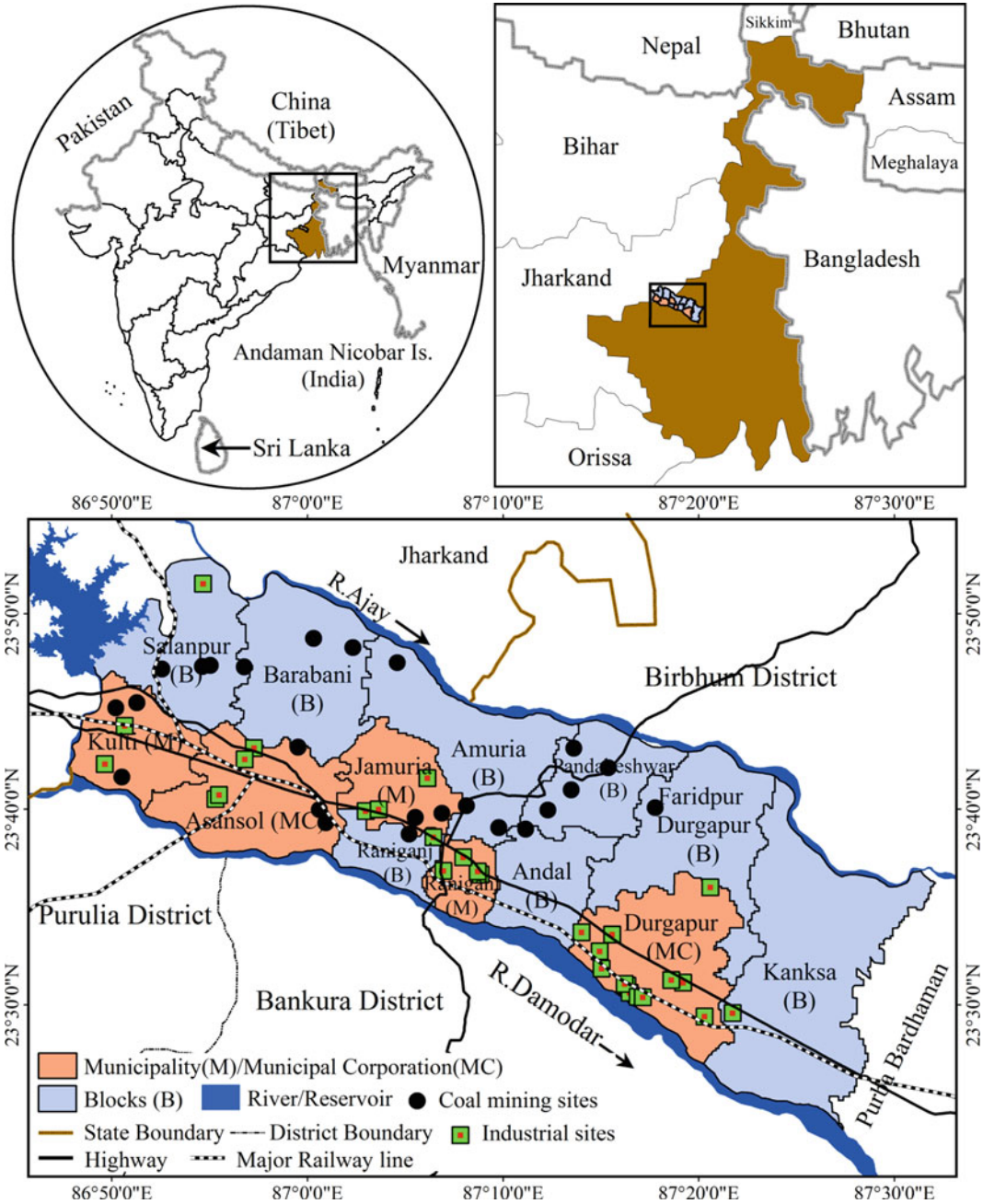
Fig. 18.1 Description of the Asansol Durgapur Development Area (ADDA)

thermal band, Q_{CAL} refers the digital number (DN) of each pixel. $Q_{CAL_{min}}$ denotes minimum DN value, and $Q_{CAL_{max}}$ is the maximum DN value of the concerned image.

Satellite brightness temperatures (SB_T) can be obtained from sensor-derived spectral reflectance using Eq. (18.2) (Artis and Carnahan 1982).

$$SB_T = \frac{C_2}{\ln\left(\frac{C_1}{Ls_\lambda} + 1\right)} \qquad (18.2)$$

where SB_T refers to at-satellite brightness temperature, Ls_λ is the spectral radiance of the thermal band (W m^{-2}sr^{-2}μm^{-2}), C_1 and C_2 are the calibrations constant in W m^{-2}sr^{-2}μm^{-2} (for Landsat-5 TM, $C_2 = 1260.56$, $C_1 = 607.76$ separately), and value of C_2 and C_1 gave in the metadata document.

Satellite brightness temperature corrected by land surface emissivity (ε) through the expression is given below in Eq. (18.3) (Snyder et al. 1998).

$$\varepsilon = 0.004 * P_{RO_V} + 0.986 \qquad (18.3)$$

where P_{RO_V} indicate as the proportion of vegetation, which can be determined with the assistance of Eq. (18.4).

$$P_{RO_V} = \left(\frac{NDVI_{jr} - NDVI_l}{NDVI_h + NDVI_l}\right)^2 \qquad (18.4)$$

where $NDVI_{jr}$ denotes NDVI score, $NDVI_h$ and $NDVI_l$ refer to maximum and minimum NDVI score.

Retrieval of LST utilizes the satellite brightness temperature and land surface emissivity. LST is figured through Eq. (18.5) (Artis and Carnahan 1982).

$$LS_T = \frac{SB_T}{[1 + \{(\lambda \times SB_T/\rho) \times \ln\varepsilon\}]} \qquad (18.5)$$

where LS_T denotes surface temperature (scale-kelvin), $\lambda =$ frequency of radiated radiance in meters (Markham and Barker 1985) is utilized, $\varepsilon =$ land surface emissivity, $\rho = h * c/\sigma(1.438 * 10^{-2} mK)$, $h =$ Planck's constant ($6.626*10^{-34}$ J K^{-1}), $\sigma =$ Boltzmann constant ($1.38 * 10^{-23}$J/k), and $c =$ speed of light ($2.998 * 10^8$ m/s)

The estimated LS_T by Eq. (18.5) is the Kelvin unit. So, converted LS_T from Kelvin to Celsius by the conversion relation is $0\,°C$ equals 273.15 K.

18.3.2 Accuracy Assessment of the LST Maps

It is very challenging to survey the precision level of the computed LST maps without having multi-point ground temperature information of the comparing time frame. Due to the absence of field LST for the period between 1991, 2000, and 2010 LST maps of those periods were not taken for accuracy assessment. Field measurements were done for the year 2019. The assessment of satellite gathered LST with that of ground-assessed values was done over comparable GPS areas using a thermal infrared thermometer. The air temperature was also measured from the same GPS locations. Pearson's correlation coefficient (r) was figured between computed LST and measured LST of the selected sites. The significance level of the same was also done for making an inference. It was assumed that if these LST maps represent actual temperature satisfactorily, the non-validated maps of the rest period could be treated as acceptable.

18.3.3 Methods of Anthropogenic Heat Estimation from Landsat Images

Heat fluxes are estimated over the entire study region for the summer months of 2000, 2010, and 2019. For assessing anthropogenic heat flux, different solar radiation parameters are should be taken into consideration (Fig. 18.2).

Nowadays, many researchers estimated heat flux spatially by using surface energy balance algorithms and also remote sensing data. For the natural land surface, the equation provided by the surface energy balance is expressed in Eq. (18.6).

$$
\begin{aligned}
Net radiation(R_n) = {} & Ground heat flux(G_{HF}) \\
& + Sensible heat flux(S_{HF}) \\
& + Latent heat flux(L_{HF})
\end{aligned}
$$
$$(18.6)$$

In the account of the urban region, the condition of surface energy balance was redressed by the
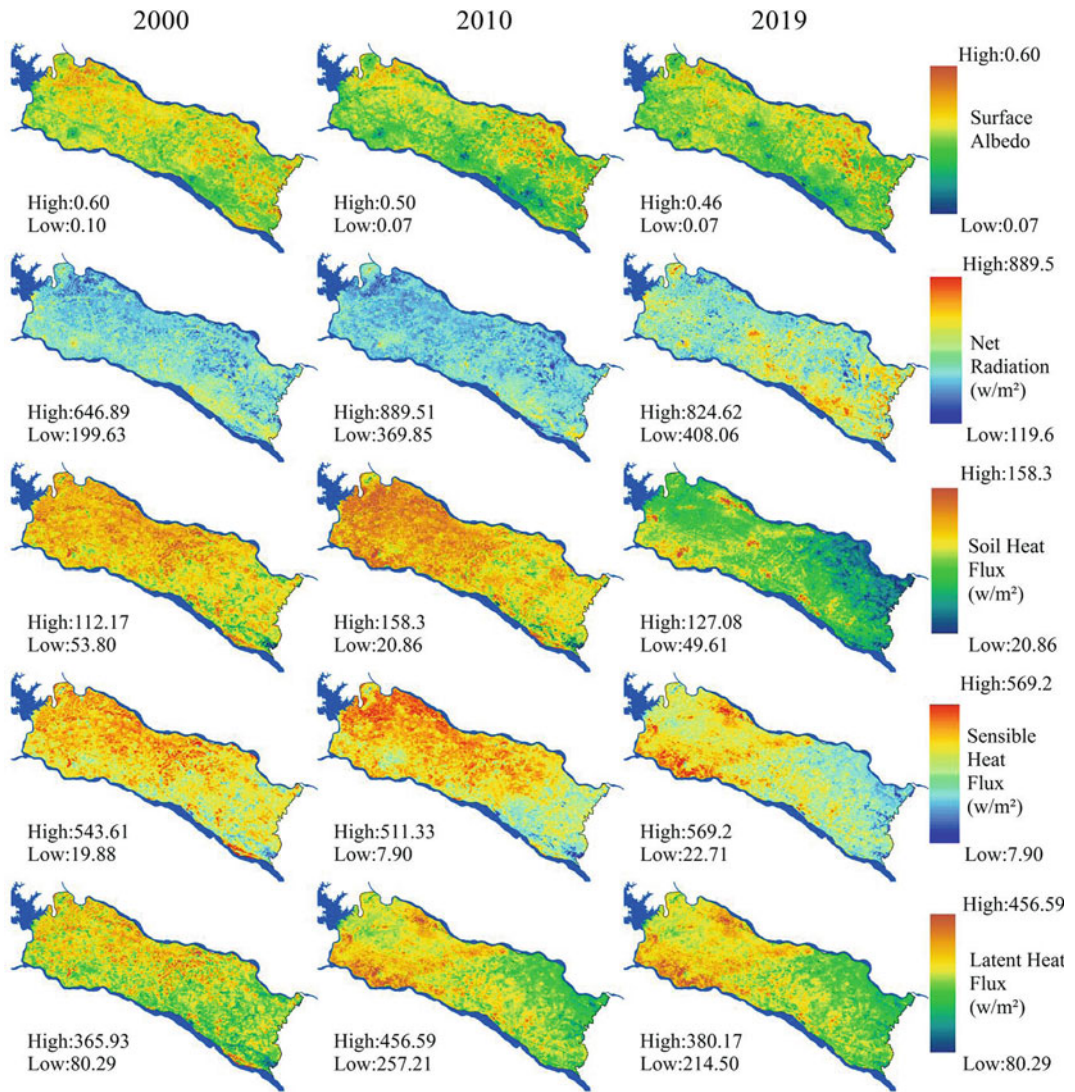
Fig. 18.2 Solar parameters used for computed Anthropogenic Heat Flux (AHF)

impact of anthropogenic heat. Therefore, the modified equation is expressed in Eq. (18.7) (Oke 1987).

$$\text{Netradiation}(R_n) + \text{Heatflux}(A_{HF}) = \text{Groundheatflux}(G_{HF})$$
$$+ \text{Sensibleheatflux}(S_{HF})$$
$$+ \text{Latentheatflux}(L_{HF})$$

$$(18.7)$$

Therefore, A_{HF} is the prime vector for enhancing the urban heat island (UHI) effect.

Net radiation (R_n) is the genuine radiant energy accessible at the surface. Net radiation is processed by using Eq. (18.8)

$$R_n = (1 - \alpha) \times R_s + \text{EaRl} - \varepsilon\sigma T_s^4 \qquad (18.8)$$

where R_s means incoming shortwave radiation (W/m²), α refers to surface albedo (dimensionless), which is trailed by Tasumi et al. (2008), Rl is the incoming longwave radiation (Watt/m²), Ea and ε is the air and surface emissivity

(dimensionless), σ is the Stefan Boltzmann constant, and T_s is the surface temperature.

The incoming shortwave radiation (R_s) is processed by Eq. (18.9).

$$R_s = G_{sc} \times \cos \theta \times d_r \times \tau_{at} \qquad (18.9)$$

where G_{sc} denotes solar constant (1367 W/m^2), $\cos \theta$ refers sun elevation angle, d_r is the inverse square relative distance between earth and sun and τ_{at} refers to air transmissivity.

The air transmissivity (τ_{at}) is determined as:

$$\tau_{at} = 0.75 + 2 \times 10^{-5} \times h \qquad (18.10)$$

where h refers to the height of an area

The incoming longwave radiation (Rl) is figured at every pixel involving the recipe as:

$$Rl = \sigma \times T_{air}^4 \qquad (18.11)$$

where σ is the Stefan Boltzmann constant and T_{air} refers to the air temperature.

Atmospheric emissivity (Ea) is computed from the following Eq. (18.12) as given by Brutsaert (1982).

$$Ea = 1.24 \left(\frac{VP_{air}}{T_{air}} \right)^{1/7} \qquad (18.12)$$

where VP$_{air}$ represents the vapor pressure of air in hPa.

Ground heat flux is connected with net radiation. Ground heat flux refers to the pace of energy sent by the soil per unit of time and area. Numerous researchers laid out relapses to estimate the ground heat transition of various surfaces. Ground heat flux is processed involving the condition as:

$$G_{HF} = C_g \times R_n \qquad (18.13)$$

where C_g denote the fixed coefficient, which is based on the different seasons and various types of surfaces. In this study, C_g values are assigned as referred by Kato and Yamaguchi (2005) for all surface types.

Sensible heat flux (S_{HF}) alludes to the pace of heat loss because of temperature inclinations which depend on the hypothesis of mass transport of heat and force between the surface and the near-surface climate (Chakraborty et al., 2015). The outflow of S_{HF} can be composed as

$$S_{HF} = \rho S_H \frac{T_1 - T_2}{r_a} \qquad (18.14)$$

where ρ is the air density, S_H is specific heat, $T_1 - T_2$ is the near-surface temperature difference (δT) which can be calculated following by Bastiaanssen et al. (1998), and r_a is the aerodynamics to heat flux which is calculated using Eq. (18.15) followed by Brutsaert (1982).

$$r_a = \frac{\left\{ \ln\left(z_{avg} - d_h \right) z_{rou} \right\}^2}{k^2 \times U_w} \qquad (18.15)$$

where z_{avg} addresses the height (average) of the tree, z_{rou} denotes surface roughness height, k is Von Karman constant, d_h refers to zero plane displacement height, and U_w denotes the speed of the wind.

The height at which zero wind speed is accomplished is signified as zero displacements (d_h). Here, d_h is inferred after Eq. (18.16)

$$d_h = \frac{2h}{3} \qquad (18.16)$$

where h refers to the obstacle's height

Surface roughness height (z_{rou}) is usually defined by a length scale called the length of the roughness. It is assessed as (Eq. 18.17):

$$z_{rou} = \frac{h}{8} \qquad (18.17)$$

An additional parameter of surface energy balance is latent heat flux (L_{HF}). The latent heat flux is determined by the articulation (Monteith and Unsworth 2013) given in Eq. (18.18).

$$L_{HF} = \rho S_H \frac{e_s - e_a}{\gamma(r_a + r_s)} \qquad (18.18)$$

where e_s is the saturation vapor pressure (hPa) at the surface temperature, γ the psychrometric constant (hPa/K), r_s is the stomatal resistance

(s/m) which relies upon the environmental circumstance, vegetation, and meteorological conditions

Radiant heat balance and anthropogenic heat discharge together to effect sensible heat flux, which is expressed as H_n. It is assessed through the articulation given in Eq. (18.19).

$$H_n = R_n - G_{HF} - L_{HF} \qquad (18.19)$$

The distinction between total sensible heat flux (S_{HF}) and H_n is known as anthropogenic heat flux (A_{HF}). Hence, the condition is:

$$A_{HF} = S_{HF} - H_n \qquad (18.20)$$

If S_{HF} is greater than or equivalent to H_n, we can use Eq. (18.20) to calculate A_{HF}; if not, then it is a substitute H_n.

18.3.4 Spatial Linkages Between LST and AHF

Earlier, it was stated that most of the previous studies that tried to compute anthropogenic heat flux from satellite image data did not yield identical results and therefore not comparable quantitatively. But the relative spatial pattern can be assessed between LST and AHF to assess whether such heat flux contributes anything to intensifying the heat island effect. The spatial correlation coefficient was computed between LST and image-specific AHF maps of the corresponding period. Statistically significant high correlation coefficient values could help to infer the influence of AHF on to heat island effect.

Apart from this, ordinary least square (OLS) regression Eq. (18.21) was conducted between AHF and LST to evaluate the spatial character of the influence of AHF on temperature. AHF was treated as the independent variable in this process. Relevant statistics like multiple R^2, and standard error were computed to justify the acceptability of the regression model.

$$\hat{\beta} = \left(x^T x\right)^{-1} x^T y \qquad (18.21)$$

where $\hat{\beta}$ ordinary least squares estimator, x matrix regressor variable x, T matrix transpose, y vector of the value of the responsive variable.

18.3.5 Assessing the Connection Between LULC and LST and AHF Maps

LULC maps were ready for the years 2000, 2010, and 2019. A supervised image classification technique with a maximum likelihood classification method was taken on for the image classification. For the precision evaluation of the classified image, overall accuracy and Kappa coefficient (K) (Eq. 18.22) were determined. For this reason, 100 reference sites were gathered from the field investigation utilizing GPS, and 900 sites were collected from the high-resolution Google Earth image.

$$k = \frac{N \sum_{i=1}^{r} Xii - \sum_{i=1}^{r}(Xi+ *Xi+i)}{N^2 - \sum_{i=1}^{r}(Xi+ *Xi+i)} \qquad (18.22)$$

where r = number of rows in the matrix; N = total number of pixels Xii = number of observations fin row i and column i; $Xi+$ and $X+i$ are the marginal totals for row i and column i.

18.4 Result and Analysis

18.4.1 Land Surface Temperature and Heat Island

Figure 18.3 depicts the spatial as well as temporal variation of land surface temperature for April, representing the summer season, and January, representing the winter season, of 1991, 2000, 2010, and 2019. In January 1991, the range of LST was 12.80 °C to 30.80 °C which was increased to 10.57–37.54 °C in January 2019. It does signify that in the last 28 years maximum limits of LST were enhanced significantly in some patches (Fig. 18.3). But when

mean LST was considered, the temperature increased from 18.49 °C to 19.15 °C. These statistics signify that only a very small proportion of the target area has encountered an exorbitantly high rise in temperature. Practically, it is conceivable predominantly because of the transformation of land use and land cover (LULC). If a water body turns into a concrete area, there is a high possibility to raise the temperature to >10 °C (Nimish et al. 2020). In April 1991, the recorded range of LST was 21.98–39.08 °C, but it was increased to 26.91–46.91°C in 2019 indicating both rising temperatures about upper and lower limits.

Figure 18.3 also depicts the phase-wise decadal pictures of LST in the summer and winter seasons for the last 28 years (from 1991 to 2019). This attempt was taken to provide a generalized view of LST change over the decades instead of year specific view. For this, average LST maps were prepared for three consecutive decades (1991–2000 as phase 1; phase 2 from 2001 to 2010, and year 2011 to 2019 considered as phase 3) and the entire period as a whole (1990–2019) taking yearly LST images of winter and summer seasons separately. During the summer season, Decadal change was remarkably high over the study region. From the 1st phase (1991–2000) to the 3rd phase (2001–19), mean LST increased from 31.34 °C to 35.20 °C. The annual increasing rate of LST in the summer season was 0.13 °C. In the winter season, the mean LST was increased from 18.53 °C to 22.91 °C between the 1st and 3rd phases. Municipal areas, industrial areas, and coal mining areas recorded maximum LST in all the years for both seasons. These areas can be treated as heat islands and hotspots. In the study area, since all the industrial areas, and mining areas are not located within the urban area, the heat island state was also identified even in the peripheral belt of the urban areas. Over the period, some
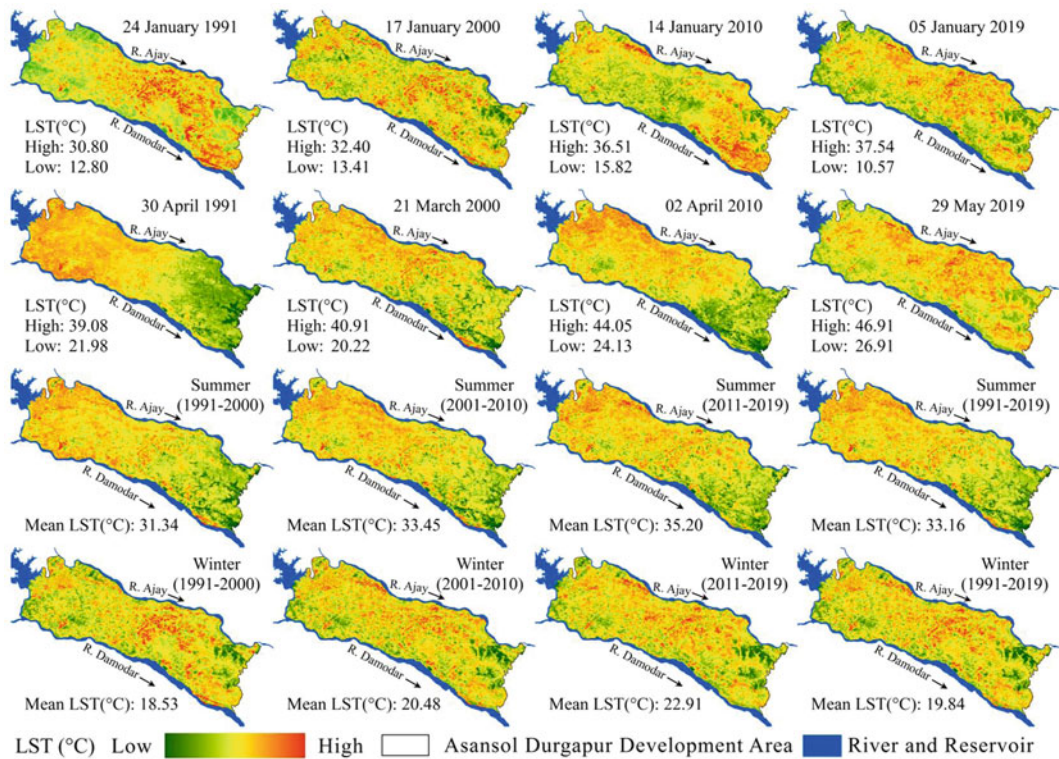

Fig. 18.3 Spatiotemporal variation of LST (°C) for Asansol Durgapur Development Area (ADDA)

new areas were identified as temperature hotspots
due to the establishment of new industries and
land use transformation. Figure 18.4 depicts the
dispersion of maximum, minimum, and average
LST in two thermally extreme seasons (summer
and winter). Dispersion of maximum temperature
was found much greater than the minimum, and
it was found greater in the summer season than in
winter. However, over the progress of time, the
dispersion remarkably increased in summer.
Table 18.1 provides detailed statistics of the
change of area under different temperature
intensity zones. For instance, in the ADDA
region, the total area that experienced LST >30°
C was 909.78 km^2 on 30 April 1991 and it was
increased to 1591.25 km^2 in 2019. In January,
the area under LST between 20°C and 25°C was
1.90 km^2 which was enhanced to 168.60 km^2.
The rising trend of areal extension under a high
range of temperature was also recorded in
municipal areas like Asansol municipal corpo-
ration (MC), Durgapur MC, Raniganj, Jamuria,
and Kulti municipalities.

Phase-wise decadal change of LST in sum-
mer and winter seasons also illustrates

encroachment of more area under higher tem-
perature intensity zones. For instance, in the
winter season, an area under a temperature
zone > 20 °C was 55.92 km^2 in the 1991–2000
decade and it was excessively increased to
1355.17 km^2 in phase 2011–19. This trend was
also found true in the case of municipal corpo-
rations and municipalities. In the summer sea-
son, an area under a temperature zone >30 °C
was 1461.70km^2 in phase 1(1991–2000) and it
was enhanced to 1554.75 km^2 in phase 2 (2001–
2010). In phase 3, this area under tempera-
ture > 30 °C was dramatically reduced to
815.06km^2 (Table 18.2). Relatively greater
rainfall in the summer months in these periods
was the major reason behind this. The amount of
rainfall in summer months for the years 2012,
2017, and 2018 were respectively 61.14, 55.67,
and 67.21 mm, which was higher than the
average amount of rainfall in summer months
(29.96 mm) from 1990 to 2017. This result
indicates that rising temperature effects not only
prevailed during the summer period of this
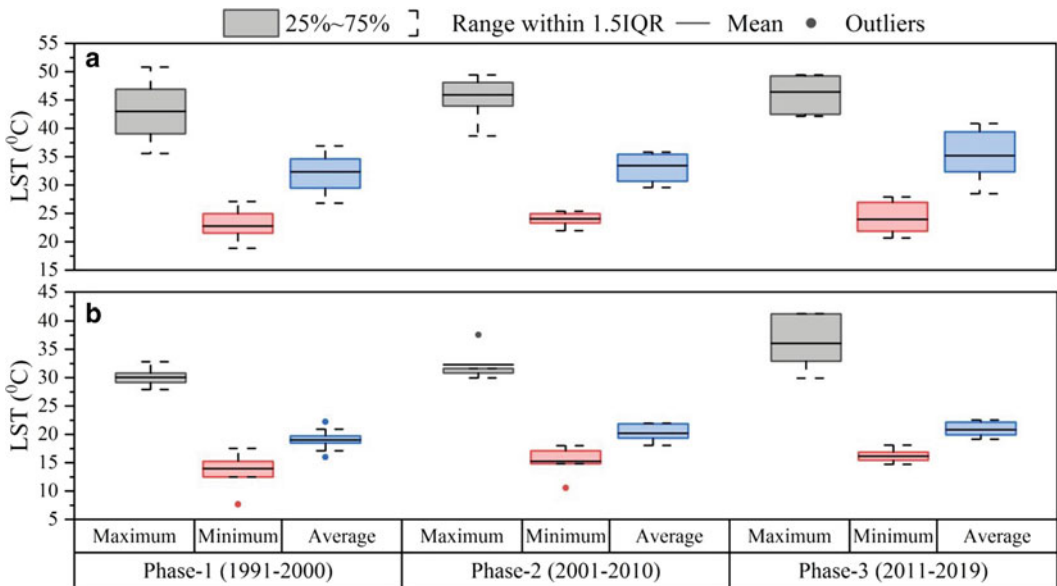region, but the winter season also witnessed the
same.

Fig. 18.4 Box plot showing variation of the land surface temperature (°C) in two thermally extreme seasons **a** summer season and **b** winter season

Table 18.1 Areal (km^2) coverage under different LST classes for the years 1991, 2000, 2010, and 2019 of both summer and winter months

Month	LST (°C)	ADDA Region	Asansol MC	Durgapur MC	Raniganj (M)	Jamuria (M)	Kulti (M)
30 April (1991)	< 25	76.67	0.96	41.23	0.55	0.19	6.10
	25–30	616.73	33.39	72.80	17.18	12.36	32.65
	>30	909.78	90.65	40.17	7.26	66.65	57.25
21 March (2000)	< 25	28.91	0.39	3.41	0.20	0.05	0.81
	25–30	344.73	17.89	66.54	9.56	8.59	11.92
	> 30	1229.53	106.72	84.25	15.23	70.56	83.27
02 April (2010)	< 25	3.13	0	0	0	0	0.09
	25–30	27.25	0.32	4.27	0.34	0.14	1.39
	> 30	1572.79	124.68	149.93	24.65	79.06	94.52
29 May (2019)	< 25	0.83	0	0	0	0	0
	25–30	11.09	0	0.85	0	0	0.11
	> 30	1591.25	125.00	153.35	24.99	79.20	95.89
24 January (1991)	< 20	1601.27	124.78	153.40	23.89	79.1	96
	20–25	1.90	0.22	0.80	1.10	0.10	0
	> 25	0	0	0	0	0	0
17 January (2000)	< 20	1460.93	121.20	136.88	22.67	76.06	89.55
	20–25	142.20	3.80	17.28	2.32	3.14	6.45
	> 25	0.04	0	0.04	0	0	0
14 January (2010)	< 20	1303.35	120.18	93.82	24.16	76.82	89.73
	20–25	299.19	4.81	60.20	0.83	2.38	6.26
	> 25	0.63	0.01	0.18	0	0	0.01
05 January (2019)	< 20	1262.42	75.75	65.15	19.83	59.75	82.70
	20–25	168.60	1.26	40.10	0.11	0.89	2.09
	> 25	172.15	47.99	48.95	5.05	18.56	11.21

18.4.2 Accuracy Assessment of the LST Maps

The correlation coefficient (r) value between computed and measured LST for 2019 (summer) was 0.87 which is statistically significant at a 0.01 level. Measured air temperature from the ground was also compared with the LST. In this connection, it is to be mentioned that the date of image acquisition and field LST and air temperature collection is not the same. The date of image acquisition was May 1, 2019, and field data collection was May 3, 2019. Since no major change in weather events like rainfall or Storm did not happen, data were taken for correlation.

The outcome shows that the R^2 value between measured air temperature and computed LST for 2019 (summer) was 0.79 with a 0.01 level of significance. Between air temperature and estimated LST, the difference was very clear. Based on this, the LST map of May 2019 (summer) could be treated as accepted.

18.4.3 Spatio-Temporal Distribution of Anthropogenic Heat Flux

The spatial distribution of AHF (w/m^2) was shown in Fig. 18.5 for the years 2000, 2010, and 2019. The

Table 18.2 Decadal-wise areal (km²) coverage of different LST classes for summer and winter seasons (Value within parenthesis indicate % of area)

Season	Phase	LST (°C)	ADDA area	Asansol MC	Durgapur MC	Raniganj (M)	Jamuria (M)	Kulti (M)
Summer	1991–2000	< 25	7.72 (0.48)	0	0.24 (0.02	0	0	0
		25–30	133.75 (8.34)	1.93 (0.12)	26.78 (1.67)	1.41 (0.09)	1.22 (0.08)	2.33 (0.16)
		> 30	1461.7 (91.18)	123.06 (7.68)	127.18 (7.93)	23.58 (1.47)	77.98 (4.86)	93.66 (5.84)
	2001–2010	< 25	5.6 (0.35)	0	0	0	0	0
		25–30	42.83 (2.67)	0.63 (0.04)	8.56 (0.53)	0.3 (0.02)	0.21 (0.01)	0.88 (0.05)
		> 30	1554.75 (96.98)	124.37 (7.76)	145.64 (9.09)	24.69 (1.54)	78.99 (4.93)	95.12 (5.93)
	2011–2019	< 25	11.15 (0.70)	0	0.86 (0.05)	0.05 (0)	0	0.02 (0)
		25–30	776.96 (48.46_	0.12 (0.01)	120.06 (7.49)	0.17 (0.01)	0.17 (0.01)	0.65 (0.04)
		> 30	815.06 (50.84)	124.87 (7.79)	33.28 (2.08)	24.77 (1.55)	79.03 (4.93)	95.33 (5.95)
	1990–2019	< 25	5.15 (0.32)	0	2.17 (0.14)	0.02 (0)	0	0
		25–30	655.42 (40.88)	1.11 (0.07)	100 (6.24)	0.35 (0.02)	1.02 (0.06)	14.1 (0.88)
		> 30	942.6 (58.80)	123.89 (7.73)	52.03 (3.25)	24.62 (1.54)	78.18 (4.88)	81.9 (5.11)
Winter	1991–2000	< 20	1547.25 (96.51)	123.05 (7.68)	146.24 (9.12)	24.67 (1.54)	78.4 (4.89)	95.14 (5.94)
		20–25	55.92 (3.49)	1.95 (0.12)	7.96 (0.50)	0.32 (0.02)	0.8 (0.05)	0.86 (0.05)
		> 25	0	0	0	0	0	0
	2001–2010	< 20	602.66 (37.59)	59.37 (3.70)	60.9 (3.80)	15.44 (0.96)	19.35 (1.21)	50.78 (3.17)
		20–25	1000.32 (62.40)	65.6 (4.09)	93.19 (5.81)	9.55 (0.60)	59.85 (3.73)	45.2 (2.82)
		> 25	0.19 (0.01)	0.02 (0)	0.12 (0.01)	0	0	0.03 (0)
	2011–2019	< 20	248 (15.47)	19.56 (1.22)	22.24 (1.39)	3.34 (0.21)	4.55 (0.28)	24.04 (1.50)
		20–25	1353.92 (84.45)	105.37 (6.57)	131.87 (8.23)	21.64 (1.35)	74.61 (4.65)	71.89 (4.48)
		> 25	1.25 (0.08)	0.06 (0)	0.08 (0.01)	0.01 (0)	0.04 (0)	0.07 (0)
	1990–2019	< 20	815.24 (50.85)	41.79 (2.61)	67.25 (4.20)	11.79 (0.74)	22.89 (1.43)	31.85 (1.99)
		20–25	787.32 (49.11)	83.17 (5.19)	86.9 (5.42)	13.19 (0.82)	56.29 (3.51)	64.1 (4)
		> 25	0.61 (0.04)	0.03 (0)	0.05 (0)	0.01 (0)	0.02 (0)	0.05 (0)

result shows that a high value of heat flux over urban and mining areas was observed. A considerable amount of heat is released for the activities from the mining areas, commercial areas, and urban areas causing an emphatically high amount of energy footprint. It is considerably low in dense vegetation and water cover areas. In the current study, the high value of anthropogenic heat flux (569.22 w/m^2) was estimated in 2019, while 2000 and 2010 were recorded as 357.58 and 436.65 w/m^2, respectively. However, high AHF was found in a very small patch of the mining area. Mean AHF was 39.59 W/m^2 in 2000, and it increased to 98.86 w/m^2 in 2019. Both Asansol and Durgapur municipal corporation areas and mining areas registered to grow anthropogenic heat flux (Fig. 18.5). Mining and heavy industrial unit-dominated areas among other urban morphological units were found highly susceptible to rising AHF.

Areal coverage under different anthropogenic heat flux classes for the years 2000, 2010, and 2019 was represented in Table 18.3. AHF was classified into three categories (100, 100–200, and > 200 W/m^2) and the area under each sub-class was computed in all the selected years. Over the progress of time, the wider area experienced higher AHF. For example, in the year 2000, the area under AHF > 200 W/m^2 was 0.41, which was increased to 10.89 km^2 in 2019 in ADDA. An almost similar picture was sketched in different urban centers under Asansol Durgapur Development Area (Table 18.3).

18.4.4 Accuracy of the Anthropogenic Heat Flux with the Help of Previous Literature

For the accuracy assessment of the estimated anthropogenic heat flux previous works of literature was taken as reference. Here, in situ heat flux data were not available; therefore, this approach was quite good.

Table 18.4 represented the ratio of different solar parameters of this study and previous studies for the validation of the AHF model. The *H/Rn* ratio of this study was 0.51, 0.36, and 0.29 in 2000, 2010, and 2019, respectively. These values were almost similar to reference studies like Christen and Vogt (2004), Moriwaki et al. (2006), and Zhang et al. (2013). Then again, the *G/Rn* ratio was 0.18 in 2000, which was very like the estimated value by Moriwaki et al. (2006), and Ziaul and Pal (2018b) in their investigation. In the case of the *LE/Rn* ratio, similarities were found between the present study and the previous studies by Zhang et al. (2013), Moriwaki et al. (2006), and Ziaul and Pal (2018b). The same result could not be found since the emission strength is not similar in all the regions. Despite a few departures of results from the predecessors, as in most of the cases, almost identical results were found; hence, AHF models from image data could be treated as representative.
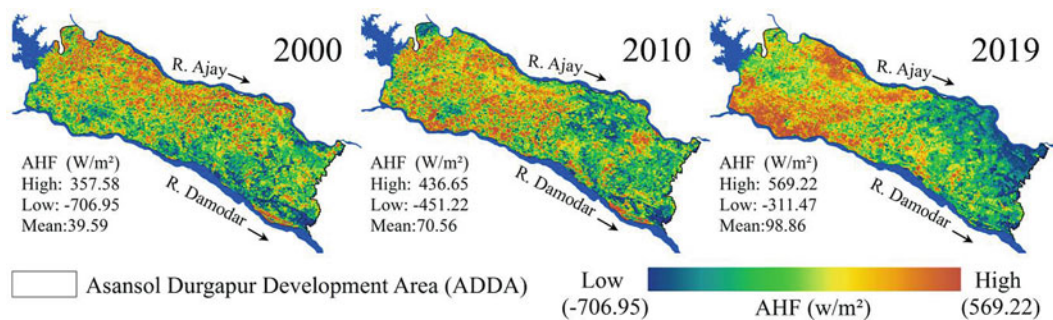

Fig. 18.5 Spatial variation of AHF (W/m^2) for the years 2000, 2010, and 2019

Table 18.3 Areal coverage (km²) under different AHF classes for the respective years (Value within parenthesis indicates % of area)

Year	2000			2010			2019		
AHF (W/m²)	< 100	100–200	> 200	< 100	100–200	> 200	< 100	100–200	> 200
ADDA area	1601.53 (99.90)	1.22 (0.08)	0.41 (0.03)	1580.08 (98.56)	18.69 (1.17)	4.4 (0.27)	1359.86 (84.82)	232.42 (14.50)	10.89 (0.68)
Asansol MC	124.48 (7.76)	0.37 (0.02)	0.16 (0.01)	119.81 (7.47)	4.07 (0.25)	1.13 (0.07)	116.88 (7.29)	8.05 (0.50)	0.07 (0.004)
Durgapur MC	154.19 (9.62)	0.01 (0.001)	0	150.48 (9.39)	2.73 (0.17)	0.99 (0.06)	146.72 (9.15)	6.98 (0.44)	0.5 (0.03)
Raniganj (M)	24.99 (1.56)	0	0	24.61 (1.54)	0.39 (0.02)	0	23.75 (1.48)	1.23 (0.08)	0.01 (0.001)
Jamuria (M)	79.19 (4.94)	0.01 (0.001)	0	78.33 (4.89)	0.87 (0.05)	0	65.78 (4.10)	13.23 (0.83)	0.19 (0.01)
Kulti (M)	95.98 (5.99)	0.02 (0.001)	0	95.12 (5.93)	0.82 (0.05)	0.06 (0.004)	86.37 (5.39)	9.54 (0.60)	0.09 (0.01)

Table 18.4 Ratio of heat flux to the net radiation of the current examination and estimated already

Original reference	Land use	Observation period	H/Rn	LE/Rn	G/Rn
Present study	Dominated by urban area	March, 2000	0.51	0.34	0.18
		April, 2010	0.36	0.42	0.17
		May, 2019	0.29	0.38	0.13
Ziaul and Pal (2018b)	Urban	April, 1990	0.37	0.29	0.17
	Urban	April, 2010	0.42	0.4	0.28
	Urban	April, 2017	0.53	0.51	0.34
Zhang et al. (2013)	Fuzhou, China (Landuse: Urban)	March, 2001	0.53	0.04	0.57
Kato et al. (2007)	Nagoya, Japan (Landuse: Urban)	July, 2000 (Summer)	0.2	0	0.8
Moriwaki et al. (2006)	Tokyo, Japan (Landuse:Urban)	July, 2001 (Summer)	0.49	0.28	0.26
Grimmond et al. (2004)	Marseille, France (Landuse: Urban)	June–July, 2001 (Summer)	0.69	0.17	0.27
Christen and Vogt (2004)	Basel, Switzerland (Landuse: Urban)	June–July, 2002 (Summer)	0.48	0.18	0.38

18.4.5 Spatial Linkages Between LST and AHF

Spatial correlation between LST and Landsat image-based AHF in 2000, 2010, and 2019 years were, respectively, 0.56, 0.64, and 0.77 with a significance level of < 0.01. Increasing correlation value over time signifies growing adjacency as well as the contribution of AHF to LST. When the relationship was generated for an individual urban area, a significant relation was found. For instance, these were 0.62 and 0.57, respectively, in the case of Asansol and Durgapur municipal corporations. Based on this, it can be stated that there was a spatial adjacency between the AHF hotspot and the location of the heat island. So, it can be stated that although the share of AHF to LST was not estimated; however, AHF

increasingly contributed heat to intensifying heat islands.

Figure 18.6 depicts the spatial pattern of OLS between AHF and LST signifying how far AHF and LST were related. In 2000, 58.40% area was identified within an urbanized and mining-dominated landscape where OLS residual was very low (0.5–−0.5) (Table 18.5). The almost normal distribution curve and residual plot also reflected the same. Over the period, increasing heterogeneity in land use composition was caused for slackening down the strangeness of control. More area was identified within 0.5–1.5 standard regression residual (Fig. 18.6) signifying underfitting of relation.

18.4.6 Association of Different LULCs with LST and AHF

Six leading LULC classes were generated from the supervised image of the year 2019. The ultimate classified image provides the major LULC features of the ADDA region (Fig. 18.7). The areal statistics of the major LULC features of the ADDA region show that the settlement area was the leading LULC feature in the ADDA region covering 34.15% of the total area while agricultural area, vegetation area, dense vegetation area, mining area, and waterbody covered respectively 30.76%, 10.63%, 9.11%, 8.83%, and 2.75% of total ADDA region. Open-cast mining areas were increased in the ADDA region (Singh and Ghosh 2021; Dey et al. 2019). It has been a significant impact on the LST (Dey et al. 2019). Two municipal corporations and three municipalities were found mostly in the dominant urbanized areas of the ADDA region. Time series change of LULC areas revealed that built area (settlement), and mining areas were increased over time. On the other hand, green and blue spaces were degraded (Fig. 18.7).

The validation of the classified images was assessed based on data of the field survey (100
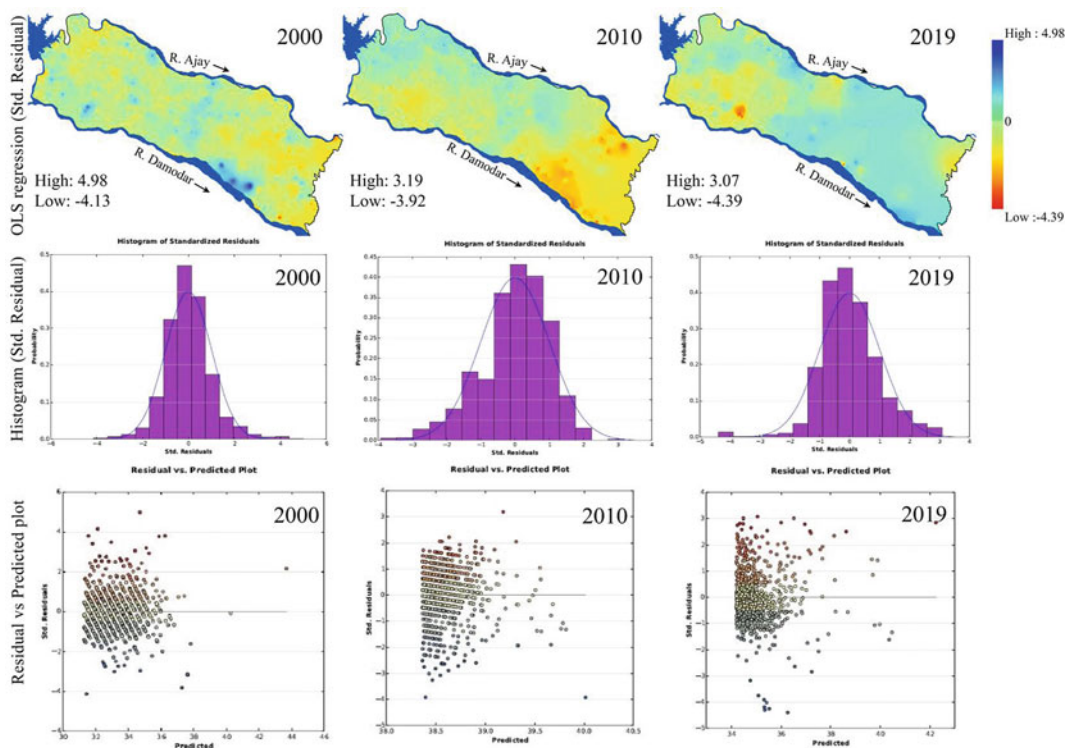
Fig. 18.6 OLS result between AHF and LST for the years 2000, 2010, and 2019

Table 18.5 Areal inclusion of standard regression residual zones of AHF and LST

Standard residual regression zone	2000		2010		2019	
	Area in km²	% of the area to total area	Area in km²	% of the area to total area	Area in km²	% of the area to total area
< −2.5 Std. Dev	1.9	0.12	5.03	0.31	4.29	0.27
−2.5–−1.5 Std. Dev	14.05	0.88	159.99	9.98	5.92	0.37
−1.5–−0.5 Std. Dev	336.43	20.99	397.92	24.82	125.11	7.8
−0.5–0.5 Std. Dev	936.22	58.4	588.32	36.7	448.07	27.95
0.5–1.5 Std. Dev	247.37	15.43	443.52	27.67	731.24	45.61
1.5–2.5 Std. Dev	49.26	3.07	8.3	0.52	285.48	17.81
>2.5 Std. Dev	17.93	1.12	0.1	0.01	3.07	0.19
Total	1603.17	100	1603.17	100	1603.17	100
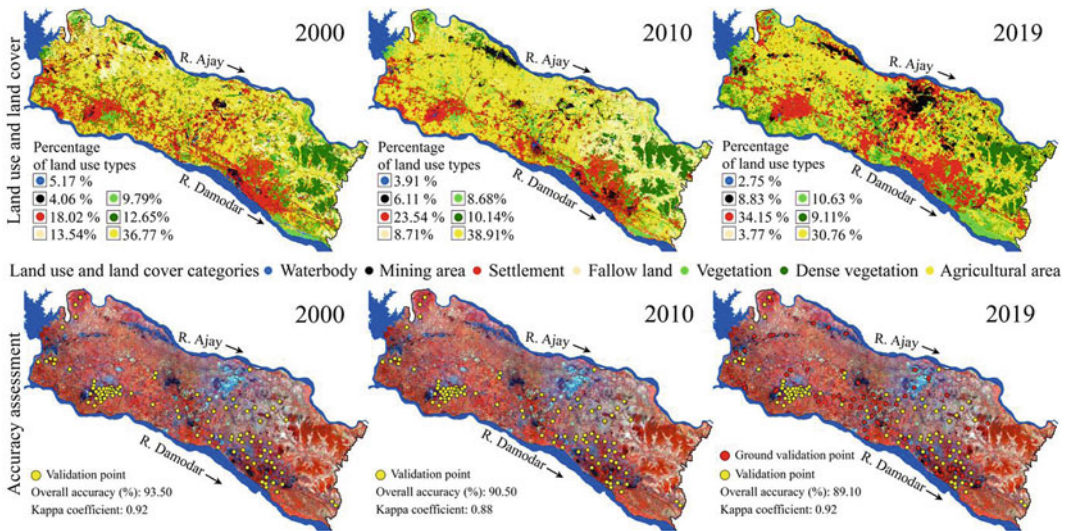
Fig. 18.7 Different land use/land cover types of the ADDA region for the year 2000, 2010, and 2019 and validation points used for accuracy assessment (in LULC maps, values against the legend indicates the percentage of area under each class)

points in the case of the year 2019) and Google Earth image (900 points) (Fig. 18.7). The overall accuracy of the classified image was between 89 and 93.5%, and the Kappa coefficient (K) was 0.88–0.92 (Fig. 18.7). Therefore, it tends to be expressed that there was an excellent agreement between ground reality and the classified image in every one of the chosen years.

Land surface temperature and heat flux results fluctuate from different LULC classes. Hence, the computation was done for five leading LULC classes. Various LULC classes with their mean AHF (W/m²) and mean LST (°C) are shown in Table 18.6.

Figure 18.8 illustrates different LULC classes and their mean AHF and LST value for the year 2019. The results show that in the mining area mean AHF and LST were recorded at 174.36 (W/m²) and 44 °C. Mean AHF was 117.77 (W/m²) in the built area and mean LST was recorded at 39 °C. Both less LST and negative AHF were found over the water body area. Due to the heterogeneous surface of the ADDA region, the overall mean value of AHF in the year 2019 was 98.86 W/m².

Table 18.6 Calculate mean AHF (W/m^2) and mean LST (°C) over the leading five LULC types in the year 2019

Land use and land cover types	Mean AHF (W/m^2)	Mean LST (°C)
Waterbody	−30.75	27
Mining area	174.36	44
Settlement	117.77	39
Vegetation	61.95	31
Agricultural area	72.12	33.7

Fig. 18.8 Mean AHF (W/m^2) and Mean LST (°C) over different LULC classes in the year 2019
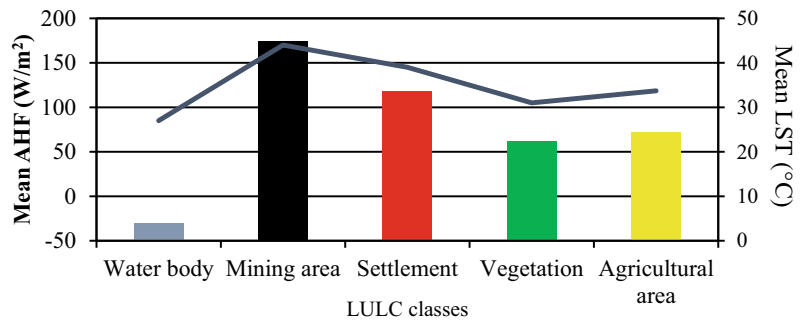
18.4.7 Minimizing Heat Island Effect

Among several other approaches to heat island effect minimization, management of green and blue space in the urban area is a nature-based solution. Population control, developing smaller towns, checking on energy footprint, etc., are some good steps toward this. However, there is a such initiative in this regard. Existing urban areas have been inflating over time instead of the formation of new urban spaces, especially in a country like India (Dutta et al. 2020). There is no such initiative regarding checking energy footprint. In this backdrop, land use/land cover engineering may be a good approach for minimizing the temperature effect. Green and blue space management, and the development of green and blue infrastructures can to some extent minimize such climate change effects (Xue et al. 2019; Sharifi 2020). To prove this distance, respective temperature profiling from different types of blue and green spaces was done. Similarly, to know how canopy density and thickness of water (water depth) can control LST were also analyzed.

18.4.7.1 Effect of Blue and Green Space Proximity on Temperature

Temperature away from both green and blue spaces of different kinds depicted that irrespective of types of green and blue space, the temperature at very proximity was found low and increased gradually away from this (Table 18.7). The degree of increase varied among green/blue space types. For instance, the temperature at the centroid of dense vegetation was 29.67 °C which is almost 3 °C greater at 500 m away from this. Pal and Ziaul (2017), Xue et al. (2019), and Ziaul and Pal (2020) also reported a similar trend of temperature change in their studies. From these statistics, it was further resolved, the size, nature of vegetation, water depth, and shape of blue and green space are also crucial for determining the temperature change. Large size, higher canopy density, and non-elongated shape have a greater impact on minimizing the temperature.

NDVI value indicates canopy density and with the change of this temperature varies (Prohmdirek et al. 2020). A similar result was reported in this present study. With the increase

Table 18.7 Change of temperature away from different types of blue and green space (temperature in °C)

Green/blue space types	At the centroid	At the fringe	At 100 m away from fringe	At 300 m away from fringe	At 500 m away from fringe	At 1000 m away from fringe
Dense vegetation	29.67	30.81	31.53	33.23	33.3	35.56
Sparse vegetation	30.03	31.58	32.59	32.71	34.25	33.75
Linear vegetation	31.15	32.72	34.43	35.23	37.1	36.21
Ecological park	28.95	31.29	33.65	35.13	36.58	34.89
Play ground	31.98	32.12	33.65	34.65	34	33.83
Agriculture field	33.16	35.63	32.65	34.45	35.61	36.68
River	28.3	29.1	29.73	31.13	31.45	34.85
Reservoir	21.95	23.8	24.44	26.63	25.44	25.83
Ponds	26.4	27.55	27.61	31.1	33.28	33

Table 18.8 Relationship between NDVI and LST and NDWI and LST

Parameter	Classes	YC = a + bx	R^2	P-value	r
NDVI versus LST	Low canopy density (0–0.15)	$-7.161x + 33.67$	0.014	< 0.001	−0.12
	Moderate canopy density (0.15–0.25)	$-21.45x + 36.08$	0.112	< 0.001	−0.34
	High canopy density (>0.25)	$-10.44x + 33.48$	0.042	< 0.001	−0.21
NDWI versus LST	Low water depth (<0.05)	$-35.17x + 33.34$	0.025	< 0.001	−0.16
	Higher water depth (>0.05)	$-76.81x + 35.11$	0.544	< 0.001	−0.74

of NDVI value, temperature decreases signifying the fact that quality vegetation can minimize temperature strongly. The linear regression between NDVI and LST exhibited that NDVI negatively controls LST; however, its degree was less in the case of the vegetation with low canopy density. The same was true in the case of depth of water (Table 18.8).

Considering the result of the present study and previous works of literature, it can be stated that conservation and creation of blue and green spaces are good alternatives for minimizing the temperature effect (Xue et al. 2019; Yu et al. 2020). Management of green and blue space can also reduce other air pollutants that are also noxious to human well-being and improve the ecosystem goods and services for making a

resilient urban ecosystem (Mavoa et al. 2019; Cameron et al. 2020; de Macedo et al. 2021).

18.5 Discussion

Results showed that the intensity of the surface heat was expanded and the areal spread was likewise multiplied. The sprawl of urban areas, intensification, and expansion of mining and industrial area are the major reason behind this in this area. This result is concomitant with previously declared results by many internationally reputed researchers like Henits et al. (2017), Mohajerani et al. (2017), Mushore et al. (2017), Firozjaei et al. (2018). The rate of change was not found as high as reported by other scholars

despite the highly industrialized and urbanized nature of the present study areas. For instance, Arekhi (2018) reported that LST was increased by 9 °C in 30 years, and Hereher (2017) exhibited a 1 °C increment of land surface temperature in 11 years. In the present study area, the rate of mean temperature rise was almost confined to 3.5 °C for the summer and winter seasons for 28 years. Land use transformation specifically, the spread of built-up area was found to be the major reason behind this. Peng et al. (2018a, b), Qiao et al. (2020), Mahato and Pal (2021) also condemned that the proliferation of built area, an increase of concrete materials, loss of forest, and water bodies are the major reasons behind temperature rise in the urban and rural area. In the region where industrial and urban growth was not in a full-fledged state, a high change of temperature is very much evident in those regions. Some places were identified where the urban area was transformed into urban land or rural scape was transformed into industrial land, those patches were witnessed a 5–6 °C rise in temperature which is very much accordant with the result of the growing urban areas (Sejati et al. 2019).

Anthropogenic heat sources and energy footprint in the ADDA region were found high and it was in an increasing trend over the advance of time but the rate of change was high in the last 28 years since the history of AHF was increased sufficiently well before the study period when the process of urbanization and industrialization had started. Nonetheless, according to the census report between 2001 and 2011, the number of inhabitants in this region was increased from 2,552,781 to 2,882,031. The increase of building space (horizontal or vertical rise of the building), vehicle density, transport infrastructure, and enhancement of industrial production directly or indirectly influenced the energy footprint of the study unit. Although, no quantitative data on energy footprint was cited, however, an increase in population density and meeting their needs, and increasing energy consumption are very evident not only in this area but beyond (Mohsin et al. 2019). The increasing population also causes growing heat flux from metabolism. The increasing contribution of AHF over time is very obvious from different internationally reputed studies conducted by Zhang et al. (2013), Yang et al. (2014), Ogunjobi et al. (2018), and Ayanlade and Howard (2019). They also clearly reported that urban, industrial, and mining areas are the major sources of AHF. In the present study, Landsat image-based AHF was computed with the quite varying result as also found in some works conducted by Zhang et al. (2013), Ziaul and Pal (2018a, b), Chen et al. (2019), Yu et al. (2018a, b), Ayanlade and Howard (2019). So, the further scope is there to upheave the accuracy of this work.

The relationship between AHF and LST clarifies the fact that AHF plays an understandable part in expanding heat island power in urban regions. Here, the share of AHF to temperature was not computed. But computation may provide the degree of its share. Within the study area, mining, industrial, and highly urbanized patches recorded the highest AHF and high spatial proximity between temperature and AHF. It does indirectly signify that the relative share of AHF is high in these areas due to energy-intensive anthropogenic activities. One question may be raised regarding making a linkage between LST and AHF since AHF directly influx into the atmosphere, it does not affect LST. However, it is also true that Peng et al. (2018a, b) established a positive relation between LST and air temperature. High temperature and AHF in an area can create discomfort situations which are very essential concerning the mental and physical health of the people living there.

The study further revealed that green and blue spaces can minimize the urban heat island effect (Ziaul and Pal 2020; Liu et al. 2021). Within 500 m distance from the blue and green spaces, temperature may reduce up to 2.5 °C. Yu et al. (2018a, b) also reported the same trend. Apart from this, so many other valuable services they can tender. Chiefly four kinds of services they can offer (1) provisioning (2), regulating, (3) habitat, and (4) culture. All these are inclusively linked with human likelihood, health, and well-being. Shah et al. (2021) directed a decent survey on urban environment ecosystem services
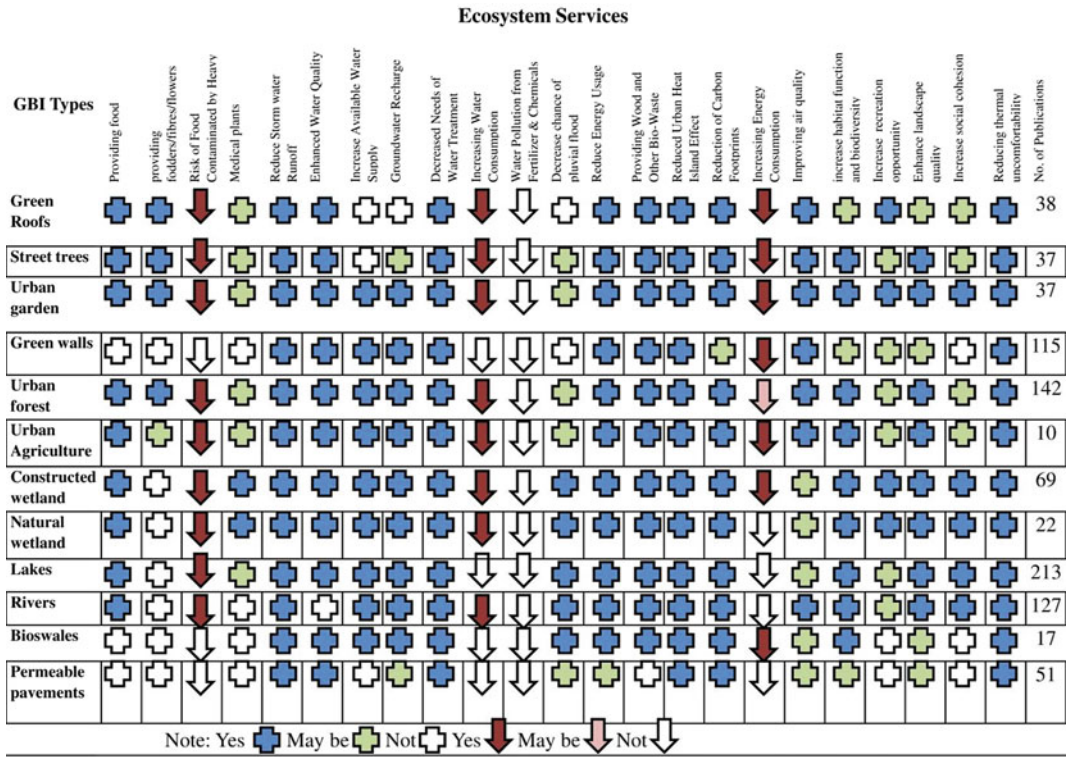
Fig. 18.9 Different forms of services and dis-services from green and blue infrastructures based on literature and field experiences. Values within parenthesis in each column indicate the number of the literature surveyed, reports of literature were taken from Shah et al. (2021) in most of the cases

(positive) and dis-services (negative) of various green and blue space types from the perspective of food, energy, and water nexus. They reported that these can enhance ecosystem urban sustainability and resilience. Some developed countries executed their green and blue infrastructures (GBIs) to reduce surface runoff (Brazil, Netherland, USA), the urban heat effects (Germany, Australia), food production (Singapore), and carbon storage (South Africa) (Astee and Kishnani 2010). Table 9 presented a connection between GBI typology and ecosystem services received. It was presented following Shah et al. (2021) with some modifications. Discomfortability caused by AHF can be reduced by enhancing green and blue spaces. Accessibility to these services can encourage people to bear even some inconvenience caused due to the greater energy footprint effect. Increasing and maintaining green and blue space into fallow public land,

street side, railway corridor, park, playground, the courtyard of academic and administrative institutions, even household, and rooftops are highly necessary in this regard (Fig. 18.9).

18.6   Conclusion

The present study deliberately highlighted the increasing trend of heat island intensity and its spatial spread although its rate was not sufficiently high as usually found in the newly growing urban areas. High-temperature zone was identified as hot spots in urban areas, mining areas, and industrial areas. AHF was also in a rising trend in the urban and industrial areas showing spatial adjacency with heat island areas. This spatial association signified that AHF has a discernible role to enhance the heat island effect. Mining, industrial, and built areas were the major

sources of AHF. People have no such control over incoming solar radiation, but people can mediate the temperature and AHF effect to some extent. To combat this situation, the emission of heat should be restricted. Partial restriction on a personal car, encouraging people to use public transport facilities, economic demand, and application of energy-efficient advanced technology both in transport and industrial sectors are some fruitful steps on this. Land use/land cover management is a good alternative as mentioned. Increasing green and blue space, and developing such infrastructures can minimize the heat island effect, control pollution levels, provide priceless goods and services and help to build a resilient urban ecosystem. Since the space crisis is a real problem, small-scale initiatives, street-side greening, encouraging peri-urban agriculture, and water bodies are very necessary for this initiative.

Since the issue of temperature rise is exceptionally connected with human physiology and psychology in a specific and urban environment, as a rule, the review figured out the spatial pattern of temperature, AHF, and their degree of association, this work could support adopting appropriate steps to mediate heat effect. The study also highlighted the mediating role of green and blue space. So, while making a plan for this, the planner can adopt this proven way where possible. Linking AHF and temperature is a novel approach, however, research is further needed for quantifying the share of AHF to temperature. Moreover, AHF was computed only for three specific years. Since the study tried to link between LST and AHF, it would be better to compute decadal average AHF for greater credibility. This study recommends adopting such an approach for making the nature of relation more prominent and universal.

References

Aithal BH, Chandan MC (2019) Assessing land surface temperature and land use change through spatio-temporal analysis: a case study of select major cities of India. Arabian J Geosci 12(11):1–16

Arekhi M (2018) Investigating land surface temperature (LST) change using the LST change detection technique (Gomishan District, Iran). In: Conference of the Arabian journal of geosciences. Springer, Cham, pp 135–139

Artis DA, Carnahan WH (1982) Survey of emissivity variability in thermography of urban areas. Remote Sens Environ 12(4):313–329

Astee LY, Kishnani NT (2010) Building integrated agriculture: utilising rooftops for sustainable food crop cultivation in Singapore. J Green Build 5(2):105–113

Ayanlade A, Howard MT (2019) Land surface temperature and heat fluxes over three cities in Niger Delta. J Afr Earth Sc 151:54–66

Bastiaanssen WG, Menenti M, Feddes RA, Holtslag AAM (1998) A remote sensing surface energy balance algorithm for land (SEBAL). 1 Formulation. J Hydrol 212:198–212

Brutsaert W (1982) Evaporation into the atmosphere: theory. History Appl 1

Cameron RW, Brindley P, Mears M, McEwan K, Ferguson F, Sheffield D, Richardson M et al (2020) Where the wild things are! Do urban green spaces with greater avian biodiversity promote more positive emotions in humans? Urban Ecosystems 23(2):301–317

Chakraborty SD, Kant Y, Mitra D (2015) Assessment of land surface temperature and heat fluxes over Delhi using remote sensing data. J Environ Manage 148:143–152

Christen A, Vogt R (2004) Energy and radiation balance of a central European city. Int J Clim: J Royal Meteorol Soc 24(11):1395–1421

Colding J, Barthel S (2017) An urban ecology critique on the "Smart City" model. J Clean Prod 164:95–101

de Macedo LSV, Picavet MEB, de Oliveira JAP, Shih WY (2021) Urban green and blue infrastructure: a critical analysis of research on developing countries. J Clean Prod 313:127898

Dey D, Salui CL, Biswas B (2022) Impact assessment of open cast mining activity in ADDA region, Paschim Barddhaman on land surface temperature. In: Geospatial technology for environmental hazards. Springer, Cham, pp 63–74

Dhar RB, Chakraborty S, Chattopadhyay R, Sikdar PK (2019) Impact of land-use/land-cover change on land surface temperature using satellite data: a case study of Rajarhat Block, North 24-Parganas District, West Bengal. J Indian Soc Remote Sens 47(2):331–348

Dissanayake DMSLB, Morimoto T, Ranagalage M, Murayama Y (2019) Land-use/land-cover changes

and their impact on surface urban heat islands: Case study of Kandy City Sri Lanka. Climate 7(8):99

Dutta D, Rahman A, Paul SK, Kundu A (2020) Estimating urban growth in peri-urban areas and its interrelationships with built-up density using earth observation datasets. Ann Reg Sci 65(1):67–82

Firozjaei MK, Kiavarz M, Alavipanah SK, Lakes T, Qureshi S (2018) Monitoring and forecasting heat island intensity through multi-temporal image analysis and cellular automata-Markov chain modelling: a case of Babol city Iran. Ecol Indicators 91:155–170

Gaur A, Eichenbaum MK, Simonovic SP (2018) Analysis and modelling of surface Urban Heat Island in 20 Canadian cities under climate and land-cover change. J Environ Manage 206:145–157

Grigoraş G, Uriţescu B (2019) Land use/land cover changes dynamics and their effects on surface urban heat island in Bucharest, Romania. Int J Appl Earth Obs Geoinf 80:115–126

Grimmond CSB, Salmond JA, Oke TR, Offerle B, Lemonsu A (2004) Flux and turbulence measurements at a densely built-up site in Marseille: heat, mass (water and carbon dioxide), and momentum. J Geophys Res: Atmospheres 109(D24)

Henits L, Mucsi L, Liska CM (2017) Monitoring the changes in impervious surface ratio and urban heat island intensity between 1987 and 2011 in Szeged Hungary. Environ Monitor Assess 189(2):1–13

Hereher ME (2017) Effect of land use/cover change on land surface temperatures-The Nile Delta Egypt. J African Earth Sci 126:75–83

IPCC (2013) Working group I contribution to the IPCC fifth assessment report climate change 2013. The physical science basis -summary for policymakers. World Bank, 2011. World Bank database. http://data.worldbank.org/

Kalnay E, Cai M (2003) Impact of urbanization and land-use change on climate. Nature 423(6939):528–531

Kato S, Yamaguchi Y (2005) Analysis of urban heat-island effect using ASTER and ETM+ data: separation of anthropogenic heat discharge and natural heat radiation from sensible heat flux. Remote Sens Environ 99(1–2):44–54

Khandelwal S, Goyal R, Kaul N, Mathew A (2018) Assessment of land surface temperature variation due to change in elevation of area surrounding Jaipur, India. Egyptian J Remote Sens Space Sci 21(1):87–94

Lakra K, Sharma D (2019) Geospatial assessment of urban growth dynamics and land surface temperature in Ajmer Region, India. J Indian Soc Remote Sens 47(6):1073–1089

Mahato S, Pal S (2018) Changing land surface temperature of a rural Rarh tract river basin of India. Remote Ses Appl: Soc Environ 10:209–223

Mahato S, Pal S (2021) Land surface thermal alteration and pattern simulation based on influencing factors of rural landscape. Geocarto Int 1–29

Markham BL, Barker JL (1985) Spectral characterization of the Landsat Thematic Mapper sensors. Int J Remote Sens 6(5):697–716

Mathew A, Khandelwal S, Kaul N (2018) Investigating spatio-temporal surface urban heat island growth over Jaipur city using geospatial techniques. Sustain Cities Soc 40:484–500

Mavoa S, Davern M, Breed M, Hahs A (2019) Higher levels of greenness and biodiversity associate with greater subjective wellbeing in adults living in Melbourne, Australia. Health Place 57:321–329

Meng Q, Zhang L, Sun Z, Meng F, Wang L, Sun Y (2018) Characterizing spatial and temporal trends of surface urban heat island effect in an urban main built-up area: a 12-year case study in Beijing, China. Remote Sens Environ 204:826–837

Mohajerani A, Bakaric J, Jeffrey-Bailey T (2017) The urban heat island effect, its causes, and mitigation, with reference to the thermal properties of asphalt concrete. J Environ Manage 197:522–538

Mohsin M, Abbas Q, Zhang J, Ikram M, Iqbal N (2019) Integrated effect of energy consumption, economic development, and population growth on CO_2 based environmental degradation: a case of transport sector. Environ Sci Pollut Res 26(32):32824–32835

Monteith J, Unsworth M (2013) Principles of environmental physics: plants, animals, and the atmosphere. Academic Press

Mushore TD, Mutanga O, Odindi J, Dube T (2017) Linking major shifts in land surface temperatures to long term land use and land cover changes: a case of Harare, Zimbabwe. Urban Climate 20:120–134

Nimish G, Bharath HA, Lalitha A (2020) Exploring temperature indices by deriving relationship between land surface temperature and urban landscape. Remote Sens Appl: Soc Environ 18:100299

Ogunjobi KO, Daramola MT, Akinsanola AA (2018) Estimation of surface energy fluxes from remotely sensed data over Akure Nigeria. Spatial Inf Res 26(1):77–89

Oke TR, Cleugh HA (1987) Urban heat storage derived as energy balance residuals. Bound-Layer Meteorol 39(3):233–245

Pal S, Ziaul SK (2017) Detection of land use and land cover change and land surface temperature in English Bazar urban centre. Egyptian J Remote Sens Space Sci 20(1):125–145

Peng J, Ma J, Liu Q, Liu Y, Li Y, Yue Y (2018a) Spatial-temporal change of land surface temperature across 285 cities in China: an urban-rural contrast perspective. Sci Total Environ 635:487–497

Peng J, Jia J, Liu Y, Li H, Wu J (2018b) Seasonal contrast of the dominant factors for spatial distribution of land surface temperature in Urban areas. Remote Sens Environ 215:255–267

Prohmdirek T, Chunpang P, Laosuwan T (2020) The relationship between normalized difference vegetation index and canopy temperature that affects the urban heat Island phenomenon. Geographia Technica 15(2):222–234

Ranagalage M, Estoque RC, Murayama Y (2017) An Urban heat island study of the Colombo metropolitan area, Sri Lanka, based on Landsat data (1997–2017). ISPRS Int J Geo Inf 6(7):189

Santamouris M, Haddad S, Fiorito F, Osmond P, Ding L, Prasad D, Wang R et al (2017) Urban heat island and overheating characteristics in Sydney, Australia. An analysis of multiyear measurements. Sustainability 9 (5):712

Sarangi C, Tripathi SN, Qian Y, Kumar S, Ruby Leung L (2018) Aerosol and urban land use effect on rainfall around cities in Indo-Gangetic Basin from observations and cloud resolving model simulations. J Geophys Res: Atmos 123(7):3645–3667

Sejati AW, Buchori I, Rudiarto I (2019) The spatio-temporal trends of urban growth and surface urban heat islands over two decades in the Semarang Metropolitan Region. Sustain Cities Soc 46:101432

Shah AM, Liu G, Meng F, Yang Q, Xue J, Dumontet S, Casazza M et al (2021) A review of urban green and blue infrastructure from the perspective of food-energy-water nexus. Energies 14(15):4583

Sharifi A (2020) Trade-offs and conflicts between urban climate change mitigation and adaptation measures: a literature review. J Clean Prod 276:122813

Silva JS, da Silva RM, Santos CAG (2018) Spatiotemporal impact of land use/land cover changes on urban heat islands: A case study of Paço do Lumiar, Brazil. Build Environ 136:279–292

Snyder WC, Wan Z, Zhang Y, Feng YZ (1998) Classification-based emissivity for land surface temperature measurement from space. Int J Remote Sens 19(14):2753–2774

Son NT, Chen CF, Chen CR, Thanh BX, Vuong TH (2017) Assessment of urbanization and urban heat islands in Ho Chi Minh City, Vietnam using Landsat data. Sustain Cities Soc 30:150–161

Sultana S, Satyanarayana ANV (2020) Assessment of urbanisation and urban heat island intensities using landsat imageries during 2000–2018 over a subtropical Indian City. Sustain Cities Soc 52:101846

Shi Y, Katzschner L, Ng E (2018) Modelling the fine-scale spatiotemporal pattern of urban heat island effect using land use regression approach in a megacity. Sci Total Environ 618:891–904

Singh P, Kikon N, Verma P (2017) Impact of land use change and urbanization on urban heat island in Lucknow city, Central India. A remote sensing based estimate. Sustain Cities Soc 32:100–114

Singh RS, Ghosh P (2021) Geotourism potential of coal mines: an appraisal of Sonepur-Bazari open cast project, India. Int J Geoheritage Parks 9(2):172–181

Tafesse B, Suryabhagavan KV (2019) Systematic modeling of impacts of land-use and land-cover changes on land surface temperature in Adama Zuria District Ethiopia. Model Earth Syst Environ 5(3):805–817

Tasumi M, Allen RG, Trezza R (2008) At-surface reflectance and albedo from satellite for operational calculation of land surface energy balance. J Hydrol Eng 13(2):51–63

Willie YA, Pillay R, Zhou L, Orimoloye IR (2019) Monitoring spatial pattern of land surface thermal characteristics and urban growth: A case study of King

Williams using remote sensing and GIS. Earth Sci Inf 12(4):447–464

Xiao H, Weng Q (2007) The impact of land use and land cover changes on land surface temperature in a karst area of China. J Environ Manage 85(1):245–257

Xue Z, Hou G, Zhang Z, Lyu X, Jiang M, Zou Y, Liu X et al (2019) Quantifying the cooling-effects of urban and peri-urban wetlands using remote sensing data: case study of cities of Northeast China. Landsc Urban Plan 182:92–100

Yang W, Chen B, Cui X (2014) High-resolution mapping of anthropogenic heat in China from 1992 to 2010. Int J Environ Res Public Health 11(4):4066–4077

Yang J, Sun J, Ge Q, Li X (2017) Assessing the impacts of urbanization-associated green space on urban land surface temperature: a case study of Dalian, China. Urban Forestry Urban Greening 22:1–10

Yu Z, Guo X, Zeng Y, Koga M, Vejre H (2018a) Variations in land surface temperature and cooling efficiency of green space in rapid urbanization: the case of Fuzhou city, China. Urban Forestry Urban Greening 29:113–121

Yu Y, Liu J, Shao W (2018b) The estimation and effect of anthropogenic heat flux in Beijing. Energy Procedia 152:302–306

Yu Z, Yang G, Zuo S, Jørgensen G, Koga M, Vejre H (2020) Critical review on the cooling effect of urban blue-green space: a threshold-size perspective. Urban Forestry Urban Greening 49:126630

Zhang Y, Balzter H, Wu X (2013) Spatial–temporal patterns of urban anthropogenic heat discharge in Fuzhou, China, observed from sensible heat flux using Landsat TM/ETM+ data. Int J Remote Sens 34 (4):1459–1477

Zhang F, Tiyip T, Kung H, Johnson VC, Maimaitiyiming M, Zhou M, Wang J (2016) Dynamics of land surface temperature (LST) in response to land use and land cover (LULC) changes in the Weigan and Kuqa river oasis, Xinjiang China. Arabian J Geosci 9(7):1–14

Zhang X, Estoque RC, Murayama Y (2017) An urban heat island study in Nanchang City, China based on land surface temperature and social-ecological variables. Sustain Cities Soc 32:557–568

Zheng Z, Ren G, Wang H, Dou J, Gao Z, Duan C, Yang Y et al (2018) Relationship between fine-particle pollution and the urban heat island in Beijing, China: observational evidence. Bound-Layer Meteorol 169 (1):93–113

Zhou Y, Weng Q, Gurney KR, Shuai Y, Hu X (2012) Estimation of the relationship between remotely sensed anthropogenic heat discharge and building energy use. ISPRS J Photogramm Remote Sens 67:65–72

Zhou B, Rybski D, Kropp JP (2017) The role of city size and urban form in the surface urban heat island. Sci Rep 7(1):1–9

Zhou D, Bonafoni S, Zhang L, Wang R (2018) Remote sensing of the urban heat island effect in a highly

populated urban agglomeration area in East China. Sci Total Environ 628:415–429

Ziaul S, Pal S (2018a) Analyzing control of respiratory particulate matter on land surface temperature in local climatic zones of English Bazar Municipality and surroundings. Urban Clim 24:34–50

Ziaul S, Pal S (2018b) Anthropogenic heat flux in English Bazar town and its surroundings in West Bengal, India. Remote Sens Appl: Soc Environ 11:151–160

Ziaul S, Pal S (2020) Modeling the effects of green alternative on heat Island mitigation of a meso level town, West Bengal India. Adv Space Res 65(7):1789–1802

Zu Y, Huang L, Hu J, Zhao Z, Liu H, Zhang H, Chen M et al (2017) Investigation of relationships between meteorological conditions and high PM10 pollution in a megacity in the western Yangtze River Delta, China. Air Qual Atmos Health 10(6):713–724

Impact of Urbanization on Land Use and Land Cover Change and Land Surface Temperature in a Satellite Town

19

Manisha D. Malcoti, Hina Zia, and Chitrarekha Kabre

Abstract

Urban Heat Island, the phenomenon synonymous with urbanization and change in local climate, is a grave threat to the energy balance and resources of a city. This paper presents a study of one of the fastest-growing satellite towns of Delhi, Gurugram, using remote sensing techniques to establish if the fast pace of urban expansion influenced air and surface temperatures. The temperature trends were studied using remote sensing and ArcGIS software. Satellite images for the years 2000 (Landsat 7 ETM+), 2010 (Landsat 5, TM) and 2019 (Landsat 8, OLI/TIRS) were downloaded and analyzed for LST ArcGIS using the mono-window algorithm. The year 2019 revealed a maximum LST of 47.68 °C for June in comparison with an LST of 44.8 °C for June 2010 and 40.4 °C for May 2000. The city's temporal and spatial changes over the past decades (2000–2019) were studied by the technique of change detection. To study land use

and land cover changes, supervised classification using ERDAS was done. The supervised classification (maximum likelihood classifier) has been used to identify the five major categories of LULC for the period years 2000, 2010 and 2019. The study found that since 2000, the city's most abundant resource of agricultural land 2000 saw a sharp decline of 60% in 2019. This seems to be utilized by the urban built-up because the urban areas also saw an increment of more than 62% for the same time frame. The classification had accuracy of 96.67%, 94% and 86.67% for the years 2000, 2010 and 2019, respectively. Studies involving LULC classification are important because they represent how human activities are modifying ecology. The classification helped establish that the agricultural areas of Gurugram are on a rapid decline, whereas urban built-up areas have significantly doubled in the past two decades. The study helps in understanding the impacts of urbanization patterns for a fast-expanding metropolis and the possible interventions to be made by urban planners and policy managers to prevent further aggravation of UHI and plan mitigation strategies.

M. D. Malcoti (✉) · H. Zia
Faculty of Architecture and Ekistics, Jamia Millia Islamia, New Delhi, India
e-mail: dabralm11@gmail.com

H. Zia
e-mail: hzia@jmi.ac.in

C. Kabre
Faculty of Architecture, School of Planning and Architecture, New Delhi, India
e-mail: chitrarekha.kabre@spa.ac.in

Keywords

Urban heat island · Remote sensing · Land surface temperature (LST) · Land use and land cover (LULC) · Normalized differential built-up index (NDBI)

19.1 Introduction

The process of urbanization is a natural and inevitable consequence of economic development. India, an emerging and developing country, is experiencing rapid economic development which in turn is changing the urban and rural landscape. The country has more than 31.2% of the total population living in 7935 towns/cities (census 2011). It is estimated by 2050, India will house 14% of the world's urban population in its cities causing a major landscape modification (Swerts et al. 2014). The existing urban landscape is becoming over-stressed and populous causing the spill over in suburban and rural hinterlands bringing about change in the land use and land cover pattern. What is often ignored is that due to the continuous replacement of natural ecosystems with urban infrastructure, the environment suffers irreplaceable damage and modification of microclimate leading to UHI development (Stone and Rodgers 2001). A study of urban areas has shown that the land use/land cover (LULC) change due to urbanization and the declining natural land cover has significantly altered their climate over the past few decades (Montazeri and Masoodian 2020). The rapid transformation of the urban landscape can be said to be due to the continuous growth in the urban population (Bharath et al. 2018). Due to this, the pervious surface is converted into non-pervious urban surfaces, changing almost the whole urban landscape. The result is an increase in the land surface temperature (LST) in the urban areas which ultimately leads to the development of the urban heat island (UHI) phenomenon (Shahfahad et al. 2020). Analysis of current trends of increased extreme heat exposure felt by urban populations from both climate change and the urban heat island effect presents a grave threat (Tuholske et al. 2021).

The UHI can be grouped into three categories based on the methods of measurement. These are boundary layer heat island (BLUHI) which is studied using the air temperature above the average building height, canopy layer heat island (CLUHI) which is studied using the air temperature between the rooftop and ground surface and surface urban heat island (SUHI) which is studied using the LST (Voogt 2009). Among these, researchers consider SUHI as the most popular and commonly used method of studying the urban thermal environment because of the availability of a wide variety of thermal remote sensing data (Voogt and Oke 2003). Numerous studies have underlined that in any urban area the land surface temperature (LST) correlates with open areas, built up and green areas and their density (Erell et al. 2014; Golany 1996; Johansson 2006; Kumari et al. 2018; Mohan, Pathan, et al. 2011a, b; Voogt and Oke 1998). The findings of these studies can be related to the process of urbanization with changes in local climate patterns including an increase in LST. Voogt had presented that remote sensing is a valid and positive approach to measuring surface urban heat islands (Voogt 2009). The cause-and-effect relationship between built-up and LST can now be easily confirmed by studying multi-temporal LANDSAT data for any urban area. The thermal band/s of Landsat satellites help in calculating LST for any region of interest over the surface of the earth (Du et al. 2015; Verma et al. 2009; Weng 2014). With technological advancement, together with GIS, satellite data can help identify urban land processes and detect temporal and spatial changes (Weng 2001; Rahman and Netzband 2007). Further, temporal analysis of the correlation between LST with normalized differential built-up index (NDBI) suggests that the relationship varies temporally and can be a reliable tool to understand the variation of LST over a time period for an urban area (Chen et al. 2006). Land surface temperature (LST) is representative of the radiative temperature of land surfaces and is directly affected by albedo, vegetation cover and soil moisture (Oke et al. 2017). Historic LST data can be extremely useful in monitoring the increasing UHI patterns of individual cities over time and thus reveals the impact of urbanization on the local climate. With the latest developments in urban remote sensing, it is possible to understand the relationship between LST, land

use and land cover (LULC) and normalized difference built index (NDBI) to evaluate the impact of urban growth on the surface temperature of any urban area (Shahfahad et al. 2021).

The past few decades have seen the trend of increased UHI studies in countries globally to assess the factors and consequences. Chapman et al. (2017) presented a literature survey on urbanization and climate change-induced increase in temperature to the tune of 5 °C. Further, Zhou et al. (2014) did a comprehensive study on climate changes due to urbanization in China and concluded that the temperature of China is experiencing a decadal increase of 0.5 °C. In the case of India, a developing country many similar types of research are taking place. Veena et al. (2020) presented a review of the UHI studies done in the Indian cities and presented that the Indian cities have experienced an increase of about 2–6 °C in the temperature over the past decades. Megacities like Delhi, Mumbai, Chennai and Bangalore were also studied by many researchers and confirmed the trend of increasing temperatures over the year (Grover and Singh 2015; Javed Mallick and Bharath 2008; Mohan Kandya et al. 2011a, b; Rose et al. 2011; Shahfahad et al. 2021). A study on Mumbai has examined the pattern of LULC change in Mumbai metropolitan city from 1991 to 2018 and quantified its impact on the UHI dynamics (Shahfahad et al. 2021).

Further studies on cities like Jaipur, Nagpur and Guwahati also confirmed the UHI trend (Borbora and Das 2014; Gupta 2012; Surawar and Kotharkar 2017). A scoping study review by Lall et al. (2014) for various studies done on Indian cities has verified that maximum studies deal with establishing the presence of UHI as an environmental issue by recording its temperature intensity only, but aspects of causative factors and impact due to urbanization have not been comprehensively studied. Another study by Kotharkar et al. (2018) reviewing UHI studies done on South Asian cities presented that Delhi, Chennai and Colombo were the most studied cities. No study was found for upcoming metro cities or satellite towns that are also bearing the pressure of urbanization spilled over from the megacities. Further, very few studies in India analyzed the impact of urban sprawl through biophysical parameters like normalized difference vegetation index (NDVI) and normalized difference built-up index (NDBI) following LULC change study. Therefore, the main goal of this paper is to understand the relationship between LST, LULC for an urban area over two decades and study the impact of biophysical indices like NDBI and NDVI to evaluate how urbanization influences surface temperature for a satellite town, Gurugram of the capital city Delhi.

19.2   Materials and Methods

19.2.1   Study Area: Gurugram City, India

Earlier known as Gurgaon till 2016, Gurugram is one of the prominent cities of the Delhi NCR region and has shown the maximum decadal population growth among all cities. This urban and industrial development in India's "millennium city" has been facilitated by an uneven process of land acquisition, exemption and agrarian transformation (Cowan 2018). The city also boasts of having the third-highest per capita income in the country.

The study area, Gurugram city (previously known as Gurgaon) is just 32 km southwest of the capital city of India, New Delhi, and is located in the northern state of Haryana. It lies between latitude 28.457523 and longitude 77.026344. Gurugram with approximately 432 square km city area is known as a financial and technology hub of Haryana (Fig. 19.3). As per the census 2011, the population of the city was 876,824 which is growing manifold. Thanks to private sector-led urbanization, the city has witnessed phenomenal urban growth in the past two decades. The population of the city was 902,112 during the census 2011 and projected scenario of the city is 3,700,000 as per Gurgaon Manesar Master Plan 2021 (Fig. 19.1).

The city is still expanding and areas like the new Gurgaon are luring the population with compact apartments in high-rise residential
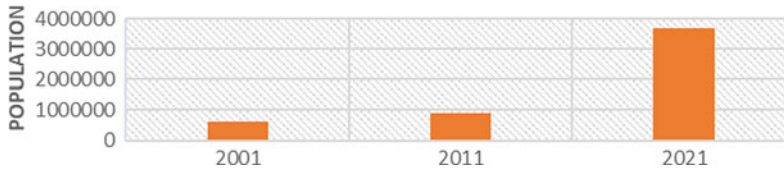
Fig. 19.1 Population growth chart for Gurugram

societies aping the Western culture. The city has an overlap between monsoon-influenced humid subtropical and semi-arid climates. It has a high variation between summer and winter temperatures and precipitation patterns. Summers usually start in early April and peak in May continuing till June. The peak summer temperature may reach 45 °C accompanied by heat waves. The monsoon starts in June and July mid and lasts until mid-September. From November onwards, the city starts experiencing lower temperatures, and by December, the city experiences fog episodes. January is the month of lowest temperatures dropping to 5 °C easily, again accompanied by cold wave spells. The temperature trend for Gurugram city for the past two decades is shown in Fig. 19.2.

19.2.2 Material Used

The study has downloaded satellite data from http://earthexplorer.usgs.gov. For the period between 2000 and 2019, the years 2000, 2010 and 2019 were taken as representative years to analyze decade long variations. Good quality imageries, with zero cloud cover of Landsat 7 ETM+ (2000), Landsat 5 TM (2010) and Landsat 8 OLI_TIRS (2019) and having 30 m spatial resolution, have been used for this study (Table 19.1). Thermal infrared bands, band 6 of Landsat TM and ETM+ and band 10 of Landsat 8 were used to calculate LST for specified years using ArcGIS 10.3 software. The digital numbers DN are converted to at-satellite radiance to retrieve the brightness temperature. The master plans for the city for the year 2031 from the TCP department Haryana were used. Google Earth imagery was also used to identify and validate surfaces and LULC changes. Long-term temperature data for the city was taken from gridded data available at the IMD Web site.

Post–pre-processing, the LULC classification was done using the maximum likelihood classifier (MLC). The land use indices (NDVI and NDBI) were generated from the optical bands of Landsat data by using raster calculator tool in ArcGIS software (version 10.2). LST was calculated using the thermal bands (band 6 in the Landsat TM and ETM+ while band 10 in the Landsat OLI/TIRS). The details of the methods used have been presented in the flowchart (Fig. 19.4).
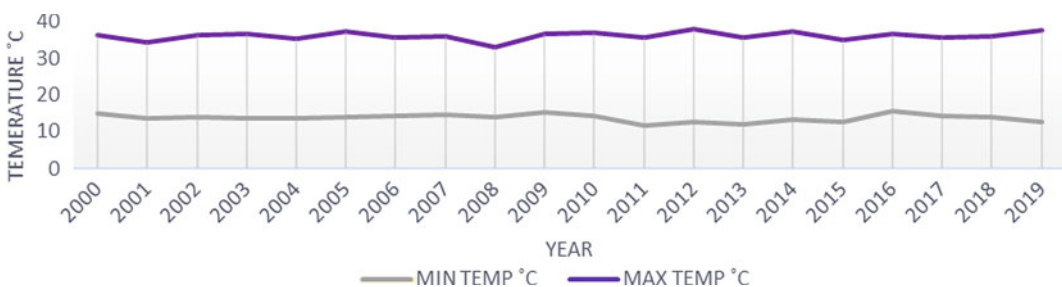
Fig. 19.2 Historical air temperature data for Gurugram. *Source* https://www.imdpune.gov.in/Clim_Pred_LRF_New/Grided_Data_Download.html
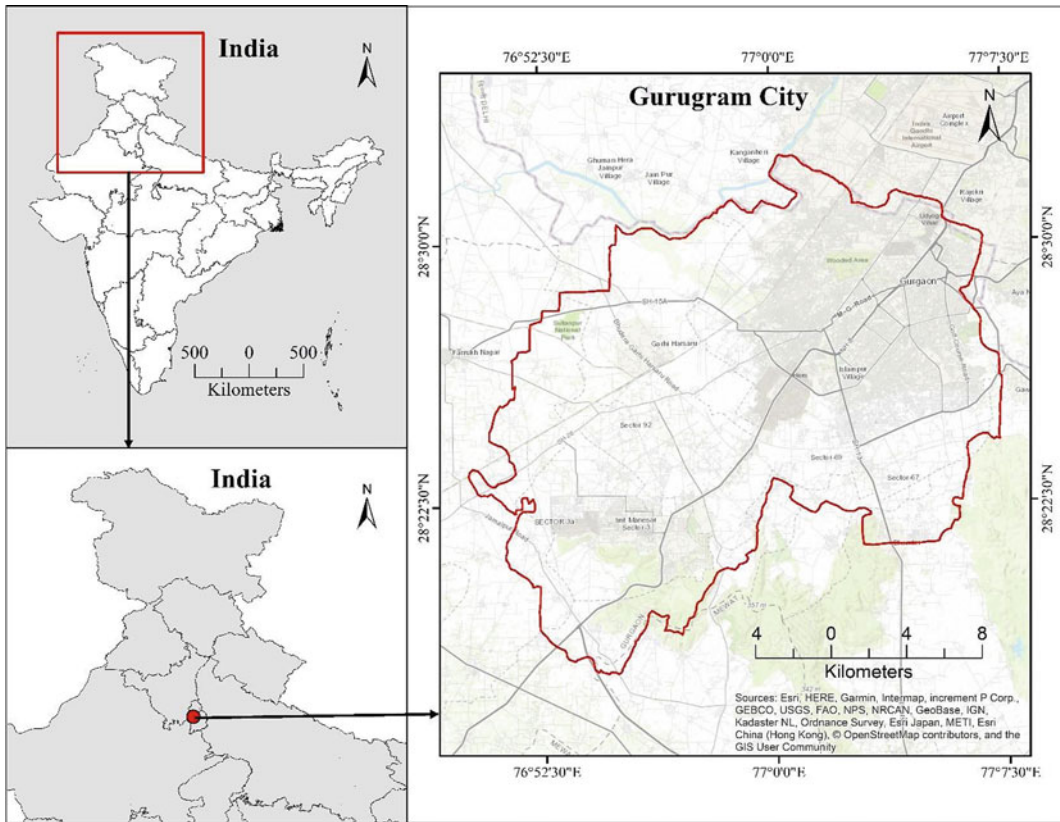
Fig. 19.3 Study area Gurugram, Haryana

Table 19.1 Satellite sensors and date of data retrieval

Satellite	Sensors	Date of acquisition	Path/Row	Cloud cover (%)	Sun elevation (in degrees)	Sun Azimuth (in degrees)
Landsat 7	Enhanced thematic mapper (ETM+)	24.5.2000	147/040	0.0	67.152	105.25
Landsat 5	Thematic mapper (TM)	13.6.2010	147/040	0.0	67.125	98.567
Landsat 8	Operational land imager (OLI), thermal infrared sensor (TRS)	22.6.2019	147/040	0.0	68.793	99.525

19.2.3 Methodology

19.2.3.1 Image Pre-Processing

The images downloaded from Landsat (5, 7 and 8) are of the highest quality (L1TP), These images are already systematically, geometrically and radiometrically corrected. However, area of Interest (AOI) was clipped in ArcGIS 10.3 for the LST map and in ERDAS, only stacking and sub setting was done to generate LULC maps.

19.2.3.2 LULC Classification

LULC classification has evolved to be the most widely used application in remote sensing. To
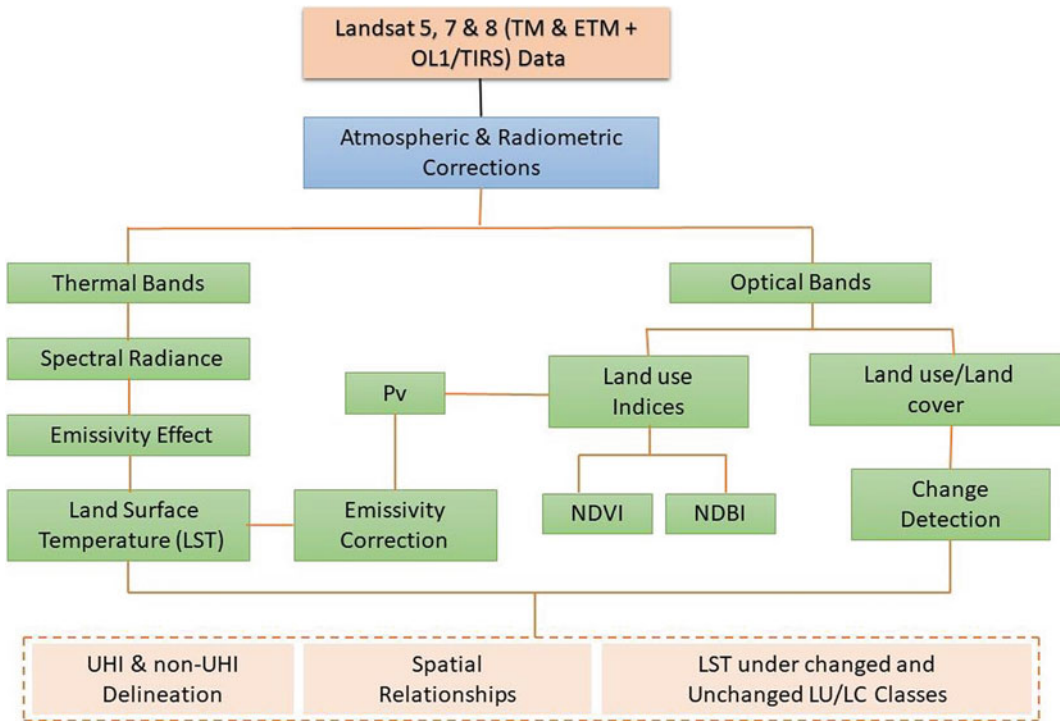
Fig. 19.4 Flowchart to calculate LST from satellite imagery

study LULC change over Gurugram city, multi-temporal data is used for representative years 2000, 2010 and 2019, showing decadal variation. Using ERDAS 2014, the stacked and subset images of AOI are used to identify land use classes. Supervised classification was done on ERDAS 2014 using the maximum likelihood scheme (MLC). Five different land use classes were made, namely urban built-up, agricultural, vegetation, open land and water body/wetland, for the years specified, and LULC classes map was created for respective years. Accuracy assessment was done for the classified maps, land use/land cover map of 2000, 2010 and 2019 through physical surveys, field visits and also study of Google Earth imagery. Further accuracy assessments were done using kappa coefficient and results have been given in Table 19.3. Thereafter, a change detection map was created in ArcGIS to assess the land use/land cover change from 2000 to 2019.

19.2.3.3 Retrieval of LST from Landsat Images

Analysis of historic LST data was obtained using mono-window (MWA) and split window algorithm (SWA). For the years 2000 and 2010, mono-window algorithms were used (Kumari et al. 2018). The split window algorithm was used to generate the LST map for 2019 (Landsat 8). The split window algorithm can be used only for data that have two thermal bands (B10 and B11) as in Landsat 8 (Du et al. 2015).

19.2.3.4 Retrieval of LST from Landsat 5(TM) and Landsat 7 (ETM+)

The retrieval of LST from Landsat thematic mapper (TM) and Landsat 7, enhanced thematic mapper (ETM+) was done in four steps as per Landsat User handbook (Ihlen and USGS 2019). In the first step, the digital number of the image is converted into spectral radiance using Eq. 19.1.

$$L_\lambda = \min(\max - \min) \times DN/255 \qquad (19.1)$$

where L_λ = spectral radiance, Min = 1.238 (spectral radiance of DN value 1), Max = 15.600 (spectral radiance of DN value 255) and DN = digital number.

In the second step, spectral radiance is converted into sensor radiance value by using the following Eq. 19.2.

$$L_\lambda = \left\{ \frac{LMAX\lambda - LMIN\lambda}{Qcal\,MAX - Qcal\,MIN} \right\} (Qcal - Qcal\,MIN) + LMIN\lambda \qquad (19.2)$$

where L_λ = spectral radiance at the sensor's aperture, Qcal = quantized calibrated pixel value [DN], QcalMin = minimum quantized calibrated pixel value corresponding to LMIN, QcalMax = maximum quantized calibrated pixel value corresponding to LMAX, LMINλ = spectral at-sensor radiance that is scaled to QcalMin and LMAXλ = spectral at-sensor radiance that is scaled to QcalMax

Further, in Step 3, the sensor effective radiance is converted into sensor brightness value temperature (in Kelvin) by using Eq. 19.3.

$$TB = \frac{K2}{\ln(\frac{K1}{L_\lambda} + 1)} \qquad (19.3)$$

where TB = effective at-sensor brightness temperature [K], K2 = calibration constant 2, K1 = calibration constant 1, L_λ = spectral radiance at the sensor's aperture [W/(m^2 sr μm)] and ln = natural logarithm.

The values of K1 and K2 are constant for every satellite image as per Landsat 5, 7 and 8. These are displayed in Table 19.5. Finally, in the final step, the effective at-temperature in Kelvin is converted into °C by using the equation, as shown below.

$$T(^\circ C) = T - 273.15 \qquad (19.4)$$

19.2.3.5 Retrieval of LST from Landsat 8 OLI/TIRS

This study uses the mono-window algorithm for estimating LST from Landsat 8 imagery for calculation of LST as per the description provided. As per the recommendation of USGS (after January 6, 2014) of not using TIRS Band 11 due to its larger calibration uncertainty, the study used only band 10 in the algorithm (Avdan and Jovanovska 2016). This study utilizes TIR band 10 to estimate brightness temperature and bands 4 and 5 for calculating the NDVI. The metadata of the satellite images used in the algorithm is presented in Table 19.1. The first step is retrieving the top of atmospheric (TOA) spectral radiance using Eq. 19.5.

$$L_\lambda = ML \cdot Qcal + AL \qquad (19.5)$$

where L_λ = temperature of atmosphere spectral radiance, M_L = band-specific multiplicative rescaling factor from the metadata (0.000342), A_L = band-specific additive rescaling factor for Band 10 from the metadata (0.1) and Qcal = quantized and calibrated standard product pixel values (DN) of band 10.

In the second step, TIRS band data is converted into BT from spectral radiance using thermal constants as per metadata file (MTL) using Eq. 19.3. The third step involves calculating NDVI. As per Weng (2004), it is mandatory to estimate the NDVI because the amount of vegetation is a significant factor for LST estimation. The NDVI was calculation using Eq. 19.6.

$$NDVI = \frac{NIR - R}{NIR + R} \qquad (19.6)$$

where NIR is the near-infrared band and R is the red band. For the fourth step, the proportion of vegetation (Pv) is calculated using Eq. 19.7.

$$Pv = (NDVI - NDVIMIN/NDVIMAX - NDVIMIN)^2$$

$$(19.7)$$

Further, in the fifth step, land surface emissivity LSE is calculated to estimate LST. As per Planck's law "LSE is the proportionality factor that scales blackbody radiance, which predicts emitted radiance." The land surface emissivity LSE (ε) is calculated using Eq. 19.7 as proposed by Sobrino et al. (2004).

$$\varepsilon = 0.004 \times Pv + 0.986 \qquad (19.8)$$

where ε is emissivity and Pv is the proportion of vegetation. Finally, the last step of calculating LST or emissivity corrected LST is done using Eq. 19.9.

$$T = \frac{TB}{1 + (\lambda.TB/P)\ln(\varepsilon)} \qquad (19.9)$$

where BT = brightness (at-satellite temperature), W = wavelength of emitted radiance (11.5 µm) and = 14,380 (constant).

19.2.3.6 Calculation of NDVI and NDBI

NDVI is calculated by using the equation suggested by Kriegler et al. (1969) as shown below.

The ratio of the NIR and red band is used for the calculation because of the highest EM spectrum of absorption by chlorophyll of these two bands. The NDVI was calculated using Eq. 19.6. Calculation of NDBI is done by Eq. 19.10 as suggested by Zha et al. (2003) using the mid-infrared (MIR) and near-infrared (NIR) bands of Landsat data.

$$NDBI = \frac{MIR - NIR}{MIR + NIR} \qquad (19.10)$$

19.3 Results and Discussion

19.3.1 Analysis of Variation of LULC Pattern

Due to rampant urbanization, agricultural and pervious land in Gurugram was converted to impervious areas. This is evident from the LULC classification maps generated for the years 2000, 2010 and 2019 (Fig. 19.5). The results indicated that temporally urban built-up areas have increased manifold as indicated in Table 19.2.
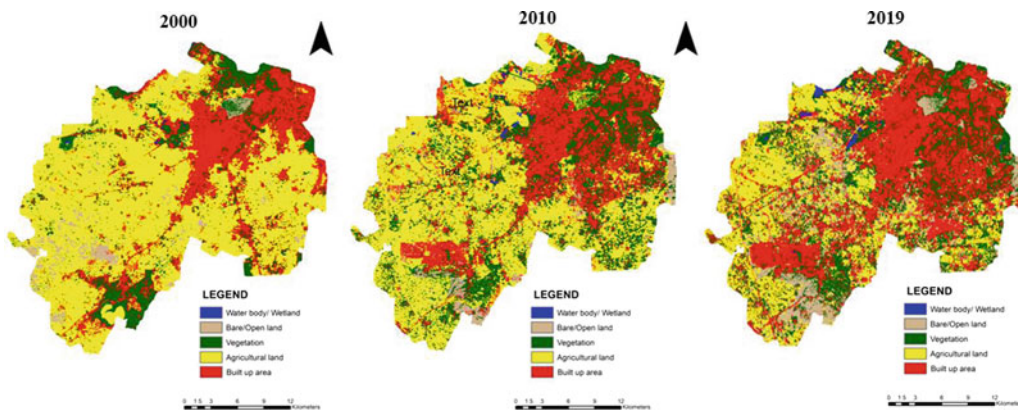
Fig. 19.5 LULC classes image of Gurugram, 2000–2019

Table 19.2 LULC classes with area coverage (in acres)

Year	Water body/wetland	Vegetation	Open land	Urban built-up	Farmland
2000	153	15,123	5455	25,343	66,621
2010	356	29,069	6183	30,463	46,239
2019	552	27,650	17,869	40,554	25,685

The urban built-up area since 2000 had increased by 20% till 2010 and 60% till 2019. It is evident from LULC maps that a major percentage of farmlands were converted into impermeable areas of urban built-up since they also decreased by approximately 61% in the last two decades. It is encouraging to see the area of vegetation or the green area of the city is also on increase. This may be attributed to the fact that the farmlands have been converted into urban residential pockets that are judiciously planned with due regard to green areas. The absence of optimum green and permeable areas may choke a city eventually. As the city grew, water treatment plants and sewage treatment plants were set up in the city area accompanied by the increased flow in the Najafgarh drain that flows in the northwest part of Gurugram. This is the reason why the water body area has seen an increased manifold. Studying Table 19.2 we can summarise that it is all the agricultural land of the city that eventually got converted into various other land use classes. Table 19.3 below presents the accuracy assessment of the land use classification of Gurugram which was done using the Kappa coefficient.

19.3.2 Analysis of LST Pattern

Urban surfaces in dense areas are observed to make those pockets in a city warmer than neighboring areas (Mohan et al. 2012). With the rapid increase in urban built-up areas, roads and flyovers the pervious, green area of Gurugram has decreased significantly. This has led to an increase in anthropogenic heat release also. Studies present that an increase in impervious areas and a change or reduction in the distribution of green cover can increase land surface temperatures gradually (Kumari et al. 2018; Shahfahad

et al. 2022). Land surface temperature (LST) is representative of the radiative temperature of any land surface, such as soil, grass, pavements, asphalt and is directly affected by albedo, vegetation cover and soil moisture. Historic LST data can be extremely useful in monitoring the increasing UHI patterns of individual cities over some time and thus reveals the impact of urbanization on local climate (Tran et al. 2006).

In the present study, LST maps were created for the years 2000, 2010 and 2019 for the city of Gurugram to analyze the spatial and temporal trends of temperature (Fig. 19.6). The temperature range classification in LST maps was divided into 5 equal classes with a defined interval of 5 °C by managing symbology of the maps in ArcGIS. The same range was used in all three LST maps of representative years to bring more clarity in comparison. The city, once an agrarian economy, is now a leading economic center of the country and the hub of call centers of many MNCs. The city has grown up considerably from being a sleepy and dusty town of Haryana. Initially, the city lacked basic infrastructure facilities for its population, but slowly with the influx of younger working-class, the authorities started improving these facilities since the city witnessed a boom in real estate. On one hand, the city saw better connectivity with the capital city and a wide network of roads, and on the other hand, the Gurugram city area kept on growing within the district with each master plan.

The analysis of historic data revealed that LST has increased significantly in the last twenty years (Table 19.4). The LST map was generated for the peak summer months for the city for each year. The year 2000 saw a summer temperature range of 27.0–40.4 °C (May 2000). Large parts of the city (84%) exhibited a high-temperature range of 36–40 °C. While the vegetated area

Table 19.3 Accuracy assessment for LULC classes

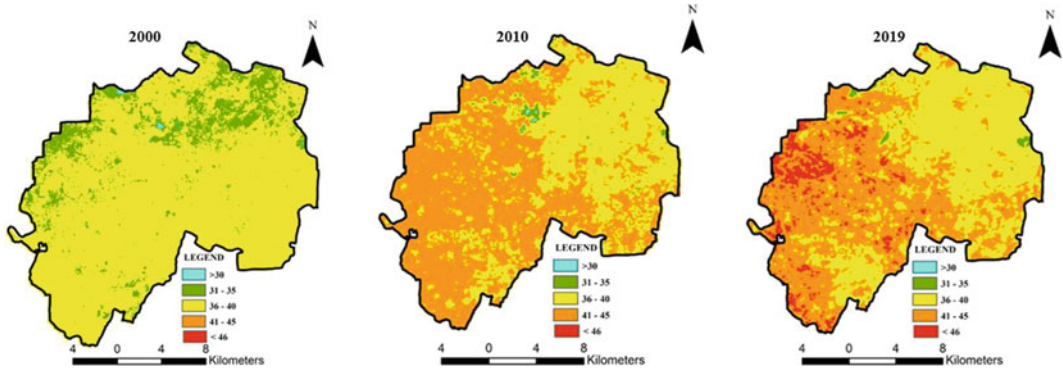| Year	Accuracy percentage (%)	Kappa coefficient
2000	96.67	0.91
2010	94.00	0.95
2019	86.67	0.82

Fig. 19.6 LST image of Gurugram, 2000–2019

around the water body (near Najafgarh Lake) were the lower temperature zones in the city, the area of the city in a north-eastern range having vegetation and agricultural land displayed a warm temperature range of 31–35 °C. A decade later in 2010 when Gurugram was at peak of urbanization, LST range analysis of the city revealed a temperature range of 44.8–28 °C. The temperature range of 31–35 °C was only observed for a mere 1% area of the city as against 15% during previous observation. While the south-western and north-western parts of the city were exhibiting a maximum temperature range of 41–45 °C, the north-Eastern part of the city, majorly a residential area exhibited a temperature range of 36–40 °C. Lastly, LST analysis for the

city was done for the year 2019. As expected, the city surface temperature increased further, whereas for June 2019, more than 6% of the city was witnessing LST in the range of 46–48 °C, these areas lie in the north-western part of the city. Table 19.4 below gives a comparative analysis of how over the years the city area saw different temperature range. The maximum LST observed for the city saw a jump of 7.28 °C in the past 20 years. The historical LST dataset suggests that the city is experiencing more severe summer heat and gradually the greater city area is falling victim to it. This is in line with the temporal monthly average maximum temperature (gridded data from IMD Web site) as presented in Table 19.5.

Table 19.4 LST comparative analysis for the city over the past two decades

Year	Area of city(percent) that falls in land surface temperature range				
	≥ 30 °C	31–35 °C	36–40 °C	41–45 °C	≤ 46 °C
2000	0.05	15.48	84.43	0.01	0
2010	0.07	1.27	50.85	47.6	0
2019	0	0.84	42.77	50.29	6.1

Table 19.5 Temporal monthly average maximum temperature (gridded data from IMD Web site)

Year	Minimum (Monthly average)	Maximum (Monthly average)
2000	14.92	36.39
2005	13.73	37.29
2010	14.37	37.14
2015	12.65	35.06
2019	12.71	37.54

19.3.3 Analysis of NDVI and NDBI

In the present study for Gurugram, NDVI and NDBI were calculated to assess the relationship between it and the physical features of the study area. The result shows that there is higher NDVI in 2000, 2010 and 2019 around the northern part of the city along with few patches in the southern and eastern side which also boasts of the golf course (Fig. 19.7). The lowest NDVI is found in built-up dominating the industrial and high-density residential areas in the central part of the city. NDVI values vary from −0.09 to −0.35 in 2000, and in 2019, it is −0.10 to 0.52 (Fig. 19.7). The values of these NDVI suggest that sparse vegetation is dominant such as shrubs or farmland in the city except for thick vegetative regions of Najafgarh Lake and Sultanpur national park. The NDVI value of 0.1 or less than that represents non-vegetated land, bare rock or it may be built-up or fallow land area. Analyzing the large extent of residential areas, private developers have given due importance to planning green areas in their projects owing to local authority byelaws and marketing trends.

The NDVI ranges from +1 to −1. The positive values are representative of healthy green vegetation, while the negative NDVI values indicate non-vegetative and impermeable cover. NDVI representing vegetation of an urban area is associated with the properties of the ground surface in the urban regions and influences the surface temperature significantly (Zhang and Wang 2008). Correlational analysis of NDVI and LST was done to understand how they influence each other in urban conditions. Scatter plots were prepared for the representative years and a negative degree of correlation (low) was established as given in Fig. 19.10. The pictorial representation of scatter plots helps in understanding the correlation. The correlation was negative but low for the year 2000; however gradually over the years by 2019, the negative correlation became very weak. It may also suggest that in the current scenario the city LST was not directly influenced by NDVI but was governed by some other physical factor. Also, dry, diseased or deciduous non-greenish vegetation, which are also referred to as non-photosynthetic vegetation (NPV), has different reflectance properties in comparison with green vegetation and result in lower NDVI value (Tetali et al. 2022). For the year 2000, a negative correlation was low represented by $r2 = 0.3545$; this further reduced to $r2 = 0.217$ in the year 2010, and finally, 2019 was represented by $r2 = 0.122$ presenting a very weak negative correlation.

Analysis of NDBI images shows that there is a much increase in the area under built-up from 2000 to 2019. In 2000, NDBI ranges from 0.09 to 0.39, and in 2019, it increased from − 0.36 to 0.39 (Fig. 19.8). In 2000, a high NDBI value was seen in the central, eastern and southern parts of the study area. Generally, a high NDBI value is recorded in the area which has a high concentration of built-up and open land with bare soil and rocks. In 2019, it is observed that the central and northern areas of the city have high values of
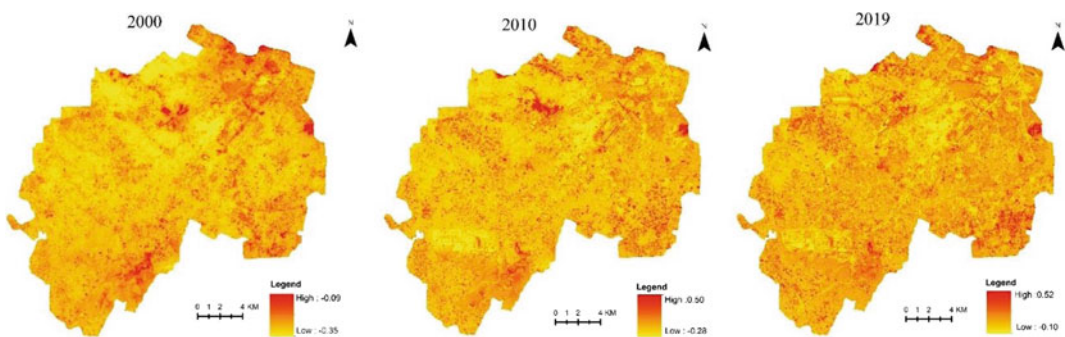

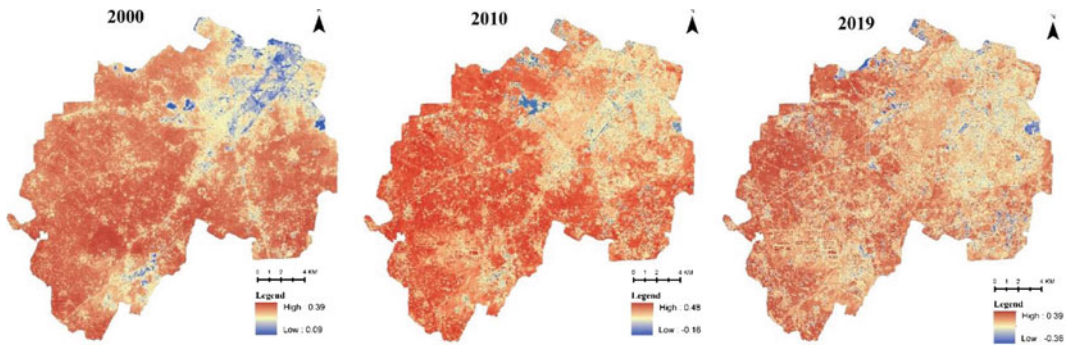
Fig. 19.7 NDVI image of Gurugram, 2000–2019

Fig. 19.8 NDBI image of Gurugram, 2000–2019

NDBI owing to densely built-up areas. Much large extent of the city has now moderate NDBI value owing to the extent of built-up reaching new zones also dry bare soil when gets heated displays similar NDBI values as built up.

For the years 2000, 2010 and 2019, a correlation study was done to establish the variability of LST with NDBI. As stated, earlier NDBI is an index that represents the degree of urbanization for any area, explained by the percentage of urban built-up. Scatter plots were also prepared for the representative years and a positive degree of correlation (medium and high) was established as given in Fig. 19.11. A positive correlation between LST and NDBI in a scatter plot means that the area which has a high NDBI value has a high LST value and an increase in NDBI causes an increase in LST. There is a change in the degree of correlation among the LST and NDBI over the years. In 2000, there is a moderate degree of positive correlation between NDBI and LST ($r2 = 0.418$). In 2010 a strong degree of correlation between NDBI and LST ($r2 = 0.569$) exists. In 2019, the correlation between LST and NDBI is moderate where $r2 = 0.457$. Different land use/land cover classes have different values of LST and NDVI and NDBI.

19.3.4 Association Between LULC Changes and LST

Cities like Gurugram are the main engines of urban growth alongside the national capital city.

With the rapid pace of urbanization, the city is bound to witness an increase in pollution, waste generation, changes in the vertical and horizontal surfaces. It is observed that the urban surfaces absorb a large number of radiations, unlike the traditional surface materials. Since these urban materials are generally water-resistant, the area they cover becomes impervious and gets heated up easily. This is the reason why surface temperatures in urban areas are higher. Similarly, the open, fallow land which is devoid of any plants or crops also shows high temperatures because of the low emissivity of dry soil.

Analysis of the historic temperature data of the city also validates our findings of LST. The summer temperatures have increased substantially over the years. The temperature data was downloaded from the gridded data, identified for Gurugram city from the IMD Web site.

City transects were drawn to analyze the temperature variation between two decades (Fig. 19.9). Examining the transects of the city in East to West and North to the south under the "Then and Now" criteria, it was concluded that various pockets of the city have seen a total transition in terms of LST. This can be attributed to the fact that LULC of the city saw a huge makeover following urban sprawl. From being a village in Haryana to the most sought-after place by MNCs for their head offices, the city has seen it all but at a cost that the environment, and thus, the health of its population is paying.
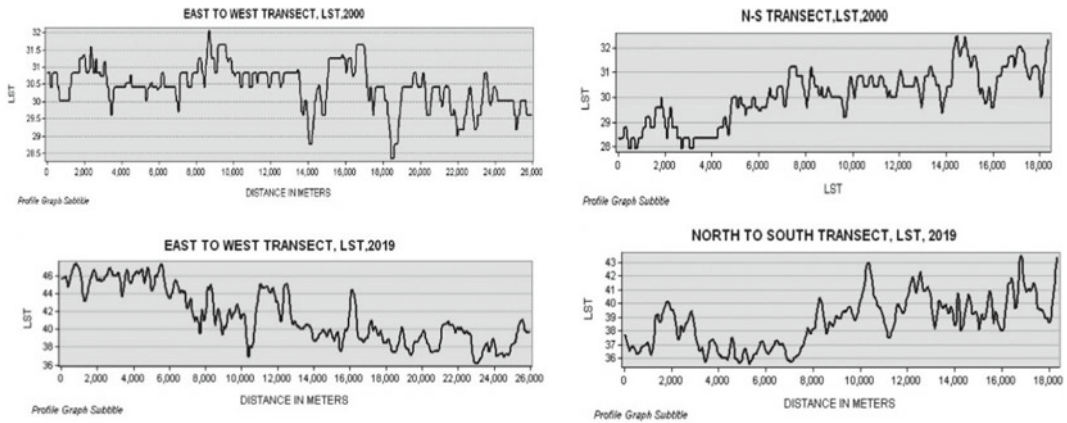
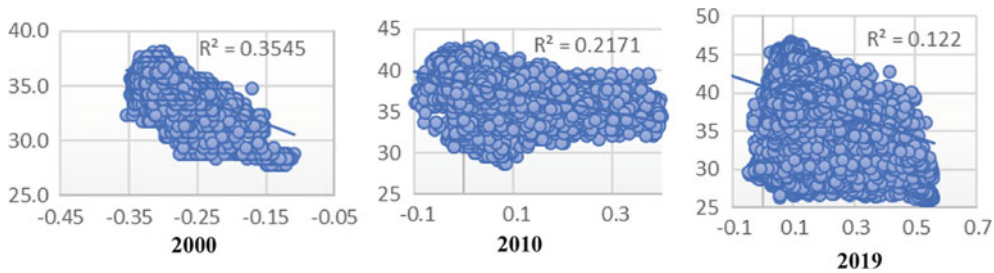**Fig. 19.9** City transects of Gurugram, 2000 and 2019

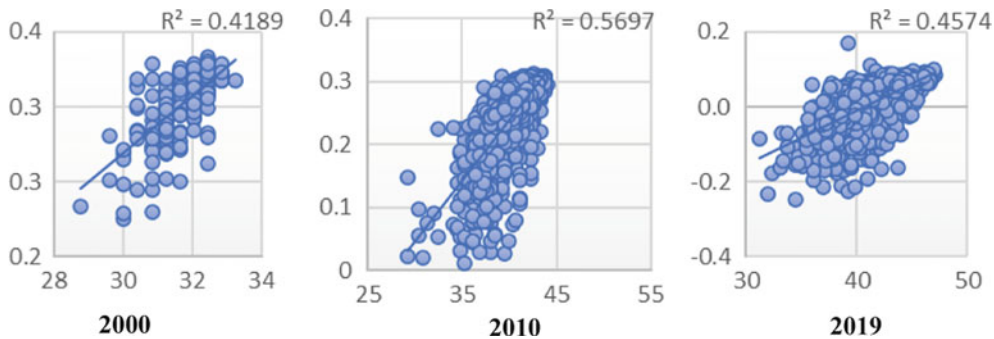**Fig. 19.10** Scatter plots for NDVI and LST

Fig. 19.11 Scatter plots for NDBI and LST

19.4   Conclusion

To date, Gurugram is witnessing the process of urbanization at an unprecedented rate, with further change in land use of agricultural land to residential land use. An example is coming up of new urban neighborhoods such as the New

Gurgaon area, with seamless connectivity to IGI airport and Dwarka expressway (Delhi). Development of infrastructure, stretching of administrative boundary, increasing residential density and addition of new SEZs are some steps taken by the administration to manage sprawl and upgrade civic amenities not to forget luring more investors. As a result, the influx of the immigrant

population does not stop and the pressure on residential sectors remains as it is. The present study confirms this trend that over the past two decades significant percent of urban built-up land has increased causing a decrease in farmland areas. Following this, permeable areas are sacrificed to propose impermeable areas causing noteworthy land cover changes in city boundaries. This leads to an increase in surface temperature and gives rise to UHI effects. As more and more farmlands get converted into commercial industrial or residential plots, the intensity of UHI will keep on increasing. Through this study, the authors using Landsat 5, 7 and 8 datasets established the presence of UHI in Gurugram city and also successfully established a relationship between LST and LULC. By studying the temporal and spatial variability of LST, it was concluded that the city is slowly warming up due to the change in LULC. The abundance of urban surface materials, reduction in permeable surfaces and change in land use pattern of the city are said to be the reason for such high variability in LST of the city.

References

Avdan U, Jovanovska G (2016) Algorithm for automated mapping of land surface using LAND-SAT 8 satellite data

Bharath HA, Chandan MC, Vinay S, Ramchandra TV (2018) Modelling urban dynamics in rapidly urbanising Indian cities. Egyptian J Remote Sens Space Sci 21(3):201–210

Borbora J, Das AK (2014) Summertime Urban Heat Island study for Guwahati City, India. Sustain Cities Soc 11:61–66. https://doi.org/10.1016/j.scs.2013.12.001

Chapman S, Watson JE, Salazar A, Thatcher M, McAlpine CA (2017) The impact of urbanization and climate change on urban temperatures: a systematic review. Landscape Ecol 32(10):1921–1935

Chen X, Zhao H, Li P, Yin Z (2006) Remote sensing image-based analysis of the relationship between urban heat island and land use / cover changes. 104:133–146. https://doi.org/10.1016/j.rse.2005.11.016s

Cowan T (2018) The Urban Village, Agrarian transformation, and rentier capitalism in Gurgaon India. Antipode 50(5):1244–1266. https://doi.org/10.1111/anti.12404

Du C, Ren H, Qin Q, Meng J, Zhao S (2015) A practical split-window algorithm for estimating land surface temperature from landsat 8 data. Remote Sens 7 (1):647–665. https://doi.org/10.3390/rs70100647

Erell E, Pearlmutter D, Boneh D, Kutiel PB (2014) Effect of high-albedo materials on pedestrian heat stress in urban street canyons. Urban Clim 10(P2):367–386. https://doi.org/10.1016/j.uclim.2013.10.005

Kriegler FJ, Malila WA, Nalepka RF, W R (1969) Preprocessing transformations and their effects on multi-spectral recognition. In: Proceedings of the sixth international symposium on remote sensing of environment, University of Michigan, Ann Arbor, MI, USA, pp 97–131

Golany GS (1996) Urban design morphology and thermal performance. Atmos Environ 30(3):455–465. https://doi.org/10.1016/1352-2310(95)00266-9

Grover A, Singh R (2015) Analysis of urban heat Island (UHI) in relation to normalized difference vegetation index (ndvi): a comparative study of Delhi and Mumbai. Environments 2(4):125–138. https://doi.org/10.3390/environments2020125

Gupta R (2012) Temporal and spatial variations of urban heat Island effect in Jaipur city using satellite data. Environ Urban ASIA 3(2):359–374. https://doi.org/10.1177/0975425312473232

Ihlen V, USGS (2019) Landsat 7 (L7) Data users handbook. USGS Landsat User Services 7(November):151. https://landsat.usgs.gov/sites/default/files/documents/LSDS-1927_L7_Data_Users_Handbook.pdf

Javed Mallick YK, Bharath BD (2008) Estimation of land surface temperature over Delhi using Landsat-7 ETM +. J Ind Geophys Union 12(3):131–140. http://www.igu.in/12-3/5javed.pdf

Johansson E (2006) Influence of urban geometry on outdoor thermal comfort in a hot dry climate: a study in Fez Morocco. Build Environ 41(10):1326–1338. https://doi.org/10.1016/j.buildenv.2005.05.022

Kotharkar, R., Ramesh, A., & Bagade, A. (2018). Urban Heat Island studies in South Asia: A critical review. Urban Climate, 24(October 2017), 1011–1026. https://doi.org/10.1016/j.uclim.2017.12.006

Kumari B, Tayyab M, Mallick J, Khan MF, Rahman A (2018) Satellite-driven land surface temperature (LST) using landsat 5, 7 (TM/ETM + SLC) and Landsat 8 (OLI / TIRS) Data and its association with built-up and green cover over Urban Delhi, India 7

Lall BA, Talwar S, Shetty S, Singh M (2014) Scoping study for policy initiatives to minimise urban heat island effect for low carbon urban growth. October 1–79. https://shaktifoundation.in/wp-content/uploads/2017/06/Scoping-Study-for-Policy-Initiatives-to-Minimize-Urban-Heat-Island-effect1.pdf

Mohan M, Kandya A, Battiprolu A (2011a) Urban heat island effect over national capital region of india: a study using the temperature trends. J Environ Protect 02(04):465–472. https://doi.org/10.4236/jep.2011a.24054

Mohan M, Kikegawa Y, Gurjar BR, Bhati S, Kandya A, Ogawa K (2012) Urban heat Island assessment for a Tropical Urban Airshed in India. Atmos Clim Sci 02 (02):127–138. https://doi.org/10.4236/acs.2012.22014

Mohan M, Pathan SK, Narendrareddy K, Kandya A, Pandey S (2011b) Dynamics of urbanization and its impact on land-use/land-cover: a case study of Megacity Delhi. J Environ Prot 02(09):1274–1283. https://doi.org/10.4236/jep.2011.29147

Montazeri M, Masoodian SA (2020) Tempo-spatial behavior of surface urban heat island of Isfahan metropolitan area. J Indian Soc Remote Sens 48:263–270

Oke TR, Mills G, Christen A, Voogt JA (2017) Urban climates. Cambridge University Press. https://doi.org/10.1017/9781139016476

Rahman A, Netzband M (2007) An assessment of urban environmental issues using remote sensing and GIS techniques an integrated approach: a case study: Delhi, India Atiqur. PRIPODE workshop on urban population, development, and environment dynamics in developing countries, June, 1–25

Rose L, Horrison E, Venkatachalam LJ (2011) Influence of built form on the thermal comfort of outdoor urban spaces. In: The 5th international conference of the international forum on urbanism (IFoU), Oke 1987

Shahfahad, Kumari B, Tayyab M, Ahmed IA, Baig MRI, Khan MF, Rahman A (2020) Longitudinal study of land surface temperature (LST) using mono- and split-window algorithms and its relationship with NDVI and NDBI over selected metro cities of India. Arabian J Geosci 13(19). https://doi.org/10.1007/s12517-020-06068-1

Shahfahad, Naikoo MW, Towfiqul Islam ARM, Mallick J, Rahman A (2022) Land use/land cover change and its impact on surface urban heat island and urban thermal comfort in a metropolitan city. Urban Clim 41 (November 2021):101052. https://doi.org/10.1016/j.uclim.2021.101052

Shahfahad, Rihan M, Naikoo MW, Ali MA, Usmani TM, Rahman A (2021) Urban heat island dynamics in response to land-use/land-cover change in the coastal City of Mumbai. J Indian Soc Remote Sens 49 (9):2227–2247. https://doi.org/10.1007/s12524-021-01394-7

Sobrino JA, Jiménez-Muñoz JC, Paolini L (2004) Land surface temperature retrieval from LANDSAT TM 5. Remote Sens Environ 90(4):434–440

Stone B, Rodgers MO (2001) Urban form and thermal efficiency: how the design of cities influences the urban heat island effect. J Am Planning Assoc 67(2):186–198. https://doi.org/10.1080/01944360108976228

Surawar M, Kotharkar R (2017) Assessment of urban heat island through remote sensing in Nagpur urban area using landsat 7 ETM+ satellite images. Int J Urban Civ Eng 11(7):868–874. http://waset.org/publications/10007350

Swerts E, Pumain D, Denis E (2014) The future of India's urbanization. Futures 56:43–52

Tetali S, Baird N, Klima K (2022) A multicity analysis of daytime surface urban heat islands in India and the US. Sustain Cities Soc 77:103568. https://doi.org/10.1016/j.scs.2021.103568

Tran H, Uchihama D, Ochi S, Yasuoka Y (2006) Assessment with satellite data of the urban heat island effects in Asian mega cities. Int J Appl Earth Obs Geoinf 8(1):34–48. https://doi.org/10.1016/j.jag.2005.05.003

Tuholske C, Caylor K, Funk C, Verdin A, Sweeney S, Grace K, Peterson P, Evans T (2021) Global urban population exposure to extreme heat. Proc Natl Acad Sci USA 118(41):1–9. https://doi.org/10.1073/pnas.2024792118

Veena K, Parammasivam KM, Venkatesh TN (2020) Urban heat island studies: current status in India and a comparison with the International studies. J Earth Syst Sci 129(1). https://doi.org/10.1007/s12040-020-1351-y

Verma R, Kumari K, Tiwary R (2009) Application of remote sensing and GIS technique for efficient urban planning in India. Geomatrix conference proceedings, March, 1–23. https://www.researchgate.net/publication/234097016%0AApplication

Voogt J (2009) Epa-how to measure a UHI. Epa Website 5463:236–240. https://doi.org/10.1007/978-3-642-00887-0_19

Voogt JA, Oke TR (1998) Effects of urban surface geometry on remotely-sensed surface temperature. Int J Remote Sens 19(5):895–920. https://doi.org/10.1080/014311698215784

Weng Q, Lu D, Schubring J (2004) Estimation of land surface temperature-vegetation abundance relationship for urban heat is- land studies. Remote Sens Environ 89(4):467–483

Weng Q (2014) A remote sensing—GIS evaluation of urban expansion and its impact on surface temperature in the Zhujiang Delta China. Int J Remote Sens 22 (10):1999–2014

Wenq Q (2001) A remote sensing-GIS evaluation of urban expansion and its impact on surface temperature in the Zhujiang Delta, southern China. Inter J Rem Sens 22(10):1999–2014

Zha Y, Gao J, Ni S (2003) Use of normalized difference built-up index in automatically mapping urban areas from TM imagery. Int J Remote Sens 24(3):583–594. https://doi.org/10.1080/01431160304987

Zhang J, Wang Y (2008) Study of the relationships between the spatial extent of surface urban heat islands and urban characteristic factors based on landsat ETM+data, 7453–7468. https://doi.org/10.3390/s8117453

Zhou D, Zhao S, Liu S, Zhang L, Zhu C (2014) Surface urban heat island in China's 32 major cities: spatial patterns and drivers. Remote Sens Environ 152:51–61. https://doi.org/10.1016/J.RSE.2014.05.017

Identifying the Flood Hazard Zones in Urban Area Using Flood Hazard Index (FHI)—A Case of Capital City of India

Nitin Rathi, Susanta Mahato,
Deep Narayan Pandey,
and Pawan K. Joshi

Abstract

Floods are one of the most destructive natural catastrophes due to the extensive damage to property, infrastructure, and human lives. It is difficult to forecast which areas will be flooded due to the dynamic and intricate nature of floods. As a result, flood hazard zones can be identified early and flood disasters can be managed more effectively. The flood extent map of the Yamuna River flood in Delhi in 2010 was utilized to determine the inundated area in this study. In Delhi, the Flood Hazard Index (FHI) was also employed in a multi-criteria decision-making strategy to spatially demarcate the distinct flood zones. To establish the relationship between flood inundation and influential factors, multicollinearity diagnostics test was used. Receiver Operating Characteristic Curve (ROC) was used to validate the flood hazard zones model. The entire inundated area was 5.7% (about 79.85 km^2), with agriculture being the most affected by the flood, with a 63% area under flood. According to the flood hazard map, 8.75% of Delhi is in a very high flood hazard zone. Built-up regions made up 39.66% of the zone with a very high flood threat, while agricultural made up 32.9%. The approach and solution-oriented results presented in this chapter will aid regional and municipal authorities and policymakers in lowering flood risks and developing appropriate mitigation measures to prevent potential harm.

N. Rathi
Centre for the Study of Regional Development (CSRD), Jawaharlal Nehru University, New Delhi 110 067, India
e-mail: sudhadevinitin@gmail.com

S. Mahato · D. N. Pandey · P. K. Joshi (✉)
Special Centre for Disaster Research (SCDR), Jawaharlal Nehru University, New Delhi 110 067, India
e-mail: pkjoshi27@hotmail.com; pkjoshi@mail.jnu.ac.in

S. Mahato
e-mail: susantamahato@jnu.ac.in

D. N. Pandey
e-mail: deepudai@gmail.com

P. K. Joshi
School of Environmental Sciences (SES), Jawaharlal Nehru University, New Delhi 110 067, India

20.1 Introduction

Floods are one of the most devastating natural disasters on the planet, causing infrastructure damage, including critical public infrastructure,

and often resulting in fatalities. It is a recurring event in the areas occupied for agriculture and human settlements. Because of the abundance of water, all civilizations thrived near rivers' banks. However, when the same water in large quantities inundates the normally dry inhabited area, resulting in the loss of life and property, it is referred to as a 'flood' disaster. According to the International Charter for Space and Major Disasters, flooding on the earth's surface is the most common hazard type and is often natural in origin; however, it becomes a disaster because of human activities. As per the World Health Organization (WHO), these occur when an overflow of water resulting from heavy rainfall, rapid snowmelt, or a storm surge from a cyclone, among other things, submerses land that is usually dry. The floods can be broadly categorized as flash floods (rapid and excessive rainfall that raises water heights quickly, and rivers, streams, channels, or roads may be overtaken), river floods (consistent rain or snowmelt forces a river to exceed capacity), and coastal floods (storm surges associated with tropical cyclones and/or tsunami). Among these, river floods are the ones that may last for days or weeks, having consistent and long-term challenges that could be studied, documented, and managed. These floods are increasing in frequency and intensity because of the extreme precipitation as a result of climate change.

The majority of flood problems occur in developing countries as a result of a lack of infrastructure, poor management, low income, and the lack of advanced early warning systems (Ghent 2013; Jonkman 2005). Flood risk is a measure of vulnerability to flooding-related damage and loss that is commonly calculated by considering physio-climatic, hydrodynamic, economic, social, and ecological factors (Dash and Sar 2020). Calculating risk is a difficult task due to the involvement of numerous factors in the process. However, the combination of geographical information system (GIS) and multi-criteria decision-making (MCDM) is successful for natural hazard analysis, (Rashed and Weeks 2003; Fernández and Lutz 2010). The MCDM Analytic Hierarchy Process (AHP) method is a

structured and very flexible approach to solving complex decision-making problems involving multiple criteria or parameters. AHP is a straightforward and well-proven method for resolving multi-criteria decision-making issues to identify Flood Hazard Index (FHI), which can be used to create flood hazard zone map. Flood hazard zone refers to the geographical area that can be inundated by flood events and has a high possibility of being equalled and exceeded at any given time and space. In this context, the Flood Hazard Index (FHI) is an indicator used to explain flood risk hotspots through a comparative analysis of different intensities or frequencies of the given flood in a specific geographical setting and at a given time. Currently, the FHI method is used in the majority of flood hazard zonation and assessment studies (Das 2018; Dash and Sar 2020; Kabenge et al. 2017; Kazakis et al. 2015; Papaioannou et al. 2015). A validation process is generally carried out after comparing the FHI results to an index-based flood inundation map to ensure that the FHI results are the probable representation of flood hazard in space and time. Previous research has found that using a spatial map of historical floods to validate AHP results is a better option (Dash and Sar 2020). Several studies were done on Indian cities regarding flood hazard/risk zonation (Table 20.1).

Along with the GIS environment which is used for assessment and integration of parameters, remote sensing inputs are taken for spatial flood mapping and collection of relevant parameters for such analysis. Though Synthetic Aperture Radar (SAR) data is an excellent source for flood mapping (in the cloudy environment), appropriate selection of optical remote sensing data often provides opportunities for such mapping. Flooding may also occur due to excessive rainfall in the upper hilly areas (upstream), and in such scenarios, optical remote sensing data stands out to be efficient and effective. In the tropical countries like India, every year during the monsoon season, low-lying areas near the river are inundated resulting in flood situations in the immediate catchment. This chapter focuses on the flood hazard zonation mapping of Delhi, India's capital city. This is accomplished by

Table 20.1 Literature on urban flood risk and zoning in Indian cities

References	Study area	Objective	Findings
Sarmah et al. (2020)	Guwahati	Urban flood hazard map and human vulnerability index (HVI) of Guwahati are being developed	Flooding threatens 38.70% of the Guwahati municipal area
Saha and Agrawal (2020)	Prayagraj	Calculating the flood inventory and assessing the impact of flooding on different land use classes	According to the flood risk map, 701.71 km^2 (12.80%) of the study area is at high danger, while 1273 km^2 (23.22.8%) is at moderate risk
Mundhe (2019)	Pune	Using multi-criteria decision-making tools, identify flood-prone locations and develop a vulnerability zonation	Flood-prone zones were found to cover 5% (12.50 km^2) of the total area, indicating a high flood-risk zone
Dhiman et al. (2019)	Mumbai, Kolkata, Chennai, Surat	After delineating hazard prone zones, city-scale mitigation and adaptation plans were developed	In consideration of anthropogenic flood threats, Mumbai, followed by Surat, is the most susceptible of the four cities
Singh et al. (2018)	Bangalore	Road network vulnerability assessment from urban flood risk map	The very high flood risk category affects 5.8–9.6% of total road length
Zope et al. (2017)	Poisar River basin, Mumbai	The flood plain and hazard map was developed using hydrological and hydraulic models, using GIS and remote sensing	The major reason for the rise in flood peak discharge and reduction in lag time is the influence of urbanization
Sowmya et al. (2015)	Cochin	To identify flood extent areas and urban flood vulnerable zonation	High and very high vulnerable zones affected 8.6% of the city's area
Singh and Singh (2011)	Noida	To identify the flood-affected areas in Noida city	Severely flood affected areas are in eastern and western sections and moderately affected forest area

combining actual mapping of the spatial extent of Yamuna River (during the Flood event of 2010) using optical remote sensing data with the creation of a flood hazard zone map utilizing FHI along with the combination of MCDM/AHP in a GIS environment. During times of high precipitation, the city also experiences urban flooding throughout its road network; yet, it is still important to map, model, and communicate the flooding that occurs along the Yamuna basin.

20.2 Study Area

This chapter focuses on the capital city of India, Delhi (Fig. 20.1). It is located in the northern part of India and shares borders with Haryana and Uttar Pradesh. The longitude and latitude of Delhi are respectively $77°13'$ and $28°38'$. According to the Census of India (2011), the total population of Delhi is 16753235 (approx.

16 million), and its area is 1484 km^2 (Census of India 2011). The city is situated on the right bank of Yamuna River, and Gangetic Plain lies in its north and east, Aravalli Hills in south and Thar Desert in the west (Kumar et al. 2019). Elevation in Delhi varies from 137 to 325 m, and its average elevation is 204 m. In fact, Yamuna River flows through Delhi clipping the eastern part of city. The climate of Delhi is semi-arid, and temperature varies in summer from 27.6 to 44.2 °C and in winter from 3.5 to 22.2 °C (Kumar et al. 2019).

20.3 Materials and Methods

The chapter demonstrates the utility of secondary data collected from a variety of sources. Thematic layers for the study 'Flood Hazard Zoning (FHZ)' were created using satellite remote sensing images and a satellite-driven digital elevation
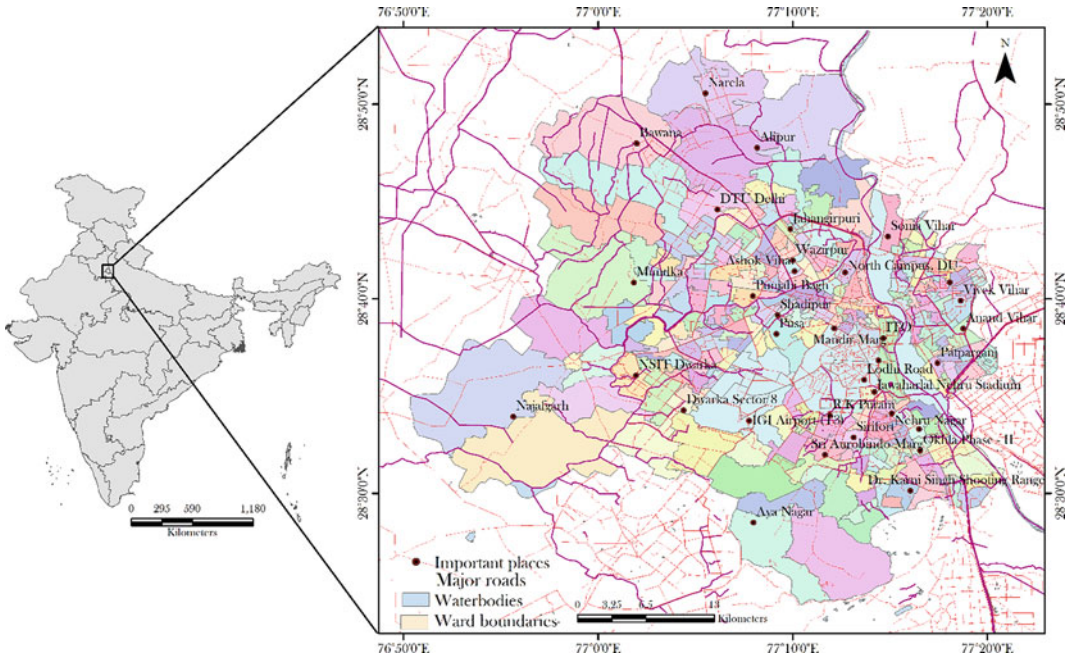
Fig. 20.1 Study area

model (DEM). The weights to the selected spatial layers of different parameters for FHZ were calculated using the AHP method of MCDM. Using ArcGIS, the spatial layers of the selected parameters were created and categorized into five categories to give each parameter a specific rating. On the basis of Jenks' natural break clustering technique, the values of all parameters were divided into five groups (Jenks 1967). Only quantitative parameters could be classified as natural breaks, so qualitative parameters were categorized based on their influence on flooding, and ratings were assigned to the manually defined classes based on their contribution to flooding.

20.3.1 Flood Extent Mapping

Landsat-5 Collection 2 Level-2 data of September 26, 2010, (one of the known flooding incidence dates) was used to map the pre-flood extent and the peak flood situation. The Landsat-5 data of October 22, 2008, was used to map the Yamuna River's normal extent. The two date

mapping was compared before and after flooding and used to determine Yamuna River's normal spatial extent in Delhi. The water and non-water classes were separated using the Modified Normalized Difference Water Index (MNDWI). MNDWI is an improved version of McFeeters' 1996 Normalized Difference Water Index (NDWI) (Xu 2006). Both the NDWI and MNDWI use multiple bands, and a band ratio approach helps in separating the water class from the other classes. However, NDWI is less accurate in comparison to MNDWI in urban areas or where the built-up is heavily mixed with water. Thus, in terms of overall accuracy for the urbanized locations like Delhi, MNDWI is better for studying floods because it easily reduces non-water pixels while increasing water pixels when compared to other indices. As a result, only one index was used to determine the flood's spatial extent (Du et al. 2016; Gautam et al. 2015; Sun et al. 2012; Szabó et al. 2016). In the ArcGIS software, the green band and the Shortwave Infrared (SWIR) band were used to calculate MNDWI (Gautam et al. 2015; Xu 2006).

$$\text{MNDWI} = \frac{\text{GREEN} - \text{SWIR}}{\text{GREEN} + \text{SWIR}} \qquad (20.1)$$

where GREEN and SWIR refer to data collected in green (0.52–0.60 μm) and Shortwave Infrared (1.55–1.75 μm) wavelengths. MNDWI values were categorized into two classes and threshold value manually defined zero, whereas the potential range of MNDWI is between −1 and 1 (Sun et al. 2012). The pixel values below zero denote the built-up class including other classes, and positives values show the water class. Finally, MNDWI was classified as a binary raster layer with water and non-water classes.

20.3.2   Identification of Flood Causative Parameters

On the basis of physiographic, hydrologic, and geological attributes, eight parameters were identified to create the flood hazard zone map. The most important aspect of the MCDA method is the parameter or criteria selection, because the entire result is dependent on the influence of these parameters. Based on previous studies that have been conducted to create a flood hazard zone map using AHP, it is concluded that they have all chosen criteria that correspond to local geographical settings that influence the physical process of flood mechanism (Das 2018; Dash and Sar 2020; Kabenge et al. 2017; Kazakis et al. 2015; Papaioannou et al. 2015). The eight parameters chosen are flow accumulation, draining capacity, elevation, ground water depth, slope, potential runoff coefficient, land use, and geology. The description of each parameter is given in Table 20.2.

The density of the drainage network in the study area influences flow accumulation, which is an important factor in influencing flooding. The spatial layer of flow accumulation was created using Advanced Spaceborne Thermal Emission and Reflection Radiometer (ASTER) DEM data with a spatial resolution of 30 m. Drainage capacity is determined by the drainage network. The drainage density raster layer was created using the drainage network vector layer. The drainage network vector layer was downloaded for free from OpenStreetMap, and the watershed layer was created using the Delhi vector layer (downloaded from IGIS maps https://map.igismap.com/). Elevation is another important parameter that affects the flow of water, drainage capacity, and runoff coefficient, among other things. The ASTER Global DEM (GDEM) datasets were used to create a raster layer of elevation zones, which were then

Table 20.2   List of parameters used in the analysis and their description

Parameter	Description
Flow accumulation	A cumulative count of the number of pixels that naturally drain into outlets (unitless)
Draining capacity	The amount of liquid that can be discharged at the open channel end (categorical)
Elevation	Height above the surface of the ground, or an area that is higher than the surrounding land (metres)
Ground water depth	The depth or elevation above or below sea level at which the surface of ground water stands (below the surface in metre)
Slope	describing steepness of the earth surface (degree)
Potential runoff coefficient	The portion of rain that becomes surface runoff during a rain even (unitless)
Land use	The human use of land (unitless)
Geology	Distribution of rock and stone types (unitless)

classified into five zones using Jenks' Natural Break classification techniques (Jenks 1967). The water-holding capacity of the land and the rate of infiltration were determined by ground water depth. To achieve maximum accuracy, the ground water depth map was created during the pre-monsoon period (Dash and Sar 2020). The ground water depth map raster layer was created by digitizing and reclassifying a map published in the Central Ground Water Board (CGWB) of India's annual report (Central Ground Water Board 2015; Shekhar et al. 2009). The flow of water, drainage capacity, and infiltration rate were all controlled by the slope. The thematic layer of slope map was created using the ASTER GDEM (30 m spatial resolution). The slope value was converted to percentage and divided into five categories. Through the intersection of vector layers of land use, slope, and soil texture, the thematic layer of potential runoff coefficient was created. Soil texture (Mallick et al. 2015) and land use map (Sharma et al. 2020) were taken from previous studies and converted into five classes before being reclassified and converted into a vector layer for overlaying. Values for runoff coefficients were manually entered into the intersected map from table (Liu and Smedt 2004; Mahmoud et al. 2014; Merz et al. 2006). The land use spatial layer was derived from previous research (Sharma et al. 2020). The geology thematic layer was created by digitizing a published map by the Geological Survey of India (Central Ground Water Board 2015; Shekhar et al. 2009). The flood conditioning parameters were chosen using a multicollinearity analysis (Table 20.3). The parameters were deduced using a VIF less than 2 threshold in this study.

20.3.3 Rating the Values of Different Parameters

The values of spatial layers were divided into five categories for rating purposes. Each geological layer has only four units, which are divided into four classes. The maximum slope rating is 10, and the minimum runoff rating is 2 (Table 20.4). A rating was assigned based on the influence of qualitative parameters on flooding (Dash and Sar 2020).

20.3.4 Expert Advice for Parameters Weights

The weights of all parameters were calculated using the AHP method. On the advice of concerned experts in this field, a pairwise comparison matrix for the weights was created after comparing these parameters to each other. The effectiveness of AHP methods is dependent on the experts' understanding and knowledge (Dash and Sar 2020). For the AHP matrix table, all of these parameters were ranked in order of increasing importance for flood hazard zoning. On a scale of 1–9, parameters were preferred, with 1 being equally preferred and 9 being extremely preferred (Saaty 2013; Saaty and Wind 1980) (Table 20.5).

20.3.5 Consistency Check

As AHP is based on the opinions of various experts, the most important step in validating this method is to check its consistency (Eq. 20.1). The consistency check is crucial for proving that

Table 20.3 Selection of the parameters for flood hazard zones determination using multicollinearity test

Parameters	Flow accumulation	Draining capability	Elevation	Ground water depth	Slope	Runoff coefficient	Land use	Geology
Multicollinearity test (VIF)	1.57	1.04	1.63	1.88	1.97	1.24	1.04	1.15

Table 20.4 AHP ranking of parameters

Parameters	FA	DC	EL	GWD	SL	RC	LU	GEO
FA	1	2	3	4	5	7	7	9
DC	1/2	1	1	3	4	6	7	8
EL	1/3	1	1	2	4	5	6	6
GWD	1/4	1/3	1/2	1	3	4	5	6
SL	1/5	1/4	1/4	1/3	1	2	4	5
RC	1/7	1/6	1/5	1/4	1/2	1	3	4
LU	1/7	1/7	1/6	1/5	1/4	1/3	1	2
GEO	1/9	1/8	1/6	1/6	1/5	1/4	1/2	1

FA—Flow accumulation; DC—Draining capability; EL—Elevation; GWD—Ground water depth; SL—Slope; RC—Runoff coefficient; LU—Land use; GE—Geology

judgments are correct or acceptable; if the consistency ratio (CR) value (Eq. 20.2) is less than 0.1, the judgments are acceptable (Saaty 2013).

$$\text{Consistency Ratio}(CR) = \frac{\text{Consistency Index (CI)}}{\text{Random Index (RI)}}$$

$$(20.1)$$

$$CI = \frac{\lambda_{\max} - n}{n - 1} \qquad (20.2)$$

where $\lambda_{\max}$ is the average priority vector, n is number of parameters, and the value of Random Index (RI) has already been defined in the Random Index table by Saaty. Here, $\lambda_{\max} = 8.506$, $n = 8$, CI = 0.072, RI = 1.41 (mentioned by Saaty 1987), and CR = 0.051 were calculated after all mathematical calculations. The AHP method is thus validated and authentic in the case of study, as evidenced by the value of CR < 0.1.

20.3.6 Flood Hazard Zonation/Zoning

To spatially demarcate the flood hazard zones in Delhi, FHI was used (Eq. 20.3). The GHI uses weights of selected parameters as an input to generate flood hazard zone map, so the AHP method of MCDA was used to solve this problem. In some previous studies, the Flood Hazard Index method was used to validate the results obtained from satellite images and the AHP method based on MCDA (Das 2018; Dash and

Sar 2020; Kabenge et al. 2017; Kazakis et al. 2015; Papaioannou et al. 2015).

$$FHI = \sum_{i=1}^{n} r_i \times w_i \qquad (20.3)$$

where r_i = rating of the parameter in each point, w_i = weight of each parameter, n = number of the criteria.

20.4 Results

20.4.1 Flood-Causative Parameters

All of the parameters were categorized into five risk zones based on a scale of 2–10, with 2 being the least vulnerable to flooding and 10 being the most vulnerable. The following are the outcomes of all spatial layers.

Flow Accumulation

The water concentration is depicted on the thematic map of flow accumulation. One of the most important parameters for displaying the pattern of water accumulation is flow accumulation (Mahmoud and Gan 2018). The flow accumulation in the study area was calculated for the National Capital Region (NCR) because it provides more accuracy in water concentration than the Delhi subset. Between 0 and 1,506,163, the flow accumulation values range. In Fig. 20.2a, pixels with values in dark green and green colour

Table 20.5 Subclasses of criteria, rating, and weights of the parameters

Parameters	Class	Rating	Weights
Flow accumulation	584,747–1,506,163 425,271–584,746 230,355–425,270 59,066–230,354 0–59,065	10 8 6 4 2	0.324
Draining capability E = elevation; D = drainage Density	Very low (E) to very low to moderate (D) Low (E) to low to moderate (D) Moderate (E) to low to high (D) High (E) to very low to high (D) Very high (E) to low to very high (D)	10 8 6 4 2	0.210
Elevation (m)	137–206 206–220 220–239 239–265 265–325	10 8 6 4 2	0.176
Ground water depth (m)	< 5 5–10 10–20 20–40 > 40	10 8 6 4 2	0.119
Slope (%)	0–6 7–11 12–18 19–29 30–96	10 8 6 4 2	0.071
Runoff coefficient	0.83–1 0.58–0.82 0.43–0.57 0.28–0.42 0.03–0.27	10 8 6 4 2	0.049
Land use	Water Built-up Agriculture Barren Forest	10 8 6 4 2	0.029
Geology	Delhi Supergroup Aeolian deposit Older alluvium Newer alluvium	8 6 4 2	0.021

indicate areas with low water concentrations, while pixels with red and orange colour indicate areas with higher water concentrations.

Draining Capability

The presence of fewer drains, a poor, outdated, and old drainage system, and the presence of fewer drains in urban areas are rapidly increasing the problem of flooding and water logging. Drainage capacity is an important factor in flood control (Ouma and Tateishi 2014). Both drainage density and elevation played a significant role in determining the draining capability range. The findings show that areas with low to moderate elevation and low to high drainage density have a high flood risk. Values in red pixels represent
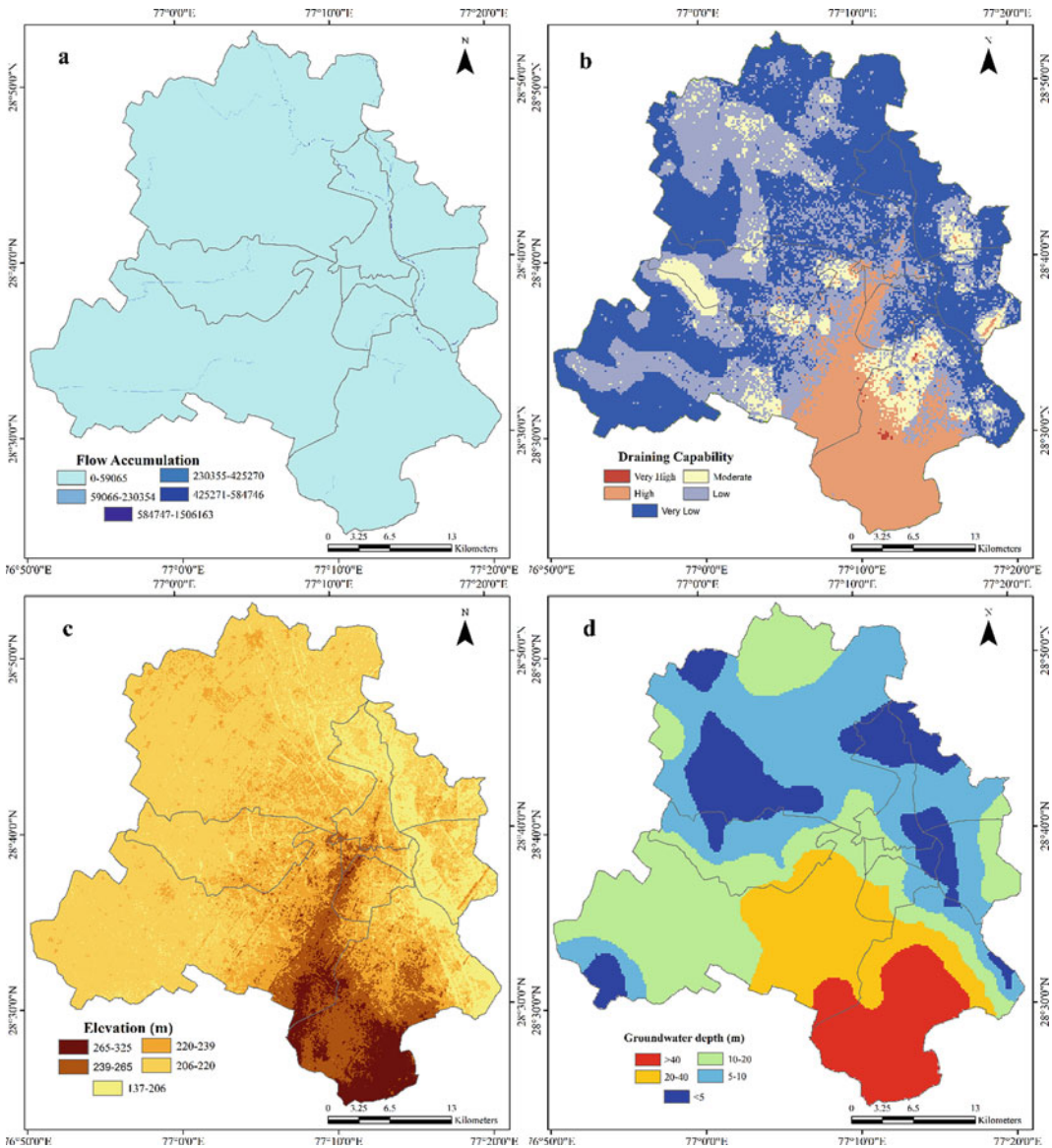
Fig. 20.2 Flood-causative parameters (**a**—Flow accumulation, **b**—Draining capability, **c**—Elevation, **d**—Ground water depth)

low draining capability, while values in dark green colour represent high draining capability with very high elevation values in Fig. 20.2b.

Elevation

It is one of the most important parameters for flood hazard zoning because it influences other parameters such as slope, runoff coefficient, and so on. In flood plains, elevation determines flood susceptibility, with higher elevations indicating less vulnerability and lower elevations indicating greater vulnerability. Low-lying areas are more susceptible to both water logging and river flooding. The red pixels in the study area Fig. 20.2c indicate an area near the Yamuna River with low elevation values, indicating a high risk of flooding and inundation. In the flooding, the elevation data is divided into five

classes in decreasing order of elevation and given a value ranging from 2 (lower elevation means maximum influence) to 10 (higher elevation means minimum influence).

Ground Water Depth

The depth of water below the ground surface is referred to as ground water depth. This parameter is strongly linked to areas where flooding is a common occurrence due to rainfall. If the ground water depth is less at any palace, there is a greater risk of flooding and water logging because the area's ability to hold water through porosity is reduced, and it will be saturated in less time than areas with greater ground water depth. Because areas with shallower ground water depths became saturated during the pre-monsoon rains and lack the capacity to hold more water, infiltration rates are lower and runoff is higher in these areas. The study assigns a score of 10 to the category of water depths less than 5 m and a score of 2 to the category of water depths greater than 40 m. It is possible to conclude that the lower the ground water depth, the greater the vulnerability, and vice versa (Fig. 20.2d).

Slope

The study area's flood susceptibility is defined by the slope per cent. Water will flow more quickly, and there will be fewer chances of water logging if the slope percentage is higher, and vice versa if the slope percentage is lower. The ability to drain is also excellent in high-slope areas. Based on previous research, it is possible to conclude that low surface slopes and low elevated zones are particularly vulnerable to flooding (Das et al. 2021; Dash and Sar 2020; Mahmoud and Gan 2018). Because of the lower percentage of slope, plain areas are more vulnerable to flooding and inundation. Figure 20.2 shows areas with low elevation and greater flooding influence as red pixels with high rating values. The results in Fig. 20.3a show that approximately 40% of the total slope is less than 20%.

Runoff Coefficient

The total depth of runoff divided by the total depth of rainfall is the ratio. Rainfall is one of the main causes of flooding, so runoff is an important parameter to consider when estimating flooding. "For estimating flood occurrences from rainfall frequencies, runoff coefficients can be used in event-based derived flood frequency models" (Mahmoud et al. 2014). The runoff coefficient is determined by the study area's soil type, slope, and land use. The runoff coefficient ranges from 0 (the least influence) to 1 (the most influence) (maximum influence). The high hazard zone for flooding is depicted in Fig. 20.3b by the red value.

Land Use/Cover

Land use is one of the most important factors that affects a region's hydrological processes (Fig. 20.3c). For example, forest cover increases infiltration and lowers runoff coefficient. Because of the low infiltration rate and high flow of water, the area covered by water and the built-up categories are more prone to flooding. Water received the highest rating in the study area due to its high flow and runoff coefficient, while forest and plantation received the lowest rating (2).

Geology

The control of the hydrological process is also aided by lithological structure. There are four major lithological groups in Delhi. Each group was given a rating from 2 (minimum) to 10 (maximum) influence in flooding based on porosity and infiltration capacity. The higher the values indicate the greater the flood hazard. In the study area, there is no such lithological group as shown in Fig. 20.3d that has a significant impact on flooding in Delhi.

20.4.2 Flood Extent Mapping

Flood extent mapping was done using satellite data from Landsat-5 C2 L2, which was acquired on September 26, 2010. Water and non-water classes have been calculated from MNDWI with different threshold values for pre- and post-flooding situations in Fig. 20.4. These inundation maps show the extent of the Yamuna River and the flood-prone areas in Delhi in comparison.
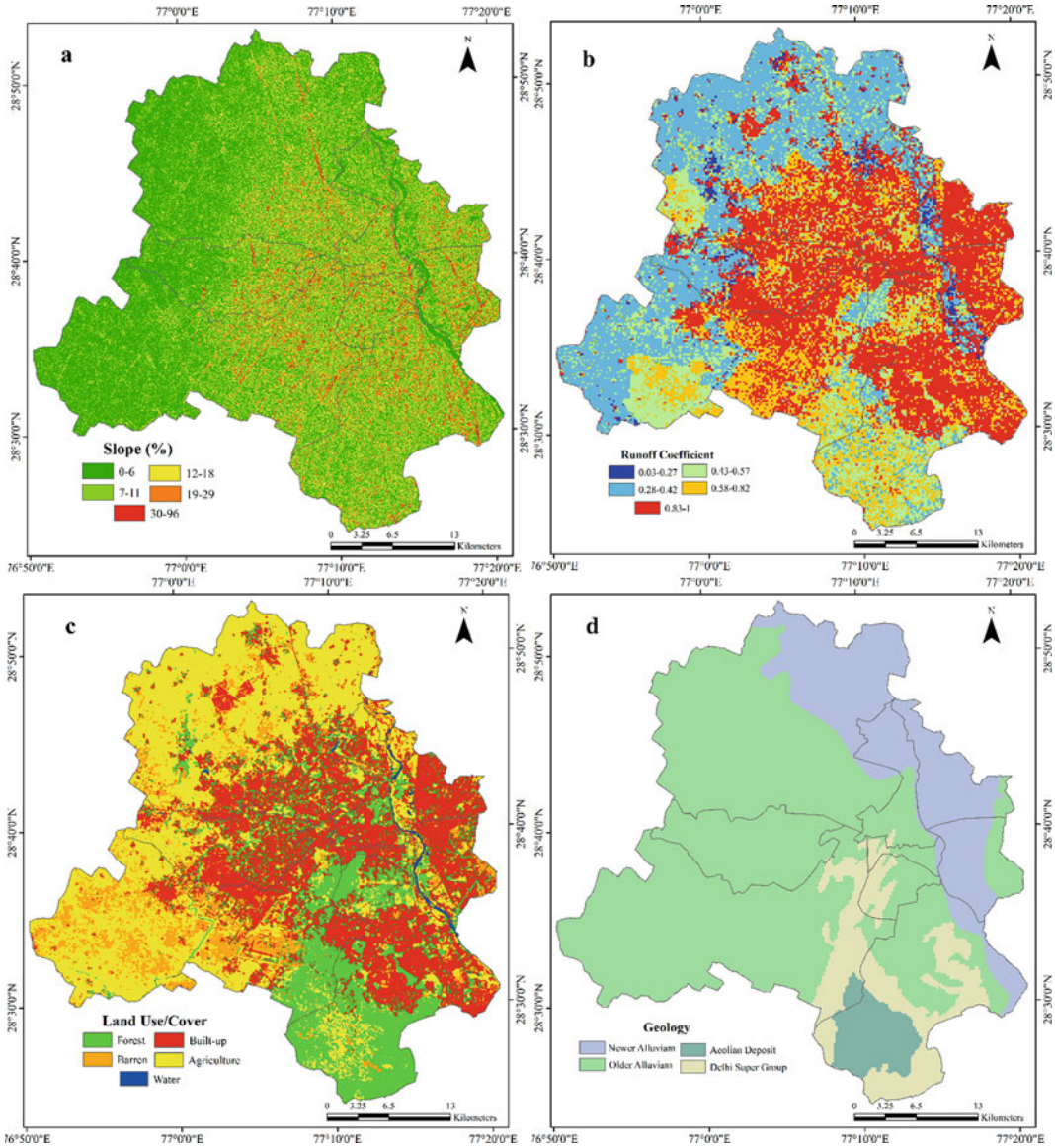
Fig. 20.3 Flood causative parameters (**a**—Slope, **b**—Runoff coefficient, **c**—Land use/cover, **d**—Geology)

Before the flood, the area of water bodies was 20.32 km^2, which is the normal size of water bodies. The area of water bodies or inundating area calculated on the basis of satellite image during the flood (on September 26, 2010) was 79.85 km^2. The total area inundated was calculated to be 59.53 km^2 (excluding the normal extent of water bodies). In this net inundated area, agricultural land was 62.89%, built-up (24.54%), forest (19.38%), and barren land (8.83%).

20.4.3 Flood Hazard Index

The Flood Hazard Index was calculated by multiplying the eight parameters listed in Table (20.3) by their weights and applying the Flood Hazard Index formula. The flood hazard map was divided into five categories: very low, low, moderate, high, and extremely high. About 8.75% of the study area is in the very high hazard zone, 13.18% in the high hazard zone, 33.82% in
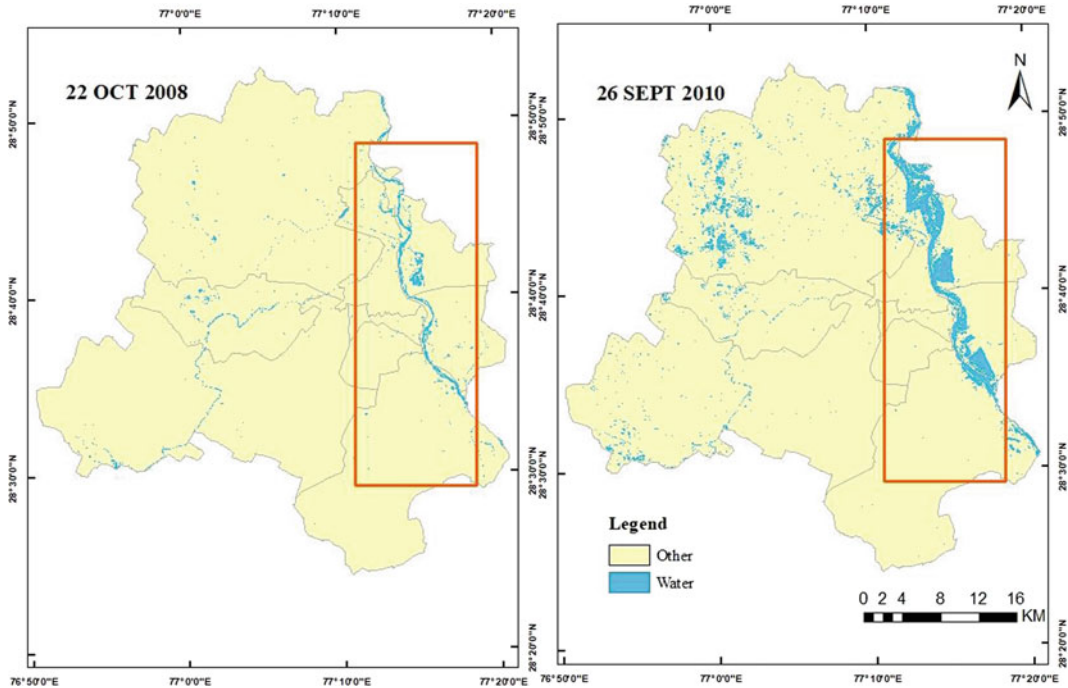
Fig. 20.4 Delhi before (2008) and during flood of 2010

the moderate hazard zone, 22.31% in the low hazard zone, and 21.92% in the very low hazard zone. Approximately 79% of the area is outside of the high and very high flood hazard zones, indicating that flooding is not a major concern in Delhi. According to analysis of areas with very high flood hazard, approximately 39.66% of the area is built-up, 32.91% is agriculture, 12.03% is forest, and 10.73% is barren land. The built-up category is the most vulnerable in all zones, according to the results.

20.4.4 Validation

Validation is an important part of spatial analysis and modelling so as in order to prove the validity of the MCDA's AHP method, which was used to create a flood hazard zone map of Delhi. Validation was carried out using a flood map of Delhi that was created using satellite data from the flood of September 26, 2010. To validate the model, the area under the curve (AUC) of the Receiver Operating Characteristics Curve

(ROC) was calculated and validates flood hazard zone models with an AUC of 0.872 (Fig. 20.5). According to the findings, approximately 66% of the inundation area falls within the very high flood hazard zone (Fig. 20.6). The comparison of land use on both maps reveals that agriculture is the most vulnerable class on both maps. In the very high flood hazard zone and inundation map, the share of forest and water class is respectively 21.25 km^2 and 18.90 km^2, indicating a similarity in both maps.

20.5 Discussion

The flood extent demarcated and flood hazard zones in the city provide accurate and reliable data. The study concluded that the AHP method of MCDA is an important tool for integrating multiple parameters for decision-making after validation of the flood hazard zones mapped using actual flood distribution. The tool is extremely useful for solving complex decision-making problems involving multiple parameters.
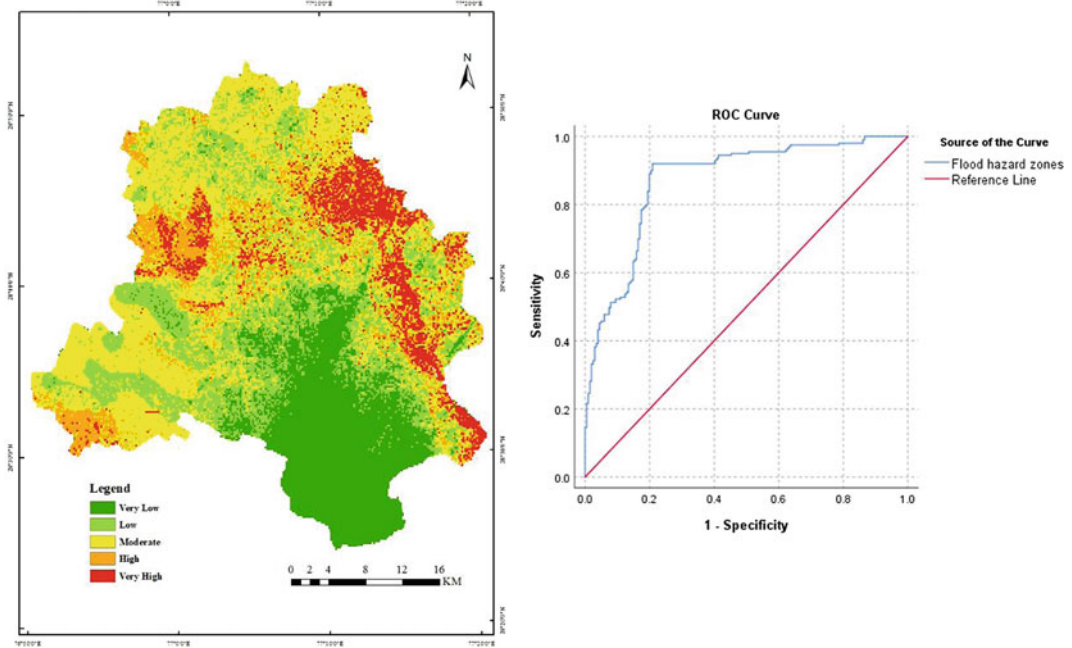
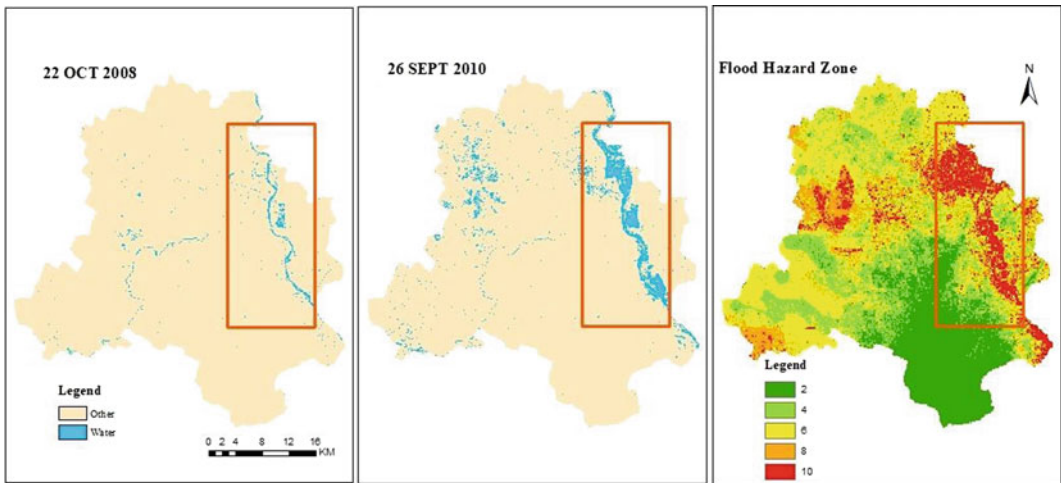**Fig. 20.5** Flood hazard zones in NCT Delhi and the ROC Curve

Fig. 20.6 Delhi before flood, during flood, and flood hazard zones

The index-based approach is reported to be suitable for understanding flood susceptibility and vulnerability in this study (Dash and Sar 2020). According to Dash (2020) and Kazakis, the most important parameters to assess flood vulnerability are flow accumulation and draining capability (2015). Because the Yamuna River flows through the study area and the area has low elevation and slope, the final flood hazard zone map shows a very high flood hazard zone in the eastern and northeastern parts of the study area. Preparedness and mitigation plan for areas in very high and high flood hazard zones should be developed based on the findings of this study.
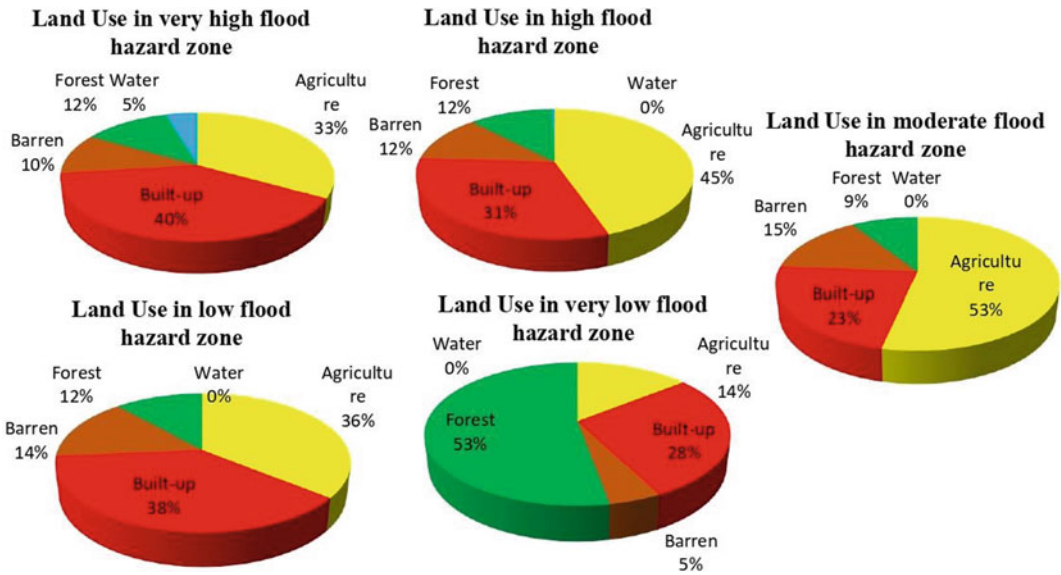
Fig. 20.7 Shows the proportion of land use in different flood hazard zones

The study also shows how much land is used for different purposes in each zone. Such studies can be carried out on a local scale for flood hazard mapping. Such data is extremely useful for decision-makers in planning and implementing mitigation measures. As a result, FHI can help vulnerable communities reduce flood damage and build resilience (Kabenge et al. 2017).

The study is based on the AHP method, which completely relies on expert advice to assign values to different parameters of the comparison matrix, ensuring that the final results are similar to their perceptions of those parameters. Because the AHP-based method has some qualitative parameters, rating them based on their characteristics proved less accurate when compared to quantitative parameters in the study.

The use of remote sensing data in this study yielded positive results, but it also has some drawbacks, such as the fact that remote sensing data was not as accurate prior to 1980. As a result, remote sensing limits the study and mapping of historical floods. Another limitation is that the spatial resolution of free and openly available satellite imagery is medium to coarse. However, such research necessitates data with a very high spatial resolution. Another significant

limitation was the lack of satellite data during the flood peak, which prevented researchers from measuring the full extent of flooding and inundation. Remote sensing data was used in the study to prepare two classes using MNDWI. Intermixing occurs as a result of such broad classification, for example, pixels of agricultural fields that were filled with water rather than water logged due to flooding. As a result, many of the pixels in the inundation map are not flooded.

The flood hazard map was overlaid with a land use map to extract data on different land uses in different flood zones (Fig. 20.7). Integrating data on hospitals, schools, population, and other important service infrastructure distribution can improve this information even more. The inundation map is directly related to the data of the river's water level during peak flooding, so it will be possible to estimate the water extent at various water levels in the case of future flood scenarios. Incidentally, there is limited detailed knowledge of the Yamuna flood plains in Delhi. Although at a relatively medium resolution, such studies and tools provide valuable information on flood hazard zones. Usage of this information for potential human impacts at district level and application of tools by different organizations is needed.

The results can be used by urban and housing development organizations as one of their considerations in selecting conduction site locations to avoid very high and high flood hazard zones and flooded areas. The FHI could be used by people who care about water resources and river system improvements to find places that need migration infrastructure. The department dealing with disaster management can use it for better planning, both before and after the flood events. These are precursors to the potential damage assessment. The method to calculate FHI could consider other parameters that influence floods, though our approach could capture the actual flood distribution using Landsat data and the potential hazard risk using MCDM. Such assessment approaches can be upscaled using geo-computational technologies to provide online and real-time assessments. This enables a wide range of stakeholders to use such information, particularly in the context of developing countries and for disaster risk reduction.

20.6   Conclusion

The chapter presents multiple learning items for the readers. For example, flood extent map of the Yamuna River flood in Delhi on September 26, 2010, was created using Landsat-5 C2 L2 satellite data. MNDWI was used to distinguish between water and non-water classes, as well as to map the inundated area. The total inundated area was 5.7%, according to satellite images (approx. 79.85 km^2). Furthermore, the total flooded area was divided into various land use categories. Agriculture was the hardest hit by the flood, with 63% of its land inundated. It provides a comprehensive list of parameters which can influence flood hazard in a city in tropical countries. The weights for all eight thematic layers were calculated using the AHP method of MCDA, and the rankings of parameters were determined based on expert advice. Finally, these layers were combined using GIS to create a flood hazard map. According to the flood hazard map, 8.75% of Delhi is in a very high flood hazard zone. Built-up areas accounted for 39.66% of the flood hazard zone, while agriculture accounted for 32.91%. This study demonstrates that combining

FHI and AHP to create a flood hazard zone map is an important and reliable method. We compared the actual flood coverage of the Delhi flood of 2010 to the modelled flood hazard zones.

Application of remote sensing data coupled with a GIS tool is efficient for preliminary and reliable analysis of flood hazard. Developing databases at 1:50,000 scale (with spatial resolution of 30 m) may be considered coarser for city level planning, but this gives an overall snapshot for planning and development. The analysis could be fine-tuned with higher resolution data for the selected pockets while preparing operational action items. Researchers and practitioners in the field can benefit from learning GIS-based MCDA methods for effective flood hazard mapping, which will aid in flood management decision-making. The methodology employed herewith demonstrates the data-limited approach, which can be applied to cities of similar size and can be enhanced with more information. Lastly, the approach and results that focus on finding solutions that are described in this chapter will help regional and municipal authorities and policymakers lower the risk of flooding and come up with the right ways to prevent damage.

References

Central Ground Water Board (2015) Ground water year book, National Capital Territory, Delhi

Das A, Santra PK, Bandyopadhyay S (2021) The 2016 flood of Bihar, India: an analysis of its causes. Nat Hazards 107(1):751–769. https://doi.org/10.1007/s11069-021-04604-0

Das S (2018) Geographic information system and AHP-based flood hazard zonation of Vaitarna basin, Maharashtra, India. Arabian J Geosci 11(19). https://doi.org/10.1007/s12517-018-3933-4

Dash P, Sar J (2020) Identification and validation of potential flood hazard area using GIS-based multi-criteria analysis and satellite data-derived water index. J Flood Risk Manage 13(3):1–14. https://doi.org/10.1111/jfr3.12620

Dhiman R, VishnuRadhan R, Eldho TI, Inamdar A (2019) Flood risk and adaptation in Indian coastal cities: recent scenarios. Appl Water Sci 9(1):1–16

Du Y, Zhang Y, Ling F, Wang Q, Li W, Li X (2016) Water bodies' mapping from Sentinel-2 imagery with modified normalized difference water index at 10-m

spatial resolution produced by sharpening the swir band. Remote Sens 8(4). https://doi.org/10.3390/rs8040354

Fernández DS, Lutz MA (2010) Urban flood hazard zoning in Tucumán Province, Argentina, using GIS and multicriteria decision analysis. Eng Geol 111(1–4):90–98. https://doi.org/10.1016/j.enggeo.2009.12.006

Gautam VK, Gaurav PK, Murugan P, Annadurai M (2015) Assessment of surface water dynamicsin bangalore using WRI, NDWI, MNDWI, supervised classification and K-T transformation. Aquatic Proc 4 (Icwrcoe):739–746. https://doi.org/10.1016/j.aqpro.2015.02.095

Ghent EO (2013) Application of remote sensing and geographical information systems in flood management: a review. Res J Appl Sci Eng Technol 6(10):1884–1894. https://doi.org/10.19026/rjaset.6.3920

Jenks GF (1967) The data model concept in statistical mapping. Int Yearbook Cartogr 7:186–190

Jonkman SN (2005) Global perspectives on loss of human life caused by floods. Nat Hazards 34(2):151–175. https://doi.org/10.1007/s11069-004-8891-3

Kabenge M, Elaru J, Wang H, Li F (2017) Characterizing flood hazard risk in data-scarce areas, using a remote sensing and GIS-based flood hazard index. Nat Hazards 89(3):1369–1387. https://doi.org/10.1007/s11069-017-3024-y

Kazakis N, Kougias I, Patsialis T (2015) Assessment of flood hazard areas at a regional scale using an index-based approach and analytical hierarchy process: application in Rhodope-Evros region, Greece. Sci Total Environ 538:555–563. https://doi.org/10.1016/j.scitotenv.2015.08.055

Kumar M, Sharif M, Ahmed S (2019) Flood risk management strategies for national capital territory of Delhi India. ISH J Hydraulic Eng 25(3):248–259. https://doi.org/10.1080/09715010.2017.1408434

Liu YB, Smedt FD (2004) WetSpa extension, a gis-based hydrologic model for flood prediction and watershed management documentation and user manual. March, 1–126

Mahmoud SH, Gan TY (2018) Multi-criteria approach to develop flood susceptibility maps in arid regions of Middle East. J Clean Prod 196:216–229. https://doi.org/10.1016/j.jclepro.2018.06.047

Mahmoud SH, Mohammad FS, Alazba AA (2014) Determination of potential runoff coefficient for Al-Baha Region, Saudi Arabia using GIS. Arab J Geosci 7(5):2041–2057. https://doi.org/10.1007/s12517-014-1303-4

Mallick J, Singh CK, Al-Wadi H, Ahmed M, Rahman A, Shashtri S, Mukherjee S (2015) Geospatial and geostatistical approach for groundwater potential zone delineation. Hydrol Process 29(3):395–418. https://doi.org/10.1002/hyp.10153

Merz R, Blöschl G, Parajka J (2006) Spatio-temporal variability of event runoff coefficients. J Hydrol 331 (3–4):591–604. https://doi.org/10.1016/j.jhydrol.2006.06.008

Mundhe N (2019) Multi-criteria decision making for vulnerability mapping of flood hazard: a case study of Pune City. J Geograph Stud 2(1):41–52

Ouma YO, Tateishi R (2014) Urban flood vulnerability and risk mapping using integrated multi-parametric AHP and GIS: Methodological overview and case study assessment. Water (switzerland) 6(6):1515–1545. https://doi.org/10.3390/w6061515

Papaioannou G, Vasiliades L, Loukas A (2015) Multi-criteria analysis framework for potential flood prone areas mapping. Water Resour Manage 29(2):399–418. https://doi.org/10.1007/s11269-014-0817-6

Rashed T, Weeks J (2003) Assessing vulnerability to earthquake hazards through spatial multicriteria analysis of urban areas. Inter J Geogr Inf Sci. https://doi.org/10.1080/1365881031000114071

Saaty RW (1987) The analytic hierarchy process—what it is and how it is used. Math Model 9:161–176. http://dx.doi.org/10.1016/0270-0255(87)90473-8

Saaty TL (2013) The modern science of multicriteria decision making and its practical applications: the AHP/ANP approach. Oper Res 61(5):1101–1118. https://doi.org/10.1287/opre.2013.1197

Saaty TL, Wind Y (1980) Marketing applications of the analytic hierarchy process. Manage Sci 26:641–658. https://doi.org/10.1287/mnsc.26.7.641

Saha AK, Agrawal S (2020) Mapping and assessment of flood risk in Prayagraj district, India: a GIS and remote sensing study. Nanotechnol Environ Eng 5(2):1–18

Sarmah T, Das S, Narendr A, Aithal BH (2020) Assessing human vulnerability to urban flood hazard using the analytic hierarchy process and geographic information system. Int J Disaster Risk Reduct 50:101659

Sharma S, Nahid S, Sharma M, Sannigrahi S, Anees MM, Sharma R, Shekhar R, Basu AS, Pilla F, Basu B, Joshi PK (2020) A long-term and comprehensive assessment of urbanization-induced impacts on ecosystem services in the capital city of India. City Environ Interactions 7:100047. https://doi.org/10.1016/j.cacint.2020.100047

Shekhar S, Purohit RR, Kaushik YB (2009) Groundwater management in NCT Delhi, 1–10

Singh RB, Singh S (2011) Rapid urbanization and induced flood risk in Noida India. Asian Geogr 28 (2):147–169

Singh P, Sinha VSP, Vijhani A, Pahuja N (2018) Vulnerability assessment of urban road network from urban flood. Int J Disaster Risk Reduct 28:237–250

Sowmya K, John CM, Shrivasthava NK (2015) Urban flood vulnerability zoning of Cochin City, Southwest Coast Of India, using remote sensing and GIS. Nat Hazards 75(2):1271–1286

Sun F, Sun W, Chen J, Gong P (2012) Comparison and improvement of methods for identifying waterbodies in remotely sensed imagery. Int J Remote Sens 33 (21):6854–6875. https://doi.org/10.1080/01431161.2012.692829

Szabó S, Gácsi Z, Balázs B (2016) Specific features of NDVI, NDWI and MNDWI as reflected in land cover

categories. Landscape Environ 10(3–4):194–202. https://doi.org/10.21120/le/10/3-4/13

Xu H (2006) Modification of normalised difference water index (NDWI) to enhance open water features in remotely sensed imagery. Int J Remote Sens 27 (14):3025–3033. https://doi.org/10.1080/0143116060 0589179

Zope PE, Eldho TI, Jothiprakash V (2017) Hydrological impacts of land use–land cover change and detention basins on urban flood hazard: a case study of Poisar River basin, Mumbai India. Nat Hazards 87(3):1267–1283

An Assessment of Traffic Noise Level in Agartala Municipal Corporation Using Geo-spatial Technology in Tripura, India

21

Prajnamita Debnath, Sajal Ghosh, Debasish Kundu, Jatan Debnath, Tuhin Kanti Ray, and Eshita Boral

Abstract

Vehicular noise greatly affects the population who are exposed to it, particularly the road users or those who are located alongside transport lines. Though noise pollution does not have an immediate health impact, long-term exposure to it might be detrimental for human physical as well as mental health. In Agartala Municipal Corporation, there has been a significant rise in the number of vehicles over a period of last ten years; therefore, the noise created by them also has become an issue of concern. The present study is an attempt to evaluate the level of traffic noise along twelve major roads in Agartala Municipal Corporation. This study would not only throw an insight into the vulnerable areas affected by noise pollution in the city but also address the population most likely to be affected by it. An effort has been made to show the relationship of traffic noise level with traffic volume and road character like the carriageway width, and it could be established that the nature of road and traffic composition has a positive relation with noise level in the city. In order to optimize the level and efficiency of noise effect in the city, geospatial techniques were used to prepare a noise map through IDW interpolation method.

Keywords

Noise pollution · Equivalent noise level · Traffic volume · Geospatial technology

21.1 Introduction

The environmental noise climate is influenced drastically by road traffic noise as a continuous sound is produced by passage of each vehicle which fluctuates hourly in an irregular drift (Halim and Abdullah 2014). Thus, noise pollution due to vehicular traffic has become one of the growing environmental problems of urban centers that needs to be addressed (Bhosale et. al. 2010; Chauhan et al. 2010). With the increase in population numbers, travel demand has also significantly amplified. Thus, in order to meet the increasing need for mobility more and more vehicles, both public and majorly private have started playing on roads. The resultant effect is that motor vehicles in the cities have become the

P. Debnath · S. Ghosh · D. Kundu · E. Boral (✉)
Department of Geography and Disaster Management, Tripura University, Suryamaninagar, Tripura 799022, India
e-mail: eshitaboral@tripurauniv.ac.in

J. Debnath
Department of Geography, Gauhati University, Guwahati, Assam 781014, India

T. K. Ray
Department of Geography, Vidyasagar College, Kolkata, West Bengal 700006, India

main source of urban noise emission (Tiwari et al. 2013), contributing about 55% to the total noise (Sinha and Sridharan 1999). This not only causes irritation to the road users and those occupying space alongside roads but it also slowly and adversely affects human health (Das and Jamatia 2014). It has been found in several researches that the threshold of listening was affected by long-term exposure to noise (Coles et al. 1968; Passchier-Vermeer 1974; Ward 1975; Berger et al. 1978; Stevin 1982; Alberti 1998; Nash 2000). So, noise pollution caused by traffic has appeared as a fundamental issue to urban people and planner (Halim and Abdullah 2014).

The northeastern state of Tripura has been experiencing steady urban growth over the decade. The environmental condition of Agartala Municipal Corporation (AMC), the capital of the state, has been changing abruptly along with the rapid growth of urbanization (Sen et al. 2014). AMC has about 4.95% of area under transport services, and the number of registered vehicles has increased by 58.8% over a period of last five years. Among all the vehicles, the highest growth rate was recorded in auto rickshaws followed by two-wheelers and personalized vehicles. Furthermore, of the total length of road network about one fifth witness peak traffic flows of more than 4000 PCU (Government of Tripura 2006). Consequently, noise levels are quite high in the city.

Under such situation, this work aims to study the status of vehicular noise level along twelve major roads within Agartala Municipal Corporation and to assess the vulnerable zones affected by noise pollution in the city. An attempt has also been made to categorize the population who are most likely exposed to noise pollution along the selected twelve roads. This would help in better understanding the adversity of traffic noise pollution at these areas.

21.2 Methods and Materials

21.2.1 Study Area

Agartala Municipal Corporation is located on the major corridors of movement in the state and is connected to the rest of the country by surface through a single road, i.e., the Assam-Agartala-Sabroom road (NH8/44). The city has a high population growth rate and the density in the city core to that of the peripheral areas is highly variant. The city core area accounts to about 17% of the total area which accommodates about 50% of the population of the city, enhancing the travel demand in the core areas of the city by manifold. Further popularity of personalized vehicles and intermediate para-transit modes in intra-city travel causes stress to the pollution levels in the city. The vehicular noise level of 12 selected roads under Agartala Municipal Corporation was surveyed. The roads were selected on the basis of its carrying capacity and importance. All these roads are the major roads of the Municipal Corporation and support highest traffic volume.

21.2.2 Data Collection Process

The data for the study has been collected through an extensive field survey. Traffic Noise was recorded on two time periods, i.e., peak hour (9:30–10:30 a.m.) and lean hour (2:00–3:00 p.m.) for duration of five minutes at an interval of fifteen minutes for a period of one hour at road junctions with the help of handheld noise meter.

Assessment of traffic volume and composition was also measured to ascertain their influence on traffic noise level. For this purpose, traffic count was carried out at junctions of each road for one hour at an interval of fifteen minutes both for peak and lean hour. Carriageway width for each of the roads was measured at major and minor junctions with the help of 100-m measuring tape, and the average of the values was considered as width of the road.

In order to assess the variation of traffic noise at different land use zones, namely industrial zone, commercial zone, residential zone, and silent zones in the city, the maximum, minimum, and equivalent noise level of two locations under each of these zones at four different time periods, i.e., 9:30–11 a.m., 2–2:30 p.m., 5–6:30 p.m., and 7:30–9 p.m. from the month of January to March, 2019, was monitored. The land use

components along the roads were assessed through field survey using 100-m measuring tape at 20-m interval. The affected population has been estimated with the help of land use survey considering a buffer of 100 m along the roads. Target group discussion with a structured schedule following random sampling technique was undertaken for 10 persons under different sections along each road.

21.2.3   Data Analysis

The Equivalent Noise Level for each of the roads was calculated to find out the status of traffic noise pollution in the city using the following formula which had been developed based on Sen et al. (2014)

$$L_{eq} = 10 \log \sum_{i=1}^{n} (10) * L_i/10 * t_i \qquad (21.1)$$

where L_{eq} = Equivalent Noise Level, n = Total number of sound samples, L_i = The noise level of any ith sample, and t_i = Time duration of ith sample.

Noise pollution indices were calculated using Gaussian percentile to obtain the noise pollution level. Different percentile values like L_{10}, L_{50}, and L_{90} were computed from the sampled data, and the parameters were used for the evaluation of Noise climate (NC) and Noise pollution Level (LPL) (Tripathi et al. 2006).

Noise climate (NC) is the range over which the sound levels are fluctuating in an interval of time and was assessed using the following formula

$$NC = (L_{10} - L_{90}) \qquad (21.2)$$

where NC is Noise Climate, L_{10} is the level of sound exceeding for 10% of the total time of measurement or Peak noise level, L_{50} is the level of sound exceeding for 50% of total time of measurement or mean sound level, and L_{90} is the level of sound exceeding for 90% of total time of measurement or background or residual noise level (Hunashal and Patil 2012).

As L_{eq} is an insufficient descriptor of the annoyance caused by fluctuating noise, therefore

Noise pollution level expressed in dB was calculated by using the following formula.

$$NPL = L_{eq} + NC \qquad (21.3)$$

NPL is the noise pollution level, L_{eq} is Equivalent noise level, and NC is the noise climate.

Another noise descriptor used to measure traffic noise pollution is Traffic noise index (TNI). TNI can be measured by using the following equation.

$$TNI = 4(L_{10} - L_{90}) + L_{90} - 30 \text{ dB (A)} \qquad (21.4)$$

Traffic noise index (TNI) is another parameter, which indicates the degree of variation in a traffic flow. This is also expressed in dB (A) and can be computed by the following formula (Pradhan et al. 2012).

21.2.4   Noise Mapping Using Geospatial Techniques

In order to estimate the overall noise pollution scenario of Agartala Municipal Corporation, noise contours are computed in GIS by spatial interpolation method. The noise data obtained from the twelve selected roads were mapped by interpolating noise levels computed on a raster of points (de Kluijver and Stoter 2003; Esmeray and Eren 2021). Among the various spatial interpolation techniques, Inverse Distance Weighted (IDW) interpolations were used for the study which estimates the noise level L_p at each point p, as an average of the noise levels collected at the M fixed samples (Can et al. 2014) and the map was prepared in QGIS software.

21.3   Results and Discussion

21.3.1   Noise Level in Different Roads of AMC

The issues of noise pollution across the world's cities have been organized in many research (Singh and Daver 2004; Li et al. 2002; Morillas et al. 2002; Zannin et al. 2002; Alberola et al.

2005; Lebiedowska 2005; Pucher et al. 2005; Tansatcha et al. 2005) and have identified the sources of city noise (Dursun et al. 2006; Ausejo et al. 2010; Al-Qdah 2014). Noise of vehicle's engine and traffic horns are the main source of noise pollution related to transportation and other responsible factors of traffic noise are traffic speed, composition, volume, and management system (Cohen and McVoy 1982; Banerjee et al. 2008; Al-Mutairi et al. 2009; Swain et al. 2012). Noise level has been measured at 12 selected roads (Table 21.1) within Agartala Municipal Corporation, and attempt has been made to establish its relationship with volume of traffic and the type of vehicles that occupy the roads.

21.3.1.1 Noise Descriptors Used in Assessment of Traffic Noise Level

The statistical equivalent sound pressure level was measured at different time intervals during peak hour and lean hour traffic conditions. Table 21.2 depicts the equivalent noise level (L_{eq}) and statistical sound level descriptors such as L_{10}, L_{50}, and L_{90}. L_{eq} is the constant sound level while the statistical equivalent sound pressure level was measured at different time intervals of 10%, 50%, and 90% to calculate the traffic indices.

21.3.1.2 Noise Climate

The greater the difference between L10 and L90, the traffic noise index (TNI) will increase even more and subsequently, noise level to the recipient environment results in more annoyance (Nassiri et al. 2016). During peak hour, it has been observed that Agartala-Sabroom road, Akhaura road, and Dhaleswar A.A road record NC value more than 10 dB. Even during lean hours, NC value exceeds 8 dB for all the selected roads except GB-ITI road, Airport road, and Jail-Ashram road. So, it could be stated that the noise climate of the selected roads depicts relatively high fluctuation of noise level during peak hour and also in lean hour which create significant amount noise pollution.

21.3.1.3 Noise Pollution Level

Noise pollution level (NPL) values at different road stretches are displayed in Table 21.3. Noise pollution results reveal that during peak hours maximum NPL of 87.10 dB was observed in Dhaleswar A.A road followed by Agartala-Sabroom road (82.26 dB), Akhaura road (82.07 dB), and Motorstand road (80.43 dB). The prime causes are traffic congestion, horning from vehicles and noise from shops and markets located along these roads. During lean hours, average noise level in the previously mention road remains

Table 21.1 Selected roads within AMC

S. No.	Road name	Extension	
		From	To
1	VIP road	North gate	Secretariat
2	GB-ITI road	GB Bazar	Up to Jail-Ashram Road
3	Airport road	Bhati Abhoynagar	Narsinghgarh
4	Bamutia road	Music college	Bamutia Market
5	Jail-Ashram road	m/s Sarada Iron B.K Road	Satadal Sangha, Dhaleswar
6	Dhaleswar A.A road	Motorstand Shani Temple	Chandrapur Bazar
7	Barjala road	Durga Chowmohani bridge	Panchabati Kali Bari
8	TG road	Ramnagar Rd no.4	Up to Ramnagar Rd no.9
9	HGB road	Battala Bazar	Kaman Chowmohani
10	Akhaura road	Old RMS Chowmohani	Akhaura check post
11	Motorstand road	Motorstand Shani Temple	Kaman Chowmohani
12	Agartala-Sabroom road	Battala Bazar	Amtali (within AMC)

Table 21.2 Noise level (dB) variation at selected roads of AMC

Road name	Time							
	Peak hour traffic flow				Lean hour traffic flow			
	L_{eq}	L_{10}	L_{50}	L_{90}	L_{eq}	L_{10}	L_{50}	L_{90}
VIP road	68.35	71.20	65.61	61.51	60.70	63.25	58.27	54.63
GB-ITI road	60.00	62.52	57.6	54.00	50.76	52.91	48.73	45.68
Airport road	60.10	62.62	57.69	54.09	55.90	58.26	53.66	50.31
Jail-Ashram road	65.78	68.53	63.15	59.20	53.90	56.17	51.74	48.51
Bamutia road	63.58	66.24	61.04	57.22	59.70	62.21	57.31	53.73
Barjala road	68.20	71.05	65.47	61.38	51.78	53.97	49.70	46.60
T.G road	68.78	71.65	66.02	61.90	61.90	64.49	59.42	55.71
Dhaleswar A.A road	76.30	79.47	73.24	68.67	68.90	71.77	66.14	62.01
Motorstand road	70.45	73.38	67.63	63.40	64.89	67.60	62.29	58.40
Akhaura road	71.89	74.88	69.01	64.70	67.45	70.26	64.75	60.70
H.G.B road	69.90	72.81	67.10	62.91	61.78	64.37	59.31	55.60
Agartala-Sabroom road	72.40	75.42	69.50	65.16	64.96	67.67	62.36	58.46

Table 21.3 Variation of noise descriptors (NC, L_{np}, TNI) at selected roads of AMC

Road name	Time					
	Peak hour traffic flow			Lean hour traffic flow		
	NC (dB)	NPL (dB)	TNI (dB)	NC (dB)	NPL (dB)	TNI (dB)
VIP road	9.69	78.04	70.27	8.62	69.32	59.11
GB-ITI road	8.52	68.52	58.08	7.23	57.99	44.60
Airport road	8.53	68.63	58.21	7.95	63.85	52.11
Jail-Ashram road	9.33	75.11	66.52	7.66	61.56	49.15
Bamutia road	9.02	72.60	63.30	8.48	68.18	57.65
Barjala road	9.67	77.87	70.06	7.37	59.15	46.06
T.G road	9.75	78.53	70.90	8.78	70.68	60.83
Dhaleswar A.A road	10.8	87.10	81.87	9.76	78.66	71.05
Motorstand road	9.98	80.43	73.32	9.20	74.09	65.20
Akhaura road	10.18	82.07	75.42	9.56	77.01	68.99
H.G.B road	9.90	79.80	72.51	8.77	70.55	60.68
Agartala-Sabroom road	10.26	82.26	76.20	9.21	74.17	65.30

high (more than 60 dB). GB-ITI road and Barjala road are the only two roads among the twelve selected roads where noise pollution level is less than 50 dB during lean hours.

21.3.1.4 Traffic Noise Index

The maximum TNI value was observed in the peak hours due to maximum number of traffic accompanied by traffic congestion and other background sound originating from surrounding areas as the selected areas are the arterial roads connecting busy intersections of the city. During peak hour traffic, maximum TNI value has been observed in Dhaleswar A.A. road (81.87 dB), Agartala-Sabroom road (76.20 dB), and Akhaura road (75.42 dB). Whereas minimum TNI value

has been observed in GB-ITI road (58.08 dB), Airport Road (58.21 dB), and Bamutia road (63.30 dB) primarily due to less traffic congestion and comparatively fewer number of vehicles compared to other selected roads (Table 21.3). During lean hour traffic scenario, it has been observed that GB-ITI road (44.60 dB), Barjala road (46.06 dB), and Jail-Ashram road (49.15 dB) have less TNI value due to fewer vehicle number. Whereas in the case of Dhaleswar road, Akhaura road, Agartala-Sabroom road, and Motorstand road, TNI values are relatively high even in lean hours.

21.3.2 Noise Level and Traffic Volume

Traffic volume refers to the number of vehicles that pass by a road at a given time period. There exists a strong relationship between traffic volume and noise level (Ma et al. 2006; Swain et al. 2012). It has been found that the level of discontentment has increased in urban residential area with the increase in traffic congestion (Tapia Granados 1998). As traffic volume increases, noise level also increases. Traffic volume not only includes noise from vehicles but also from road signaling system, which creates waiting period for moving vehicles. It has been observed that during peak hour the noise level of all the roads is high owing to high traffic volume as compared to the lean hour. In peak hour, the number of vehicles is quite high in Agartala-Sabroom road, Motor stand road, Akhaura road, H.G.B road, Barjala road, and VIP road, and consequently, the noise level of these roads is also higher which establishes that in the case of these roads noise level and traffic volume are directly correlated. However, in the case of GB-ITI road and Dhaleswar A.A. road, the noise level and the traffic volume show negative corelation. In the case of GB-ITI road, traffic volume is significantly less but noise level during peak hour though lesser compared to other roads yet is considerably high as compared to traffic volume. Similarly in the case of Dhaleswar A.A. road which has traffic volume lesser than the ones mentioned above yet it has recorded maximum noise level not only in peak hour but also in lean hour (Fig. 21.1).

In both the roads therefore, the noise could be attributed to something else other than mere traffic volume. The presence of traffic terminal point located in the vicinity of Dhaleswar A.A. road where the noise level has been recorded can be considered to have an impact on the level of noise. It is because during waiting period at traffic signals many vehicles do not switch off the engine and further immediately after the signal turns green drivers tend to start honking to allow them space. While in the case of GB-ITI road the presence of commercial sector is responsible for the high noise level. In the case of lean hour as well, the noise level of Akhaura road, Agartala-Sabroom road, Motorstand road, T.G. road, and HGB road was high and the traffic volume was also high comparatively, but in the case of other roads traffic noise level is much more even when the traffic volume is low. This may be attributed to the other activities that carry on along the road, specifically commercial services which contribute to the noise during lean traffic hours.

21.3.2.1 Relation Between Noise Level and Traffic Volume

Traffic volume is one of the most important factors of traffic noise pollution in urban areas (Crocker 2007; Sulaiman et al. 2018), and Agartala is no exception. The scatter diagram shows the relation between traffic volume and traffic noise, the prior being the independent variable and later the dependent variable. In Fig. 21.2 (a and b), the relationship is clearly established that more the traffic volume more is the noise level. However, in the case of AMC it can be seen that peak hour R^2 value is 0.742, which means both the elements are moderately positively correlated. But in the case of lean hour, the R^2 value is 0.917 that is means; the traffic volume and noise level are strongly positively correlated with one another more than that in the peak hour. It may be interpreted that during peak hour other noises may also have a significant influence on the total noise level.

Fig. 21.1 **a** Noise level (dB) and traffic volume on different roads (peak hour); **b** Noise level (dB) and traffic volume on different roads (lean hour)
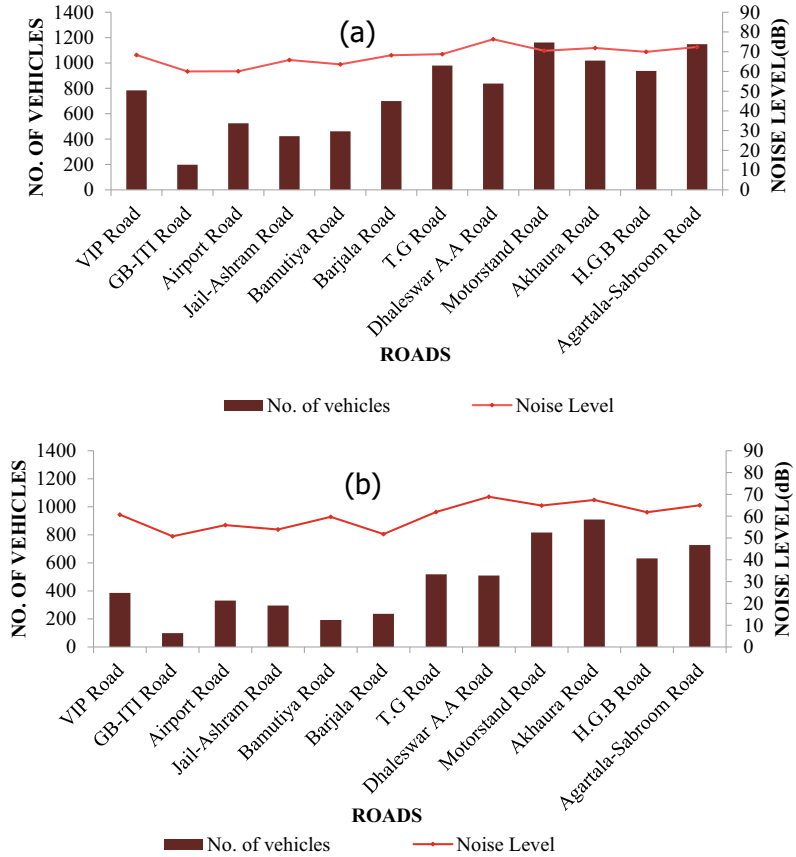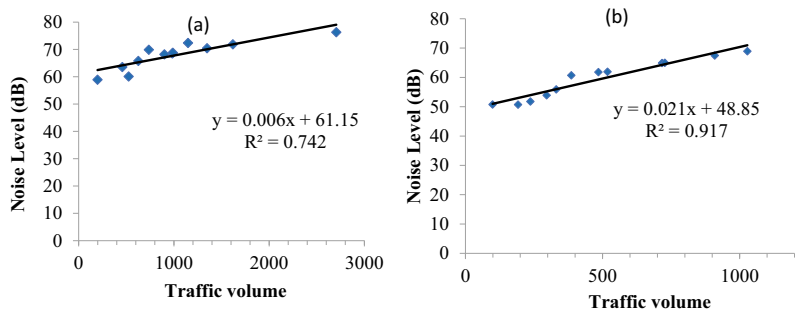

Fig. 21.2 **a** Relation between traffic noise and traffic volume (peak hour); **b** Relation between traffic noise and traffic volume (lean hour)

21.3.2.2 Noise Level and Category of Vehicles

Not only does the traffic volume have an impact on the noise level but also the category of vehicles does affect the level of noise in an area (Alves Filho et al. 2004). This part of the work has been devoted to establishing a comparison between the noise level and the type of vehicle

dominating the area. It has been observed in Tables 21.4 and 21.5 that in the case of roads where L_{eq} is very high like that of Dhaleswar A. A. road, that even though total vehicular number plying along this road is low, the number of auto rickshaws and magic cars is significantly high. Contrarily in the case of GB-ITI road and Jail-Ashram road where the numbers of auto

Table 21.4 Peak hour vehicle strength and noise level

Roads	Equivalent noise level (dB)	Bus	Car	Toto	Magic	Auto	Two-wheeler	Jeep	Rickshaw	Truck	Pickup van	Cycle	Total
VIP road	68.35	10	179	2	5	218	293	31	10	0	18	18	784
GB-ITI road	60.00	1	28	1	0	17	125	0	1	0	6	19	198
Airport road	60.10	15	91	5	0	163	219	2	4	0	15	11	525
Jail-Ashram road	65.78	4	32	0	17	147	159	17	16	4	27	0	423
Bamutia road	63.58	14	91	0	2	126	147	13	27	0	22	19	461
Barjala road	68.20	06	21	5	20	252	43	4	64	4	110	171	700
T.G road	68.78	03	143	149	2	220	245	2	19	2	146	48	979
Dhaleswar A.A road	76.30	11	25	53	39	229	275	6	137	3	2	58	838
Motorstand road	70.45	7	144	160	3	245	375	6	138	3	38	42	1161
Akhaura road	71.89	8	68	147	42	135	284	14	77	27	182	35	1019
H.G.B road	69.90	11	72	184	3	267	334	7	54	0	2	3	937
Agartala-Sabroom road	72.40	16	124	201	12	243	374	13	102	5	47	11	1148

Table 21.5 Lean hour vehicle strength and noise level

Roads	Equivalent noise level (dB)	Bus	Car	Toto	Magic	Auto	Two-wheeler	Jeep	Rickshaw	Truck	Pickup van	Cycle	Total
VIP road	60.70	6	79	10	2	116	155	2	1	0	5	10	386
GB-ITI road	50.76	5	17	2	0	27	40	2	1	2	0	3	99
Airport road	55.9	07	50	0	07	81	180	5	0	0	1	0	331
Jail-Ashram road	53.90	39	4	0	12	97	97	0	39	6	2	0	296
Bamutia road	59.70	2	12	30	22	53	19	13	28	0	9	4	192
Barjala road	51.78	5	16	14	0	43	125	1	10	1	7	15	237
T.G road	61.90	2	41	78	0	109	205	10	49	5	9	10	518
Dhaleswar A.A road	68.90	7	45	97	0	10	207	2	36	3	10	0	510
Motorstand road	64.89	16	45	135	132	135	201	11	66	11	51	14	817
Akhaura road	67.45	14	101	150	30	204	243	40	99	4	17	7	909
H.G.B road	61.78	5	24	160	41	76	163	26	110	6	10	11	632
Agartala-Sabroom road	64.96	0	22	20	3	144	283	3	210	2	25	15	727

P. Debnath et al.

rickshaws are less, L_{eq} is also low. Again in the case of Akhaura road and Agartala-Sabroom road total vehicular number being high, mention may be made of truck, magic cars, auto rickshaws, buses, and private cars. L_{eq} is also quite high.

21.3.2.3 Traffic Noise and Carriageway Width

A carriageway consists of a width of road on which a vehicle is not restricted by any physical barriers or separation to move laterally. A carriageway generally consists of a number of traffic lanes together with any associated shoulder, but may be a sole lane in width, for example, a highway off ramp.

Carriageway width reflects the number of vehicles on road at a time. It is considered that more the vehicles running along a road at a time more will be the noise level. Figure 21.3 shows that relationship between noise level and carriageway width depicts a R^2 value is 0.424, which means the relationship between the carriageway width and noise level is positively correlated, but their degree of correlation is not very strong in the case of AMC.

21.3.3 Noise Mapping

Geospatial technologies could provide great potential to optimize the quality of noise effect studies because traffic noise and its environmental effect have numerous spatial components. Spatial noise contour maps are useful to urban planning agencies, traffic engineers, cities, and governmental agencies and can be used as
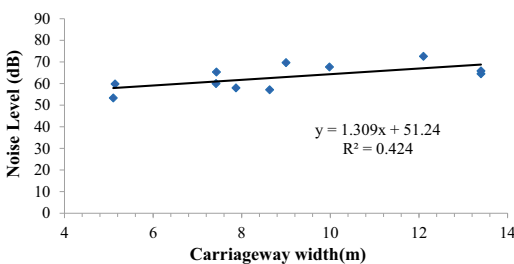
indicators to identify factors that influence traffic noise levels (Obaidat 2011). A noise map has been prepared using Inverse Distance Weighted (IDW) interpolation method to depict the overall character of noise pollution within AMC incorporating the previously collected field data on noise level at traffic intersections (Fig. 21.4). It reflected a distance decay effect where noise level has shown to decrease from CBD toward the peripheral areas of the city. The map reflects that the highest noise level was along Agartala-Sabroom road, TG road, Akhaura road, and HGB road, medium noise level has been recorded in and along Barjala road, Bamutia road, etc. This complies with the research findings that along these roads not only is the vehicular population high but also the concentration of commercial activities is greater. The lowest level of noise was observed in the outer parts of the city, which may be attributed to the less movement of vehicles, human crowd, and less busy commercial areas in the periphery of the city.

21.3.4 Traffic Noise at Terminals

The relationship between mobility in transport sector and noise level is well established. In this section, attempt has been made to assess the noise level at terminals of the three modes of transport available in the city, i.e., Road transport, Rail transport, and Air transport. Not only does the movement of vehicles along roads or rail lines creates noise pollution, but the terminals of surface transport as well as aviation sector create quite considerable noise pollution. With this perspective, the noise level at three selected terminal stations and their approach roads have been recorded (Table 21.6). Noise level has been measured for 20-m distance from these terminal points at an interval of 5 m both for morning and evening peak hours.

21.3.4.1 Noise Level at Nagerjala Bus Stand

Nagerjala bus stand is one of the busiest bus stands in the city of Agartala. It is observed that noise level is showing a decreasing trend from
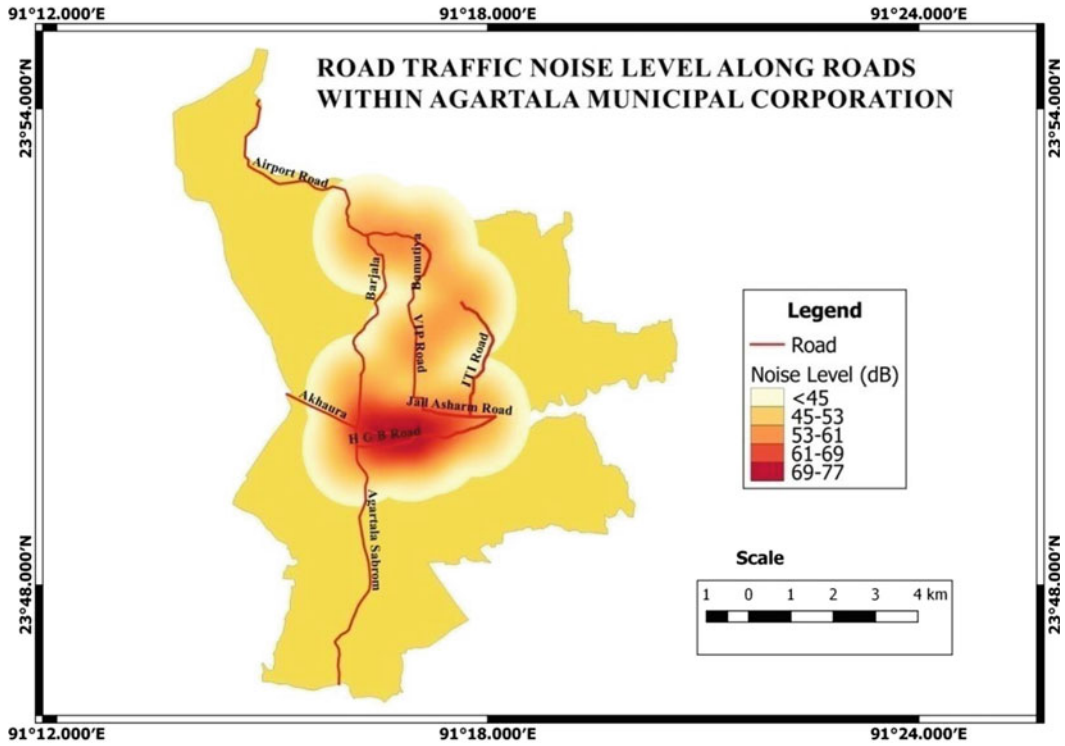

Fig. 21.3 Carriageway width of the study area

Fig. 21.4 Road traffic noise level along the roads of the Agartala Municipal Corporation

Table 21.6 Selected terminals for assessing noise level

Sector	Location	Approach roads
Road	Nagerjala bus stand	Agartala-Sabroom road Toward Battala
Rail	Agartala railway station	Toward Agartala-Sabroom road
Airway	Agartala airport	Airport road (toward Narsinghgarh) Airport road (toward Usha Bazar)

the bus stand outwards (Fig. 21.5). From the bus stand-up to a distance of 10 m, noise level is quite high, particularly toward the Battala side, as the vehicles moving out of the terminus wait here to accommodate some additional passengers, but at 15 m it is significantly reduced and the trend is followed in both the time period for the rest of the distance with the increase in distance from the bus stand.

Toward Bishalgarh road noise level also showed decreasing trend during morning peak hour, but in the case of evening peak hour noise level was higher at 5-m distance from the bus

stand due to heavy congestion in this route during evening hours. However, beyond 5 m it again showed a decline in noise level.

21.3.4.2 Noise Level at Agartala Railway Station

Unlike bus terminus where congestion and honking of vehicles add to the noise pollution, in the case of rail services whistle of train, period of arrival and departure of train and hiring connecting vehicles to destinations, shouting of vendors on and off the platforms are the major causes of noise pollution. Since its inception, the

Fig. 21.5 Noise gradient along Nagerjala bus stand at morning and evening peak hour
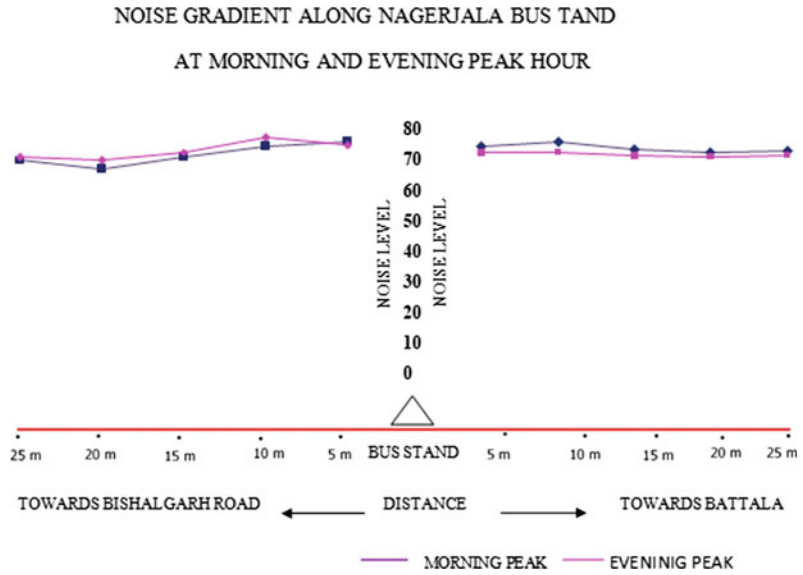
Fig. 21.6 Noise gradient at Agartala railway station at morning and evening peak hour
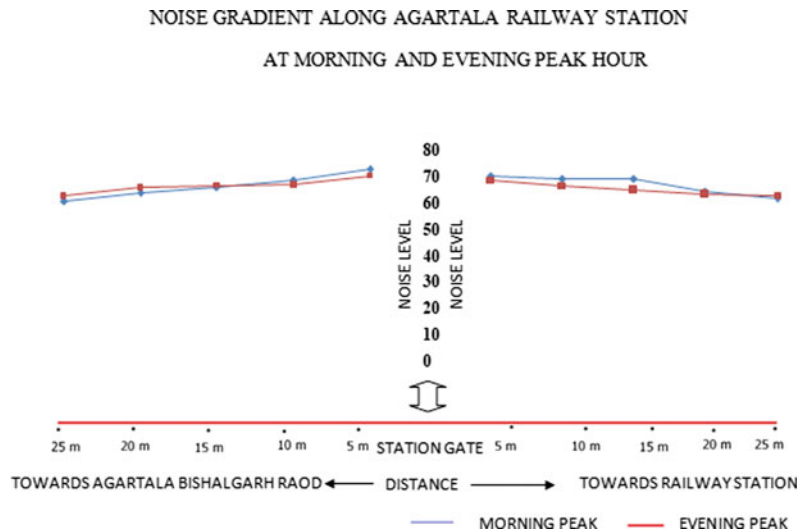
Agartala Railway station has seen a steady increase in the passenger numbers. But being located outside the main center of the city the approach roads show a clear decline in the noise level away from the rail station. The noise level is decreasing for both the approach roads (Fig. 21.6). The noise level at railway station is high because of noise of train, human crowd, other vehicular movements those ply as Para-transit mode of transport, but with the increasing distance the noise shows a decreasing trend from railway station.

21.3.4.3 Noise Level at Maharaja Bir Bikram Airport

Aviation sector also has its share in causing noise pollution. Those residing near an airport are well aware of the sound of takeoff and landing of an aircraft. Figure 21.7 shows the noise gradient along the roads connecting to Agartala Airport. From the diagram, it can be observed that noise level is declining from the airport toward both the approach roads toward Usha Bazar as well as toward Narsinghgarh.

Fig. 21.7 Noise gradient at Agartala airport at morning and evening peak hour

NOISE GRADIENT ALONG AGARTALA AIRPORT AT MORNING AND EVENING PEAK HOUR
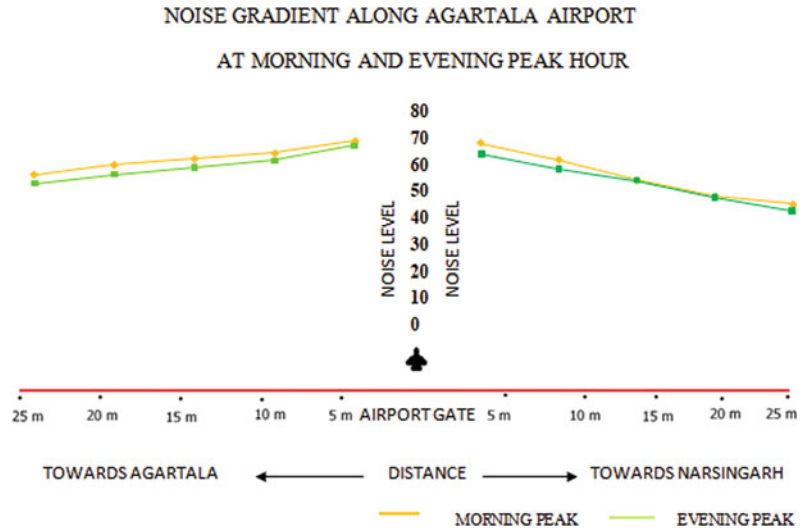
These roads are located at the periphery of the city and therefore cater to lesser traffic numbers and encounter much less congestion therefore recording lower noise levels. Further, the noise generated from airplane decreases with the increase in distance away from airport. Contrarily human crowd and noise of other Para-transit modes of transport are responsible for increasing the noise level at airport.

21.3.5 Land Use and Traffic Noise Level

In this section, the traffic noise level has been considered at areas with different land use character, mainly industrial area, commercial area, residential area, and silent zones like hospitals and schools. There exists a standard limit for noise (Table 21.7) for each of these zones with which the present noise level of the city has been compared. Two areas from each of these land use zones have been selected for the study, i.e., for industrial zone AD Nagar and Chandinamura, for commercial zone MG Bazar and Battala Bazar, for residential zone Ramnagar 4 and Indiranagar, and two locations for silent zone selected were IGM hospital and GB hospital.

The data available from the Pollution Control Board depicts (Fig. 21.8) that in 2018, the noise level of AD Nagar industrial area is less than the standard level in both day and nighttime but the noise level is comparatively higher at nighttime, whereas in 2019, the level of noise crossed the standard level, it may be due to the increase in industrial activities. But in the case of Chandinamura industrial area, it has been observed that the noise level is very low in both the years, which is lesser than its standard level, it may be because of the lesser industrial activities in the area coupled with less movement of vehicles as this industrial area is not linked with a major road; thus, being less affected by other traffic noise or human crowd, this industrial area records lower level of noise.

In the case of commercial zone, it has been observed that noise level of two commercial zones, i.e., Battala Bazar and MG Bazar, is higher than its standard level, which may be a result of very high commercial activities in the region. Furthermore, these commercial hubs are near to the CBD of a city and lie alongside the busiest roads in the city, so that vehicular movement as well as pedestrian mobility is higher in these commercial zones. For identifying the noise pollution level in residential area, two areas, i.e., Ramnagar lane 4 and Indiranagar,

Table 21.7 Ambient air quality standards in respect of noise

Category of zone/area	Standard limit of noise (dB) (A)	
	Day time	Night time
Industrial zone	75	70
Commercial zone	65	55
Residential zone	55	45
Silent zone	50	40

Notes
1. Day time shall mean 6:00 a.m.–10 p.m.
Nighttime shall mean from 10:00 p.m.–6:00 a.m.
2. Silence zone is an area comprising not less than 100 m around hospitals, educational institutions, courts, religious places, or any other area which is declared as such by the competent authority
3. Mixed categories of areas may be declared one of the four above mentioned categories by the competent authority
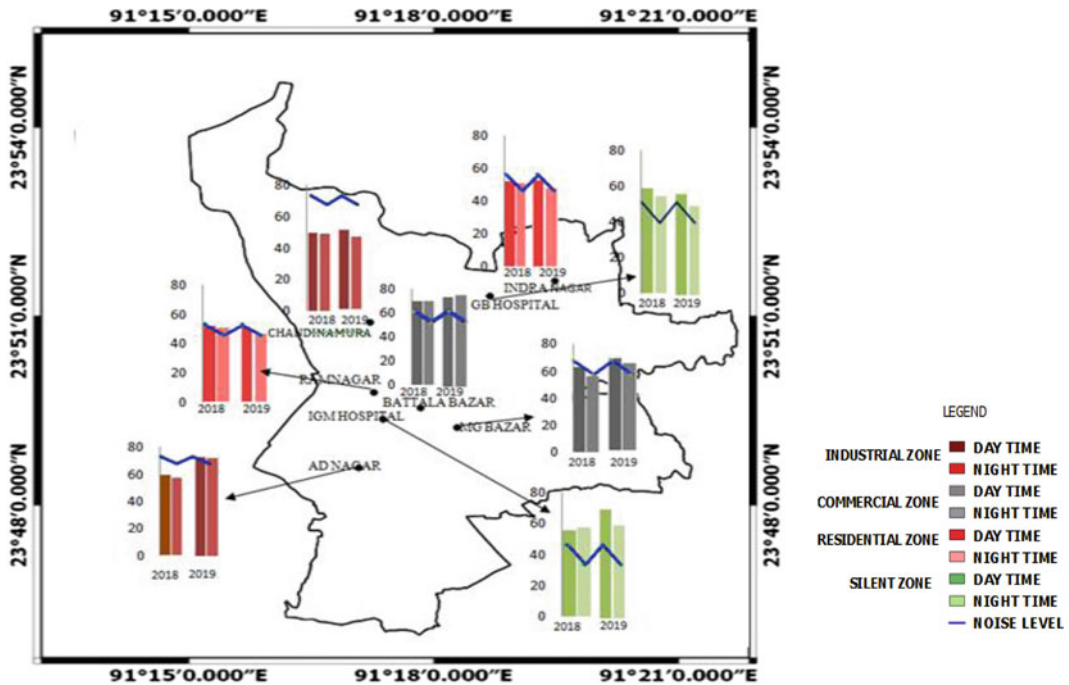
Fig. 21.8 Annual record of noise level at different zones (2018 and 2019)

area were considered and it depicted that in both the year noise level is almost equal to its standard level. The noise level is quite high in both hospital zone areas, which is more than its standard level in both the years. This may be attributed to its location at the busiest traffic intersection nodal points of the city.

21.3.6 Temporal Variation in Traffic Noise Level at Areas with Different Land Use Category

Temporal as well as spatial dimensions of noise level was monitored to identify the relation between Noise pollution and Land use pattern, at
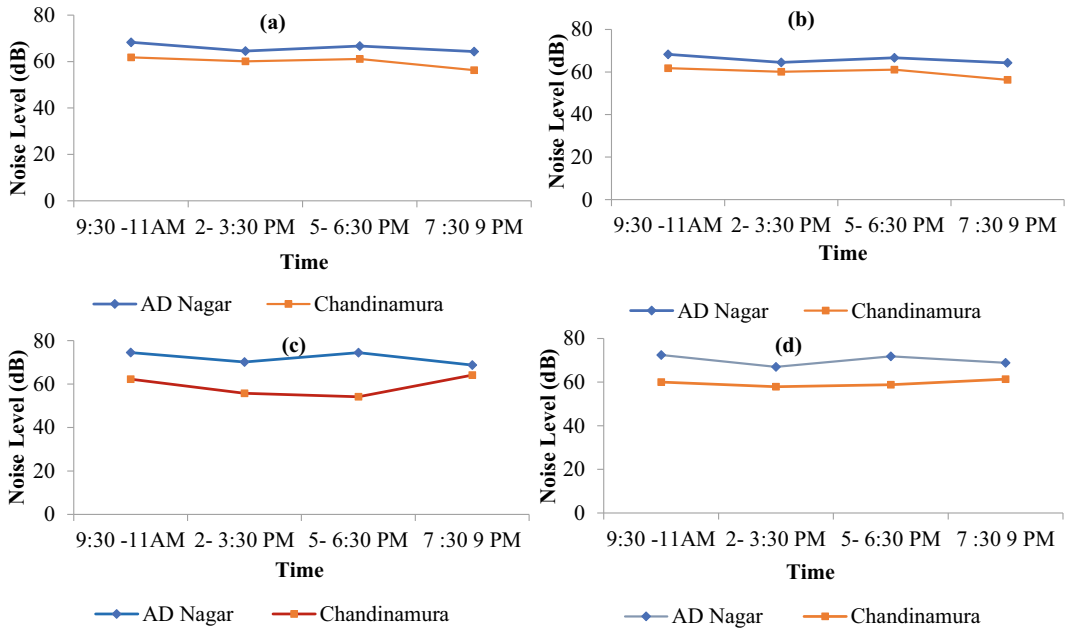
Fig. 21.9 a Equivalent noise level in industrial area for January; **b** Equivalent noise level in industrial area for February; **c** Equivalent noise level in industrial area for March; **d** Equivalent noise level in industrial area for April

industrial, commercial, residential, and silent zones. Areas was selected which belongs to four, i.e., A D Nagar industrial zone, Battala Bazar from commercial zone, Ramnagar road No. 5 area from residential zone, and for silent zone IGM hospital area was surveyed.

In the month of January 2019 in A.D. Nagar industrial zone, the highest noise level was recorded during 7:30–9 p.m. with 74.0 dB may be because this industrial zone lies along the NH 8/44 and trucks enter the city through this road at this hour. The lowest noise level was recorded during 2–2:30 p.m. with 69.4 dB, but the maximum equivalent level of noise 68.89 dB was recorded at the peak hour 9:30–11 a.m. (Fig. 21.9a). In Chandinamura, the highest noise level is recorded at 9:30–11 a.m. with 68.0 dB at the same time minimum noise level was 59.5 dB, and the lowest noise level record at 2–2:30 p.m. with 62.9 dB, at the same time minimum noise level was 54.9 dB much lower than the AD Nagar area, for reasons stated above. However, the equivalent noise level is high at 5–6:30 p.m. (65.90 dB). In the case of February, 2019, in A. D Nagar industrial zone the highest

noise level was recorded at morning peak hour (9:30–11 a.m.) with 75.4 dB and likewise the maximum equivalent level of noise was recorded at 9:30–11 a.m. (72.34 dB). In Chandinamura, the highest noise level was recorded at 9:30–11 a.m. with 69.3 dB as well as the equivalent noise level was also high 65.40 dB (Fig. 21.9b) during the same period. It is observed that the noise level is higher for the month of February in both the industrial areas. In the month of March 2019, the highest noise level was 78.7 dB and the maximum equivalent level of noise was 674.5 dB in the morning peak hour at A. D Nagar area. While in Chandinamura the highest noise level, 65.8 dB was recorded during 9:30–11:00 a.m. but the highest equivalent noise level of 64.12 dB was seen during 7:30–9 p.m. (Fig. 21.9c), the evening lean period may be because of the movement of trucks during this time frame.

In the month of April, 2019, in A. D Nagar area the highest noise level was recorded at 5–6:30 p.m. with 76.9 dB at the same time minimum noise level was 70.7 dB, which is relatively higher than all the previous months.

The maximum equivalent level of noise was also recorded at 9:30–11 a.m. (72.45 dB). In Chandinamura, the highest noise level and the equivalent noise level are was recorded at 9:30–11 a.m. with 63.7 dB and 62.05 dB values, respectively (Fig. 21.9d). From the four-month noise monitoring result, it is observed that the noise level is comparatively high in AD Nagar area than Chandinamura which may be due to industrial activities being more in AD Nagar, and the most important reason is AD Nagar industrial area is located in Agartala–Sabroom Highway, so that the movements of vehicles is more than Chandinamura, that's why AD Nagar is more noisy zone than Chandinamura. Overall, in both the industrial areas within the city limits the noise level was more or less in parity with the standard limits since heavy industries are not located here.

The two selected commercial areas are MG Bazar and Battala, the busiest commercial zones within the city. In MG Bazar commercial zone, the highest noise level was recorded at 9:30–11 a.m. with 78.6 dB while the maximum equivalent level of noise was recorded at 7:30 –9 p.m. with value74.26 dB. In the case of Battala Bazar area, the highest noise level 74.5 dB was recorded at 5–6:30 p.m. and the maximum equivalent noise level of 71.30 dB was observed during the same time frame indicating that the commercial areas in the city remain busy throughout the day. In February MG Bazar commercial zone, the highest noise level 76.0 dB was recorded between 9:30 and 11 a.m. and minimum noise level 70.9 dB was seen at 5–6:30 p.m., both being high because of the activities in the region as well as the traffic movement. The maximum equivalent level of noise was recorded at 5–6:30 p.m. (73.10 dB). In Battala Bazar, the highest noise level was recorded at 5–6:30 p.m. with 79.1 dB, but the equivalent noise level 75.05 dB was recorded between 9:30 and 11 a.m., the peak hour. In MG Bazar area, the highest noise level recorded was 78.9 dB at 9:30–11 a.m. and the lowest noise level recorded was 70.1 at 7:30–9 p.m. The maximum equivalent level of noise recorded was77.76 dB at 9:30–11 a.m. In the case of Battala Bazar, the highest noise level reading was 82.0 dB between

9:30 and 11 a.m. and the lowest noise level reading was recorded 71.3 dB between 7:30 and 9 p.m. but the equivalent noise level was also recorded highest during 9:30–11 p.m. (79.99 dB). It is observed that subsequently the noise level recorded shows an increasing trend with every month. In April, MG Bazar recorded highest noise level between 9:30 and 11 a.m., the morning peak hour, i.e., 80.3 dB, and the lowest noise level was recorded at 7:30–9 p.m. with a value of 67.3 dB while the maximum equivalent level of noise was recorded at 5–6:30 p.m. (74.20 dB). In Battala Bazar, the highest noise level observed was 80 dB during the morning peak and the minimum noise level was 65.7 dB, but the equivalent noise level recorded was highest at 5–6:30 p.m., i.e., 74.2 dB (Fig. 21.10). For the commercial areas in the city, the noise level recorded was always higher than the standard limit both for day and nighttime unlike the industrial areas.

The residential areas in all cases recorded noise level that was within the permissible limits for all the four months. While in January Indiranagar recorded the highest noise level of 62.2 dB between 5 and 6:30 p.m. lowest noise level of 58.0 dB between 2 and 2:30 p.m. for obvious reasons of it being the lean traffic period, the maximum equivalent noise level of 59.26 dB was recorded at again the evening peak hour. In Ramnagar road no 4 area, the highest noise level of 61.5 dB and the lowest noise level of 49.9 dB were recorded at the evening peak and morning lean hours, respectively, but strangely the equivalent noise level showed highest readings at 9:30–11 a.m. of 55.7 dB may be because of the festivities that occurred during the republic day celebrations in this region. In February for Indiranagar, the highest noise level was recorded evening peak hour and the lowest noise level at morning lean hour and the maximum equivalent level of noise 52.50 dB was recorded at evening peak hour. It is observed that noise level in this area decreased from the month of January. In Ramnagar road no. 4 area, except the highest noise level of 59.4 dB being recorded during morning peak hour the minimum noise level and the maximum equivalent noise level were recorded in the same time period as before with values
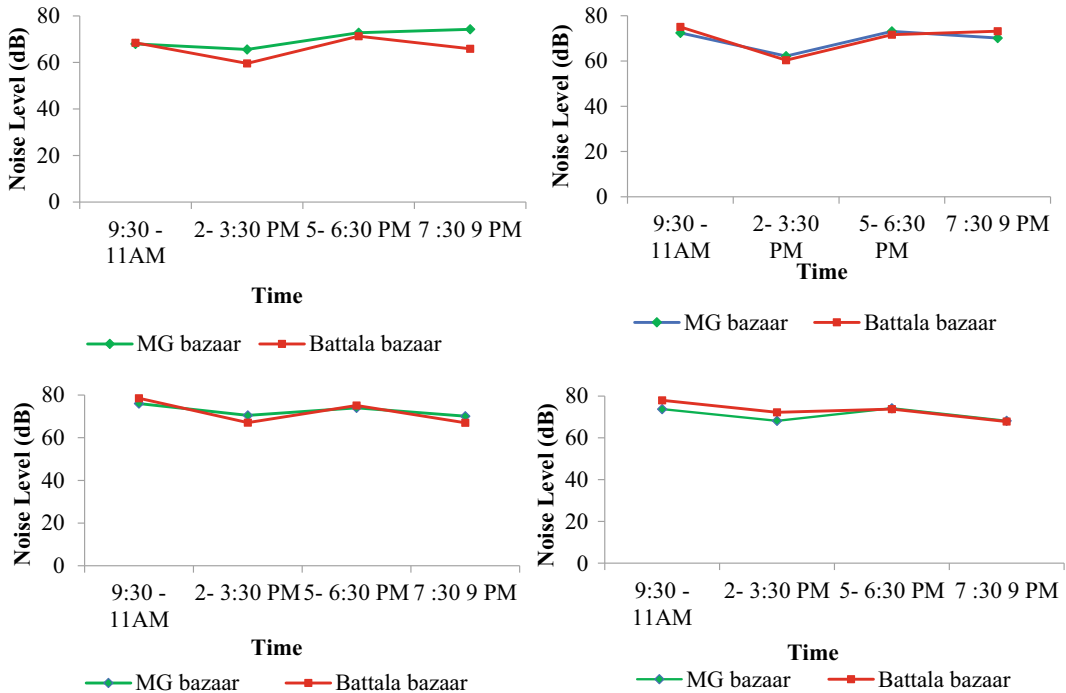
Fig. 21.10 **a** Equivalent noise level in commercial area for January; **b** Equivalent noise level in commercial area for February; **c** Equivalent noise level in commercial area for March; **d** Equivalent noise level in commercial area for April

of 47.4 dB and 56.24 dB, respectively. In the month of March, the maximum equivalent noise level recorded was during the morning peak hour for both the selected residential areas reading a value of 54.5 dB and 57.9 dB, respectively, and unlike the other cases in Ramnagar lane no. 4 area the lowest noise level in March was observed during night lean hour (Fig. 21.11).

In April however, the maximum equivalent noise level for Indiranagar was recorded during morning peak hour but for Ramnagar it was observed to be during the evening peak hours with values 55.2 dB and 57.0 dB, respectively. Comparatively, it appears that Indiranagar area is noisier than the Ramnagar area. It may be due to the presence of IT sector, Silk processing, unit, and Gomati milk dairy farm in this region.

Contrary to the industrial and residential areas, the selected silent zones are quite noisy. As GB hospital area is a multi-sector area, being a commercial area alongside a hospital zone area and also because it supports bus and auto stands, while IGM hospital is located on Akhaura road,

one of the busiest road of the city as well as it connects to the Office Lane, where many of the government offices are located, resulting in higher vehicular movements, traffic noise and human crowd thus the noise level recorded in most cases are higher than the permissible limits. In GB Hospital area, the highest noise levels in January and February were witnessed during evening peak hours whereas for March and April it was in the morning peak hour. The lowest noise level on the other hand was seen in afternoon lean hour except for the month of January when it was recorded in the evening lean hour.

The maximum equivalent level of noise recorded was 75.8 dB, 76.62 dB, 78.9 dB, and 76.0 dB for January, February, March, and April, respectively, at 5–6:30 p.m. except for March when it was in between 9:30 and 11 a.m. For IGM Hospital area, the highest noise level for all the four months varied between morning peak and evening peak hours ranging from 79.0 to 80.0 dB while the lowest noise level varied between afternoon and evening lean hours
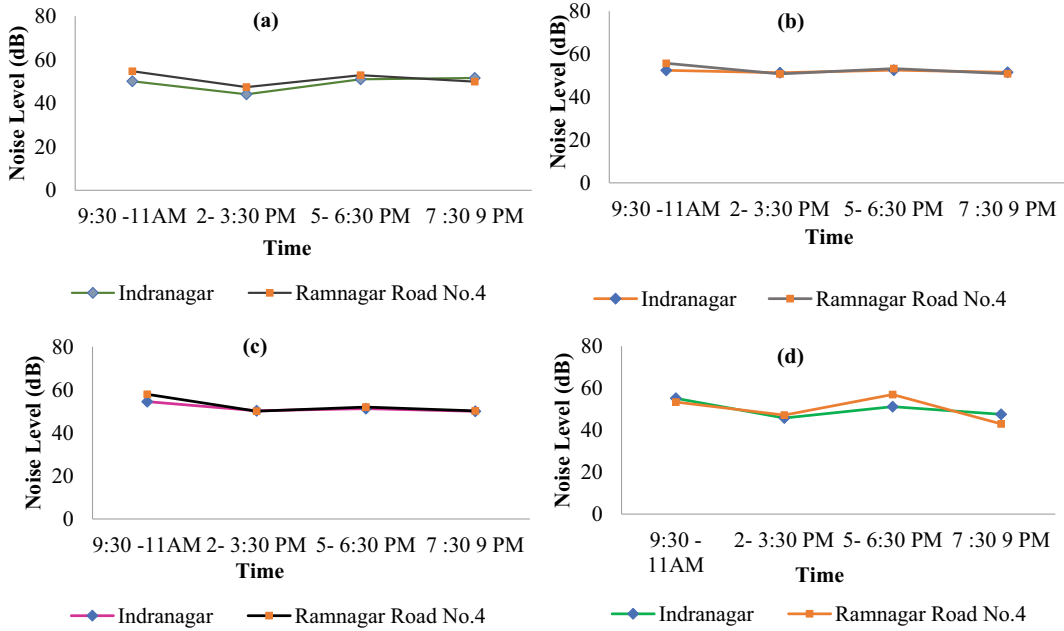
Fig. 21.11 **a** Equivalent noise level in residential area for January; **b** Equivalent noise level in residential area for February; **c** Equivalent noise level (Indiranagar and Ramnagar road no. 4); **d** Equivalent noise level (Indiranagar and Ramnagar road no. 4

ranging from 63.1 to 68.0 dB. The equivalent noise level for January and February was 76.35 dB and 77.0 dB and was recorded in the evening peak hour (Fig. 21.12a, b). However, for March and April the values were 75.56 dB and 78.9 dB and were recorded in the morning peak hour (Fig. 21.12c, d).

21.3.7 Spatial Variation in Traffic Noise Level at Areas with Different Land Use Category

In order to identify the nature of land use along the approach roads to each of the zones, which is in turn indicative of any external noise that may impact the total noise level of the zones, field survey was conducted for one selected area under each type of zones. Under industrial zone A.D. Nagar industrial area, commercial zone Battala

Bazar area, Residential zone Ramnagar area and for Silent zone IGM hospital area was chosen.

21.3.7.1 Industrial Zone (A.D Nagar Industry)

A.D. Nagar industrial zone mainly comprises industrial units, zones of commercial activities, and major parts of police ground and police quarter. From the land use map (Fig. 21.13), it can be observed that the noise level decreases from Industry gate toward Battala, indicating that the distance decay effect occurs for distances away from the industry. Further, most part toward Battala till 100 m is occupied by police quarter, so that the noise level is lower at this region toward Battala. In the case of toward Bishalgarh, the noise level is also showing a decreasing trend. It may be due to the presence of a Montessori school; however, between 80- and 100-m distance noise level was quite high maybe due to the presence of CNG station, so the vehicular noise is more.
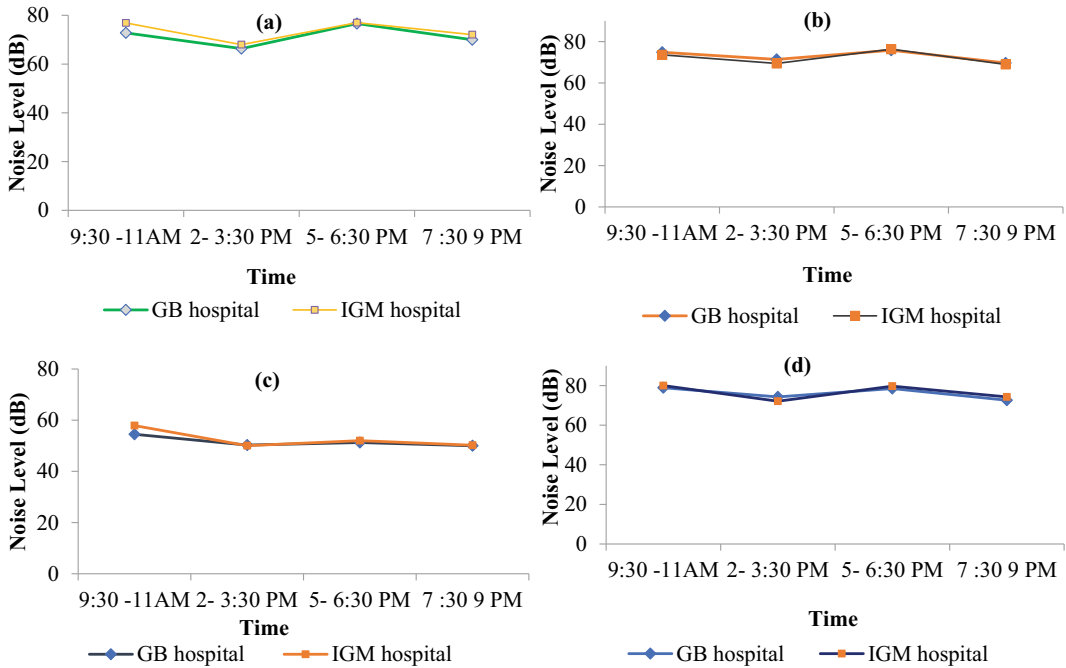
Fig. 21.12 **a** Equivalent noise level in silent zones for January; **b** Equivalent noise level in silent zones for February; **c** Equivalent noise level in silent zones for March; **d** Equivalent noise level in silent zones for April

21.3.7.2 Commercial Zone (Battala Bazar)

From the conducted survey and the prepared land use map, it was observed that 90 percent of the area in Battala Bazar is dominated by commercial activities, and the level of noise is showing slightly increasing trend away from the center, which may be because of the high number of mixed traffic movement in the area. Toward H.G. B. road, the noise level recorded increased from 60-m to 100-m distance. H.G.B road houses all the retail shops of electronics and other essential items because of which human crowd in this area remains high throughout the day (Fig. 21.14).

21.3.7.3 Residential Zone (Ramnagar Road no. 4 Area)

Ramnagar road no. 4 being a residential area is mainly dominated by human settlement. From Fig. 21.15, it can be observed that the noise level of Ramnagar road no. 4 changed with its land use pattern, here noise level increases from the first noise monitoring point toward main road, because of commercial activities toward main roads, and

vehicular movement on the main roads, but toward the interior though noise level was high up to 40 m distance, it slightly goes down up to 80 m.

However, from 80 to 100 m, may be due to the presence of some shops slight increase in noise level is documented. In the case of the road toward Ramnagar road 3 noise level showing quite a fluctuating trend, here the higher noise level is observed from 80- to 100-m distance. In the case of the road toward Ramnagar road no. 05, the noise level is showing decreasing trends from the first monitoring point toward the interior, and it may be due to lesser human crowd and lesser vehicular movement.

21.3.7.4 IGM Hospital (Silent Zone)

IGM hospital area is the one of noisy area of Agartala City. From the survey, it was seen that the noise level of IGM hospital area is much more than any other traffic intersection point and other crowded areas. The land use map (Fig. 21.16) of the existing land use pattern and noise level observed that the noise level was high at IGM gate, but showed a slightly decreasing

Fig. 21.13 Spatial variation in traffic noise level at industrial zone with different land use category
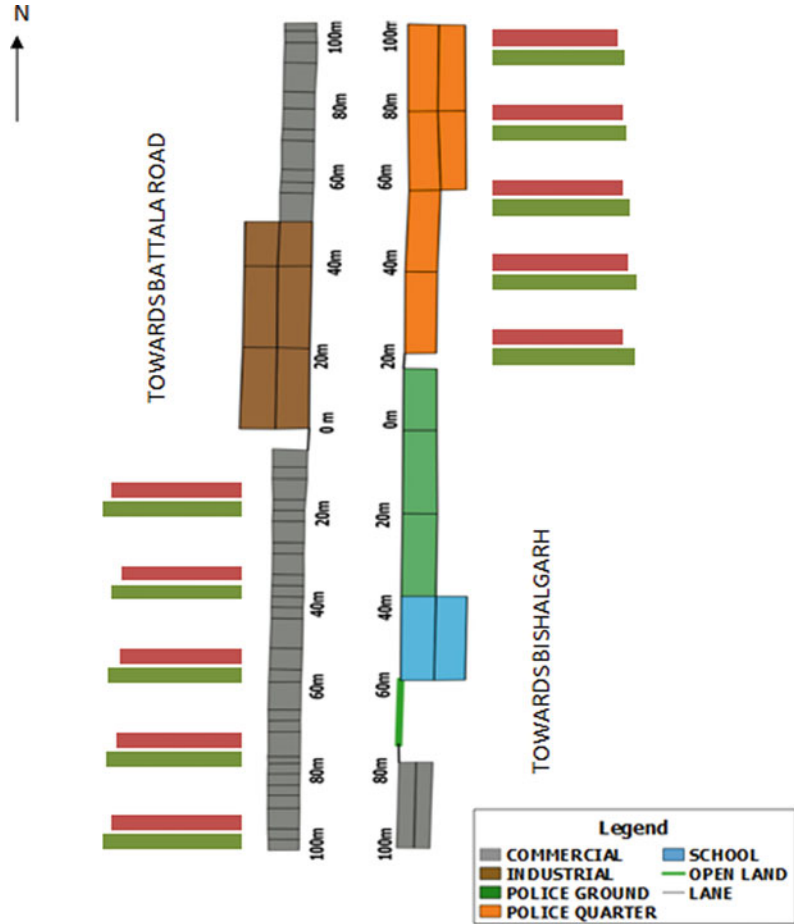
trend, till 80 m after which up to 100 m the noise level was quite high (Fig. 21.16). It may be attributed to the presence of IGM traffic intersection point, where heavy vehicular movement is recorded. Contrarily toward Paradise crossing noise level shows a decreasing trend, which may be due to the presence of administrative offices along the road. However, on the first 20 m along this road the noise is quite high because of the human crowd at the hospital gate as well as due to the entry and exit of vehicles and ambulance from the hospital premises. In the case of the road toward Office Lane from the hospital gate, the noise level was reduced during peak hour quite obviously because of the presence of most of the administrative offices in the area like the Agartala Municipal Corporation, Higher Education Department, etc.

21.3.8 Population Affected by Noise Level in AMC

The detrimental effects of exposure to noise pollution are well established, ranging from annoyance, hearing loss to cardiovascular diseases (Banerjee et al. 2008). Apart from these diseases hypertension, high-stress levels and sleep disturbances have been experienced by local people around the highways. Negative impact of road traffic noise on psychological and physiological health of humans have established in many studies (Anees et al. 2017; Helbich 2018; Klompmaker et al. 2019).

Road traffic noise pollution has a harmful impact on human work efficiency at Agartala city, Tripura (Pal and Bhattacharya 2012). An attempt had been made to estimate the percentage

Fig. 21.14 Spatial variation in traffic noise level at commercial zone with different land use category
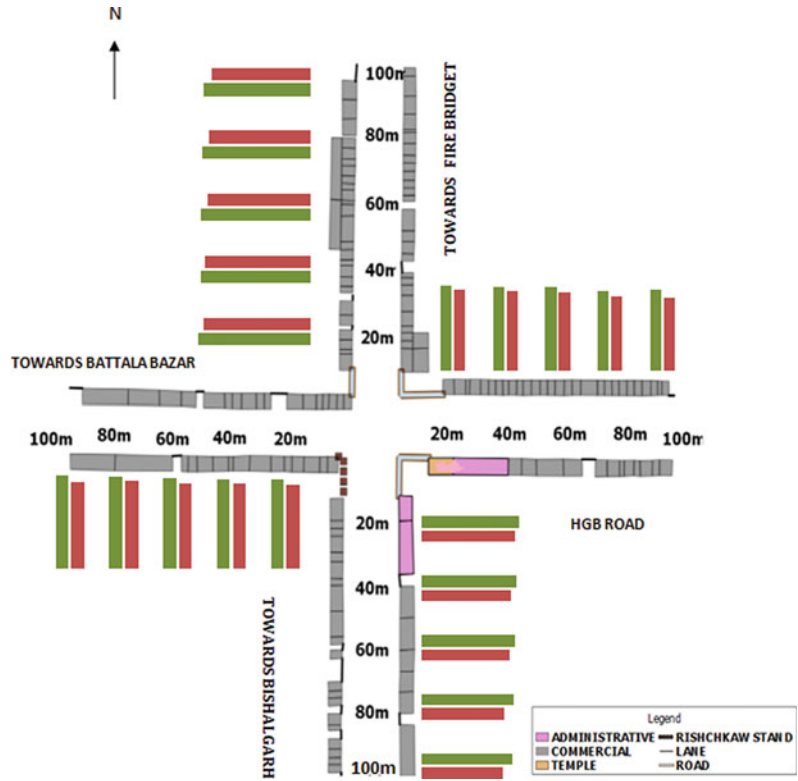
of population affected by this vehicular noise along the selected roads with the help of the land use of the area and target group discussion. Each of the selected roads has distinct land use along them, and thus, the population affected are of different age groups, gender, income levels, etc. Akhaura road has the highest level of noise where 40% office goers, 30% school students and teachers, and 20% hospital visitors are likely to be affected (Table 21.8). Similar is the case for VIP road where the most affected sections are office goers and residential population and comparatively less affected are shop-owners and school children. While in HGB road, Motorstand road, Agartala-Sabroom road, T.G road, and Dhaleswar A.A road, shop owners are the most exposed section, for that of Barjala road vehicle noises mainly cause problem to the residential

population. In the case of Airport road, GB-ITI road, and Bamutia road where noise pollution is comparatively less, shop owners are mainly affected, but hospital visitors, individuals going to office, and educational institutions also confirmed their discomfort with the noise pollution in the area.

21.4 Conclusion

Noise pollution is a major environmental pollution. It is a major source of disturbances in daily life of people particularly living in a congested and crowded area. So, assessment of the noise pollution of an area is important to understand the environmental condition of a particular place. Further, the GIS-based noise map has great

Fig. 21.15 Spatial variation in traffic noise level at residential zone with different land use category
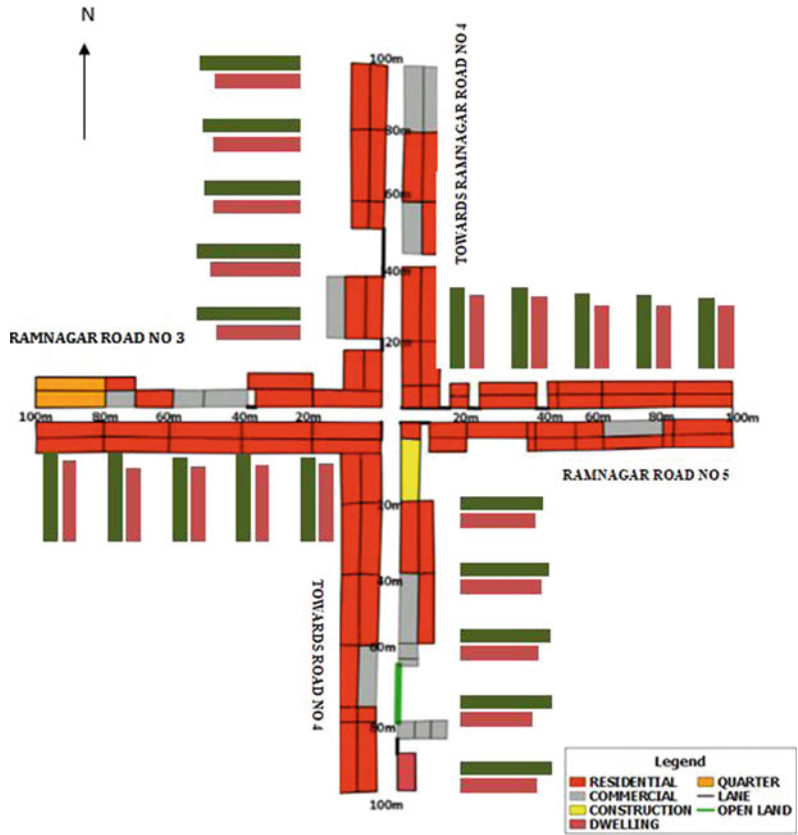
potentiality mapping traffic noise levels. The study revealed that roadside noise level in AMC is mainly dependent on total vehicular volume and category of vehicles. The spatial contour map generated based on collected field data shows that noise levels read maximum values at or near major traffic intersections and are relatively high all along the busiest roads in the central part of the city, i.e., Motor stand road, T.G road, HGB road, Agartala-Sabroom road, etc., while the noise level decreases toward peripheral areas. In the case of some roads, numbers of vehicles movement are less but recorded noise level is high which may be due to other sources of noise in the area like the presence of market or commercial activities along the road. It may be mentioned that most of the major roads in AMC have a mixed land use pattern along them; therefore, vehicular noise level is amplified at many areas because of other activities. Therefore, strict enforcement of existing law is necessary not only to prohibit unnecessary use of horns particularly around the silence zones and at traffic intersections but also to ensure that
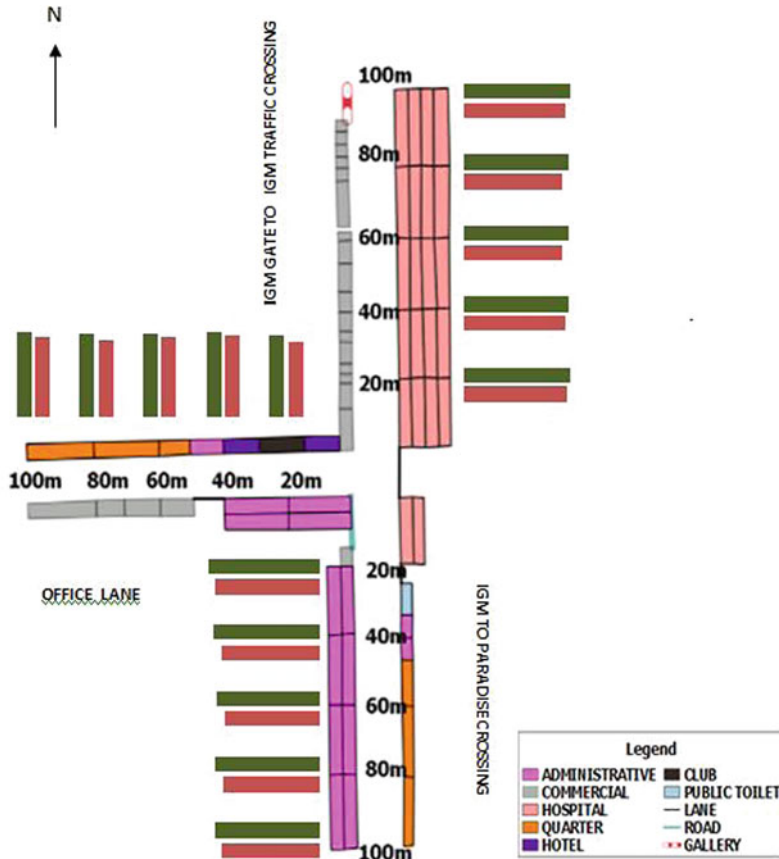
Fig. 21.16 Spatial variation in traffic noise level at Indira Gandhi memorial hospital with different land use category

Table 21.8 Impact of noise pollution along different roads in AMC

Road name	Average noise level of a day (dB)	Estimated affected population (in percent)				
		Settlement	Shop owner	Office	Educational institute	Hospital
VIP road	64.52	20	10	40	5	0
GB-ITI road	53.33	10	50	15	5	20
Airport road	58.00	30	40	20	0	10
Bamutia road	59.84	20	40	10	30	0
Jail-Ashram road	57.14	40	50	0	10	0
Dhaleswar A.A road	60.00	40	60	0	0	5
Barjala road	65.34	60	40	0	0	0
TG road	72.60	30	70	0	0	0
HGB road	67.67	0	100	0	0	0
Akhaura road	69.67	0	10	40	30	20
Motorstand road	65.84	0	100	0	0	0
Agartala-Sabroom road	68.68	10	80	5	5	0

people are aware about the hazards of loud sound so that total noise pollution levels are under control within a growing city like Agartala where vehicular population is inevitably intended to rise.

References

Alberola J, Flindell IH, Bullmore AJ (2005) Variability in road traffic noise levels. Appl Acoust 66(10):1180–1195

Alberti PW (1998) Noise, the most ubiquitous pollutant. Noise Health 1(1):3

AlMutairi N, AlsRukaibi F, Koushki P (2009) Measurements and model calibration of urban traffic noise pollution@@. Am J Environ Sci 5(5):613

AlQdah KS (2014) The assessment and analysis of traffic noise pollution in the city of Amman. Int J Environ Prot 4(5):68

AlvesFilho JM, Lenzi A, Zannin PHT (2004) Effects of traffic composition on road noise: a case study@@. Transp Res Part d: Transp Environ 9(1):75–80

Anees MM, Qasim M, Bashir A (2017) Physiological and physical impact of noise pollution on environment. Earth Sci Pak 1(1):08–11

Ausejo M, Recuero M, Asensio C, Pavón I, López JM (2010) Study of precision, deviations and uncertainty in the design of the strategic noise map of the macrocenter of the city of Buenos Aires, Argentina. Environ Model Assess 15(2):125–135

Banerjee D, Chakraborty SK, Bhattacharyya S, Gangopadhyay A (2008) Evaluation and analysis of road traffic noise in Asansol: an industrial town of eastern India. Int J Environ Res Public Health 5(3):165–171

Berger EH, Royster LH, Thomas WG (1978) Presumed noise-induced permanent threshold shift resulting from exposure to an A-weighted Leq of 89 dB. J Acoust Soc Am 64(1):192–197

Bhosale BJ, Late A, Nalawade PM, Chavan SP, Mule MB (2010) Studies on assessment of traffic noise level in Aurangabad city, India. Noise Health 12(48):195

Can A, Dekoninck L, Botteldooren D (2014) Measurement network for urban noise assessment: comparison of mobile measurements and spatial interpolation approaches. Appl Acoust 83:32–39

Chauhan A, Pawar M, Kumar D, Shukla SK, Bainola PK, Gupta MK, Chauhan SPS (2010) Assessment of noise levels in different zones of Haridwar city, Uttarakhand. Researcher 2(7):56–59

Cohn LF, McVoy GR (1982) Environmental analysis of transportation systems

Coles RRA, Garinther GR, Hodge DC, Rice CG (1968) Hazardous exposure to impulse noise. J Acoust Soc Am 43(2):336–343

Crocker MJ (2007) Fundamentals of acoustics, noise, and vibration. In: Handbook of noise and vibration control, pp 1–16

Das V, Mishra DU, Kumar Jamatia S (2014) Evaluation of noise pollution: a case study of Udaipur, Tripura, India. Int J Eng Res Technol (IJERT) 3

de Kluijver H, Stoter J (2003) Noise mapping and GIS: optimising quality and efficiency of noise effect studies. Comput Environ Urban Syst 27(1):85–102

Dursun S, Ozdemir C, Karabork H, Koçak S (2006) Noise pollution and map of Konya city in Turkey. J Int Environ Appl Sci 1(1):63–72

Esmeray E, Eren S (2021) GIS-based mapping and assessment of noise pollution in Safranbolu, Karabuk, Turkey. Environ Dev Sustain 23(10):15413–15431

Government of Tripura (2006) City development plan—Agartala, Urban Development Department, Agartala

Halim H, Abdullah R (2014) Equivalent noise level response to number of vehicles: a comparison between a high traffic flow and low traffic flow highway in Klang Valley, Malaysia. Front Environ Sci 2:13

Helbich M (2018) Toward dynamic urban environmental exposure assessments in mental health research. Environ Res 161:129–135

Hunashal RB, Patil YB (2012) Assessment of noise pollution indices in the city of Kolhapur, India. Procedia Soc Behav Sci 37:448–457

Klompmaker JO, Hoek G, Bloemsma LD, Wijga AH, van den Brink C, Brunekreef B, Lebret E, Gehring U, Janssen NA (2019) Associations of combined exposures to surrounding green, air pollution and traffic noise on mental health. Environ Int 129:525–537

Lebiedowska B (2005) Acoustic background and transport noise in urbanised areas: a note on the relative classification of the city soundscape. Transp Res Part D: Transp Environ 10(4):341–345

Li B, Tao S, Dawson RW (2002) Evaluation and analysis of traffic noise from the main urban roads in Beijing. Appl Acoust 63(10):1137–1142

Ma G, Tian Y, Ju T, Ren Z (2006) Assessment of traffic noise pollution from 1989 to 2003 in Lanzhou city. Environ Monit Assess 123(1):413–430

Morillas JB, Escobar VG, Sierra JM, Gómez RV, Carmona JT (2002) An environmental noise study in the city of Cáceres, Spain. Appl Acoust 63(10):1061–1070

Nash JL (2000) What's wrong with hearing conservation? Occupational Hazards 62(1):41–44

Nassiri P, Karimi E, Monazzam MR, Abbaspour M, Taghavi L (2016) Analytical comparison of traffic noise indices—a case study in District 14 of Tehran City. J Low Freq Noise Vib Active Control 35(3):221–229

Obaidat MT (2011) Spatial mapping of traffic noise levels in urban areas. J Transp Res Forum 47(2)

Pal D, Bhattacharya D (2012) Effect of road traffic noise pollution on human work efficiency in government

offices, private organizations, and commercial business centres in Agartala City using fuzzy expert system: a case study. Adv Fuzzy Syst

PasschierVermeer W (1974) Hearing loss due to continuous exposure to steady-state broad-band noise@@. J Acoust Soc Am 56(5):1585–1593

Pradhan AC, Swain BK, Goswami S (2012) Measurements and model calibration of traffic noise pollution of an industrial and intermediate city of India. The Ecoscan 1(1):1–4

Pucher J, Korattyswaropam N, Mittal N, Ittyerah N (2005) Urban transport crisis in India. Transp Policy 12(3):185–198

Sen P, Bhattacherjee A, Das A, Das D (2014) Noise pollution assessment in greater Agartala city: a case study. IJRET: Int J Res Eng Technol 3(9)

Singh N, Davar SC (2004) Noise pollution-sources, effects and control. J Hum Ecol 16(3):181–187

Sinha S, Sridharan PV (1999) Present and future assessment of noise level in the Neyveli region. J Environ Stud Policy 2(1):1–14

Stevin GO (1982) Spectral analysis of impulse noise for hearing conservation purposes. J Acoust Soc Am 72 (6):1845–1854

Sulaiman FS, Darus N, Mashros N, Haron Z, Yahya K (2018) Traffic noise assessment at residential areas in Skudai, Johor. E3S Web Conf 34:02024

Swain BK, Goswami S, Panda SK (2012) Road traffic noise assessment and modeling in Bhubaneswar, India: a comparative and comprehensive monitoring study. Int J Earth Sci Eng 5(1):1358–1370

Tansatcha M, Pamanikabud P, Brown AL, Affum JK (2005) Motorway noise modelling based on perpendicular propagation analysis of traffic noise. Appl Acoust 66(10):1135–1150

Tapia Granados JA (1998) Reducing automobile traffic: an urgent policy for health promotion. Rev Panam Salud Publica 3(4):227–241

Tiwari AV, Kadu PA, Mishra AR (2013) Study of noise pollution due to railway and vehicular traffic at level crossing and its remedial measures. Am J Eng Res 2 (4):16–19

Tripathi BD, Pathak V, Upadhyay AR (2006) A case study of noise pollution in the city of Varanasi. Indian J Environ Prot 26(8):737

Ward WD (1975) Acoustic trauma and noise-induced hearing loss. Human

Zannin PHT, Diniz FB, Barbosa WA (2002) Environmental noise pollution in the city of Curitiba, Brazil. Appl Acoust 63(4):351–358

Part IV

Urban Environmental Planning and Waste Management

Solid Waste Management Scenario of Raiganj Municipality, West Bengal, India

22

Bhaswati Roy

Abstract

Solid waste management is a significant aspect of urban services and environmental sustainability. In the past, enormous land masses made trash disposal easy, but today's growing population, changing lifestyle, technological advancements, and fast urbanization make it harder. Solid waste management is crucial for a healthy and vibrant society. In this paper, attempts have been made to analyze the solid waste management scenario of Raiganj municipality using geospatial technology in terms of solid waste generation, collection, transportation, and disposal. All necessary information was gathered from both primary and secondary sources. These included field research, interviews, and municipal data collection. Data were evaluated statistically and qualitatively using Arc GIS 10.2.1, Microsoft Office Excel, and Microsoft Office Publisher. The cartographic maps were used to analyze the data. The findings of this investigation show that Raiganj's present waste management system cannot handle the growing number of urban residents. This city has growing challenges with solid waste collection, treatment, and disposal. The unavailability of scientific landfill sites hinders Raiganj's welfare. Solid waste management in the Raiganj Municipal area needed to be improved. The ramifications of prospective solutions for municipal solid waste (MSW) at the centralized and decentralized level must be emphasized via the conjunct initiative of different scientific treatment procedures. As a result, municipalities, in collaboration with the informal sector and commercial organizations, must concentrate on developing potential prospects to fulfill the long-term aim of municipal solid waste management (MSWM) sustainability for this municipality.

Keywords

Solid waste · Solid waste management · Solid waste generation · Geospatial technology · Cartography

B. Roy (✉)
Department of Geography, Raiganj University, Raiganj, India
e-mail: bhaswatidaspara@gmail.com

22.1 Introduction

Man is a formal creature; every man has his duty toward society and nature. The Earth's extensive regeneration capacity is not satisfactory for

human beings (Patterson 2006). In the words of Mahatma Gandhi, "Earth has enough to satisfy every man's need, but not every man's greed." For their selfish desire to improve their socio-economic well-being, they are destroying nature through deforestation, greenhouse gas emissions, and excessive use of chemical fertilizers, paving the way for irreversible environmental degradation. Among the various problems faced by the inhabitants of urban society, the problem of solid waste generation and management is one of the most crucial ones. Throughout the world, the problem of solid waste presents a wide variety of complex challenges daily (Singh and Gupta 2012). So, it has become an emergency to study and learn about the hazardous outcomes of solid waste and its management. First, it becomes necessary to understand "what is solid waste?".

According to the World Health Organization (W.H.O.), any unwanted, useless, discarded material that is not a liquid or gas that arises out of man's activity that is not free flowing is called solid waste. Solid waste identification comprises organic and inorganic waste materials such as grass clippings, bottles, furniture, product packaging, kitchen refuse, appliances, paper, batteries, paint cans, which do not carry any value to the first user (Ramachandra 2006). In pure microeconomic terms, it is utterly "bad" or "nasty," and nobody likes to consume it (Singh and Gupta 2012). These waste materials can have an unfavorable impact on public health and severe environmental consequences if not arranged or managed thoroughly (Alam and Ahmade 2013; Tariq 2012). As a result, the municipality or government authority and residents at their level must take precautions to manage solid waste and the resulting contamination (Vij and Aggarwai 2012). Solid waste management is used as a system for operating all garbage, waste collection, waste storage, waste transfer and transport, processing, recycling programs, and disposal of waste in a way that is in harmony with the best principles of human health, conservation, economics, and environmental considerations (Srivastava and Srivastava 2012). The literature survey has found that the disposal

problem is a vital issue of discussion among the researchers, but too few of them are vocal about the overall characteristics of solid waste management like collection, segregation, transportation, and disposal (Khanlaria et al. 2012; Prasad 2016; Roy 2017). However, solid waste management has become an imposing threat for every country (Dungdung and Gurjar 2012) because of the population explosion, rising economy, the boom in community living standards, rapid urbanization, etc. (Sharholy et al. 2008). However, it is one of the neglected areas of development in India (Dungdung and Gurjar 2012; Mohanty et al. 2021). In India, municipal solid waste management is going through a chronic phase due to poor collection, insufficient transportation, and unavailability of suitable facilities for disposal and treatment. However, the government has taken several initiatives in this regard (Dandabathula et al. 2019). Unscientific disposal negatively influences public health and all other components of the environment (Rana et al. 2015; Singh et al. 2012). This situation will change people's attitudes toward consumption (Sakai et al. 1996). India should embrace an out-and-out federal initiative to promote the concept of waste minimization, reuse, and recycling.

With the assistance of the Geographic Information System (GIS), the current research is an exhaustive investigation that aims to analyze the current condition of waste production, sources, and composition and identify the reasons and challenges of municipal solid waste management in Raiganj municipality. In addition, the study intends to inspire academics, planners, and authorities to devise solutions congruent with the sustainable enhancement of the existing system.

22.2 Materials and Methods

22.2.1 Study Area

Uttar Dinajpur is a predominantly agricultural district that is one of the least developed districts in West Bengal, India, with a high level of

illiteracy, rapid population growth, limited health care and livelihood access, and widespread rural poverty. There are four municipalities in Uttar Dinajpur, namely Raiganj, Kaliaganj, Dalkhola, and Islampur. Raiganj is the district town of Uttar Dinajpur and also one of the old municipalities. The substantial role of the municipality entails the maintenance of the cleanliness of the town, providing pollution-free urban areas and providing basic infrastructure like water supply, sanitation, and solid waste management, along with the facilities as per standards. I am a native resident of Uttar Dinajpur and am also a research scholar at Raiganj University. As a concerned citizen, the unscientific method adopted by the municipality to dispose of solid waste bothered my mind. The disposal site is located in ward no. 20 near the river Kulik, which has degraded the river's quality of water and the people who live near the disposal site are affected by several skin diseases. The Raiganj wildlife sanctuary is situated near the Raiganj municipality (around 5 km) and it's popularly known as the Kulik bird sanctuary because the river Kulik flows beside this sanctuary. Actually, the Kulik River is the heartline of the Kulik bird sanctuary. If we don't take this matter seriously in the future, it might take an alarming shape. There has been a lack of infrastructure to manage solid waste in a proper way. This study attempts to explore the present solid waste management conditions of the study area and presents a conceptual analysis with the help of a Geographical Information System (GIS). Raiganj municipality is located in the south-western part of Uttar Dinajpur district. The absolute location of this municipality lies between 88°6′ 23.812″ E to 88°9′5.932″ E longitude and 25°38′ 27.102″ N to 25°34′57.153″ N latitude. The area of the municipality is 10.75 km^2, consisting of 25 wards (shown in Fig. 22.1), situated 425 km from the state capital Kolkata. The total population of the area is 183682. As a result of rapid growth, according to the 2011 census record, 96,565 are male and 87,092 are female. At present, the number of wards has been increased in Raiganj municipality, but proper maps are not available on the municipality website.

22.2.2 Materials

The method of this paper rests upon gathered data from the primary field and different secondary sources. These included preliminary field investigation, face-to-face interviews, and municipality data collection.

22.2.3 Methods

Data were analyzed both quantitatively and qualitatively using different softwares such as Arc GIS 10.2.1, Microsoft Office Excel, and Microsoft Office Publisher. A stepwise normative approach will be adopted to understand the solid waste management process of study area. The methodology of this study is a bifold system.

First step to study the existing situation analysis includes the pilot survey, information collection about waste management situation of the municipality, description of the factors which are influencing the solid waste generation of this area.

Second step is analysis of existing situation with the help of GIS technique comprised of result and discussion, finally the conclusion. To create maps in Arc GIS 10.2.1 software, spatial data and attribute data are entered into a database. Theses include ward map of Raiganj municipality, solid waste management related data like ward wise generation of solid waste, collection of waste and worker distribution for solid waste collection, etc. I have collected the ward map of this municipality from the municipality office. Registration and transformation were done to convert the collected ward map image into real-world image. After that I have used the digitization technique for R to V conversion (raster to vector). Necessary additional field was added in attribute table of these vector file. Different thematic mapping techniques like choropleth map and pie diagram have been incorporated with the help of this Arc GIS software. Choropleth map mainly shows the ward wise generation and collection of solid waste. Whereas, pie diagram reveals the ward wise

Fig. 22.1 Location of the study area
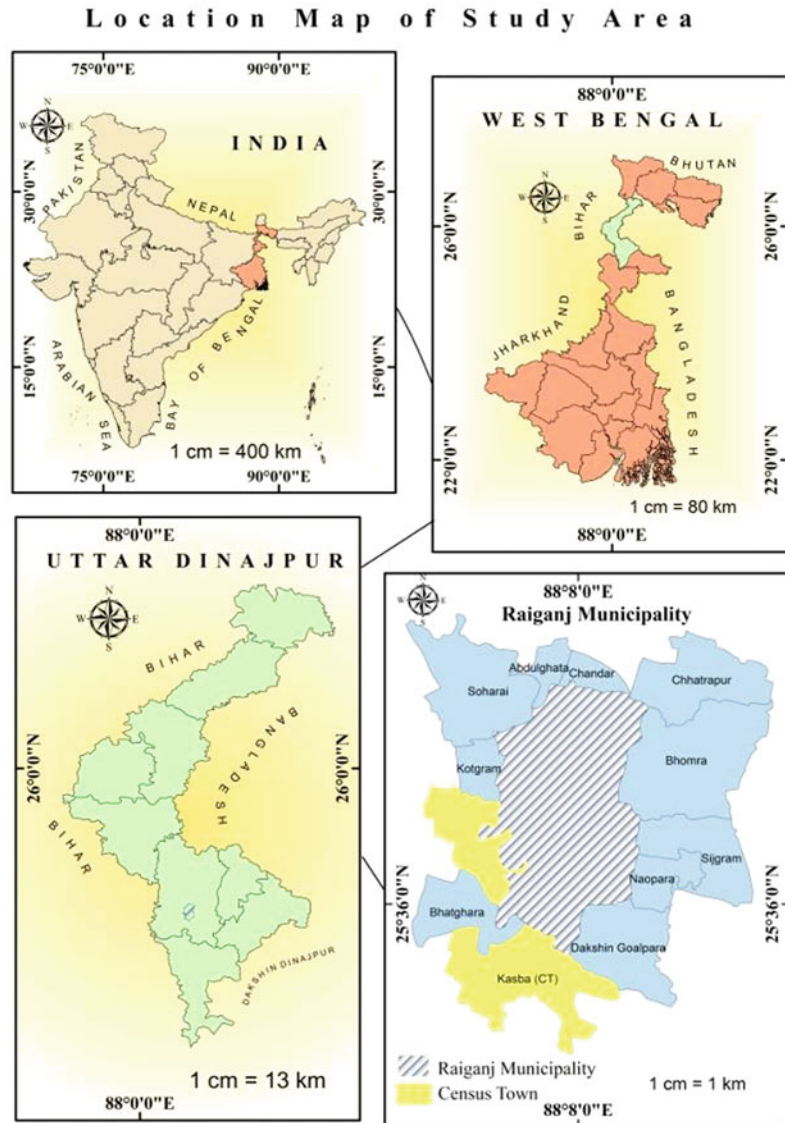
worker distribution as well as the difference between collection and generation.

22.3 Result and Discussion

22.3.1 MSW Generation of Study Area

The generation of MSW comprises household waste, market waste, sanitation residue, construction, demolition debris, etc. The amount of

MSW has been increasing rapidly due to changing lifestyles, rapid urbanization, and an increasing population. It can be said that solid waste is the inevitable upshot of human activity. The proposition can be asserted by citing a beautiful example. When we purchase articles from shops, the shopkeepers pack the goods in plastic, which is not destroyable and, more importantly, not biodegradable; we leave the plastic packet here and there. In this way, solid waste is generated. Raiganj generates approximately 97 MT of waste per day (per capita

400 g) from various sources, with 51% biodegradable waste and 49% non-biodegradable waste. About 63% of trash comes from homes, and the other 37% comes from hotels, markets, farms, and other places. Domestic solid waste contains about 60% organic matter, and the remaining 40% is inert materials. The moisture that is contained in organic matter is about 50%. Market SW contains about 70% biodegradable matter, and 30% is non-biodegradable. It is assumed that agricultural waste contains about 100% biodegradable matter, neglecting the very few inert materials, and clinical waste contains about 100% non-biodegradable materials. Figure 22.2 represents the ward wise solid waste generated in MTPD. It has been shown that waste production varies from ward to ward. Most of the time, the inner wards produce more waste than the outer wards, and wards 9, 10, 13, and 16

are the most important ones for the Raiganj municipality. Commercial activities and many people living in these areas are primarily to blame.

22.3.2 Collection and Transportation

Solid waste management begins with the collection. Garbage is picked up from residences, business areas, and collection points. The success of any SWM system largely depends on the critical components of the collection, transportation, and disposal. The success of the effective solid waste management system, particularly the primary collection system, largely depends on the proper coordination between the dwellers, the generators, and the staff, the collectors.

Fig. 22.2 Ward wise solid waste generation
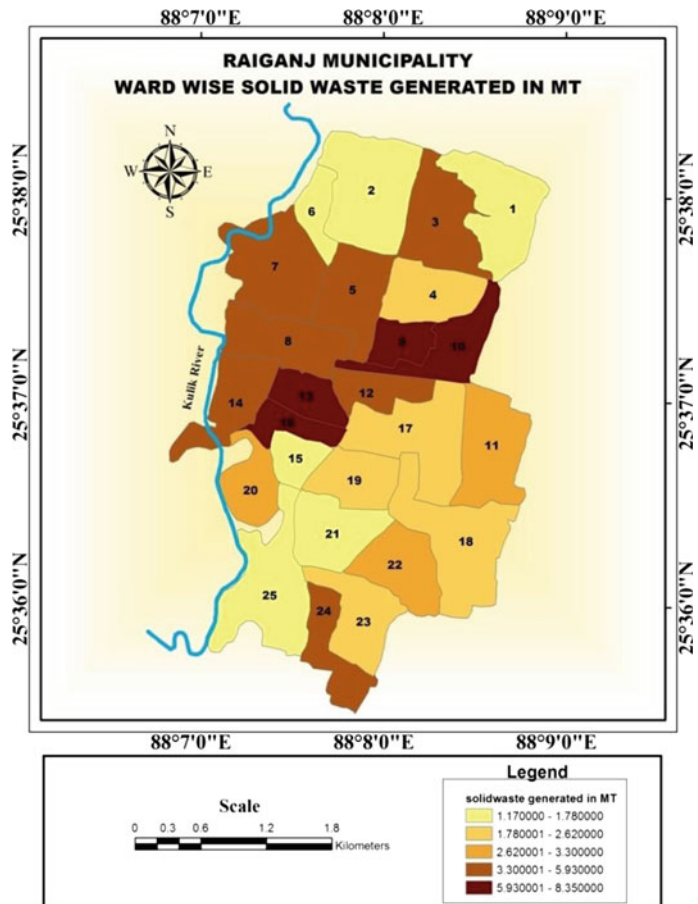
Raiganj municipality used a systematic method in the collection process (Fig. 22.3). Raiganj municipality collects waste from door to door daily except Sunday. The municipality pays for around 185 staff engaged in the collection process, and the municipality pays 112.018 lakh for 185 staff (as given in Table 22.1). Every morning, the collection staff blows the whistle, announcing his arrival at the place, and the people put their domestic waste into the handcart or tricycle of the staff (Tables 22.2 and 22.3).

According to Raiganj municipality, the door to door collection system serves about 60% of households without charges. It has been seen that the municipality collector plays a dominant role in the core area rather than the outer area. The NGO, namely Green Zen, the best NGO in North Bengal, executes the crucial task of collection and disposal of biomedical waste. The NGO collects waste from the district hospital, five nursing homes, and 21 clinics. Waste is transferred to the transfer station from waste generating points through tractor tippers, tractor trailers, refuse collectors, dumper placers, and tricycles, along with hand carts. There is a lack of separate compartments or separate vehicles for biodegradable and non-biodegradable waste. There can be a massive discrepancy between the existing numbers of vehicles and the required ones (Figs. 22.4 and 22.5; Table 22.4).

22.3.3 Disposal of Waste

The disposal of waste is an essential aspect of the SWM process, as unscientific disposal of waste
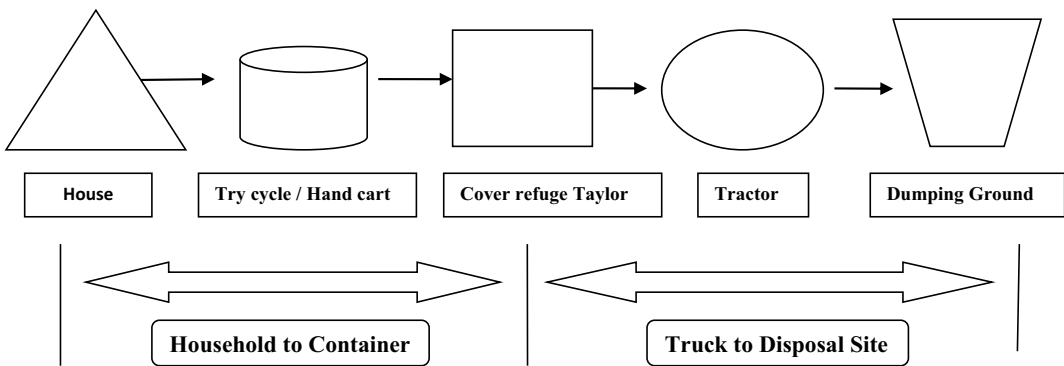
Fig. 22.3 Systematic model of collection system in RMC. *Source* Author creation

Table 22.1 No of staff engaged in collection process

Type of workers	No. of staffs	Salaries and overheads (Rs. Lakh)
Door to door collectors	64	39.3578
Street sweepers	56	33.30275
Transportation personal	65	39.3578
Total	185	112.01835

Source Raiganj municipality office

Table 22.2 Coverage of door to door collection system

Total no of wards	House to house collection		
25	No of wards covered	Collection schedule (daily/alternative day)	Cost for collection
	25	Daily	Nil

Source Based on municipality data

Table 22.3 Ward wise distributions of workers, generation, and collection of SW

Ward No.	Solid waste generation in MT	Solid waste collection in MT	Workers engaged in collection		
			Door to door collector	Street sweeper	Transportation personal
1	1.54	1	1	1	2
2	5.59	4.3	3	2	2
3	2.37	1.37	2	1	2
4	1.75	1.1	1	1	2
5	4.57	2.44	3	3	2
6	1.78	1.07	1	1	2
7	5.2	3.33	3	2	2
8	5.16	4.12	3	3	2
9	6.58	4	5	4	2
10	8.35	6.55	8	6	4
11	2.85	2	1	4	2
12	5.61	4.4	3	6	4
13	8.01	7	7	6	4
14	5.14	4.42	3	2	2
15	1.57	0.97	1	1	2
16	7.07	6.8	6	5	2
17	2.62	1.55	1	3	2
18	2.48	1.95	1	3	2
19	2.27	1.76	1	1	2
20	3.19	2.91	2	1	2
21	1.17	0.9	1	1	2
22	3.3	2.3	2	2	2
23	2.19	1.12	1	2	2
24	5.93	3.21	3	2	2
25	1.23	0.9	1	2	2
Total	97.52	71.47	64	65	56

Source Based on municipality data

can cause irreparable damage to the environment, human health, and subsoil strata. Raiganj currently has one dumping ground covering approximately 7 acres of land near the River Kulik in Bander Ward No. 20, approximately 1.5 km from the town center. At present, the open dumping method is used in this area. The land is low lying, so it cannot contain much solid waste collected for dumping. The eastern side of the Kulik River is becoming increasingly filled with waste. As per requirements, the space is becoming confined.

22.4 Conclusion

The colossal amount of solid waste generated by human efforts, consciously or unconsciously, has now become a universal phenomenon, culminating in significant health-related issues for civilization. As the famous axiom goes, "Prevention is better than cure;" here, too, it is relevant in association with the prevention of these practices is superior to mitigating the toxicity of their pernicious effects on the living

Fig. 22.4 Ward wise
collection of solid waste

Fig. 22.4 Ward wise collection of solid waste
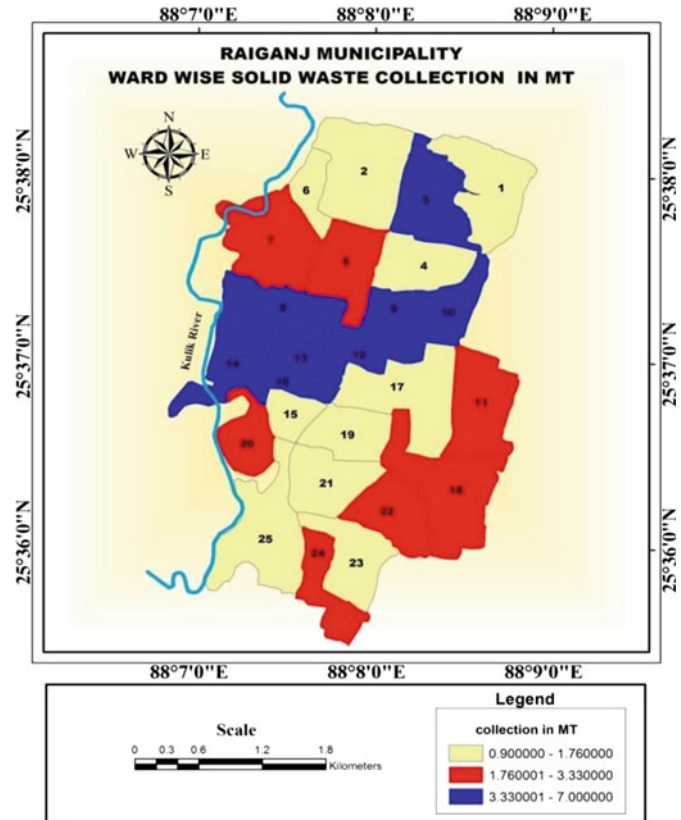
system and environment. However, to achieve a sustainable solution to this problem, a proper waste management system and significant public awareness are highly instrumental. Waste management is a multifaceted system that deals with its treatment and disposal; it is a holistic approach with a wide range of complementary activities that integrate reduction of waste generation, collection, segregation, and proper transportation to its corresponding recycling hub. Through this analysis, we can conclude that the selected study area suffers from different disposal-related problems in this present study. The surrounding area's inhabitants face various problems due to unscientific landfilling in low-lying areas near the river Kulik. As per field survey data, the economic condition of the people and the generation rate of solid waste are entwined in this area. The wards inhabited by high-income groups of people generate more garbage than those of people with low incomes. The commonly observed findings in this area are (1) the waste collection frequency is less in comparison with the amount of waste generated in the municipality; (2) there is a lack of workforce, trained staff, modern machinery, and equipment; (3) there are no facilities for implementing recycling processes; (4) lack of private participation or involvement of community-based organizations; (5) insufficient fund allocation to process and dumping is a challenging problem in this area; (6) a few of the wards face water logging problems such as wards 1, 2, 17, etc.; (7) there is no separation of solid waste such as plastic, food waste, metal, and so on; (8) lack of public awareness about the need for solid waste segregation; and (9) lack of proper dumping facilities in this area is also a significant problem. The dumping site is near the river Kulik, degrading the river's health and
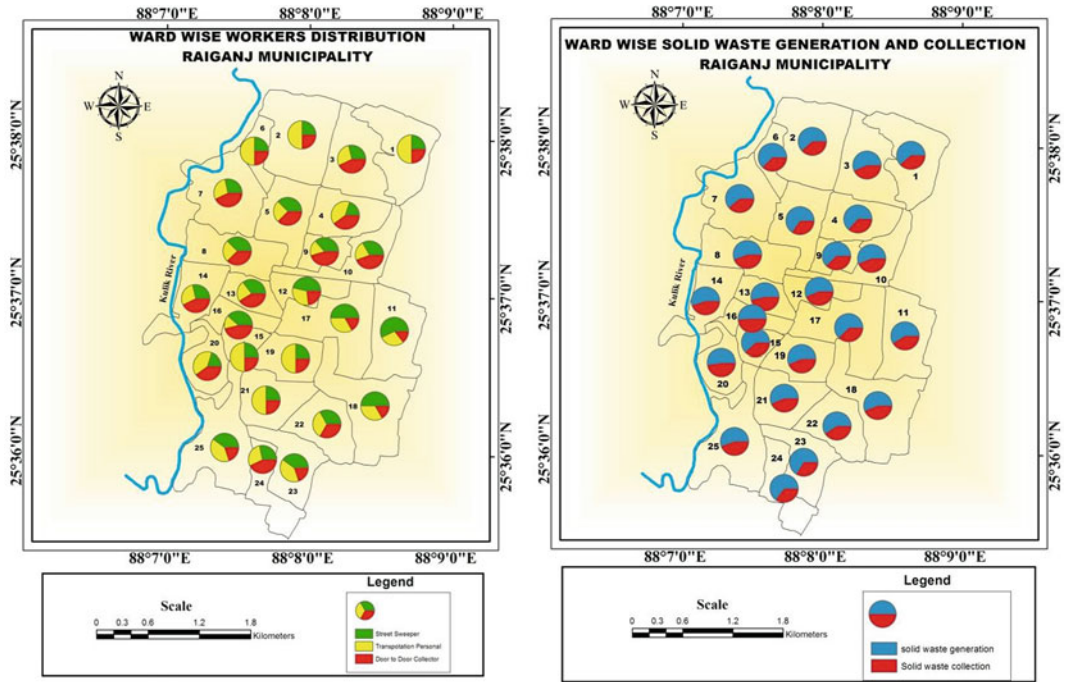
Fig. 22.5 Ward wise distributions, generations, and collection of solid waste

Table 22.4 Total no and type of vehicles used in Raiganj municipality

Type of vehicles	Existing numbers	Actually require/proposed	Avg. no of tips per day
Tractor tipper	2	3	1
Tractor trailer	20	35	1
Refuse collector	4	60	2
Dumper placers	10	12	1
Try cycle	35	55	2
Hand carts	20	100	2

surrounding environment. Adopting centralized and decentralized strategies to facilitate solid waste management at various sources could be workable for tangible sustainability in the municipal solid waste management (MSWM) system. Also, the optimum involvement of organized informal waste management sectors, along with dedicated ventures from private and government agencies, can be an effective tool to combat the MSWM challenges and put forth good scopes for the future of this municipality. If we take some initiatives, it can minimize the impact of solid waste. These steps are

- Generation of municipal solid waste should be decreased.
- 4R (reduce, recycle, recovery and reduced) of solid waste management should be introduced in every part of municipality. Increase the people awareness about 4R.
- Municipalities should increase their level of service as well as the number of staffs to provide the good service to the public.
- People participation as well as awareness program regarding hazardous waste is essential.
- Collection of hazardous waste at collection points shall be safe and secure. Promotion of

the use of less hazardous alternatives. Segregation of solid waste is very essential in collecting points.

References

Alam P, Ahmade K (2013) Impact of solid waste on health and the environment. Int J Sustain Dev Green Econ 2:4

Dandabathula G et al (2019) Impact assessment of India's Swachh Bharat Mission—Clean India Campaign on acute diarrheal disease outbreaks: yes, there is a positive change. J Family Med Primary Care 8(3):1202–1208. https://doi.org/10.4103/jfmpc.jfmpc_144_19

Dungdung A, Gurjar E (2012) Solid waste: management and related health hazards—an Indian perspective. In: Bhatt M, Illiyan A (eds) Solid waste management: an Indian perspective. Synergy Books of India, New Delhi, p 155

Khanlari G, Abdilor Y, Babazadeh R, Mohebi Y (2012) Land fill site selection for municipal solid waste management using GSI method, Malayer, Iran

Mohanty S, Saha S, Santra GH, Kumari A (2021) Future perspective of solid waste management strategy in India. In: Baskar C, Ramakrishna S, Baskar S, Sharma R, Chinnappan A, Sehrawat R (eds) Handbook of solid waste management. Springer, Singapore. https://doi.org/10.1007/978-981-15-7525-9_10-1

Patterson S (2006) http://greenliving.lovetoknow.com/How_Do_Humans_Affect_the_Environment. Retrieved 27 Jan 2016, from www.google.com

Prasad MSG (2016) Applicability of geospatial technology and a measure of information for assessing the suitability of land fill sites: a case study of Mysore city. Int J Emerg Technol Eng Res 4:6

Ramachandra T (2006) Management of municipal solid waste. TERI Press, New Delhi

Rana R, Ganguly R, Gupta AK (2015) An assessment of solid waste management system in Chandigarh city, India. EJGE 20(6):1547–1572

Roy B (2017) Towards scientific management of solid waste through suitable landfield site selection for Raiganj municipality West Bengal, India: a model based approach. Int J Trend Sci Res Dev (IJTSRD) 1 (6):892–901. ISSN 2456-6470. https://www.ijtsrd.com/papers/ijtsrd4692.pdf

Sakai S, Sawell SE, Chandler AJ (1996) World trends in municipal solid waste management. Waste Manage 16:341–350

Sharholy M, Ahmad K, Mahmood G, Trivedi R (2008) Municipal solid waste management in Indian cities—a review. Waste Manage 28:459–467

Singh J, Laurenti R, Singha R, Frostell B (2014) Progress and challenges to the global waste management. Waste Manage Res 32(9):800–812

Singh AK, Gupta V (2012) Management of solid waste & its effects on health: a case study of South Delhi. In: Bhatt M, Illiyan A (eds) Solid waste management: an Indian perspective. Synergy Book India, New Delhi, pp 177–192

Srivastava R, Srivastava A (2012) Municipal solid waste management: a case study of "The City of Taj". In: Bhatt M, Illiyan A (eds) Solid waste management: an Indian perspective. Synergy Book India, New Delhi, pp 239–240

Tariq M (2012) Sustainable decentralized solid waste management. In: Bhatt M, Illiyan A (eds) Solid waste management: an Indian perspective. Synergy Book India, New Delhi, pp 208–209

Vij D, Aggarwai B (2012) Domestic solid waste management: a case study of Gazibad District of U. P. In: Bhatt M, Illiyan A (eds) Solid waste management: an Indian perspective. Synergy Books India, New Delhi, pp 228–229

Integration of Advanced Technologies in Urban Waste Management

23

Parvez Hayat

Abstract

It is pertinent to distinguish between urban solid waste when compared to its rural counterpart. Rural areas generate almost negligible waste when compared to the urban areas as till recently they led frugal and minimalistic lifestyle. Basically, there are four types of solid waste in urban areas, one is the household waste, which we commonly refer to as garbage, the second is the biomedical/hospital waste, the third is the e-waste and the fourth is Construction & Demolition Waste. It is indeed very surprising to note that till date most of the developing countries have not prepared an inventory of urban solid waste. In fact, it does not seem to be a priority of either the citizens or the urban local bodies. Technology will be the key to tackle the challenges of urban solid waste management in India. Through satellite imagery/remote sensing techniques to utilizing machine learning and artificial intelligence (AI), it is possible to identify hotspots where different types of waste are accumulating and also in tracking movement of bins and trucks. It would then be possible to develop an optimal strategy to transfer these wastes using GIS to appropriate treatment facilities for their ultimate disposal. One of the major issues faced in solid waste management is the existence of dumpsites, which must be closed, and the legacy waste appropriately disposed as it has now become a mountain of waste and cannot take in any fresher waste. To initiate the closure, an environmental impact assessment (EIA) needs to be done, which is hampered by the lack of past data regarding the activities at the dumpsite. Therefore, the analysis of multitemporal remote sensing images and aerial photography is a useful tool for conducting the EIA. Finally, the Government of India needs to develop a standardized policy to dispose of household waste, e-waste and medical waste. It is the need of the hour and should be done in mission mode on a war footing. The need of a central ministry on solid waste management may be set up without any further delay.

23.1 Introduction

Unprecedented levels of urbanization and population growth led to produce massive amounts of waste, most of which is generated in the large

P. Hayat (✉)
Centre for Disaster Management, Department of Geography, Faculty of Natural Sciences, Jamia Millia Islamia, New Delhi 110025, India
e-mail: phayatips@gmail.com

metropolitan cities (Zhang 2016; Ramachandra et al. 2018). Every day, the problems related to the inefficient waste management are a serious threat to environment and health of integral components of a sound ecosystem (Vergara and Tchobanoglous 2012). Critical factors which include rapid urbanization, alteration in the pattern of consumption which can be linked to the economic growth and mechanization have resulted in augmentation of waste generation (Liu et al. 2019). The pace of accelerated growth of these factors has in fact rather surpassed the pace of advancement required in the technological space that could handle such a downpour of waste (Pal and Bhatia 2022). Hence, this widened gap can be observed at the level of urban local bodies (ULBs), where many are still practicing waste management in the traditional ways (De and Debnath 2016; Kumar et al. 2017).

In India management of urban waste comes under the purview of Ministry of Environment, Forests and Climate Change (MoEFCC) which keeps on releasing time-to-time guidelines for the management of urban waste (Reymond et al. 2020). Recently, the MoEFCC released new guidelines in the form of SWM Rules 2016 that replaced Municipal Solid Waste Rules 2000 which was further amended in 2018 (Mandal 2019). These rules were framed and put in action in order to make waste management achievable in a sustainable sense. However, due to lack of enforcement of these rules at the Urban Local Bodies (ULB) level or at the level like gram panchayats, the waste management has remained relatively unchanged (Joseph et al. 2012). In addition to this, tools and technologies which should be there in the market to address the issue of surging waste generation are missing (Vanapalli et al. 2021). Cities and urban villages are already overwhelmed and will continue to be burdened with the problem of increasing waste generation due to lack of space to form further landfills (Mandal 2019). As a result, unwillingly, dumping points in and around cities will be formed and always grow in numbers (Malav et al. 2020).

The future generations are expected to be smart and may adopt advanced technologies like geospatial techniques and artificial intelligence (AI) in the urban waste management (Allam and Dhunny 2019; Andeobu et al. 2022). For this, the prospects of smart and advanced technologies in waste management may be researched and developed for ensuring a better waste management approach at a lower cost and in short time period (Dhanwani et al. 2021; Al-Ruzouq et al. 2022). The remote sensing and GIS techniques have been already utilized in the municipal waste management practices in developing countries like India (Ali and Ahmad 2020). Moreover, the researchers may also look after the applicability of machine learning and AI in the urban waste management (Ni et al. 2020). As an example, satellite imagery with machine learning can identify hotspots where waste has been accumulating or automatic sensors that notify every time a dustbin or a container is full, etc. (Glanville and Chang 2015). Therefore, this exploratory study is aimed to understand the need of sustainable management of urban waste in the cities of developing countries like India and how the advanced technologies can be utilized for it. The advanced techniques and tools may assist the urban planners and waste managers to increase the resource recovery, recycling and reuse of solid and other waste (Zorpas 2020) beside identifying the illegal accumulation of waste to avoid problems arising from it (Abdallah et al. 2020).

23.2 Waste Generation and Classification

Understanding the characteristics of the waste around us is crucial in developing technologies and strategies for effective solid waste management (Mohanty et al. 2021). In the context of an urban setting, waste can be classified as solid, liquid or gaseous (Abdel-Shafy and Mansour 2018). All these categories of waste will include household, industrial, biomedical, municipal and radioactive wastes and have a different method of treatment and disposal (Selvan Christyraj et al. 2021). In India, approximately, 1.4 lakh MT of municipal solid waste (MSW) is being generated

daily (Kumar et al. 2017). MSW is primarily produced by domestic households with a little fraction being generated from commercial and industrial establishments. The entire catalogue of the sources of waste, therefore, can be described under five major classifications of waste (Miezah et al. 2015).

23.2.1 Municipal Solid Waste

MSW includes all the garbage discarded by general public and is mostly generated from households, colonies, institutions, offices, shops, schools, hotels, etc., in the form of papers, plastic, metal, glass, food waste, small quantities of batteries, lights and bulbs, etc.

23.2.2 Industrial Solid Waste

It generally comprises waste from industries, factories and workshops such as food processing, packaging waste, solvents, chemical and toxic waste, oils and paints.

23.2.3 Agricultural Waste

This type of waste typically consists of livestock waste, residues from agriculture crops, etc.

23.2.4 Hazardous Waste

Such hazardous and toxic waste mostly comprises waste from the wide spectrum of activities and processes related to nuclear establishments, healthcare facilities and hospitals, manufacturing industries, energy production plants, etc.

23.2.5 Construction and Demolition Waste

Since large-scale construction activities continue to grow with expansion of urbanization, demolition waste is generated as and where any construction/demolition activity takes place, with the result, building roads and bridges, fly over, subway, retrofitting, redesigning, etc. It includes most of inert and non-biodegradable materials such as concrete, plaster, wood and even metals plastics and so on.

23.3 Current Waste Management Practices in India

23.3.1 Collection and Transfer

Collection and transfer are the most cost-intensive step in the entire waste management system (Hazra and Goel 2009). In India, it considerably varies between regions of low income to high income. In many cities, approach of waste collection ranges from municipality being directly involved and having total control in waste collection and transportation to having contracted private waste collection agencies and making them responsible for collection and disposal (Sharma et al. 2018). Since municipality is responsible for a city's waste management, the system of having concessionaire becomes an inefficient way of collection, as it has been observed in many cities (Hazra and Goel 2009; Sharma and Chandel 2017). High-income cities may have standardized and dedicated vehicles and compactors for collection and transportation, while low-income cities or areas, generally, tend to work with non-mechanized rickshaws working on contractual basis. Currently, many cities in India face shortage of storage bins, necessary transport service or well-designed transfer stations equipped with necessary technologies to manage and process waste (Kumar et al. 2017). The existing system, to a large extent, is inefficient in collecting waste in a proper segregated manner, as it should for maximum resource recovery (Sudha 2008).

By knowing collection rate of a geography, the broader picture regarding waste management can be known. Cities like Delhi and Mumbai have achieved collection rates of over 50% while for many other cities, this rate is far below (Prajapati et al. 2021). India largely depends on

informal sector for the collection of its waste and recycling (Wilson et al. 2006). This large informal space is not governed by rules and policies formed at the municipality level and, thus, lacks control over the waste management (Kumar and Agarwal 2020).

23.3.2 Disposal

Throwing away or disposal is the final destination to most of the urban solid waste in India (Rajput et al. 2009). Either the waste will be dumped or landfilled. Only a little fraction of the waste finds its way back into economy via methods like recycling and composting. Disposal options in use are:

23.3.2.1 Open Dumping
This is the most commonly observed waste disposal method involving uncontrolled throwing of waste with no provision to check leachate, odour, dust, rodents, gas, etc. (Ferronato and Torretta, 2019). The waste remains for relatively longer periods and contaminates components of the environment (Pandey et al. 2012).

23.3.2.2 Sanitary Landfill
It is disposal of urban solid waste in a semi- or fully engineered landfill and is one of the most attractive disposal options. Comparatively, the harmful effects can be minimized and various processes and parameters too can be controlled by the operator (Meegoda et al. 2016). In fact, it becomes an integral part of urban waste management and will continue to be adopted at wider scale widely an effective method for disposal of waste (Abdel-Shafy and Mansour 2018).

23.3.2.3 Incineration
Incineration is a well-established and mature waste treatment process wherein combustible materials which are rejected are burned to high temperatures to leave behind ash and noncombustible (Buekens 2012). The volume reduction by almost 75–95% is accompanied by

weight reduction. Treatment technology like Incineration, unless they truly deal with residual waste (rejects), which they not in most cases, will undermine recycling and composting and many valuable resources that can be recycled and composted will be burnt in the incinerators adding to the already piling up problem of pollution (Buekens 2012). In addition to this, it is not a clean technology and may produce pollution of air by releasing toxic ash into the atmosphere (Manisalidis et al. 2020).

23.3.3 Recycling and Composting

23.3.3.1 Recycling
This is one of the traditional methods that has been known to us in the form of reprocessing of waste into new and innovative products. India depends on informal sector for recycling of waste, and therefore, not many such facilities are under authoritative control (Annamalai 2015). Due to this, these sectors do not follow any regulations and emission standards and pose serious threat to the health of environment and mankind.

23.3.3.2 Composting
It is, in fact, a biological treatment of biodegradable waste to convert waste into compost or manure under controlled conditions of temperature and moisture. Although this process is all natural and easy to implement in a decentralized system, the support is limited from the municipalities and there is the absence of reward/incentive schemes to motivate citizens to shift to this green alternative (Vergara and Tchobanoglous 2012). While natural composting tends to preserve and protect soil quality, this is direct benefit, especially in India where significant fractions of the waste are biodegradable (Ferronato and Torretta 2019). Only caution here is to ensure that the quality of compost produced should adhere to the standards; thus, segregated waste collection plays crucial role in improving quality of compost (Luttenberger 2020).

23.3.4   Critical Problems and Inadequacies and Limitations of Current Waste Management System

Waste management in the context of urban areas is a problem in India. From political structure to grass roots, range of shortcomings are present. There is inadequate enforcement of law and policies and execution of environmental legislation, lack of long-term planning, insufficient finances, lack of skilled personnel and poor monitoring (Kumar et al. 2007). Truly speaking the existing infrastructure for solid waste management in India has not been in sync with the development elsewhere in advanced countries and, therefore, has resulted in making operations inefficient and difficult to manage (Ferronato and Torretta 2019). At the same time, little advancement visible is confined to metro cities and a few other cities so far (Mohsin et al. 2022).

Problems related to collection of waste, transportation and disposal remain unanswered in metropolitan cities (Kala and Bolia 2021). Inadequate number of vehicles, that too are usually in bad shape, are often carrying the old design statement which have not been efficient in collecting and transporting waste in the right way. At times, in many areas, there is perceptible absence of provision of collection of waste by vehicles in a segregated format and they are not even fitted with compactors, leading to the transfer of loose waste and, hence, imposing a restriction on the overall capacity of overall existing system (Jimenez et al. 2015; Gu et al. 2017). The technological aspects have been almost missing from the urban waste management. Regular monitoring on the real-time basis and collection of data are two major components of any solid waste management and to have an efficient system and processes, emerging technologies and tools need to be adopted at ULB level (Asnani and Zurbrugg 2007). Technologies like AI, Machine learning, GIS as well as remote sensing have the capacities to drive waste management towards efficiency and sustainability (Abdallah et al. 2020). However, these technical competencies have been conspicuously missing resulting the system to work in conventional way.

23.4   Need for Advanced Technologies in Urban Waste Management

The existing infrastructure is incapable of managing and disposing the waste being tremendously generated every day, and therefore, it remains a challenging task for all nations to efficiently run a waste management system (Mohanty et al. 2021). New and advanced technologies like Remote sensing, GIS and GPS can govern route optimization, identifying dump sites, selection of landfills and information related to waste generation. GIS can be combined and remote sensing and GPS in recording spatial data and using the data directly for analysis and cartographic representation (Karsauliya 2013). GIS has proved to be very helpful in reducing time and is cost-effective as well (Khan and Samadder 2014).

AI can surely be incorporated into the waste management practices for achieving efficiency and optimization by taking better decisions. AI can analyse and process extensive information at a much faster rate than human reasonings and decisions, thereby, reducing time. It may also help in detection of waste, trash space and overcome issues as regards sustainability (Sharma and Vaid 2021). The technology can be employed at the sorting site where AI-powered robots can segregate different items efficiently with almost four to five times the speed of sorting than human labour (Castro and New 2016). IoT can be implemented widely to enable real-time monitoring by creating a platform in which physical objects are connected digitally to sense, process and interact within the network (Ashri 2019).

23.5 Applications of Technologies in Municipal Solid Waste Management

23.5.1 Generation of Solid Waste

The generation of waste includes those exercises where materials are recognized as being of worth and are either discarded or assembled for removal. What is significant in generation of waste is to take note of that there is an ID step and that this progression changes with every person. Waste generation is, as of now, a movement that is not truly controllable. Dealing with the gigantic measures of strong waste created has turned into a major issue, and in such manner, GIS has ended up being a help for Planners (Dutta and Goel 2017). The distribution of population data and information for how much solid waste produced in a specific region are gathered and various population layers and solid waste data are made in GIS. Then, every one of the layers is stacked (or superimposed) over the review region for resulting examination (Shrivastava et al. 2015). Investigation of layers should be possible, and regions with expanded solid waste age can be recognized and classified into various classifications, and appropriate measures can be applied. In this manner, RS and GIS can be utilized for the recognizing and classification of regions based on the generation of solid waste rates and spotting the sites for removal of the Solid waste.

23.5.2 RFID Enabled Door-to-Door Waste Collection Monitoring

By introducing RFID labels at every property, the experts in the municipal corporation can guarantee that the waste gets picked from every single house consistently (Purohit and Bothale 2011). Likewise, using similar technology there can be regular checks on the duties performed by the staff (Ramadan et al. 2012).

23.5.3 Smart Bins

Sensors are being introduced in public garbage cans, also called as Smart bins, to keep a continuous track of the situation with the storage level of the Canisters (Fig. 23.1). Container level sensors in these trash boxes give signs to the organization's order and control centre whenever garbage in cans exceeds the certain threshold limit. Therefore, the system contacts the closest waste collection vehicle drivers with respect to the storage level of container. These cans are then immediately cleared by the vehicle drivers without wasting any time. PC vision annotation and AI calculations permit these sensors to recognize various kinds of trash as the containers are being filled. For instance, a smart and intelligent waste bin uses ML to identify, categorize and sort waste in shortest span of time after the same is thrown away (Kannangara et al. 2018). Smart bins are frequently matched with an application that tells the users about the area's closest waste bin, keeping the containers from spilling over (Bano et al. 2020).

23.5.4 Collection

Collection vehicles can be installed with sensors, aside from the standard set-up of sensors incorporated into trucks, there are a few sensors explicit for the waste business, for example, an equilibrium checking the weight of the gathered waste, RFID sensors for the ID of individual trash containers or GPS sensors to track the area of the vehicle (Fig. 23.2). GPS vehicle is another smart offering, by which Garbage authorities' entire fleet of vehicles is fitted with GPS gadgets as a component of the GPS Vehicle Tracking System. It helps municipal corporations, and waste collection companies in acquiring real-time information about waste collection vehicles and checking the routes that vehicles are crossing through. This, in turn, brings about additional vehicle efficiency and bringing down the costs.
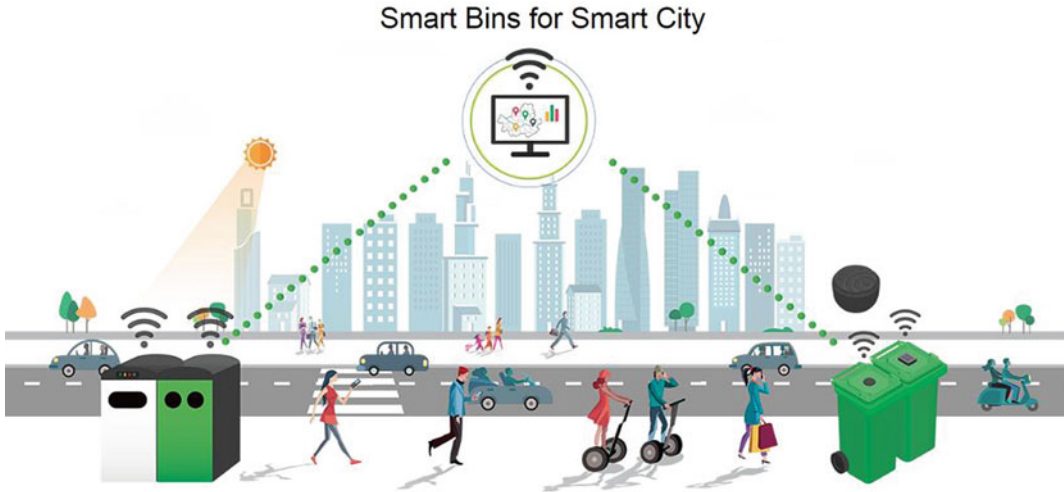
Smart Bins for Smart City

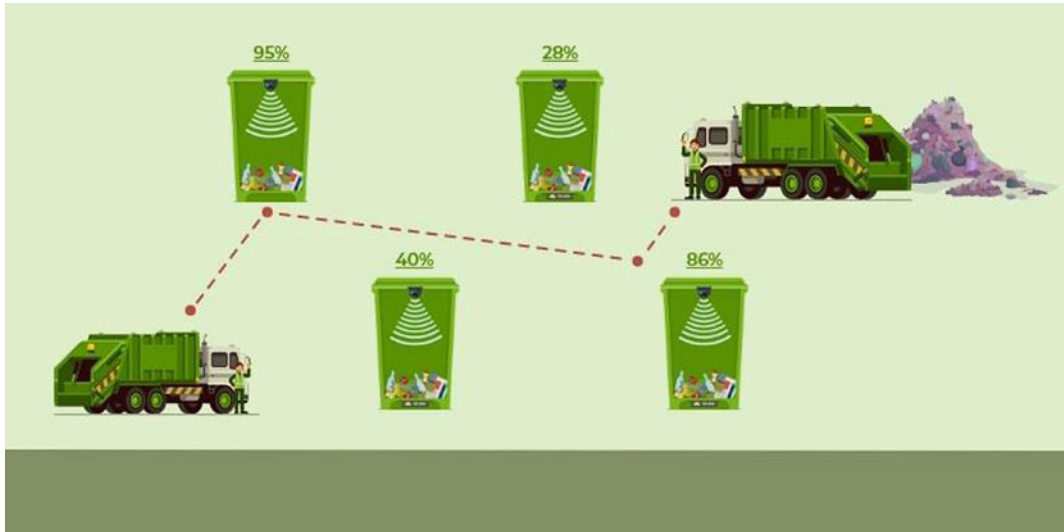**Fig. 23.1** Proposed smart bins for smart city. *Source* Tech Briefs (2022)

Fig. 23.2 Re-route efficiency for timely pickup of waste. *Source* Excellent Web World (2022)

23.5.5 Transportation

The transportation and collection services ought to be sufficient in collecting waste daily on time. Transportation of waste expands the carbon footprint, and viable utilization of AI in this part helps in upgrading the carbon emission by proposing best routes (Wang et al. 2021). An efficient and fruitful incorporated SWM plan requires appropriate routes for waste collection, and it costs regularly represent 70–85% of the absolute strong waste management cost. Hazardous, toxic and infectious waste should not be collected in a similar truck since general waste through and also not at the same time. The storage capacity has to be avoided patients and the common public. It should preferably be very much ventilated and also liberated from vertebrate pests. Another advancement in waste management is the wise dumpster, which is

loaded with AI programmes and IoT sensors (Anh Khoa et al. 2020). The sensors on these dumpsters measure the waste levels of the trash dumped inside and move this data to the principal removal framework for handling by means of intermediate servers. The dump trucks/vans can move as per the message received and gather the waste from the filled-up containers. Quite a few researchers off late have optimized models made for waste collection frequency and designing of the route, and most of them depend on Genetic Algorithm (GA) and also its hybrid variations. GA enhanced the course for the collection of electrical and electronic home waste as conveyed by Kroll and its co-workers (—). The collection costs were diminished by GA due to the streamlined route distance and the number of collection trucks and staff. Clients were urged to take an interest in the scheduling of trash collection demands in order to foster better routes (Sharma and Vaid 2021).

23.5.6 Smart Sorting

The role of AI in sorting the waste in a smart manner is like the role of AI in assembling things on a conveyor belt. Whether that incorporates waste or new items is examined with cameras and analysed by deep learning or algorithms. Robot arms and other devices then, at that point, pull the things off the belt for additional handling which, on account of waste management, incorporates sorting. They can identify things produced using various materials as well as subtleties between things of similar material, including whether a thing has been synthetically debased, guaranteeing virtue of the waste stream (Schneider 1970).

23.5.7 Smart Recycling

As indicated by a report from the UN that every day, 50 million tonnes of e-waste is produced, As the quantity of electronic gadgets ending up in landfills is expanding constantly, e-waste has been recognized as a critical issue in solid waste

management. Disposed electronic devices frequently contain unsafe chemical substances, such as lithium from a cell phone battery, which can leach into groundwater (Needhidasan et al. 2014). Simultaneously, these gadgets present a valuable chance to recover valuable and base metals, like gold and copper, in a proficient way. The systematic management of IOT considers a digital record that will be made up of electronic devices and batteries. IoT sensors and other electronic gadgets can be enacted, with makers or waste directors booking a pickup and even bringing a replacement, long before they ever end up in a landfill (Nižetić et al. 2020). The capacity to instal IoT technologies into repositories additionally considers the utilization of AI, AI and computer vision that can interact the kind of material in the cane. Prompting better arranging and reduced the labour force. As well as a simpler occupation downstream at recycling centres. Furthermore, arising smart containers can easily recognize and sort waste into classifications like glass, paper, plastic and metal, compression of it and advise sanitation labourers of fill levels of each waste class, empowering a more economical and sustainable society (Suvarnamma and Pradeepkiran 2021).

23.5.8 Disposal

Smarter the bin, smarter the sorting; it is only natural to want the transporter—the midway point—to be smarter as well. This is the drive behind a few initiatives to make AI-enabled smart waste management and disposal vehicles, including the Intelligent Internet of Things Integration Consortium (I3), sent off by the University of Southern California (USC). The I3 seeks to be able to integrate garbage trucks into the city's entire sensory system and cameras so that they are not only informed of the reliable and effective routes they must take, but also have the data needed to carry out other strategic steps. Future I3 applications for smart waste trucks include marking graffiti for cleaning teams and detecting waste left outside bins. By using AI to automate and extend the performance of garbage trucks,

another important step in the waste management cycle can be greatly improved and permanently (World Future Energy Summit 2022).

23.5.9 Landfill Management

Waste disposal is very important, and we know that it is still considered one of the most important and inexpensive ways to dispose of waste that can never be reused or reused. A well-managed landfill site is important for solid waste management. At times, informal waste disposal in existing landfills and in landfills too can be hazardous in the locations where humans and wildlife are an important part of it. Therefore, the use of GIS, RS as well as AI becomes quite evident in the management of dumping and dumping sites (Ali et al. 2021).

23.5.9.1 Landfill Site Selection with the Integration of GIS and AI

Selecting of a landfill site is a difficult and time-consuming task that includes geological, environmental, water and technological boundaries and government regulations. It requires a good amount of geospatial data processing and requires multiple conditional tests (Ali et al. 2021). The landfill site must be strong enough to withstand current waste and is considered to be installed within at least 5 years. GIS and AI have grown into a powerful tool that can integrate continuous types of local data and perform a variety of spatial analysis. This evolution is driven by major advances in computer technology and data acquisition. Therefore, these five layers (land use, slope, water features, soil and geology) should be considered, and overlay analysis should be available to determine the suitability for solid waste disposal sites, and the analysis result indicates potential landfill sites and waste, identified as high, medium, small and insignificant (Mussa and Suryabhagavan 2021).

The main purpose of site selection is to ensure that potential sites are suitable for the protection of public health and the environment. The use of GIS on a landfill site is a simple method based on

data coverage and areas that meet certain eligibility criteria. Using GIS in selecting appropriate waste disposal sites can be an effective development in the obvious accepted steps regarding waste management (Rahimi et al. 2020).

The most important considerations for setting up a landfill are as follows: slope; land use; geology; ground data; roads; and body/river. The above conditions will vary from place to place depending on the distribution of people, climatic, geological and water conditions. Multi-conditional decision-making (MCDA) and overlay analysis using GIS may be used to determine appropriate waste disposal sites. Different layers with themes were made and integrated to obtain information such as soil type, drainage pattern, geology, topography, composition and network and the area designed to determine the best landfill sites. GPS will issue direct links to selected dump sites. Based on initial GIS testing and final non-invasive multi-conditional testing (FMCDM), the most appropriate site for a new waste disposal site may be selected (Alkaradaghi et al. 2019).

23.5.9.2 Using AI Drones for Landfill Management

Advances in technology have made the drone an affordable tool for workplaces. Although they may look like pieces of luxury equipment, drones are no longer as common as the GPS rover, but they have become more important in recent years (Sliusar et al. 2022). Waste Management Organization makes many tasks easier using drones such as garbage collection, wastewater treatment, mapping of landfills, dumping and cell counting.

23.5.9.3 Landfill Monitoring

Managing and monitoring landfill sites can be a complex process that requires planning, equipment and compliance with government regulations. This process aims to build landfill sites that do not pollute the surrounding area or enter water sources. Environmental engineers can use drones to monitor waste disposal. Drones can collect data on waste disposal in real time. Drones can take high-resolution images and create 3D waste disposal models. They can check the site for any

problems such as leaks or other problems that may escape the naked eye. Such arrangements are least expensive and safer compared to traditional flight methods for gathering disposal data (Filkin et al. 2021).

23.5.9.4 Landfill Mapping

In order to build a safe waste disposal facility, companies need to make sure that they are properly planned so that it will not damage the environment. Creating a drone map reduces the time it takes to plan and design a new waste management area. The bird's eye view of drones also gives these businesses information that they may not otherwise have (Wyard et al. 2022).

23.5.9.5 Calculating Landfill Capacity

Rules require waste disposal sites to keep waste below a certain height, so it sometimes has to overload cells. Drones can help land fillers decide which cells to fill up without falling. Since drones can travel in all directions, they can provide companies with accurate 3D models to visualize the process (Ali and Frimpong 2018).

23.5.9.6 Monitoring Methane Emissions

The third largest cause of increased production of methane solid waste disposal sites. Drones provided with thermal-duty cameras are used in landfills to monitor colourless and odourless gas. Too much methane in the area is dangerous, and with the help of drone technology, companies can monitor and maintain methane emissions under control from a protected range (Gålfalk et al. 2021).

23.6 Application of Technologies in Biomedical Waste Management

Hospital waste management process begins from generation of waste to its disposal. The hospital waste generated undergoes appropriate decontamination treatment before being disposed. In developing countries like India, the waste management is done manually by the healthcare workers. It is a very tedious and time-consuming process and since done manually exposes the hospital waste handlers to various infection risks and other health hazards. In Hospitals a variety of materials are generated as waste, ranging from used disposables like needles and syringes, soiled dressings, pharmaceuticals, chemicals, pathological samples, body tissues and parts, blood, medical devices accessories and radioactive materials. Usually, 10–15% of the total quantity of waste generated is considered hazardous and it maybe it may be toxic, radioactive and quite infectious and the remaining 85% is general waste (WHO 2018). It is essential that all medical waste is segregated at the source point, appropriately treated, and safely disposed. Therefore, it is necessary that medical waste collected should never be stored for more than 24 h, in the hospital. It is therefore important to follow regular and safe disposal of waste to ensure that such hospitals maintain a safe and clean environment for the patients, health workers and visitors.

Majority of hospital waste collection systems in India are manual except metro cities and smart cities such as Allappy in Kerala and Mysore Indore; it very often exposes healthcare workers to infections. Currently, COVID-19 pandemic also has given rise to fear and apprehensions of infection risks to bio-waste handlers. Further, the task is tedious and time-consuming. To reduce worker's stress and minimize infection risks, an autonomous hospital waste-collecting robot was conceptualized.

23.6.1 Design Requirement for Robot

A design conceptualized to minimize possible occupational hazards and/infection rates if any due to biomedical waste handling; and to reduce travel hours of staff; a design solution/device with following features is required:

- Can move autonomously and is able to locate departments on its own.
- Is accident proof; that automatically waits if any human being or obstacle in its path.

- Ensures collection and segregation at its source point and collects bio-waste in its respective colour
- Coded bins from its source point.
- Minimizes direct contact points with biomedical waste.
- Is not only user friendly and affordable but also serves the purpose.

23.6.2 Design Solution for AI-Enabled Robot

After COVID-19 has hit our world, the collection and treatment of COVID waste have become a key part of the biomedical waste management. Here, AI techniques can be deployed to achieve optimized routes for biomedical/clinical waste collection. Modelling biomedical waste management processes is extremely complex due to nonlinear behaviour of several variables. Artificial Neural Networks (ANN) are capable of efficiently modelling such processes, which have not so precise data and involve human actions, that are complex to model. For conventional waste management, ANNs have been successfully used to predict optimized routes of collection (Bányai et al. 2019). In COVID-19 like pandemics which are affecting the entire globe, the prediction of frequency of collection can help tune the models related to the factors like economics, population in optimizing the collection process. After collection, classification is another key factor that needs to be carefully studied to effectively handle and dispose of COVID waste. Artificial intelligence via application of image classification can be used to identify the different type of waste. This capability of automated sorting systems will eliminate the need of manual separation of COVID waste and, therefore, will prove critical in handling such type of infectious waste where virus can live on for extended periods on material surfaces (Fig. 23.3). ANNs have proved to be highly effective technique in identification of materials to almost 99% (Rubab et al. 2022).

23.7 E-Waste and Its Management

The whole world has witnessed a massive technological revolution over the past two decades, and this has boosted the production of

Fig. 23.3 COVID-19 waste management aspects for AI smart intervention. *Source* Rubab et al. (2022)
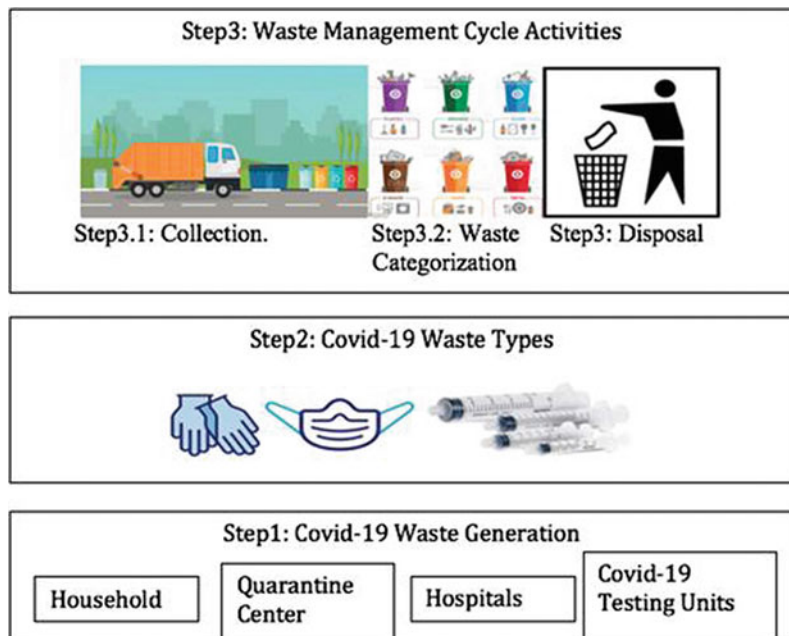
electronic products in manufacturing markets around the globe. The generation of electronic waste has become a grave concern in the digital ecosystem due to exponential growth observed in the production of electrical and electronic equipment, which only happen to increase every year.

In India, it is estimated that the total quantity of waste increases at the annual rate of 2.6 million tonnes. While India produced, 3.2 million tonnes of E-waste in 2020, it ranks fifth among e-waste producing countries after US, China, Japan and Germany. The estimation of global production of E-waste for the year 2030 is at 74.8 million tonnes. This is extremely concerning when looking at the low recycling rate of approximately 17%. Cities like Delhi, Bangalore and Mumbai are leading the list with high E-waste production and low recycling capacities (Dutta and Goel 2021). In a country like India, a large portion of E-waste comes from the level of households apart from industries and commercial. While solutions for E-waste have been in the spotlight for industries and commercials, solutions have been limited from individual households (Shreyas Madhav et al. 2022). In developing countries like India, close to 55% is the significant portion of consumer and household electronics combined.

Electronic waste, commonly known as E-waste, is categorized into 21 types under two broad categories, namely, Information Technology and communication equipment, and Consumer electrical and electronics. The e-waste includes discarded air conditioners, television sets, refrigerators, computers, motherboards, mobile phones and chargers, headphones, printers, tube lights and bulbs, cameras LED lamps, etc. More than 95% of this waste in India is managed and recycled by informal sector and scrap dealers in an unscientific and crude manner by burning or dissolving in acids (Kumar 2018). From the legislation point of view, regulations and policies are in the basic stage compared to other laws and rules governing solid waste

management. Laws for managing e-waste have been there in place since 2011 that mandated only recyclers and authorized dismantlers for collecting e-waste. A more structured and detailed, in the form of E-waste management rules 2016, was passed in 2017 (CPCB 2016). These rules, for the first time, made producers responsible for collecting back e-waste or for its exchange under EPR (Extended Producer Responsibility). DRS (Deposit Refund Scheme) was introduced wherein the producer charges an additional amount at the time of sale of product and returns it to the consumer when the end-of-life product is returned. These schemes and policies, out of other many, were definitely introduced with a view to establish proper channels and bring in accountability; however, this space still needs special attention for constant vigilance. Close to 80% of e-waste continues to be broken down by the informal sector at huge environmental and health cost, polluting soil and ground water (Lahiry 2019).

India accommodates nearly 178 registered e-waste vendors or recyclers that have been accredited by the state governments for processing e-waste, but they are not recycling at all. While some are storing e-waste in hazardous conditions, others do not have capacities to handle such waste as per report by the Union Environment Ministry (Lahiry 2019). Therefore, technologies for monitoring and vigilance should be developed and promoted for which data is easily accessible for assessment.

23.7.1 Indian Initiatives to Tackle E-Waste

On a positive side, a slow momentum shift is being built to promote new and cleaner technologies for tackling the huge problem created by mismanagement of e-waste. Laboratory-scale technologies are coming up and testing is being carried out to promote it to commercial scale. Apart from this, advanced IT technologies are

also being observed as potential solutions to minimize the errors caused by human interference and ill treatment of e-waste by constant monitoring and advanced sorting based on artificial intelligence integrated with ML (machine learning) algorithms.

23.7.1.1 Pyrolysis Technology to Recover Precious Metals by IIT Delhi

This technology is developed by Chemical Engineering department of IIT Delhi under the waste management programme of DST (Department of Science and Technology). The technology, which is under pilot scale testing and validation, will be useful to the waste management sector, particularly electrical, electronic industries and metal production industries. Currently, it is on a laboratory scale; however, design considerations are being discussed to scale it to a capacity of 50 kg/day for recycling e-waste.

The process makes use of a thermal treatment process, known as pyrolysis, wherein, the e-waste is treated under high temperatures to obtain products in the form of liquid, gas and solid residue. The liquid and the gaseous product can be used as fuel while solid residue contains metals. Further extraction of metals from the residue is carried out via hydrometallurgy process using different leaching agents. For individual metal recovery, process of electro-deposition can be used. The patent for this technology has been filed, and the scientists and researchers are working on the process to recover metals, like Copper, Silver and Gold, and to transfer the technology to industries.

This technology holds an excellent market potential due to its integrated approach of complete recycling of e-waste and recovery of metals which are precious in nature without causing damage to the environment. However, there are still concerns associated with the process of recycling due to the presence of hazardous substances present in e-waste such as antimony, cadmium, arsenic and lead.

23.7.1.2 E-Parisaraa Recycling Facility, Bangalore

The project E-Parisaraa is supported by Indo-German E-Waste initiative. The pilot project to manage e-waste has been set up in the city of Bangalore with the backing of Karnataka State Pollution Control Board with a vision to replicate similar model in other countries of India as well. The business model is simple, and the entire process converts a product waste into raw materials by following four-step approach of Manual Dismantling, Hands on Segregation, Shredding and Density Separation. Using these defined techniques, Waste Electronic and Electrical Equipment are converted into raw materials like plastics, metals and glass. What sets this model apart is that there is no burning or melting involved throughout the process. The entire process of recycling is clean to the environment and follows the principle of minimum landfill.

Lately, company has developed simple and low-cost machines like Printed Circuit Board Shredder, CRT Cutting set-up and Tube light crusher, at their facility in Dobbespet in the outskirts of the city. The leftover printed circuit boards and glass items such as tube lights and picture tubes go to the next stage where they are then cut into strips and powdered (Pandve 2010). The company exports shredded components and circuit boards for copper smelting to Umicore Precious Melting Refining, Belgium.

23.7.1.3 SDMC Facility for E-Waste Collection

To ensure scientific disposal of e-waste, the SDMC (South Delhi Municipal Corporation) has started an online facility for the e-waste collection. For this, South Delhi Municipal Corporation has partnered with RBH E-waste recycle Hub for disposing of unserviceable and old IT devices and equipment from RWAs, Markets, offices and also from residents falling under its jurisdiction. As the procedure, online request can be submitted by the consumers and as per the agreement, the company will purchase e-waste from citizens and ensure its proper disposal (Rajput 2021).

23.7.2 Deployment of Advanced Technology in E-Waste Sector Globally

23.7.2.1 Remote Sensing and Image Analysis for E-Waste Contamination

E-waste is known for releasing a variety of hazardous compounds like heavy metals, and organic pollutants including dioxins and furans. The multi-spectral remote sensing imagery can help identify and monitor release of heavy metal contaminants released during e-waste processing. The similar techniques have been used for studying contamination from heavy metal from activities like mining and large industrial work. However, these techniques are of great value in detecting contamination from a more dispersed, impromptu and shifting kinds of release typical of processing of e-waste. Given the effective price of multi-spectral imagery and enhanced resolution, these techniques can offer a swiftly responsive means to assess and monitor contamination of this kind (Garb and Friedlander 2015).

23.7.2.2 Using Machine Learning and Artificial Intelligence for E-Waste Sorting

Technological advancements will provide waste workers with additional tools to clear the way for smooth waste management by delivering E-waste to the well-established E-Waste recycling centres. Machine learning combined with automation is visioned as a technology of tomorrow in achieving an environmental waste reduction. At the industrial or commercial level, channelisation is easy to establish for recycling e-waste; however, proper channels are not existing in collecting and segregating waste from civilian homes and individual consumers. The automated robots, enabled by artificial intelligence using ML algorithms, will be an addition to the existing workforce, thereby reducing the manual intervention by learning disassembly operation using a dedicated physical training environment. Machine learning can progressively improve specific tasks using finite and increasing data captured through computer vision. Intelligent robots' systems will be able to 'intelligently' identify e-waste and dismantle the items and categorize the components without any intervention from humans (Shreyas Madhav et al. 2022).

The integration of Internet of things (IoT) with Machine Learning has also gained grip for automating the process of waste classification (Fig. 23.4). The systems equipped with such a technology have been proven efficient in attaining automated segregation of non-biodegradable and biodegradable materials. Smartphones connected to the IoT-based bins on the network can provide real-time updates and feedback while maintaining proper management of waste. The IoT sensors on the bins have the capability to measure the levels of waste inside. With the aid from intermediate servers, it sends this data for processing to the actual disposing system.

23.7.2.3 Using Augmented Reality (AR) in Operations

Augmented Reality is yet another interesting and emerging technology of this decade with tremendous potential to transform operations side of businesses. With the help of AR glasses that are equipped with cameras, depth sensors and motion sensors, supplementary information can be augmented and displayed in the real-world environment during work. It is basically superposition of virtual world and real world. This way, workers or operators can be instructed in real time about how to dismantle the products that have met end-of-life (Chen et al. 2019).

23.7.2.4 Technologizing the Electronic Market for Long-Term Usage

Hybrid Design for Electronic Gadgets

A large part of the e-waste is dedicated to the category that comprises mobile phones and gadgets, laptops, etc. Many people ditch their old laptops or smartphones for the newer model or version of software that has arrived in the market without even releasing the need of upgrade. This is a great concern as this results in large waste generation. To counter this, manufacturers
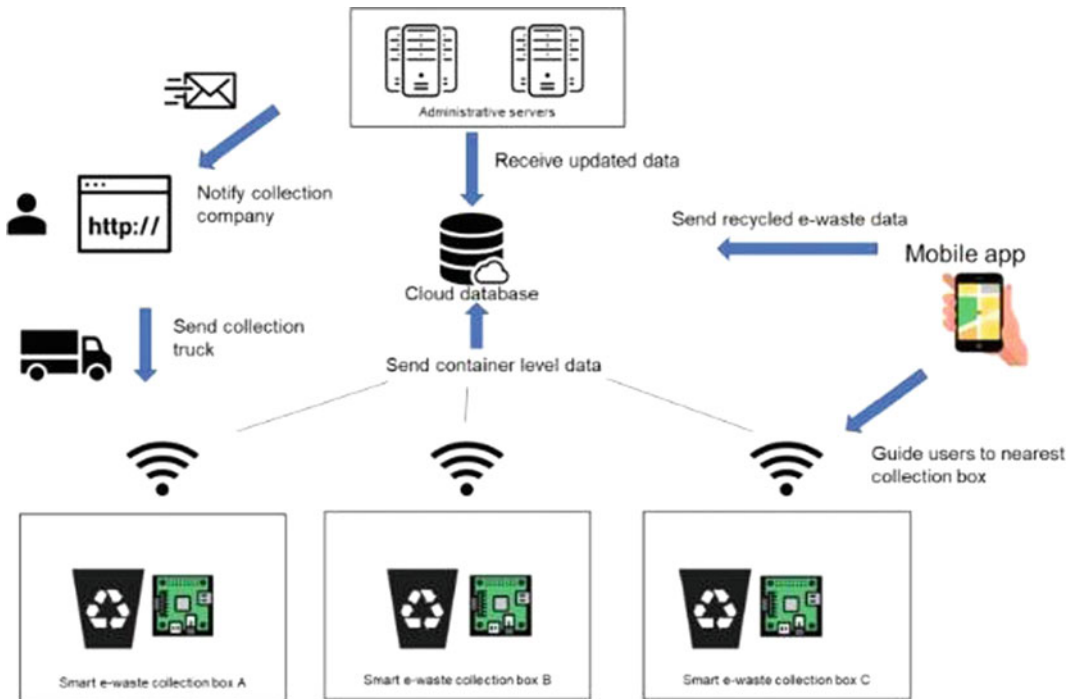
Fig. 23.4 Proposed smart E-waste management. *Source* Chen et al. (2021)

should work on hybrid design of the smartphones and tech gadgets. This will be like replacing all the incompatible components with the newer or updated software, without having to change the entire chassis of the device. For an example, the old camera in a smartphone, built in a detachable format, might be swapped with another newer or better set-up with higher specifications on the same smartphone. Since software does not need any physical entity attached to it, upgrading it will not be a problem. For an instance, the memory space can be enhanced or processor can be changed to a powerful one, etc. Also, manufacturers can easily upgrade old smartphones/laptops into new ones by changing the required components, at a much-reduced costing.

Another simple way to efficiently manage e-waste is to charge an additional amount on the electronic product at the time of selling and returning equal amount back as part of a reward scheme when consumer brings back for exchange. The manufacturer of electronic and gadgets can also introduce a reward scheme

where they may give additional discount on the new products for an exchange of an old/used product that consumer brings to the table.

Reuse and Remanufacturing

At the end-of-life of a product, the entire product need not be a waste and disposed of. Some components or modules can be perfectly fine for reuse. As a fact, it is more energy efficient to salvage a component from a dismantled device and reuse it than it is to invent a new one from raw materials. Since, second hand or reused products are comparatively cheaper than new ones, using salvaged components can reduce the cost of ownership.

23.8 Application in Construction and Demolition Waste

Construction and demolition of waste are carried out whenever any construction demolition work is done, such as building roads, bridges, flying

over a railroad, subway and rehabilitation. It contains mainly an inert and non-perishable materials such as concrete, metal, wood and plastics. Some part of this waste goes to city sewers.

India's construction industry is estimated to generate around 10–12 million tonnes of waste annually (Kolaventi et al. 2020). Forecasts of housing demand for building materials indicate an aggregate shortage of approximately 55 million cubic metres (CPHEEO 2022). Measures will be required to achieve the goal of an additional 750 million cubic metres road sector. Recycled aggregate from construction and demolition waste can close the supply and demand gap in both sectors.

23.8.1 IOT in Construction and Demolition Waste Management

GIS and GPS

It offers great advantages for data collection, storage, correlation, processing and analysis. In addition to its function to facilitate the assessment of the resulting demolition waste, GIS can also be used as an environmental impact assessment tool. For example, we used GIS to create a bottom-up material inventory model that integrates with life cycle assessment (LCA) for urban-scale environmental impact assessment and integrates with GPS technology to find materials and determine when they arrive on site in real-time locations. More recently, GIS has been used to identify illegal dumping sites where C & D waste is at potential risk (Ratnasabapathy et al. 2019).

RFID

RFID tags are another data-gathering technology that can be used to track building materials and components, equipment and tools, and construction personnel. RFID can encourage reuse of building components and reduce waste. Integrating RFID with BIM can help develop sustainable resource management. A framework was

proposed for tracking, planning and intelligently handling waste movement incidents by combining rule-based reasoning technology with RFID technology.

BIM (Building Information Modelling)

BIM comes from two technologies: space technology and data communication technology. It is largely used in India in the field of architecture, engineering and construction (AEC), and it can be effectively integrated with identification and data collection technologies such as RFID, GIS and GPS. Integrating these technologies with BIM provides definitely many benefits so far as facilitating location-based management, building material tracking and remote data collection. BIM in fact was used to estimate the amount of demolition waste during the design phase of the building. BIM offers a potential capacity in 3D coordination, design review and phase planning for managing waste more efficiently throughout the project life cycle. A system based upon BIM is used for demolition and renovation waste planning and estimation. This developed model poses the capability to deal with the estimates of the detailed volume information of each element category and material type, total inert as well as noninert demolition and retrofitting and renovation waste volumes, demolition and renovation waste disposal charging fees and the total number of pickup trucks for demolition and renovation waste. A BIM-based analysis to minimize the waste rate of the structural reinforcement applicable for a two-storey reinforced concrete structure. Therefore, BIM-based systems/models and integration of other digital technologies with BIM can provide wide solutions to minimize waste generation and optimize materials use (Ratnasabapathy et al. 2019).

23.9 Liquid Waste and Its Management

Grey water is less contaminated as compared to black water. Reusing of greywater is the most favourable possible solution with benefits in vegetable raising, flower gardening, vehicle

washing and even our home gardening and helps in reducing the usage of drinkable water. Around 50–60% of the discharged household water is grey water and its reuse assists to reduce the demand of more drinking water with reducing the expenses and enlarging the effective supply of water in areas where the water demand is high in present.

Treatment of greywater basically diminishes the demand of human being in certain areas, and it is the utmost step to alleviate the depletion of fresh water dispense in some areas with the mitigation plan for future requirements. Even some of the water-spotlighted countries planned their strategies for recycling and treatment of grey water to satisfy the needs, demand and to overcome the storage of water. In the past times, people used to satisfy their demand of water themselves and made excellent use of their greywater instead of not knowing what greywater is. They have built the proper domestic infrastructure (tub) in the manner that after bathing, the same grey water is collected for washing clothes and other household activities like flushing, vegetable raising and animal bathing. The shift from past to present is changing very drastically, people are moving towards urban areas, and their demand on water is speedily increasing, with urbanization the relocation of people towards easy lifestyle and modern technologies increased their dependency. At present in India, the people that comes under high-income group leads to ingest 150 L of water every day and it is estimated that more that 5 million people will suffer from water scarcity by 2050 worldwide. With this fact in future the water-stressed countries have to shift towards sustainable water management techniques to recycle greywater at home or at the community.

Increasing Demand of Water

In India, water security is a considerable issue, 30% potable water can be saved easily using available technologies by cleaning and reusing grey water from domestic sinks, kitchen wash basin, water from washing machines and washrooms where only soap and detergent is found as sediments called grey water. Such recycled water can be used in kitchen garden, and also wastewater is any water that has been used and discharged into closed system like drainage or sewage system or discharged in open surrounding exposed or environment. Broadly, it can be categorized as sewage and non-sewage. Sewage is wastewater that is generated from domestic activities and includes wastewater from public toilets, houses, restaurants, schools, hospitals and hotels. Non-sewage wastewater includes rainwater or flood water, used water from garages or from industrial plants. The major fraction of wastewater is produced from domestic activities in households.

At the household level, wastewater can further be categorized into:

1. Blackwater
2. Greywater
3. Yellow water.

Among these, blackwater is the most highly contaminated and can potentially cause serious diseases. The sources of blackwater includes toilet, kitchen sink, etc., and therefore, chemicals, urine, faeces, food scraps and cleaning liquids are found in this category of waste. Greywater, on the other hand, is the domestic wastewater usually produced from bathroom sinks, baths or washing machines, etc. This is much more suitable for reuse because of absence of any type of pathogens (Alemayehu 2004).

Water is a finite resource; however, rapid urbanization, change in consumption pattern and industrial demand have resulted in the overconsumption of freshwater. Due to this, many places around the globe are facing scarcity of freshwater. This is very strong indication to establish systems and technologies that can effectively make use of wastewater, especially greywater, for activities that can easily integrate its usage in place of demand for freshwater and also since to effectively deal with climate-triggered heat leading to scarcity of water, green hydrogen has great potential as alternative source of non-fossil fuel energy. In producing one litre of green hydrogen fuel, seven litres of water are consumed in electrolysis methodology. Thus, even

green hydrogen can be produced by recycled grey waste and fresh water can be immensely saved. The reuse of greywater will be an effort to address one strong point, i.e., it will reduce the demand of freshwater required for household activities and gardening purposes and also in agriculture, drip irrigation and also producing green hydrogen which helps reaching out SDG target by 2050. Naturally, the composition of greywater favours the situation as it contains many nutrients that may turn to be a beneficial fertiliser. Since greywater is one of the cleanest in the category of wastewaters, there could be numerous applications to it; however, sometimes greywater may also contain compounds like fats and oils, detergents and soaps, in large quantities. Therefore, greywater must be processed through natural filtration process to make it suitable for use and quality monitoring should be there for ensuring fit use.

23.9.1 Reuse Through Recycling Using IoT

Greywater is an excellent resource for activities like gardening and cleaning. The treatment process is low cost from operational point of view and needs assessment on the quantity of BOD (Biological oxygen demand), COD (Chemical oxygen demand) and TSS (Total dissolved solids). The addition of chlorine, along with other disinfecting additives, checks the growth of disease-spreading microorganisms. The proposed idea is to use multi-filtration process that includes three processes in series, i.e., sand filtration ≫ Reed bed Technology ≫ Distillation by natural material. As a working principle, the process starts with first step of sand filtration. The sludge, along with tiny sediment impurities and soap, is removed in this step. The filtered water is then allowed to move to second stage of filtration. The controller working on Internet of things, checks the level of water periodically and further extends to the next step of filtration, that is, reed bed technology. This is the stage where first stage filtered water is passed through aquatic plants. Here, the biodegradable and potentially

higher-end solvents break down to simple one. This step helps greywater lose its strength of contamination. Finally, the water from reed bed moves to the third stage for removal of compounds like nitrates and iron. This third stage known as natural distillation is carried out by agricultural waste like corn, seed and plants waste. At the end, the quality check is carried out (Gokul et al. 2018). This is a long and time-consuming process and, therefore, can be implemented at a community level.

Hardware Utilization

pH Sensor

pH sensor is used for measurement of acidity and alkalinity, or the caustic and base present in a given solution. It is generally expressed with a numeric scale ranging from 0 to 14. The value 7 represents neutrality. Numbers on the scale increase with increasing alkalinity, while the numbers on the scale decrease with increasing acidity. In the proposed project, pH sensor is used to measure the pH value of the grey water before filtration in the Collection tank and also used to measure the pH of the treated water after Filtration in the Storage tank (Usha AND Anslin 2019).

Turbidity Sensor

Turbidity is the haziness or cloudiness of a fluid generated by a large number of suspended particles that may be invisible to the naked eyes. The measurement of turbidity is a key test of water quality. Turbidity sensor detects the amount of scattered light that by the suspended particles in water. As there is an increase in the amount of total suspended solids (TSS) in water, there is an increase in water's turbidity level. In the proposed model, the sensor projects a focussed beam into the monitored water. The light beam reflects off particles in the water, and the resultant light intensity is measured by the turbidity sensor's photodetector positioned at 90 degrees to the light beam. The light intensity detected by the turbidity sensor is directly proportional to the turbidity of the water (Gokul et al. 2018).

Ultrasonic Sensor

In the proposed model, each tank in the different stages has an ultrasonic sensor for measurement of the level, except for the storage tank. This sensor emits high-frequency sound waves in the direction of liquid in the tank. On hitting the liquid's surface, it gets reflected back. This reflected wave is received by the Receiver of the Ultrasonic sensor. The time taken by wave through this process is directly proportional to the distance between sensor and the level of liquid. When the time reading is recorded to be fairly low, the level sensor directs solenoid valve to open using microcontroller, Arduino. This is how the level is detected in all the tanks of three stage (Gokul et al. 2018).

23.10   Conclusion

Traditionally, waste management has largely involved manual workforce. As per the demand and industry needs, waste management is ready to be revolutionized by AI-enabled smart recycling and monitoring systems. This will go a long way in conserving and preserving the environment for a more sustainable future which will be based on a circular economy model. The SWM systems working on AI are still in the stage of development and are being researched for more exploration. Smart city system will be very useful for garbage collection in areas where smart trash bins already exist. User can explore nearby trash bins so that all garbage in the city will be collected and India will be clean and healthy, that is our goal. GIS, as a decision support tool for landfill location, has proven to be useful and feasible in identifying potentially suitable sites for landfills and demonstrates its ability, using spatial data and ambition, to address the selection of a potential niche site to locate a landfill. GIS and AI software are useful for locating landfills by creating map layers based on different criteria taken into account. The processes involved in determining the location of a landfill include the integration of multiple criteria and spatial data processing. GIS is a cost-effective tool for locating landfills and creating maps for environmental management of pollution assessment. Drones with AI technology have combined to provide accurate real-time data that can be viewed and, in some cases, even a solution to separate recyclable recommendations on how to fix the problem. Try. For liquid wastewater management, a system is proposed that includes a pH sensor, a turbidity sensor and a level sensor to continuously test and monitor the water quality in the primary and tertiary stages, and an electric valve. Magnetic will control water flow. The main advantage of this system is that it not only monitors the water quality, but also recycles the water using a carbon filter and alum treatment. The system also displays real-time water quality data on the Blynk app to take the necessary actions. The final application of recycled water can be for purposes such as gardening, flushing toilets and washing cars. This monitoring and recycling can be done in various places such as home kitchens, schools, offices, colleges and hotels. Therefore, for IoT to continue to promote effective waste management, we need more support from the public and private sectors, which includes more regulations and incentives, as well as more innovation and commitment with various government agencies to use IoT applications to build a better, more sustainable future.

References

Abdallah M, Talib MA, Feroz S, Nasir Q, Abdalla H, Mahfood B (2020) Artificial intelligence applications in solid waste management: a systematic research review. Waste Manage 109:231–246

Abdel-Shafy HI, Mansour MS (2018) Solid waste issue: sources, composition, disposal, recycling, and valorization. Egypt J Pet 27(4):1275–1290

Alemayehu E (2004) Solid and liquid waste management. Ethiopia Public Health

Al-Ruzouq R, Abdallah M, Shanableh A, Alani S, Obaid L, Gibril MBA (2022) Waste to energy spatial suitability analysis using hybrid multi-criteria machine learning approach. Environ Sci Pollut Res 29 (2):2613–2628

Ali D, Frimpong S (2018) Artificial intelligence models for predicting the performance of hydro-pneumatic suspension struts in large capacity dump trucks. Int J Ind Ergon 67:283–295

Ali SA, Parvin F, Al-Ansari N, Pham QB, Ahmad A, Raj MS, Ahn DT, Ba LH, Thai VN (2021) Sanitary landfill site selection by integrating AHP and FTOPSIS with GIS: a case study of Memari Municipality, India. Environ Sci Pollut Res 28(6):7528–7550

Ali SA, Ahmad A (2020) Suitability analysis for municipal landfill site selection using fuzzy analytic hierarchy process and geospatial technique. Environ Earth Sci 79(10):1–27

Allam Z, Dhunny ZA (2019) On big data, artificial intelligence and smart cities. Cities 89:80–91

Alkaradaghi K, Ali SS, Al-Ansari N, Laue J (2019) Landfill site selection using GIS and multi-criteria decision-making AHP and SAW methods: a case study in Sulaimaniyah Governorate, Iraq. In Conference of the Arabian Journal of Geosciences (pp. 289–292). Springer, Cham.

Andeobu L, Wibowo S, Grandhi S (2022) Artificial intelligence applications for sustainable solid waste management practices in Australia: a systematic review. Sci Total Environ 834:155389

Anh Khoa T, Phuc CH, Lam PD, Nhu LMB, Trong NM, Phuong NTH, Dung NV, Tan YN, Duc DNM (2020) Waste management system using IoT-based machine learning in university. Wirel Commun Mobile Comput

Annamalai J (2015) Occupational health hazards related to informal recycling of E-waste in India: an overview. Indian J Occup Environ Med 19(1):61

Ashri R (2019) The AI-powered workplace: how artificial intelligence, data, and messaging platforms are defining the future of work. Apress

Asnani PU, Zurbrugg C (2007) Improving municipal solid waste management in India: a sourcebook for policymakers and practitioners. World Bank Publications

Bano A, Ud Din I, Al-Huqail AA (2020) AIoT-based smart bin for real-time monitoring and management of solid waste. Sci Progr

Bányai T, Tamás P, Illés B, Stankevičiūtė Ž, Bányai Á (2019) Optimization of municipal waste collection routing: impact of industry 4.0 technologies on environmental awareness and sustainability. Int J Environ Res Public Health 16(4):634

Buekens A (2012) Incineration technologies. In: Meyers RA (eds) Encyclopedia of sustainability science and technology. Springer, New York, NY. https://doi.org/10.1007/978-1-4419-0851-3_92

Castro D, New J (2016) The promise of artificial intelligence. Center Data Innov 115(10):32–35

Chen Y, Wang Q, Chen H, Song X, Tang H, Tian M (2019) An overview of augmented reality technology. J Phys Conf Ser 1237(2):022082)

Chen J, Huang S, BalaMurugan S, Tamizharasi GS (2021) Artificial intelligence based e-waste management for environmental planning. Environ Impact Assess Rev 87:106498

CPCB (2016) Central Pollution Control Board. https://cpcb.nic.in/displaypdf.php?id=RS1XYXN0ZS9FLVdhc3RlTV9SdWxlc18yMDE2LnBkZg==. Accessed on 29 June 2022

CPHEEO (2022) Construction and demolition waste. Central Public Health & Environmental Engineering Organisation.http://cpheeo.gov.in/upload/uploadfiles/files/chap4.pdf. Accessed on 29 June 2022

De S, Debnath B (2016) Prevalence of health hazards associated with solid waste disposal—a case study of Kolkata, India. Procedia Environ Sci 35:201–208

Dhanwani R, Prajapati A, Dimri A, Varmora A, Shah M (2021) Smart earth technologies: a pressing need for abating pollution for a better tomorrow. Environ Sci Pollut Res 28(27):35406–35428

Dutta D, Goel S (2017) Applications of remote sensing and GIS in solid waste management—a review. Adv Solid Hazard Waste Manage, 133–151

Dutta D, Goel S (2021) Understanding the gap between formal and informal e-waste recycling facilities in India. Waste Manage 125:163–171

Excellent Web World (2022) An innovative smart waste management solution using IoT, Mayur Panchal. https://www.excellentwebworld.com/smart-waste-management-solution-using-iot/. Accessed on 28 June 2022

Ferronato N, Torretta V (2019) Waste mismanagement in developing countries: a review of global issues. Int J Environ Res Public Health 16(6):1060

Filkin T, Sliusar N, Ritzkowski M, Huber-Humer M (2021) Unmanned aerial vehicles for operational monitoring of landfills. Drones 5(4):125

Glanville K, Chang HC (2015) Remote sensing analysis techniques and sensor requirements to support the mapping of illegal domestic waste disposal sites in Queensland, Australia. Remote Sens 7(10):13053–13069

Gålfalk M, Nilsson Påledal S, Bastviken D (2021) Sensitive drone mapping of methane emissions without the need for supplementary ground-based measurements. ACS Earth Space Chem 5(10):2668–2676

Garb Y, Friedlander L (2015) Detection and monitoring of e-waste contamination through remote sensing and image analysis. In: EGU general assembly conference abstracts, p 14232

Gokul AKR, Rajalakshmi NR, Saranya P, Vidhya P (2018) Active utilization of grey water in residential buildings using IOT. Int J Creative Res Thoughts 6(2)

Gu F, Guo J, Yao X, Summers PA, Widijatmoko SD, Hall P (2017) An investigation of the current status of recycling spent lithium-ion batteries from consumer electronics in China. J Clean Prod 161:765–780

Hazra T, Goel S (2009) Solid waste management in Kolkata, India: practices and challenges. Waste Manage 29(1):470–478

Jimenez J, Latrille E, Harmand J, Robles A, Ferrer J, Gaida D et al (2015) Instrumentation and control of anaerobic digestion processes: a review and some research challenges. Rev Environ Sci Bio/technol 14(4):615–648

Joseph K, Rajendiran S, Senthilnathan R, Rakesh M (2012) Integrated approach to solid waste management in Chennai: an Indian metro city. J Mater Cycles Waste Manage 14(2):75–84

Kala K, Bolia NB (2021) Analysis of citizen's perception towards segregation and composting. Environ Dev Sustain 23(7):10763–10786

Kannangara M, Dua R, Ahmadi L, Bensebaa F (2018) Modeling and prediction of regional municipal solid waste generation and diversion in Canada using machine learning approaches. Waste Manage 74:3–15

Karsauliya S (2013) Application of remote sensing and GIS in solid waste management: a case study of surroundings of River Yamuna, India. Int J Environ Eng Manage 4(6):593–604

Khan D, Samadder SR (2014) Municipal solid waste management using Geographical Information System aided methods: a mini review. Waste Manage Res 32(11):1049–1062

Kolaventi SS, Tezeswi TP, Siva Kumar MVN (2020) An assessment of construction waste management in India: a statistical approach. Waste Manage Res 38(4):444–459

Kumar R (2018) Unorganised e-waste disposal: alarming situation. Deccan Herald. Read more at: https://www.deccanherald.com/opinion/panorama/unorganised-e-waste-disposal-708093.html. Accessed on 29 June 2022

Kumar A, Agrawal A (2020) Recent trends in solid waste management status, challenges, and potential for the future Indian cities—a review. Curr Res Environ Sustain 2:100011

Kumar S, Smith SR, Fowler G, Velis C, Kumar SJ, Arya S, Rena RK, Cheeseman C (2017) Challenges and opportunities associated with waste management in India. R Soc Open Sci 4(3):160764

Kumar S, Mukherjee S, Chakrabarti T, Devotta S (2007) Hazardous waste management system in India: an overview. Crit Rev Environ Sci Technol 38(1):43–71

Lahiry S (2019) Recycling of e-waste in India and its potential. DownToEarth. https://www.downtoearth.org.in/blog/waste/recycling-of-e-waste-in-india-and-its-potential-64034. Accessed on 29 June 2022

Liu J, Li Q, Gu W, Wang C (2019) The impact of consumption patterns on the generation of municipal solid waste in China: evidences from provincial data. Int J Environ Res Public Health 16(10):1717

Luttenberger LR (2020) Waste management challenges in transition to circular economy—case of Croatia. J Clean Prod 256:120495

Malav LC, Yadav KK, Gupta N, Kumar S, Sharma GK, Krishnan S, Rezania S, Kamyab H, Pham QB, Yadav S, Bhattacharyya S, Yadav VK, Bach QV (2020) A review on municipal solid waste as a renewable source for waste-to-energy project in India: current practices, challenges, and future opportunities. J Clean Prod 277:123227

Mandal K (2019) Review on evolution of municipal solid waste management in India: practices, challenges and policy implications. J Mater Cycles Waste Manage 21(6):1263–1279

Manisalidis I, Stavropoulou E, Stavropoulos A, Bezirtzoglou E (2020) Environmental and health impacts of air pollution: a review. Front Public Health 8:14

Meegoda JN, Hettiarachchi H, Hettiaratchi P (2016). Landfill design and operation. Sustain Solid Waste Manage, 577–604

Miezah K, Obiri-Danso K, Kádár Z, Fei-Baffoe B, Mensah MY (2015) Municipal solid waste characterization and quantification as a measure towards effective waste management in Ghana. Waste Manage 46:15–27

Mohanty S, Saha S, Santra GH, Kumari A (2021) Future perspective of solid waste management recent strategy in India. In: Baskar C, Ramakrishna S, Baskar S, Sharma R, Chinnappan A, Sehrawat R (eds) Handbook of solid waste management. Springer, Singapore. https://doi.org/10.1007/978-981-15-7525-9_10-1

Mohsin M, Ali SA, Shamim SK, Ahmad A (2022) A GIS-based novel approach for suitable sanitary landfill site selection using integrated fuzzy analytic hierarchy process and machine learning algorithms. Environ Sci Pollut Res 29(21):31511–31540

Mussa A, Suryabhagavan KV (2021) Solid waste dumping site selection using GIS-based multi-criteria spatial modeling: a case study in Logia town, Afar region, Ethiopia. Geol Ecol Landscapes 5(3):186–198

Needhidasan S, Samuel M, Chidambaram R (2014) Electronic waste—an emerging threat to the environment of urban India. J Environ Health Sci Eng 12(1):1–9

Ni D, Xiao Z, Lim MK (2020) A systematic review of the research trends of machine learning in supply chain management. Int J Mach Learn Cybern 11(7):1463–1482

Nižetić S, Šolić P, González-de DLDI, Patrono L (2020) Internet of Things (IoT): opportunities, issues and challenges towards a smart and sustainable future. J Clean Prod 274:122877

Pal MS, Bhatia M (2022) Current status, topographical constraints, and implementation strategy of municipal solid waste in India: a review. Arab J Geosci 15(12):1–26

Pandve H (2010) Some initiative in e-waste disposal, management and recycling. Indian J Occup Environ Med 14(1):20

Pandey PC, Sharma LK, Nathawat MS (2012) Geospatial strategy for sustainable management of municipal solid waste for growing urban environment. Environ Monit Assess 184(4):2419–2431

Prajapati KK, Yadav M, Singh RM, Parikh P, Pareek N, Vivekanand V (2021) An overview of municipal solid waste management in Jaipur city, India—current status, challenges and recommendations. Renew Sustain Energy Rev 152:111703

Purohit SS, Bothale VM (2011) RFID based solid waste collection process. In: 2011 IEEE recent advances in intelligent computational systems. IEEE, pp 457–460

Rahimi S, Hafezalkotob A, Monavari SM, Hafezalkotob A, Rahimi R (2020) Sustainable landfill site selection for municipal solid waste based on a hybrid decision-making approach: fuzzy group BWM-MULTIMOORA-GIS. J Clean Prod 248:119186

Rethinking the Urban Form and Quality of Walking Experience Using Geospatial Technology

24

Kulsum Fatima

Abstract

This study represents the service area analysis for a school-going community scenario in North American context. It focuses over the prevalent street typology and its impact over urban form and quality and safety of walking experience. The main emphasis is on the use of GIS walkshed analysis tool to address underlying problems with urban form and planning. The idea underlines the interdependence between urban form and walkability scenario. Based on the GIS spatial analysis, the findings are interpreted to offer design improvements and enhance pedestrian experience. This study will be useful to support future planning proposals, which intend to develop opportunities for expanding activities that encourage walkability and pedestrian accessibility in a community-scale urban intervention. This approach offers insights to city planners, environmental designers, public health practitioners, strategist for pedestrian enhancement programs and engineers, who are striving to achieve sustainability principles for land use and mobility planning.

24.1 Introduction

The geospatial technology has a wide applicability to convey spatial complexities within the built environment and its interconnectedness with land use information in a user-friendly and easy-to-interpret means. It facilitates understanding through its ability to create interactive maps, measure distances, travel times and define extents of natural and spatial relationships. In particular, maps are "accepted as a factual representation of an area" and are widely used to "validate competing perspectives of the spaces and places" (Wood 2016). Due to the multitude of geographic information systems (GIS) applications, it has been actively employed in health research and public health sectors as it offers a better understanding for land use implications and influences of urban and built environments over issues concerning human health. There is an abundant set of literature that targets GIS application that investigates walking behaviours to help individuals to adopt an active lifestyle, health

K. Fatima (✉)
Department of Architecture, Faculty of Architecture and Ekistics, Jamia Millia Islamia, New Delhi, India
e-mail: kfatima@jmi.ac.in

K. Fatima
SAPL, University of Calgary, Calgary, AB, Canada

practitioners to monitor outcomes, propose interventions and support planning authorities in policy framing. The GIS applications are successfully utilized to acquire relevant, easy-to-comprehend and reliable measurable characteristics of the built environment to fully understand its impact and potential over walkability scenario.

This chapter discusses and uses two GIS methods, namely walkability indices (WI) and network/walkshed analysis—to create walkshed areas (Fig. 24.4), walking distances (Fig. 24.5) and walk wrap (Fig. 24.6) maps to measure walkability for Tuscany school in Tuscany community in Calgary (Alberta, Canada). WI is the "employment of composite measures which provides opportunities to walk to various destinations" (Agampatian 2014, p. 11) and the network/walkshed analysis "models the mobility or transportation network and performs a variety of analysis on them" (Wenhao 2018). Both of these methods are innovative and leading-edge to support interdisciplinary research in health sector, urban planning and environmental design. This chapter represents the usefulness of a walkshed analysis created by utilizing the efficacy of GIS analysis tools to estimate the potential accessibility and connectivity benefits of walkability in a community neighbourhood. This walkshed analysis will assess the quantitative and qualitative aspects of community walkability, including:

- the degree to which urban form forces students to take indirect paths or force them to wrap their movement through the neighbourhood; and
- the quality and safety of the walking experience for the school-going community.

This analysis will be useful to support future planning proposals, which intend to develop opportunities for expanding activities that encourage walkability and pedestrian accessibility in a community-scale urban intervention. This chapter underlines urban design and modelling approach for effective reshaping and influencing the built environment based on walkshed shapes. The maps created using walkshed analysis may be utilized to generate public perspectives on equity and safety, within the urban environment that will affect individual route choices and preferred walking distance that will define the local mobility scenario. These perspectives will help to create the possibilities to rethink and re-innovate the importance of walking and pedestrian experiences in local community through urban GIS modelling and analysis.

This chapter is divided into eight sections. Section 24.1 provides an overview of the subject and objective for this study. Section 24.2 gives a background on concept of urban walkability. Section 24.3 reviews the importance of walkshed analysis for schools to underline safe walking scenarios and experiences. Section 24.4 describes the reason for selecting Tuscany school for the GIS analysis and highlights the pattern for traffic on streets and biking paths. Section 24.5 tries to depict through map (Fig. 24.4) the Tuscany school walkshed for three different sizes of 250 m (immediate walk), 500 m (intermediate) and 1200 m (reasonable distance for a 10-min walk), alongside the walking and driving distances with respect to major landmarks. Section 24.6 highlights walking distances within and outside Tuscany community through map (Fig. 24.5), that the student population of Tuscany school is expected to walk in order to daily commute back and forth. Section 24.7 gives the walk wrap assessment and tries to identify the high traffic volume intersections near Tuscany school area through map (Fig. 24.6). This section also discusses the findings of walkshed analysis performed on Tuscany school which identify factors that promote or hinder a walkable environment. This section is followed by the conclusion and recommendation for future studies.

24.2 Background to Walkable Urban Environments

For decades, urban planners and environmental designers have been advocating the creation of urban forms and spaces to enhance the quality of human experiences. A vast literature exhibits efforts around walkability scenario in urban

spaces. Walking comes as a natural extension to individuals and is additionally considered for both leisure as well as transportation purposes. Irrespective of the need and purpose of walking, an individual is always looking for a safe and dedicated walking environment, which is governed by its urban form. It is also "believed that the degree to which an environment allows or encourages walking can be related to certain health measures such as obesity, diabetes and cardiovascular disease" (Hynes 2006). The urban environmentalist has usually been targeting to reach a preferred destination as part of daily mobility needs and "assume that on average, a person can be expected to walk about ten minutes" (Swanson et al. 2019). There have been some examples where urban planners like Clarence Perry ("ideal" neighbourhood, 1930), Douglas Farr (new suburban typology neighbourhood, 1980) and Andres Duany (walkable community, 2008) designed neighbourhoods where the amenities were in the walking circle of within a 5- to 10-min walk.

The National Highway Traffic Safety Administration (NHTSA) of the US Department of Transportation (DOT) conducted a National Survey of Bicyclist and Pedestrian Attitudes and Behaviours (NSBPAB) in 2012, which assessed "graphic and typological descriptions of bicyclists and pedestrians, attitudes and perceptions about bicycling and pedestrian activity; the availability and use of bike paths and lanes in the community; knowledge of various laws pertaining to bicyclists and pedestrians; and changes in bicycling and pedestrian behaviour and attitudes since 2002" (Transportation 2012, p. 1). Based on the detailed findings of this survey, most people agree that a "1200 m (about a 10-min walk) is a reasonable distance to access local destinations" (Transportation 2012, p. 2). This 10-min distance is typically half mile in a straight line which offers a safe, comfortable and direct walking trip. But usually this straight trip is not the case in most of the walking scenarios, due to physical obstructions and "barriers like roadways or highways [buildings, derelict land, etc.] that obstruct direct path" (Strupp 2020). Such obstructions force people to walk through the expanded pedestrian infrastructure, which creates a walk wrap in pedestrian movement.

In addition, based on literature-based evidences, it is a well-known fact that individuals do not always follow the shortest path. Various studies have identified conditions influencing human mobility and route choices based on urgency and purpose, for example, the "regular workday routines versus serendipitous or circumstantial travel" (Bolten and Caspi 2021, p. 1) and the heterogeneous preferences—governing path attributes, including static and transient attributes. Static attributes include examples of physical inaccessibility like staircase being inaccessible to wheelchair or stroller users. Transient attributes include examples like rain, crowds or lightning conditions that make walking undesirable at times. It is therefore understood that there are a wide variety of factors influencing the individual route choice in addition to the preferred walkable distance. However, it is also recognized that route choice is an individual perspective, whereas the preferred distance is a collective urban perspective that defines the human mobility patterns and walk wraps for pedestrian movement in an urban environment.

As per the available literature, there has been a significant research in studying neighbourhood spatial accessibility which measures community residents ease in accessing community amenities and the role of urban design in effective reshaping of the built environment based on walkshed analysis. The literature also highlights that there is a significant bias involved based on the assumption that residents have a preference to mobilize in road networks, which helped them ignore other travel networks, including pedestrian and biking modes. In addition to that, taking aggregation of neighbourhood blocks instead of single points of origin is another reason for the evident biases. In most of the existing methods "measures of walkability use straight-line distances for ease of calculation" (Holbrow 2010). It has also been observed that "despite well-established studies that explore pedestrians route choice priorities and the many factors affecting route preferences, very few studies or

methods apply any criteria other than minimizing travel time or distance in models to forecast individual choices at large scales of urban networks" (Bolten & Caspi 2021, p. 2). Therefore, this study will present different walkshed methods to eliminate the identified biases as discussed in the literature review.

24.3 Defining Walksheds

On a community scale, people chose to walk for multiple reasons including, health reason, destination travelling towards amenities, recreations or daily errands. Possibilities for walking and the walkability scenario for a neighbourhood are "influenced by the combination of morphological and experiential aspects of the environment" (Sandalack and Alaniz Uribe 2013, p. 7). It is governed by the presence of services or amenities that are destination for a pedestrian and helps in influencing the individual route choice as well as the preferred walkable distance. In most of the residential communities, safe access to schools is a priority and therefore neighbourhood designs are focused on achieving a walkable scenario back and forth from school locations. Usually, school's premises are a major concern for parents and school administration, as it attracts high traffic volumes with children being driven to school rather than walking. This accumulates larger than usual amounts of traffic around schools, making them unsafe for walking and biking opportunities. Therefore, efforts towards safe walking and pedestrian-friendly infrastructure around schools are important to encourage active as well as safe modes and reduce the amount of vehicular traffic around schools. In order to access and evaluate the walkable conditions in school-oriented neighbourhoods walkshed analysis is the most effective technique available to urban planners.

A "walkshed (or pedshed) refers to the area that a pedestrian potentially has access to from a particular point and within a specified distance" (Sandalack and Alaniz Uribe 2013, p. 7). In general, it is also understood as a "good measure of the walking network around a destination" (Foundation). For decades, several methods have

been utilized to accurately measure walksheds. This study uses two methods—airline walkshed and network walkshed—to compare the conceptual as well as practical walkable scenario and to influence neighbourhood development policies at urban scale and the individual choice of route at local neighbourhood scale.

The airline walkshed is described conceptually as a consistent-radius circle around a point of origin, within which a pedestrian would be able to walk and reach any destination in a desired "straight-line" similar to a bird-fly approach. However, this does not offer a practical walkability scenario, as it does not consider any physical obstruction and spatial conditions constrained by street patterns or ground realities. Whereas, the network walkshed method accurately reflects walkable area and utilize the access to land uses that influence walking. This method utilizes the ground realities impacted by the urban form, density, street pattern, connectivity issues and the land use pattern and therefore more effective than the airline method.

24.4 Community Characterization

In order to understand the relationship between urban form and pedestrian experiences, it is important to assess neighbourhood street patterns and their influence over walksheds. In June 2011, Rifaat et al. classified street patterns into five categories, namely "grid-iron, fragmented parallel, warped parallel, loops and lollipops, and lollipops on a stick" (Rifaat et al. 2011, p. 277). As per this classification, the loops and lollipops street design has become the new preferred street pattern in upcoming North American communities in the last fifty years. This preference is mainly for the following reasons: firstly due to the "decreased injury risk of crashes involving two-vehicle" (Rifaat and Tay 2009) and secondly, due to the findings of a research, that claims "parents and caregivers are more willing to let children play on the roads" (Veitch et al. 2005) in a curvilinear design as compared to a traditional right-angled corner street design similar to grid-iron pattern. Another study in 2009

claimed that "fewer crashes are associated with loops and lollipops pattern as compared to a traditional grid-iron street pattern" (Rifaat and Tay 2009) due to its curvilinear nature and traffic calming effects. As the loops and lollipops pattern is generally preferred in North American communities, this pattern is the first criteria for selecting Tuscany school community. The second criteria for selecting Tuscany school community is that its 100% households have children walking to schools, as per Census Canada 2011 data (Calgary 2019).

Tuscany is among one of the newest residential communities in northwest quadrant of Calgary, "built in the year 2000" (Calgary 2019). It is known for its walking paths that connect the community with nature within their neighbourhood. It is famous for its scenic views and independent town homes offering close proximity to "Twelve Mile Coulee Natural Environment Park" and Two-toed pond. As per the Best Neighbourhoods Ranking by Avenue Magazine, "Tuscany ranks 57th in 2020 with a Public recreation facility access points: 37 and Parks and green space points: 25" (Magazine 2020). The Tuscany community characteristics are represented in Fig. 24.1, showing its location within the city, its demographic data and street characteristics. This community has a 1-463 ratio for car crashes/year and a residential street density of 17,109.18 (m/km^2) against a land area 6.878004474 km^2 and 117,677.006808 m of total length of streets.

As per the GIS analysis, the longest street within Tuscany neighbourhood is the "101 ST NW", which is 1576.8 m long and the shortest street is "twelve MI Coulee Rd NW", which is only 1.2 m long. For the sake of traffic planning and Urban environment assessments, it has one of the largest numbers of total street counts for 1404, a total of 17 access point counts, 991 points for pednetwork junctions, and total of 71 bus stops, which makes it a well-connected, easily accessible and transit effective layout. The urban form for Tuscany community is defined in Figs. 24.2 and 24.3, which represent the dedicated biking pathways and trails network within park system and the street pattern, respectively.

Community Details

Tuscany School

Tuscany Population %

Tuscany		
	Number	Per cent
Children in census families in private households	7,055	100%
Under 6 years of age	2,765	39%
6 – 14 years	2,840	40%
15 – 17 years	510	7%
18 – 24 years	735	10%
25 years and over	210	3%

Source: Census of Canada, 2011

Longest Street
1576.8 Mtrs
(101 ST NW)

Shortest Street
1.2 Mtrs
(Twelve MI Coulee Rd NW)

Access Points (Counts)
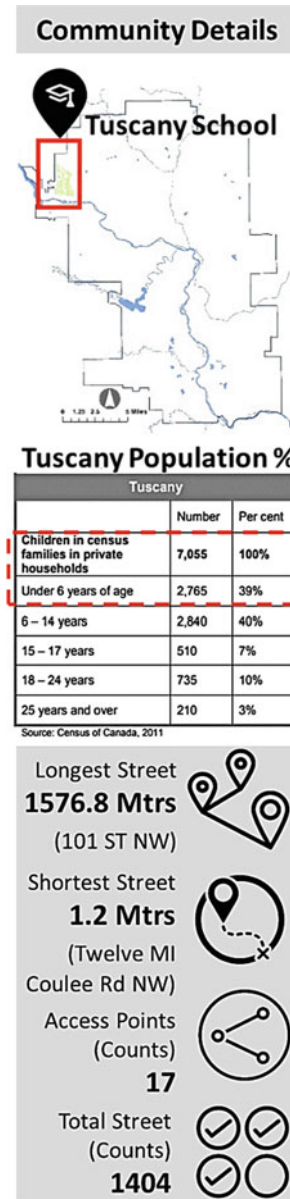**17**

Total Street (Counts)
1404

Fig. 24.1 Tuscany community characteristics (Fatima 2022b)

24.5 Tuscany School Walkshed Description

Urban planning for residential communities like Tuscany, essentially requires a safe walking and biking network around schools, these are required not only to encourage active modes of
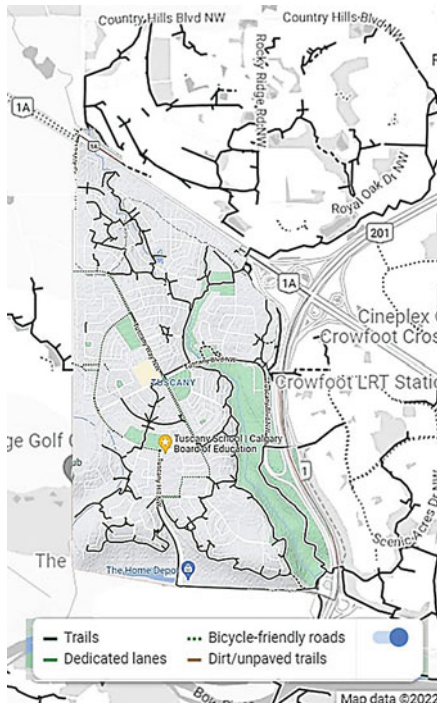
Fig. 24.2 Tuscany community area terrain and biking network pattern overlay map (Fatima, Tuscany overlay map, 2022c)

Fig. 24.3 Tuscany community Street Pattern Profile (Fatima, Tuscany overlay map, 2022c)

mobility but also to reduce the accumulation of vehicular traffics. In this case, the walkshed analysis is made specifically for the school-going population, and therefore, the Tuscany school is considered as the focal point for GIS walkshed analysis. The purpose of this selection is the school-going population which consists of junior high and high school. This set of school-going population carries a greater level of independence as compared to the students going to elementary schools, pre-schools and day care schools. This group depends on walking and cycling, with the capability, confidence, navigation skills and road knowledge to recognize direct and comfortable routes, that will eventually promote safe walkable behaviour in the community.

The objective for Tuscany school walkshed is to identify network service areas using ArcGIS applications, within which student population is expected to walk to school. The ArcGIS application intends to create a school walkshed for

three different sizes of 250 m (immediate walk), 500 m (intermediate) and 1200 m (reasonable distance for a 10-min walk), as represented in Fig. 24.4.

For the purpose of this school walkshed analysis, network analyst is used to identify "service areas", which are accessible by vehicle or by foot. A "network service area is a region that encompasses all accessible streets, for instance, the 5-min service area for a point on a network includes all the streets that can be reached within five minutes from that point" (Esri 2021). The size and shape of this service area are defined by the pattern of connections in the existing street network. The city of Calgary spatial data transportation geodatabase with linear transport shape file is used with ArcMap GIS version 10.8 (2019) to create new geodatabase, export data to pednetwork and building network dataset, which is later used in network analyst tool.

Fig. 24.4 Tuscany school walkshed for 250, 500 and 1200 m. Radius (SAND 2018a)


The service area created using the network analyst evaluates the issues concerning accessibility within the Tuscany school service area and identify factors that promote or hinder a walkable environment. These factors will also help evaluate the principle 2 of Sustainability Principles for Land Use and Mobility Plan by the City of Calgary: create walkable environments, which intends to investigate the "interconnected street network to ensure walkable access" (Calgary 2008, p. 2). As a result, this evaluation will be helpful to propose modification to strategically direct and manage redevelopment opportunities within existing areas and promotes compact development through judicious use of existing infrastructure that increases transit efficiency. This will also help to establish principles 7 and 8

from the Sustainability Principles for Land Use and Mobility Plan.

24.6 Walking Distances Within and Outside Community

Figure 24.4 represents the travel options for driving and walking times and distances in and out with respect to the walkshed analysis focal point, i.e. Tuscany school. The prominent travel destinations include Crowfoot and Tuscany LRT stations for student population travelling towards school, 44 min of walking distance from Mile Coulee, which is the main peripheral arterial road surrounding Tuscany area and shows the walking and driving time and distance required to reach

**Fig. 24.5** Walking distances from Tuscany school (SAND 2018c)
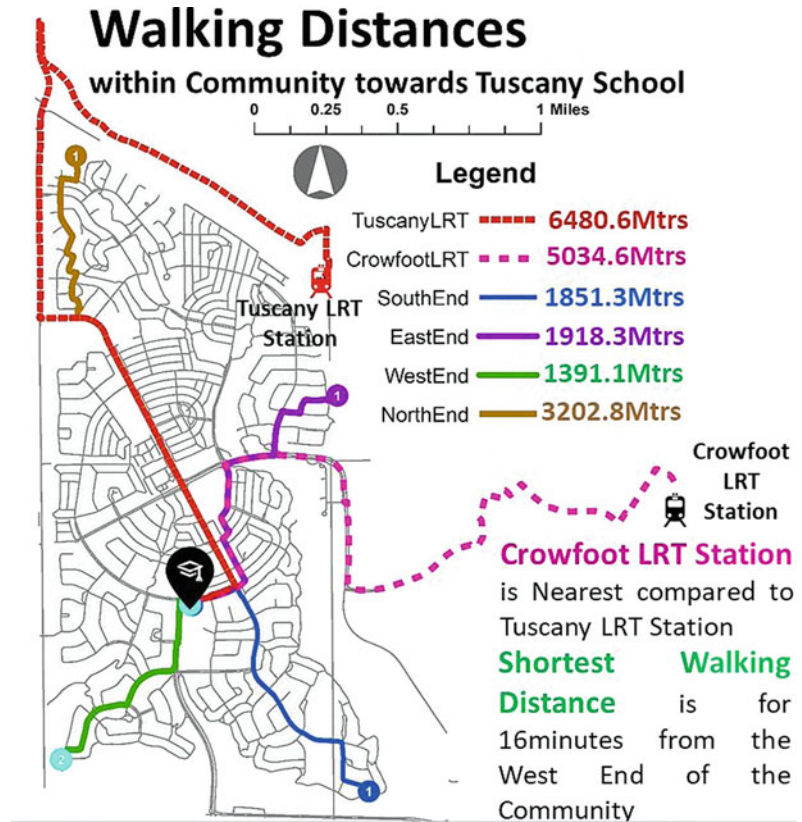
natural areas including Baker park and Bow river access areas which are outside the Tuscany community. Furthermore, a more detailed walk time assessment for travelling distance within Tuscany community is represented in Fig. 24.5. This highlights walking distances within and outside Tuscany community that the student population of Tuscany school is expected to walk in order to daily commute back and forth. Figure 24.5 shows that the shortest walking distance is a 16-min walk (green path) from the west end of community periphery, whereas the longest walking distance is approximately a 32 min walk towards the school from the north end periphery shown in brown colour path. Whereas the students walking from the south-end and east-end of the community will be walking an average between 1851 and 1918 m. Additionally, for people commuting from adjacent or outside communities, there are two LRT options, Crowfoot LRT and Tuscany LRT. As seen in

Fig. 24.5, the Tuscany LRT which is dedicated to this community is a longer walk as compared to the adjacent Crowfoot LRT station.

24.7 Walk Wrap Assessment

To better understand the street connectivity, network warp method is used to emphasize on street connectivity in relation to both walking and other types of active and passive movement within Tuscany community area. The "network warp metric compares the area accessible from a single point of origin in the presence and absence of the street network" (Galpern et al. 2018). The 1200 m circle area for walkshed is considered for this network wrap also known as walk wrap assessment analysis. This analysis identifies the resistance of urban form and to assess the quality and safety of walking experience for the population coming to Tuscany school.

Fig. 24.6 Walk warp for Tuscany (SAND 2018b)
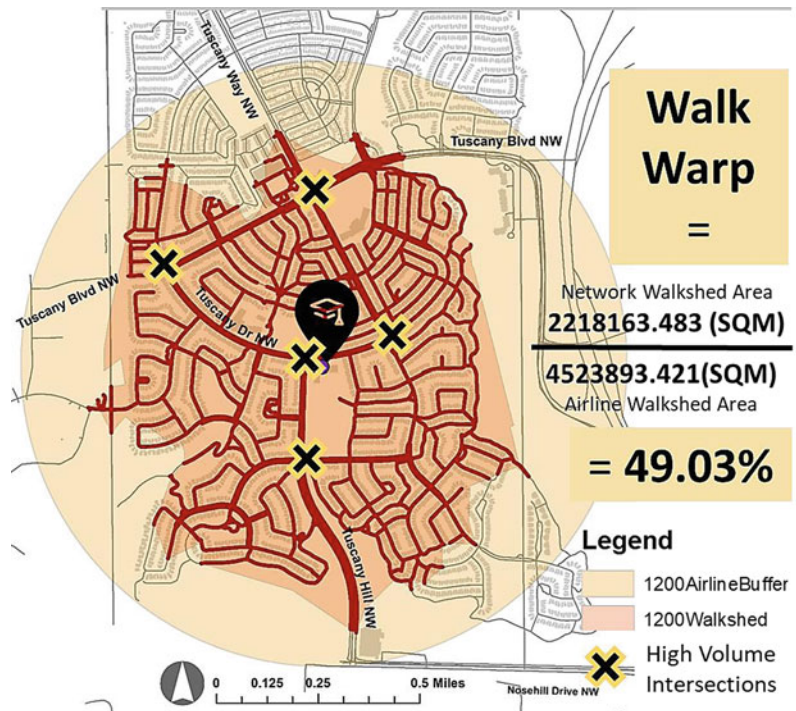
As per this analysis, the airline walkshed area is calculated along with the network walkshed area for the Tuscany school, which gives the total walk warp of 49%. Figure 24.6 represents these walksheds and walk wrap as a measure of street connectivity within Tuscany community area that plays an important role in movement behaviour. It identifies that vehicular movement appears more frequent in areas where public transit is less available and walking behaviour is evidently more frequent with dedicated pathways that encourage walking behaviour irrespective of the need for walking. This network wrap also identifies the high-volume intersection areas within the Tuscany community. As evident from Fig. 24.6, the "Tuscany school" has two prominent high traffic volume intersections within its 250 m (immediate) walkshed, one prominent high traffic volume intersections existing within its 500 m (intermediate) and two additional high-volume intersections within its 1200 m walkshed. All these high traffic junctions identified as per the walkshed analysis are represented in Fig. 24.7. This figure shows the detail of each of these traffic intersections, traffic movement

patterns and its implication over urban form. The presence of these high traffic volume intersections could be a discouraging factor enforcing indirect travel paths for the walking community. Additionally, the walk warp method indicates restriction in movement by a factor of 0.49, making an average walk extended by $1/0.49 = 2.03$ times further to reach the same destination.

As per the walk wrap analysis, the street pattern and walkshed are indicative of the following.

24.7.1   Resistance to Urban Form

This characteristic **is** indicative of the quantitative aspects that assess the degree to which urban form forces students to take indirect paths or force them to wrap their movement through the neighbourhood as follows:

• Owing to the road network configuration, residents are less likely to take public transit, increasing vehicular trips in the community.

Fig. 24.7 High-volume intersections identified in 250-, 500- and 1200-m walkshed radius (Fatima 2022a)
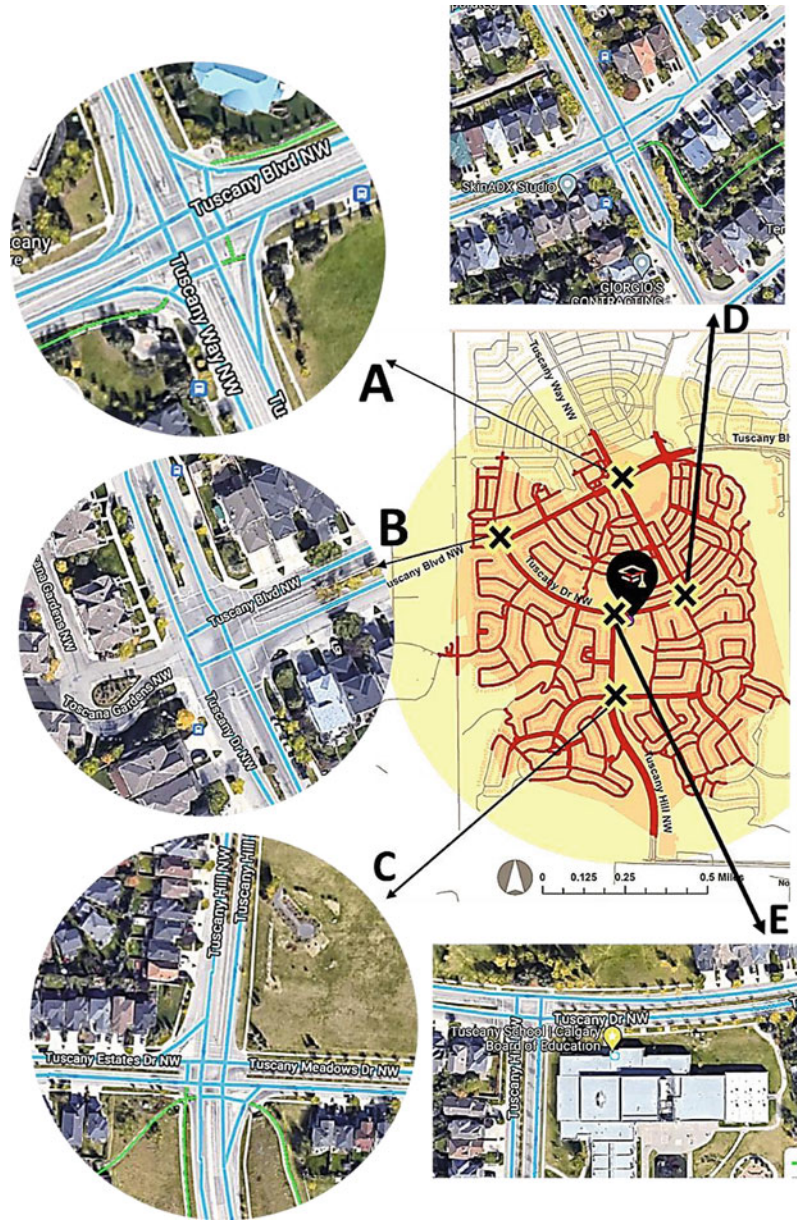
- Road pattern impedes vehicular speed due to poor sight distance, reducing the risk of vehicular crashes while increasing the risk at pedestrian crossings demanding pedestrian attention, as can be seen in Fig. 24.7.
- The network configuration encourages vehicular trips in the community where the residents are less likely to take public transit due to the extended walking distances, as indicated by walk wrap.
- Figure 24.6 represents the details of the urban form that exists within the 1200 m walkshed radius and is helpful in visualizing the indirect walking paths that resist the walking movement.

24.7.2 Quality and Safety of the Walking Experience

This characteristic is indicative of the qualitative aspects experienced by the school-going community as they walk towards the school:

- The 1200 m walkshed radius (Fig. 24.6) effectively visualizes the quality and safety of walking by offering insights through cartographic elements that convey the story of connectivity for Tuscany community.
- The high-volume intersection point A, C and D in Fig. 24.7 depicts the vehicular traffic intersections interrupting the pedestrian and biking pathways, which eventually impedes the overall pedestrian experience by introducing stress and negative experience.
- The walk towards the school from the south end and east end of the community are the safest options, crossing least number of high-volume intersections, demanding less pedestrian attention and vehicular interference.

24.8 Conclusion

The walkshed analysis identified the curvilinear street pattern, lengths and sight distances within the Tuscany community that governs the resident movement behaviour and mobility patterns. The comparison between Tuscany Community Biking Network Pattern (Fig. 24.2) and the walk warp assessment (Fig. 24.6) clearly establishes the fact that the presence of dedicated biking pathways or network exhibits no significant high-volume intersections, making the south-west quadrant within the Tuscany community the safest area for preferred walking and route choice. This quadrant is also identified for offering the shortest walking distance towards the Tuscany school, with a 16-min walk, depicted by green path in map (Fig. 24.5) walking distances from Tuscany school and therefore creates a positive experience for the school-going community.

Additionally, this walkshed analysis also identifies the presence of strong neighbourhood edges, which geographical separates the Tuscany community from major roads, adjacent neighbourhoods and surrounding natural areas inducing baker park and bow river access area (as evident in Fig. 24.4). This separation acts as a barrier which induces another scale of restricted walkshed for the resident community, impeding their walkability in and out of the community area.

Based on the issues identified within the Tuscany school service area, the impact of urban form in promoting and hindering the walkable environment is realised. These identified factors are the pointers towards the requisite modifications to create and encourage walkable environments according to the principle 2 of Sustainability Principles for Land Use & Mobility Plan by the City of Calgary. This will include traffic calming strategies, allocation of dedicated pathways and propose modification to strategically re-direct the existing traffic and infrastructure to increase transit efficiency.

For future studies, it is anticipated that this approach can offer detailed insight into the land use and spatial variables that influence an individual's decision to walk, choice of route and the preferred walkable distance. This type of urban modelling is intended to support urban design rethinking to promote regenerative modifications in community planning and design. This research is a potential example of GIS influence over the development of urban and environmental modelling and decision-making to promote more walkable neighbourhood design, and the relationships between urban forms and quality of walking experience.

References

Agampatian R (2014) Using GIS to measure walkability: a case study in New York City. Thesis. School of Architecture and the Built Environment, Royal Institute of Technology (KTH), Stockholm. Retrieved 11 June 2022 from http://www.diva-portal.org/smash/get/diva2:715646/FULLTEXT01.pdf

Bolten N, Caspi A (2021) Towards routine, city-scale accessibility metrics: graph theoretic interpretations of pedestrian access using personalized pedestrian network analysis. In: Chiabaut N (ed). PLoS One 16(3):1–20. https://doi.org/10.1371/journal.pone.0248399

Calgary Co (2008) Sustainability principles for land use & mobility plan. Retrieved from plan it Calgary: https://www.calgary.ca/content/dam/www/pda/pd/documents/municipal-development-plan/plan-it-sustainability-principles.pdf

Calgary TC (2019) Tuscany. Retrieved from the city of Calgary community profiles. https://www.calgary.ca/csps/cns/social-research-policy-and-resources/community-profiles/tuscany-profile.html

Esri (2021) Service area analysis. Retrieved from ArcMap. https://desktop.arcgis.com/en/arcmap/latest/extensions/network-analyst/service-area.htm

Fatima K (2022a) High volume intersections within 250, 500 and 1200 walkshed for Tuscany school. Google Maps, Alberta, Canada. Retrieved 14 June 2022a from https://www.google.ca/maps/@51.1185849,-114.2431637,384m/data=!3m1!1e3!5m2!1e3!1e4?hl=en

Fatima K (2022b) Tuscany community characteristics. Retrieved from https://www.calgary.ca/csps/cns/social-research-policy-and-resources/community-profiles/tuscany-profile.html

Fatima K (2022c) Tuscany overlay map. Calgary, Alberta, Canada. Retrieved 13 June 2022c from https://www.google.ca/maps/place/Tuscany,+Calgary,+AB/@51.1248591,-114.2583277,14z/data=!3m1!4b1!4m5!3m4!1s0x5371696e8c3fbbb1:0x7fce0f6820a785e4!8m2!3d51.1235364!4d-114.2448431?hl=en

Foundation H (n.d.) Appendix E—Active transportation needs assessment. Retrieved from rocky view county active transportation plan south county. https://www.rockyview.ca/Portals/0/Files/BuildingPlanning/Planning/ATP/ATP-SouthCounty-Appendix-E-Needs-Assessment.pdf

Galpern P, Ladle A, Uribe FA, Sandalack B, Doyle-Baker P (2018) Assessing urban connectivity using volunteered mobile phone GPS locations. Appl Geogr 37–46. https://doi.org/10.1016/j.apgeog.2018.02.009

Holbrow G (2010) TUFTS University. Retrieved from Department of Urban and Environmental Policy and Planning. http://sites.tufts.edu/gis/files/2013/02/Holbrow_Gabriel.pdf

Hynes RP (2006) Obesity, physical activity, and the urban environment: public health research needs. Environ Health 5:5–25. https://doi.org/10.1186/1476-069X-5-25

Magazine A (2020) Tuscany. Retrieved from best neighbourhood scores. https://www.avenuecalgary.com/best-neighbourhoods-filter/tuscany/

Rifaat SM, Tay R (2009) Effects of street patterns on injury risks in two-vehicle crashes. Transp Res Rec 2102:61–67. https://doi.org/10.3141/2102-08

Rifaat SM, Tay R, Barros Ad (2011) Effect of street pattern on the severity of crashes involving vulnerable road users. Accident Anal Prevent 43(1):276–283. https://doi.org/10.1016/j.aap.2010.08.024

Sandalack BA, Alaniz Uribe FG (2013) Neighbourhood type and walkshed size. J Urban 1–20. https://doi.org/10.1080/17549175.2013.771694

SAND (2018a) Tuscany school walkshed for 250, 500 and 1200 m. Scale not known. City of Calgary 2018a transportation geodatabase. Using Spatial and Numeric Data Services (SAND), University of Calgary (distributor). University of Calgary, Calgary, AB: generated by Kulsum Fatima, 14 Mar 2018a. Using ArcMap. Version 10.8. Environmental Systems Research Institute, Redlands, CA, 1999–2019

SAND (2018b) Walk wrap for Tuscany school. Scale 1:5000. City of Calgary 2018b transportation geodatabase. Using Spatial and Numeric Data Services (SAND), University of Calgary (distributor). University of Calgary, Calgary, AB: generated by Kulsum Fatima, 14 Mar 2018b. Using ArcMap. Version 10.8. Environmental Systems Research Institute, Redlands, CA, 1999–2019

SAND (2018c) Walking distances from Tuscany school. Scale 1:5000. City of Calgary 2018c transportation geodatabase. Using Spatial and Numeric Data Services (SANDS), University of Calgary (distributor). University of Calgary, Calgary, AB: generated by Kulsum Fatima, 14 Mar 2018. Using ArcMap. Version 10.8. Environmental Systems Research Institute, Redlands, CA , 1999–2019

Strupp J (2020) Walksheds help planners make routes to transit stops better for people on foot. Retrieved from Greater Washington. https://ggwash.org/view/78801/walksheds-help-planners-make-routes-to-transit-stops-better-for-people-on-foot-2

Swanson J, McCall N, Charlene H (2019) Walksheds show planners how easily people can walk to transit. Retrieved from Metropolitan Washington Council of Goverments. https://www.mwcog.org/newsroom/2019/07/16/walksheds-show-planners-how-easily-people-can-walk-to-transit/#:∼:text=An%20analysis%20of%20E2%80%9Cwalksheds%E2%80%9D%20can,walking%E2%80%94have%20fairly%20extensive%20walksheds.

totallycalgary (n.d.) Tuscany, Calgary. Retrieved from totallycalgary.ca: http://totallycalgary.ca/tuscany/

Transportation UD (2012) National Survey of Bicyclist and Pedestrian Attitudes and Behaviour (NHTSA) vol 2: findings report. Retrieved from National Highway Traffic Safety Administration. https://www.nhtsa.gov/sites/nhtsa.gov/files/811841b.pdf

Veitch J, Salmon J, Ball K, Bagley S (2005) Where do children usually play? A qualitative study of parents' perceptions of influences on children's active free-play. J Sci Med Sport 8:140–140. https://doi.org/10.1016/S1440-2440(17)30741-7

Wenhao W (2018) Network analysis, travel time, and accessibility. Retrieved from https://medium.com/@wenhaowu92/network-analysis-travel-time-and-accessibility-5848b4ae5f65

Wood JK (2016) Making maps: a visual guide to map design for GIS. The Guilford Press, New York and London. https://doi-org.ezproxy.lib.ucalgary.ca/10.1111/cag.12413

A Remote Sensing and GIS-Based Approach for Assessment of Drinking Water Quality and Its Association with Land-Use Land-Cover in Azamgarh City, India

Uzma Ajmal and Saleha Jamal

Abstract

Drinking water quality holds special significance as people's health and well-being are dependent on the use of pure and clean water. In this study, an effort has been done to monitor the drinking water quality and its association with land-use land-cover by using remote sensing and GIS, in Azamgarh city. A total of nine samples of drinking water were collected from various parts of the city and have been analysed for various physico-chemical parameters. Water quality index has been calculated to examine the fitness of water for drinking purposes. Spatial interpolation maps of various physico-chemical parameters as well as of the water quality index have been prepared using inverse distance weighting technique. Maximum likelihood supervised classification has been used to prepare land-use land-cover map of Azamgarh city with the help of Sentinel 2A data of 10 m spatial resolution. Results revealed that, out of the nine samples, water quality of five samples, from the areas of Bazbahadur, Har-

banshpur, Paharpur and Sarfuddeenpur, was poor for drinking. A linear correlation between water quality index and type of residential land use has been observed with compact residential areas representing poor quality of water and thin residential areas representing quality of water that was good for drinking. The study, thus, suggests an integrated RS and GIS method to assess the drinking water quality and its association with land-use land-cover which can also be applied in other studies.

25.1 Introduction

It is a very common fact that health of the humans and their survival is determined by the use of clean water for consumption and other purposes (Anwar and Aggarwal 2014). In Azamgarh city, the chief and solitary source of water is groundwater. The water that is present underneath the earth's surface in minute holes in the soil, in hollows and fissures of rocks, is known as groundwater. It is a decent source of freshwater due to its rather less susceptibility to contamination in contrast to the surface water. However,

U. Ajmal · S. Jamal (✉)
Department of Geography, Faculty of Science, Aligarh Muslim University, Aligarh, India
e-mail: salehajm@gmail.com

U. Ajmal
e-mail: uzmakhan667@gmail.com

the quality of groundwater has been worsened owing to some serious factors like population growth, industrial development as well as urbanization (Tyagi et al. 2013). Urban areas have affected the behaviour and characteristics of groundwater. Many contaminants, such as industrial and commercial diluters, salts, sediments, pesticides and faeces, have been added to both surface and groundwater. As the rate of groundwater use surpasses the rate of groundwater recharge, the risk of groundwater pollution and water-related problems rises; as a result, the groundwater table drops and contamination rates rise, posing a serious risk to human health (Asadi et al. 2007). According to data, India's groundwater level has decreased by 61% from 2007 to 2017 (Down to Earth, 09 July 2019). Each year, it is estimated that more than 500,000 people die from diarrhoea as a result of drinking contaminated water (WHO, Unsafe Drinking Water, Sanitation and Waste Management 2009). Diarrhoea, dysentery, cholera, typhoid and other diseases can be spread via contaminated water. Diarrhoea is the most commonly known disease associated with contaminated water ("10 common waterborne diseases" 2017). Schistosomiasis is another acute and chronic disease caused by consumption of infested water, affecting about 240 million people a year (WHO 2011). Therefore, analysis of drinking water quality is a valuable approach to estimate the health impacts of drinking water in Azamgarh city.

Water quality of a particular region can be examined using its physico-chemical and biological characteristics. Quality parameters of a water sample involve pH, TDS, TSS, hardness, calcium, chlorine, chloride, fluoride, nickel, magnesium, arsenic, iron, lead, BOD, COD, coliform bacteria, dissolved oxygen, etc. The concentration of these constituents is harmful to humans if they exceed the prescribed limits (BIS 2012; WHO 2012; CPCB 2013; United States EPA 2009). Water will be called safe for drinking if it lies below the standard limits defined by various agencies like WHO, BIS and the US EPA.

LULC has been believed to have a direct influence on water quality. Built-up areas have a positive relationship with water pollution, but vegetation is negatively correlated with water pollution, according to studies (Ajmal et al. 2021; Jamal et al. 2022). Asadi et al. (2007) investigated the relationship between LULC and water quality and reached to the conclusion that quality of water was poorer in densely populated parts. Chemical characteristics of groundwater such as pH, turbidity, TDS, DO, BOD and coliforms are all altered by augmented urbanization and land-use changes, leading to water-related illnesses like cholera and schistosomiasis (Marale et al. 2012; Saravanan et al. 2016). Due to illogical fertiliser use, agricultural lands are also becoming a hazard to groundwater quality (Mishra et al. 2014). Considering all these points, in this study, an attempt is made to examine the drinking water quality and its association with LULC in Azamgarh city, India.

25.2   Material and Methods

A multi-level analysis is performed for drinking water quality analysis and its association with land-use land-cover. Initially, drinking water samples from nine different locations of the city were taken and were analysed for relevant physico-chemical parameters. Inverse distance weighting (IDW) interpolation method was performed to comprehend the spatial variation of different physico-chemical parameters in the city. WQI was calculated to evaluate the appropriateness of water for drinking purposes. LULC map of Azamgarh city was prepared using sentinel 2A satellite data of 10 m spatial resolution. Further correlation between WQI and LULC was examined (methodology flowchart in Fig. 25.1).

25.2.1   Study Area

Azamgarh city, situated in the middle Ganga plain in northern part of India, with a total population of 110,983, comes under the category of medium-sized cities (Fig. 25.2). Situated on the loop line of North-Eastern railway, it is well connected with important cities of U.P., namely

Fig. 25.1 Flowchart of
methodology
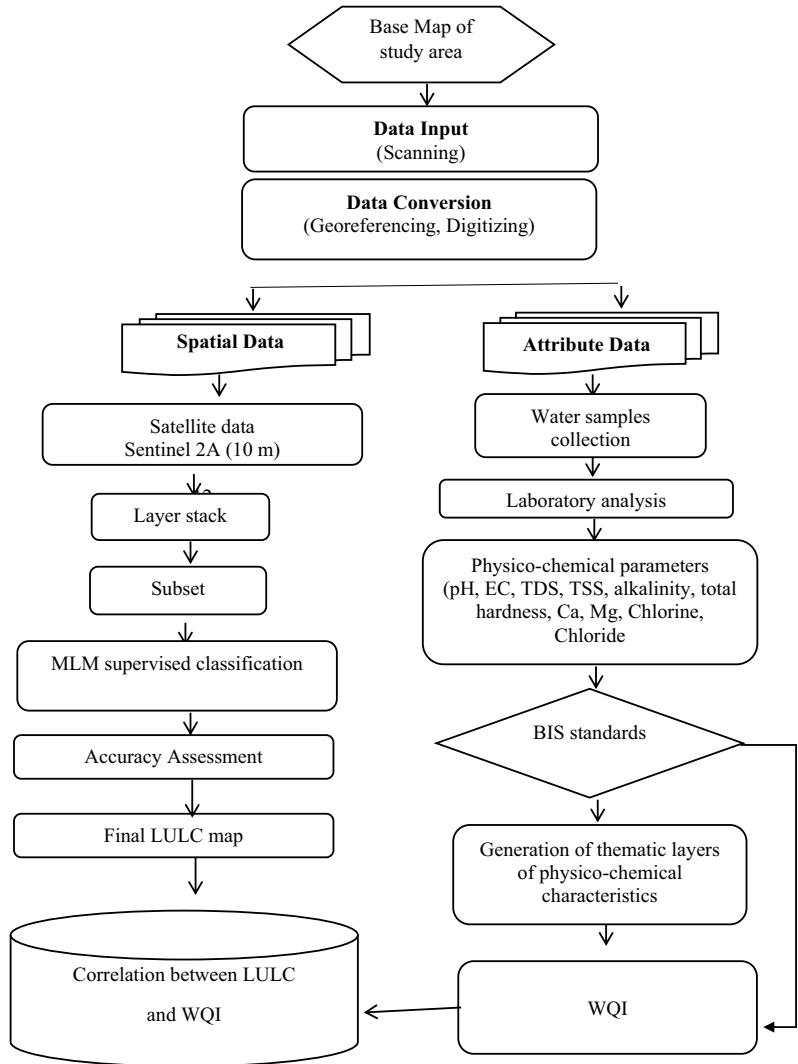
Varanasi (95 km), Gorakhpur (100 km), Alla-
habad (162 km) and Lucknow (271 km). The
city is surrounded by the river Tons on three
sides and by the seasonal Dharmu Nala on the
north and north-eastern sides. The city spreads
over an area of 12.71 sq. km. Tons River have a
great impact on the development and residential
pattern of the city. Previously, areas only north of
the Tons River were considered part of city while
in southern part rural character prevailed. Grad-
ually with the construction of bridge on Tons
River its southern counterparts started to develop
and villages got merged in the city. At present in
the northern part of Tons River, old and con-
gested character can be seen while southern part
is growing and developing towards better resi-
dential and service character. However, some of
the new colonies which are growing towards the
northern periphery are socio-economically better.
Azamgarh city has faced several outbreaks of
cholera, jaundice and diarrhoea in the past sev-
eral years. Residents have claimed unclean
drinking water as the major cause behind these
outbreaks. With increasing population, ground-
water quality has said to be deteriorated in the
city.
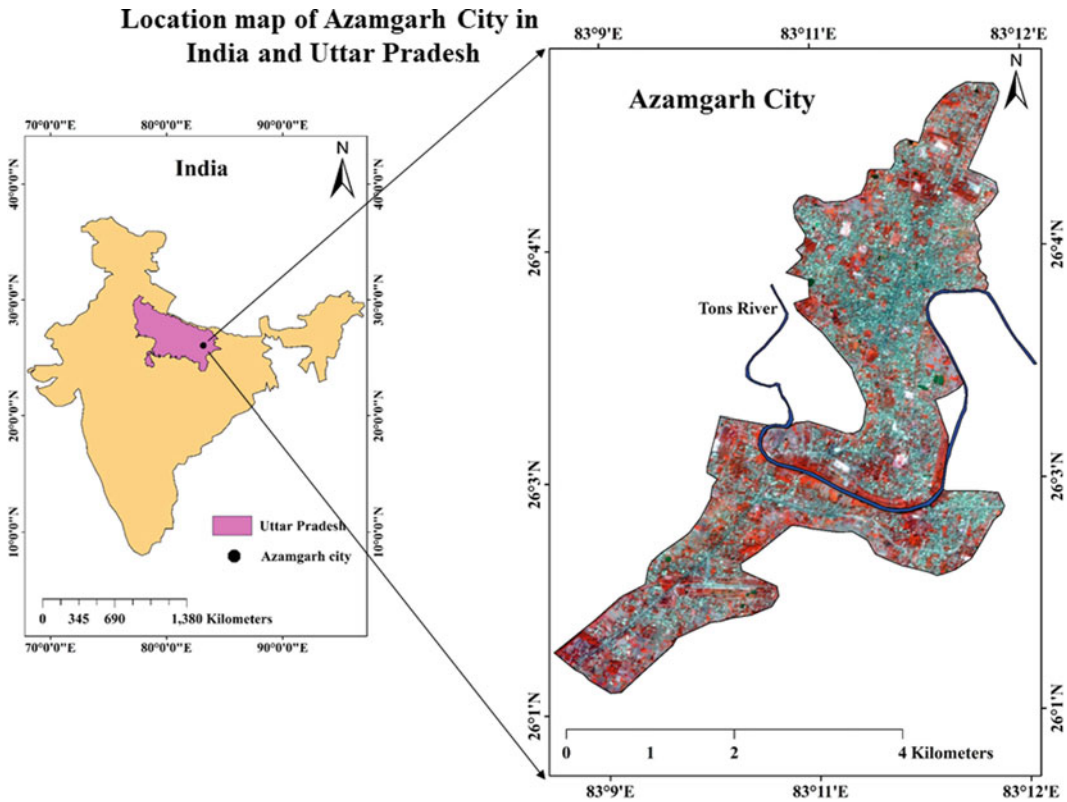
Fig. 25.2 Study area

25.2.2 Water Samples Collection and Laboratory Analysis

To examine the quality of drinking water in Azamgarh city, a total of nine drinking water samples were collected for physico-chemical analysis (Fig. 25.3). For collecting the water sample, taps and hand pumps were operated for about 5 min to flush out stagnant water in it. Then the samples were collected in clean polythene bottles, and adequate information was written on the bottles. The bottles were pre-cleaned with acid wash followed by distilled water. All samples of water quality were maintained at 4 °C temperature till transportation to the Environmental Engineering Lab, Civil Engineering, Aligarh Muslim University, Aligarh. Due care was taken such that no significant change in the composition of water samples should take place till the laboratory processing is

carried out. Tests were performed by the researcher, in Environmental Engineering Lab, under the guidance of laboratory attendants and technicians. Methods adopted for physico-chemical analysis of samples for following ten parameters, which has been shown in Table 25.1. Results of drinking water quality parameters are analysed using standard values of water quality parameters as prescribed by BIS (Table 25.2). Apart from this, BIS did not provide standard for some parameters, and for them, values of WHO and other bodies are considered (Table 25.2).

25.2.3 Inverse Distance Weighting (IDW) Interpolation for Spatial Mapping

IDW method was used to prepare interpolation map of Azamgarh City for different water quality
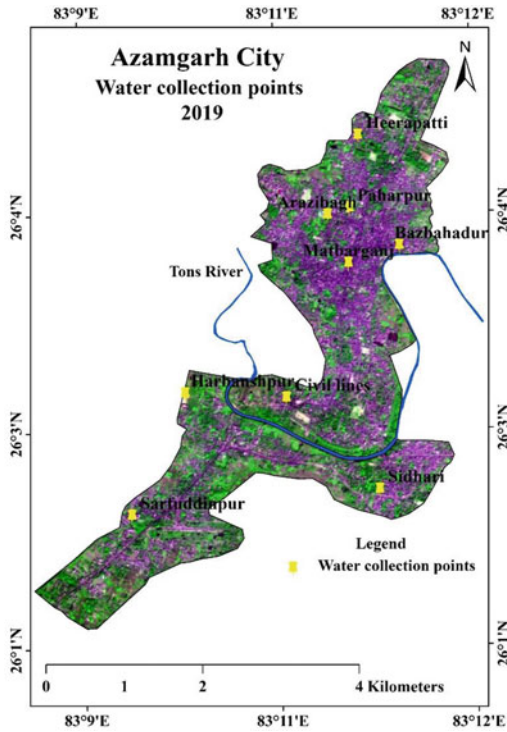
Fig. 25.3 Water samples collection points in Azamgarh city

Table 25.1 Methods used for physico-chemical analysis of water samples

Parameters	Methods
pH	pH metre
TDS	TDS metre
EC	Conductivity metre
Chloride	Argentometric titration
Alkalinity	EDTA
Total hardness	EDTA
Ca	EDTA
Mg	EDTA
Chlorine	Starch iodide test
TSS	Filtering and weighing method

parameters. IDW is the most popular method of interpolation to calculate values of unknown points using a known set of scattered points. IDW has been accepted as one of the customary spatial interpolation techniques in GIS (Burrough et al. 1998; Longley et al. 2005). The basic formula for IDW interpolation is

$$v_\mathrm{p} = \frac{\sum_{i=1}^{n} \frac{1}{d} v_i}{\sum_{i=1}^{n} \frac{1}{d}} \tag{25.1}$$

where

v_p value to be estimated
v_i known value
d_1-d_n distances from the data point to the point estimated n.

25.2.4 WQI Calculation

To examine the fitness of water for drinking, the WQI is calculated. Determination of WQI involved the following steps.

First of all, each parameter was given weights (w_i), according to their relative importance in overall quality of water (range, 1–5). (Table 25.2).

Secondly, relative weights (W_i) of the parameters (Table 25.3) are calculated (Eq. 25.2)

$$W_i = \frac{w_i}{\sum_{i=1}^{n} w_i} \tag{25.2}$$

where

W_i relative weight
w_i weight
n total number of parameters.

Later q_i is calculated by calculating concentration of each parameter with its respective standard (BIS) multiplied by 100 (Eq. 25.3).

$$q_i = \frac{C_i}{S_i} \times 100 \tag{25.3}$$

where

q_i is the quality rating,
C_i is concentration of each parameter
S_i is drinking water standard.

Table 25.2 Standard values for different parameters of water

Parameters	BIS		BIS standard	WHO standard
	Desirable limit	Permissible limit		
pH	6.5–8.5	6.5–8.5	6.5–8.5	6.5–8.5
TDS	500	2000	500	2000
EC	–	–	–	750
TSS	–	–	–	30
Alkalinity	200	600	200	–
Total hardness	200	600	200	500
Chloride	250	1000	250	200
Calcium	75	200	75	200
Magnesium	30	100	30	150
Chlorine	0.2	1	0.2	–

Table 25.3 Weights of different parameters

Parameters	Assigned weight ($\underline{w_i}$)	Relative weight (W_i)
pH	4	0.14
EC	3	0.11
TDS	4	0.14
TSS	3	0.11
Alkalinity	3	0.11
Hardness	2	0.07
Ca	2	0.07
Mg	2	0.07
Chloride	2	0.07
Chlorine	3	0.11
	$\sum w_i = 28$	$\sum W_i = 1.00$

For computing WQI, the sub-index (SI) is determined (Eq. 25.4);

$$SI_i = W_i \times q_i \qquad (25.4)$$

And lastly WQI (Eq. 25.5) is calculated

$$WQI = \sum_{i=1}^{n} S_i \qquad (25.5)$$

where

SI_i sub-index of ith parameter;

W_i relative weight of ith parameter;
Q_i is the rating based on concentration of ith parameter, and n is the number of chemical parameters

The WQI values are divided into five classes, ranging from excellent water quality to water unsuitable for drinking. If WQI is <50 water quality will be considered excellent, if it is 50–100, water will be considered good for drinking, if it ranges between 100–200, water will be considered poor for drinking, if it is 200–300, water will be considered very poor for drinking

and in the same water will be considered unfit for drinking if WQI values exceed 300.

25.2.5   LULC Preparation

The use of RS and GIS has arisen as a powerful tool for mapping of different land-use features of any area (Demuth and Radojevic 2011; Jamal and Ajmal 2020a, b; Ajmal and Jamal 2021). Sentinel 2A data of March 2017 has been used to prepare LULC map of Azamgarh city. Maximum likelihood supervised classification method has been used to find 250 spectral signatures of matching pixels from different classes. Different LULC classes were finalized by assembling spectrally similar signatures. The final LULC classes were vegetation, built-up, agricultural lands, water and open spaces as these were the prominent land-use categories found in the city.

25.3   Results and Discussion

25.3.1   Physico-Chemical Characteristics of Water Samples

The pH of water refers to the concentration of hydrogen ions in it. Normal range of pH is 0–14. A pH value of 7 is called neutral for water while it is called acidic below 7 and alkaline above 7.

Acceptable range of pH is 6.5–8.5 for drinking. pH level below 7 makes the water acidic which can corrode distribution pipes and leach metals in water. Low pH water can cause aggravation of mucous membrane and can lead to pulmonary issues as well as other diseases (Srinivas et al. 2013). From Table 25.4 and Fig. 25.4, it has been observed that the pH of the drinking water samples lies within 7.38–8.31 suggesting that pH of the water in Azamgarh city is within the desirable limit.

Electrical conductivity is known as the capability of water to pass an electric current, and it depends upon the salt content in the water as dissolved salts and other inorganic materials. Electrical conductivity ranges between 0 and 800 μS/cm which is good for consumption as there are no biological contaminants and not too much of the suspended particles. WHO has marked 750 as standard limit (Bhat and Pandit 2014) for EC, above which water is not recommended to be consumed. Table 25.4 shows that out of the total nine samples, EC is beyond the standard limit in four samples, i.e. in Matbarganj, Bazbahadur, Paharpur and Sarfuddinpur.

The term TDS, i.e. total dissolved solids, refers to the minute organic material as well as inorganic minerals found in the water. The main components are generally calcium, magnesium, sodium and potassium cations and carbonate. A certain level of these minerals in water is essential for life. Water with deficient

Table 25.4 Concentration of parameters in water samples

| Samples	Sampling point	pH	EC	TDS	TSS	Alkalinity	Total hardness	Ca	Mg	Chloride	Chlorine
1	Harbanshpur	8.31	441	239	96	184	230	148	82	16	0
2	Matbarganj	7.7	1113	615	16	384	234	82	152	121	0
3	Civil lines	7.79	614	335	46	162	192	66	81	40	0
4	Bazbahadur	7.69	1369	792	6	500	280	120	160	190	0
5	Arazibagh	7.81	400	375	36	188	184	72	112	40	0
6	Paharpur	7.61	1074	574	52	440	214	64	150	108	0
7	Sarfuddinpur	7.91	1065	543	31	252	221	81	140	192	0
8	Heerapatti	7.56	650	481	28	187	176	84	77	231	0
9	Sidhari	7.38	885	354	42	132	137	62	75	248	0
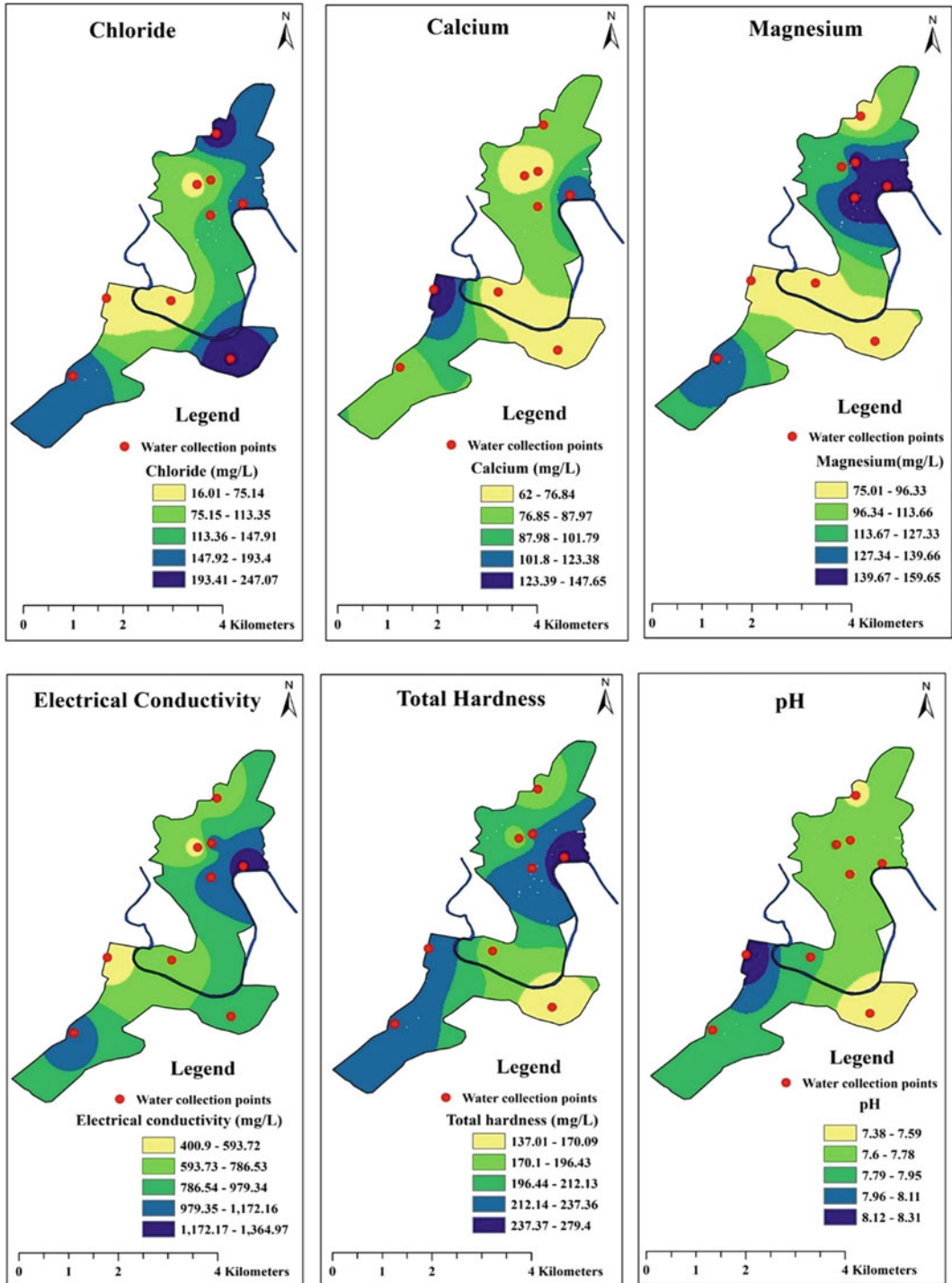
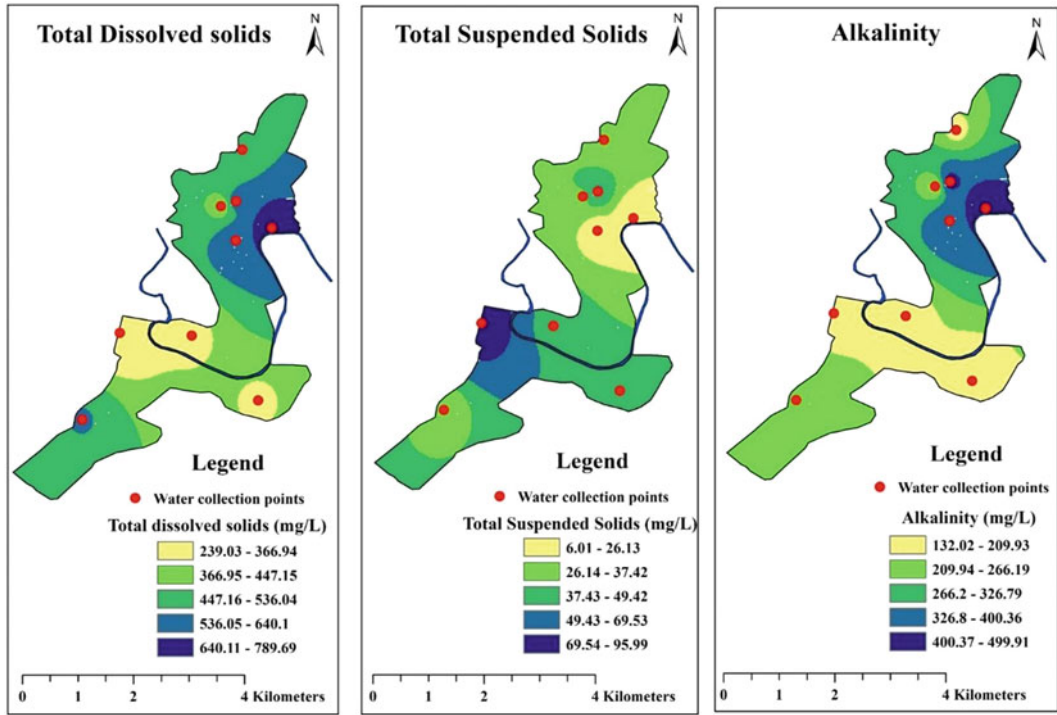**Fig. 25.4** Distribution of different parameters in Azamgarh city

Fig. 25.4 (continued)

concentrations of TDS may be unacceptable because of its flat, insipid taste and absence of desired minerals in it. Water with TDS less than 300 mg/litre is considered as excellent, 300–600 mg/L as good, 600–900 mg/L as fair and 900–1200 mg/L as poor. Early studies have linked concentration of TDS in water with increasing incidence of cancer, coronary heart diseases and mortality (Fawell et al. 2003). Desirable limit of TDS as per BIS is 500 mg/L. Table reveals that four samples surpassed the desirable limit of drinking water in terms of total dissolved solids, and these samples are from Matbarganj, Bazbahadur, Paharpur and Sarfuddinpur.

Water hardness is a total of calcium and magnesium availability in the water. Water is considered soft with a concentration of calcium carbonate below 60 mg/L, moderately hard with 60–120 mg/L, hard with 120–180 mg/L and very hard with more than 180 mg/L (McGowan 2000). The desired limit for water hardness is 200 mg/L. The hard water is unfit for consumption and can lead to stomach-related diseases (Mohsin et al. 2013). Total hardness of the sampled water from Azamgarh city ranges from 130 to 180 with an average value of 196. It has been found that water hardness crosses the desirable limit at five stations, namely Harbanshpur, Matbarganj, Bazbahadur, Paharpur and Sarfuddinpur.

Calcium and magnesium are important determinant of water hardness. Both calcium and magnesium are vital minerals and helpful to people's health in numerous respects, and an inadequate intake of any of these can result in harmful health effects. Insufficient intake of calcium can lead to kidney stones, hypertension, stroke and obesity. The desirable limit of calcium in water is recommended as 75 mg/L. Calcium concentration in the water surpasses the desirable limit in five samples of water, namely Harbanshpur, Matbarganj, Bazbahadur, Sarfuddinpur and Heerapatti. Magnesium deficiency has also

been linked with hypertension; however, an increasing concentration of magnesium can result in diarrhoea, especially in people with low kidney function. Desirable limit of magnesium in water is 30 m mg/L revealing that magnesium concentration with an average of 75 mg/l is beyond the desirable limit in all the samples.

Chlorides are inorganic minerals formed by the combination of chlorine gas and metals. Some common chlorides in the water include sodium chloride and magnesium chloride. Chlorine alone as Cl_2 in the water is poisonous; however, in a combination of metals such as sodium, it is crucial for life by providing needed salts to humans. The acceptable limit for chloride in the water is 250 mg/L, and a higher concentration is linked to heart and kidney diseases (Kumar and Puri 2012). Chloride increases the electrical conductivity of water and thus its corrosivity. The table reveals that chloride concentration is within the standard limits in all the samples. Chlorine alone as Cl_2 can be dangerous and can lead to vomiting, coma and even death (International Occupational Safety and Health Information Centre 2009); however, the concentration of chlorine is found negligible in all the samples (Table 25.4).

Alkalinity in the water is primarily due to carbonate, bicarbonate and hydroxide contents. Consumption of alkaline water may result in decreasing natural stomach acidity, which helps in killing bacteria's and ejecting unwanted pathogens. An overall surplus of alkalinity in humans can cause stomach-related diseases and skin issues. Higher alkalinity may lead to a metabolic *alkalosis* with the symptoms such as nausea, vomiting and muscle twitching. BIS has demarcated concentration of $CaCO_3$ 200 mg/L (alkalinity) as a desirable limit. The table reveals that most of the samples are within the desirable limit except four samples, i.e. Matbarganj, Bazbahadur, Paharpur and Sarfuddinpur.

Total suspended solids or TSS may include silt, decaying plants and animal substance, sewage and industrial waste. High concentration of suspended solids in the matter is generally related to elevated levels of pathogens like bacteria, germs, parasites and other microorganisms which can cause problems like nausea, twinges, diarrheal disease and headache. Neither WHO nor BIS has provided standard value of TSS in the drinking water; therefore, for the present analysis, the standard provided by National Environmental Management Authority (NEMA), Kenya, has been used. NEMA has suggested 30 mg/L of suspended solids as standard limit for drinking water which suggests that out of the total nine samples, only two samples lie within the standard limits, i.e. Matbarganj and Bazbahadur while total remaining samples have shown more suspended solids in the water which could be harmful to people consuming it.

25.3.2 LULC of Azamgarh City

LULC is the result of natural and manmade factors in any region. Nature and pattern of land use in any region are deeply associated with groundwater quality of the region. LULC data is

Table 25.5 Area under LULC classes in Azamgarh City

Azamgarh city LULC		
Land-use type	Area (km^2)	Percentage
Built-up area	5.02	39.83
open spaces	4.46	35.38
Tree cover	2.71	21.50
water body	0.24	1.90
Agriculture	0.18	1.39
Total		100.00

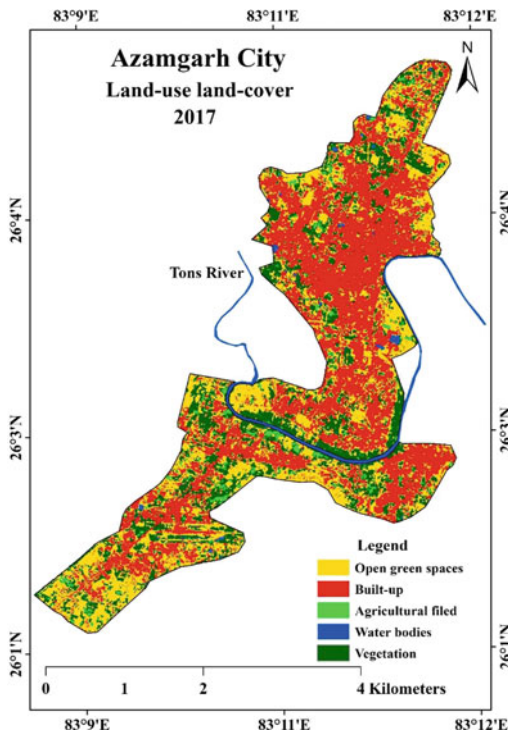*Source* Sentinel 2A (10 m resolution, 2017)

Fig. 25.5 LULC of Azamgarh City

important for sustainable management of resources and urban planning. LULC in Azamgarh city covers five categories, i.e. built-up area, vegetation, agricultural lands, open green spaces and water bodies (Table 25.5 and Fig. 25.5). The LULC map suggests that out of the total area of the city 39.83% is occupied by built-up structures. 35.38% area of the city comes under open-green spaces while tree cover occupies 21.50% area of the city. Water bodies occupy 1.90% area of the city while 1.39% area is devoted to agricultural activities (Table 25.5 and Fig. 25.5). Of the total built-up area, 65.50% represent low population density areas, 23.87% represents medium population density areas and 10.64% is occupied by high population density areas.

25.3.3 WQI and LULC

To understand the suitability of water for potable use, WQI is calculated. The obtained values of WQI and type of the different drinking water samples can be seen in Table 25.6. Interpolation map of Azamgarh city for water quality index is constructed using the data to obtain a visual representation of water quality in the city. Interpolation map using IDW technique is used to represent distribution pf WQI in Azamgarh city (Fig. 25.6). The WQI of the water samples lies within 95–147. Table reveals that, out of nine, only four samples could made it upto good category of water while remaining five water samples found their place in poor category of water. Not a single water sample could find the place in excellent category of water. The sample that was categorized into poor category were water samples from Harbanshpur, Civil lines, Arazibagh, Pahrpur and Sarfuddinpur with their WQI values ranging from 124 to 143. The WQI map is presented in Fig. 25.6.

Areas covered under built-up areas are considered as more prone for groundwater quality deterioration (Asadi et al. 2007). Therefore, to understand the impact of human interferences on water quality, all the water samples were collected from residential areas. None of the samples collected for analysis is from industrial area as there is no prominent industrial area in Azamgarh city. Therefore, the impact of different types of residential areas on the water quality has been understood with the help of correlation. The correlation of different types of residential areas and water quality has been presented in Table 25.7. Table 25.7 and Fig. 25.7 suggest that level of water quality degradation has a strong correlation with residential land uses, categorized into compact residential areas, medium residential areas and thin residential areas.

Of the total nine water samples, five samples were collected from thin residential areas, two samples were taken from medium residential areas and two samples from compact residential areas. Water samples were collected based on the proportion of density category in Azamgarh city. As major proportion of city is occupied by thin residential areas; therefore, more samples are collected from thin residential areas, and similarly, less samples are collected from compact and medium-density residential areas. Of the

Table 25.6 WQI of drinking water samples

Samples	1	2	3	4	5	6	7	8	9
Name	Harbanshpur	Matbarganj	Civil lines	Bazbahadur	Arazibagh	Paharpur	Sarfuddinpur	Heerapatti	Sidhari
Type of residential area	Thin residential	Medium residential	Thin residential	Compact residential	Medium residential	Compact residential	Thin residential	Thin residential	Thin residential
WQI value	124	129	95	147	97	143	125	98	97
WQI category	Poor	Poor	Good	Poor	Good	Poor	Poor	Good	Good

Source Computed by Researcher, 2019
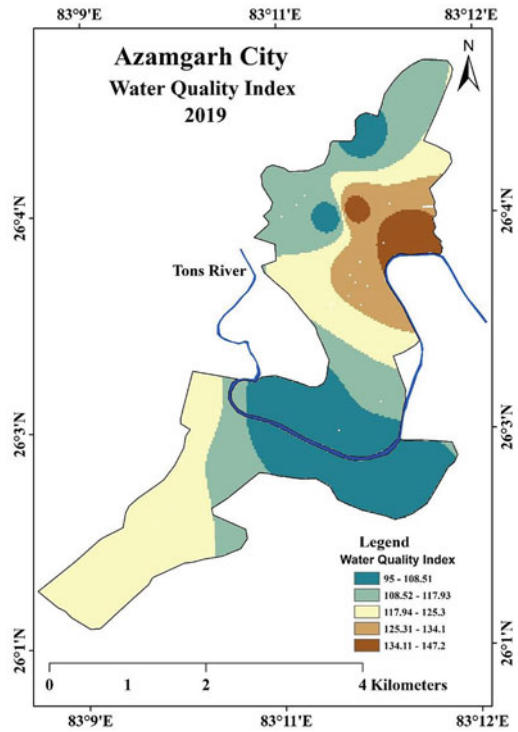
Fig. 25.6 Distribution of WQI in Azamgarh city

Table 25.7 Correlation between WQI and LULC

WQI LULC	Compact residential areas	Medium residential areas	Thin residential areas
Excellent	0	0	0
Good	0	1	3
Poor	2	1	2
V. poor	0	0	0
Unfit for drinking	0	0	0

Source Computed by Researcher, 2019

water samples collected from compact residential areas, both the samples (100%) exhibited poor water quality. Of the two water samples taken from medium residential areas, one sample (50%) displayed good water quality while the other one (50%) fell into poor category of water. Moreover, of the total five samples collected from thin residential density areas, two samples (40%) represented poor water quality while three

Fig. 25.7 Correlation of LULC with WQI

samples (60%) exhibited good quality of drinking water (Table 25.7 and Fig. 25.7).

The analysis revealed that not a single water sample from compact residential areas exhibited good water quality for drinking. Results were mixed from medium residential areas like 50% water samples represented good water quality and remaining 50% represented poor water quality for drinking. Similarly, majority of water samples (60%) from thin residential areas represented water quality th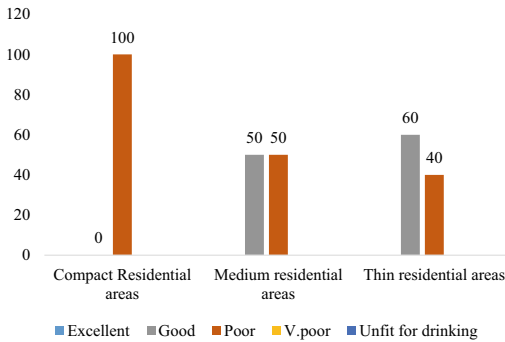at was good for drinking. Therefore, it is obvious from the outcomes that residential land-use category, with different degree of compactness, has a strong influence over the water quality of any area. Other studies conducted in Azamgarh city have also revealed that waterborne diseases like diarrhoea, typhoid and jaundice erratic significantly associated with erratic water supply and inadequate sanitation facilities (Jamal and Ajmal 2020a, b). Studies have also associated consumption of contaminated water with spread of infectious deceases as diarrhoea, cholera and skin diseases in the tropical zones (Lye 2002).

25.4 Conclusion

In the present study, physico-chemical qualities of drinking water samples, suitability of water for drinking purposes (WQI) and their association with types of residential land use has been analysed. The analysis of physico-chemical characteristics of water samples from Azamgarh city revealed that parameters like pH, chloride and chlorine were within the permissible limit for all the samples. However, values of EC, TDS, alkalinity, hardness and TSS exceeded in the water samples collected from Bazbahadur, Paharpur, Sarfuddinpur and Matbarganj, of Bazbahadur, Paharpur and Matbarganj are highly dense residential areas. WQI of the samples suggested that, out of the nine samples, the water quality of five samples was poor for drinking. A linear correlation between WQI and type of residential land use has been observed with compact residential areas representing poor quality of water and thin residential areas representing that water was good for drinking. The analysis also revealed the importance of remote sensing and GIS in preparation of various thematic maps of study area, i.e. LULC, interpolation map of water quality parameters as well as identification of problematic zones of the study area. Therefore, the study suggests a combined RS and GIS approach to appraise the influence of LULC on drinking water quality.

References

Ajmal U, Jamal S (2021) Analyzing land-use land-cover change and future urban growth with respect to the location of slaughterhouses in Aligarh city outskirts. Environ Challenges 5:100331

Ajmal U, Jamal S, Ahmad WS, Ali MA, Ali MB (2021) Waterborne diseases vulnerability analysis using fuzzy analytic hierarchy process: a case study of Azamgarh city, India. Modeling Earth Syst Environ 1–27

Anwar KM, Aggarwal V (2014) Analysis of groundwater quality of Aligarh city, (India): using water quality index. Current World Environment 9(3):851

Asadi SS, Vuppala P, Reddy MA (2007) Remote sensing and GIS techniques for evaluation of groundwater quality in Municipal Corporation of Hyderabad (Zone-V), India. Int J Environ Res Public Health 4(1):45–52. https://doi.org/10.3390/ijerp h2007010008

Bhat SA, Pandit AK (2014) Surface water quality assessment of Wular Lake, a Ramsar site in Kashmir Himalaya, using discriminant analysis and WQI. J Ecosyst

Bureau of Indian Standards (2012) Specification for drinking water. IS: 10500, New Delhi, India

Burrough PA, McDonnell R, McDonnell RA, Lloyd CD (1998) Principles of geographical information systems. Oxford University Press

Common waterborne diseases and how to prevent them, 42 May 2017. https://www.livpure.com/blog/10-common-waterborne-diseases-and-how-to-prevent-them. Retrieved on 02 Mar 2020. 31(8):1089–1099. https://doi.org/10.1093/heapol/czw039

CPCB (2009) Status of water supply, wastewater generation and treatment in Class-I cities & Class-II towns of India. Control of urban pollution, SERIES: CUPS/70/2009-10

CPCB (2013) Guide manual: Water and waste water. Central Pollution Control Board, New Delhi. http://www.cpcb.nic.in/upload/Latest/Latest_67_guidemanualw&wwanalysis.pdf. Accessed 12 July 2013

Demuth S, Radojevic B (2011) Global Change and its impact on water resources: the role of UNESCO's International Hydrological Programme. Water Resour Manage 1:7–15

Down to Earth, 09 July 2019. https://www.downtoearth.org.in/blog/water/depleting-groundwater-costs-farmers-heavily-65530. Retrieved on 26 Sept 2019

Environmental Protection Agency (EPA) of the U.S. Website (2005) http://www.epa.gov

Fawell JK, Lund U, Mintz B (2003) Total dissolved solids in drinking-water. Background document for development of WHO guidelines for drinking-water quality. World Health Organization, Geneva

International Occupational Safety and Health Information Centre (CIS) (2009) Chlorine, in International Chemical Safety Cards, 31 Mar 2009. International Programme on Chemical Safety (IPCS) and European Commission (EC). Accessed 5 Sept 2019

Jamal S, Ahmad WS, Ajmal U, Aaquib M, Ali MA, Ali MB, Ahmed S (2022) An integrated approach for determining the anthropogenic stress responsible for degradation of a Ramsar Site-Wular Lake in Kashmir, India. Marine Geodesy (just-accepted) 1–18

Jamal S, Ajmal U (2020a) Neighbourhood deprivation and health; a study of low-income neighbourhoods in Azamgarh City. Urban health risk and resilience in Asian cities. Springer, Singapore, pp 253–270. https://doi.org/10.1007/978-981-15-1205-6_15

Jamal S, Ajmal U (2020b) Assessment Of neighbourhood environmental quality using analytical hierarchy process with GIS In Azamgarh City. Planning 73(1):49–58

Kumar M, Puri A (2012) A review of permissible limits of drinking water. Ind J Occup Environ Med 16(1):40

Longley PA, Goodchild MF, Maguire DJ, Rhind DW (2005) Geographic information systems and science. Wiley

Lye DJ (2002) Health risks associated with consumption of untreatedwater from household roof catchment systems. J Am WaterResour Assoc 38(5):1301–1306. https://doi.org/10.1111/j.1752-1688.2002.tb04349.x

Marale SM, Mahajan DM, Gavali RS, Roa KR (2012) Evaluation of water quality with waterborne diseases for assessing pilgrimage impact along. Int J Environ Prot 2:8–14

McGowan W (2000) Water processing: residential, commercial, light-industrial, 3rd edn. Water Quality Association, Lisle, IL

Mishra N, Khare D, Gupta KK, Shukla R (2014) Impact of land use change on groundwater—A review. Adv Water Resour Protect 2:28–41

Mohsin M, Safdar S, Asghar F, Jamal F (2013) Assessment of drinking water quality and its impact on residents health in Bahawalpur city. Int J Humanit Soc Sci 3(15):114–128

Saravanan VS, Ayessa Idenal M, Saiyed S, Saxena D, Gerke S (2016) Urbanization and human health in urban India: institutional analysis of water-borne diseases in Ahmedabad. Health Policy Plan

Srinivas J, Purushotham AV, Murali Krishna KVSG (2013) Determination of water quality index in industrial areas of Kakinada, Andhra Pradesh, India. International Research Journal of Environment Sciences 2(5):37–45

Tyagi S, Sharma B, Singh P, Dobhal R (2013) Water quality assessment in terms of water quality index. Am J Water Res 3:34–38. https://doi.org/10.12691/ajwr-1-3-3

WHO (2011) Schistosomiasis (Bilharzia). https://www.who.int/health-topics/schistosomiasis#tab=tab_1. Accessed Jan 2020

WHO (2012) Guidelines for drinking-water quality, 4h edn. World Health Organization. ISBN 978 92 4 154815 1.

WHO (2009) Unsafe drinking water, sanitation and waste management United State EPA 816-F-09-004, May 2009. http://water.epa.gov/drink/contaminants/upload/mcl-2.pdf. Accessed 12 July 2013

Urban Planning in Perspective of UN Sustainable Development Goal-11 Using Geospatial Technology: A Case Study of Kolkata Megapolis (India)

Rajan Dev Gupta and Md. Omar Sarif

Abstract

United Nations adopted Sustainable Development Goal (SDG)-11 (sustainable cities and communities) to make cities and human settlements inclusive, safe, resilient, and sustainable. For achieving SDG-11 goals, geospatial technology is utilized to evolve a multifaceted approach in the present research to study long-term urban development trend, to model urban trajectories, to examine land surface temperature (LST) distribution, to study urbanization impact on thermal state along urban–rural directions and to carry out Urban Thermal Field Variance Index (UTFVI)-based ecological vulnerability analysis using Landsat 5 TM (1991) and Landsat 8 OLI/TIRS (2021) imageries in one of the Indian megapolis, Kolkata, during 1991–2021. Based on the supervised classification of multitemporal Landsat imageries, it is found that built-up land has expanded substantially by 32.87% leading to impervious development. The edge trajectory evolved the highest by 76.78% having adverse impact on agriculture, barren land, and food production. The infilling trajectory spread by 17.02% over the central urban sphere locations which resulted in the eradication of greenery, water bodies, and open spaces, thereby degrading the quality of life. The spatiotemporal analysis of LST dynamics found that mean LST increased from 19.76 °C in 1991 to 25.54 °C in 2021. The urban–rural gradient results show that 10–24 km buffer zones are intensified by more than 5.50 °C in each buffer zone. The ecological vulnerability analysis found that excellent ecological class declined by 9.51% affecting the landscape sustainability. The findings of this research can be suitably used for making effective policy for mitigating thermal intensification and environmental degradation along with eliminating the adverse impacts of edge and leapfrog settlements in Kolkata megapolis for sustainable urban planning so as to achieve SDG-11 goals by 2030. The geospatial technology based multi-faceted framework developed in the present research for achieving SDG-11 goals for Kolkata megapolis can also be adopted for other cities.

Keywords

Urbanization · Remote sensing · Urban trajectories · Land surface temperature · Ecological vulnerability · Kolkata megapolis · UN Sustainable Development Goal-11

R. D. Gupta (✉)
Civil Engineering Department and GIS Cell, Motilal Nehru National Institute of Technology Allahabad, Prayagraj 211004, India
e-mail: rdg@mnnit.ac.in

Md. Omar Sarif
Department of Geography, Lovely Professional University, Phagwara 144411, India

26.1 Introduction

Worldwide unprecedented transformations have been happening over the diverse sizes of the landscapes, particularly in city landscape. Populace of humans has been rising expeditiously in urban settings due to the attractions of better standard of living and economic viabilities which is transforming the city landscape at different scales from micro–macro-level (Xu et al. 2019). UN (2018) stated that 55% population of the globe has settled in the urban settings in 2018 and if the same trend continues, then 68% of global population will live in urban settings in 2050. Due to massive surge of urban population, impervious development in the form of built-up land has been spreading over all directions and this trend has been observed in almost all cities of the developing countries (Rimal et al. 2019; Tran et al. 2017). As a results, this massive urban expansion may result in loss of natural land, consumption of more energy and increase in the emission of greenhouse gas (Luo and Wu 2021).

Intergovernmental Panel on Climate Change (IPCC) (2019) reported that there has been an increase of 1.53 °C of mean land surface air temperature of the globe and 0.87 °C of mean surface (ocean and land) air temperature from pre-industrial period (1850–1900). IPCC (2021) in its AR6 report has reported 1.5 °C more global warming in next 20 years. We have also witnessed unprecedented changes in recent past which were extremely alarming and devastating in the form of glacier melting, mean sea level rising, uncertain precipitation, floods, droughts, damage of agriculture land and food shortage all around the globe.

United Nations (UN) in 2015 introduced 17 Sustainable Developments Goals (SDG) and SDG-11, in particular, lays special emphasis to make cities and human settlements inclusive, resilient, safe, and sustainable (Ravanelli et al. 2018). Sustainable Development Report of 2021 has shown that India's performance in SDG-11 is stagnating (Sachs et al. 2021). This report states that proportion of urban populace staying in slums is 35.2% in 2018 which is a decreasing target set by SDG. This report further states that India experienced annual mean concentration of $PM_{2.5}$ (particulate matter of less than 2.5 microns in diameter) as 90.6 $\mu g/m^3$ in 2019 which is a decreasing target as per SDG. Furthermore, access to improved water source to urban populace of India was 67.9% in 2017 which is also a decreasing target set by the SDG. Therefore, it is very evident that India's cities need immediate evaluation of their present development scenarios and long-term historical trends for preparing mitigation plans and initiating quick remedial actions against the said challenges.

Abastante et al. (2021) asserted that SDG-11's major indicators keywords and criteria of evaluation comprise: (1) green areas, (2) air quality (PM_{10} and NO_2), (3) temperature, (4) public transport, (5) exposure to flood risk, (6) moisture problems, and (7) structural problem. Bhatnagar et al. (2018) stated that urban population of India in 1960 was 18% that increased to 31% in 2011 and growth around cities is expected to accelerate in the future due to potential booming economy and social standards. As per Niti Aayog (2019), the State of West Bengal has scored only 34 in SDG-11 index of evaluation and it has been defined in aspirant category which means the cities of the state need high attentions as per SDG-11's driven suggestions for resilient and sustainable development.

In the perspective of SDG-11, it is prudent to adopt geospatial technology-based multifaceted approach combining urbanization, thermal adversity and ecological vulnerability for systemic assessment of the city landscape using long-term spatial transformation for efficient policy-making and urban planning. Remote sensing and Geographic Information System (GIS) are two modern technological tools which can be efficaciously utilized for this purpose. In this context, urban change dynamics have been carried out using spatiotemporal satellite datasets by the researchers (Sahana et al. 2018). Urban trajectories have been explicitly extracted for studying major threats and possible consequences on city's landscape and countryside in selected time points (Xu et al. 2007). Land

surface temperature (LST) computation has evolved as an essential approach for recognizing city's thermal state intensification and understanding the pattern of climate change (Sarif and Gupta 2019). Urban Thermal Field Variance Index (UTFVI) has been widely used to explore ecological vulnerability over the city's landscape because it spatially delineates the regions of major concerns through the scale from excellent to worst (Sarif and Gupta 2022).

Kolkata megapolis is selected as case study in the present research work due to its historical industrial and cultural heritage along with booming economy. Ghosh et al. (2018) carried out land use and land cover (LULC) dynamics along with LST distribution to depict urban heat island (UHI) scenario by incorporating different land indices to assess the biophysical properties composition over Kolkata metropolitan area during 1991–2017. However, different urban trajectories and ecological vulnerability vis-à-vis UTFVI have not been explored to assess how greenery and open space are being transformed adversely leading to ecological dysfunctions. Sharma et al. (2015) studied LULC effects on LST discourse only for Kolkata megacity but how LST has changed over landscape in urban–rural direction due to expanded urban setup was not studied.

For addressing the aforesaid research gaps, the present study is designed to monitor and mitigate severe effects on the climate by strengthening landscape transformation information for achieving the resilient and sustainable development in greater Kolkata megapolis using geospatial technological tools and techniques. In particular, objectives of the present research are: (1) to delineate the long-term urban development scenarios in multi-directions during 1991–2021, (2) to model urban trajectories and its adversity on thermal intensification, (3) to examine the state of LST distribution to analyze the change in the climate during last three decades, (4) to study urbanization impact on thermal state along urban–rural directions, and (5) to carry out ecological vulnerability analysis using UTFVI for assessment of urban environment state.

26.2   Materials and Methods

26.2.1   The Study Area

Kolkata megapolis, the study area, is the capital of West Bengal State. This covers an area of 1809.56 km^2 ranging from 22°20′52″ N to 22°46′52″ N latitude and 88°6′43″ E to 88°34′43″ E longitude (Fig. 26.1). The megapolis is one of the India's oldest industrial and cultural heritage and it is drained by Hooghly River over central portion as it flows from north direction to south-west direction (Sahana et al. 2018). Along both sides of this river, heterogeneous urban landscape has been evolved over the period of time. This megapolis is located ∼6.26 m above sea level (msl). The climate of Kolkata megapolis is tropical wet and dry type. The mean monthly temperature ranges 19–30 °C, whereas annual rainfall is 1640 mm (Sharma et al. 2015).

26.2.2   Data Used

The imageries of Landsat 5 Thematic Mapper (TM) of 1991 and Landsat 8 Operational Land Imager (OLI)/Thermal Infrared Scanner (TIRS) of 2021 are used which have spatial resolution of 30 m for both the sensors (Table 26.1). These Landsat datasets are acquired from web portal of United States of Geological Survey (USGS) (https://earthexplorer.usgs.gov/). The digital elevation data of Shuttle Radar Topography Mission (SRTM) is also acquired from same web portal of USGS.

26.2.3   Image Classification

The maximum likelihood classifier (MLC) is adopted for performing the LULC classification using supervised classification techniques to create built-up area development maps (Langat et al. 2019; Sarif and Gupta 2021a). After employing ground features as spectral signatures, LULC classification is performed (Kogo et al. 2019; Sarif and Gupta 2021b). For classification,
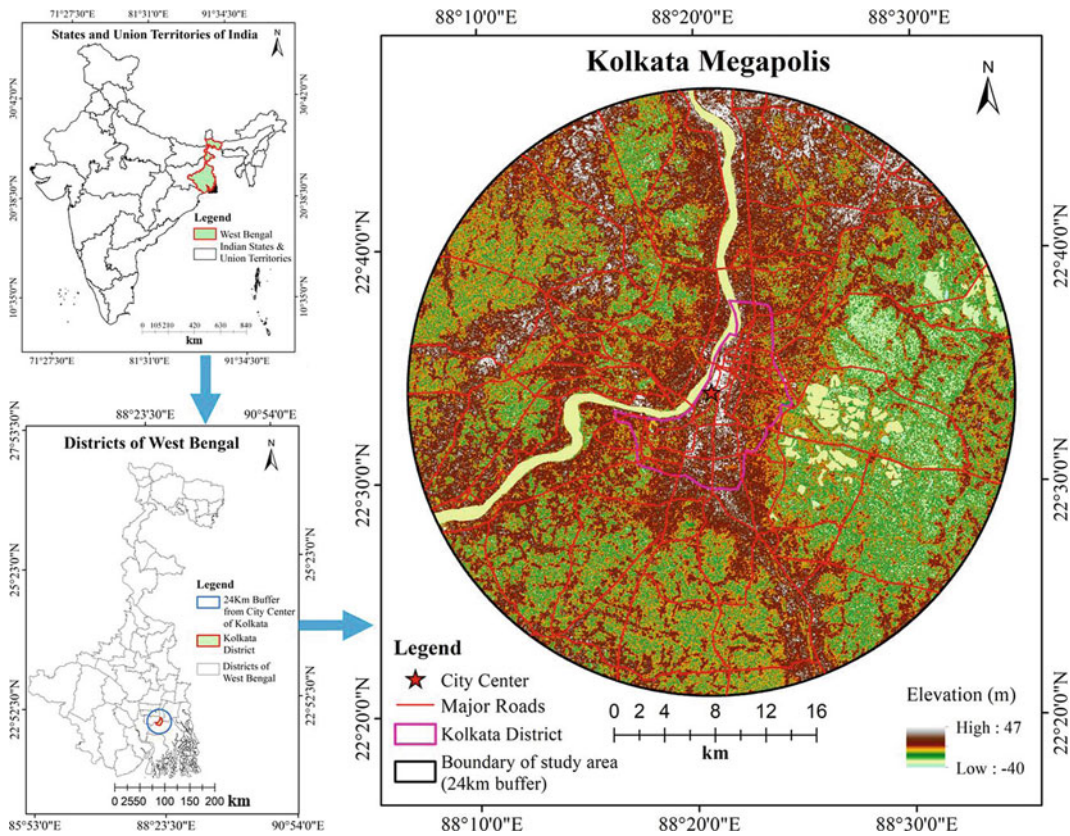
Fig. 26.1 Location map of Kolkata megapolis

Table 26.1 Data used

Satellite (sensor)	Path/Row	Acquisition date and time (GMT)	Spatial resolution (m)
Landsat 5 (TM)	138/44	06/03/1991 and 03:52:09	30
Landsat 8 (OLI/TIRS)	138/44	25/04/2021 and 04:30:36	30
SRTM	–	23/09/2014	30

we utilized band compositions of red band (band 3), near-infrared (IR) band (band 4), and short-wave IR (SWIR) band (band 5) for Landsat 5 TM of 1991 imagery which has been commonly adopted by researchers as standard form of selection of bands for Landsat 5 (TM) data. The band compositions of Coastal blue band (band 1), (Near-Infrared band (band 5), SWIR 1 band (band 6), SWIR 2 band (band 7), Cirrus band (band 9) (), Thermal IR 1 band (band 10), and Thermal IR 2 band (band 11) () for 2021 imagery of Landsat 8 (OLI/TIRS) is utilized to perform

LULC classification because it has the best band combination as it has produced best results (Liu and Zhang 2019). Anderson's LULC multi-level classification system is followed for delineating five distinct classes at level-I, viz. built-up land, agriculture land, forest land, water body, and barren land (Anderson et al. 1976). We used ERDAS IMAGINE 2014 software for carrying out this whole execution.

The accuracy assessment of LULC maps of 1991 and 2021 is carried out based on the spectral signatures selected for total 500 points

for both the images through random sampling method. Then, we carried out the validation based on authors' interpretation knowledge by using false color composite (FCC) for 1991 and the images of Google Earth for 2021. The classified maps are also validated with published work of Kolkata Metropolitan Area (KMA) (Sahana et al. 2018; Khan et al. 2019) where LULC map was produced of 1990, 2010, 2015, and 2016. The accuracy assessment is carried out by creation of confusion matrix for 1991 and 2021 for computation of overall accuracy, producer accuracy and user accuracy as well as kappa coefficient (Sarif and Gupta 2022).

26.2.4   Modeling of Urban Trajectories

Xu et al. (2007) modeled sprawl pattern index (SPI) to distinguish leapfrog trajectory, edge

trajectory, and infilling trajectory to highlight in depth urban discourse. This can distinguish between urban patches that are newly developed and pre-growth urban patches (Fig. 26.2a). We have identified newly developed patches between two time points, viz. 1991 and 2021. Figure 26.2b shows the sketch of adopted classification scheme. The SPI is calculated using Eq. 26.1.

$$S_p = \frac{L_p}{P} \qquad (26.1)$$

where S_p is SPI, L_p is the length of common boundary of new urban patches area and pre-growth existed urban patches area, P is perimeter of urban patches that are newly developed. The S_p value falls between 0 and 1.

We adopted categorized sprawl pattern index given by Xu et al. (2007) in their proposed three classes as follows:

Fig. 26.2 Urban trajectories: a Area of pre-growth patches and newly developed patches, b Sketches of urban trajectories. Source Sarif and Gupta (2021b)

Leapfrog trajectory: $S_p = 0$.
Edge trajectory: $0 < S_p < 0.5$
Infilling trajectory: $0.5 \leq S_p \leq 1$.

26.2.5 LST Retrieval

For LST computation, to achieve spectral radiance values, the raw thermal band values (Band 6 in Landsat TM and Band 10 in Landsat 8 OLI/TIRS) were converted using Eqs. 26.2 and 26.3, respectively (Xiong et al. 2012; Sultana and Satyanarayana 2020):

$$L_\varphi = \text{``gain''} \times \text{QCAL} + \text{``offset''} \quad (26.2)$$

where L_φ denotes spectral radiance [watts/(m^2 * sr * µm)] of top of atmosphere (TOA) "gain" denotes the rescaling factor on the basis of band specific information from the metadata, QCAL denotes quantized calibrated pixel digital number (DN) of the standard product, and "offset" denotes additive rescaling factor from the metadata of a specific band.

$$L_\varphi = \frac{L_{\max} - L_{\min}}{\text{QCAL}_{\max} - \text{QCAL}_{\min}} \times (QCAL - QCAL_{\min}) - L_{\min} \quad (26.3)$$

where $\text{QCAL}_{\min}$ denotes minimum DN and $\text{QCAL}_{\max}$ denotes maximum DN of the images; $L_{\min}$ and $L_{\max}$ denotes TIR band's spectral radiance at $\text{QCAL}_{\min}$ and $\text{QCAL}_{\max}$, respectively. These values can be obtained from metadata file of respective Landsat image.

The sensor's brightness temperature was then achieved using Eq. 26.4 (Ranagalage et al. 2018):

$$T_b = \left[\frac{K_2}{\ln\left(\frac{K_1}{L_\varphi} + 1\right)} \right] \quad (26.4)$$

where T_b denotes at sensor brightness temperature in Kelvin (K); and K_1 and K_2 are the values of the constants of thermal conversion provided in respective metadata file Landsat 6 and Landsat 8.

To calculate LST (°C), i.e. emissivity corrected images, Eq. 26.5 is used (Ranagalage et al. 2017).

$$\text{LST}(°C) = \left[\frac{T_b}{1 + (\lambda \times T_b/\rho)\ln(\varepsilon)} \right] - 273.15 \quad (26.5)$$

Where λ is emitted radiance wavelength (11.5 and 10.8 µm for Band 6 and Band 10, respectively); ρ is $h \times c/\sigma$ (i.e., 1.438×10^{-2} m K), σ represents Boltzmann constant (i.e., 1.38×10^{-23} J/K), h is Planck's constant (i.e., 6.626×10^{-34} J * s), c as velocity of light (i.e., 2.998×10^8 m/s), and ε denotes land surface emissivity (LSE) which is calculated utilizing normalized difference vegetation index (NDVI) using Eq. 26.6 (Sobrino et al. 2004).

$$\varepsilon = \{m\rho_v + n\} \quad (26.6)$$

where $m = (\varepsilon - \varepsilon) - (1 - \varepsilon\sigma) F\varepsilon_v$ and $n = \varepsilon_s + (1 - \varepsilon_s) F\varepsilon_v$, where ε_s and ε_v denote soil emissivity and vegetation emissivity, respectively. In the present work, the results from the study of Sobrino et al. (2004) are taken and we used $m = 0.004$ and $n = 0.986$.

ρ_v denotes proportion of vegetation and is calculated by NDVI using Eq. 26.7 (Zhang et al. 2009).

$$\text{NDVI} = \frac{\rho_{\text{NIR}} - \rho_{\text{Red}}}{\rho_{\text{NIR}} + \rho_{\text{Red}}} \quad (26.7)$$

where ρ_{NIR} represents Band 4 surface reflectance DN value in Landsat 5 TM and Band 5 DN value in Landsat 8 (OLI/TIRS); and ρ_{Red} represents DN values of Bands 3 in Landsat 5 TM and DN value of Band 4 in Landsat 8 (OLI/TIRS).

ρ_v is computed using Eq. 26.8:

$$\rho_v = (((\text{NDVI} - \text{NDVI}_{\min})/(\text{NDVI}_{\max} - \text{NDVI}_{\min})))^2 \quad (26.8)$$

where NDVI represents NDVI values calculated using Eq. 26.7, $\text{NDVI}_{\min}$ and $\text{NDVI}_{\max}$ denote minimum and maximum NDVI values from respective images.

26.2.6 Urban Thermal Field Variance Index (UTFVI)

In this research, UTFVI is used for quantifying the environment of the megapolis and for exploring UHI phenomena through the assessment of prevailing ecological status (Liu and Yuanzhi 2011; Luo and Wu 2021). This index provides the information on how the urbanization has affected the environment of the city and is computed using Eq. 26.9:

$$\text{UTFVI} = \left[\frac{T_s - T_{\text{mean}}}{T_{\text{mean}}}\right] \qquad (26.9)$$

where T_s denotes LST (°C) of a certain point and T_{mean} denotes mean LST of the study area. The threshold values of six defined UTFVI classes in the present work are given in Table 26.8.

26.3 Results

26.3.1 Built-Up Land Expansion and Its Trends

The expansion of built-up land is depicted through maps as shown in Fig. 26.3a. The overall built-up was observed 437.49 km^2 in 1991 which increased to 1032.28 km^2 in 2021 over the Kolkata megapolis and its surroundings. The development of multi-directional urban growth is found very high in northern direction. This is followed by west, east, and south while the least spread is observed in south-east direction during 1991–2021 (Fig. 26.3b and Table 26.2). This significant growth in built-up area has resulted in high urbanization which has affected environment of the suburban/rural areas adversely. Consequently, the temperature and air pollution of the megapolis got increased due to the depletion of forest land and arable land. During 1991–2021, the study area observed an overall growth of built-up area by 594.79 km^2 (32.87%) from non-built-up area.

26.3.2 Modeling of Urban Trajectories

The results show massive transformation in urban sprawl during 30 years from 1991–2021. The three-urban trajectory expansion map or classified sprawl is portrayed in Fig. 26.4 for the time period of 1991–2021, i.e., for 30 years duration. During this period, the megapolis got transformed significantly as reflected by three trajectories, i.e., leapfrog, edge, and infilling by 36.88 km^2 (6.20% of total sprawl), 456.69 km^2 (76.78% of total sprawl), and 101.22 km^2 (17.02% of total sprawl), respectively (Table 26.3). This means remarkable built-up development has been observed due to edge trajectory along the edges of the city, particularly, in north-east and south-west directions. This is followed by infilling which is found over the urban core areas or the inner city. This infilling development happened at the cost of greenery and open space. The leapfrog trajectory although has grown noteworthy; however, no giant sizes of patch are found in this class. In fact, the edge trajectory has resulted in massive growth along roadsides, especially in south-west directions.

26.3.3 Thermal State Intensification Induced by Urbanization

The spatiotemporal distribution of LST dynamics for Kolkata megapolis is shown in Fig. 26.5 for summer time points of 06th March 1991 and 25th April 2021 while their statistics are presented in Table 26.4. The overall mean LST witnessed was 19.76 °C in 1991 which increased to 25.54 °C in 2021. This means the overall mean LST has increased by high amount of 5.78 °C in last three decades leading to adverse environmental effects. In 1991, the foremost area of warm temperature was central city space and some patches over north-east direction while the

Fig. 26.3 Built-up area development during 1991–2021: **a** spatial distribution of built-up land; **b** direction-wise its growth (km^2)
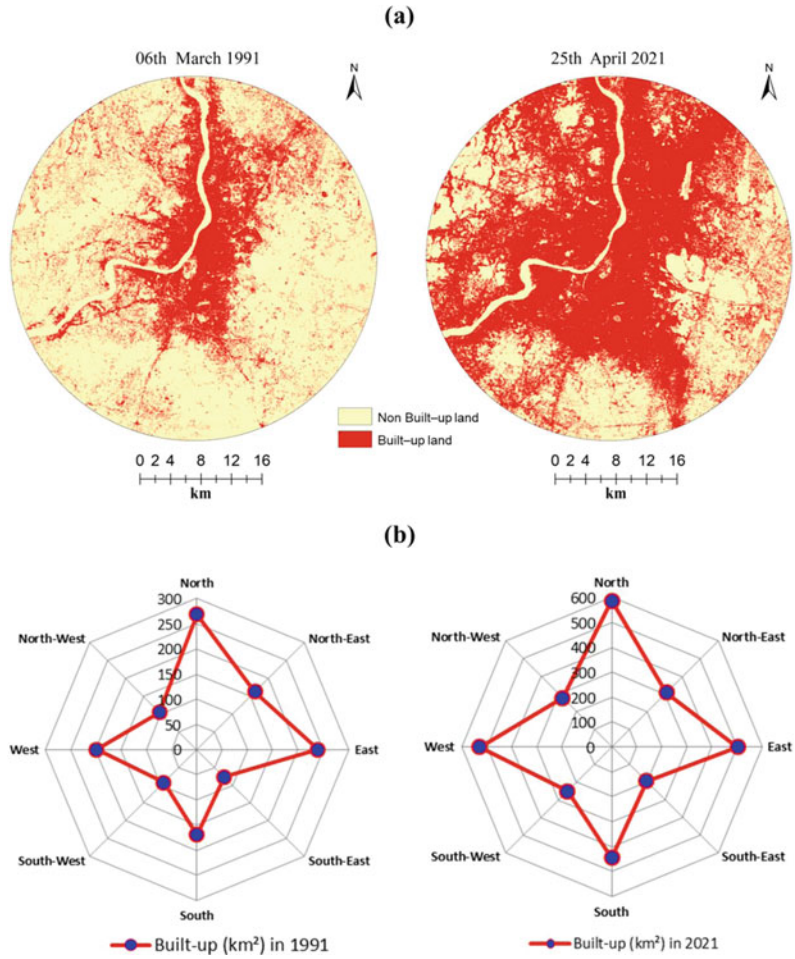
Table 26.2 Direction-wise growth of built-up area during 1991–2021

Direction-wise distribution	Built-up (1991)		Built-up (2021)		Change in built-up growth (1991–2021)	
	Area (km^2)	Area (%)	Area (km^2)	Area (%)	Area (km^2)	Area (%)
North	267.89	61.23	586.61	56.83	318.73	−4.41
South	169.61	38.77	445.68	43.17	276.07	4.41
East	239.61	54.77	503.19	48.75	263.58	−6.02
West	197.88	45.23	529.10	51.25	331.22	6.02
North-East	162.97	37.25	308.80	29.91	145.83	−7.34
South-East	76.64	17.52	194.39	18.83	117.75	1.31
North-West	104.92	23.98	277.81	26.91	172.89	2.93
South-West	92.96	21.25	251.29	24.34	158.32	3.09
	Total built-up area = 437.49 km^2		Total built-up area = 1032.28 km^2			

Fig. 26.4 Spatial growth of urban trajectories during 1991–2021
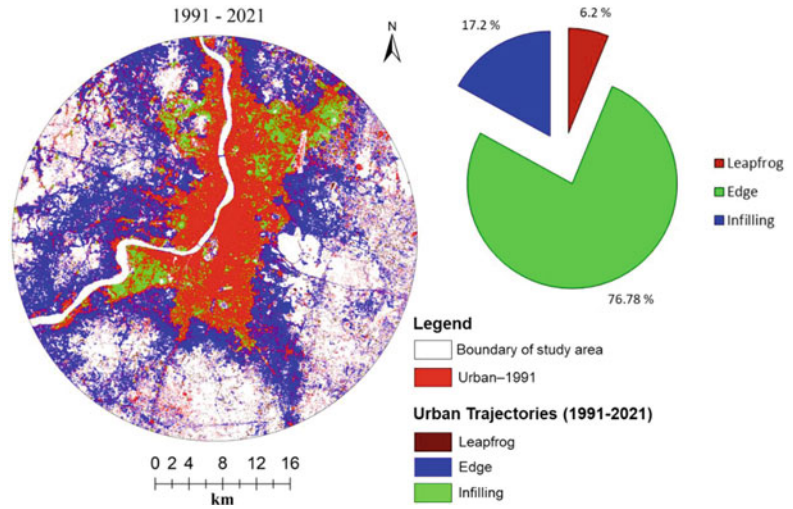
Table 26.3 Urban trajectories growth during 1991–2021

Urban trajectories	During 1991–2021	
	Area (km^2)	Area (%)
Leapfrog	36.88	6.20
Edge	456.69	76.78
Infilling	101.22	17.02

foremost area of cool temperature was over south direction. In 2021, the foremost area of warm temperature was central city, north-east and south-west, whereas the foremost area of cool temperature was south-east and up to 100 m on both the sides along Hooghly River.

The Kolkata megapolis was categorized into six zones based on LST from comfortable zone to extreme zone (Fig. 26.5). These six classes categorized based on LST for Kolkata megapolis are given in Table 26.5. The *comfortable class* has experienced severe loss of 1035.32 km^2 (57.21%) of areal coverage during 1991–2021 while the *low class* has witnessed loss of 449.28 km^2 (24.83%). The *moderate class* has found insignificant growth of 5.13 (0.28%) during 1991–2021. The *high class* has shown high growth of 736.18 (40.68%) during the same period. The *very high class* is increased by 611.45 km^2 (33.79%) while the *extreme class* has surged by 131.85 km^2 (7.29%) of areal coverage during 1991–2021. These results are indicating that thermal state of Kolkata megapolis has been severely intensified, and it has affected nearly three-fourth of the area.

The magnitude of built-up area along the mean LST distribution pattern based on multiple ring profiling was extracted at an interval of 1 km from the center of the city to rural/suburban periphery at different time point, i.e., 1991 and 2021 (Table 26.6 and Fig. 26.6). The percentage of built-up area in each buffer zone has been found significantly increasing in the range of 3.48% – 48.39%. It has been found that each zone between said time points witnessed higher temperature in comparison with its preceding time point ranging from 4.61 to 6.15 °C. This means that substantial amount of temperature intensification has been experienced at each distinct buffer zone from city center to rural/suburban periphery (Fig. 26.6). The urban–rural gradient results show that 10–24 km buffer zones were adversely intensified by more than 5.50 °C in each buffer zone due to growth of built-up land by nearly 30% in each zone. This shows that higher percentage of built-up land has strongly

Fig. 26.5 Spatial growth of LST during 1991–2021

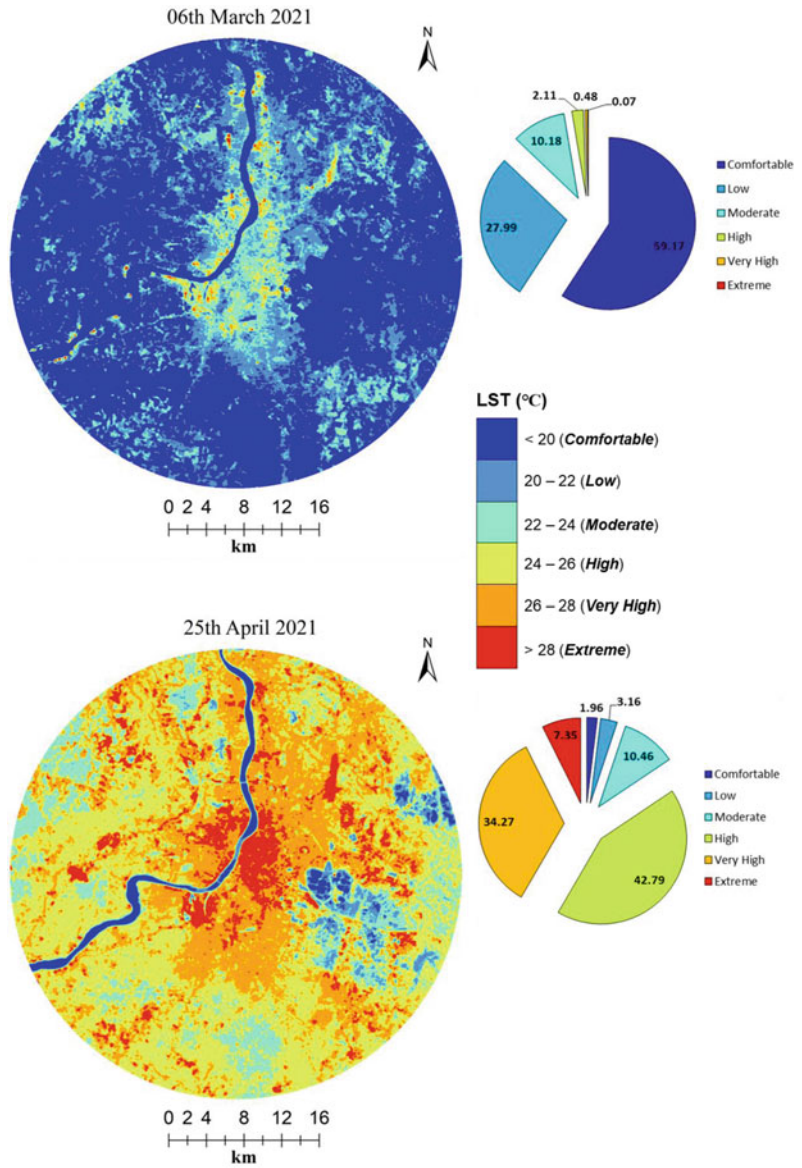**Table 26.4** Details of LST

| Date	Minimum (°C)	Maximum (°C)	Mean (°C)	Standard deviation	Overall mean LST change (°C) (1991–2021)
06th March 1991	16.00	33.61	19.76	1.95	5.78
25th April 2021	19.21	33.69	25.54	1.88	

Table 26.5 Growth of LST classes between 1991 and 2021

LST class	06th March 1991		25th April 2021		Mean LST change of LST classes (1991–2021)
	Area (km^2)	Area (%)	Area (km^2)	Area (%)	Area (%)
<20 (Comfortable)	1070.74	59.17	35.42	1.96	−57.21
20–22 (Low)	506.55	27.99	57.27	3.16	−24.83
22–24 (Moderate)	184.21	10.18	189.34	10.46	0.28
24–26 (High)	38.23	2.11	774.40	42.79	40.68
26–28 (Very High)	8.61	0.48	620.06	34.27	33.79
>28 (Extreme)	1.22	0.07	133.07	7.35	7.29

Table 26.6 Percentage of built-up area and Mean LST along urban–rural direction

Buffer zones	Mean LST (1991)	Mean LST (2021)	Mean LST change (1991–2021)	Built-up (%) in 1991	Built-up (%) in 2021	Built-up (%) change (1991–2021)
1	21.48	26.42	4.95	56.07	68.22	12.15
2	22.09	26.70	4.61	68.34	75.01	6.68
3	22.49	27.31	4.82	82.83	86.67	3.84
4	22.58	27.45	4.88	85.34	91.61	6.27
5	22.42	27.37	4.95	79.70	90.35	10.65
6	22.01	27.19	5.18	70.77	86.06	15.29
7	21.65	27.06	5.41	64.03	88.47	24.44
8	20.84	26.29	5.45	51.91	84.49	32.58
9	20.34	25.99	5.65	45.36	82.75	37.39
10	20.12	25.79	5.68	39.52	82.09	42.57
11	19.88	25.42	5.54	32.84	77.80	44.96
12	19.61	25.18	5.57	28.42	73.39	44.97
13	19.53	25.44	5.91	23.94	72.34	48.39
14	19.60	25.65	6.05	19.72	61.61	41.89
15	19.39	25.54	6.15	18.35	59.01	40.66
16	19.33	25.33	6.00	18.12	55.26	37.14
17	19.45	25.46	6.02	17.71	49.77	32.05
18	19.44	25.50	6.06	17.21	47.17	29.96
19	19.51	25.36	5.85	15.74	44.18	28.44
20	19.42	25.27	5.85	12.76	42.83	30.07
21	19.51	25.26	5.74	13.07	42.30	29.24
22	19.37	25.15	5.78	12.50	42.90	30.41
23	19.28	25.19	5.91	12.74	43.48	30.74
24	19.31	25.11	5.80	11.55	42.46	30.90

Fig. 26.6 Growth of urban development along LST from urban to rural/suburban periphery during 1991–2021: **a** 06th March 1991; **b** 25th April 2021
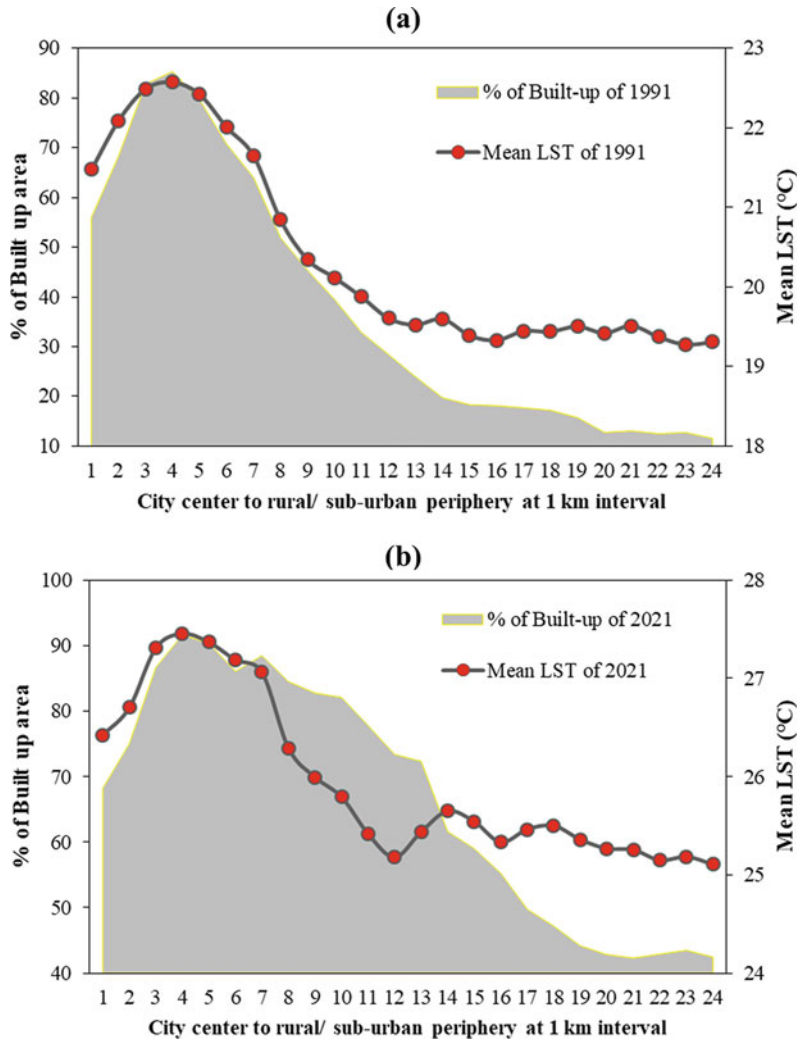
supported the intensification of LST distribution in Kolkata megapolis.

The urban trajectories have also played significant role in intensification of LST during 1991–2021 (Fig. 26.7 and Table 26.7). The mean LST in three urban trajectories, i.e., leapfrog, edge, and infilling is found to be 32.35 °C, 33.15 °C, and 33.94 °C, respectively. This means infilling trajectory that is found over the inner city or urban core areas has the highest LST observation. This is due to the high-density growth of concrete structures that is devoid of high-density greenery and significant size water bodies. The edge trajectory has seen massive
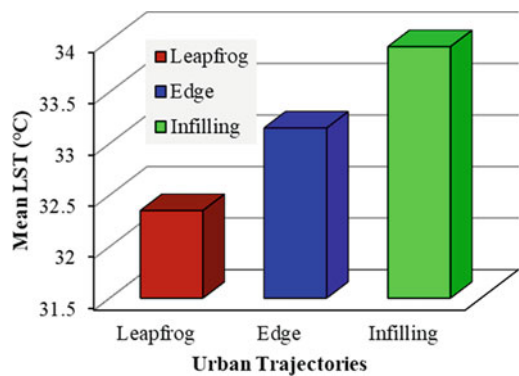

Fig. 26.7 Urban trajectories effects on LST intensification during 1991–2021

Table 26.7 Mean LST in different urban trajectories (1991–2021)

Urban trajectories	Area (km^2)	Mean LST (°C)
Leapfrog	36.88	32.35
Edge	456.69	33.15
Infilling	101.22	33.94

growth along roadsides especially in south-west direction which is second strong observing trajectory as it is lacking in significant amount of green space. The leapfrog has been found far distant from edge and over the rural settings which have substantial presence of trees and ponds that help this trajectory to keep itself the coolest.

26.3.4 Ecological Vulnerability Growth

UTFVI dynamics provides spatial state of UHI with ecological environmental viability for urban environment for sustainable development. Ecological vulnerability analysis in Kolkata megapolis is carried out using UTFVI in summer season during 1991 and 2021. The Kolkata megapolis is delineated into six ecological classes, namely excellent class, good class, normal class, bad class, worse class and worst class. The different ecological classes of UTFVI have their own importance to showcase different ecological states of the landscape, viz. excellent class (< 0) defines no urban heat island (UHI) effects, good class (0–0.005) defines weak UHI effects, normal class (0.005–0.010) defines middle UHI effects, bad class (0.010–0.015) defines strong UHI effects, worse class (0.015–0.020) defines stronger UHI effects, worst class (>0.020) defines strongest UHI effects (Sarif and Gupta 2022). The spatiotemporal UTFVI dynamics of Kolkata megapolis are presented in Fig. 26.8 for summer time points of 06th March 1991 and 25th April 2021 while their statistics are shown in Table 26.8.

Accordingly, the ecological evaluation index is categorically classified into six classes to study the real ecological state. The excellent class has found severe loss of 172 km^2 (9.51%) of areal

coverage during 1991–2021. This means the best space for living is deteriorated, and this is the biggest loss to both humans and animals. The *good class* has observed marginal gain of 32.09 km^2 (1.77%) of areal coverage during 1991–2021. The *normal class* has experienced insignificant growth of 33.47 km^2 (1.85%) during 1991–2021. The *bad class* has shown high increment of 36.29 km^2 (2.01%) during 1991–2021. The *worse class* also has adversely increased by 35.21 km^2 (1.95%) during 1991–2021. The *worst class* has also surged of 34.94 km^2 (1.93%) of areal coverage during 1991–2021. Thus, it can be observed that three deteriorating classes, viz. bad, worse, and worst together have nearly spread by 6% of the landscape. Further, best liveable classes have decreased significantly by nearly 9.50% which is a matter of high concern keeping in mind the SDG-11 goals along with the increase in deteriorating ecological classes as this will have adverse UHI effect on both living organism and animal.

26.4 Discussion

26.4.1 Urbanization: A Perspective of SDG-11

The main context of SDG-11 is making cities sustainable and mostly focused on how vulnerable land covers of city landscape are and how these are transforming and by what land use. To cater this challenge, a multifaceted approach is proposed in this research for depicting possible real landscape scenario through the use of urban trajectories. The multi-directional urban development has found that northern direction has evolved the highest, and the least development is over south-eastern.

Fig. 26.8 Spatial growth of ecological state during 1991–2021
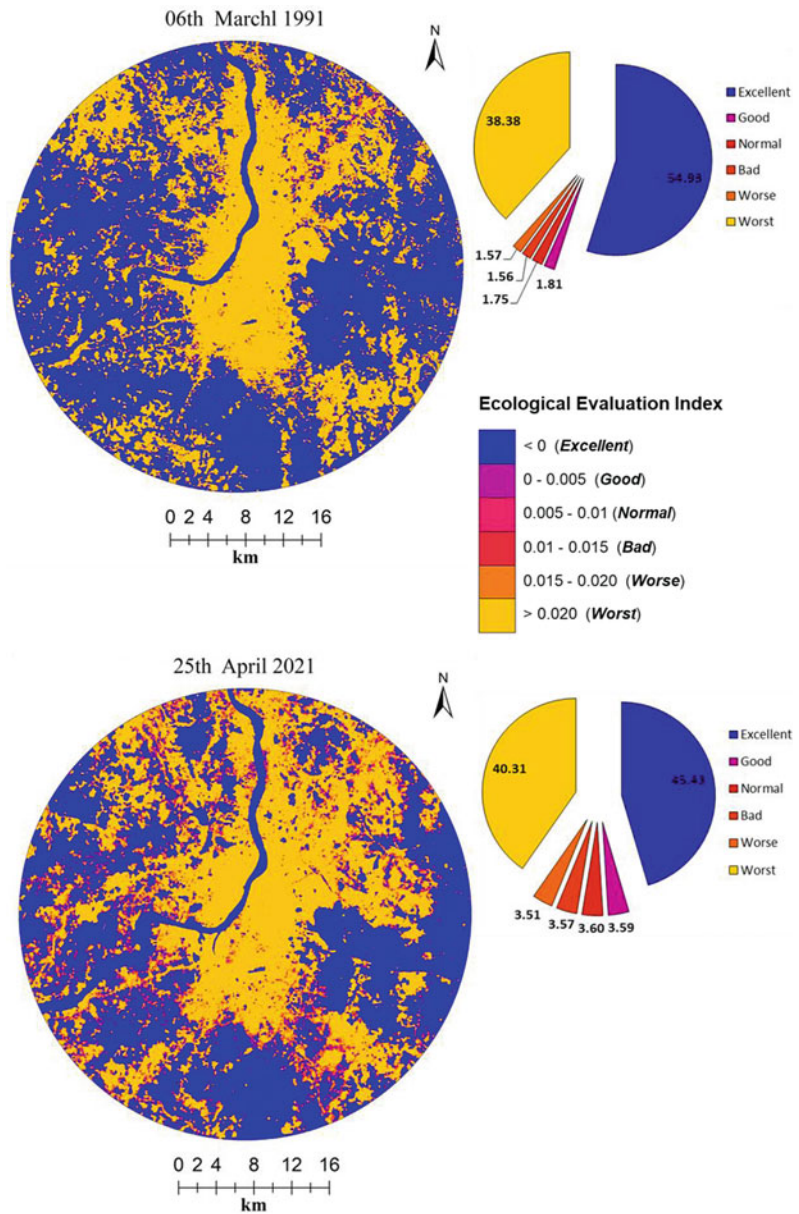
Based on the results of urban trajectories, it is found that edge and infilling trajectories are the two most accountable built-up expansions that have adversely affected the landscape. The edge trajectory has played extreme role in the decrease of agriculture land on the periphery and along the road. The food production is dependent on agriculture land, and hence increase in edge trajectory will result in reduction of food production and thereby may result in food shortage in long run. The infilling trajectory results are mostly responsible in reduction of greenery and water bodies of varying sizes leading to elimination of open spaces over the urban central sphere. The

Table 26.8 Spatial ecological growth during 1991–2021

UTFVI	UHI phenomenon	Ecological evaluation	1991		2021		Spatial areal change (%) (1991–2021)
			Area (km^2)	Area (%)	Area (km^2)	Area (%)	
<0	None	Excellent	994.06	54.93	822.06	45.43	–9.51
0–0.005	Weak	Good	32.81	1.81	64.90	3.59	1.77
0.005–0.010	Middle	Normal	31.61	1.75	65.08	3.60	1.85
0.010–0.015	Strong	Bad	28.25	1.56	64.54	3.57	2.01
0.015–0.020	Stronger	Worse	28.33	1.57	63.54	3.51	1.95
>0.020	Strongest	Worst	694.50	38.38	729.44	40.31	1.93

reduction in open spaces may also lead to the shortage of land bank for futuristic developments. All these will adversely impact the climatic and will lead to formation of UHI, disturbance in precipitation cycle and increase in air pollution due to high-density impervious development for residential and commercial purposes along with the development of health care, educational, and other infrastructural facilities.

Based on our findings, the monitoring of direction-wise urban development and urban trajectories for restoring and enhancing the urban landscape is proposed. The direction-wise urban development can help in knowing the trend of urban spread directions from the city center for addressing the adverse transformations that are occurring. The leapfrog trajectory can aid in the delineation of growth of built-up land in the megapolis at the cost of agriculture land as it mostly occurs over abandoned agriculture land. The edge trajectory is mostly spread over the edge of the city areas and along spaces adjacent to highway network and hence can help in measuring existing built-up setup, in particular, in the peripheral area of the megapolis. The infilling trajectory can assist in delineating the critical land parcels that are declining in urban core region due to transformation in other land use types. Thus, for achieving SDG-11 goals, all these findings can be taken into consideration for making timely and informed decisions for preservation of precise land resources for enhancing the carrying capacity of the landscape as well as for environmental sustainability.

26.4.2 Kolkata Megapolis Planning Vis-A-Vis Environmental Viability

As per IPCC (2021) AR6 report, an extreme transformation of landscape has been going on at local to global level, especially after post-industrial era, which needs to be monitored and mitigated so as to control the rise in global mean temperature leading to decrease in adverse consequences of climate change. This work has assessed long-term spatial state over Kolkata megapolis from 1991 to 2021. The effects of urban trajectories, viz. leapfrog, edge and infilling on the thermal state are assessed to inspect how different sprawl types/urban trajectories are influencing intensifying and/or cooling the LST over the city landscape. The multiple ring profiling of built-up land including mean LST to examine where, how, and what magnitude of LST is changing due to built-up area is also carried out. The findings indicate that more than 50% of built-up land has immense role in intensifying thermal state. This study will help planners and administrators in enriching carrying capacities of the landscape of Kolkata megapolis in accordance with SDG-11 city goals.

Furthermore, to minimize the adverse effects of UHI, thermal evaluation using UTFVI is carried out for addressing the number of issues such as water scarcity, air pollution, and health problems. The ecological evaluation results show that urban settings have the highest vulnerability while water bodies/ponds/river, and even forest land have the excellent comfortability along their

surroundings. Addition to it, the adverse role of infilling and edge trajectories in thermal state intensification is also found. Scientists are encouraging different mitigation strategies like creation of green cool roofs, plantation of trees on the streets, and usage of light materials and paints (Chen and You 2019). Furthermore, distinctive alleviation approaches, viz. preserving and restoring small to large size water bodies, wetlands, greeneries, plantation on open/ barren space can highly restore the local ecosystem and climate of the megapolis. The long-term spatiotemporal geospatial database can be a powerful tool for the planners to analyze the transformations of the ground based on historical development and its trends for preparing suitable strategies for environmental sustainability.

26.5 Conclusions

In the present research, geospatial technology is efficaciously used for studying long-term three decadal urbanization trends and intensity along with thermal state analysis and ecological dynamics using Landsat 5 TM and Landsat 8 OLI/TIRS imageries for Kolkata megapolis of India during 1991–2021. The spatiotemporal urbanization with directional growth of urban development over the megapolis landscape is examined including LST intensification and ecological assessment. It is observed that built-up land has grown substantially by 594.79 km^2 (32.87%) which expanded from 437.49 km^2 (24.18%) in 1991 to 1032.28 km^2 (57.05%) in 2021. The direction-wise urban development results found that spread in northern direction is the highest by 318.73 km^2 and in south-eastern direction the lowest by 117.75 km^2.

Based on the analysis of urban trajectories, it is observed that edge trajectory evolved the most by 456.69 km^2 (76.78%) on the periphery of the city boundary and along roadway networks resulting in reduction of agriculture land which has severe adverse impact on food production and security. The infilling trajectory spread by 101.22 km^2 (17.02%) which mainly eradicated greenery, water bodies, and open spaces over the

central urban areas harming the environmental sustainability. Further, infilling trajectory has shown the highest mean LST as it is primarily concentrated in concrete spaces over the central urban space while leapfrog has shown the lowest mean LST as it is mainly found in rural setup.

The findings of distinctive mean LST classes show that comfortable class severely declined by 57.21%, whereas high class, very high class, and extreme class surged by 40.68%, 33.79%, and 7.29%, respectively. The results of urban–rural gradient analysis based on multiple ring buffers show that percentage of built-up land has swiftly grown in the range 3.48–48.39% which intensely surged the mean LST by 4.61–6.15 °C. The results demonstrate that more than 50% of built-up land has adverse impact on the thermal state and the quality of human lives which is in contradiction with the goals of SDG-11.

The results of ecological vulnerability analysis revealed that excellent ecological class severely declined by 9.51% leading to adverse impact on the landscape sustainability. At the same time, the three ecological classes having most deteriorating effect on the urban environment, viz. bad class, worse class, and worst class together have surged by about 6%. These findings indicate toward ecosystem dysfunction and biodiversity damages in megapolis landscape including LST intensification, UHI formation, and enhanced health problems. Therefore, it is recommended that long-term spatiotemporal multifaceted approach of change dynamics, urban trajectories, thermal state analysis along with ecological assessment evolved in the present research can be adopted by planners for preparation of mitigation strategies so that SDG-11 goals for Kolkata megapolis can be achieved. Further, the multi-faceted framework developed in the present research for achieving SDG-11 goals for Kolkata megapolis using geospatial technology can also be adopted for other cities.

The present study has been carried out for 30 years duration from 1991 to 2021 to understand the urban dynamics including its thermal state and ecological vulnerability. It will be interesting to add more temporal coverages at an

interval of 05 years during this 30 years period based on the availability of cloud-free imageries of Landsat and/or other remote sensing satellites in the future studies.

References

Abastante F, Lami IM, Gaballo M (2021) Pursuing the SDG11 targets: the role of the sustainability protocols. Sustain 13:1–19. https://doi.org/10.3390/su13073858

Anderson JR, Hardy EE, Roach JT, Witmer RE (1976) A land use and land cover classification system for use with remote sensor data. In: A revision of the land use classification system as presented in U.S. Geological Survey Circular 671, Washington

Bhatnagar A, Nanda TP, Singh S, Upadhyay K, Sawhney A, Swamy DTVRR (2018) Analysing the role of India's smart cities mission in achieving sustainable development Goal 11 and the new urban agenda. In: Leal Filho W, Rogers J, Iyer-Raniga U (eds) World sustainability series, pp 275–292. https://doi.org/10.1007/978-3-319-73293-0_16

Chen R, You X (2019) Reduction of urban heat island and associated greenhouse gas emissions. In: Mitigation and adaptation strategies for global change, pp 1–23

Ghosh S, Chatterjee ND, Dinda S (2018) Relation between urban biophysical composition and dynamics of land surface temperature in the Kolkata metropolitan area : a GIS and statistical based analysis for sustainable planning. Model Earth Syst Environ https://doi.org/10.1007/s40808-018-0535-9

IPCC (2019) Climate Change and Land. An IPCC Special Report on climate change, desertification, land degradation, sustainable land management, food security, and greenhouse gas fluxes in terrestrial ecosystems. Summary for Policymakers. https://doi.org/10.4337/9781784710644

IPCC (2021) Climate Change 2021: the physical science basis. Available at https://www.ipcc.ch/report/sixth-assessment-report-working-group-i/

Khan A, Chatterjee S, Akbari H, Bhatti SS, Dinda A, Mitra C et al (2019) Step-wise land-class elimination approach for extracting mixed-type built-up areas of Kolkata megacity. Geocarto Int 34:504–527. https://doi.org/10.1080/10106049.2017.1408704

Kogo BK, Kumar L, Koech R (2019) Analysis of spatio-temporal dynamics of land use and cover changes in Western Kenya. Geocarto Int 1–16. https://doi.org/10.1080/10106049.2019.1608594

Langat PK, Kumar L, Koech R, Ghosh MK (2019) Monitoring of land use/land-cover dynamics using remote sensing: a case of Tana River Basin, Kenya. Geocarto Int 1–20. https://doi.org/10.1080/10106049.2019.1655798

Liu H, Zhang Y (2019) Selection of Landsat8 image classification bands based on MLC–RFE. J Ind Soc

Remote Sens 47:439–446. https://doi.org/10.1007/s12524-018-0932-6

Liu L, Yuanzhi Z (2011) Urban heat island analysis using the Landsat TM data and ASTER data: a case study in Hong Kong. Remote Sens 3:1535–1552. https://doi.org/10.3390/rs3071535

Luo H, Wu J (2021) Effects of urban growth on the land surface temperature: a case study in Taiyuan, China. Environ Dev Sustain 23:10787–10813. https://doi.org/10.1007/s10668-020-01087-0

Niti Aayog (2019) SDG INDIA (index and dashboard 2019–20). Available at https://niti.gov.in/sites/default/files/2019-12/SDG-India-Index-2.0_27-Dec.pdf

Ranagalage M, Estoque RC, Murayama Y (2017) An urban heat island study of the Colombo metropolitan area, Sri Lanka, based on Landsat data (1997–2017). ISPRS Int J Geo-Inf 6:189. https://doi.org/10.3390/ijgi6070189

Ranagalage M, Estoque RC, Handayani HH, Zhang X, Morimoto T, Tadono T et al (2018) Relation between urban volume and land surface temperature: a comparative study of planned and traditional cities in Japan. Sustain 10:1–17. https://doi.org/10.3390/su10072366

Ravanelli R, Nascetti A, Cirigliano RV, Di Rico C, Leuzzi G, Monti P et al (2018) Monitoring the impact of land cover change on surface urban heat island through Google Earth Engine: proposal of a global methodology first applications and problems. Remote Sens 10:1–21. https://doi.org/10.3390/rs10091488

Rimal B, Keshtkar H, Sharma R, Stork N, Rijal S, Kunwar R (2019) Simulating urban expansion in a rapidly changing landscape in eastern Tarai, Nepal. Environ Monit Assess 191:1–14. https://doi.org/10.1007/s10661-019-7389-0

Sachs J, Kroll C, Lafortune G, Fuller G, Woelm F (2021) Sustainable Development report 2021. Cambridge. https://doi.org/10.1017/9781009106559

Sahana M, Hong H, Sajjad H (2018) Analyzing urban spatial patterns and trend of urban growth using urban sprawl matrix: a study on Kolkata urban agglomeration, India. Sci Total Environ 628–629:1557–1566. https://doi.org/10.1016/j.scitotenv.2018.02.170

Sarif MO, Gupta RD (2019) Land surface temperature profiling and its relationships with land indices: a case study on Lucknow City. In: ISPRS annals of photogrammetry, remote sensing and spatial information sciences. Copernicus Publications, Dhulikhel, Nepal LAND, pp 89–96. https://doi.org/10.5194/isprs-annals-IV-5-W2-89-2019

Sarif MO, Gupta RD (2021a) Comparative evaluation between Shannon's entropy and spatial metrics in exploring the spatiotemporal dynamics of urban morphology: a case study of Prayagraj City, India (1988–2018). Spat Inf Res 29:961–979. https://doi.org/10.1007/s41324-021-00406-5

Sarif MO, Gupta RD (2021b) Modelling of trajectories in urban sprawl types and their dynamics (1988–2018): a case study of Prayagraj City (India). Arab J Geosci 14:1–21. https://doi.org/10.1007/s12517-021-07573-7

Sarif MO, Gupta RD (2022) Spatiotemporal mapping of land use/land cover dynamics using remote sensing and GIS approach: a case study of Prayagraj City, India (1988–2018). Environ Dev Sustain 24:888–920. https://doi.org/10.1007/s10668-021-01475-0

Sharma R, Chakraborty A, Joshi PK (2015) Geospatial quantification and analysis of environmental changes in urbanizing city of Kolkata (India). Environ Monit Assess 187:1–12. https://doi.org/10.1007/s10661-014-4206-7

Sobrino JA, Jiménez-Muñoz JC, Paolini L (2004) Land surface temperature retrieval from LANDSAT TM 5. Remote Sens Environ 90:434–440. https://doi.org/10.1016/j.rse.2004.02.003

Sultana S, Satyanarayana ANV (2020) Assessment of urbanisation and urban heat island intensities using Landsat imageries during 2000–2018 over a sub-tropical Indian City. Sustain Cities Soc 52:1–14. https://doi.org/10.1016/j.scs.2019.101846

Tran DX, Pla F, Latorre-Carmona P, Myint SW, Caetano M, Kieu HV (2017) Characterizing the relationship between land use land cover change and land surface temperature. ISPRS J Photogramm Remote Sens 124:119–132. https://doi.org/10.1016/j.isprsjprs.2017.01.001

UN (2018) The World's cities in 2018. Departmentof Economic and Social Affairs, Population Division (2018). The World's cities in 2018—Data booklet (ST/ESA/ SER.A/417). UN, pp 1–34

Xiong Y, Huang S, Chen F, Ye F, Ye H, Wang C, et al. (2012) The Impacts of Rapid Urbanization on the Thermal Environment: A Remote Sensing Study of Guangzhou, South China. Remote Sens. 4, 2033–2056. https://doi.org/10.3390/rs4072033

Xu C, Liu M, Zhang C, An S, Yu W, Chen JM (2007) The spatiotemporal dynamics of rapid urban growth in the Nanjing metropolitan region of China. Landsc Ecol 22:925–937. https://doi.org/10.1007/s10980-007-9079-5

Xu G, Jiao L, Liu J, Shi Z, Zeng C, Liu Y (2019) Understanding urban expansion combining macro patterns and micro dynamics in three Southeast Asian megacities. Sci Total Environ 660:375–383. https://doi.org/10.1016/j.scitotenv.2019.01.039

Zhang Y, Odeh IOA, Han C (2009) Bi-temporal characterization of land surface temperature in relation to impervious surface area, NDVI and NDBI, using a sub-pixel image analysis. Int J Appl Earth Obs Geoinf 11:256–264. https://doi.org/10.1016/j.jag.2009.03.001

An Introduction to Big Data and Its Possible Utility in the Urban Context

27

Sundus Samreen Wani, Salman Amin, and Qamar Irshad

Abstract

The present-day cities are growing exponentially with urbanization and so is the population. Cities are a house to a major share of the population. With this ever-increasing population, cities come across many problems which cannot easily be anticipated. This is because, the phenomena which take place in a city are complex, interlinked, intertwined and form the city systems. In order to facilitate the solutions to the complex problems, complex data handling is required. In this digital age, big data has helped in expediting the solutions to those problems and has proven to be a boon for the complex city systems by making it easy to understand them. Big data has been put to use in various sectors in a city system; from mapping assets, solving various sectoral problems, streamlining governance and administrative issues and reducing the communication gap between stakeholders in a city. This paper aims at giving an insight about big data, and how it can be beneficial and advantageous for the city. Some successful case studies where big data has been put to application in cities have also been incorporated into the paper.

27.1 Introduction to Big Data

ORACLE or Oak Ridge Automatic Computer and logical engine defines big data as the data that contains greater variety, arriving in increasing volumes and with more velocity. Big data are massive, complex, structured and unstructured data sets that are rapidly generated and transmitted from a wide variety of sources (Oracle 2022). It has its own characteristics, and there are parameters on the basis of which it is classified. It has its own merits and utilities. It is huge in volume, and it keeps on growing exponentially. Owing to its large, increasing size, complexity associated with it increases with time. From collection to processing to storing, the complexity remains (Taylor 2022).

One of the first examples of handling a large amount of data in modern human history could date back to the late 1800s (Kofa Study 2022; Krettek 2022; Marr 2015). This was a case of the United States census of 1890 where the estimated time to carry it out manually was estimated to be

S. S. Wani
Department of Physical Planning, School of Planning and Architecture, New Delhi, India

S. Amin · Q. Irshad (✉)
Department of Architecture, Faculty of Architecture & Ekistics, Jamia Millia Islamia, New Delhi, India
e-mail: qirshad@jmi.ac.in

Table 27.1 Increase in world population (in billion persons)

Year	1	1000	1500	1650	1750	1804	1850	1900	1930
Population	0.2	0.275	0.45	0.5	0.7	**1**	1.2	1.6	**2**
Year	1950	1960	1974	1980	1987	1999	2011	2020	2023
Population	2.55	**3**	**4**	4.5	**5**	**6**	**7**	7.8	**8**

1–1804 (1803 years): 0.2 to 1 billion
1804–2011 (207 years): from 1 to 7 billion
Source Worldometers.info (2022)

13 years (CrashCourse 2017). This was a predicament for the Census Bureau as the US census takes place every 10 years (United States Census Bureau 2022). The census of 1880 itself, with a resident US population of about 50 million, had taken about 7 years to compile and was published in 1888 (United States Census Bureau 2021; Anderson 2015). By the time it was completed, it had already become outdated. So, to solve this problem, the bureau had to come up with something that could handle such a large volume of data in a considerably short period of time (CrashCourse 2017).

Automation or automatic tabulation and sorting could have presented a solution. A competition was held to select a design of a machine that could best do the required job. Herman Hollerith won the competition of the US census with his tabulating machine or tabulator and sorter for its ability to count combined facts (Columbia University 2001). It used punch cards to store information of the population, and an electromechanical setup was built in the machine to read and compile the data (IBM 2022a, b). The resultant of the above was a saving of 5 million USD of 1890s taxpayers' money and compilation of the data in record time (estimates vary from 6 weeks to 3 years) (Columbia University 2001).

The US census of 1890 was a glimpse into what big data could look like, and what may be required to process it. From that time period, human civilization has only grown and grown in exponential terms. One can find examples of such growth wherever they look. The global population had taken more than 125 years to reach 2 billion in 1930 from 1 billion in 1804. The next billion was reached in 1960 after 30 years, and the next after that took only 14 years. In 1974 there were 4 billion people on the planet. So, the time period of doubling the population on the planet became 44 years from the earlier 125 years, which was a reduction, of about 80 years. In 2023, the world population is forecasted to be 8 billion as can be seen in Table 27.1. The time period of doubling may have increased to 49 years, but, where adding 1 billion people had taken 125 years, now in less than half that time, four times as many people are being added to our planet (Worldometers.info 2022). And every person comes with their own data package and information that needs to be recorded, saved and processed.

A very interesting point to note here is that the population has increased at this rate, despite the fact that the fertility rates have gone down (Roser 2014). So, the fertility rates paint a contrasting picture, and just by looking at them alone could lead one to draw a conclusion which is far from the reality. Similarly, the data increase could have pushed us to a shortage of storage, but as the amount of data increased, the capacity of our machines and computers to store it, has also gone up. On top of that, the physical sizes of our computers and the storage systems have in fact gone down. Take for example, the IBM 350 disc; it was announced in 1956, and the last model was sold till 1969. It had a storage capacity of 5 MB, while its physical size was about $1.5 \times 0.75 \times 1.75$ m^3, which is the size of a decent-sized cloth cupboard with hangers (IBM 2022a, b; SolarWinds Worldwide 2019). Today, a data storage capacity of 128 GB and 1 TB, which are respectively 25,000 times and 200,000 times larger than that of IBM 350 disc, both take equal physical space of one fingertip each ($1.5 \times 1.1 \times 0.1$ cm^3) (Western Digital Corporation or its affiliates 2022).

The scale of human systems continues to increase at an unprecedented rate. Through all this development of the last century, we have now reached a point where the rate of generation of information is very high, and the volume of data generated is very large. We can get an idea of how vast we have become, in terms of consuming and generating data, just by looking at the smart devices we have that continuously generate and record data—a smartphone, connected to a tablet, which is connected to a laptop; and all of these are in an ecosystem of other connected tech, such as smart TV, smart watches and smart homes. Big data is not just the information or structured or unstructured data sets, it is also the technologies, their evolution and usage that provide the required information at the correct time to the user seeking it from a sea of data that has been growing exponentially for a long time (Riahi and Riahi 2018). Big data is one the most popular phenomena of our time, that every industry wants to tap into and successfully use to fulfil their needs.

Big data classification has started with the Vs. Any data set which has these Vs are considered to be big data. ORACLE has defined three Vs of big data—volume, velocity and variety (Oracle 2022). "Volume" refers to the quantity of data collected and stored; "Velocity" refers to the rate of transfer of data; and "Variety" refers to the different types in which the data arrives, such as photographs, videos, audio and text (Arockia Panimalar et al. 2017).

Over the period of time, there was an increase in the number of Vs and they became four, then five. After further evolution, they became ten and then fourteen. The classification has now been extended to seventeen Vs and one C—volume, velocity, value, variety, veracity, validity, volatility, visualization, virality, viscosity, variability, venue, vocabulary, vagueness, verbosity, voluntariness, versatility and complexity (Arockia Panimalar et al. 2017). All of these represent a unique characteristic of big data, and further, it can be broken down, the better would its utility be.

The utility of big data presents itself in the form of big data analytics, which is the process of analysing this large volume of variable data arriving at a high velocity. Our ordinary, daily computers are

incapable of doing so, and specialized powerful machines are required for it (Riahi and Riahi 2018). Apart from being useful in general terms, big data analytics can be used specifically in an urban scenario in the following ways.

Big data analytics can be used to describe something. This is used to answer the question, "what" i.e. "what is happening" and is called descriptive analytics. Specifically in a city, it could be a phenomenon that is taking place, but is impossible to accurately describe due to the complexities in a city. Further, it can be used for diagnosis, i.e. to answer the question "why" or "why is it happening". This is called diagnostic analytics. Similarly, there is predictive analytics, which would forecast where might we be headed or what the future of the phenomenon taking place in the city could look like. Last utility is prescriptive analytics, which recommends a path that must be taken in order to mitigate the change that the phenomenon brings with itself (Riahi and Riahi 2018).

27.2 Complexities in a City

With industrialization in the nineteenth century, urbanization became a common phenomenon. Further technological advancements, in the latter half of the twentieth century set a pace for globalization. Urbanization, technological advancement and globalization have had an impact on the social systems, built environment and the natural environment in the city, which means the systems in a city started to get altered. Technological revolution has been strongly linked to growth and development. Figure 27.1 is taken from Freeman and Perez (1988) and Hall (1999) as published in Dodgson and Gann (2011, p. 104). It shows technologies that have aided in the growth of cities along with the type of system they could be classified under or implemented with to be successful. It also includes Hall's (1999) representative example of cities; those that have played an important role in the development of key technologies (Dodgson and Gann 2011, p. 104).

Figure 27.1 lists out technologies that developed and operated independently, over the period

Fig. 27.1 Some key
technologies affecting city
development and growth.
Source "Freeman and Perez
(1988) and Hall (1999)" in
Dodgson and Gann (2011,
p. 104)
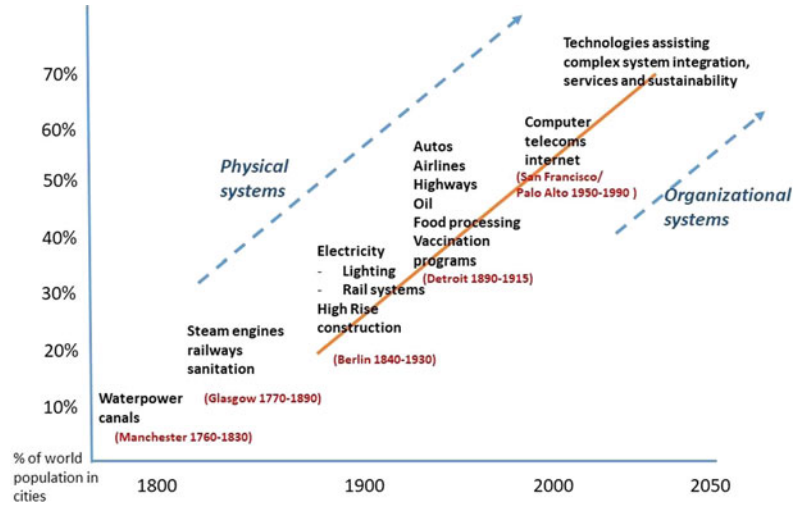
of time but they are interconnected with each other. A city thus can be called as a system of systems (Dodgson and Gann 2011). For example, if we take the transportation sector into consideration, it depends upon the energy sector. Traditionally, cars were either petrol- or diesel-based, but technological advancements take place, hybrid cars that run on electricity or any other fuel got introduced. Similarly, improved telecommunication infrastructure helps in increased opportunities of working from home, which in turn has an impact on the transport sector.

Cities are complex adaptive systems which depend upon the relationships of ecosystems, organisms and the built environment. Energy and material flows through a complex network in order to get distributed. In today's world, the problems in the cities are growing and these growing problems are complex, diverse, uncertain and huge in number just like the city networks. To deal with the problems in a city, those energy and material flows need to be assessed in depth. These complex network flows are interconnected, any change in even a single component of the networks might lead to further wanted or unwanted changes in other components or networks. With the growth of cities, and more and more people settling down in the cities, metropolitan regions came up with populations in excess of 10 million people. In 1970, there were only eight megacities on the planet, by 2010, the number had grown to

27 (Kennedy et al. 2015), and a further 45 megacities likely will exist by 2030 (United Nations Department of Economic and Social Affairs Population Dynamics 2018). In 2030, 4.9 billion people will be living in the cities according to the Population Reference Bureau. Increasing size of the cities has led to increase in complexity of cities, giving rise to enormous social and environmental challenges. Cities are perceived to be areas of high global risk because of more people living in the city, with extreme levels of poverty, vulnerability and social–spatial fragmentation. To provide essential services for this increasing population, massive developments are needed as in most of the cases, these are not sustainable and do not have an equitable distribution of the resources among rich and poor. Whether cities can develop as sustainable cities depends to a large extent on how they obtain, share and manage their energy and material resources.

Problems arising due to increasing population and further developments, lead to unanticipated problems in a city. Jane Jacobs once said, "*cities happen to be problems in organized complexity*" and "People who try to predict the future by extrapolating in a line of more of what exists [today]…are always wrong". According to him, predicting a city's future is not possible because of the complex nature of the city systems. Cities in today's world do not just face complex problems, but are stuck between wicked problems

(McFadden 2017), which are difficult or impossible to solve because of the complex interdependence (McFadden 2017). Wicked problems basically are real-world problems that acknowledge the complex interdependence of diverse factors and stakeholders, rather than simplistic, linear cause-and-effect abstractions that isolate the product of design from its context (Wahl 2017). These problems are not only limited to social systems in a city, but also to the problems associated with the reciprocal effects between social systems and natural systems that provide the basis for their existence.

If we take for instance the example of COVID-19, a very recent problem, the pandemic, one of the wicked problems that persists. It has its impact not only on the person who gets infected, but has a far-reaching multiplier impact starting from a local area level to an international level. Not only has COVID-19 impacted the health of people in various nations, but it has brought down the economy, the social status and in many cases led to pandemic-led migration. The biggest intra-country migration was seen in the Indian subcontinent since independence from the British Union in 1947 and partition of the country, when daily wage earners were forced to return to their native places from megacities due to loss of work in the sudden lockdown of 2020. An estimated 10 million workers had returned to their home state till September 2020 (Sharma 2020), i.e. within 5–6 months, which when compared to the migration at the time of Indian partition, has a higher number of migrating people per unit time. 14.5 million people had migrated over the course of 4 years at the time of independence (Bharadwaj et al. 2008). Even those who had been working formally for years in the private sector of the cities, moved back to their hometowns, in the light of lowering wages or losing jobs, the prospect of being with their family and relatives, and saving the costs pertaining to rent or higher cost of living.

The UN estimates that 55% of the global population lives in urban areas—a figure that is projected to rise to 68% by 2050. With urban sprawl, problems related to urbanization are increasing day by day. Urbanization in India has been an instrument of economic, social and political progress but it has led to serious problems. Urban population, haphazard and unplanned growth of urban areas, and a desperate lack of infrastructure are the main problems. The rapid growth of urban population both natural and through migration has put heavy pressure on public utilities like housing, sanitation, transport, water, electricity, health, education and so on. There are visible gaps between demand and supply of facilities and services in a city, also the distribution is inequitable. A very large number of people, in cities, live in a relatively small amount of space. As the population increases in a city, areas good for development get occupied, low-income group people due to low affordability have to settle down in areas which are highly vulnerable to disasters. Intensive urban growth can lead to greater poverty, with local governments unable to provide services for all people.

Human interventions have also led to changes in the city systems, which further has altered functioning of the city. Increase in population contributes to large volumes of uncollected waste left unattended, which further creates multiple health hazards and magnifies the risk of environmental hazards. Concentrated energy use has also led to increased air pollution with significant impact on human health. By reclaiming water bodies, wetlands and other eco-sensitive areas for construction purposes, there have been changes in average temperature and rainfall. Changes in rainfall along with the changes in the land use and land cover lead to frequent floods in a city. Also, with the loss of total urban tree cover, instances of soil erosion and further turning fertile land to barren have grown across cities.

While the cities are all going through all these complex processes, the issues that we face today are difficult to anticipate and many times, cosmetic solutions that are implemented, lead to more complex and difficult situations. In order to plot the issues that we are facing in the cities today, and with the available data in a city, big data has proved to be a boon for the city planners. Ongoing digital revolution that we are going through since the last decade has been applied to the cities, and it has led to improvement in the quality of life of the people and bring

about changes in the way in which people interact and experience a city.

27.3 Application of Big Data in a City

Issues in a city are both spatial and temporal. The issues in a city are spread across either a part of a city or citywide. There is a fair enough chance that a problem that exists in a city, might not be evolving from the city itself. It might be as a result a problem that exists in a neighbouring area, for example, the problem of air pollution in Delhi. The timing of the worst air quality of the city consistently coincides with the timing of crop burning in the neighbouring states of Haryana and Punjab. Temporal issues or problems existing in a city may vary from several minutes to years or decades. For instance, in case of a fire accident, it may last either for minutes or for hours, and this incident will be on a smaller spatial scale. Climate change on the other hand is a problem which has come into being as a result of human negligence towards the environment over a period of time. It has taken several decades to build up and reach to the point where it stands today. Generally, the more the spread of an issue is on a temporal and spatial scale, the more complex it is. Complexity in a city has been dealt with by the use of big data for efficient delivery of services and utilities. It has been used for mapping assets, solving various sectoral problems, streamlining governance and administrative issues and reducing the communication gap between stakeholders in a city. Some of the case studies where the application of big data has remained successful are as follows.

27.3.1 Santa Monica's Well-Being Project—California, USA

Well-being project is a medium to get deeper insights of community strengths and needs by collecting various data and analysing it. Data collection is done by multiple sources varying from a widespread resident survey and social media to measure and track citizens. The data collection is dynamic so are the following processes. The findings of the data are incorporated into the formal planning process along with the budget allocation. A dynamic process makes it easy to find out measures to make the city liveable and happier continuously. This process was aimed to make a cost-effective and a streamlined process for city well-being.

Data that is collected is turned into a Well-being Index, which further is a measure of community wellbeing. This index acts as an initiation point to the understanding of community well-being and city overall. The project encourages collaboration and broad buy-in among city leaders and local organizations (e.g. needed to convince city government departments to improve their data collection) (World Economic Forum 2020).

27.3.2 Smart Dubai Happiness Meter—Dubai, UAE

This project is on similar lines as case study 1. It is developed as a part of the vision of Dubai to become the world's happiest place. As its name suggests, it measures happiness through live sentiment capture at numerous touch points across the city. City-wide technological deployment has been made for it through all possible customer interaction channels such as websites, mobile applications and physical service centres. The design used is simple in functionality to capture maximum user data. In two and a half years, more than 22 million sentiments have been captured at 4400 touchpoints via 172 customer interaction channels. Real-time data capture is helping enhance the experience of the city, along with supporting Dubai's city transformation agenda (World Economic Forum 2020).

27.3.3 Storms of the East Coast—USA

Big Data can play an important role in mitigating the harmful effects of natural disasters through disaster management. During Hurricane Sandy of

2012, the effect it was going to have on the East Coast, was studied with the help of big data analytics. The pattern of the storm was forecasted accurately, 5 days in advance, which had not been possible earlier. This enabled the authorities to take the measures necessary and plan effective responses (Simplilearn 2019).

27.4   Conclusion

Cities are a complex system of systems, and hence, the problems within the city are also complex, which are classified as wicked. To deal with the ever-challenging and exponentially rising problems, the digital age has proven to be beneficial. Rapid digitization taking place in the urban areas gives us a huge opportunity to experiment with various different methods to improve the condition of those living in the urban areas and their sprawl. Through real-time collection of data such as sentiment capturing, those who are forced to cling to the edges due to the lack of affordability, can be integrated as a stakeholder in the system, which they actually are, and be meted out equitable treatment, provided the entity in-charge has the intent in the right place. This digital age that we are going through, lends a helping hand to organize the cities by timely providing the right information to identify and mitigate the problems in a city. The problems can range from natural disasters to man-made disasters such as poor condition of living. The aforementioned right information comes from spatial and temporal checks which are necessary but dynamic, and thus need to be checked timely. In such a scenario, big data has made it possible to easily handle this data, and accurately process it, to give the results and solutions that are much required to face the ever-evolving and unpredictable, upcoming challenges.

Data storing, collection and analyses in the form of big data are definitely beneficial for any city, but the cost incurred in this whole process is an important issue. The results that we achieve are almost accurate, but at higher costs than the traditional way of data processing. Any city administration that aims to put big data to use in the city should frame effective policies and guidelines that will help to sustain the whole process in an economical manner. If made cost-effective, big data can help to overall improve living standards and quality of life in a city overall.

References

Anderson MJ (2015) The American census—a social history. Yale University Press. ISBN: 9780300 195422, 0300195427

Arockia Panimalar S., Varnekha Shree S, Veneshia Kathrine A (2017) The 17 V's of big data. Int Res J Eng Technol (IRJET), 329–333

Bharadwaj P, Khwaja AI, Mian A (2008) The big march: migratory flows after the partition of India. Faculty Research Working Papers Series. Harvard Kennedy School—John F. Kennedy School of Government

Columbia University (2001) Herman Hollerith. Retrieved from Columbia University Computing History: http://www.columbia.edu/cu/computinghistory/hollerith.html

CrashCourse (2017) Early computing: crash course computer science #1. Retrieved from YouTube: https://www.youtube.com/watch?v=O5nskjZ_GoI

Dodgson M, Gann DM (2011) Technological innovation and complex systems in cities. J Urban Technol 8 (3):101–113

Freeman C, Perez C (1988) Structural crises of adjustment, business cycles and investment behaviour. In: Dosi G, Freeman C, Nelson R, Silverberg G, Soete L (eds) Tech Change Econ Theory pp 38–66. London, New York: Pinter Publishers

Hall P (1999) Cities in Civilization: Culture, Innovation, and Urban Order. London: Phoenix Giant

IBM (2022a) Hollerith tabulator and sorter box. Retrieved from IBM Archives: https://www.ibm.com/ibm/history/exhibits/attic/attic_071.html

IBM (2022b) IBM 350 disc storage unit. Retrieved from IBM Archives: https://www.ibm.com/ibm/history/exhibits/storage/storage_350.html

Kennedy CA, Stewart I, Facchini A, Cersosimo I, Mele R, Chen B et al (2015) Energy and material flows of megacities. PNAS 112(19):5985–5990

Kofa Study (2022) History of data processing (lesson 1, topic 3). Retrieved from Kofa Study—Data Processing (Week 1): https://www.kofastudy.com/courses/jss1-computer-studies-2nd-term/lessons/data-processing-week-1/topic/history-of-data-processing/

Krettek A (2022) The data processing evolution: a potted history. Retrieved from ITProPortal: https://www.itproportal.com/features/the-data-processing-evolution-a-potted-history/

Marr B (2015) A brief history of big data everyone should read. Retrieved from World Economic Forum: https://www.weforum.org/agenda/2015/02/a-brief-history-of-big-data-everyone-should-read/

McFadden M (2017) Medium. Retrieved 17 Aug 2021, from https://medium.com/@meganmcfadden/a-beginners-introduction-exploring-systems-thinking-for-21st-century-cities-faa91f4129fa

Oracle (2022) What is big data? Retrieved from Oracle: https://www.oracle.com/in/big-data/what-is-big-data/

Riahi Y, Riahi S (2018) Big data and big data analytics: concepts, types and technologies. Int J Res Eng, 524–528

Roser M (2014) Fertility rate. Retrieved from Our World in Data: https://ourworldindata.org/fertility-rate

Sharma YS (2020) Labour minister Gangwar clarifies his response on migrant workers in Parliament. The Economic Times. Retrieved from https://economictimes.indiatimes.com/news/economy/policy/labour-minister-gangwar-clarifies-his-response-on-migrant-labourers-in-parliament/articleshow/78142699.cms

Simplilearn (2019) Big data in 5 minutes | what is big data?| introduction to big data | big data explained | Simplilearn. Retrieved from YouTube: https://www.youtube.com/watch?v=bAyrObl7TYE

SolarWinds Worldwide (2019) Amazing facts and figures about the evolution of hard disc drives. Retrieved from Pingdom: https://www.pingdom.com/blog/amazing-facts-and-figures-about-the-evolution-of-hard-disc-drives/

Taylor D (2022) What is big data? Introduction, types, characteristics, examples. Retrieved from Guru99: https://www.guru99.com/what-is-big-data.html

United Nations Department of Economic and Social Affairs Population Dynamics. (2018). World urban prospect 2018. United Nations Department of Economic and Social Affairs Population Dynamics, New York

United States Census Bureau (2021) 1880 fast facts—history. Retrieved from U. S. Census Bureau: https://www.census.gov/history/www/through_the_decades/fast_facts/1880_fast_facts.html

United States Census Bureau (2022) Fast facts—history—U. S. Census Bureau. Retrieved from U. S. Census Bureau: https://www.census.gov/history/www/through_the_decades/fast_facts/

Wahl DC (2017) Facing complexity: wicked design problems. Retrieved 17 Aug 2021, from https://medium.com/age-of-awareness/facing-complexity-wicked-design-problems-ee8c71618966

Western Digital Corporation or its affiliates (2022) Sandisc Extreme® microSDXC™ UHS-I CARD (Micro SD Cards). Retrieved from Western Digital: https://www.westerndigital.com/en-in/products/memory-cards/sandisc-extreme-uhs-i-microsd#SDSQXAA-128G-GN6MA

World Economic Forum (2020) Smart at scale: cities to watch—25 case studies. World Economic Forum, Geneva

Worldometers.info (2022) World population. Retrieved from Worldometer: https://www.worldometers.info/world-population/

Rethinking Progress in Approaches and Techniques for the Urban Environmental Studies

28

Atiqur Rahman, Shouraseni Sen Roy, Swapan Talukdar, and Shahfahad

Abstract

As a consequence of increasing urban population, the cities around the world had experienced very fast transformation of urban landscape which has resulted in serious consequences for the urban environment, landscape quality and climate.The researchers around the world have tried to model and analyse the urban expansion and its impacts on various aspects of urban environment. This chapter describes the various approaches and models used for analysing the urban expansion and its consequences for the urban environment in the last few decades. From mapping and modelling the urban spatial forms to achieving urban sustainability and resilience, the researches on urban studies have made significant progress in the past two centuries. In the past few decades, the urban researchers have examined the urban landscape pattern, urban sprawl, future urban expansion as well as the impacts of urban expansion on urban environment, ecosystem services, ecology and biodiversity, climatic system, etc. Moreover, the techniques used for analysing urban expansion and its consequences have also developed from the conventional field-based methods to the application of geospatial techniques and artificial intelligence (AI). The advent of AI along with innovative and advanced techniques has made it possible to deal with the negative consequences of urban expansion. Now the researchers are oriented towards achieving the urban resilience, promoting green buildings and increasing thermal comfort in the cities.

28.1 Introduction

Since the pre-historic times, the world's population was predominantly agrarian and was living in smaller settlement units (Birch-Chapman et al. 2017). This scenario started changing during the eighteenth and nineteenth centuries when people started living in the large urban clusters as a consequence of industrial revolution (Williamson 1995). During this period, large-scale movement

A. Rahman (✉) · S. Talukdar · Shahfahad
Department of Geography, Faculty of Natural Sciences, Jamia Millia Islamia, New Delhi 110025, India
e-mail: arahman2@jmi.ac.in

S. S. Roy
Department of Geography and Sustainable Development, University of Miami, Coral Gables, FL, USA
e-mail: ssr@miami.edu

of labour force from the rural agrarian economy to urban industrial and service-based economy took place (Turok and McGranahan 2013; Sugihara 2019). This resulted in the large-scale transformation of urban landscape pattern and degradation of urban environmental quality (Williamson 1995; Hanlon 2020; Polovnikova et al. 2022). Since the first industrial revolution in Europe in mid-nineteenth century, the global urban population has increased many folds (Seto et al. 2013). As a consequence of this, the cities around the world had witnessed degradation of their environmental quality, rising urban heat island (UHI) intensity and heat waves, congestion, air and water pollution, urban sprawl, etc. (Chew 2001; Azam and Khan 2016). The researchers have tried to examine and model the negative consequences of urbanization for environment, ecology and society since last two centuries. However, in the past few decades, the rapid urbanization and environmental degradation, especially in developing countries have gain attention of the researchers around the world (Turok and McGranahan 2013; Bai et al. 2017).

Among the various impacts of urbanization on its environment and society, the urban sprawl (Ewing 2008; Saini and Tiwari 2020) and UHI are the most studied phenomenon across the world (Aflaki et al. 2017; Veena et al. 2020). Since last two decades, the researches in urban studies have made significant progress (Banai 2013; Mouratidis 2021) but there is a clear gap between the literatures on urban studies during twentieth century and the first two decades of twenty-first century. For instance, the literatures on urban studies during twentieth century were more oriented towards mapping and modelling the urban spatial forms while in the twenty-first century, majority of literatures are oriented towards urban sustainability and urban planning (Berke 2002; Seto et al. 2012). The main focus of researches on urbanization and its consequences in twenty-first century are urban resilience, urban spatial forms and sustainability (Ahern 2013). The primary goal of all these researches is achieving the sustainable urban development and preparing effective planning policies. The

researches on urban environment were primarily based on the monitoring and analysing the urban landscape dynamics and environmental quality using field samples as well as secondary data sources like topographical maps and aerial photographs (Forster 1985; Rahman et al. 2011; Weng and Quattrochi 2018). The advent of satellite remote sensing and artificial intelligence (AI) had enabled the researchers to examine the urban spatial forms and its environment at various spatio-temporal scales (Wu and Silva 2010; Patino and Duque 2013; Wentz et al. 2014; Wellmann et al. 2020). The application of AI in urban studies has several advantages like better and fast analysis of urban environmental quality and landscape dynamics, self-automated management of water resources, air, water and noise pollution, solid waste, etc., and providing efficient means of energy usages (Allam and Dhunny 2019; Kumar 2020).

More recently, the urban green commons, public open spaces and landscape quality have emerged as the hot topics in the context of urban planning and sustainability (Colding et al. 2013; Yung et al. 2016; Shahfahad et al. 2019). Another important aspect of urban sustainability which has emerged as a hot topic of urban studies is low-carbon city (Liu and Qin 2016) which specifically focuses on the reduction of CO_2 emissions from the cities. Although the developed countries of western Europe and North America have made significant progress in the research of low-carbon city (Coutard and Rutherford 2010; Bulkeley et al. 2012; Tan et al. 2017), the progress in developing countries of Asia and Africa is not satisfactory. Among the developing countries, China has made significant progress in the low-carbon city research (Yang and Li 2013; Khanna et al. 2014; Liu and Qin 2016). But in other developing countries, very few studies are available on the analysis and modelling of urban carbon emission and footprint (Ahmad et al. 2015; de Souza Leao et al. 2020). Thus, there is a clear gap between the researches on urban environment in the developed and developing countries.

28.2 Development in Remote Sensing Data and Approaches for Urban Studies

The urban areas are complex and dynamic systems which changes with time and space (Batty 2009). Therefore, it is essential to model and analyse the dynamic nature of urban areas and its environments to develop new planning strategies and make cities sustainable for living (Webb et al. 2018; Kourtit et al. 2022). As discussed earlier, the advent of remote sensing technology marked a remarkable change in the field of urban studies. Now, with remote sensing techniques, the researchers can model the urban spatial forms and change at various scale with precise accuracy and quantify its impacts on urban environment and climatic systems (Mobasheri 2021). Different models and approaches have been developed and applied for examining and modelling the urban landscape pattern, its environment and impact of urbanization on environment, economy and society (Berling-Wolff and Wu 2004; Nuissl and Siedentop 2021). During this period, researchers have examined the urban landscape pattern and quality, urban sprawl, consequences of urban land use change and modelled the future urban expansion.

The earliest satellite observation systems available for mapping the earth surface were CORONA, ARGON and LANYARD, which were mostly used for ground reconnaissance and area mapping (Fu et al. 2020). With the launch of Landsat 1 multispectral scanner (MSS) in early 1970s, researchers around the globe started to map the urban landscape pattern and change at various spatial and temporal scales (Phiri and Morgenroth 2017). Landsat is the longest-running earth observation satellite, extensively used for the mapping of urban landscape and its changes since past 50 years. Besides Landsat series, several other low-to-medium-resolution satellite data have been utilized for the mapping and monitoring urban landscape and environment like Moderate Resolution Imaging Spectroradiometer (MODIS), Satellite Pour l'Observation de la Terre (SPOT), IRS Resourcesat, Advanced Spaceborne Thermal Emission and Reflection Radiometer (ASTER), Sentinel (Table 28.1). In addition, some high-resolution satellite data like Quick-Bird, IKONOS and GeoEye are also available for use on paid basis. Another important revolution in urban studies came with the advent of thermal remote sensing. Although Landsat 1 multispectral scanner (MSS) was launched in 1972, it did not have a thermal band. With the launch of Landsat 4 thematic mapper (TM) in 1982, the first medium-resolution thermal satellite came into existence which has been extensively utilized for urban environmental studies, especially in the study of urban thermal environment (Chen et al. 2017; Wulder et al. 2019). More recently, the researchers have started using hyperspectral and microwave remote sensing data such as synthetic-aperture radar (SAR) and light detection and ranging (LIDAR) data for urban mapping and monitoring (Kuras et al. 2021) of urban areas.

28.3 Current Status of Urban Studies in Developed and Developing World

As discussed earlier, there is a clear gap between the researches on urbanization and urban environment in the developing and developed countries, the researchers of Western developed countries have made significant progress in the urban research. On the other hand, the researchers of developing countries of Asia and Africa are mostly dependent on the traditional approaches and methods. The focus of urban research in developed countries like Western European and North American countries are towards urban resilience and sustainability (Bush and Doyon 2019; Langemeyer et al. 2021). Contrary to this, in developing countries, the researches on urban environment are more oriented towards the case studies on quantification and assessment of urbanization and its consequences for environment, economy and society (Naikoo et al. 2020; Hatab et al. 2021; Khan and Sudheer 2022).

The differences in trend of urban studies in developed and developing countries may be

Table 28.1 List of most frequently remote sensing satellites in urban studies

Satellite series	Satellite name	Sensor	No. of bands	Resolution (m)	Launch year
Landsat	Landsat 1	MSS	4	60	1972
	Landsat 2	MSS	4	60	1975
	Landsat 3	MSS	5	60	1978
	Landsat 4	TM	7	30/120[a]	1982
	Landsat 5	TM	7	30/120[a]	1984
	Landsat 7	ETM+	8	30/60[a]	1999
	Landsat 8	OLI/TIRS	11	30/100[a]	2013
	Landsat 9	OLI-2/TIRS-2	11	30/100[a]	2021
IRS Resourcesat	LISS I	Multispectral	4	73	1988
	LISS II	Multispectral	4	36.25	1991
	LISS III	Multispectral	4	23.5	2003
	LISS IV	Multispectral	3	5.8	2003
Sentinel	Sentinel 1	SAR	1	10	2014
	Sentinel 2	SAR (multispectral & optical)	13	10	2015
	Sentinel 3	SAR (multispectral & optical)	21	10	2016
SPOT	Spot 1	High-Resolution Visible (HRV)	4	20	1986
	Spot 2	High-Resolution Visible (HRV)	4	20	1990
	Spot 3	High-Resolution Visible (HRV)	4	20	1993
	Spot 4	High-Resolution Visible and InfraRed (HRVIR)	5	20	1998
	Spot 5	High-Resolution Geometric (HRG) & High-Resolution Stereoscopic (HRS)	4	10	2002
	Spot 6	New Astrosat Optical Modular Instrument (NAOMI)	5	6	2012
	Spot 7	New Astrosat Optical Modular Instrument (NAOMI)	5	6	2014
MODIS	MODIS	Terra & Aqua	36	250, 500, and 1000	1999
ASTER	ASTER	Terra & Aqua	14	15, 30 and 90	1999
QuickBird	QuickBird	–	4	5	2001
IKONOS	IKONOS	–	4	3.2	1999

[a] Spatial resolution of the thermal band

attributed to the type and pattern of urban expansion in these countries. For instance, in developing countries, the main problems of urbanization are the rapid and unplanned urban expansion and its impacts on urban environment and urban morphology (Zhang 2016). Therefore, the focus of urban researchers in developing countries is on the environmental consequences of urbanization. Contrary to this, the urbanization in developed countries is occurring in a controlled and planned manner and most of the developed nations are experiencing de-urbanization (Eskew and Olival 2018). Thus, the focus of urban researchers in developed countries is on urban resilience and sustainable urban planning (Bautista-Puig et al. 2022). The

concept of urban resilience has emerged in these countries to make cities capable to the tolerate shocks brought on by natural catastrophes and climate change and to recover from them (Klein et al. 2003). Further, in developed nations, researchers are also focusing on how the geospatial knowledge and AI can be utilized for achieving the urban sustainability and resilient societies (Vinuesa et al. 2020). More recently, researchers have applied a new approach called nature-based solutions to make the cities resilient to the natural disasters and climate change (Bush and Doyon 2019).

In developing countries, the researchers of urban environment are more oriented towards the contemporary urban issues such as development of UHI and heat stress, loss biodiversity and ecosystem services, degrading air and water quality (Wang et al. 2008; Shahfahad et al. 2022; Morya and Punia 2022). On the other hand, in developed countries, the focus is on the vulnerability of urban population to heat waves and UHI, green building and capacity building for the urban sustainability (Carter et al. 2015; Pauleit et al. 2019). More recently, the concept of green building has also been introduced in the developing countries. For instance, China and Southeast Asian countries have encouraged the green building practices to deal with the UHI and heat waves (Gou 2019). Progress has been also noted in the UHI studies in developing countries, as focus is shifting in these countries on vulnerability to UHI and thermal comfort in the cities (Shahfahad et al. 2022). But the developed countries are more advanced as the focus of UHI research in these countries is on quantification of UHI and heat waves-induced mortality rates (Błażejczyk et al. 2022) as well as examining the thermal performances of different building materials and design (Hooshangi et al. 2016) for the UHI mitigation.

28.4 Future Scope

From conventional methods to the application of geospatial techniques and AI, the urban environmental research has made a significant progress in the last two centuries. The application of AI in urban studies had made it easier for the researchers to quickly examine and model the impact of urbanization on its environment and ecology. But in the era of global urbanization and changing environmental and climatic conditions, there is still a need of more convenient studies on urban environmental issues and their management (Hardoy et al. 2013). Further, the number of researches in developing world is much lower than its need. For instance, India had nearly 377 million population living in about 7935 urban centres including cities and towns in 2011 (Joshi and Ahmed 2016). But, most of the studies are primarily based on the larger metropolitan cities like Delhi, Mumbai, Kolkata, Chennai, Bengaluru and Hyderabad. Similar is the case of other developing nations of Asia and Africa. Hence, there is a need of studying the changing pattern of urban landscape and its important on environment, ecology and society in these medium- and small-sized cities. Further, as the global climate is changing and the number of natural disasters is increasing day by day, the researchers of the developing countries may look after the sustainable and resilient cities.

The future scope of urban research should be focused on the current and future urban issues. For example, researchers had extensively studied the problem of UHI formation and declining urban thermal comfort in both developed and developing countries (Kotharkar et al. 2018; Huang and Lu 2018). Thus, it may be an important aspect of urban environmental research to identify the UHI mitigation strategies and increasing thermal comfort of the cities. In this regard, the application of nature-based solutions and AI may be helpful for the urban researchers. Researchers may also look after the potential of green buildings and increasing urban green covers for UHI mitigation, especially in the cities of developing countries. Moreover, the identification of potential areas for increasing green and blue infrastructures to mitigate the UHI and reduce the heat stress may also be an important area of research. Recently, the developing countries have introduced the smart city mission to promote inclusive and sustainable cities which

may provide clean and sustainable living environment (Yadav et al. 2019). In this regard, the researchers may apply the geospatial techniques and AI in the planning of sustainable smart cities. Another important point in UHI research is that studies on UHI have been done either using air temperature data which is used to examine the canopy layer UHI (CLUHI) or thermal satellite data which is used to examine the surface UHI (SUHI). For a better understanding of UHI and the interaction between surface and air temperature, an integrated investigation of the UHI using both air temperature data and thermal satellite data may be beneficial. Furthermore, an important issue of the cities of developing countries is high emission of carbon. Hence, researchers may also focus on achieving low-carbon cities for the climate change mitigation and urban ecological management.

References

Aflaki A, Mirnezhad M, Ghaffarianhoseini A, Ghaffarianhoseini A, Omrany H, Wang ZH, Akbari H (2017) Urban heat island mitigation strategies: a state-of-the-art review on Kuala Lumpur, Singapore and Hong Kong. Cities 62:131–145

Ahern J (2013) Urban landscape sustainability and resilience: the promise and challenges of integrating ecology with urban planning and design. Landscape Ecol 28(6):1203–1212

Ahmad S, Baiocchi G, Creutzig F (2015) CO_2 emissions from direct energy use of urban households in India. Environ Sci Technol 49(19):11312–11320

Allam Z, Dhunny ZA (2019) On big data, artificial intelligence and smart cities. Cities 89:80–91

Azam M, Khan AQ (2016) Urbanization and environmental degradation: evidence from four SAARC countries—Bangladesh, India, Pakistan, and Sri Lanka. Environ Prog Sustain Energy 35(3):823–832

Bai X, McPhearson T, Cleugh H, Nagendra H, Tong X, Zhu T, Zhu YG (2017) Linking urbanization and the environment: conceptual and empirical advances. Annu Rev Environ Resour 42(1):215–240

Banai R (2013) Plan versus project dilemma revisited: a progress review of urban and regional studies literature. Urban Stud 50(4):807–824

Batty M (2009) Cities as complex systems: scaling, interaction, networks, dynamics and urban morphologies. In: Meyers R (eds) Encyclopedia of complexity and systems science. Springer, New York, NY. https://doi.org/10.1007/978-0-387-30440-3_69

Bautista-Puig N, Benayas J, Mañana-Rodríguez J, Suárez M, Sanz-Casado E (2022) The role of urban resilience in research and its contribution to sustainability. Cities 126:103715

Berke PR (2002) Does sustainable development offer a new direction for planning? Challenges for the twenty-first century. J Plan Lit 17(1):21–36

Berling-Wolff S, Wu J (2004) Modeling urban landscape dynamics: a case study in Phoenix, USA. Urban Ecosyst 7(3):215–240

Birch-Chapman S, Jenkins E, Coward F, Maltby M (2017) Estimating population size, density and dynamics of Pre-Pottery Neolithic villages in the central and southern Levant: an analysis of Beidha, southern Jordan. Levant 49(1):1–23

Błażejczyk K, Twardosz R, Wałach P, Czarnecka K, Błażejczyk A (2022) Heat strain and mortality effects of prolonged central European heat wave—An example of June 2019 in Poland. Int J Biometeorol 66 (1):149–161

Bulkeley H, Broto VC, Edwards G (2012) Bringing climate change to the city: towards low carbon urbanism? Local Environ 17(5):545–551

Bush J, Doyon A (2019) Building urban resilience with nature-based solutions: how can urban planning contribute? Cities 95:102483

Carter JG, Cavan G, Connelly A, Guy S, Handley J, Kazmierczak A (2015) Climate change and the city: building capacity for urban adaptation. Prog Plan 95:1–66

Chen Z, Xu B, Devereux B (2014) Urban landscape pattern analysis based on 3D landscape models. Appl Geogr 55:82–91

Chen F, Yang S, Yin K, Chan P (2017) Challenges to quantitative applications of Landsat observations for the urban thermal environment. J Environ Sci 59:80–88

Chew SC (2001) World ecological degradation: accumulation, urbanization, and deforestation, 3000 BC-AD 2000. Rowman Altamira

Colding J, Barthel S, Bendt P, Snep R, Van der Knaap W, Ernstson H (2013) Urban green commons: insights on urban common property systems. Glob Environ Chang 23(5):1039–1051

Coutard O, Rutherford J (2010) The rise of post-networked cities in Europe? Recombining infrastructural, ecological and urban transformations in low carbon transitions. In: Cities and low carbon transitions. Routledge, pp 123–141

de Souza Leao EB, do Nascimento LFM, de Andrade JCS, de Oliveira JAP (2020) Carbon accounting approaches and reporting gaps in urban emissions: an analysis of the Greenhouse Gas inventories and climate action plans in Brazilian cities. J Clean Prod 245:118930

Dutta D, Rahman A, Kundu A (2015) Growth of Dehradun city: an application of linear spectral unmixing (LSU) technique using multi-temporal Landsat satellite data sets. Remote Sens Appl: Soc Environ 1:98–111

Eskew EA, Olival KJ (2018) De-urbanization and zoonotic disease risk. Ecohealth 15(4):707–712

Ewing RH (2008) Characteristics, causes, and effects of sprawl: a literature review. In: Urban ecology, pp 519–535

Forster BC (1985) An examination of some problems and solutions in monitoring urban areas from satellite platforms. Int J Remote Sens 6(1):139–151. https://doi.org/10.1080/01431168508948430

Fu W, Ma J, Chen P, Chen F (2020) Remote sensing satellites for digital Earth. In: Guo H, Goodchild MF, Annoni A (eds) Manual of digital Earth. Springer, Singapore. https://doi.org/10.1007/978-981-32-9915-3_3

Gamanya R, De Maeyer P, De Dapper M (2007) An automated satellite image classification design using object-oriented segmentation algorithms: a move towards standardization. Expert Syst Appl 32(2):616–624

Gou Z (ed) (2019) Green building in developing countries: policy, strategy and technology. Springer

Hanlon WW (2020) Coal smoke, city growth, and the costs of the industrial revolution. Econ J 130(626):462–488

Hardoy JE, Mitlin D, Satterthwaite D (2013) Environmental problems in an urbanizing world: finding solutions in cities in Africa. Routledge, Asia and Latin America

Hatab AA, Ravula P, Nedumaran S, Lagerkvist CJ (2021) Perceptions of the impacts of urban sprawl among urban and peri-urban dwellers of Hyderabad, India: a Latent class clustering analysis. Environ, Dev Sustain, pp 1–26

Hooshangi HR, Akbari H, Touchaei AG (2016) Measuring solar reflectance of variegated flat roofing materials using quasi-Monte Carlo method. Energy Build 114:234–240

Huang Q, Lu Y (2018) Urban heat island research from 1991 to 2015: a bibliometric analysis. Theoret Appl Climatol 131(3):1055–1067

Joshi R, Ahmed S (2016) Status and challenges of municipal solid waste management in India: a review. Cogent Environ Sci 2(1):1139434

Khan A, Sudheer M (2022) Machine learning-based monitoring and modeling for spatio-temporal urban growth of Islamabad. Egypt J Remote Sens Space Sci 25(2):541–550

Khanna N, Fridley D, Hong L (2014) China's pilot low-carbon city initiative: a comparative assessment of national goals and local plans. Sustain Cities Soc 12:110–121

Klein RJ, Nicholls RJ, Thomalla F (2003) Resilience to natural hazards: how useful is this concept? Glob Environ Change Part B: Environ Hazards 5(1):35–45

Kotharkar R, Ramesh A, Bagade A (2018) Urban heat island studies in South Asia: a critical review. Urban Clim 24:1011–1026

Kourtit K, Nijkamp P, Türk U, Wahlstrom M (2022) City love and place quality assessment of liveable and loveable neighbourhoods in Rotterdam. Land Use Policy 119:106109

Kulkarni K, Vijaya PA (2022) Measuring urban sprawl using machine learning. Fundamentals and methods of machine and deep learning: algorithms, tools and applications, pp 327–340

Kumar V (2020) Smart living for smart cities. In: Smart living for smart cities. Springer, Singapore, pp 3–70

Kuras A, Brell M, Rizzi J, Burud I (2021) Hyperspectral and lidar data applied to the urban land cover machine learning and neural-network-based classification: a review. Remote Sens 13(17):3393

Langemeyer J, Madrid-Lopez C, Beltran AM, Mendez GV (2021) Urban agriculture—A necessary pathway towards urban resilience and global sustainability? Landsc Urban Plan 210:104055

Liu W, Qin B (2016) Low-carbon city initiatives in China: a review from the policy paradigm perspective. Cities 51:131–138

Luck M, Wu J (2002) A gradient analysis of urban landscape pattern: a case study from the Phoenix metropolitan region, Arizona, USA. Landscape Ecol 17(4):327–339

Martínez-Bravo M, Martínez-del-Río J (2019) Urban pollution and emission reduction. In: Leal Filho W, Azul A, Brandli L, Özuyar P, Wall T (eds) Sustainable cities and communities. Encyclopedia of the UN Sustainable Development Goals. Springer, Cham. https://doi.org/10.1007/978-3-319-71061-7_30-1

McDonald RI, Marcotullio PJ, Güneralp B (2013) Urbanization and global trends in biodiversity and ecosystem services. In: Elmqvist et al. Urbanization, biodiversity and ecosystem services: challenges and opportunities. Springer, Dordrecht. https://doi.org/10.1007/978-94-007-7088-1_3

Mobasheri A (2021) An introduction to open source geospatial science for urban studies. In Open source geospatial science for urban studies. Springer, Cham, pp 1–8

Morya CP, Punia M (2022) Impact of urbanization processes on availability of ecosystem services in National Capital Region of Delhi (1992–2010). Environ Dev Sustain 24(5):7324–7348

Mouratidis K (2021) Urban planning and quality of life: a review of pathways linking the built environment to subjective well-being. Cities 115:103229

Naikoo MW, Rihan M, Ishtiaque M, Shahfahad (2020) Analyses of land use land cover (LULC) change and built-up expansion in the suburb of a metropolitan city: spatio-temporal analysis of Delhi NCR using Landsat datasets. J Urban Manag 9(3):347–359

Nuissl H, Siedentop S (2021) Urbanisation and land use change. In Sustainable land management in a European context. Springer, Cham, pp 75–99

Patino JE, Duque JC (2013) A review of regional science applications of satellite remote sensing in urban settings. Comput Environ Urban Syst 37:1–17

Pauleit S, Ambrose-Oji B, Andersson E, Anton B, Buijs A, Haase D, van den Bosch CK (2019) Advancing urban green infrastructure in Europe: outcomes and reflections from the GREEN SURGE project. Urban Forest Urban Greening 40:4–16

Phiri D, Morgenroth J (2017) Developments in Landsat land cover classification methods: a review. Remote Sen 9(9):967

Polovnikova ES, Kyarova MA, Gazukina YG (2022) Assessment of the industrial impact on the environment. In: Popkova EG, Sergi BS (eds) Geo-economy of the future. Springer, Cham. https://doi.org/10.1007/978-3-030-92303-7_21

Rahman A, Aggarwal SP, Netzband M, Fazal S (2010) Monitoring urban sprawl using remote sensing and GIS techniques of a fast growing urban centre, India. IEEE Journal of Selected Topics in Applied Earth Observations and Remote Sensing 4(1):56–64

Rahman A, Kumar Y, Fazal S, Bhaskaran S (2011) Urbanization and quality of urban environment using remote sensing and GIS techniques in East Delhi-India. J Geogr Inf Syst 3(01):62

Sahana M, Hong H, Sajjad H (2018) Analyzing urban spatial patterns and trend of urban growth using urban sprawl matrix: A study on Kolkata urban agglomeration India. Sci Total Environ 628–629:1557–1566

Saini V, Tiwari RK (2020) A systematic review of urban sprawl studies in India: a geospatial data perspective. Arab J Geosci 13:840

Seto KC, Güneralp B, Hutyra LR (2012) Global forecasts of urban expansion to 2030 and direct impacts on biodiversity and carbon pools. Proc Natl Acad Sci 109 (40):16083–16088

Seto KC, Parnell S, Elmqvist T (2013) A global outlook on urbanization. In: Elmqvist et al. Urbanization, biodiversity and ecosystem services: challenges and opportunities. Springer, Dordrecht. https://doi.org/10.1007/978-94-007-7088-1_1

Shahfahad, Kumari B, Tayyab M, Hang HT, Khan MF, Rahman A (2019) Assessment of public open spaces (POS) and landscape quality based on per capita POS index in Delhi, India. SN Appl Sci 1(4):1–13

Shahfahad, Naikoo MW, Islam ARMT, Mallick J, Rahman A (2022) Land use/land cover change and its impact on surface urban heat island and urban thermal comfort in a metropolitan city. Urban Clim 41:101052

Sugihara K (2019) Multiple paths to industrialization: a global context of the rise of emerging states. In: Otsuka K, Sugihara K (eds) Paths to the emerging State in Asia and Africa. Emerging-economy state and international policy studies. Springer, Singapore. https://doi.org/10.1007/978-981-13-3131-2_1

Sugumaran R, Degroote J (2010) Spatial decision support systems: principles and practices. CRC Press

Talukdar S, Singha P, Mahato S, Pal S, Liou YA, Rahman A (2020) Land-use land-cover classification by machine learning classifiers for satellite observations—A review. Remote Sens 12(7):1135

Tan S, Yang J, Yan J, Lee C, Hashim H, Chen B (2017) A holistic low carbon city indicator framework for sustainable development. Appl Energy 185:1919–1930

Turok I, McGranahan G (2013) Urbanization and economic growth: the arguments and evidence for Africa and Asia. Environ Urban 25(2):465–482

Veena K, Parammasivam KM, Venkatesh TN (2020) Urban Heat Island studies: current status in India and a comparison with the International studies. J Earth Syst Sci 129(1):1–15

Venter ZS, Chakraborty T, Lee X (2021) Crowdsourced air temperatures contrast satellite measures of the urban heat island and its mechanisms. Sci Adv 7(22): eabb9569

Vinuesa R, Azizpour H, Leite I, Balaam M, Dignum V, Domisch S, Fuso Nerini F (2020) The role of artificial intelligence in achieving the sustainable development goals. Nat Commun 11(1):1–10

Wang J, Da L, Song K, Li BL (2008) Temporal variations of surface water quality in urban, suburban and rural areas during rapid urbanization in Shanghai, China. Environ Pollut 152(2):387–393

Webb R, Bai X, Smith MS, Costanza R, Griggs D, Moglia M, Thomson G (2018) Sustainable urban systems: co-design and framing for transformation. Ambio 47(1):57–77

Wellmann T, Lausch A, Andersson E, Knapp S, Cortinovis C, Jache J, Haase D (2020) Remote sensing in urban planning: contributions towards ecologically sound policies? Landsc Urban Plan 204:103921

Weng Q, Quattrochi DA (2018) Urban remote sensing. CRC Press

Wentz EA, Anderson S, Fragkias M, Netzband M, Mesev V, Myint SW, Quattrochi D, Rahman A, Seto KC (2014) Supporting global environmental change research: a review of trends and knowledge gaps in urban remote sensing. Remote Sens 6(5):3879–3905

Williamson JG (1995) Migration and city growth during industrial revolutions. In: Giersch H (eds) Urban agglomeration and economic growth. Publications of the Egon-Sohmen-Foundation. Springer, Berlin, Heidelberg. https://doi.org/10.1007/978-3-642-79397-4_3

Wu N, Silva EA (2010) Artificial intelligence solutions for urban land dynamics: a review. J Plan Lit 24 (3):246–265

Wulder MA, Loveland TR, Roy DP, Crawford CJ, Masek JG, Woodcock CE, Zhu Z (2019) Current status of Landsat program, science, and applications. Remote Sens Environ 225:127–147

Yadav G, Mangla SK, Luthra S, Rai DP (2019) Developing a sustainable smart city framework for developing economies: an Indian context. Sustain Cities Soc 47:101462

Yang L, Li Y (2013) Low-carbon city in China. Sustain Cities Soc 9:62–66

Yung EH, Conejos S, Chan EH (2016) Public open spaces planning for the elderly: the case of dense urban renewal districts in Hong Kong. Land Use Policy 59:1–11

Zhang XQ (2016) The trends, promises and challenges of urbanisation in the world. Habitat Int 54:241–252